Variable geometry turbocharging of transport diesel engines.

Baghery, A.

Award date:
1982

Awarding institution:
University of Bath

VARIABLE GEOMETRY TURBOCHARGING OF TRANSPORT DIESEL ENGINES

Submitted by: A.Baghery for the degree of Ph.D. of the
University of Bath
1982

A. Baghery.

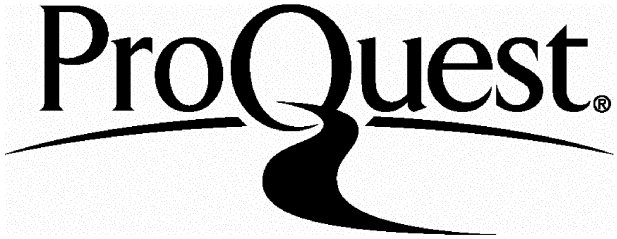

SUMMARY

A boost controlled continuously variable geometry turbocharger prototype has been designed, manufactured and tested. The prototype has been first rig tested and later fitted to a Perkins T6.354 diesel engine. The engine tests have included both steady state and transient runs.

Torque back up has been improved considerably increasing from 34.3% to 55.8%, the former occurring at 1400rpm while the latter at 1200rpm. In the experimental programme, compressor surge has been the limiting parameter while in the theoretical investigations a wide mass flow compressor has been assumed and the limiting parameter was maximum cylinder pressure. In the theoretical investigations lower compression ratio and retarded injection timing have been considered to further improve the scope for higher torque back up and improved transient response. In addition the performance of the variable geometry turbocharged engine using a simple boost controlled turbine restriction schedule has been simulated. It is concluded that a simple boost controlled system will present sfc penalties in the part load regime and thus more sophisticated multi-variable schemes will have to be studied if sfc optimization is to be achieved.

The experimental programme has been conducted using the 'zip fastener' design. This design has been found to be strongly non-linear with respect to turn down ratio in response to turbine restriction but will offer the required effects at the expense of a slight drop in turbine efficiency. However, in future investigations initial calibration studies have to be undertaken to ensure comparable swallowing capacities with the standard turbine which the variable geometry turbine replaces.

Acknowledgements

I wish to express my special gratitude to Prof. F. J. Wallace for the invaluable advice and guidance rendered throughout the supervision of this work.

At an earlier stage of the project, the writer also had many helpful discussions with the late Dr. R. J. B. Way.

Thanks are also due to Mr. B. Lang and Mr. P. Prest for their assistance with the prototype development and instrumentation of the rigs.

I would also like to thank the technical staff, in particular Mr. F. Denton, Mr. T. Elley and K. Britain for their patient cooperation.

Finally, Thanks are due to the Engineering School Office staff, particularly Mrs. H. J. Ford and J. Dyer.

Contents

Contents

Nomenclature

Symbol	Definition	Units
Ay	downstream area of a component	m2
CP	compressor power	kw
Cp	specific heat at constant pressure	kj/kg.k
CT	compressor torque	nm
Cs	compressor speed	rpm
Cv	specific heat at constant volume	kj/kg.k
es	engine speed	rpm
e	cooler effectiveness	
El	error margin on torque	nm
E2	error margin on mass flow	kg/min
hl	instantaneous turbine throat width	m
hlmax	maximum turbine throat width	m
hlmin	minimm turbine throat width	m
H	specific enthalpy	kj/kg
Hc	heat loss to coolant	kw
I	moment of inertia	kg.m2
k	combustion rate constant	
kq	heat loss correlation constant	
$\dot{M}e$	engine mass flow rate	kg/min
$\dot{M}f$	fuel mass flow rate	kg/min
Msc	scavenge air mass flow rate	kg/min
$\dot{M}c$	compressor mass flow rate	kg/min
My	downstream component mach number	
$\dot{M}ex$	exhaust mass flow rate	kg/min
Mcl,2	engine cylinder mass content	kg
M'ex,M''ex	mass content at start of successive pulse intervals	kg
$\dot{M}t$	turbine mass flow rate	kg/min

Nomenclature

$\dot{M}r$	rate of change of mass content of a receiver	kg/sec
$\dot{M}in$	rate of flow into a receiver	kg/sec
$\dot{M}out$	rate of flow out of a receiver	kg/sec
Mr	receiver mass	kg
Mf	mass of fuel prepared	kg
Mfinj	mass of fuel injected	kg
Ncyl	number of cylinders	
Pim	inlet manifold pressure	bar
Pem	exhaust manifold pressure	bar
Pl,2,3..	Pressure at 1,2,3.. in the engine cycle	bar
Pin	cooler inlet pressure	bar
Pout	cooler exit pressure	bar
Pex	exhaust manifold pressure	bar
P'ex,P''ex	pressure at the start of successive pulse intervals	bar
Pr	receiver pressure	bar
Pa	ambient pressure	bar
Pox	upstream stagnation pressure	bar
Q	rate of heat loss from a receiver	kw
Rc	compressor pressure ratio	
Rt	trapped air fuel ratio	
rslope	governor droop line slope	
r	rack position	
ri	initial rack position	
rf	final rack position	
r',r''..	rack position after t	
r'f,r''f..	'final' rack position after t	
rmin	minimum rack position	
rmax	maximum rack position	

Nomenclature

rm	boost pressure ratio	
rmjfr	boost at which turbine is just fully restricted	
rmjfo	boost at which turbine is just fully open	
resmax	maximum turbine restriction	
szero, 2	governor set points	rpm
TQc	compressor torque	nm
Tim	inlet manifold temperature	k
Tem	exhaust manifold temperature	k
Tl,2,3..	temperature at 1,2,3.. in the engine cycle	k
Tl,2	also compressor inlet and outlet temperature	k
Tox	upstream stagnation temperature	k
Tcl	mean coolant temperature	k
Tin	cooler inlet temperature	k
Tout	cooler exit temperature	k
Tex	exhaust manifold temperature	k
Tw	water jacket temperature	k
T'ex,T''ex	temperature at the start of successive pulse intervals	k
TQt	turbine torque	nm
Tr	receiver temperature	k
TQe	engine torque	nm
TQl	load torque	nm
Ta	ambient temperature	k
T	governor time constant	sec
U	internal energy	kj/kg
Vc2	cylinder volume in pulse model	m3
Vex	exhaust manifold volume	m3
Vs	swept volume	m3
V'ex,V''ex	volumes at start of each successive pulse interval	m3

Nomenclature

VOLce	cooler-engine receiver volume	m3
VOLet	engine-turbine receiver volume	m3
W	work by receiver	kw
$\dot{w}$	shaft acceleration	rev/s2
xloss	cooler pressure loss coefficient	
xeff	effectiveness coefficient	
xmf	cooler mass flow rate	kg/min
ΔPc	pressure drop across cooler	bar
Δs	speed increment over which full rack movement occurs	rpm
Δt	integration time interval also interval in exhaust pulse model	sec
ηc	compressor efficiency	
γ	specific heat ratio	
θ	crank angle	deg.

chapter i

1. Introduction

1.1 General

The indicated power of any internal combustion engine operating at a given air/fuel ratio is proportional to the air consumption. This constitutes the primary reason for the increasing level of pressure charging in modern diesel engines. Pressure charging can be administered in a number of ways. Independent pressurized air supply, mechanical supercharging, dynamic pressure exchangers, exhaust gas driven turbocharging and numerous variations on the latter including straight and differential compounding form the spectrum of available schemes. Each scheme is likely to be best suited to a particular application with considerable overlap between most of the schemes. Thus, the difficulty is in providing the boost in a manner suited to a particular application with a minimum of associated problems.

In addition to the increased engine specific output, the diesel engine performance can be improved in a number of incidental ways by pressure charging. Exhaust driven turbocharging has been widely used in the field of transport engines and is the subject of this thesis. It uses only a relatively small proportion of the energy present in the exhaust gases but is at present the most suitable method in this field. The major secondary benefits to be drawn from this scheme are better specific fuel consumption, lower noise levels and emission improvements among others. However, the specific disadvantage associated with turbocharging is the adverse effect on transient response and emission of black smoke due to turbo-lag i.e. the turbocharger's sluggish response. These are

dealt with in more detail below.

1.2 Basic features of exhaust turbocharging

As the specific output of the diesel engine is increased by turbocharging, the frictional losses increase only slightly leading to improved specific fuel consumption. This is an important aspect as regards the limited resources of fossil fuel and minimized running costs.

As it is possible to arrange for the boosting process to provide excess air at full load and speed, higher air/fuel ratios can be maintained leading to reduced levels of exhaust emission (24). This can also be extended to other speeds but at the expense of a proportional reduction in bmep. It is also possible to improve the torque characteristics of the turbocharged diesel engine over the naturally aspirated engine by arranging for reduced fuelling at higher speeds with the engine still giving adequate rated power.

A further benefit brought about by pressure charging is the reduction in the ignition delay period leading to smoother initial combustion patterns with considerable reduction in combustion noise levels. This reduced delay period will also allow injection retard such that reduced levels of NOx emissions can be obtained.

The above mentioned drawback of exhaust turbocharging is due to the fact that there is insufficient boost available at low engine speeds. The problem is clearly illustrated in Fig. 1.1. This figure shows the power requirements of the compressor over the entire speed range of a typical engine to be able to maintain a boost density ratio of 2.0, and the energy available from the

exhaust gases over the same engine speed range. The compressor curve is based on the assumption that the compression process is 100% efficient. It can be seen that if even all the available energy in the exhaust could be utilized, it would still be insufficient to obtain the required boost below 60% of full engine speed. In the real process where each component has its own inefficiencies, the problem is aggravated even further. Moreover, it is evident that at full engine speed, there is a 70% energy surplus over that required by the compressor, though clearly less for a compressor with an efficiency less than 100%. This highlights the basic problem associated with exhaust turbocharging in maintaining a constant high boost ratio over the normal speed range. Although a constant boost level over the entire engine speed range may not always be desirable, it is sufficiently close to the ideal requirements to illustrate the shortcomings of such a system. An important point emerging from this is the fact that in the lower engine speed range efficient energy conversion is essential while this is not so crucial at the higher speed end.

The increasing boost with increasing engine speed behaviour has been referred to as the 'natural' characteristics of exhaust driven turbochargers (48). The problem arises from the fact that all forms of turbine tend to have flow characteristics similar to those of fixed area nozzles with only a secondary effect due to the rotor rotation. Since the major controlling factor on the shape of the torque-speed curve of an engine is the shape of the fuel delivery characteristics, insufficient air over parts of the speed range would necessitate a cut back in fuelling over that part to avoid incomplete combustion and thus falling short of the ideal

torque-speed characteristics. Fuelling in accordance to air availability leads to a falling engine torque characteristic which is highly undesirable in transport vehicle applications, as it gives rise to the need for continuous gear changing. A measure of torque back up is thus necessary to avoid this situation. With fixed geometry turbocharging, to obtain a reasonable torque back up, it is necessary to arrange for a fuelling schedule similar in shape to that of a naturally aspirated engine which ignores the large amount of air available at high speeds and gives a peak torque at a speed usually in the region of 60% of maximum engine speed, with a limiting air/fuel ratio at this speed. In this way the need for continuous gear changing is reduced as the engine torque rises with reductions in engine speed. It is this requirement in transport engines that leads to the search for higher boost levels at lower engine speeds. Substantial improvements in this field will not only improve the 'drivability' of a vehicle but may well lead to new engine-transmission concepts where fewer gear ratios can be employed. However, moderate improvements can be effected by means of a number of options available and by revised matching considerations. First, a review of existing matching considerations will be given.

1.3 Matching considerations

It is necessary to select the flow characteristics of the turbine and compressor in a way such that the turbomachinary is suitably matched to a particular engine. This requires that the engine is not excessively penalized by back pressure from the turbine while the required boost density is obtained over as wide a range as possible. In addition to the problems presented by the 'natural'

characteristics of the turbocharger, these requirements are further aggravated by the fact that a typical turbomachinary can only work effectively over a relatively narrow range, although generally the compressor is capable of efficient operation over a wider range than the turbine.

Similarly, a number of considerations apply in selecting a suitable compressor. Since a constant horsepower non-compound engine is not likely to be a reality in the foreseable future, an engine torque characteristic having as high a peak torque as possible in the mid-speed range is highly desirable. It is thus essential for best torque back up, to ensure most efficient compressor operation in this speed range, while at higher speeds less efficient compressor operation can be tolerated. Since the best efficiency region of a compressor is normally quite close to the compressor surge line, a further consideration in compressor selection must be to avoid running into that region. It is also essential that extremely high velocities in the compressor be avoided to prevent compressor choking which can ultimately lead to engine air starvation as well as extremely inefficient compressor operation under choked conditions. This phenomenon, however, does not present as frequent a problem as compressor surging.

1.4 Options available for improved torque characteristics

The energy availability at the turbine inlet in the lower speed range can be increased by selection of a smaller turbine giving a reduced swallowing capacity. This tends to maintain a higher pressure ratio across the turbine at lower mass flow rates, but unfortunately also results in excessive back pressure on the engine

at higher engine speeds with consequential overboosting and increased pumping work by the engine in that region. This scheme, thus, cannot offer a solution without a means of limiting high engine speed overboosting. This can be achieved either by means of an exhaust waste gate or, by a tailored fuelling schedule. In the former, Fig. 1.2, some of the exhaust gases are routed round the turbine at high engine speed and load, resulting in reduced turbine work and hence boost pressure. However, this scheme will add to the complexity of the system for only a moderate improvement in the situation. With a tailored fuelling schedule engine fuelling is reduced at high engine speeds to keep turbocharger speed below a certain value corresponding to the required boost. This scheme offers the required improvement in torque characteristics comparable to the waste gate system, but at the expense of maximum power output (48).

Another development to aid low speed torque is the tuned inlet manifold reported by Cser (11) and (5). In this system resonance develops in the especially constructed intake system at low engine speed increasing the volumetric efficiency of the engine considerably. However, at high speeds the suction frequency of the engine is incompatible with the natural frequency of the intake system leading to a slight fall in performance. Thus, this system gives low speed torque improvement without overboosting at high engine speeds.

Similarly on the compressor side, a number of options are available for minor adjustments. Due to the wide speed range of transport engines very wide mass flow range compressors are needed. The mass flow range of compressors may be increased by means of imparting

prewhirl to the downstream flow at the compressor inlet. This can be effected through the use of variable inlet guide vanes (37, 44) or even aerodynamically by injecting high pressure fluid at an oblique angle into the main flow at the compressor inlet (21, 22)

Recent advances in compressor blading design such as backward swept rotors can give similar effect, and thus may be employed if exceptionally wide flow range compressors are required (43).

Finally an alternative method of turbocharging is the dynamic pressure exchanger, the Comprex supercharger (12, 15, 31). This has better low speed characteristics leading to better low speed engine torque and has a transient response almost an order of magnitude better than the fixed geometry turbocharger (31). However, this system is not fully developed as yet and remains bulky, heavier and more expensive than a turbocharger. Also the noise level, despite recent developments, is substantially higher than that of the turbocharger. Two stage turbocharging also presents an improvement on the single stage fixed geometry turbocharger (6, 26, 27, 33, 45). Other, more complex systems with secondary combustion chambers (2), Fig. 1.3, and compounding - differentially (36, 38, 51), Fig. 1.4, or straight (20, 32, 54), - are further alternatives to the single stage turbocharged engine but add considerably to the complexity of the diesel engine.

1.5 Transient response

The familiar turbo-lag has been the subject of many investigations (3, 7, 23, 46, 49). The turbocharger rotor has a finite inertia and thus takes a finite time to respond to changes in engine exhaust conditions. Under transient conditions, during this period of

time, there is insufficient air in the engine cylinders for complete combustion. Thus the sluggish response of the engine is accompanied by the emission of substantial amounts of black smoke as a result of unburnt fuel. This problem is aggravated in the case of highly rated engines, since the increase in fuel delivery to the cylinders is proportionally higher. However, in such cases boost pressure controlled rack limiters can be used to limit fuelling under low boost conditions at the expense of a further loss in the transient response (25).

Pulse turbocharging, where much of the kinetic energy of the exhaust gases leaving the engine is retained and made available for useful work in the turbine, has improved the transient response of the turbocharged diesel engine considerably. However, for highly rated engines it may be advantageous to use the constant pressure turbocharging system where under steady state conditions, the overall turbocharger efficiency may exceed the gains due to the retention of the exhaust pulse energy. In these cases, the transient response is further aggravated by the use of the constant pressure turbocharging system, where the cylinders discharge into a large exhaust manifold which takes a finite time to 'fill up' before the new conditions reach a steady state (30).

In engines in which as a result of pulse interference due to the number of cylinders and their firing order, pulse turbocharging is not possible and where constant pressure turbocharging is not acceptable, an alternative may be the adoption of pulse converters to minimize the pulse interference (47, 19, 10). This although not yet widely adopted in transport engines, has been increasingly applied to medium speed, highly rated engines.

1.6 Variable geometry turbocharging

The shortcomings of fixed geometry turbocharging have been highlighted above. In most of the schemes described, all of which offer some improvement, attempts are made to utilize the available energy in the exhaust in as efficient a manner as possible. However, from Fig. 1.1 it is evident that the energy availability in the low speed range is not sufficient to provide good low speed torque characteristics even if all the available energy could be harnessed. It is thus seen that ideally the energy availability at the turbine inlet has to be increased - similar in concept to the wastegate system, from a revised matching point of view - but at even lower engine speeds; i.e. by reduction of turbine swallowing capacity in relation to the mass flow rate to maintain the necessary pressure ratio across the turbine. This in effect is similar to having a series of volutes with different swallowing capacities, the smallest of which would be used to obtain maximum low speed torque, while at higher engine speeds a larger casing would be used to accommodate the mass flow without subjecting the engine to excessive back pressure.

The swallowing capacity of a turbine can be varied by two alternative approaches. Either a reduction in the volute inlet throat area, or a reduction in the volute exit width will both lead to a reduction in the swallowing capacity of nozzleless turbines. In the former, an increase in the inlet velocity, which is wholly tangential, occurs as the turbine has to pass the same amount of flow through the reduced area. This is due to the positive displacement action of the engine which maintains the mass flow approximately constant at a given speed. The volute exit angle,

being a function of volute geometry only, will decrease with respect to the tangential direction, resulting in increased rotor torque and hence compressor boost, Fig. 1.5. However, although a proportional reduction in the volute exit throat area would lead to a reduction in the swallowing capacity of the turbine, but this would actually lead to an increase in exit flow angle as the throughflow component has to increase to accommodate the mass flow. Nevertheless, as a result of the increase in the energy availability in the volute, it may be possible to obtain an overall improvement.

1.6.1 Previous variable geometry work at Bath

These possibilities have been investigated by a number of researchers at Bath and elsewhere. Some preliminary work was carried out by Sanwalka (28) who showed that the gains due to a reduction in the exit area of a nozzleless casing were very limited. Instead he suggested ideas for a scheme where either volute inlet area is varied or a nozzle ring is used at the volute exit.

However, before the nozzled casing scheme was investigated, tests were carried out by Ghadiri-Zareh (13, 14) using a series of differently sized volutes on turbocharged Perkins and Leyland engines. Figs. 1.6 and 1.7 show some of the results obtained. As the size of the volute is reduced, the 'equivalent' volute exit flow angle becomes tighter, thus changing the effective turbine match. With the smallest casing fitted to the Perkins engine, maximum engine torque with best air/fuel ratio and lowest sfc occurred at engine speeds down to 1550rpm, with the maximum cylinder pressure as the limiting operating parameter. This casing also presented the lowest smoke level over the greater part of this range of engine

speed. The medium size casing led to the occurrence of peak torque in the 1550 to 2300rpm engine speed range. There was also a considerable improvement in air/fuel ratio and smoke compared to the standard casing which gave moderate torque back up at an engine speed of 1600rpm. Similarly, with the Leyland tests, the smallest casing offered the best low speed torque back up with reduced smoke and improved sfc, while the medium casing gave comparable torque back up but at a higher engine speed of 1760rpm (Fig. 1.7).

At the same time, a theoretical investigation by Sivakumaran (29), the results of which are summarized in ref. (50), showed similar benefits to be gained from a variable geometry scheme where the swallowing capacity in a nozzled turbine casing is reduced by means of a change in the turbine nozzle angle.

In the next stage of the experimental programme, a series of tests were performed by Ziarati (57) on a Perkins T6.354 diesel engine restricting the volute throat area progressively by the imposition of spacers under the nozzle support ring to restrict the axial dimension in a number of discrete steps. This test programme showed that a substantial improvement in turbocharger speed in the engine mid-speed range could be achieved by a 56% reduction in volute exit axial distance. Higher restrictions showed a deterioration in performance. Similar tests using a nozzleless casing confirmed the fact that a nozzleless variable geometry scheme was unsatisfactory.

Following these investigations, attempts were made to determine the relative merits of various nozzled variable geometry schemes in an effort to approach a commercially viable design. Several versions,

including the 'sliding ring' and the present 'zip fastener' design were tested on the turbine dynamometer rig. The former consisted of a tight fit ring which moved over the nozzle ring thus presenting restriction to the flow, and the latter consisted of two nozzle rings each with half the number of original blades and each blade half the length of the original blades. These two rings could be brought to 'mesh' by imposition of spacers as with other schemes. Finally, Bahmanpoor (8) carried out a set of tests on the original 'sinking teeth' device but using triangular section nozzle blades rather than the aerodynamically shaped aerofoil section blades. This was an attempt at reducing eventual production costs, but proved unsatisfactory since the fall in turbine efficiency was found to be beyond acceptable levels. Also, from the earlier investigations it was concluded that the sliding ring configuration was not viable due to excessive loss in efficiency and that the 'sinking teeth' option offered the best performance in terms of efficiency and turn down ratio. However, from a manufacturing point of view the 'zip fastener' design offered ease of production and greatest compactness, while being only slightly inferior in terms of performance. This design was thus chosen as a compromise between production considerations and aerodynamic performance.

1.6.2 Other variable geometry investigations

Attempts have been made at developing variable geometry schemes by others such as Cummins Engine Co. and Teledyne Continental Motors. Chapple et al, (9) at Cummins have adopted a method whereby a variable geometry volute is effected by means of a movable wall inside the especially designed volute. Their objective was to create a fluid passage that would develop the same energy momentum

conversions for a variety of mass flow rates at the design pressure ratio and wheel speed. It is claimed that the variable geometry turbine efficiencies suffer only slightly and the scheme is thought to be suitable for turbocharging applications. However, no engine test data is included in ref. (9).

Berenyi et al, (4) at the Teledyne Continental Motors investigated the application of a swivelling nozzle variable geometry scheme to a very high specific output diesel engine. However, because of the very wide flow range needed in this project, a variable geometry compressor (pivoted diffuser vanes) was also developed to allow full exploitation of the turbine effect (16). The turbine efficiencies obtained during this investigation, which uses a swivelling nozzle ring upstream of turbine rotor inlet for swallowing capacity adjustments, showed a reduction of a few percentage points. However, considerable torque back up and transient response improvements have been obtained. Peak torque has been moved to 1700rpm from 2400rpm engine speed giving 16% torque back up compared with 3% at 2400rpm in the standard form. Maximum engine speed is 2600rpm.

1.7 Current work programme

The work described in this thesis consists of the following:

i) Theoretical consideration of variable geometry turbocharging

ii) Experimental investigation of variable geometry turbocharging

1.7.1 Theoretical considerations (computer program development)

This work is subdivided into the following:

i) Steady state program adaptation to the present work and inclusion of variable geometry aspects

ii) Transient program modifications including incorporation of variable geometry

An existing steady state matching program (EMAT) and the associated subroutines were metricated and adapted to the present work including provision for variable geometry simulation. The program was modified to be able to handle continuous boost controlled variable geometry operation according to a predetermined boost-restriction schedule as well as a discrete restriction option. Similarly changes were made in the transient performance prediction program (TRANIC). This program was also metricated.

1.7.2 Experimental investigations

The major part of the work reported in this thesis has been experimental and includes the design, development and testing of a variable geometry prototype. The test programme consisted of the following:

i) Rig testing of the variable geometry prototype

ii) Steady state engine testing of the prototype

iii) Transient engine testing of the prototype

After the variable geometry prototype was designed and produced, a series of turbine rig tests were carried out to establish its performance characteristics. These were performed on the high speed dynamometer (Section 2.1.1) using spacers to obtain four discrete restrictions of 0, 16.7, 33.4 and 50%, the latter constituting the maximum restriction obtainable with the 'zip

fastener' design.

The engine tests were carried out on a Perkins T6.354 engine loaded by the hydrostatic dynamometer (Section 2.2.1). The steady state tests consisted of a limiting torque and four constant bmep runs for each restriction. The restrictions were set at 0, 25, 40 and 50%. A further set of limiting torque tests was carried out using enhanced fuelling to take full advantage of variable geometry turbocharging.

The transient tests consisted of a series of 'constant' speed, fuel steps. The hydrostatic dynamometer was modified to improve its ability to keep engine speed constant under fuel steps and the tests repeated under these conditions. Enhanced fuelling was applied during the latter set of transient tests.

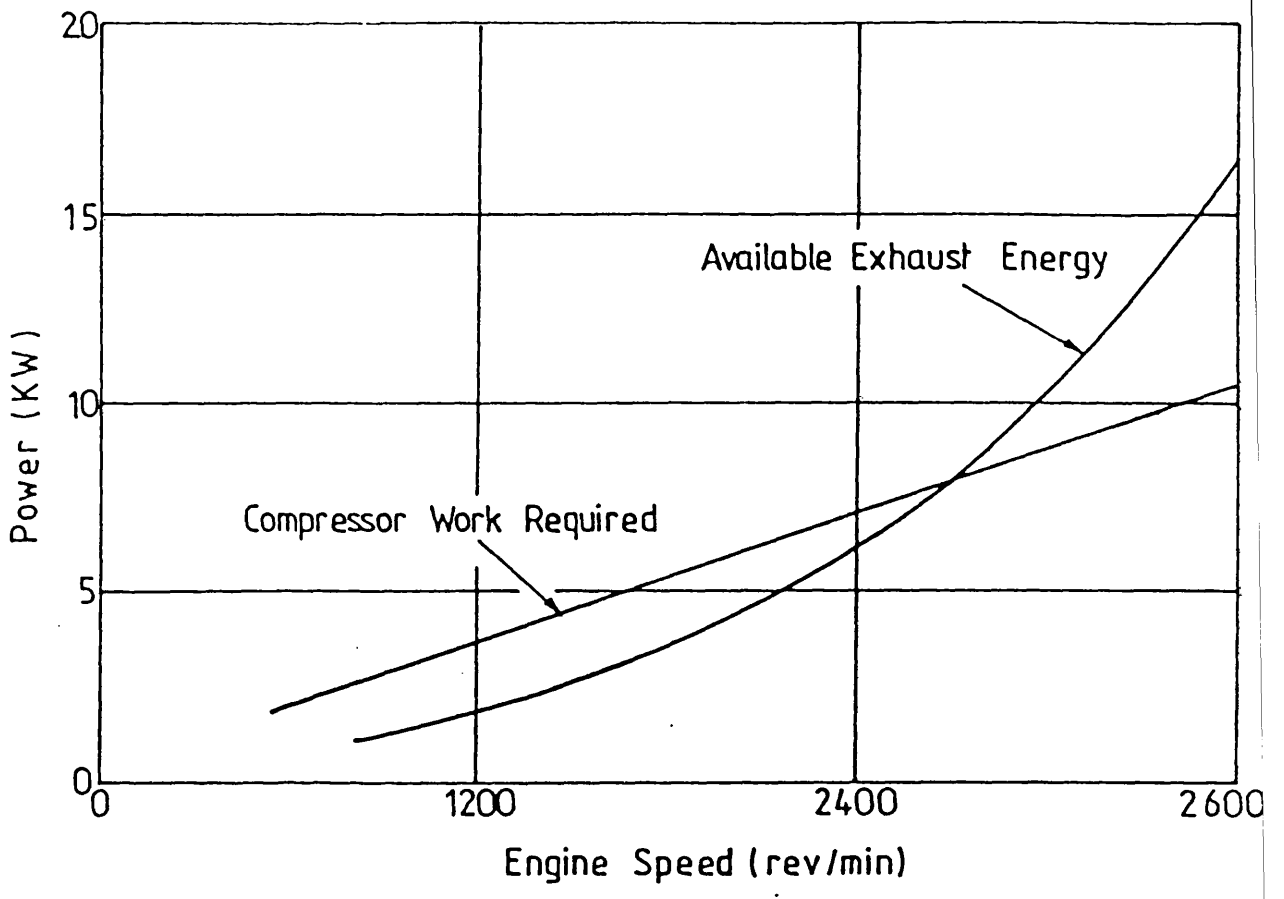

Fig. 1.1 Available Exhaust Energy and Compressor work at Full Load, Ref. (24).

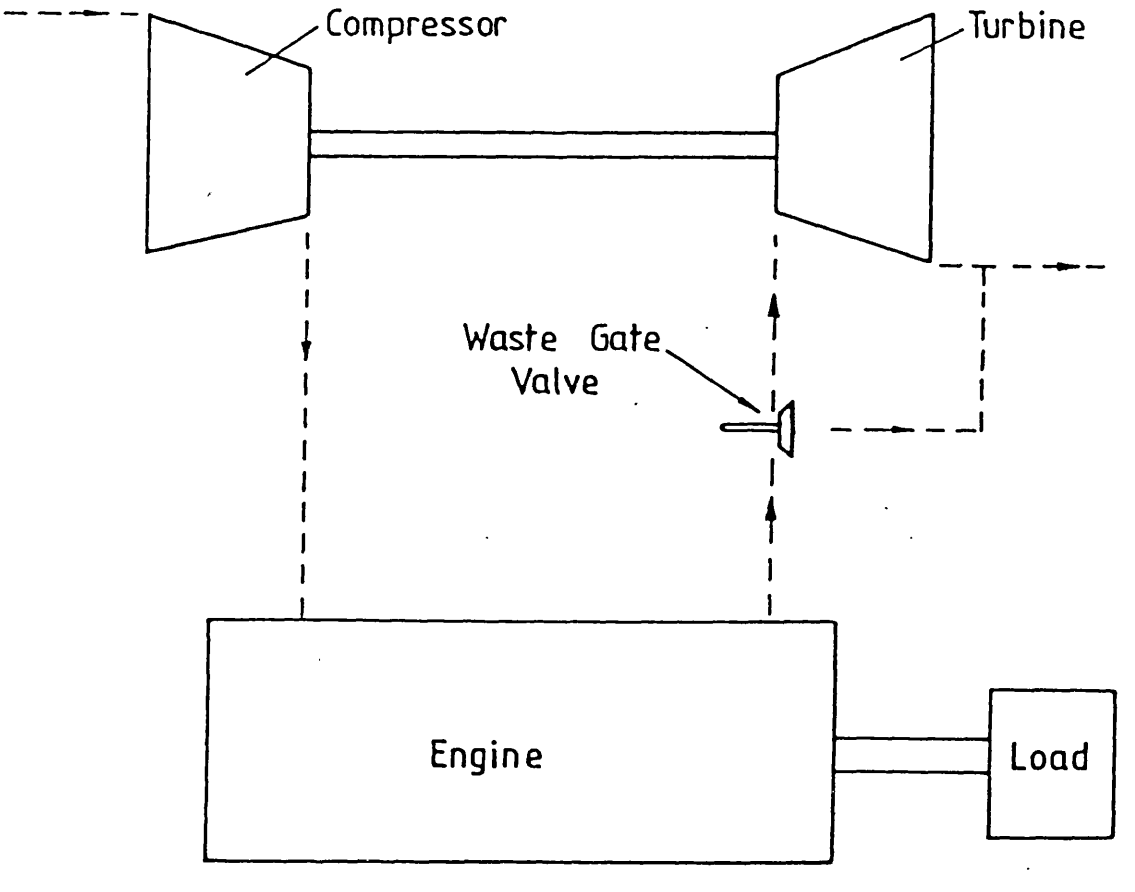

Fig. 1.2 Schematic of a Wastegate System

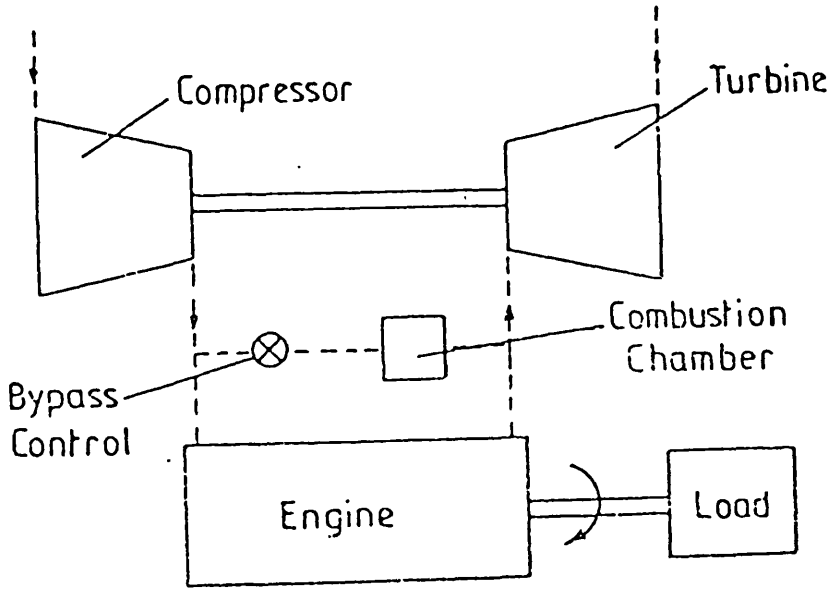

Fig. 1.3 The Hyperbar, A System With Secondary Combustion Chamber.

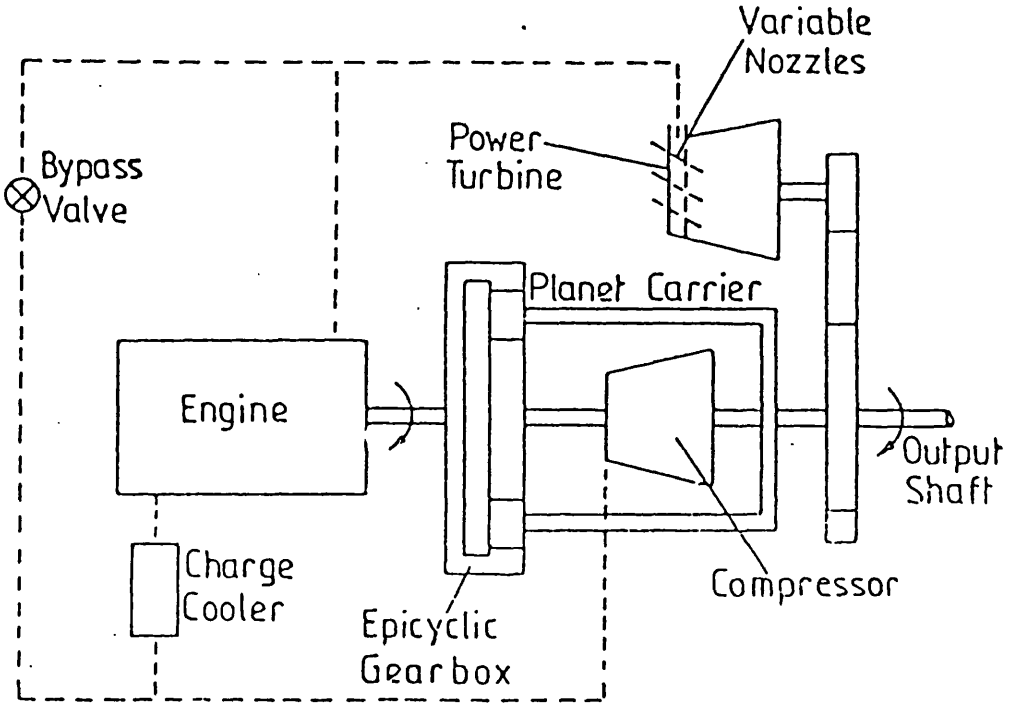

Fig. 1.4 Layout of the Differential Compound Engine.

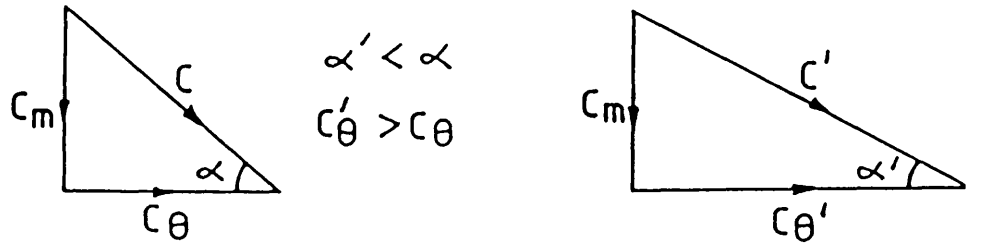

Normal Volute Restricted Volute Entry

(a) Variable Geometry Nozzleless Casing Exit Velocity Triangle

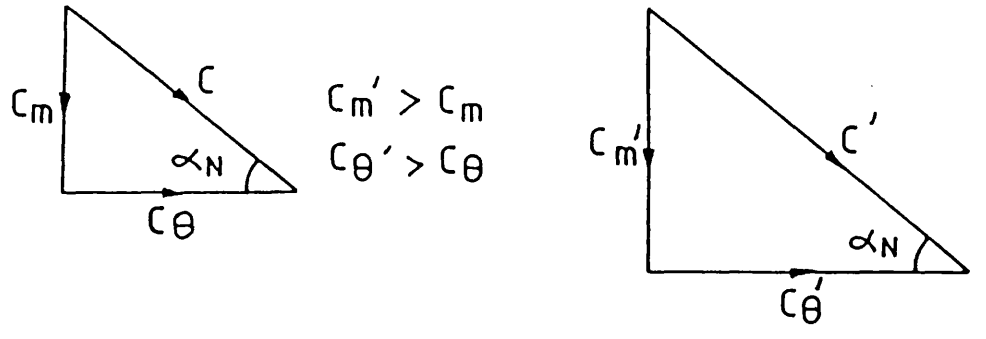

Normal Nozzled Volute Restricted Nozzle Ring

(b) Variable Geometry Nozzled Casing Exit Velocity Triangle

Fig. 1.5 Velocity Triangle For Variable Geometry Turbine.

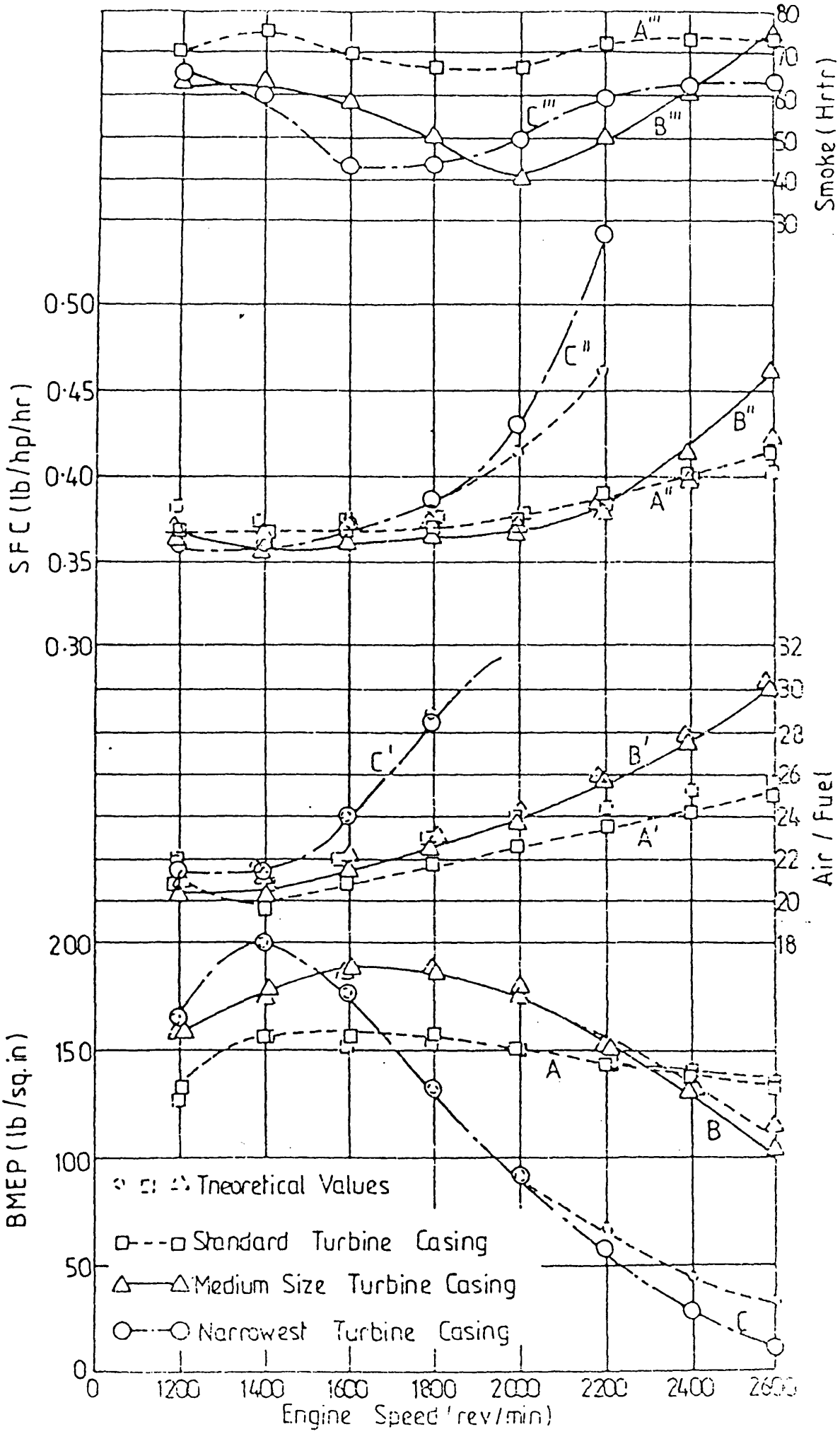

Fig. 1.6 Performance of Perkins T6.354 Engine Using Three

Different Turbine Casi

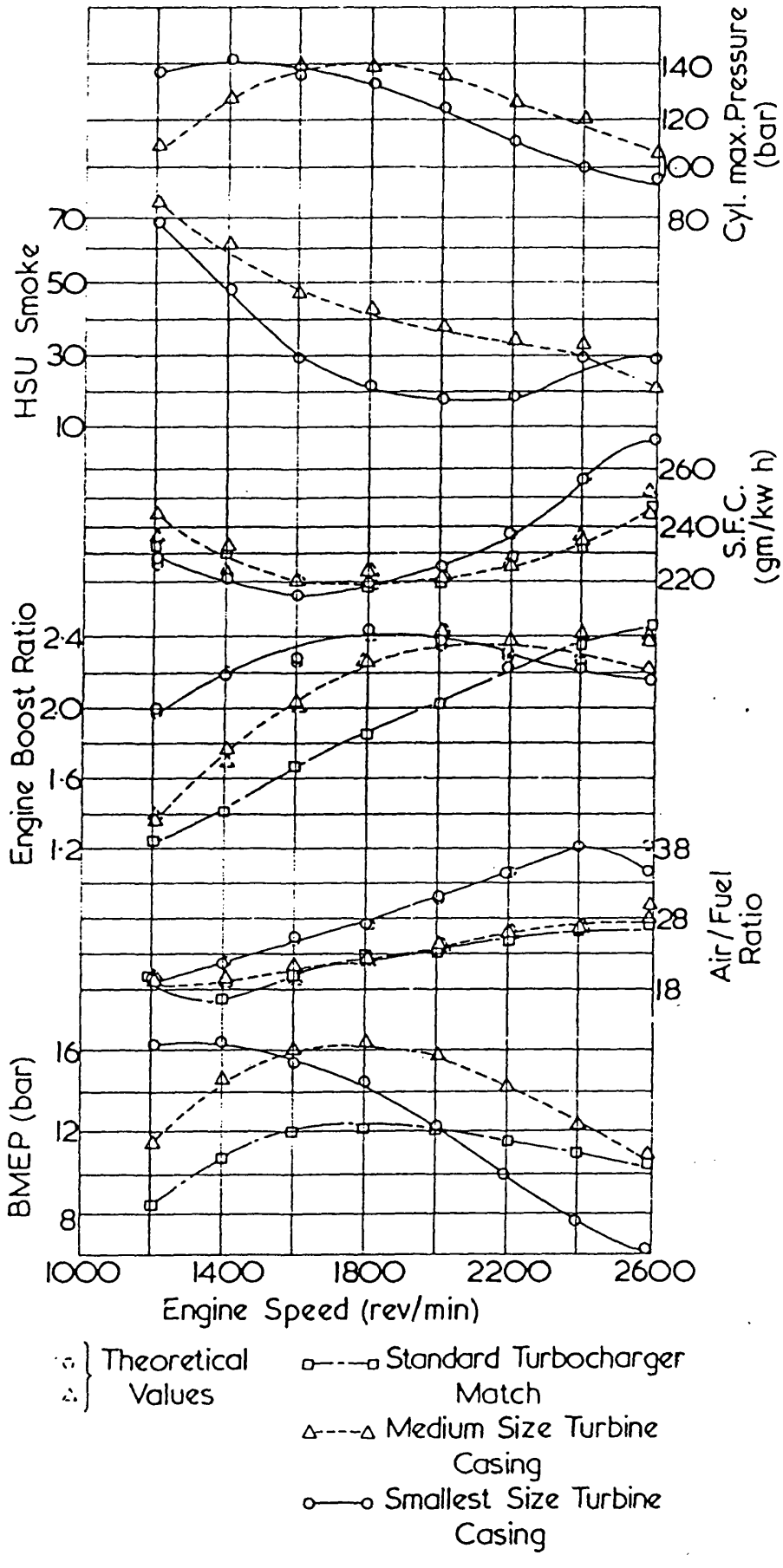

Fig. 1.7 Performance of Leyland 520 Engine Using Three Different Turbine Casings.

2. EXPERIMENTAL EQUIPMENT

2.1 Turbine test rig

2.1.1 The high speed turbine dynamometer

The variable geometry turbine assembly was fitted to the high speed turbine dynamometer, Figs. 2.1 and 2.2, especially designed to assess the performance of the turbine accurately over a broad range. The main bearing housing of the dynamometer, also supporting the brake arm, floated on air bearings to minimize frictional effects. Oil was pumped under pressure through the dynamometer absorption chamber which accommodates a cropped centrifugal compressor type rotor as the means of transferring the power developed by the turbine to the oil through viscous shear and pumping action. The oil was pumped from a settling tank passing through a filter and a heat exchanger before dividing into bearing oil, by-pass line and the rest into the dynamometer brake chamber, Fig. 2.3. The flows in the brake and by-pass lines are controlled by means of valves. These settings automatically determine the bearing oil line pressure. Load setting of the dynamometer is achieved by adjusting the valves in the brake and by-pass lines.

The power band of the brake was found to be limited by the need to maintain a minimum bearing oil pressure of 50 psi. The bearing and brake oil feeds were strongly interdependent and hence the minimum bearing oil pressure limit restricted the maximum loading capacity. This did not significantly affect the test programme, since the range available was sufficient for assessing the performance of the variable geometry turbine.

The drawbacks of this dynamometer were instability at full load and low speeds, partial seizure of the air bearings due to thermal distortion under certain conditions and inaccuracy in torque measurement due to connection of the flexible bearing oil feed hose to the floating section supporting the brake arm.

It was, however, possible with careful handling to avoid regions of instability and regular air bearing inspections overcame any seizure problems. The inaccuracy in torque measurement was minimized by recording any offset reading after every other run.

Air was supplied by the laboratory compressor which was capable of delivering a maximum of 50 m3/min. of air at a pressure of 6 bar. This was sufficient to meet the mass flow requirement of the 3-inch turbine unit up to a speed of 70,000 rpm over most parts of the power band without the need to use the combustion chamber.

The air pressure fluctuations were damped out as they passed through the arca valve. It then flowed through the gate valve and the electronically operated butterfly valve. At this stage turbine inlet pressure was regulated by an automatic reducing dome valve.

The rig was also equipped with a number of safety devices. The electronically controlled butterfly valve would shut down automatically should either bearing oil pressure fall below 50 psi or rotor speed exceed the preset value.

2.1.2 Turbine rig instrumentation

A full account of instrumentation methods concerning pressure, temperature, torque and speed measurements will be found in

subsection 2.2.2. The speed of the turbine was, however, measured by detection of electric pulses off a permanent magnet built into the dynamometer impeller shaft rotating in an open ended inductive coil fitted in an aluminium annular plate instead of the magnetic pick-off described in 2.2.2.

Air mass flow rate was measured using a BS1042 orifice plate situated in the supply line downstream of the pneumatic butterfly valve. Static pressure and temperature upstream of the orifice, the pressure drop across it and the orifice area enabled the computation of the mass flow rate.

2.1.3 Data reduction program

The quantities recorded during the turbine rig tests, i.e. static temperature, static pressure and pressure drop across the orifice, temperature and static pressure at outlet, brake load and turbine speed were all processed using an existing data reduction program. The program was modified to be able to handle these particular data.

The pressure transducer and the load cell were carefully calibrated and the calibration data was supplied to the data reduction program to convert voltages to the appropriate quantities in S.I. units. For a full listing of this program see references (57) and (8).

The program provides dimensional and non-dimensional quantities together with efficiencies. It was also modified to have relevant calculated quantities plotted on the plotter of the main frame computer. These results will be discussed in chapter 3.

2.2 Engine test bed

2.2.1 The engine test bed dynamometer

2.2.1.1 General description

The load for the engine was provided by a low inertia hydrostatic dynamometer (Figs 2.4 to 2.6). The load is controlled by the setting of a solenoid actuated valve which controls the area of the flow orifice upstream of the hydraulic pump in response to the current passing through the solenoid. The schematic layout of the dynamometer is shown in Fig. 2.7. The pump is a Lucas, fixed displacement swash plate axial piston unit. Oil is supplied to this pump by a Hamworthy gear pump driven by a 3-phase, 55 kw electric motor. The principle of operation is given in the following subsection.

2.2.1.2 Operation

The principle of operation of the dynamometer is as follows: The torque exerted on the engine shaft is approximately proportional to the pressure difference across the hydraulic pump. The pressure upstream of the pump must be maintained above zero gauge pressure for mechanical reasons. The electric motor is employed to provide this pressure by operating the gear pump upstream of the main loading pump.

The torque is, therefore, proportional to (Pl-Pb), where Pb is the upstream and Pl is the downstream fluid pressure determined by the position of the solenoid actuated load valve and the pump speed. The solenoid movement is proportional to the current flowing through

its coils. An approximate proportional relationship between solenoid current and dynamometer torque is, therefore, achieved.

The dynamometer has two basic modes of operation, namely constant torque and constant speed as well as allowing time-varying demand wave forms such as square or sinosoidally varying torque and speed schedules. For the present set of tests only the first two modes of the dynamometer were used.

Both the constant torque and constant speed modes employ proportional plus integral controllers. Torque/speed demand, set by means of potentiameters, is compared with the torque/speed feed back signal and the error between them is amplified in a circuit having proportional plus integral characteristics. The output is used to drive the solenoid and hence effect the desired load/speed.

The integral element is required to maintain the supply of power to the solenoid when the error signal approaches zero. A steady supply of energy is required under these conditions, since the valve is not driven through a hydraulic actuator which would maintain a steady state position without further need for power from the control circuit.

A further feature of the dynamometer is that it can produce 'negative torque' to motor the engine if necessary or to crank the engine for starting. This is facilitated by means of the electric motor which supplies the gear pump with enough power to raise Pb above Pl and result in a negative pressure difference across the pump (now motor), turning the engine.

Finally, the power inputs from the engine and the electric motor are dissipated as heat in the oil. This heat is transferred to the cooling water in a tubular heat exchanger.

2.2.2 Engine test bed instrumentation

Conversion of physical changes to calibrated digital or analogue quantities normally involves three stages. Namely, when a transducer is used as part of a measuring system, electronic signal conditioning and some form of display or data processing device form the other parts of the system. The following description is, therefore, presented with reference to all three parts of the measuring system.

i) Temperature measurement

The chromel-alumel thermocouple which is the most widely used device for temperature measurement was employed. No specific signal conditioning is required with this transducer. A Jenways unit, i.e. a standard digital voltmeter calibrated in units of degrees centigrade, was employed as the display unit. This device has built in cold junction compensation.

ii) Pressure measurement

For steady state pressure measurement, mercury or water manometers were used. For transients, semi-conductor strain gauge (piezoresistive) pressure transducers were used which make use of the strain dependent resistance of certain semi-conductors. These are highly sensitive with their outputs in the hundreds of millivolts range. Hysteresis is less than 0.1%.

The bridge formed by the gauges is supplied from a bridge regulator voltage supply and the output is fed into an instrumentation amplifier. The signal conditioning is performed by the plug-in card containing the appropriate circuitry.

After calibration, the output is interfaced with the A/D converter of the transient data acquisition system.

For cylinder peak pressure measurement, a piezoelectric transducer was used. These have a high frequency response making them suitable for this application. They also have very low hysteresis and a wide temperature range.

Since the surface of the quartz crystal in the transducer becomes charged in proportion to the applied pressure, they require careful signal conditioning equipment to minimize charge leakage. The charge amplifier, in conjunction with a storage osilloscope, was used to display the cylinder pressure variations. The traces or indicator diagrams stored had no provision for TDC marking. The diagrams were photographed by a purpose built camera.

iii) Speed measurement

The commonly used magnetic pick-off was used for measuring the speed of rotation of both the turbocharger and engine speed. The probe consists of a coil wound round a magnet. When a metalic 'tooth' passes through the magnetic field an electrical pulse is produced. The pulses so generated by the compressor wheel proved to be small due to the aluminium blading. Before conditioning these signals, a buffer amplifier with a gain of 10 was used to magnify the incoming

waveform.

The waveforms are converted to a stream of fast edged pulses by a trigger circuit. These are then fed directly to an orbit counter which detects the pulses and displays the appropriate reading in revolutions per minute.

However, during the transient tests, the on-line PDP-8L computer which was used for data acquisition, had to be supplied with analogue voltages. To this end, a frequency to voltage converter was used. The fast edged pulses were converted to fixed length and height rectangles. An integrator then provides a mean voltage proportional to the area of these rectangles. The more frequent the pulses, i.e. the higher the speed, the higher will be the mean voltage.

This technique is satisfactory for most applications but proved to be slow when used as the engine speed feed back signal to the dynamometer operating under speed demand mode. A d.c. tachogenerator which has an almost instantaneous analogue output, was used to improve the dynamometer response. The tachogenerator was calibrated against the rpm readings given by the magnetic pick-off placed near the wheel with 60 circumferential teeth.

iv) Air mass flow measurement

Air mass flow rate was measured using a British Standard bell-mouth nozzle (BS1042) attached to the compressor inlet. A water in U-tube manometer was used to display the depression caused by the flow of air. The necessary measured information together with the BS calculation procedure enabled the data reduction program to

calculate the air mass flow rate.

v) Fuel flow rate

Fuel flow rate was measured by timing a certain quantity of fuel drawn from a bucket placed on a balance. A two way valve, Fig. 2.8, allowed oil to be either drawn from the overhead fuel tank or from the bucket. The sudden change in head occasionally caused a slight instability in engine speed but was overcome by drawing fuel from the bucket for a while before a known quantity was timed. No attempt was made to measure transient fuel flow rates.

2.2.3 Data reduction program

The following quantities were recorded in the course of the steady state engine tests: BS nozzle pressure, compressor exit pressure, inlet manifold (i.e. cooler exit) pressure, turbine inlet and exit pressure, ambient pressure, compressor exit temperature, inlet manifold temperature, turbine inlet and exit temperature, ambient temperature, engine and turbocharger speed, engine torque and the time for a certain quantity of fuel to be consumed. These data were processed using an existing data reduction program (expl) modified to handle these particular sets of data. A full listing of this program can be found in ref.(57).

The output from this program is an array containing a wide range of calculated quantities such as power, sfc, air to fuel ratio, boost pressure ratio etc. The program was modified to have these quantities plotted by the main frame computer, mostly against engine speed. These results will be discussed in the next chapter.

2.3 Transient data acquisition system

The various quantities of interest during a transient test, such as the engine and turbocharger speed, load torque, various pressures and the metering valve position, which appear as analogue voltages at the output of the signal conditioning cards, were fed into the A/D converter of an on-line PDP-8L computer, Fig. 2.9. The computer was loaded with a simple data reduction program in machine code language. This together with the various calibration factors reproduced the original quantities and a teleprinter recorded these values at every tenth of a second during the time taken for one complete transient test to be performed. From the output of the teleprinter, various quantities were plotted against time. These will be discussed in the next chapter.

2.4 Description of the variable geometry turbocharger prototype

2.4.1. General description, Fig. 2.10 to 2.13

The device described below was the proposed first prototype, for experimental purposes, of a turbocharger in which the inlet area to the turbine could be varied whilst the engine was running. It was to be based on the main components of the Holset 3-inch turbocharger unit while use was to be made of the previous research work information obtained with a succession of discrete fixed restriction positions.

The inlet area of the turbine was to be restricted by as much as 50% of its original value. This was achieved by forming vanes on the adaptor ring, Fig. 2.10, linking the volute to the bearing housing

and a similar set of vanes on a piston or annulus able to move in an annular recess in the volute casting.

As the piston is moved forward out of its recess its vanes move into the spaces between the opposing fixed vanes, the span of each set of vanes being equal to one half of the width of the inlet passage. The solid annulus of the piston closes off the inlet area by reducing its width until the desired degree of restriction has been reached. This design has been referred to as the 'zip fastener' design for apparent reasons.

Although previous investigations had shown that the 'zip fastener' design will offer marginally inferior performance to the 'sinking teeth' version, it was nevertheless selected for the first prototype as a compromise between performance, simplicity and reliability. However, it is noted that this design is only capable of a maximum of 50% axial restriction, since the half blades on each ring would come into contact with the opposite ring surface giving a maximum travel of half the total throat width. Nevertheless, since at 50% axial restriction, the total blade blockage forms a larger proportion of the unrestricted throat area, it will result in a maximum restriction, in terms of throat area, in excess of 50%.

The design presents three main problem areas viz. guidance of the moving parts, sealing of the gases and positional control. Each of these is strongly influenced by the high temperatures involved and the corrosive properties of the exhaust gases.

2.4.2 Guidance

The moving parts had to be guided in such a way as to achieve consistent positioning in response to the control without sticking and throughout an acceptable life. To avoid possible sticking problems caused by thermal distortion it was decided to provide guidance on the control piston where temperatures are quite low and to leave clearances around the vaned piston in its recess in the volute casting. In the early stages of design, it was thought that the leakage past the piston would be negligible in view of the fact that at least 50% of the inlet area would still be open even in the most severe throat restriction case. However, as it will be mentioned later, the clearance around the vaned piston did pose serious leakage problems which were eventually solved.

2.4.3 Sealing

The piston rods carrying the vaned piston had to be sealed also. These seals had to cope with eccentricity between the rods and the bores in which they run and were exposed to high temperatures. The constraint of using the existing volute casting necessitated sealing in a region of high temperature. However, this would not be economical for a production device where suitable design of the volute and control system could facilitate much cheaper sealing in a less hot region.

The sealing involved the use of piston rings mounted in pairs in the casting, with the control rods sliding through them. Each pair consists of a ring tensioned to spring outwards on to the casing and another to spring inwards onto the rod. Large radial clearances are, therefore, acceptable without losing seal effectiveness. The

rings used were made of stellite but in a cooler environment cheaper materials could be used. The control rods are made of stainless steel with a very fine finish to improve the rubbing characteristics. No lubrication was used due to the hostile working environment.

The major sealing problem, however, was the main piston which was exposed to boost pressure on one side. The piston experienced very high temperatures in excess of 300 C. The inside and outside of the annular piston was sealed using piston ring shaped PTFE ring and a U-cross sectioned sealing ring on each section. These seals were only a first attempt and melting and extrusion problems were expected when the prototype was mounted on the engine. The problems encountered during the tests will be mentioned as each particular set is being discussed in the next chapter.

2.4.4 Control

The boost control system employed for the prototype consisted of an annular piston exposed to compressor delivery or cooler exit pressure such that the force due to this would act in opposition to a spring force. The chamber in which the control piston operated was formed around, and supported by, an extension attached to the volute casing which replaced the first few inches of the exhaust pipe. The diameter of this part, called the tail-piece, was slightly smaller than the original exhaust pipe and as it proved later, had an adverse effect on turbine performance since it acted as a nozzle at the turbine exit. The area reduction ratio was 1.4:1.

Since the force exerted on the vaned ring due to exhaust gas pressure also affects the boost-restriction schedule, provision was made to minimize this effect. The force due to the exhaust pressure on the vaned ring acted in the same direction as the force due to boost. Therefore, the effective area for boost pressure action was chosen to be considerably larger than the vaned ring face area which was exposed to the exhaust pressure. The effect of the exhaust pressure was minimized to an upper limit of 4.5%.

By the appropriate selection of spring lengths and rates, any linear variation of boost with piston position is possible. However, the space available for the springs lends itself perfectly to the use of diaphragm (Hauserman) springs, which can be made to give almost any force - displacement pattern. It is therefore possible to produce the optimum restriction for any given boost pressure. Initially, however, by using a set of ordinary coil springs the assembly was calibrated to follow a linear schedule from a fully restricted (50%) position at 1.5 boost ratio to gradually unrestricting the throat area up to 0% at a boost ratio of 2.0. A certain amount of stiction and backlash was observed which were improved greatly but impossible to eliminate.

2.5 Prototype modifications

In the very beginning, it was realized that excessive stiction prevented the piston from smooth movement and hence unintrupted restriction of the turbine. The U-sectioned rings were replaced by a similar set of PTFE rings to reduce this effect. The stiction was considerably reduced but at the expense of unacceptable boost air

leakage past the piston. Since it was envisaged that for the major part of the experimental programme, discrete restriction positions would be used, it was decided to supply the 'boost' air from an external supply. Any leakage from this air would be insignificant. As it proved later, this air helped to cool the seals and prevented them from premature destruction. A vent hole was also drilled at the back of the assembly to allow the leakage air to escape freely.

Later in the test programme, the 4 seals (2 on each side) were further reduced to 2 (1 on each side) to deliberately increase the leakage air and thus improve the seal life.

The turbine dynamometer tests showed a great deal of air leakage past the vaned piston, discharging directly to the downstream side of the rotor blades. The problem was almost totally eliminated by the insertion of a set of in and out-springing piston type sealing rings. The set contained two in-springing and one out-springing rings which together formed a very effective sealing arrangement. As a result of the leakage, the first set of turbine dynamometer tests were discarded and are not included in the thesis. A further set of tests was carried out after the leakage problem had been solved.

Finally to achieve consistent nozzle plug positions for various discrete restrictions, a set of accurately ground distance pieces were used. In the turbine dynamometer tests, spacers were made to give 16.7% and 33.4% restriction in addition to the 0% and 50% restrictions obtained by having the air supply fully 'on' and fully 'off' respectively.

In the engine tests, a set of distance pieces were made to give 0, 25, 40 and 50% restrictions including the 'on' and 'off' positions. However, the manner in which these pieces were placed between the moving plate and the body of the assembly to achieve the required restriction varied during the first and the repeat set of tests. In the first set of tests the pieces were placed between the moving plate and the body of the turbine casting and the air supply then shut. Since it was impractical to have support in more than one place, the inevitable tilt of the moving plate under spring force resulted in a further restriction of the turbine throat area beyond the nominal values. In contrast, in the repeat set of tests, to ensure constant flow of leakage air past the seals, the distance pieces were placed between the moving plate and the body of the variable geometry device while having the air supply 'on' all the time. This resulted in the actual restriction to be less than the nominal values. This is the reason for the relative effectiveness of the 25 and 40% restrictions in the first set of tests and the marked deterioration in effectiveness of the 25 and 40% restrictions in the repeat set of tests.

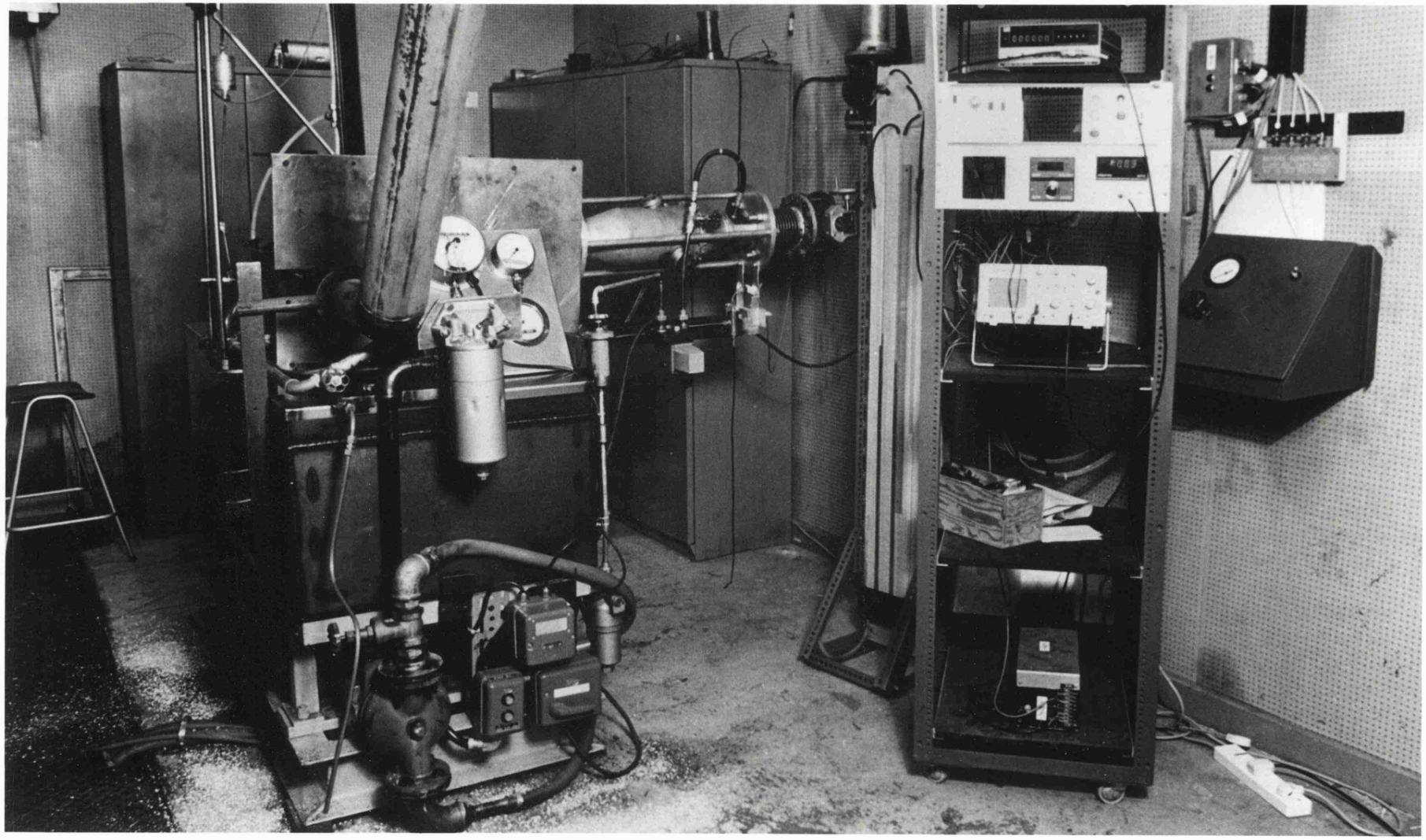

FIG. 2.1 TURBINE RIG AND INSTRUMENTATION PANEL

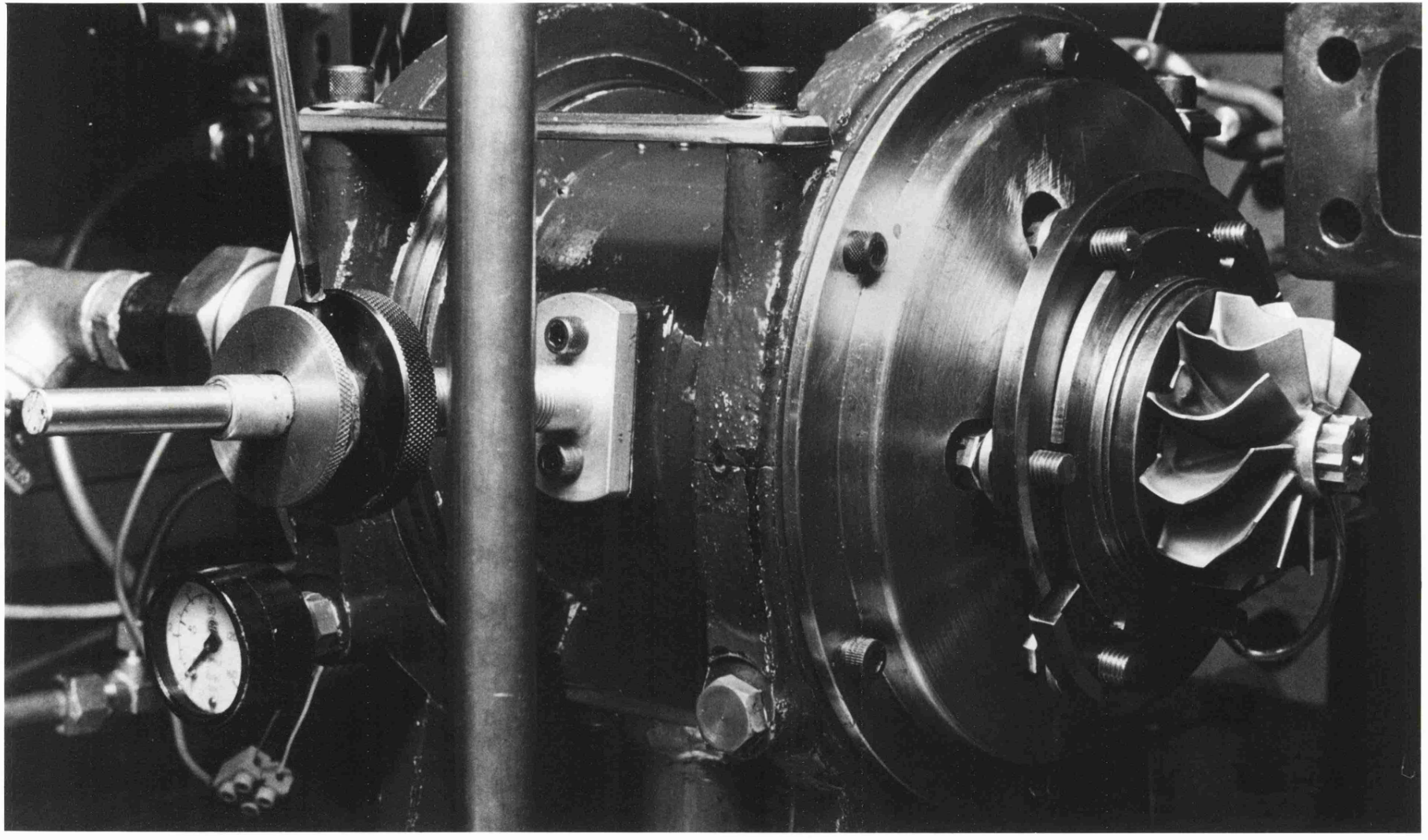

FIG. 2.2 TURBINE ROTOR AND DYNAMOMETER ASSEMBLY

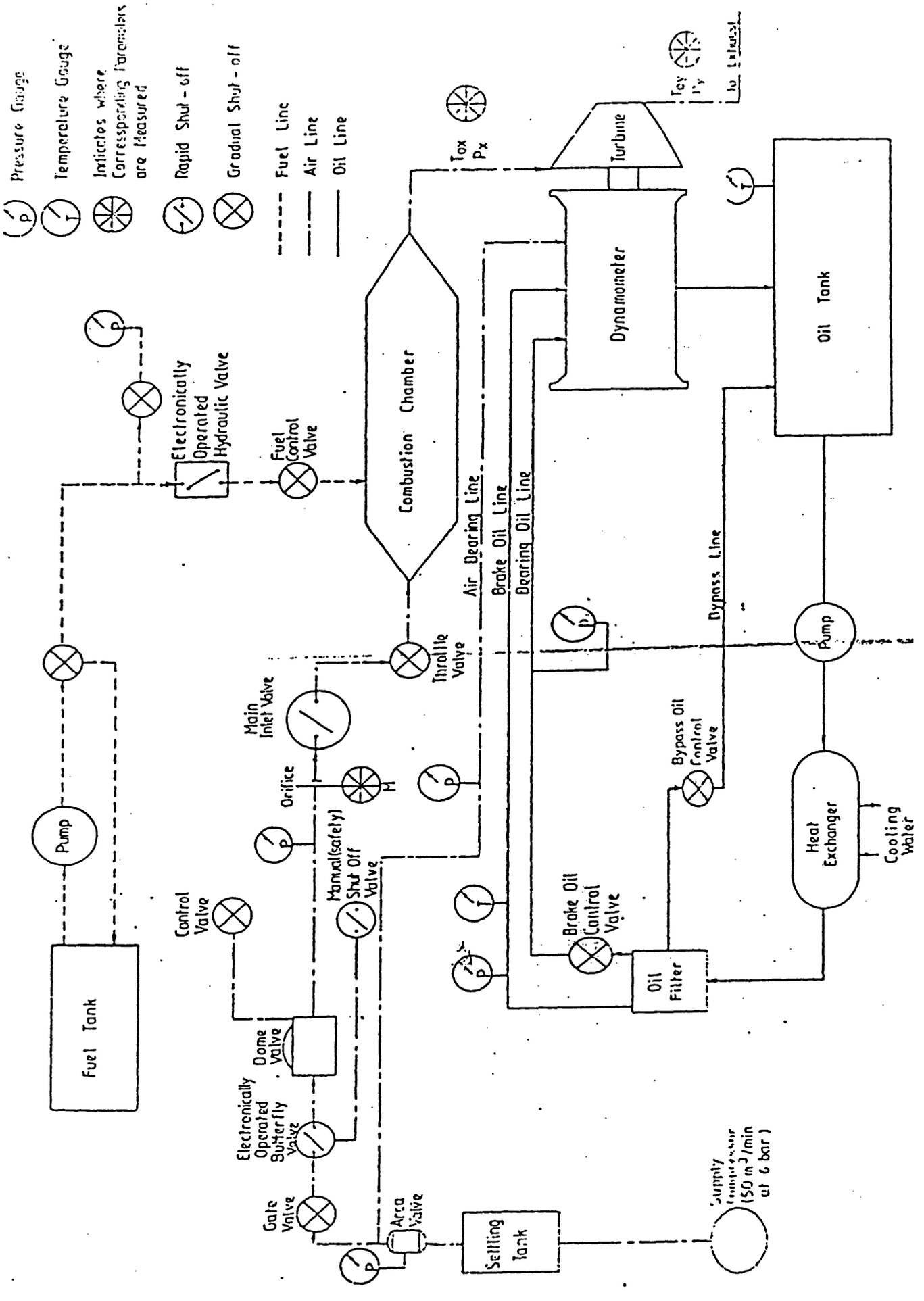

Fig. 2.3 Schematic Layout of the Turbine Dynamometer Rig.

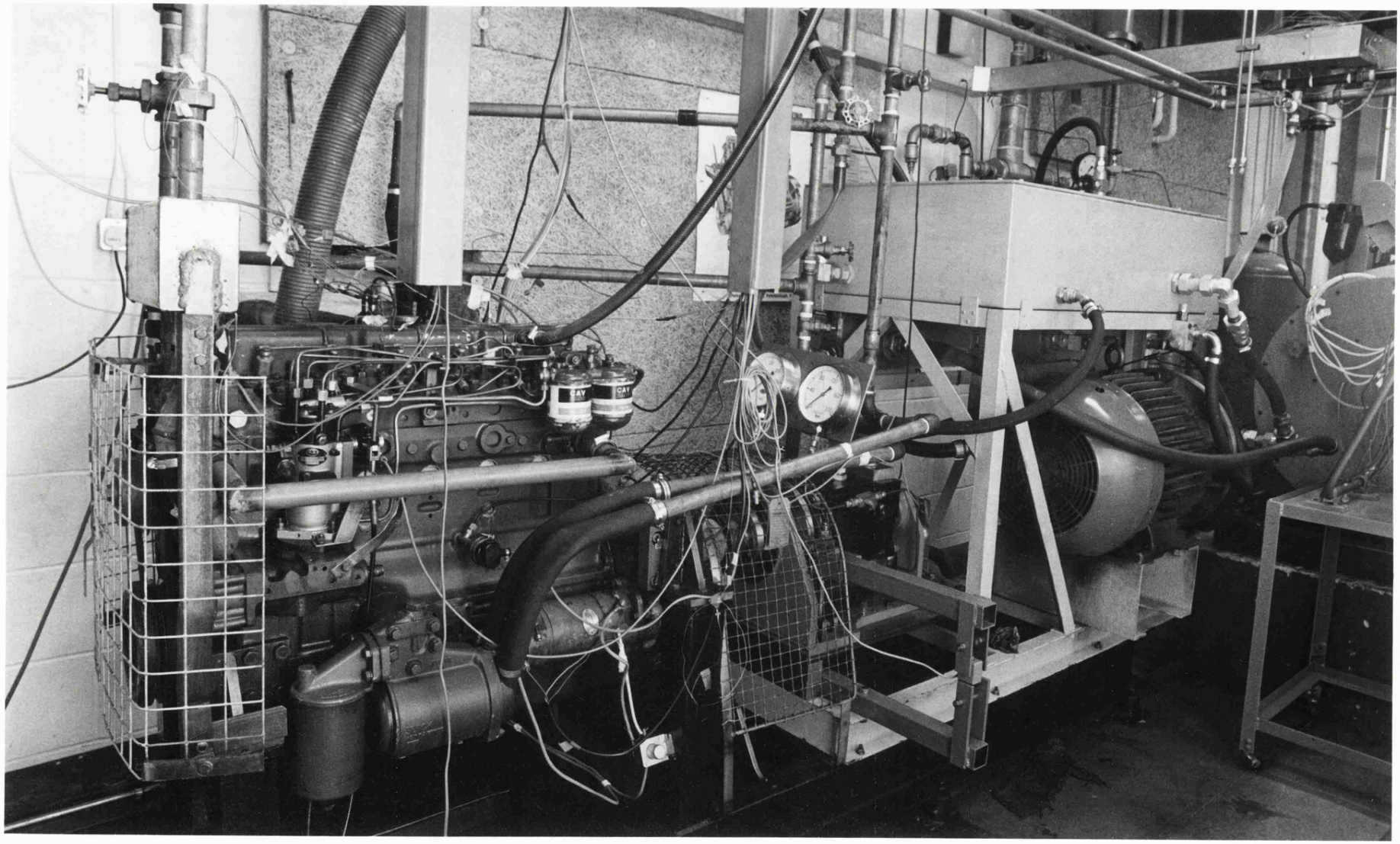

FIG. 2.4 ENGINE-DYNAMOMETER ASSEMBLY

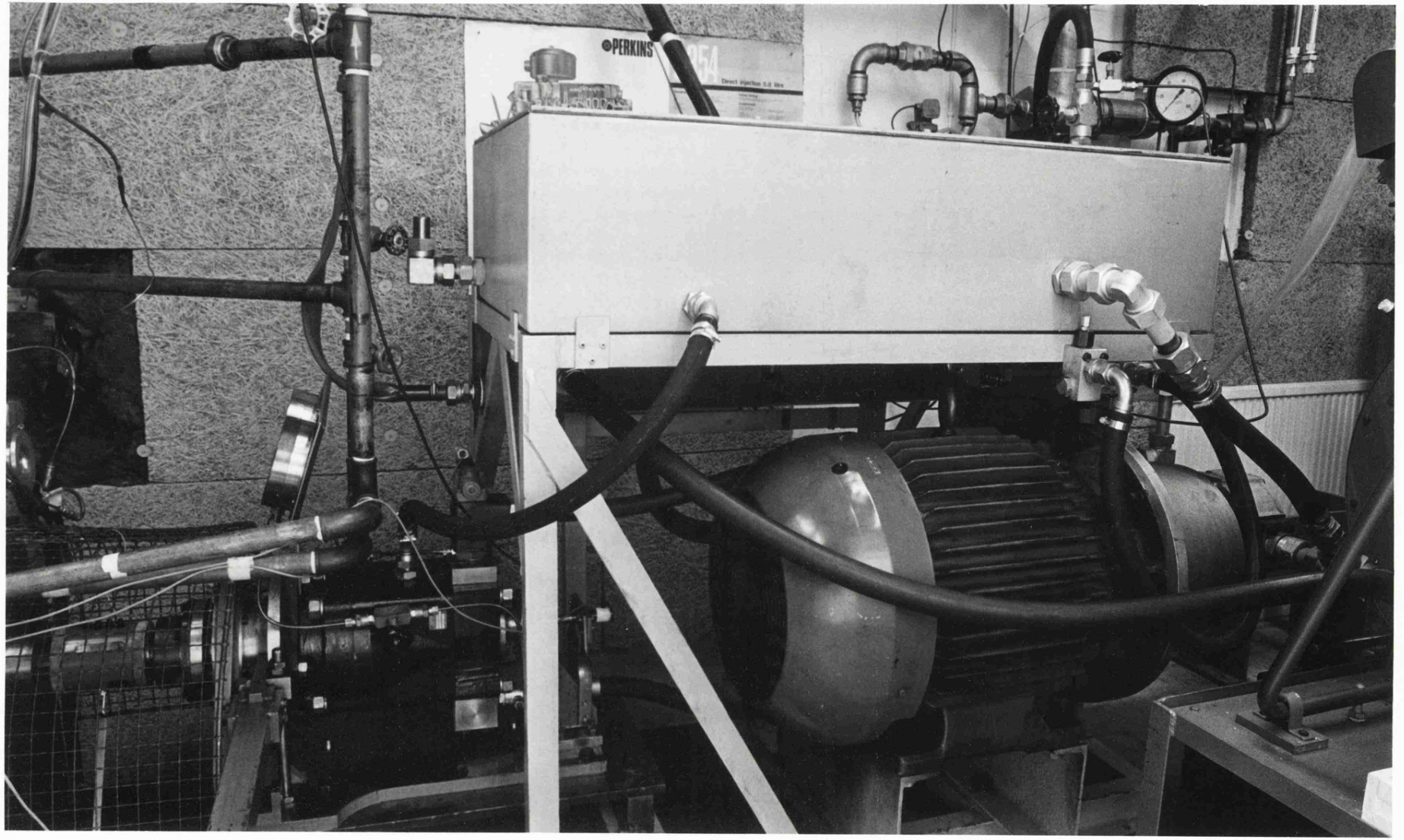

FIG. 2.5 HYDROSTATIC DYNAMOMETER

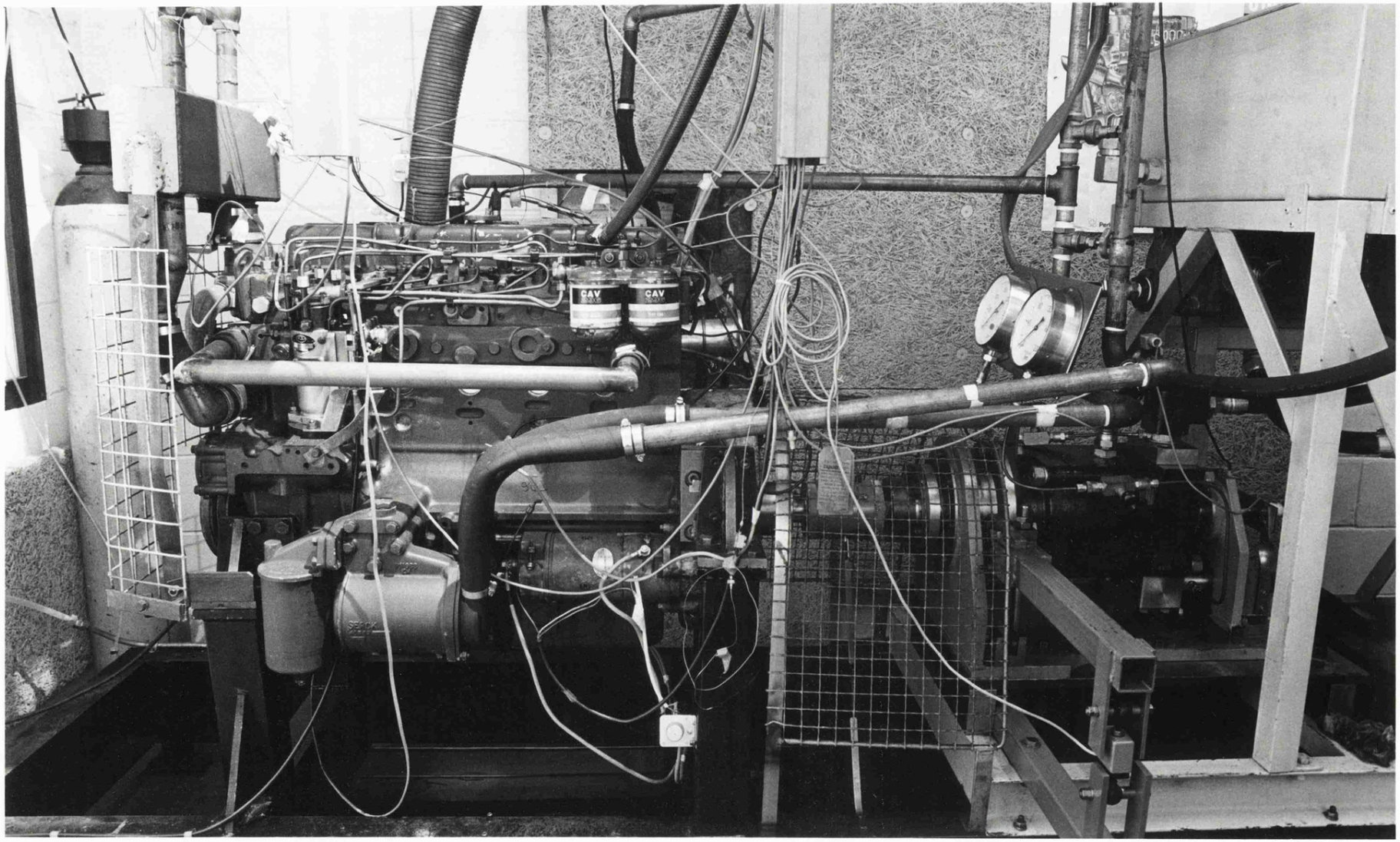

FIG. 2.6 PERKINS T6.354 ENGINE

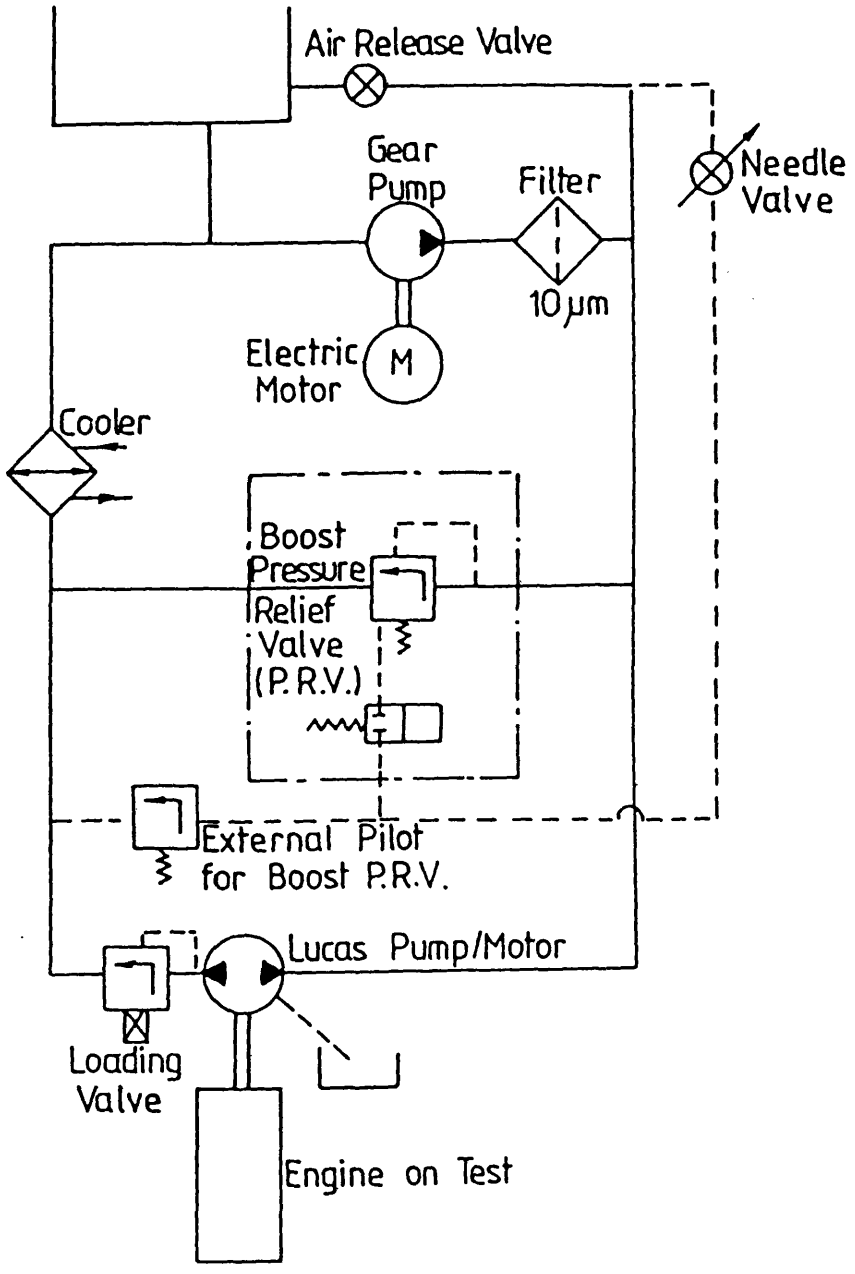

Fig. 2.7 Hydrostatic Dynamometer Hydraulic Ciruit.

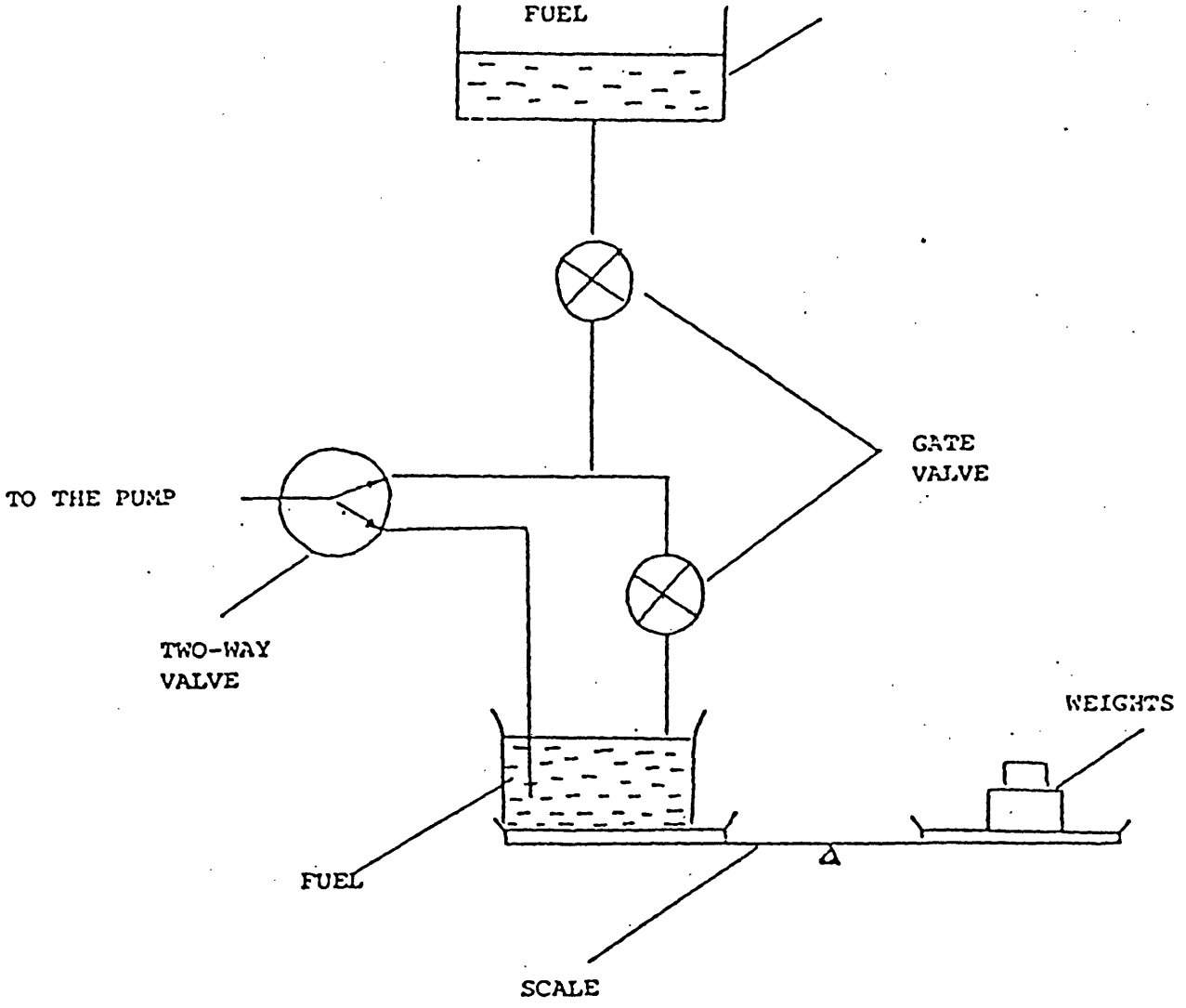

Fig. 2.8 Steady State Engine Fuel Flow Measurement.

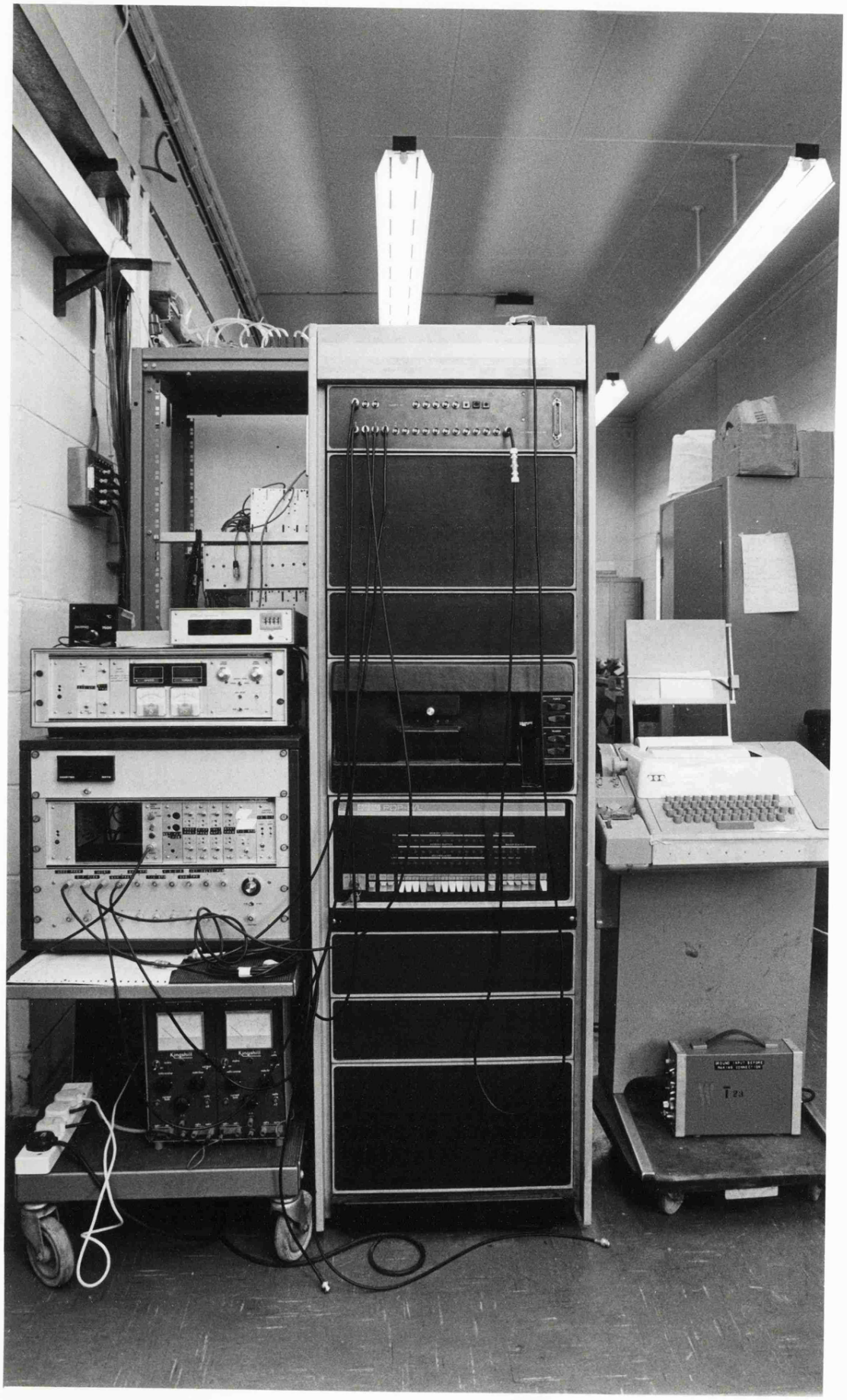

FIG. 2.9 ENGINE DATA ACQUISITION SYSTEM

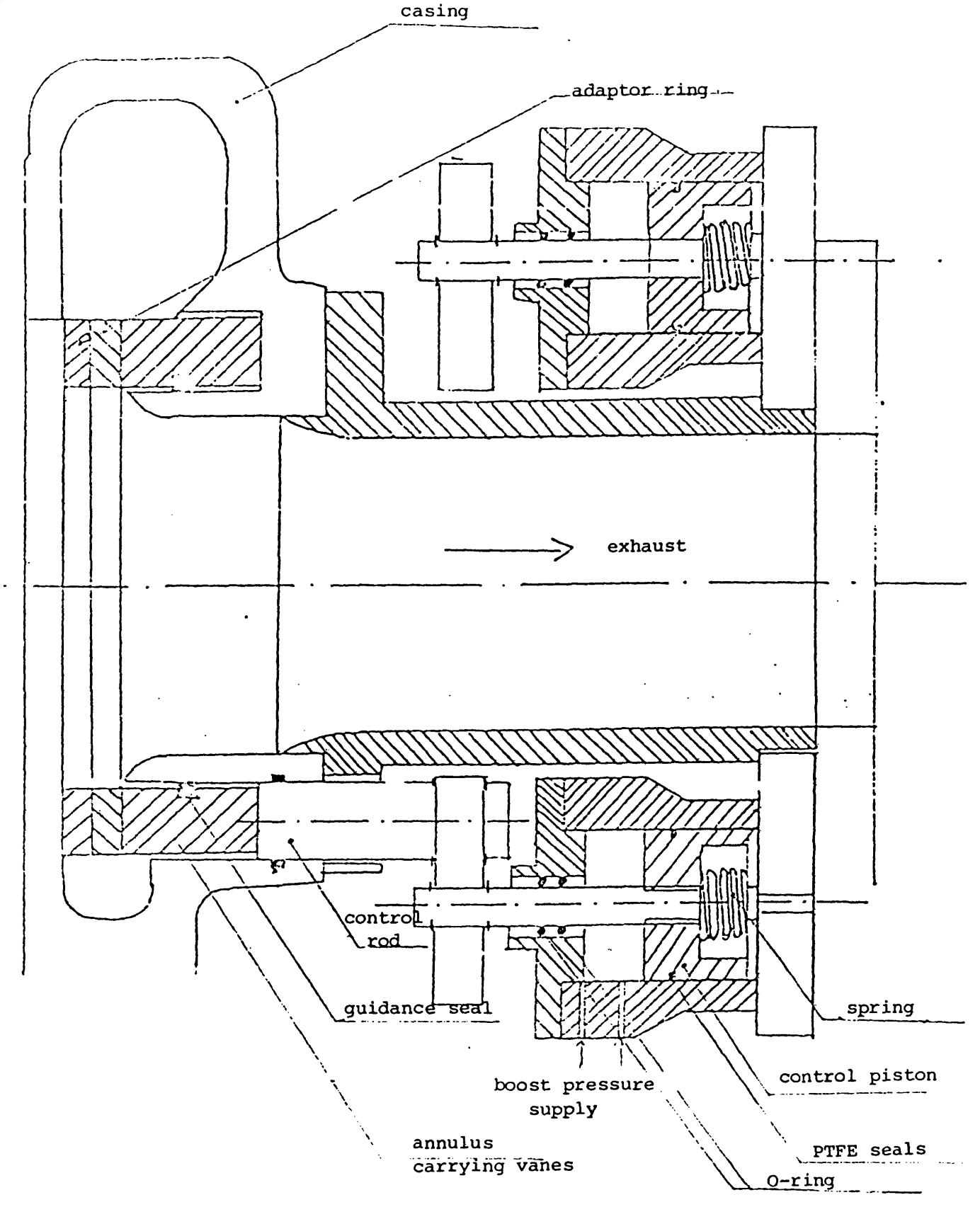

Fig. 2.10 Schematic of Variable Geometry Turbine Assembly.

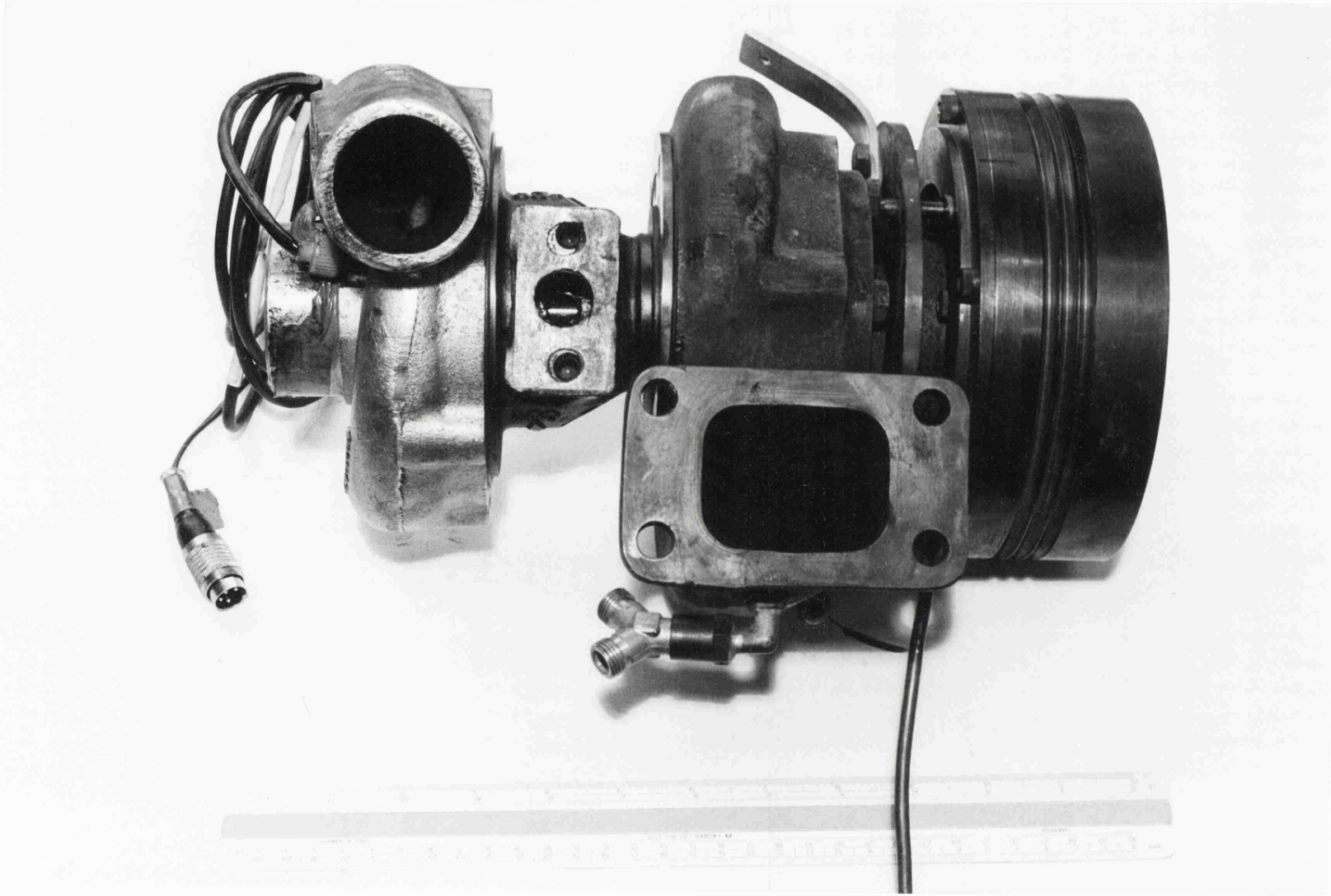

FIG. 2.11 VARIABLE GEOMETRY TURBOCHARGER ASSEMBLY

FIG. 2.12 VARIABLE GEOMETRY COMPONENTS

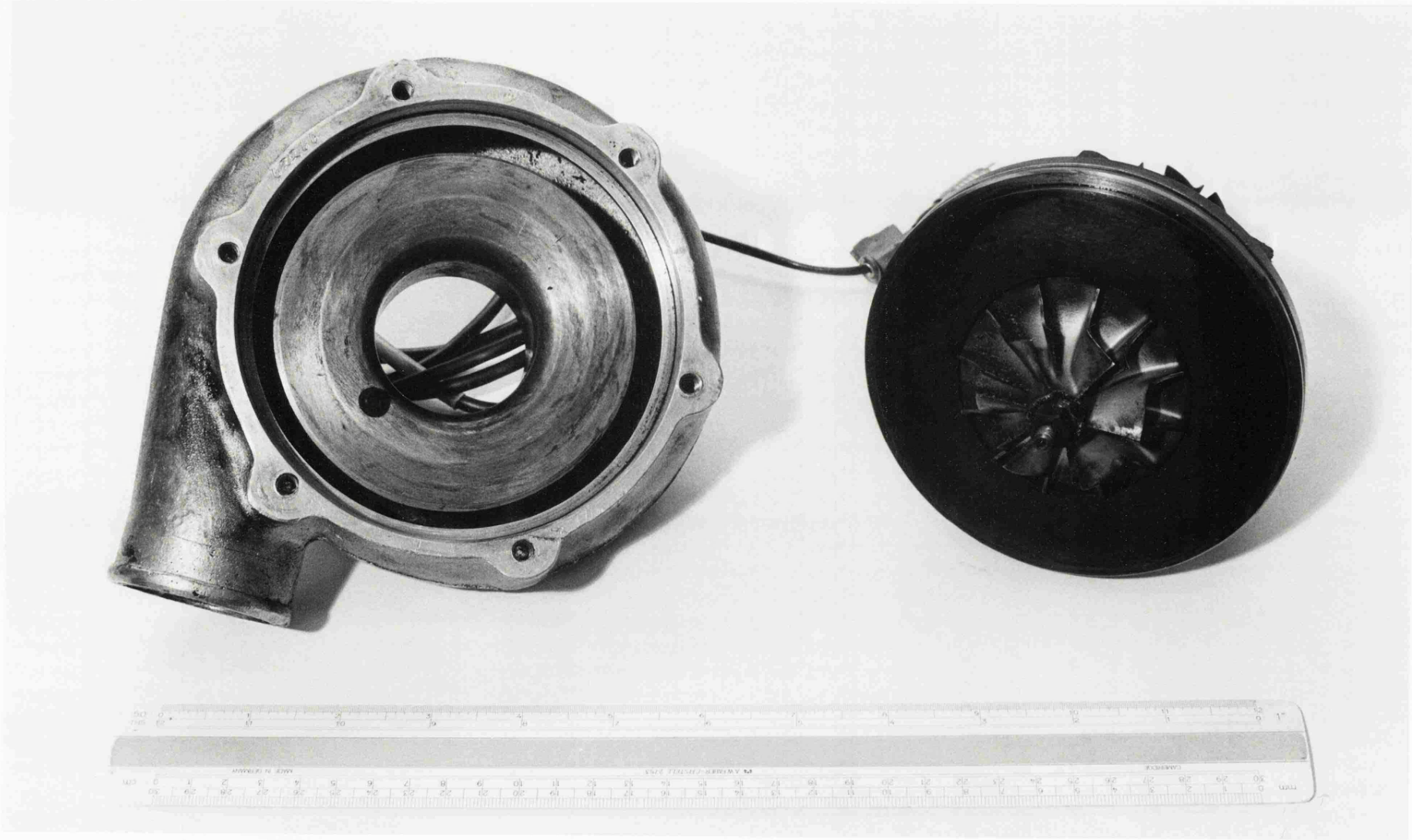

FIG. 2.12 H1 SERIES COMPRESSOR

chapter iii

3. EXPERIMENTAL PROGRAMME

3.1 Turbine dynamometer tests

3.1.1 General

As it was stated in the introduction, following the work carried out by Ziarati (57) and Bahmanpoor (8), it was concluded that it was necessary to carry out further work on the 'zip fastener' prototype which was chosen as a compromise between performance and production merits. To this end, the device which was described in section 2.4 was fitted to the high speed turbine dynamometer and a final set of tests was carried out to assess the performance of the prototype unit. It should be remembered that this design will only give a maximum of 50% axial restriction. As mentioned earlier the first set of tests were found to be unacceptable as a result of the excessive leakage past the moving nozzle ring, allowing the flow to bypass the rotor blades and discharge directly to the downstream side of the blades. The results of these tests are not included in the thesis, since their contribution to the project is minimal.

A further set of tests was carried out after the leakage problem was solved by the insertion of the 'in and out' springing sealing rings in the prototype. For this series of tests, the distance pieces were used to keep the variable geometry device in a number of discrete restriction settings. A linear distribution from 0 to 50% axial restriction was chosen at 0, 16.7, 33.4 and 50%, (actual restrictions in terms of 'throat area' are slightly higher due to the blockage effect of the vanes in this particular design).

Since a similar set of tests had previously been carried out on the preceding 'simulated' prototype (57, 8), it was decided, in the interest of time, to perform the present tests only at turbine speeds of 30000, 50000 and 70000rpm over the permissible dynamometer load range. This, as it proved later, was sufficient to represent the prototype's performance characteristics.

A further complication arose as a result of the narrow tail piece which resulted in high exit kinetic energy losses. The piece acted as a nozzle at the exit from the turbine with the adverse effects to be discussed shortly.

3.1.2 Present tests

A brief account of the chronological development of the variable geometry concept was presented in section 1.6.1. A fuller account can be found in refs. (57, 8). The present tests are a repetition of the simulated zip fastener tests, the difference being that these are performed on the final prototype capable of continuously moving the nozzle ring assembly from no restriction to full restriction pneumatically. Simulated zip fastener tests were those where the restrictions were achieved by dismantling the turbine and placing flat rings under the nozzle ring to produce restrictions. These had already shown that the efficiency penalty was within acceptable limits.

3.1.3 Major components

The turbine used, was a Holset 3 inch H1 series which consisted of a single entry nozzled volute with a rotor of the following

particulars.

Turbine	Holset, Radial inflow
Inlet diameter	69.6 mm
Mean exit diameter	41.7 mm
Blade channel depth at exit	19.1 mm
Blade channel depth at inlet	11.68 mm
Blade inlet angle	0 deg.
Blade exit angle at mean diameter	45 deg.
Blade thickness at inlet	0.835 mm
Blade thickness at exit	1.2 mm
Rotor cone angle	90 deg.

The volute had the following dimensions.

Inlet area	1963.44 mm2
Mean inlet radius	77 mm
Inlet angle	tangential

3.1.4 Discussion of experimental results

It is worth remembering that the intention was to achieve a corresponding mass flow turn down ratio for each restriction without excessive penalty on efficiency at all speeds.

The results are shown in Figs. 3.1 to 3.10. Each of the 3 sets of results shows the variation of non-dimensional mass flow rate, non-dimensional torque and efficiency against pressure ratio with speed as parameter. Each figure also shows the corresponding results of the unrestricted case for comparison purposes. Numbers 3, 5 and 7 correspond to a turbine speed of 30000, 50000 and

70000rpm respectively. These results have also been discussed in ref. (53). In contrast to previous designs, it is evident from the figures that a linear reduction in axial width does not result in a linear reduction in the turbine swallowing capacity. The relationship is strongly non-linear, small restrictions resulting in almost no mass flow turn down ratio, while the effect becomes more pronounced with increasing axial restriction. Fig. 3.1 shows a 2.5% reduction in mass flow rate for 16.7% axial restriction, while a 33.4% restriction has resulted in 12.2% reduction in mass flow, as shown in Fig. 3.4. Similarly, Fig. 3.7 shows a 45% turn down ratio for a 50% axial restriction, all at a turbine speed of 70000rpm.

It is evident that the most effective area of operation of the turbine, in terms of mass flow reduction, is in the 30 to 50% restriction regions. For continuously variable operation, provision may have to be made to have a non-linear restriction schedule since it would be necessary to achieve a minimum restriction of approximately 30%, fairly early on in the schedule while the rest of the schedule can be of a more gradual nature. This will prove difficult to achieve with a simple boost controlled scheme. More sophisticated control systems may have to be considered if this design is to be pursued beyond the scope of the present project.

Figs. 3.2, 3.5 and 3.8 show the effect of the restrictions on turbine torque. This effect can be appreciated more readily from Figs. 3.3, 3.6 and 3.9 showing the corresponding turbine efficiencies. Fig. 3.3 indicates a small penalty on turbine efficiency at the higher speeds of 50000 and 70000rpm, while in Fig.

3.6 the deterioration in efficiency only occurs at 50000rpm but with an improvement in efficiency at the other speeds. The maximum deterioration, as a result of throat area restrictions of up to 50%, is under 5%. Fig. 3.9, however, shows quite a substantial improvement in efficiency at every speed over the entire pressure ratio range. These efficiencies are also shown on a basis of rotor speed with pressure ratio as a parameter in Fig. 3.10.

The zip fastener design, by its nature cannot guide the flow closely before it is almost fully restricted, and thus will result in inefficient operation of the turbine in the intermediate positions when compared to the performance obtained with a nozzle ring assembly such as the sinking teeth unit. However, when it is fully restricted it will guide the flow according to the vane angle and result in more efficient operation. This is confirmed by a comparison between the zip fastener results and the fully open sinking teeth design results presented in ref. (57).

A further likely cause for the slightly inferior performance of the fully open zip fastener design compared to the standard nozzle ring is the enhanced volute losses due to much rougher flow paths in the modified turbine volute caused by the movable nozzle blade ring. However, as stated earlier, this design was chosen, believing the drop in performance will be justified by the simplicity in production and the operational reliability of this design.

The enhanced exit kinetic energy losses due to the considerably smaller tail piece area (an area reduction ratio of 1.4:1) have also contributed towards the slightly inferior performance of the

variable geometry prototype device. The results presented are based on the exit static pressure being measured at the tail piece. If, however, the static pressure is taken at the immediate exit from the turbine and calculations performed on that basis, slightly better efficiencies will be obtained throughout.

Finally, the strong non-linearity in turn down ratio is caused by the nature of the zip fastener configuration. Flow guidance is incomplete and large flow angles with respect to the tangent are set up locally offsetting part of the reduction in the geometric flow area and hence the swallowing capacity. The relative sizes of the volute throat area and the rotor exducer area can also contribute towards this phenomenon.

In view of the above findings, it is concluded that the objective is achieved to a satisfactory degree at all restrictions and an actual improvement in performance is achieved at 50% restriction. Nevertheless, it must be borne in mind that the performance of the zip fastener design falls short of the standard nozzle ring throughout the range of operation mainly due to the nature of the design.

3.2 Steady state engine tests

3.2.1 General

The results of the turbine dynamometer tests were summarized above. This section deals with the assessment of the performance of the variable geometry turbocharged T6.354 Perkins engine. The engine was fitted with the variable geometry prototype replacing the

standard H1 series turbocharger which is normally fitted to these engines. Details of the hydrostatic dynamometer providing the necessary load for the engine were given in the previous chapter.

It was decided to carry out a series of constant bmep tests, namely at 2, 4, 6 and 8 bar corresponding to torque levels of 92, 184, 276 and 368 nm. A limiting torque test was then carried out to complete the engine performance map. These tests were performed at fixed values of variable geometry restriction. Although, the variable geometry prototype was connected to an external pressurized air supply, no provision was made to have a continuously varying turbine throat area in relation to boost as envisaged earlier. This decision was made as a result of the following two factors: a) As already described, to have acceptably smooth operation of the variable geometry device, an excessive rate of air leakage had to be tolerated, making a direct boost controlled scheme i.e. a physical connection between the device and the inlet manifold, impractical. This would have led to unacceptable loss of inlet manifold air. As a result it was envisaged to employ, at a later stage, fast response 'Norgren' valves which would respond to boost pressure and proportionally supply the prototype with air from an external source; b) It was of genuine interest to assess the performance of the variable geometry turbocharged engine at a number of discrete restrictions regardless of boost considerations.

Experience from the turbine tests had shown the non-linear nature of the effect of throat restrictions on turbine swallowing capacity. Thus, a non-linear restriction pattern was adopted to obtain the necessary information from the areas of more effective operation.

Four positions, at 0, 25, 40 and 50% of the total turbine throat width were adopted.

Originally, the engine had a CAV DPA fuel pump which incorporated a speed dependent fuel limiting device known as the 'chopper'. The function of the chopper was to restrict fuelling below 1600rpm engine speed corresponding to 800rpm pump speed to avoid overfuelling and hence excessive smoke emission. This was achieved by means of the fuel pressure being proportional to the engine speed. This pressure acted on a spring loaded lever which was overcome by the spring below 1600rpm and hence activated the fuel limiting mechanism. The pump was mechanically governed by means of internal centrifugal weights.

As a result of the chopper device, it was found in practice, that the engine operation under torque control was not stable enough to allow accurate performance data collection over the lower engine speed range, particularly at 1200, 1400 and occasionally at 1000rpm. This was due to the low inertia dynamometer since these pumps are normally employed for high inertia applications. This was later confirmed by the manufacturers. Under speed control, however, it was possible to reduce the instability, but not sufficiently to allow reliable measurements.

A further consideration in the course of these tests was the fact that lack of experience with the PTFE seals necessitated a cautious approach (regarding the extent of heat to which the seals were exposed inside the moving assembly). It was, therefore, decided to start the tests from the lower torque levels and progress towards

the limiting torque curve while making each test as short as possible to protect the seals. As a result of this, fuel flow measurements were not conducted to a very high standard, so that the sfc curves lacked sufficient accuracy. The fuel flow was measured by means of a bucket and weighing scale. This method can be of extreme accuracy if large quantities of fuel are timed giving a representative average over the period of measurement. Conversly, over short periods, speed fluctuations and other possible influencing factors will be reflected to an unacceptable level.

It is worth noting, however, that the PTFE seals withstood the heat much better than expected. In addition, the end piece on which the assembly was mounted was carefully lagged. Furthermore, a cooling effect was achieved by means of the constant flow of cold air leaking past the seals. These helped to keep the immediate seal temperatures sufficiently low to prevent frequent extrusion of the seals. Under extreme conditions of maximum fuelling over sustained periods of time, however, extrusion did take place necessitating replacement by a new set of seals.

A full set of tests was carried out despite the above mentioned shortcomings. These results are presented in ref. (53). Having found more confidence with the seals, however, allowed a repetition of these tests, particularly the constant bmep tests, at a later data.

As envisaged, the complete schedule of tests was repeated after carrying out the necessary modifications of which more will be said below. It is proposed to include only the latter set of results

since they are identical with the original set of results with the exception of the improved fuel flow measurements and hence sfc curves. No loss of information will occur from the omission of the original results.

To overcome the limitations imposed by the original chopper fuel pump, during the second set of tests a similar pump but which did not incorporate a chopper mechanism was further modified to override the action of the governor by giving direct access to the fuel metering valve. This was particularly suitable for the later transient tests. Further, as a result of much more stable operation and prolonged PTFE sealing ring life, readings at 1200 1400rpm were possible and more accurate sfc results were obtained.

In the figures to be discussed shortly, the symbol O corresponds to 0%, X to 25%, Y to 40% and Z to 50% restrictions. Data has been recorded between 1000 and 2500rpm inclusive at intervals of 300rpm or between 1000 and 2600rpm inclusive at intervals of 200rpm. Each set of constant torque test consists of the following, all plotted on a base of engine speed Ne (with the exception of 'b' below).

a) Turbocharger speed (rpm)

b) Compressor map with engine operating lines
   for different engine speeds.

c) Engine boost pressure ratio

d) Compressor delivery pressure ratio

e) Specific fuel consumption (kg/kw-hr)

f) Trapped air fuel ratio

g) Mean turbine inlet pressure ratio

h) Turbine inlet temperature (deg. C)

i) Air mass flow rate through the engine (kg/sec.)

j) Fuel mass flow rate (kg/sec.)

k) Inlet manifold temperature (deg. C)

The limiting torque tests have the following parameters plotted in addition to the above.

l) Brake mean effective pressure (bar)

m) Engine torque (nm)

n) Engine brake power (kw)

3.2.2 Major components

a) Engine specification

Type: Perkins T6.354, 6 cylinder in line, 4 stroke, direct injection diesel engine.

Bore : 98.4 mm (3.875 in)

Stroke : 127.0 mm (5.0 in)

Swept volume : 5.8 litres (354 cu. in)

Effective compression ratio : 16:1

Geometric compression ratio : 20:1

Stroke ratio : 0.87

Valve timing : EVO 52 BBDC EVC 16 ATDC

IVO 19 BTDC IVC 49 ABDC

b) Engine operating limits

Maximum cylinder pressure : 2000 psi (138 bar)

Maximum turbocharger speed : 100000rpm

Maximum turbine inlet temperature : 750 deg. C

c) Fuel injection equipment

Fuel injection pump : CAV rotary pump

Type : DPA 3268 L 3835

Static timing : 26 BTDC nominal

d) Cooler

Type : Serk series 7, air/water cooler

Fitted between compressor and inlet manifold

Calibration curves are shown in Figs. 3.11 and 3.12

e) Dynamometer : See subsection 2.2.1.

3.2.3 Discussion of the steady state results

i) 2 bar bmep results

The constant torque tests were carried out by setting the torque demand potentiameter and altering fuelling via metering valve adjustment to achieve the required speeds.

The results for the 2 bar bmep curves are shown in Figs. 3.13a to 3.13k. The order of these figures is such as to demonstrate the effect of variable geometry on the turbocharger performance first and then to show the overall performance of the engine turbocharger as a whole.

Fig. 3.13a shows turbocharger speed variation with engine speed. The strongly progressive - i.e. non-linear - action of the variable geometry device is apparent from the fact that the 'Z' curve for fully restricted variable geometry position is well removed from the remaining curves. The increase in turbocharger speed at this very low bmep level is considerable particularly at higher engine speeds. In general, turbocharger speed virtually doubles over the full

engine speed range, with the corresponding favourable effect on compressor delivery pressure and hence on boost to be discussed shortly.

First, however, the movement of the engine operating points in the compressor performance map is considered. This is shown in Fig. 3.13b. Due to the very low energy levels associated with this engine torque, movement of the operating points in the compressor map is quite small, particularly in the low engine speed range, and is in line with the increase in the turbocharger speed described above. The largest movement occurs (O to Z) at an engine speed of 2600rpm. It is also evident that the efficiency of the compressor improves with every restriction, the highest improvement being of the order of 7 percentage points.

Figs. 3.13c and 3.13d show the engine boost pressure ratio and compressor delivery pressure ratio respectively. The small difference between these two sets of curves is due to the pressure drop across the aftercooler. The trend of turbocharger speed is followed closely by these pressures, resulting in a boost ratio rise from 1.15 to 1.77 corresponding to a compressor delivery pressure ratio rise from 1.25 to 1.9 at the maximum engine speed of 2600rpm. In the lower engine speed range, where it is most desirable to have an improvement in engine boost, the effect is rather small, particularly so at variable geometry restrictions below 50%. However, it becomes appreciable towards the engine mid-speed range.

Specific fuel consumption (sfc) is depicted in Fig. 3.13e. There is a clear deterioration of fuel consumption as a result of higher

engine back pressures caused by the severe turbine flow restriction at 50%. A comparison of Fig. 3.13c with Fig. 3.13g reveals the negative pressure gradient across the engine leading to an increase in pumping work and possible interference with the scavenging process. The adverse effect on sfc suggests that the restricted variable geometry setting should only be used as an aid to better transient response at very low bmep levels. Under such conditions, the extra air will ensure a more rapid acceleration together with less smoke emission. This will be dealt with in more detail in subsections 3.3 and 3.5.

Fig. 3.13f shows the engine air fuel ratio at this bmep level. At the lowest engine speed of 1000rpm, the air/fuel ratio has increased from 60.5 to 62.5 while at the maximum engine speed of 2600rpm it has increased from 47 to 57. The increase in air/fuel ratio at this torque level is of no benefit to steady state operation. Particularly, since it is achieved at the expense of engine sfc. The only benefit that variable geometry operation can offer at very low torque levels will be seen to be in the transient response.

Fig. 3.13g shows the mean turbine inlet pressure. As mentioned earlier, these pressures are consistently higher than the engine inlet manifold pressures shown in Fig. 3.13c imposing a negative pressure gradient across the engine. The implication on sfc has already been mentioned. A point worth noting is the fact that these pressures are a mean of the actual pressure pulses whose lows and peaks are below and above this mean value. Therefore, while it is possible that the scavenging process is unaffected, it nevertheless is likely that some interference does occur. No

provision was made to ascertain this fact to a definitive degree.

Turbine inlet temperature is represented in Fig. 3.13h. Despite the higher air/fuel ratio, Fig. 3.13f, no appreciable amount of cooling has taken place. This is due to the higher sfc values which result in a greater proportion of the heat released by the fuel to go through the exhaust. Furthermore, part of the potential cooling effect is offset by the much higher engine inlet temperatures for the restricted cases as shown in Fig. 3.13k.

Fig. 3.13i and 3.13j show the air and the fuel mass flow rates through the engine. The extra air delivered by the compressor is apparent in Fig. 3.13i and a maximum increase of some 40% occurs at the maximum engine speed of 2600rpm. Fig. 3.13j clearly shows the amount of extra fuel injected at each speed to maintain the required torque level. This has been necessary because of the adverse effect of the variable geometry turbine on sfc at this torque level.

ii) 4 bar bmep results

These are presented in Figs. 3.14a to 3.14k. Fig. 3.14a shows the effect of each restriction on turbocharger speed. As expected, the effect of variable geometry below 50% restrictions is minimal but a substantial improvement takes place at 50% restriction. At 1000rpm engine speed, the turbocharger speed has increased from 23000rpm to 35000rpm, a 52% improvement, while a 87% improvement at 2150rpm engine speed has increased the turbocharger speed from 53000rpm to the limiting value of 100000rpm. It is also evident that, 50% restriction test runs beyond 2150rpm engine speed, have not been possible as a result of the turbocharger speed limit.

The position of the engine operating points in the compressor map is depicted in Fig. 3.14b. It is evident that as the torque level increases, the movement of the operating points becomes greater. Even at the lowest engine speed of 1000rpm the 'Z' point is reasonably higher than the 'O' point. At the maximum engine speed of 2500rpm 'Z' is substantially raised above 'O'. All points are again moved to the more efficient operating region as a result of the variable geometry turbine operation. The most notable improvement is at 1900rpm engine speed where the compressor operating point has moved to the most efficient region with a compressor efficiency of 72%.

Fig. 3.14c represents the variation of boost with engine speed for the different restrictions. As expected, these follow the same trend as the turbocharger speeds shown in Fig. 3.14a; a maximum improvement of 65% occurring at 2150rpm engine speed, while at 1000rpm engine speed, boost ratio has increased from 1.02 to 1.1, some 8% improvement. It is evident that at this torque level too, the improvement in air availability to the engine is quite modest in the low engine speed range where it is needed most under transient conditions. Compressor delivery pressure ratio is shown in Fig. 3.14d. It follows the same trend as boost and is higher than it by the amount of pressure dropped in the cooler.

Engine sfc variations with engine speed is presented in Fig. 3.14e. It is evident that as the engine torque level is increased, the adverse effect of variable geometry on sfc decreases, particularly so in the low engine speed range. Although, sfc has deteriorated by more than 0.06 kg/kw-hr at an engine speed of 2150rpm, at 1300rpm

and 1600rpm it is almost unaffected, while at 1000rpm there is a small improvement. It is, therefore, possible at low engine speeds and increasing loads, to operate the variable geometry device during steady state running of the engine for fuel economy in addition to improving the transient performance. This gives rise to the possibility of sfc optimization over the entire engine load-speed range using some form of sensing and control mechanisms. This will become more apparent with higher load levels to be discussed shortly.

Fig. 3.14f shows the effect of variable geometry restriction on trapped air/fuel ratio. The improvement on air/fuel ratio is more pronounced here than at 2 bar bmep. At the lowest engine speed of 1000rpm, the air/fuel ratio has increased from 37 to 40 while at the maximum permissible engine speed, under variable geometry operation, of 2150rpm, the air/fuel ratio has increased from 37 to over 50. The implication of the increased air/fuel ratio, however modest at low engine speeds, is evident on the transient response of the engine.

Fig. 3.14g depicts the mean turbine inlet pressure variation with engine speed. Although, there still remains a negative pressure gradient across the engine, it is less in magnitude with a smaller resultant adverse effect on sfc.

Turbine inlet temperature is shown in Fig. 3.14h. The more generous air/fuel ratios shown in Fig. 3.14f together with the less adverse effects on sfc have resulted in a reduction in the turbine temperature. The reduction is more pronounced at higher engine

speeds with air/fuel ratios in the region of 50 and is of the order of 50 deg. C at an engine speed of 2150rpm. The reduction in the cycle mean temperature leads to less heat transfer to the cooling water, hence offsetting part of the adverse effect on sfc due to negative loop work.

Air mass flow through the engine is shown in Fig. 3.14i. The increase due to a 50% restriction over the fully open case is quite modest at low engine speeds, particularly at 1000rpm, while at 2150rpm the increase is quite appreciable, increasing from 0.115kg/sec to 0.175kg/sec, resulting in a 52% improvement. This is responsible for the much more generous air/fuel ratios depicted in Fig. 3.14f.

Fig. 3.14j shows the delivered fuel mass flow in g/sec. It is self evident that to maintain the constant 4 bar bmep level, particularly with the 50% restriction, at lower engine speeds slightly less fuel and at higher speeds more fuel has had to be injected; in the latter to overcome the higher pumping work at the higher engine speeds. As seen before, this has also been reflected in the sfc curves which showed similar behaviour in Fig. 3.14e.

Inlet manifold temperatures are shown in Fig. 3.14k. These show expected trends, with temperature rising as the compressor delivers air at a high pressure ratio. It should be noted that, despite this increase in inlet temperature, the effect on air/fuel ratio, Fig. 3.14f, has been substantial enough to result in a nett reduction in engine exhaust temperature. This is in addition to offsetting the increase in exhaust temperature due to higher sfc

values.

iii) 6 bar bmep results.

Turbocharger speed, presented in Fig. 3.15a, shows the familiar pattern but with more pronounced improvements. At 1000rpm engine speed it has increased from 30,000rpm to 42,000rpm, a 40% improvement while at 2000rpm engine speed, where the turbocharger speed reaches its limiting value of 100,000rpm, the improvement is 77% over the unrestricted value of 56,500rpm. Although, an upper limit of 100,000rpm for the turbocharger speed has been set, it is possible to run up to 125,000rpm with this compressor wheel. However, this was avoided, since in practice, for reliability reasons, 100,000rpm is set as the upper limit for turbocharger speed. In a practical boost controlled, continuously varying variable geometry device, the moving nozzle ring could begin to open up the nozzle throat area to avoid over-speeding.

The much more pronounced effects on turbocharger performance are similarly reflected on the compressor map, shown in Fig. 3.15b. The 'Z' movement, even at the minimum engine speed of 1000rpm, is quite appreciable while at 1900rpm the 'Z' point is far removed from the 'O' point representing the unrestricted configuration. Similarly all the 'Z' points now lie in a much more efficient region of compressor operation, the largest movement being from the 62% to the 72% efficient region.

The corresponding effect of higher turbocharger speeds on engine boost is shown in Fig. 3.15c. Engine boost pressure ratio at the lowest engine speed of 1000rpm has increased by 7.5% from 1.06 to

1.14, while at 2000rpm the improvement is 56%, caused by an increase from 1.19 to 1.86 pressure ratio. Again the effect of this on the transient performance of the engine in self evident. This will be considered in subsections 3.3 and 3.5. Fig. 3.15d shows similar trends for compressor delivery pressure before any pressure is dropped in the cooler.

Fig. 3.15e shows the sfc variation with engine speed. The sfc improvement range though modest, has now extended up to 1500rpm engine speed while at 4 bar bmep it only extended up to 1100rpm engine speed. Furthermore, the sfc penalty beyond 1500rpm is now much less pronounced than the 4 bar bmep runs. It is evident that at this load level the variable geometry device can present steady state benefits as well as transient response improvements. This however, will necessitate a sfc optimization mechanism to achieve, which may not be justified by such modest sfc improvements. However, as will be seen shortly, the sfc improvement will be quite reasonable for higher load levels.

The effect on air/fuel ratio is shown in Fig. 3.15f. Again the improvement is quite considerable even at 1000rpm engine speed. The air/fuel ratio has increased from 27 to 29 at this speed, while at 2000rpm there is a 45% improvement from an unrestricted value of 29 to a fully restricted value of 42.

Fig. 3.15g shows the variation of mean turbine inlet pressure ratio with engine speed. A comparison of this figure with Fig. 3.15c shows that the engine back pressure is still higher than the boost pressure causing negative loop work. It is important to notice,

however, that in the lower engine speed range where variable geometry application is considered more appropriate, the negative pressure gradient across the engine is almost insignificant.

As expected, the variable geometry device presents excessive restriction to the large volume flow at higher engine speeds causing excessive engine back pressure. This will in turn have an adverse effects on the engine sfc in that region.

The consistently lower turbine inlet temperatures are shown in Fig. 3.15h. At 1000rpm engine speed, a modest drop from 425 deg. C to 412 deg. C takes place, while at 2000rpm the drop is over 70 deg. C. In general, a drop in the exhaust temperature under variable geometry conditions does not necessarily mean a reduction in exhaust enthalpy, calculated as a percentage of the total energy released by the fuel. This is because, although the temperature may have dropped, the total mass flow per unit time has increased, and the flow of energy through the exhaust is proportional to the product of these two quantities.

Fig. 3.15i shows the air mass flow rate through the engine. Wholly expected trends are seen. Again, the increase in air mass flow rate in the low engine speed range is more appreciable than the 4 bar bmep runs. At 2000rpm the increase is quite substantial and a 47% increase is obtained.

The delivered fuel mass per second is presented in Fig. 3.15j. This is in line with sfc curves discussed in Fig. 3.15e. The extra amount of fuel needed at higher engine speeds to maintain the 6 bar bmep level is now very small while at lower engine speeds a very

slight reduction in fuel delivery has taken place. Small variations are, however, within the experimental error margin and cannot result in definitive conclusions. Later tests at higher torque levels, though, will confirm the trend towards sfc improvement in the low engine speed range and its deterioration in the higher speed range.

Finally Fig. 3.15k represents the inlet manifold temperature variation. Trends similar to those for the 4 bar bmep runs are seen, ie, increasing inlet manifold temperature for increasing variable geometry restrictions.

iv) 8 bar bmep results.

This torque level is the last of the constant torque tests and is followed by the limiting torque tests to be presented in the following section. The 8 bar bmep results are shown in Fig. 3.16a to 3.16k.

Fig. 3.16a shows the variation of turbocharger speed with engine speed for each restriction. At this bmep level the maximum engine speed with 50% restriction has been limited to 1900rpm due to the fact that the turbocharger speed limit is reached at this engine speed. The speed has increased from 37,000rpm to 48,000rpm at 1000rpm engine speed while at 1900rpm engine speed there is a 54% improvement from 65,000rpm to the turbocharger limiting speed. It is again evident that restrictions below 50% have minimal effect of the turbocharger speed and hence on all other parameters.

The compressor map together with the engine operating points

superimposed on it is shown in Fig. 3.16b. It is clear that the fully restricted 'Z' points are now well inside the high efficiency regions of the compressor map while still being well removed from the surge line. The movement, as in previous cases, is very large at higher engine speeds while quite substantial at the lowest engine speed of 1000rpm.

The corresponding boost pressure ratio available to the engine is shown in Fig 3.16c. Similar improvements in boost as in turbocharger speed have taken place. An 8% improvement in boost at 1000rpm engine speed has been caused by an increase from 1.1 to 1.19, while at 1900rpm engine speed boost has increased from 1.3 to 1.9 corresponding to a 46% improvement. Fig. 3.16d shows similar trends for compressor delivery pressure.

Fig. 3.16e shows the engine sfc variation with engine speed. The substantial improvement in sfc in the low and mid-speed range is apparent. The improved sfc region has now extended up to an engine speed of 1800rpm beyond which sfc starts to deteriorate due to excessive engine back pressure. The variable geometry device, therefore, can be of considerable benefit during steady state operation in the lower half of the engine speed range where it is primarily designed for. This indicates that a sfc optimization scheme will be worth considering in future.

Fig. 3.16f represents the air/fuel ratio variations. With the unrestricted turbine configuration, it is evident that in the lower part of the engine speed range, particularly at 1000rpm, the air/fuel ratio is already too tight for complete combustion.

However, with the application of the 50% restriction it has increased by 19% from 18.5 to 22 which results in much better combustion. At 1900rpm it is also increased from 24 to 34, a 41.5% improvement. This will have positive implications on the transient performance.

Mean turbine pressure ratio is shown in Fig. 3.16g. Comparison of this figure with Fig. 3.16e shows that at 1000rpm engine speed there now is a positive pressure gradient across the engine indicating that there is no negative loopwork as well as a better scavenging process, while at higher engine speeds, the negative pressure gradient across the engine is gradually restored leading to excessive pumping work. The negative pressure difference is of the order of 0.25 bar. This has again adversely affected the sfc values.

Fig. 3.16h shows the turbine inlet temperatures. The cooling effect is now quite considerable throughout the speed range. A 25 C temperature drop at 1000rpm engine speed is followed by a progressively increasing drop to a final value of 475 C from 575 C at 1900rpm. In general, lower temperatures will lead to prolonged valve life especially at the limiting torque level to be discussed next.

The increase in air mass flow, shown in Fig. 3.16i, is now quite appreciable throughout the engine speed range, resulting in a 44% increase from 0.112 kg/sec to 0.161 kg/sec at 1900rpm.

Fig. 3.16j illustrates the actual reduction in the fuel delivered up to 1800rpm engine speed, resulting in improved sfc values.

Finally, Fig. 3.16k shows the inlet manifold temperatures against engine speed.

v) Limiting torque results

This is the most important set of tests which was performed under maximum fuelling conditions, ie maximum governor set point. It should be noted that the results discussed here are the original limiting torque tests carried out using the original 'chopper' limited fuel pump arrangement. These have also been presented in ref.(53). The chopper device behaved in a slightly uncertain manner due to the fact that it is subject to a number of forces including friction, fluid pressure, spring force and even electro-static forces. Most inconsistent of these is the force due to frictional effects, making the achievement of identical fuel rate positions for the same governor set point impossible. It is, therefore, impractical to expect to achieve exactly the same fuelling under maximum governor set point for different tests. This phenomenon has affected the results to a small degree, whereby the 'full throttle' characteristics of the engine are not truly representative of the performance which could be achieved when a more appropriate fuel pump, such as that used for the later set of tests, is fitted.

The tests were carried out using the constant speed demand facility of the dynamometer.

The limiting torque results are presented in Figs. 3.17a to 3.17l. The power developed by the engine is shown in Fig. 3.17a. It is demonstrated that the rated performance of 115 kw (155 bhp) is

achieved at the maximum engine speed of 2600rpm and that at lower speeds a significant increase in power is available with progressively restricted nozzle throat area. A feature of these tests is the enhanced effectiveness of restrictions below the maximum 50% configuration. For an explanation of this see subsection 2.5.

Engine torque and bmep are shown in Figs. 3.17b and 3.17c. The effect of the chopper fuel limitation is apparent, particularly on the unrestricted '0' line, where the curve reaches a maximum at 1600rpm engine speed and rises again with increasing engine speed. It should be noted, that at this stage of the experimental schedule, no deliberate attempt was made to take advantage of the extra air available due to the variable geometry turbocharger operation. However, as a result of the initial mismatch between the engine and the turbocharger, slight overfuelling of the engine has occurred, making any gains in torque and consequently in power a result of more efficient operation of the engine together with more efficient combustion due to the extra air. In the later set of tests, however, 'deliberate' enhanced fuelling has been applied to show the full potential of the variable geometry device.

Normally, in high performance engines, peak torque is restricted by the maximum cylinder pressure of 2000 psi (138 bar) for most engines. The turbocharger match is, therefore, such as to ensure this and hence achieve maximum torque back up. The drawback with this matching technique, is the limited range by which the peak torque can be moved to lower engine speeds. A match to give high torque back up at very low engine speeds would necessitate a very

small turbine swallowing capacity which would impose excessive engine back pressures at the higher engine speeds together with turbine over-speeding. This will further necessitate a by-pass mechanism such as the wastegate system to avoid over-speeding and hence over-boosting of the engine at high speeds. Normally, however, a wastegate is not employed and a match is chosen such that this latter drawback is avoided while peak torque takes place at speeds closer to the engine maximum speed than ideally desirable.

However, as it was mentioned above and will be discussed in more detail later, the engine-turbocharger match in this case was not 'ideal' and basically a larger than necessary swallowing capacity together with incomplete flow guidance in the unrestricted configurations was presented by the turbine. It has, therefore, resulted in a peak torque, dictated by air fuel ratio rather than peak cylinder pressure. This does not undermine the effectiveness of the chopper device, since the latter will only prevent overfuelling for a normal engine-turbocharger match, and because it has no means of taking into account the boost level, in this particular case some overfuelling has occurred.

The resulting improvement in torque is apparent in Fig. 3.17b. This is wholly due to the extra air made available to the engine resulting in more complete combustion of the fuel. Although maximum cylinder pressures were not measured at this stage of the tests, it is quite possible that the maximum cylinder pressure is only reached under fully restricted variable geometry configurations. Nevertheless, a very badly defined peak torque of 465 nm at 1800rpm engine speed has been raised to 518 nm at 1400rpm engine speed.

Torque back up has, thus, increased from 8.1% at 69.2% maximum engine speed to 20.5% at 53.8% maximum engine speed.

Fig. 3.17d shows the turbocharger speed variation with engine speed. The effect of variable geometry on the speed is quite remarkable at every restriction. At the highest engine speed of 2600rpm, the variable geometry facility would not be used, since turbocharger speed and hence boost are adequate, and the former would exceed its limiting value if more than 25% restriction were applied. Similarly, at 2400rpm the 40% restriction leads to the limiting turbocharger speed of 100,000 rpm with the corresponding boost improvement. Similar improvements can be observed at 2200 and 2000rpm engine speed. At 1800rpm it is possible to apply the full restriction of 50% with a resultant increase, from the unrestricted position, in turbocharger speed from 66,000rpm to 96,000rpm. It will also be observed that at 1200 and 1000rpm, the gains in turbocharger speed are still considerable. Although these will not be of much benefit from a standpoint of increase in torque back up, they will be highly significant in improving the transient response.

The engine operating points superimposed on the compressor performance map are shown in Fig. 3.17e. The initial mismatch of the turbocharger to the engine is evident. Had the turbocharger been an ideal match, the 'O' points would have been situated further up in the more efficient regions of compressor operation. However, a perfect initial match will entail other difficulties with respect to variable geometry operation unless an exceptional wide flow range compressor is available. Had the 'O' points been closer to the compressor surge line they would have presented a very small margin

for movement due to turbine restrictions before the compressor would run into surge. Indeed, one of the conclusions to be drawn from this exercise is to find compressors with the surge line well to the left of the best operating region. Certain modified compressors are already obtainable though these cannot eliminate the problem totally.

It is clear that with the existing compressor, surge has been avoided, though at low engine speeds the 'Z' points lie very close to the surge region. Compressor surge would have set in for the 50% restriction had the original match been a better one.

Figs. 3.17f and 3.17g show the engine boost and compressor delivery pressure ratio variations with engine speed. Fig. 3.17f demonstrates that over the engine speed range 2600 to 1800rpm, boost pressure ratio can be maintained constant at approximately 1.8 by progressive application of the variable geometry device. At 1400rpm the unrestricted setting compressor pressure ratio is 1.205 and is raised by the fully restricted variable geometry device to 1.54 (Fig. 3.17g).

Fig. 3.17h shows the sfc variations with speed. It is clear that with every restriction, the sfc improves up to an engine speed of 1900rpm then it begins to deteriorate as also seen in the previous bmep cases. The largest improvement occurs at 1600rpm engine speed where sfc is reduced from 0.24kg/kw-hr to slightly over 0.2 kg/kw-hr at 50% restriction. This improvement is almost entirely due to the better combustion of the fuel made possible by the extra air which is available under variable geometry operation. The

deterioration in sfc at higher engine speeds under variable geometry conditions is a result of the excessive back pressure imposed on the engine by the very small swallowing capacity of restricted turbine.

Further evidence for the slight mismatch between the engine and turbocharger is provided by the air/fuel ratios shown in Fig. 3.17i. The fuel pump was set on a Hartridge meter by Lucas representatives and any maladjustment of the pump can be ruled out. Air fuel ratios as low as 16 occur at 1000rpm engine speed and an air/fuel ratio of approximately 17 persists up to an engine speed of 1600rpm. The manufacturer's tests results show a minimum air/fuel ratio of 18 at 1400rpm and air/fuel ratios near 20 elsewhere in the low to mid-speed range. The improvements in the air/fuel ratios in this region due to variable geometry operation is responsible for the improved sfc curves. The mean turbine inlet pressure was not monitored during this test, but it is possible to extrapolate, from previous trends, the behaviour of the engine back pressure. It is certain that in the low engine speed region the pressure gradient across the engine is favourable, crossing over at about 1600rpm, from where it begins to adversely affect the engine sfc.

Turbine inlet temperature variation is shown in Fig. 3.17j. The progressive reduction in temperature as a result of more generous air/fuel ratios is evident. A reduction of just under 100 C occurs at 1800rpm, while at 1000rpm the reduction is quite modest. This reduction in temperature will ensure better mechanical endurance of engine valves and valve seats.

Fig. 3.17k shows how the air mass flow through the engine has been

affected as a result of the variable geometry device. The progressive increase in air flow for each restriction is evident. The largest improvement occurs at 1800rpm engine speed and is of the order of 33%, increasing from 0.105 to 0.14 kg/sec.

Fig. 3.171 shows the fuel flow variation at each running condition despite the nominal constant position of the fuel pump governor set point. Part of the inconsistency must be ascribed to the error involved in the fuel flow measurement technique. The rest, however, is a result of the genuine inability of the chopper governor pump to deliver completely consistent amounts of fuel.

3.3 Transient tests

3.3.1 General

As already stated, the dynamometer had a constant speed mode of operation which allowed the application of step fuel inputs at constant engine speed. This facility, however, proved to be unsatisfactory because of the slow response of the dynamometer resulting in excessive engine acceleration on the application of the fuel steps. This led to unacceptably large speed excursions, affecting the overall transient behaviour of the engine-turbocharger. It was, nevertheless, decided to proceed with the transient test schedule, while improvements in the dynamometer response were carried out to allow a second series of tests at a later date. The reasons for selecting the constant speed type of 'unit test' was to obtain the clearest possible indication of the effect of the variable geometry turbine on transient response while eliminating all other influencing factors such as an increase in

mass flow rate through the engine due to an increase in speed. As will be seen in the second set of tests, this was a particularly severe test which did not allow the variable geometry potential to be fully appreciated.

These series of tests were carried out using the modified fuel pump already described. Thus most of the instabilities experienced with the chopper pump were eliminated by using this pump which allowed direct control of metering valve position, also overriding the influence of the mechanical governor. This has the additional advantage that governor response was eliminated as a variable, and that true fuel steps could be applied.

As with the steady state tests, the transient tests were conducted at fixed settings of the variable geometry device, rather than under boost control, viz. fully restricted (50% restriction) and fully open (0% restriction). The other two restrictions of 25 and 40% are excluded from the present set of tests due to the fact that their effect was very limited, but all four restrictions were applied for the later transient tests conducted after the dynamometer had been modified to reduce the speed excursions. The upper fuel step limit for higher engine speed settings was varied so as not to exceed the turbocharger speed limit of 100,000rpm. The tests were conducted at nominal engine speeds of 1200, 1400, 1600, 1800 and 2000rpm, with the variable geometry device in the maximum restricted or fully open position, and with maximum permissible metering valve step at each speed, from an initial value corresponding to a torque of approximately 160 nm. This lower limit was dictated by the dynamometer characteristics, since at

lower torques it would have necessitated the high hydraulics boost mode of operation. This would have interfered with the transient tests; but for the later set of transient tests, this limit was lowered by readjusting the dynamometer so as to get a lower limit of 92 nm corresponding to 2 bar bmep.

The appropriate information was recorded by the high speed digital data acquisition system. The following four variables are presented in Figs 3.18 to 3.22 for five test series, (a) engine speed, (b) turbocharger speed, (c) dynamometer torque and (d) boost pressure ratio.

Finally, it should be noted that throughout this series of transient tests, the size of the fuel step at each speed remained constant while the variable geometry device was restricted. However, as will be seen, a significant amount of overfuelling has taken place, particularly at the lower engine speeds, which has led to final torque values well above the steady state limiting torque values.

3.3.2 Discussion of the transient results

a) Nominal engine speed Ne=1200rpm (Fig. 3.18)

All parameters have been plotted against time in seconds. Although the actual recording time for all transient tests was 7 seconds, for greater clarity the period shown in each figure has been restricted to 2.5 seconds.

At the top of Fig. 3.18, the engine speed excursion is shown. It is evident that the excursion is unacceptably large and is more so for the 50% restricted case than the unrestricted case.

In the later set of tests, however, a substantial reduction in the speed excursion was achieved by the modifications carried out on the dynamometer control circuit. The increase in engine speed has increased the mass flow rate through the engine, hence accelerating the turbocharger artificially. This is clearly reflected in the turbocharger speed behaviour. Turbocharger speed, shown below the engine speed curve, has a distinctive peak for the 50% restriction case and begins to drop slightly beyond 1.7 secs. This is due to the sudden increase in air mass flow due to engine acceleration which is forced through the small swallowing capacity of the restricted turbine, leading to the turbine speed 'overshoot'. Had engine acceleration been prevented, the turbocharger response would have been more sluggish, though still more rapid than the unrestricted configuration, ie the 'O' curves. The turbocharger speed has responded faster for the restricted turbocharger setting, showing an increase from an initial value of 41,000rpm to 99,500rpm in 1.5 seconds and finally settling at 94,000rpm, as opposed to 23,000rpm to a final value of 48,000rpm for the unrestricted configuration.

The next pair of curves below the speed curve show the dynamometer response in terms of the load it presents to the engine. The base line torque for the unrestricted case is 200 nm as opposed to the nominal 160 nm. This was again due to dynamometer instability which was rectified for the second set of transient tests. However, it is clearly evident that the response of the dynamometer is far too slow to prevent engine acceleration. It should ideally present a very large torque at the onset of engine acceleration to keep the latter

to as low a level as possible. This has been achieved in the later set of tests. The final equilibrium values of torque are indicated by arrows on the right hand side of these figures. In Fig. 3.18 the final torque values for the fully restricted and fully open configurations are respectively 693 nm and 537 nm, the difference being directly due to lack of available air in the latter case, since the same fuel step was applied in both cases.

A comparison of these torque values with the steady state values of the limiting torque shown in Fig. 3.17b, shows the extent of the overfuelling which has occurred during the transient tests. It is, therefore, misleading to compare these two sets of performance curves, though it is sound to compare the relative improvement of the two transient curves due to variable geometry operation. It is evident that there is quite a substantial amount of benefit to be gained from variable geometry operation. This is particularly true, since at this speed peak cylinder pressures are not reached under normal turbocharger operation. Although the higher torques associated with variable geometry operation will ensure faster vehicle acceleration, particularly so at this engine speed, an additional and important effect of the variable geometry device is to provide a much higher initial turbocharger speed, hence reduced levels of smoke emission during the transient period. Also, turbocharger speed is maintained at a much higher level throughout the transient period resulting in a continuously higher supply of air to the engine.

The consequent boost pressure improvements are shown at the bottom of Fig. 3.18. The benefit of the variable geometry device on boost

is clearly shown, reaching a peak value of 1.99 for the 50% restricted configuration, and only 1.20 for the unrestricted case. Air availability is thus substantially improved throughout the transient period.

It is pointed out that, although a higher final torque value has similar advantages as a more powerful or 'uprated' engine, the more significant factor is the rate at which instantaneous engine torque is developed; this being responsible for the transient response of a vehicle. The higher this rate of increase of torque, the higher will be the rate of increase of engine speed, ie acceleration. It is with view to this important parameter that the overall performance of the variable geometry device can be assessed. Therefore, an engine acceleration of approximately 2000 rev/min/sec for the restricted case compares favourably with an unrestricted setting acceleration of approximately 1500 rev/min/sec and the advantage of the former is thus emphasized. (Although, ideally there should be no engine acceleration during these tests).

It should also be noted that actual engine torque is substantially higher than the measured dynamometer torque shown, since only a surplus of engine torque over the dynamometer torque will result in engine acceleration. Thus, the measured load torque excludes the engine inertia term.

b) Nominal engine speed Ne=1400rpm

Fig. 3.19 shows the four variables for 1400rpm engine speed against time. The discrepancy between the two engine speed excursions is now smaller, making a direct comparison more accurate, though the

interference with the turbocharger acceleration still occurs in both cases.

The turbocharger response is clearly improved, increasing from an initial value of 50,000rpm to a peak of 99,500rpm after 1.5 secs and dropping slightly beyond that point for the fully restricted case, while in the unrestricted case the turbocharger accelerates from 27,000rpm to a final value of 50,000rpm. The rate of increase of turbocharger speed is quite clearly much higher for the restricted case than for the unrestricted case leading to better instantaneous air availability at engine inlet. This will ensure a more rapid rate of torque development by the engine, though this is not quite apparent from the dynamometer torque curves. However, from the engine speed excursions it can be seen that only a larger instantaneous engine torque could have resulted in a higher engine speed peak despite the higher dynamometer torque.

Also because of slight overfuelling in this case, the final torque value for the restricted case is higher than the 'O' case for the same fuel step, though a small proportion of this can be attributed to possible sfc improvements due to a more favourable pressure gradient across the engine. The final torque values for the two cases are respectively 610 nm and 530 nm.

Finally, the effect on boost pressure ratio is also shown in Fig. 3.19. A value of 2 is reached from an initial value of 1.23 in 1.5 secs for the restricted case while in the unrestricted case a value of 1.23 is reached in the same time from a virtual no boost initial condition.

c) Nominal engine speed Ne=1600rpm (Fig. 3.20)

The fuelling for this transient test was limited by permissible turbocharger speed, although it has not quite reached the 100,000rpm limit. The maximum turbocharger speed reached is 98,000rpm after 1.3 sec from an initial value of 62,000rpm for the 50% restricted case. As the size of the fuel steps is reduced, the engine speed excursion has also become smaller leading to a much less pronounced turbocharger speed overshoot. In the unrestricted case, it is evident that the turbocharger response is considerably more sluggish and only rising from an initial value of 34,000rpm to a final speed of 53,000rpm.

The engine is quite clearly not overfuelled in this case and a final steady state torque of 464 nm and 430 nm is achieved for the restricted and unrestricted cases respectively. The difference is solely due to more efficient operation of the engine, due to variable geometry (cf 515 and 450 nm in Fig 3.17b).

The dynamometer torque curves fail to show any improvement in the rate of change of torque development by the engine, but a closer look at the engine speed excursions will reveal the more rapid rate of instantaneous torque development which is responsible for the higher and more steep speed excursion. Boost, shown at the bottom of Fig. 3.20, has improved quite considerably too, rising from 1.3 to 1.85 in 1.5 seconds for the restricted case while in the unrestrticted case boost only rises from 1.05 to 1.2 in over 2.0 seconds.

d) Nominal engine speed Ne=1800rpm (Fig. 3.21)

Fig. 3.21 shows the variation of the four parameters with time. The size of the fuel step is also limited by the permissible turbocharger speed. Although the size of fuel steps is becoming increasingly limited, the benefits of variable geometry turbocharger are still clearly apparent. For approximately the same loading of the engine, the speed excursion is considerably higher for the restricted case, indicating the much higher instantaneous torque developed by the engine due to the higher air availability in the engine cylinders.

An initial turbocharger speed of 76,000rpm is accelerated to the limiting value of 100,000rpm for the restricted case, while in the unrestricted case, the initial value of 38,000rpm has only increased to a final value of 55,000rpm. This corresponds to a similar improvement in boost pressure ratio, rising from 1.42 to 2.1 in 1.3 secs and to a final value of 1.9 for the restricted case. The boost rises from 1.05 to only 1.2 in the unrestricted case.

e) Nominal engine speed Ne=2000rpm (Fig. 3.22)

The result of this set is less significant due to the extremely small size of the fuel step limited by the permissible turbocharger speed limit. Similarly the larger speed excursion for the restricted case indicates the higher level of torque produced by the engine in the first few fractions of a second. Similar effects on the turbocharger speed and hence boost can be observed.

3.4 Final steady state engine tests

3.4.1 General

Since the first set of tests was accompanied by a number of difficulties as regards the fuel pump and possible fuel flow measurement inaccuracies, a further series of tests using a similar pump, but without the chopper mechanism was performed. The action of the mechanical governor was also overridden to allow direct control of the metering valve position in the pump. The movement of the metering valve was monitored by using a 360 fine resolution position transducer. Full travel of the metering valve was calibrated to correspond to about 7 volts. The new pump helped to overcome most of the limitations imposed by the original CAV DPA mechanically governed fuel pump incorporating the chopper mechanism. This particularly helped to ensure more stable operation of the engine in the low speed range. Having direct access to the metering valve also allowed a greater degree of freedom in the selection of fuelling schedules.

During this set of tests, enhanced fuelling was applied to take advantage of the extra air made available by the variable geometry device, and therefore to demonstrate the capabilities of the latter to a greater degree. To this end, the engine manufacturer's standard fuelling schedule as represented by air/fuel ratio, was chosen as the basis for fuelling the engine under different test conditions, ie the air/fuel ratio was maintained constant corresponding to the manufacturer's schedule irrespective of the degree of variable geometry restrictions. This will be a more appropriate criterion for comparison of the engine performance under different restriction conditions. This criterion was also of

great value in determining the limiting torque curve. In the absence of a correctly set governed fuel pump in which maximum governor set point is maintained throughout the speed range, it was extremely difficult to decide what the limiting torque should be, particularly in the low and midspeed range, all the more since smoke measurements were not made during any part of the test programme. In the low and mid-speed range, smoke limited fuelling was much more probable than peak cylinder pressure limited fuelling since the original match was short of ideal, see Fig. 3.17e. This is what led to the overfuelling in the original test series.

As a result of the slight initial mismatch, and the adherence to the air/fuel ratio schedule, the engine has been derated as compared to the manufacturer's data. With a better initial match this initial derating need not occur.

Each air/fuel ratio was arrived at by trial and error using a PET computer to assess the air/fuel ratio at each speed. This was achieved by feeding fuel mass, fuel time and air nozzle pressure drop in conjunction with B.S. information on calculation of air flow rate to the computer, programmed in Basic. This program is not separately described since it is a shorthand version of the main data reduction program mentioned elsewhere. However, if the air/fuel ratio was found to differ from the standard schedule, the fuelling was altered accordingly and this process repeated enough times to arrive within a reasonable distance from the standard schedule. This process was assisted by the use of the metering valve position transducer as a guide to the magnitude of each adjustment.

Finally, since no provision was made for measuring smoke emission, no objective assessment of the latter was possible. However, frequent visual inspections, though subjective, were made at the exit of the exhaust pipe to check for unusual smoke emission. To eliminate any adverse combustion effects, the fuel injection equipment was cleaned and checked on a Hartridge machine before the start of the test programme.

A number of refinements were also carried out on the hydrostatic dynamometer. The speed feed back signal originally obtained from the pulses off a 60 tooth wheel, was instead supplied by a d.c. tachogenerator which has a considerably faster response than the pulse system. This helped to improve the dynamometer response. Also, the proportional plus integral control system was optimized to minimize the magnitude of the speed excursions during the transients.

Throughout these tests, cylinder pressures were measured using the piezoelectric transducer. (Fig. 3.29).

3.4.2 Discussion of final steady state results, ref. (56)

The constant torque results of this series of tests were presented in subsection 3.2.3. Here it is proposed to complete the discussion by presenting the 'enhanced fuelling' limiting torque results. The same parameter as on page 41 are plotted against engine speed. These are shown in Figs. 3.23a to 3.23n.

Although it is envisaged that, ultimately, the variable geometry device will operate under fully automatic control, either using a

mechanical system with boost as the controlling variable, or as a full multi-variable microprocessor system implementing a schedule of fuel pump metering valve, turbine variable geometry setting and possible injection timing, it was decided at this stage of the test programme as in the previous tests, to run the unit in a series of fixed nozzle ring positions rather than under continuous control.

The tests cover the following conditions:-

i) Engine speed Ne=1000 to 2600rpm in steps of 200rpm

ii) Variable turbine geometry : four fixed settings 0, 25, 40 and 50% restricted configurations (code O, X, Y, Z respectively).

Due to the strongly progressive action of the variable geometry device, the increase in fuelling to maintain the standard air/fuel ratio schedule is slight for the X and Y settings, whereas for the maximum restriction, fuelling was determined by the limits of maximum cylinder pressure (Pmax ≯ 138 bar), and turbocharger speed (Nt/c ≯ 100,000rpm). In the low to mid-speed range, the compressor surge line imposed fuelling restriction, leading to air/fuel ratios being higher than the standard schedule.

Fig. 3.23a shows the engine brake power variation with engine speed. It is evident that due to the turbocharger mismatch, a considerable amount of derating has occurred, the maximum engine power being 88 kw as opposed to the rated 115 kw. This will have to be avoided in future investigations. The improvement in engine power due to variable geometry is, however, quite evident up to an engine speed of 1800rpm. Beyond this speed the power begins to fall quite

abruptly due to excessive back pressure imposed on the engine. The point to notice is the relative ineffectiveness of the X and Y settings. The discussion is therefore pursued with emphasis on the O and Z settings for the rest of the subsection. The largest increase in power occurs at 1200 rpm engine speed and is of the order of 12 kw. At this speed full advantage of the extra air delivered by the variable geometry device is taken and an air/fuel ratio of 20 is maintained.

Figs. 3.23b and 3.23c show engine torque in nm and engine bmep in bars. The unrestricted peak torque is 431 nm and occurs at 1400rpm engine speed corresponding to a 34.3% torque back up at 53.8% maximum engine speed. Torque back up is calculated in relation to engine torque at maximum engine speed with the unrestricted variable geometry turbocharger and not the torque specified by the manufacturer's standard data. It is noted that due to the slight mismatch, peak torque was not accompanied by maximum permissible cylinder pressure and hence an improvement in torque back up without a reduction in compression ratio or retardation of injection timing has been possible. This is in addition to the shift in peak torque to the left leading to a 55.8% torque back up at 46.1% engine speed to have been achieved. Engine peak cylinder pressure was monitored throughout this set of tests and only for the new torque level, the pressure limit of 2000 psi was nearly reached at 1200rpm.

Turbocharger speed is shown in Fig. 3.23d. Again the strongly progressive action of the variable geometry is apparent from the fact that the 'Z' curves for the fully restricted variable geometry

position are well removed from the remaining curves. The maximum turbocharger speed increase occurs at 1800rpm engine speed where the turbocharger speed increases from 64,000rpm to the permissible value of 100,000rpm corresponding to a 56% improvement. The increase in turbocharger speed is quite appreciable even at the lowest engine speed to 1000rpm. It is over 51%.

The compressor map with the engine operating points superimposed on it is shown in Fig. 3.23e. It is again quite clear that the match for the unrestricted turbine 'O' is considerably short of ideal. This is mainly due to the slightly excessive turbine nozzle area in the fully open position and the lack of close guidance of the flow by the variable geometry blade configuration resulting in larger effective blade angles which present a bigger swallowing capacity turbine. However, as stated earlier, a better match would have resulted in a very small surge margin hence restricting variable geometry operation to an unacceptable degree. In future investigations compressors with as large a surge margin as possible have to be employed to overcome this difficulty. Nevertheless, it is evident that the 'Z' points in 4 cases, are on or slightly beyond the nominal surge line. Surge was observed during these tests characterized by a soft whistling noise increasing and diminishing in amplitude at a few tens of times per second. There is no great compressor efficiency gains in the 'Z' locations since efficiency drops sharply as the compressor approaches surge.

Figs. 3.23f and 3.23g represent the engine boost and compressor delivery pressure ratio against engine speed. The improvements seen in the turbocharger speed are clearly reflected in compressor

delivery and hence boost pressure ratio; the difference between them being due to pressure losses in the aftercooler. A maximum boost ratio of over 1.9 is achieved at 1800rpm, a 46.1% improvement over the 1.3 in the 'O' case. At low engine speeds the improvement is less but still substantial at 14.5% from 1.1 to 1.26 at 1000rpm.

Fig. 3.23h shows the sfc variation with engine speed. The substantial improvements at this torque level is quite appreciable, though not strictly comparable with the other cases since in the 'Z' case air/fuel ratio was not maintained at the pre-set schedule. Nevertheless, the benefits that variable geometry can actually have on fuel consumption is considerable. However, due to excessive back pressure, the deterioration in sfc at higher engine speeds is quite marked, indicating that beyond 1800rpm the application of variable geometry should be moderated.

Air fuel ratio is depicted in Fig. 3.23i. The 'O' curve represents the basic standard air/fuel ratio schedule. This figure also shows the discrepancy between the air/fuel ratios for different variable geometry settings. Although more accurate air/fuel ratios could have been obtained for the X and Y cases, in the interest of time the present values were tolerated, particularly since it was known that the X and Y cases are less significant in any case. The line for the 'Z' case also shows how much the fuelling had to be restricted to avoid surge or turbocharger over-speeding beyond the 1200rpm engine speed. The lowest air/fuel ratio occurs at 1400rpm engine speed and is of the order of 18, while the most generous air fuel ratio for the unrestricted case is 28 and occurs at the maximum engine speed of 2600rpm. In the case of the 'Z' setting the

biggest air fuel ratio is over 35 and occurs at 2000rpm engine speed.

Fig. 3.23j demonstrates the mean turbine pressure ratio against engine speed. A comparison of this figure with Fig. 3.23f reveals that in the lower engine speed range the pressure gradient across the engine is positive for all variable geometry settings and gradually becomes negative. Beyond 1800rpm the pressure difference across the engine is considerable leading to adverse effects on engine sfc. Although the mean turbine inlet pressure is higher than the boost pressure in the mid-speed range, the pulse nature of the exhaust discharge process will mean that over a sizeable proportion of the pulses, inlet pressure will be higher than exhaust pressure with less adverse effects overall, than those demonstrated by the mean values of exhaust pressure.

Turbine inlet temperature variation is shown in Fig. 3.23k. The reduction in temperature beyond 1250rpm engine speed is mainly due to the more generous air/fuel ratios. Substantial temperature reductions are not expected from this series of tests due to the fact that a constant air/fuel ratio was chosen as the criterion for performance comparison.

Air and fuel mass flow rates are shown in Figs. 3.23l and 3.23m. The considerable amount of extra air delivered by the variable geometry turbocharger is quite clear in Fig. 3.23l. Fig. 3.23m shows the amount of extra fuel which has been allowed to be injected due to the extra air made available by the variable geometry device. The biggest increase is over 21% and occurs at 1200 rpm.

Finally, inlet manifold temperature is shown in Fig. 3.23n. The successive increase in the temperature is a result of the hotter air at intake to the compressor since the test cell becomes hotter in time and also as a result of the higher temperatures associated with higher pressures delivered by the compressor.

3.5 Final transient tests

3.5.1 General

In this set of tests too, the same letters, O, X, Y and Z correspond to 0, 25, 40 and 50% turbine throat area restrictions respectively. The two intermediate value are nominal rather than actual settings of the variable geometry device as already explained in subsection 2.5.

In these figures, the discontinuity in the curves indicates a change in the time scale. Each division corresponds to 0.2 sec before the discontinuity and 0.5 sec beyond it.

Despite the modifications mentioned in section 3.4.1, the dynamometer could not respond instantaneously to changes in fuelling and a maximum speed excursion of about 11% was tolerated. For smaller fuel steps, the excursion is smaller. The speed excursions do not affect the results of the transient tests to any significant degree. This is partly because of the very short time over which the excursions occur. 0.3 to 0.4 sec is a typical interval which is insignificant when compared to the total transient time of approximately 5 seconds. The main reason, however, is the small magnitude of the excursion over this time.

To avoid over-crowding of the figures, only the most significant parameters are plotted, ie only one engine speed excursion is shown. The others follow approximately the same pattern. Similarly, the load torque curves for the 25% and 40% restriction settings have been omitted.

It was decided to perform the transient tests, keeping the final air/fuel ratio comparable with the steady state values as far as possible, thus taking full advantage of the extra air made available by the variable geometry device. With regard to the steady state results, where the improvements in torque for restrictions of up to 40% were small, and at the same time, the resolution of the mechanism by which the position of the metering valve was adjusted, was too coarse to allow fine incrementing of the metering valve, it was decided to apply similar metering valve steps to the 0, 25 and 40% configurations. In the 50% restriction case, however, fuelling was incremented so as to achieve final torque values comparable to those obtained during the steady state limiting torque tests with 50% restriction. These will be seen to be slightly higher than the steady state results which is acceptable for transients. A further implication of fixed air/fuel ratios is that the overall levels of smoke emission will be similar.

An initial torque value of approximately 92 nm was chosen in the pre-transient state. This torque level was the lower limit of stable operation of the dynamometer over the full speed range while making cross-correlation with steady state results possible.

Similarly, the high speed digital data acquisition system, in

addition to the same parameters as before, recorded fuel pump metering value settings.

Fuel steps were applied at engine speeds of 1000, 1200, 1400, 1600 and 1800rpm, for the O, X, Y and Z settings of the variable geometry device. Figs. 3.24 to 3.28 show the following five variables plotted against time.

a) engine speed

b) turbocharger speed

c) dynamometer torque

d) boost pressure ratio

e) metering valve position

3.5.2 Discussion of the transient results

a) Engine speed Ne=1000rpm (Fig. 3.24)

Performing the transient tests under the constant speed mode of the dynamometer has resulted in quite a long transient time of over 5 seconds. This is due to the fact that keeping the engine speed and hence the displaced volume per unit time constant leads to very sluggish turbine acceleration, since the increase in turbocharger speed and hence boost is dictated largely by the increase in exhaust temperature rather than by an increase in the mass flow rate. Under road conditions, however, the engine speed slowly increases as the vehicle accelerates, leading to a consistent increase in air mass flow rate. The transient results must, therefore, be interpreted with regard to the particularly severe nature of the constant speed unit tests.

The engine speed excursion is shown at the top of Fig. 3.24. There is a maximum engine speed increase of 11% and a return to within 2% of the nominal speed over a 0.4 sec period. The effect of these speed excursions is negligible on the overall transient response of the engine; particularly the effect on turbocharger speed is insignificant.

Next is shown the turbocharger speed variation with time. There clearly is an initial variable geometry (50% restricted) advantage over the fully open case. The initial turbocharger speed has been raised from 17,000 to 27,000rpm and the improvement is maintained throughout the transient by the end of which the turbocharger speed for restricted and fully open cases is 56,000 and 38,000rpm respectively; a 60% increase. However, at this low engine speed, turbocharger acceleration rates are inevitably slow although the improvement in turbocharger acceleration is evident.

The dynamometer load torque is shown next. It is apparent that the dynamometer control system is now underdamped leading to a number of over and under-shoots, but converging on the right torque level to bring back the engine speed to its nominal value in a very short period of time when compared with the first series of transient tests.

The higher dynamometer torque levels associated with the 'Z' curve are mainly due to the higher engine torque, developed due to the extra fuelling, under 50% restricted operation. The higher instantaneous engine torque will lead to a faster response when such a unit is installed in an appropriate vehicle.

Boost can also be seen to have been improved in line with turbocharger speed. Final boost values are 1.093 and 1.26 for the unrestricted and restricted cases respectively.

At the bottom of the figure, the size of the fuel steps applied in the 'O' and 'Z' cases, is shown. The metering valve step is virtually instantaneous from the given minimum up to the respective limiting values for the 'O' and 'Z' positions.

b) Engine speed Ne=1200rpm (Fig. 3.25)

The fuel steps are slightly larger than at 1000rpm for both 'O' and 'Z' cases corresponding to the higher limiting torque levels at 1200rpm.

The speed excursion is still of the same order of magnitude as at 1000rpm. Turbocharger speed response in the 'Z' position is now greatly improved compared with the 'O' position, starting from 36,000 (cf. 18,500rpm) and rising to its final value of 72,500rpm, while in the 'O' position, the final value of 35,500rpm is reached more sluggishly. However, response times are again artificially extended due to the nature of the constant speed transients.

Boost can also be seen to have improved considerably. A no boost situation for the 'O' case is raised to just under 1.1 for the 'Z' case before the fuel step is applied, and at the end of the recorded transient period the boost has increased from just under 1.1 to 1.45 in the 'O' and 'Z' cases respectively.

c) Engine speed Ne=1400rpm (Fig. 3.26)

The fuel steps are further increased to achieve final torque levels comparable to the steady state values at 1400rpm. Turbocharger speed is still below the permissible limit of 100000rpm when fully restricted. It accelerates from an initial value of 44,000rpm to a final value of 90,000rpm for the 'Z' case, while for the 'O' case the initial turbocharger speed of 24,000rpm is raised to a final speed of 47,000rpm. The higher torque developed by the engine due to the larger fuel steps is clearly shown by the dynamometer response torque.

At this speed, however, the two air/fuel ratios for the 'O' and 'Z' cases are no longer equal as indicated by the steady state results. Fuelling had to be restricted in the 'Z' case to avoid compressor surge. The most marked improvement is evident from the boost curves. The final boost value for the 'Z' case is 1.64 and compares very favourably with 1.16 for the 'O' case. The improvement is over 41%.

d) Engine speed Ne=1600rpm (Fig. 3.27)

The fuel steps applied at this speed correspond to steady state torque levels which are past the peak torque at 1400rpm. Similar trends as those for the previous cases can be observed. Turbocharger speed is substantially increased and now has reached the limiting value of 100,000rpm at the end of the transient period in the case of the 50% restriction, while for the 'O' case a final value of only 55,500rpm is reached. Before the step is applied, however, the turbocharger speed is maintained at 55,000rpm for the 50% restriction setting compared with 30,000 for the fully open

case. Due to the extra fuel injected, the dynamometer has had to prevent engine acceleration by applying a larger resisting torque. The extra engine torque would normally result in faster vehicle acceleration under road conditions. Since it has not been possible to adhere to the air/fuel ratio schedule due to the turbocharger speed limit, smoke emission is bound to be reduced by the application of the variable geometry device. However, it should be remembered that had the initial turbocharger match been ideal, there would have been a much smaller scope for increase in fuelling and hence torque at 1400 and 1600rpm, except with the introduction of lower compression ratio pistons or variable injection timing equipment to retard the timing appropriately.

Boost ratio has also improved in response to higher turbocharger speed levels. It is increased from 1.2 to 1.9 for the 'Z' case while in the 'O' case, it rises from 1.0 to just over 1.2.

e) Engine speed Ne=1800rpm (Fig. 3.28)

As the engine speed increases the significance of variable geometry application diminishes since it is most appropriate in the low to mid-speed range. However, the benefits at this speed are still substantial and worth considering. The fuel steps have coincided since no extra fuelling has been applied to prevent the turbocharger speed from exceeding the 100,000rpm limit. Turbocharger speed has increased substantially from 65,000rpm to the limiting value of 100,000rpm in the 50% restriction case while in the 'O' position, it has risen from 33,000rpm to 61,000rpm in the same time.

The dynamometer torque curves are most significant in that, although the size of the steps are now the same, the dynamometer has had to apply a larger torque to keep the speed excursions approximately the same. This indicates that the instantaneous torque developed by the engine under 50% restriction conditions is substantially higher leading to much better vehicle acceleration under road conditions.

Boost ratio is similarly improved from 1.32 to 1.98 in the 'Z' case while it only rises from 1.02 to 1.26 for the 'O' case in the same time. The rate of increase is, however, quite improved under variable geometry operation.

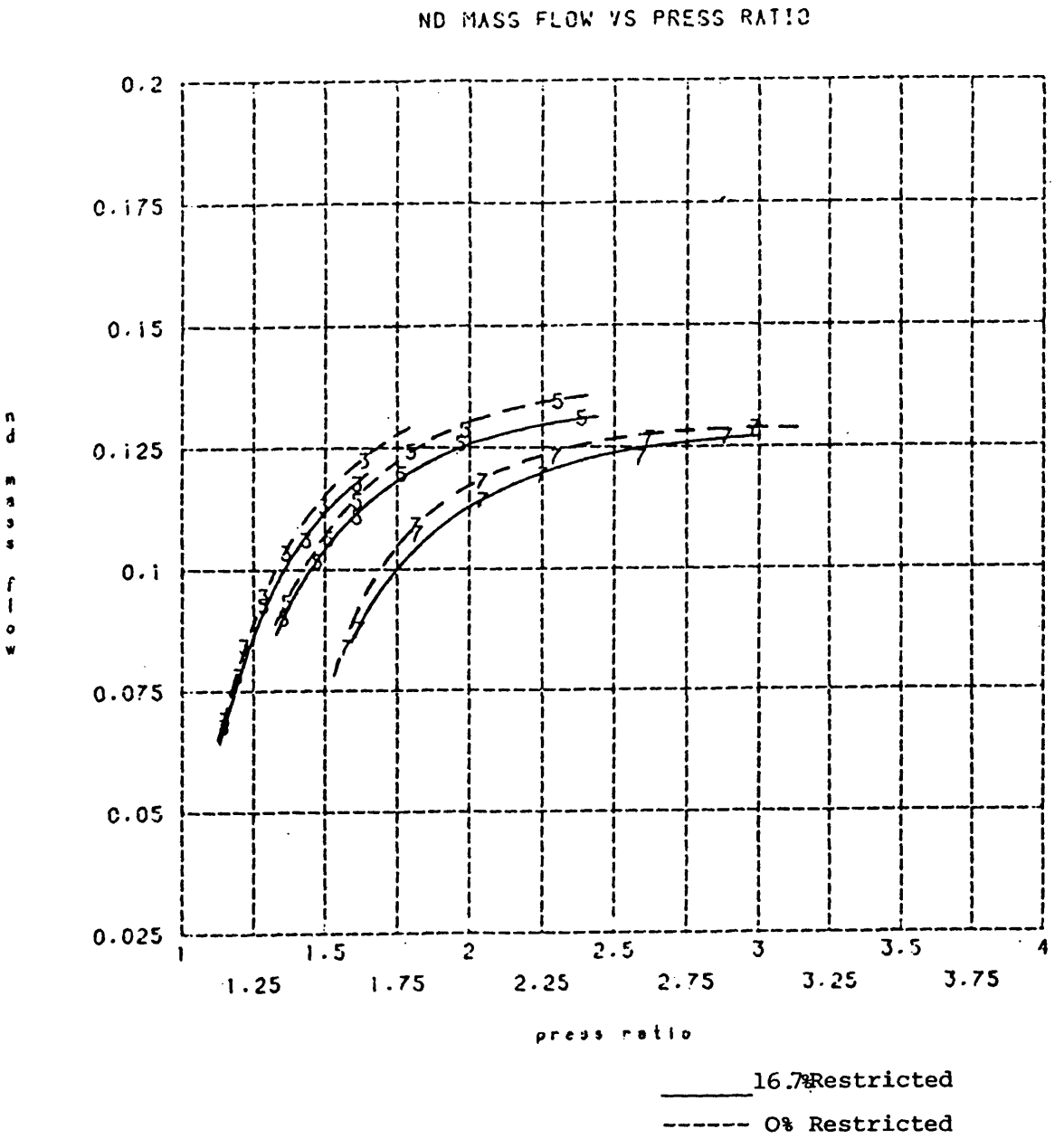

Fig. 3.1 Zip Fastener Variable Geometry Turbine Dynamometer Results, 16.7% Restriction. 3 = 30000 rpm etc.

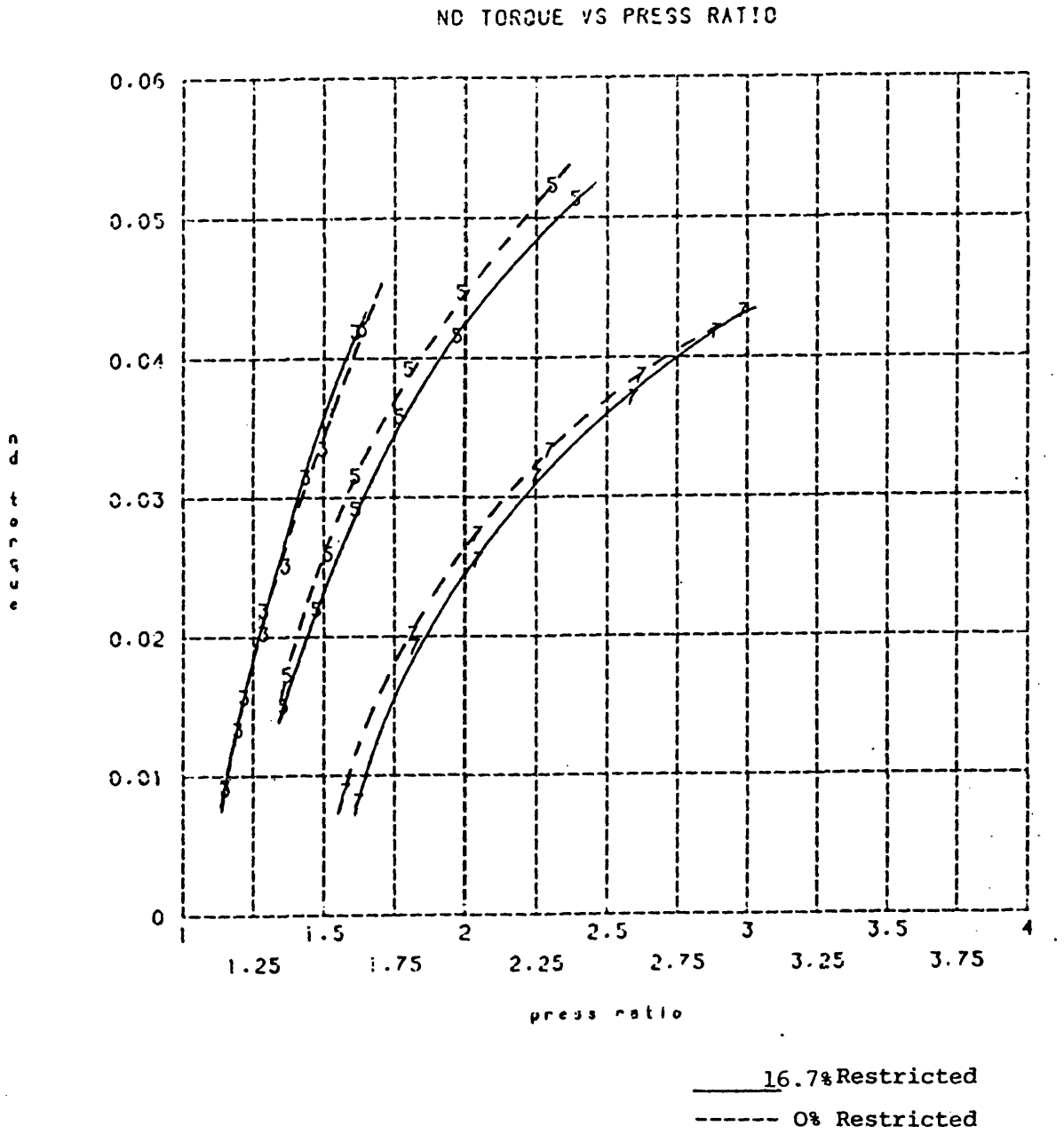

Fig. 3.2 Zip Fastener Variable Geometry Turbine Dynamometer Results, 16.7% Restriction. 3 = 30000 rpm etc.

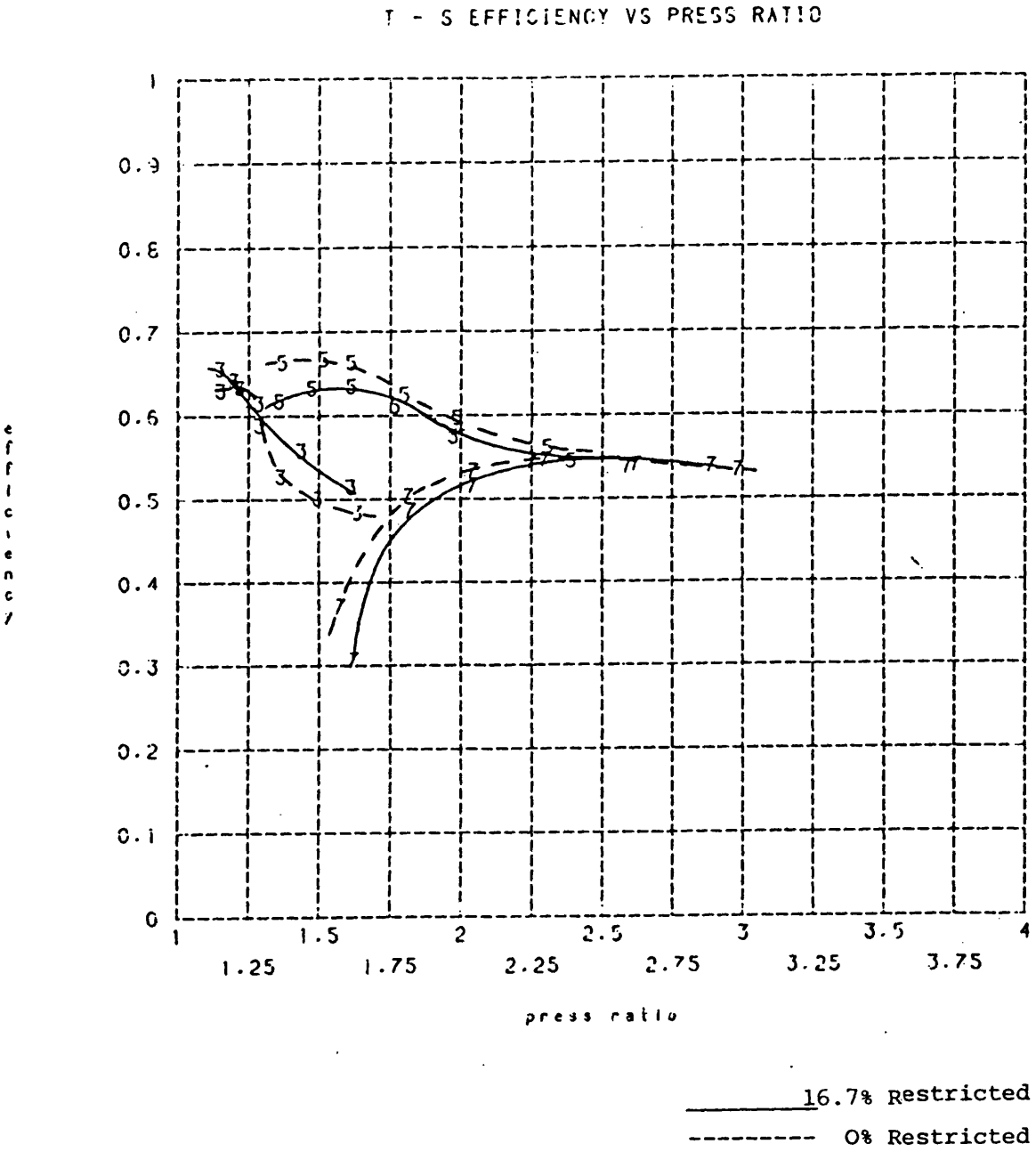

Fig. 3.3 Zip Fastener Variable Geometry Turbine Dynamometer Results, 16.7% Restriction. 3 = 30000 rpm etc.

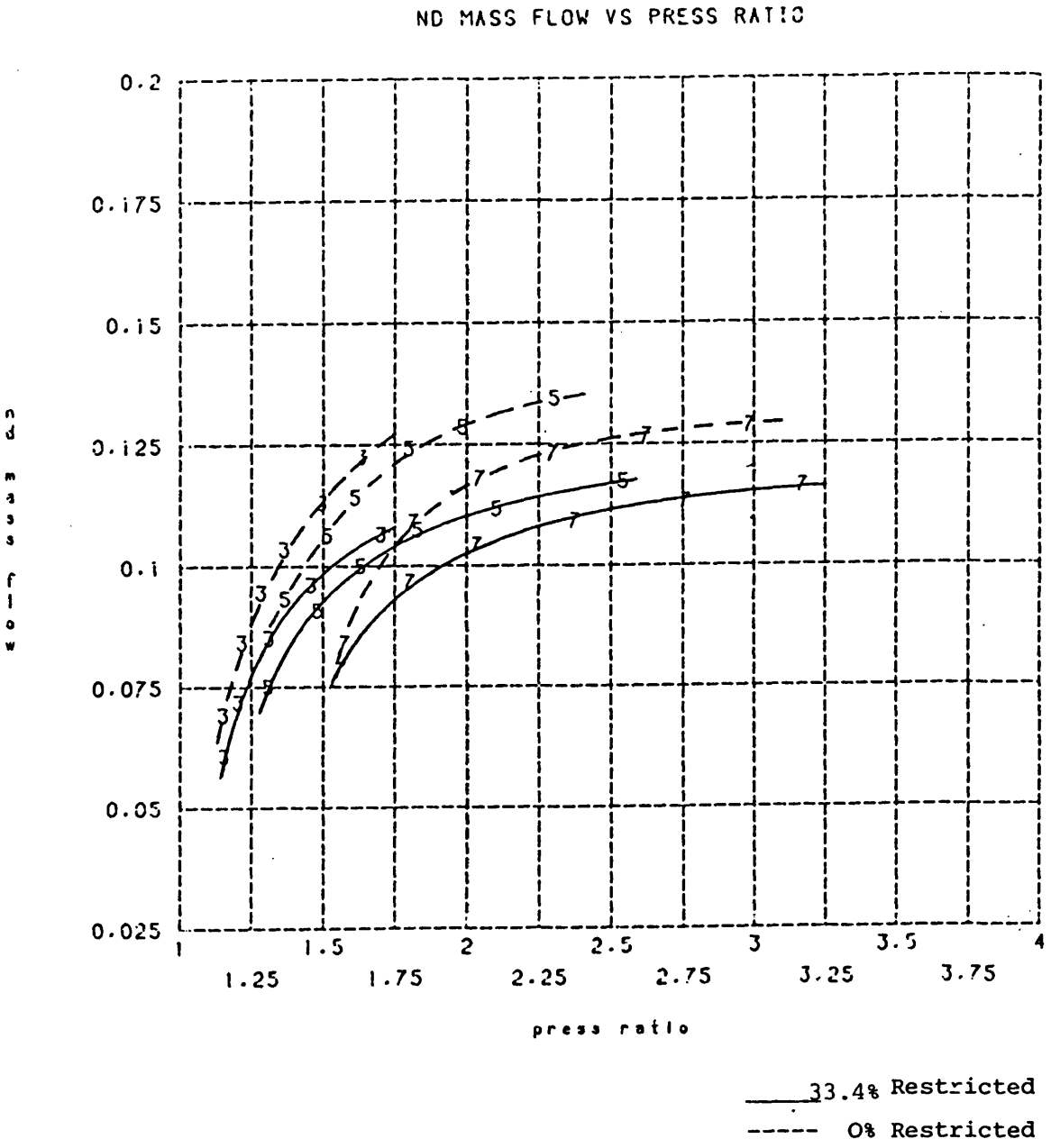

Fig. 3.4 Zip Fastener Variable Geometry Turbine Dynamometer Results, 33.4% Restriction. 3 = 30000 rpm etc.

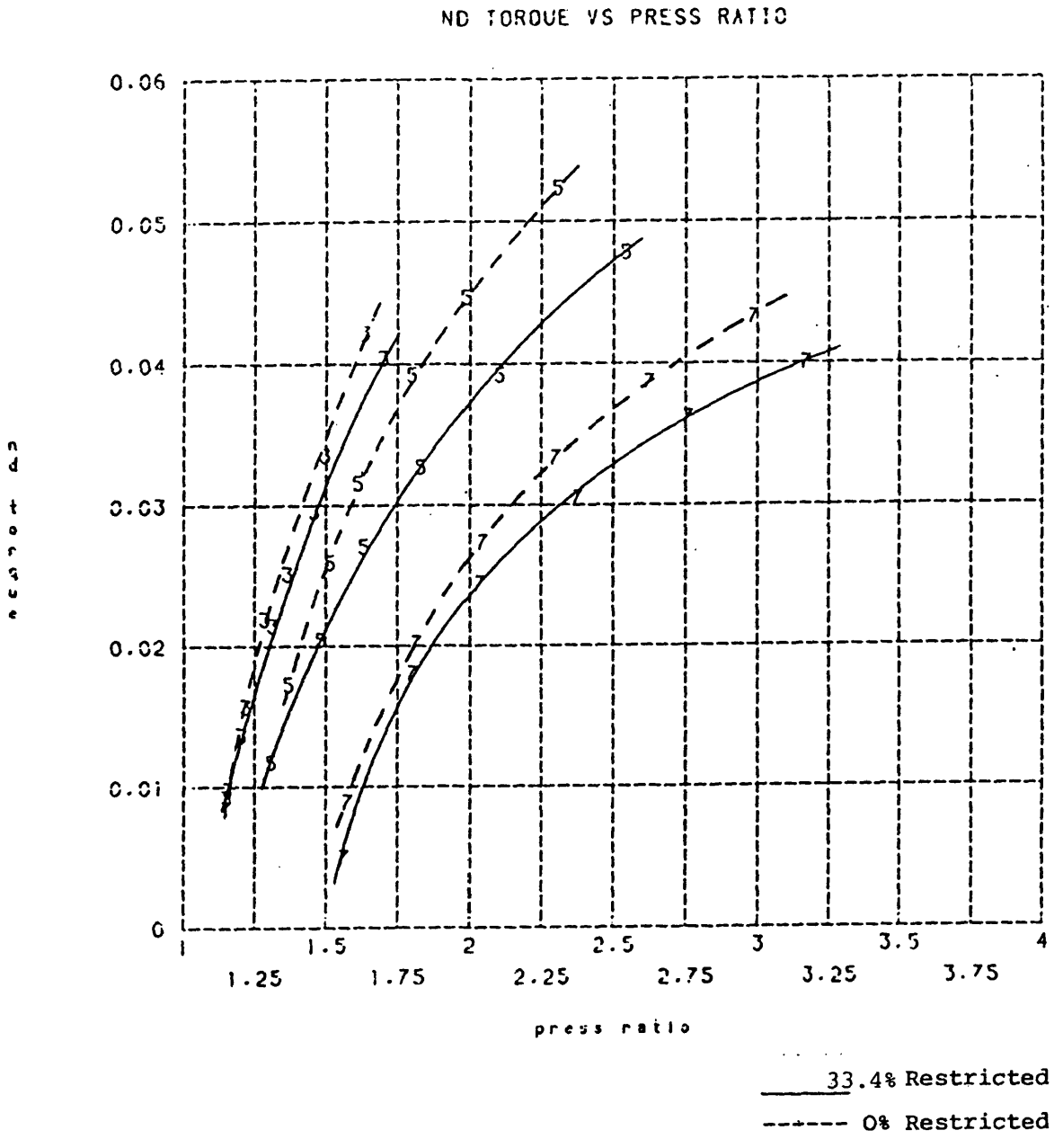

Fig. 3.5 Zip Fastener Variable Geometry Turbine Dynamometer Results, 33.4% Restriction. 3 = 30000 rpm etc.

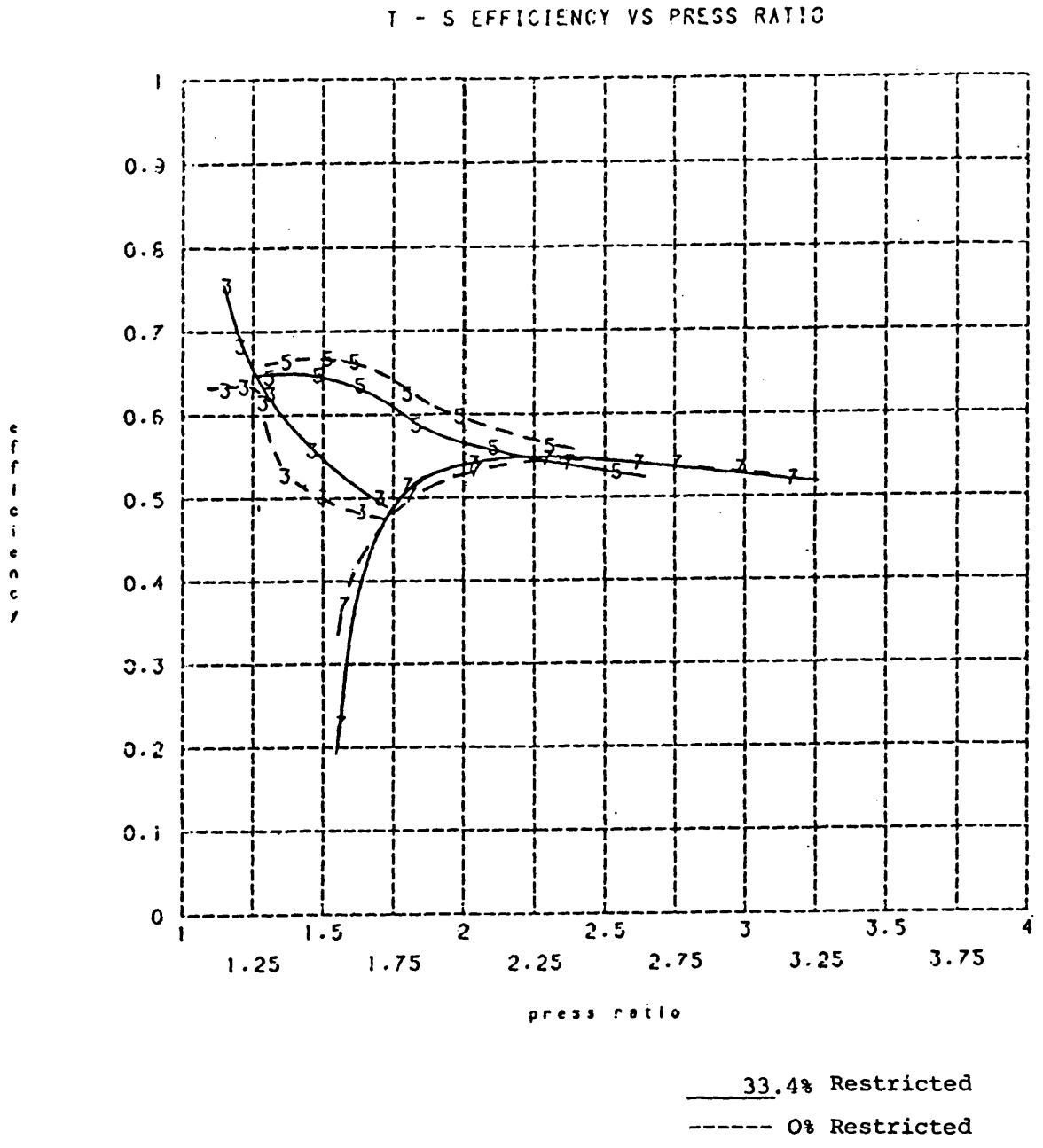

Fig. 3.6 Zip Fastener Variable Geometry Turbine Dynamometer Results, 33.4% Restriction. 3 = 30000 rpm etc.

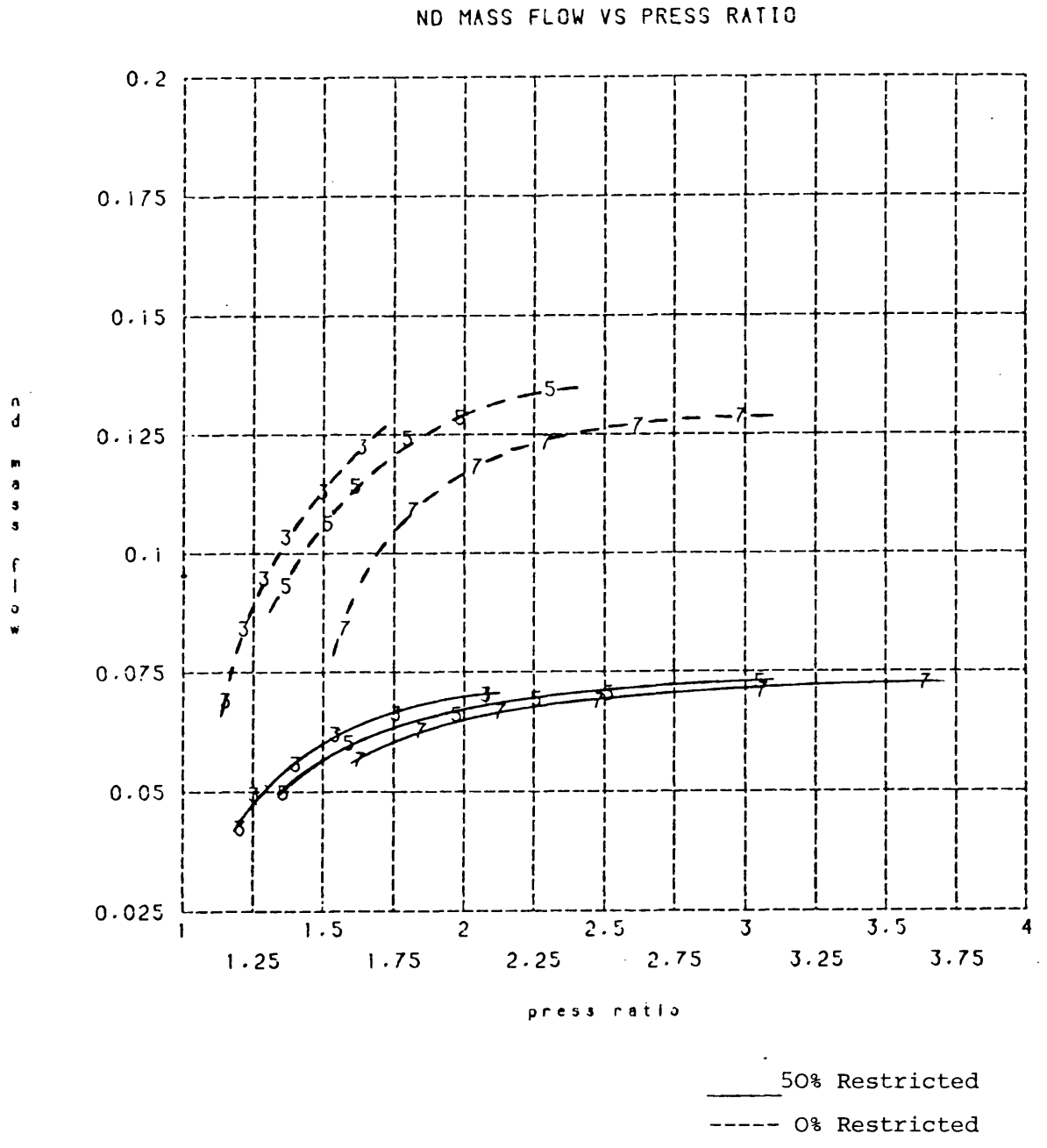

Fig. 3.7 Zip Fastener Variable Geometry Turbine Dynamometer Results, 50% Restriction. 3 = 30000 rpm etc.

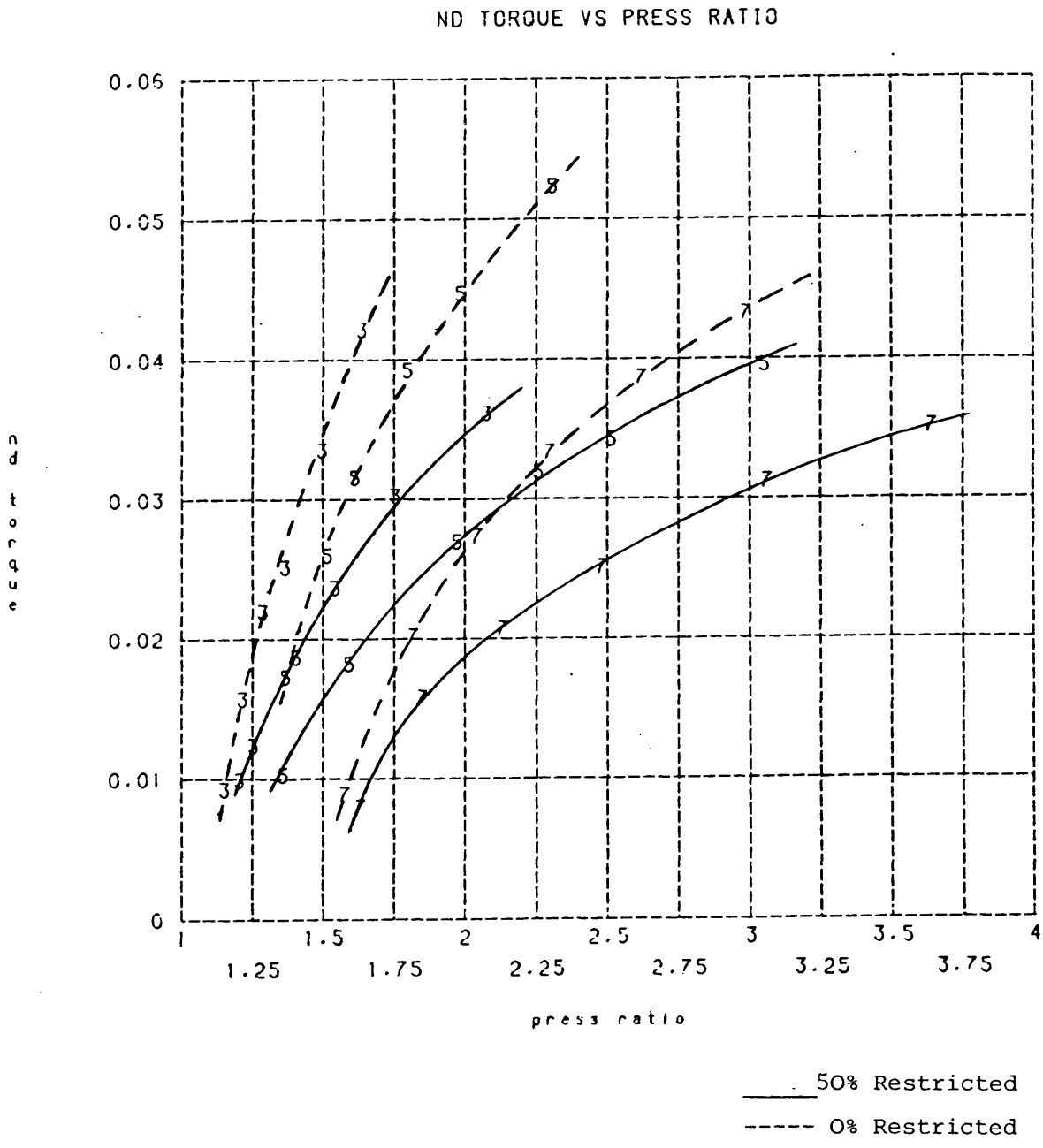

Fig. 3.8 Zip Fastener Variable Geometry Turbine Dynamometer Results, 50% Restriction. 3 = 30000 rpm etc.

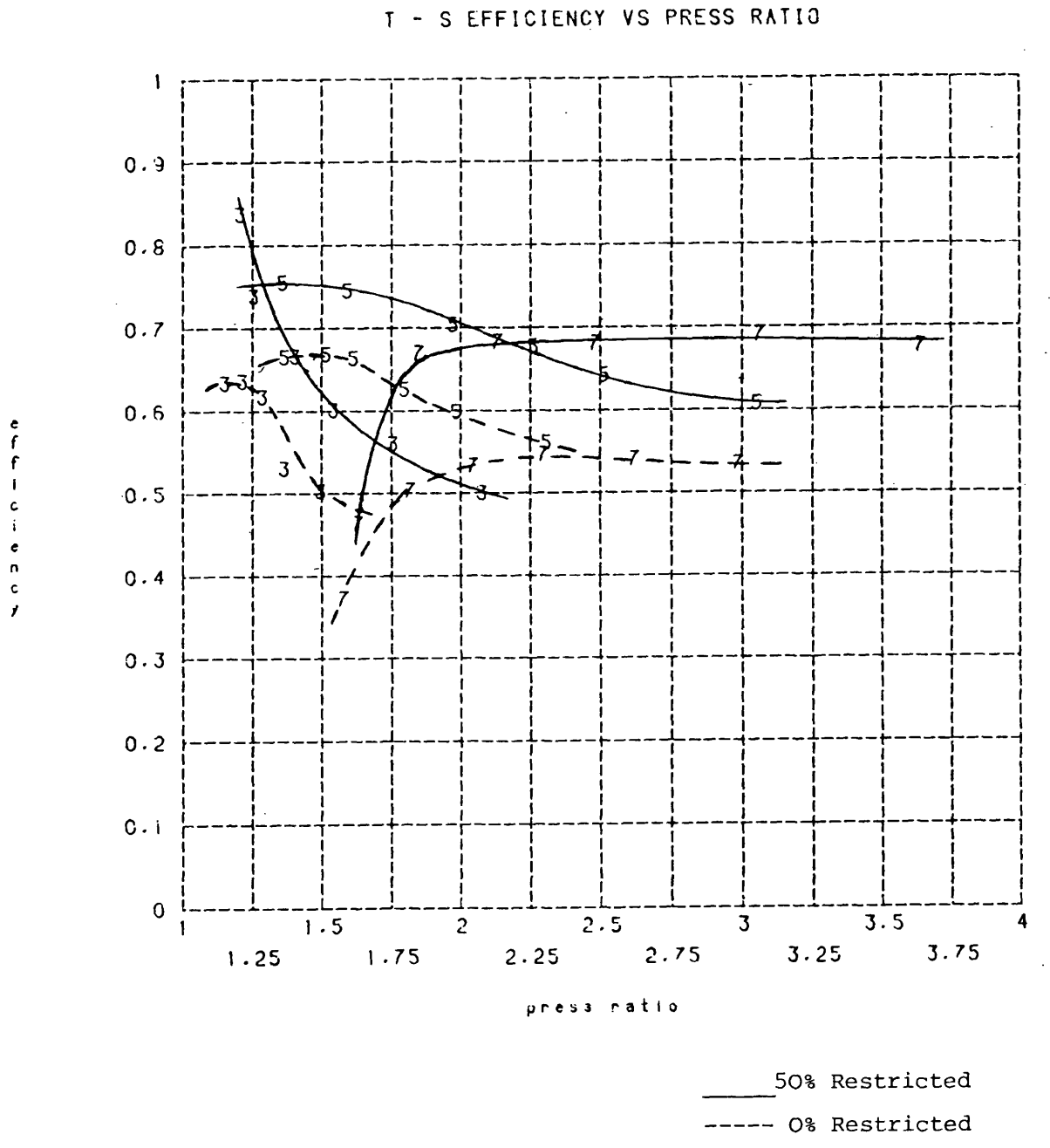

Fig. 3.9 Zip Fastener Variable Geometry Turbine Dynamometer Results, 50% Restriction. 3 = 30000 rpm etc.

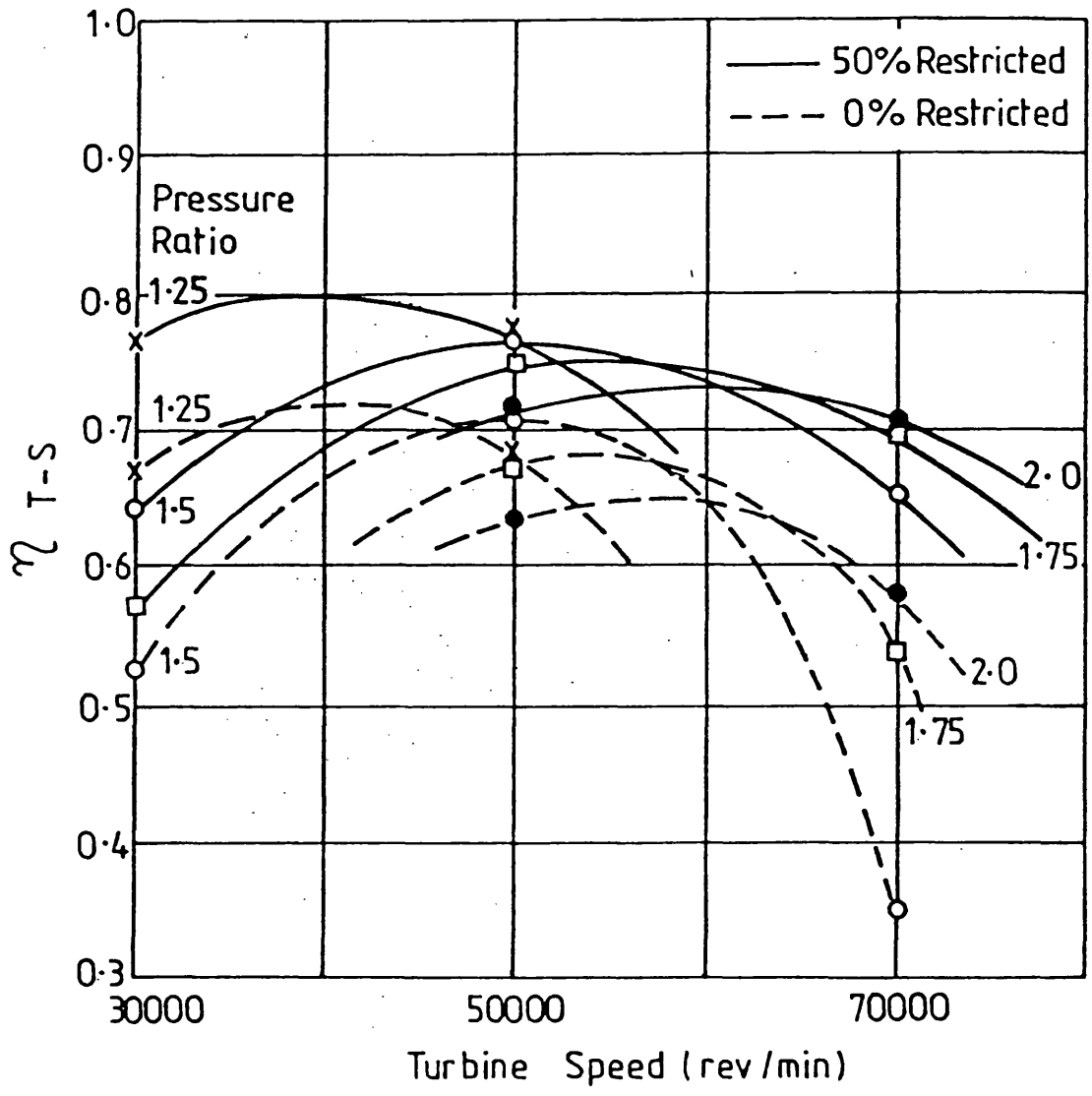

Fig. 3.10 Zip Fastener Variable Geometry Turbine Efficiency Against Turbine Speed.

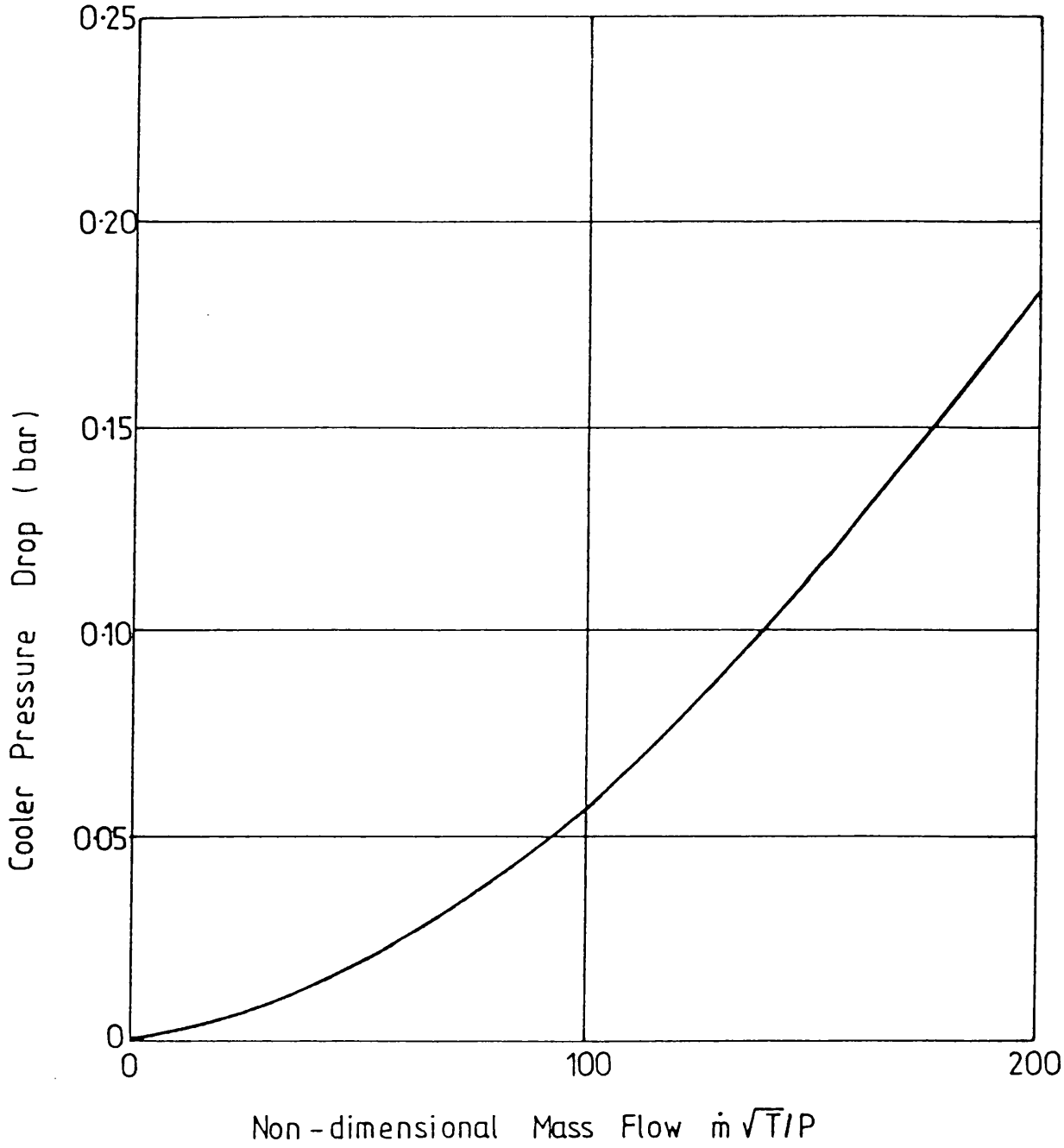

Fig. 3.11 Cooler Pressure Drop Against Non-Dimensional Mass flow.

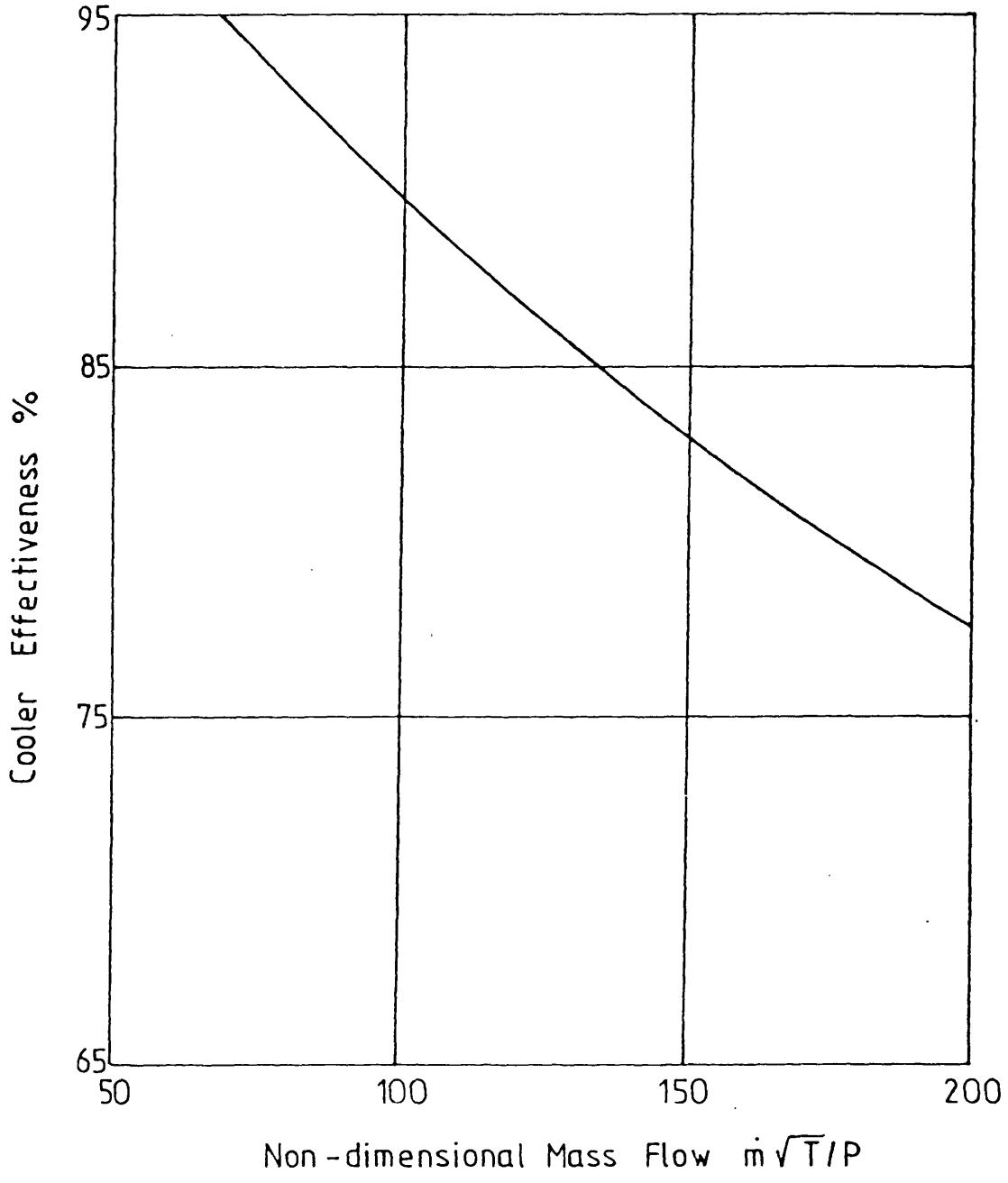

Fig. 3.12 Cooler Effectiveness Against Non-Dimensional Mass Flow.

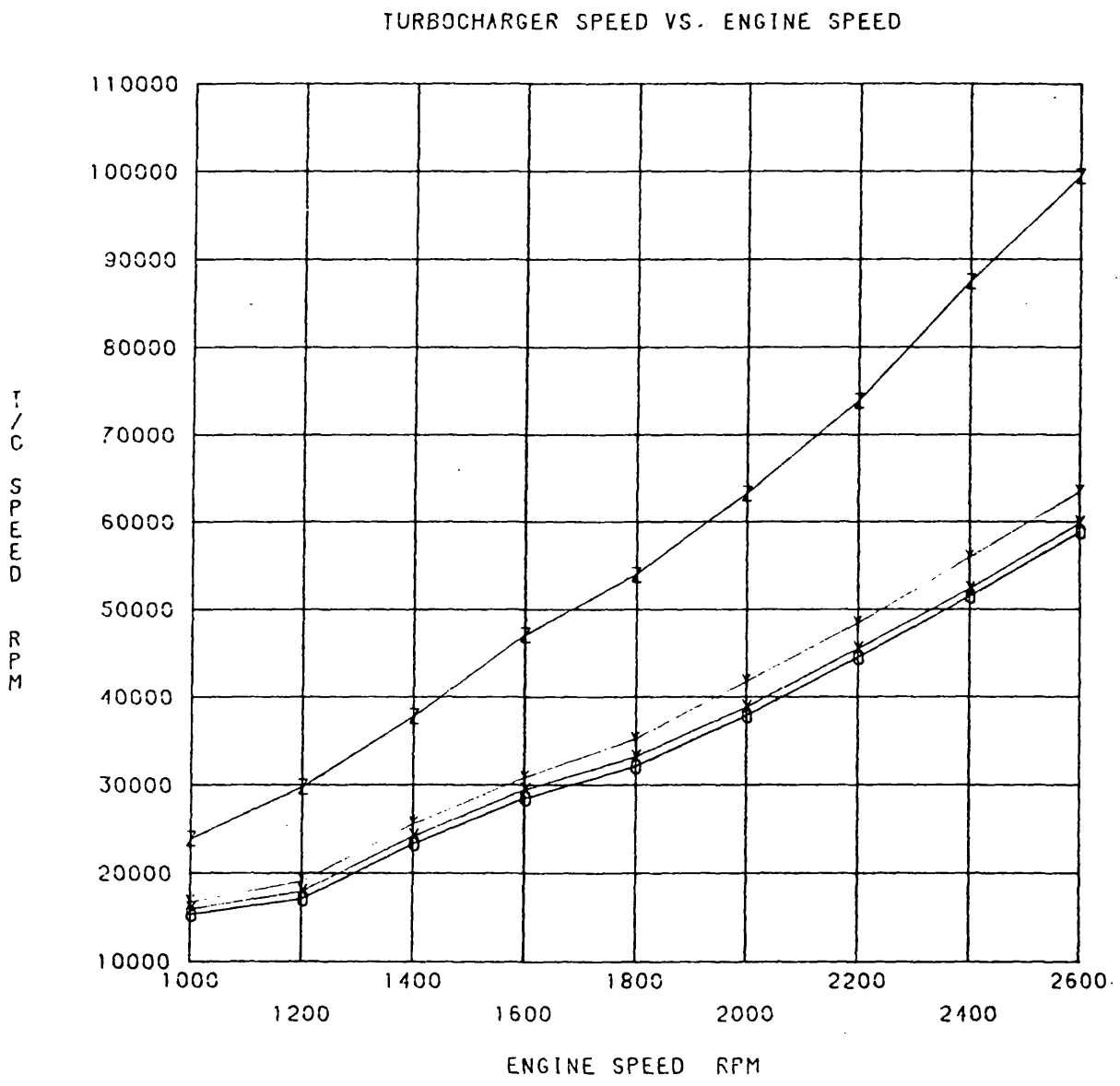

Fig. 3.13a 2 Bar BMEP Variable Geometry Engine Results,

O = 0%, X = 25%, Y = 40% and Z = 50% Restriction.

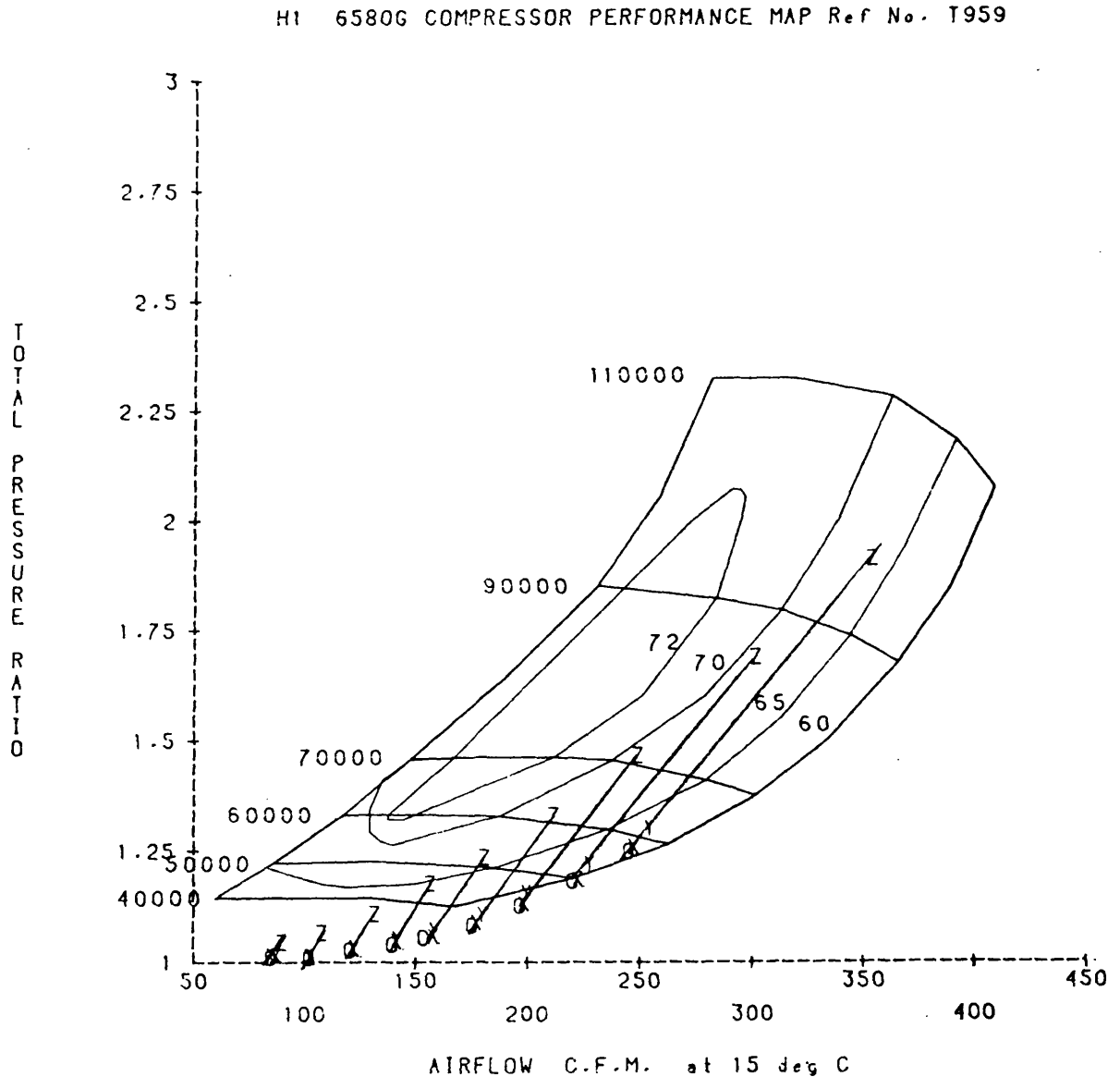

Fig. 3.13b 2 Bar BMEP Variable Geometry Engine Results,

O = 0%, X = 25%, Y = 40% and Z = 50% Restriction.

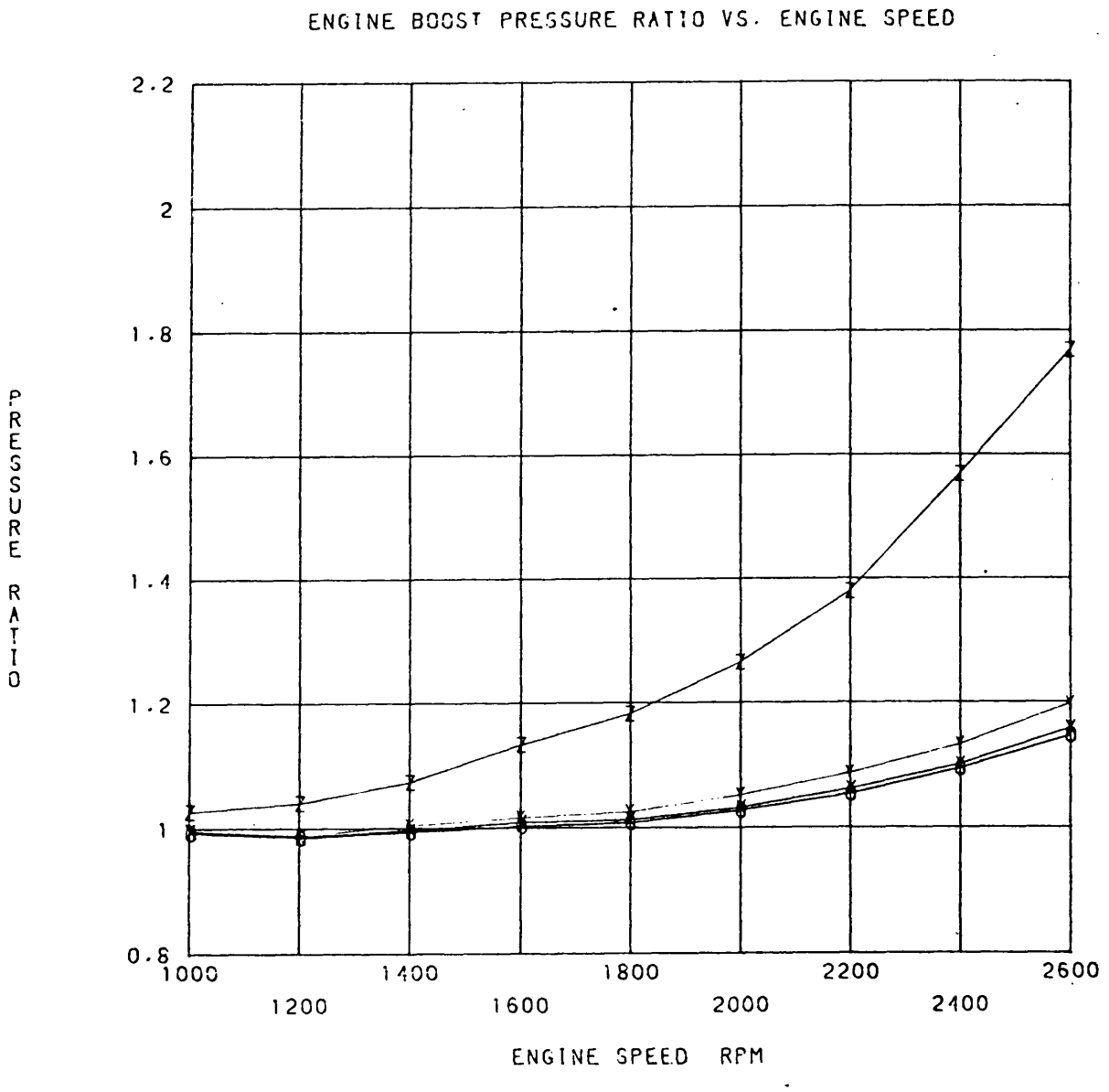

Fig. 3.13c 2 Bar BMEP Variable Geometry Engine Results,

O = 0%, X = 25%, Y = 40% and Z = 50% Restriction.

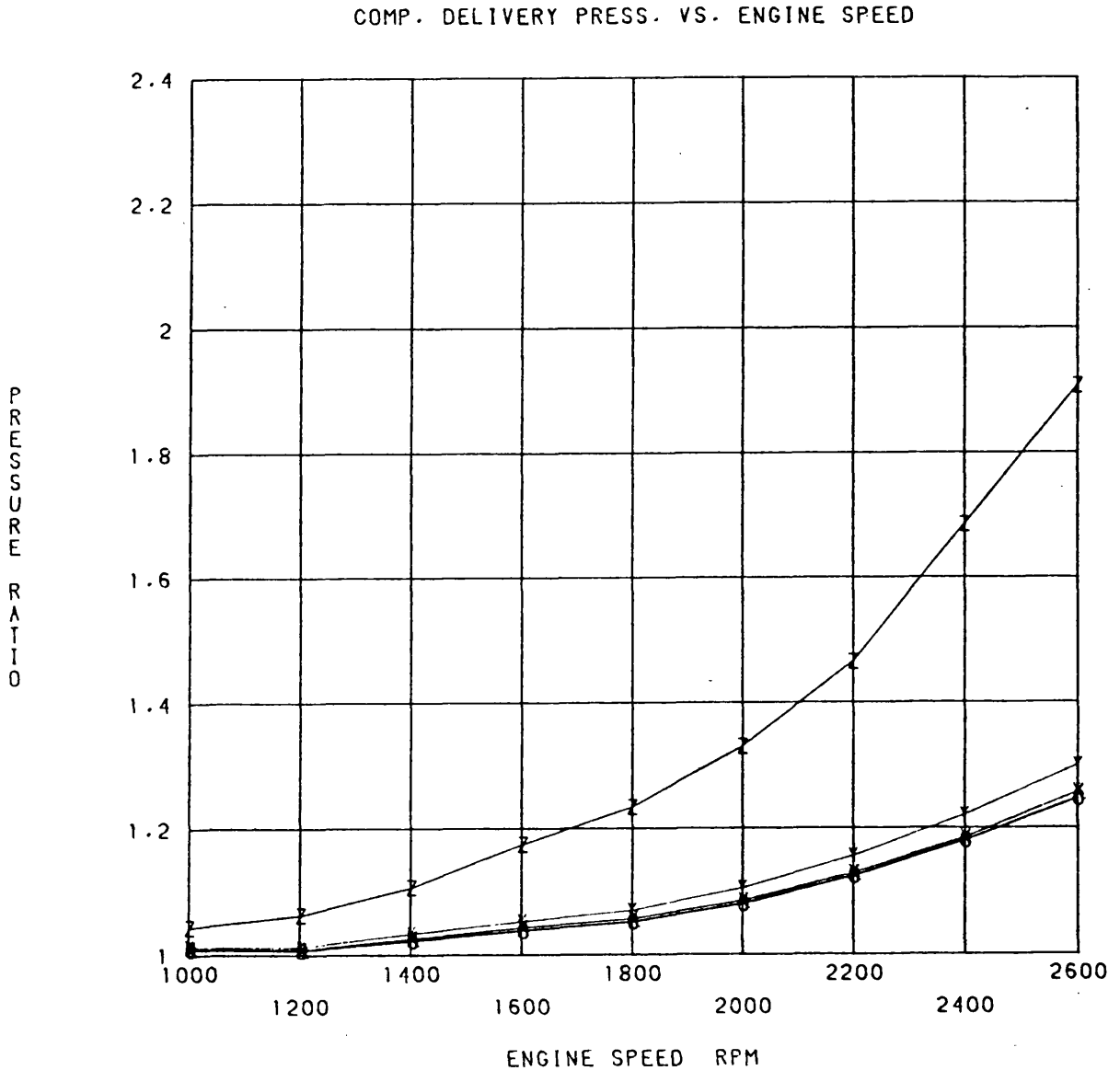

Fig. 3.13d 2 Bar BMEP Variable Geometry Engine Results,

O = 0%, X = 25%, Y = 40% and Z = 50% Restriction.

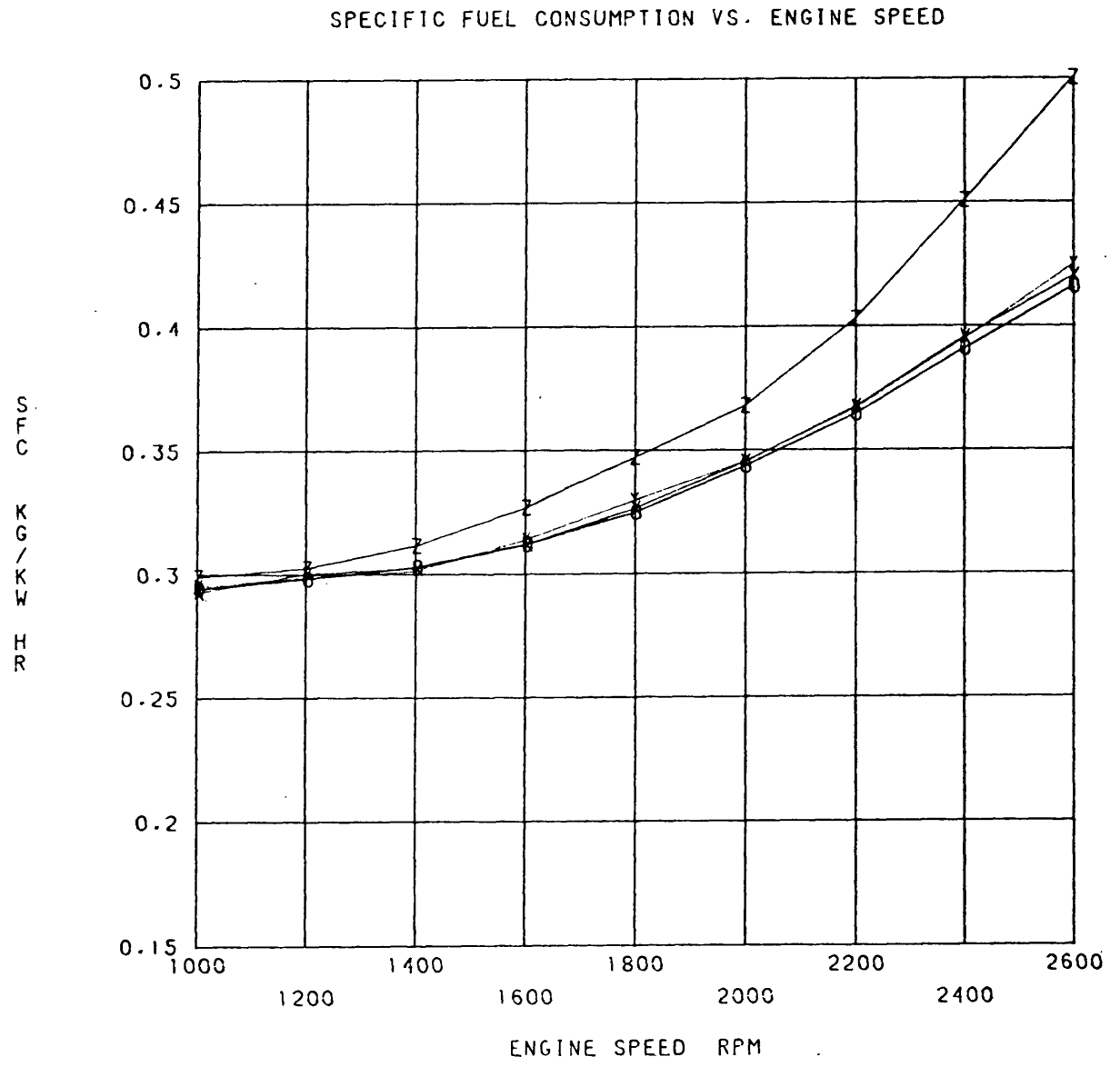

Fig. 3.13e 2 Bar BMEP Variable Geometry Engine Results,

O = 0%, X = 25%, Y = 40% and Z = 50% Restriction.

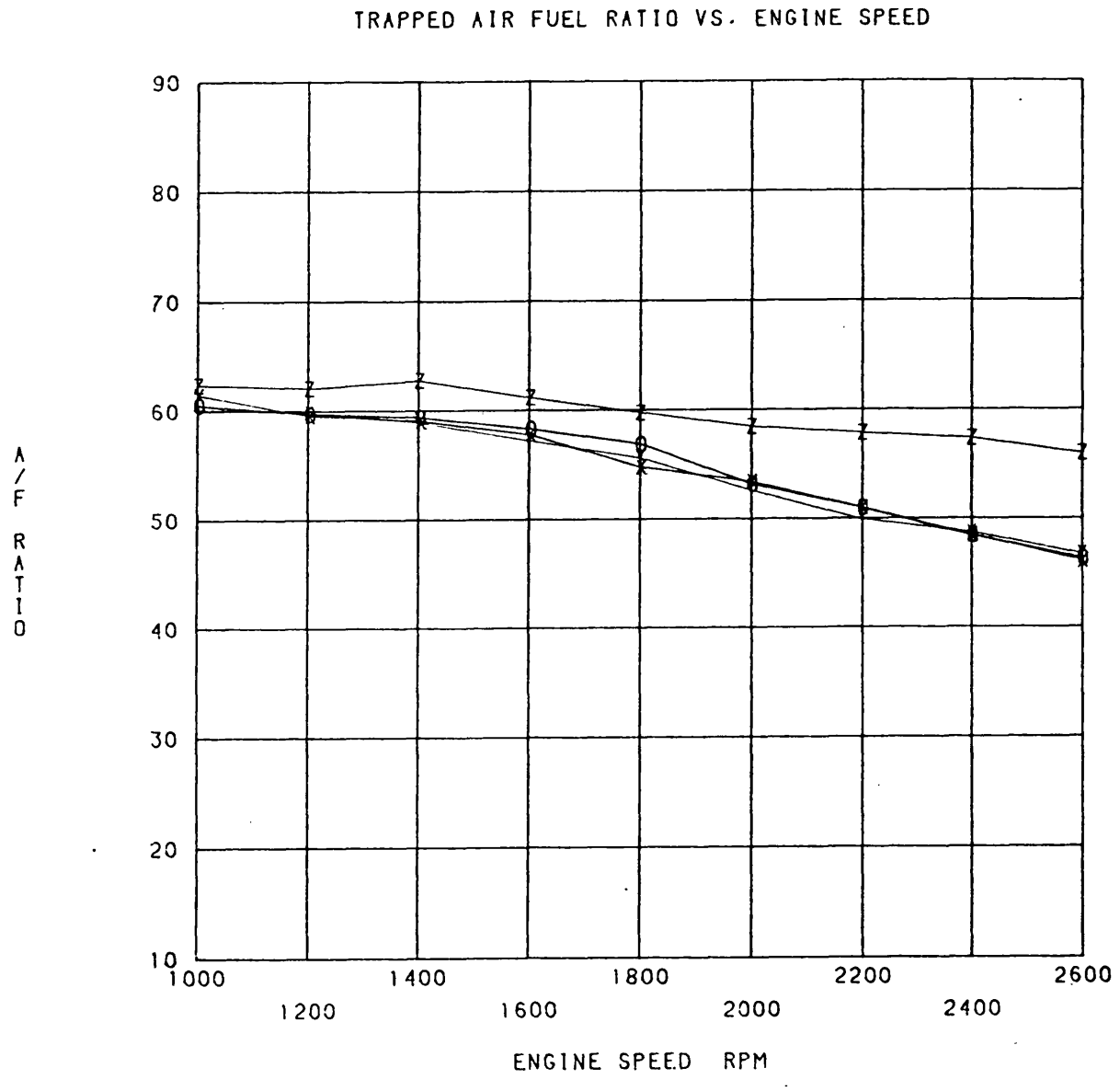

Fig. 3.13f 2 Bar BMEP Variable Geometry Engine Results,

O = 0%, X = 25%, Y = 40% and Z = 50% Restriction.

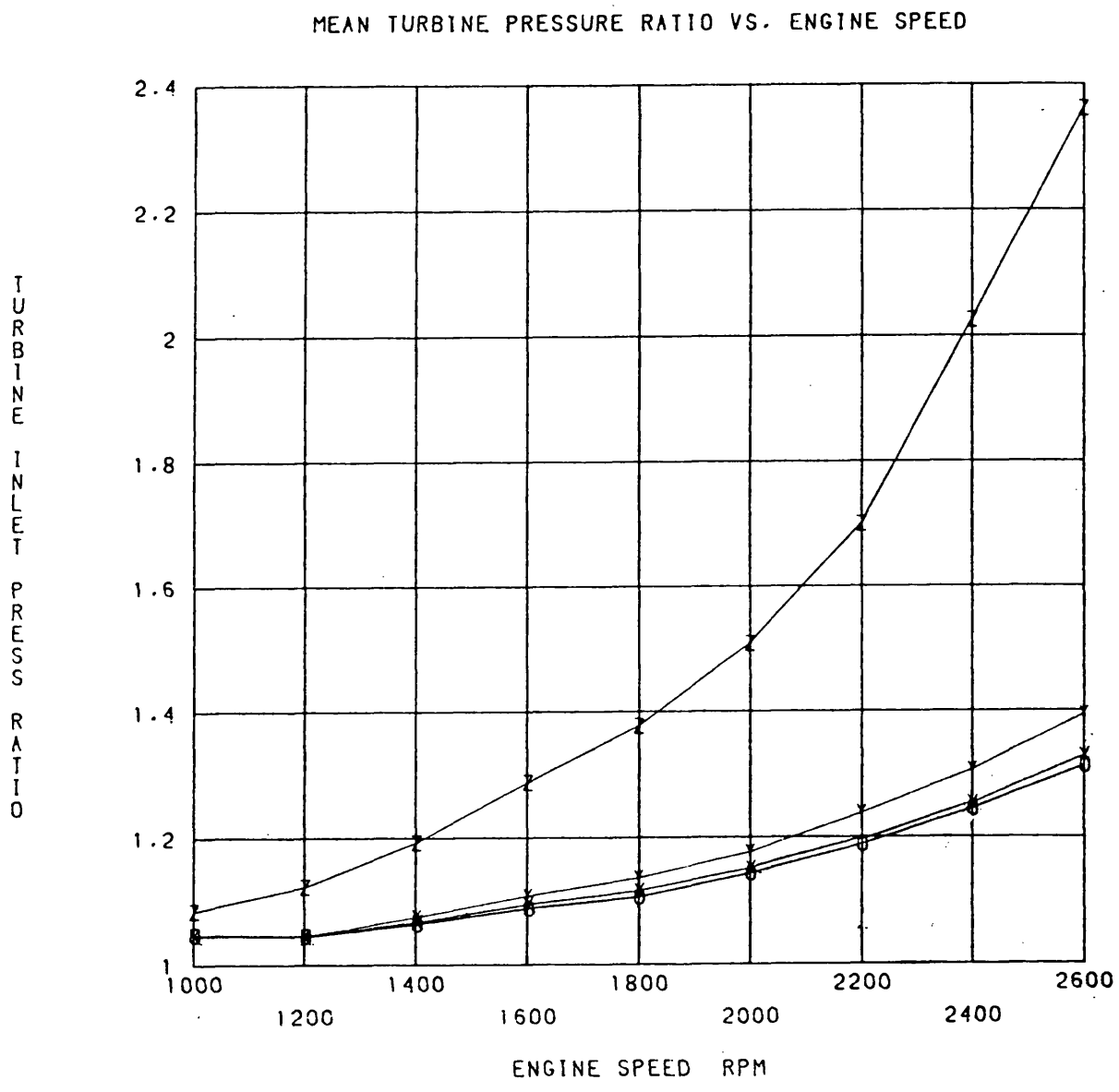

Fig. 3.13g 2 Bar BMEP Variable Geometry Engine Results,

O = 0%, X = 25%, Y = 40% and Z = 50% Restriction.

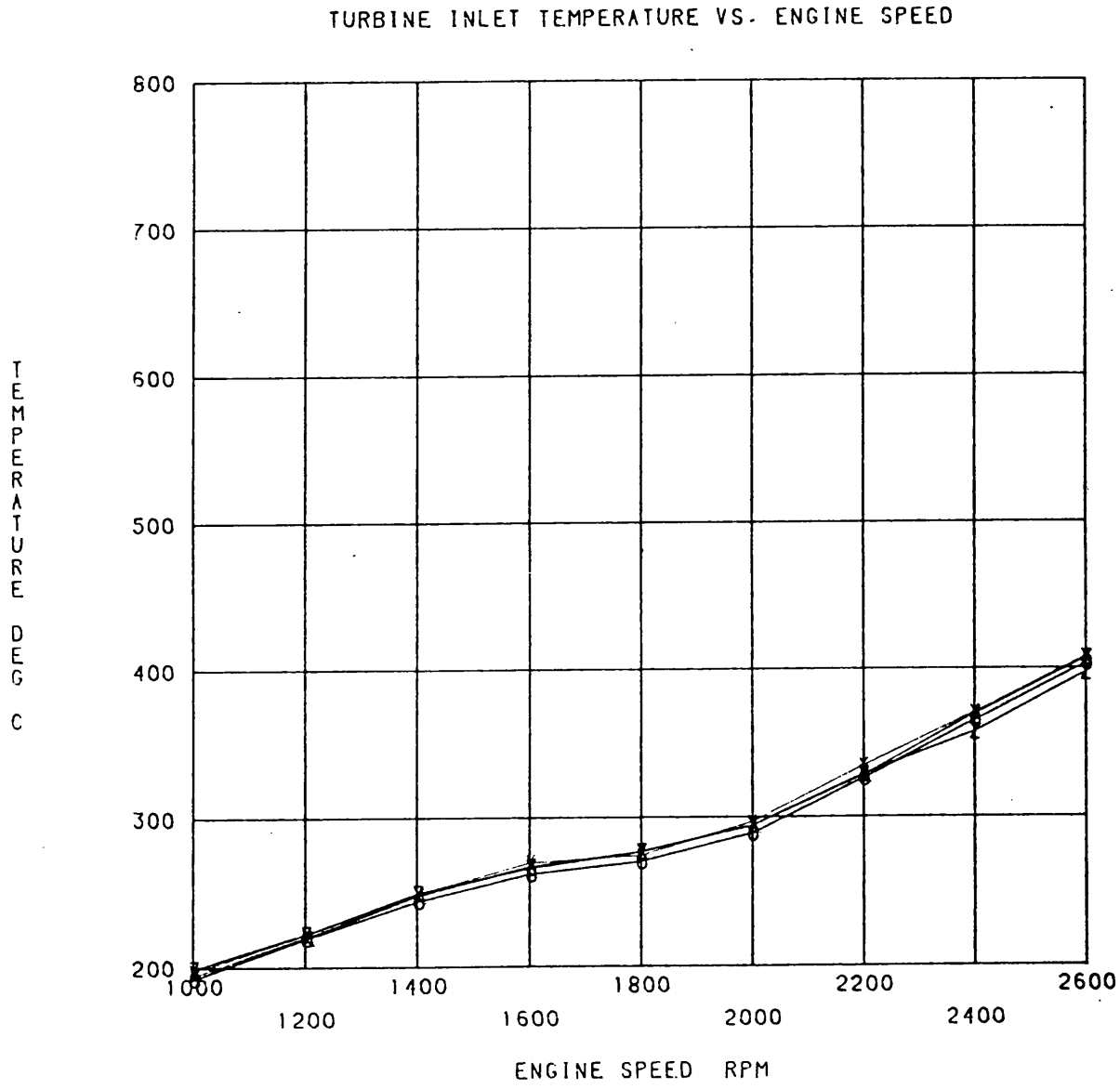

Fig. 3.13h 2 Bar BMEP Variable Geometry Engine Results,

O = 0%, X = 25%, Y = 40% and Z = 50% Restriction.

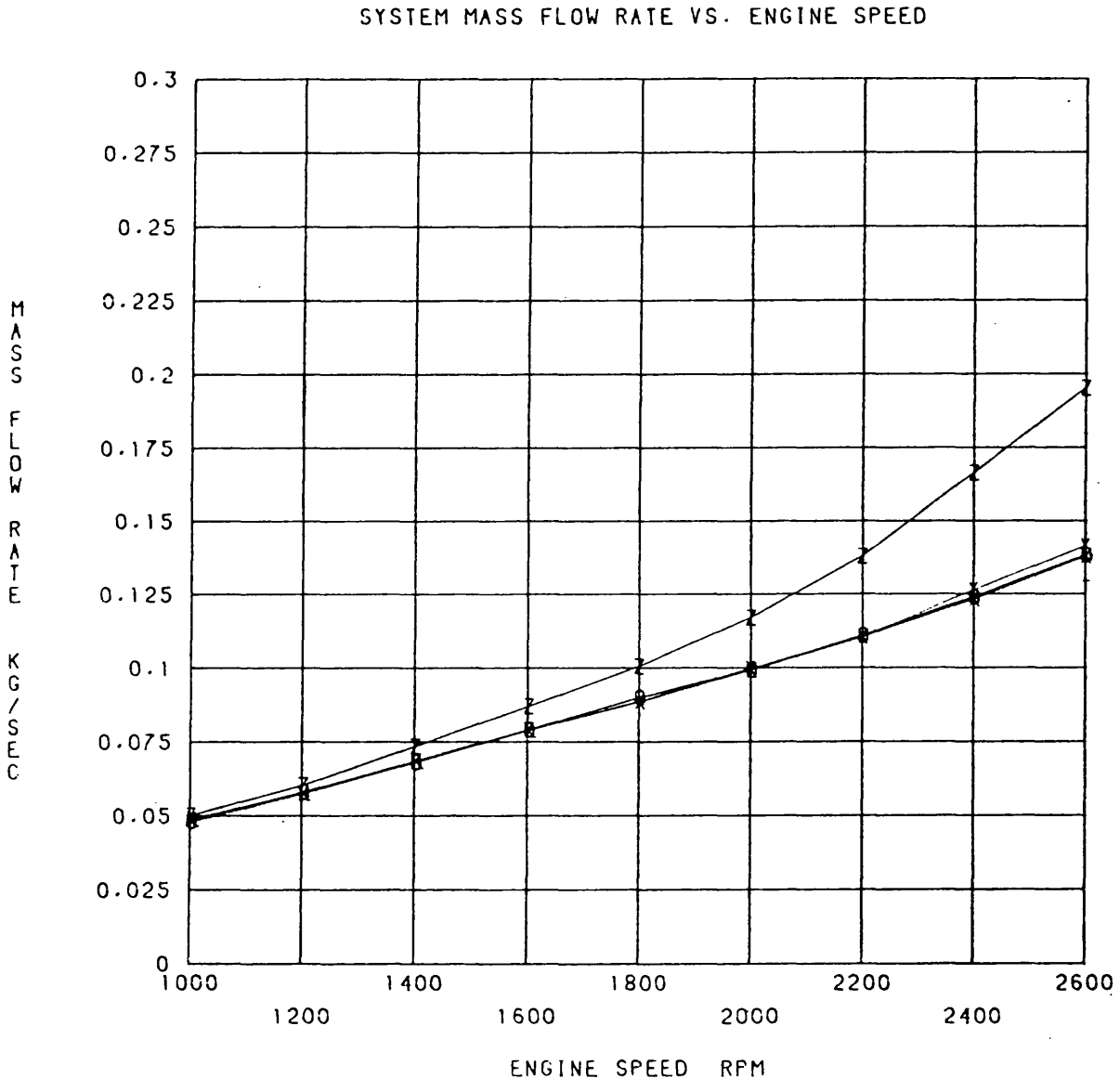

Fig. 3.13i 2 Bar BMEP Variable Geometry Engine Results,

O = 0%, X = 25%, Y = 40% and Z = 50% Restriction.

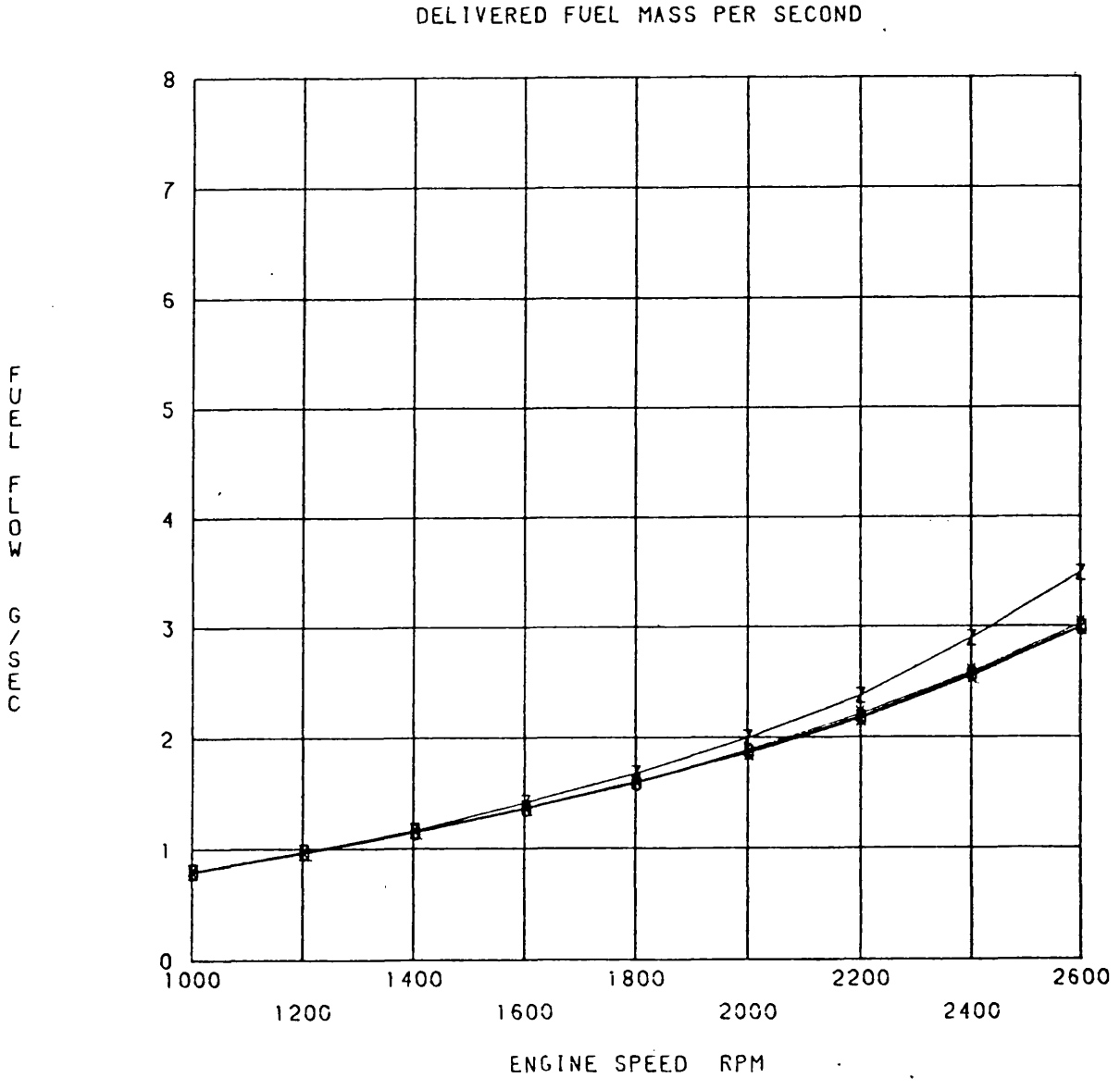

Fig. 3.13j 2 Bar BMEP Variable Geometry Engine Results,

O = 0%, X = 25%, Y = 40% and Z = 50% Restriction.

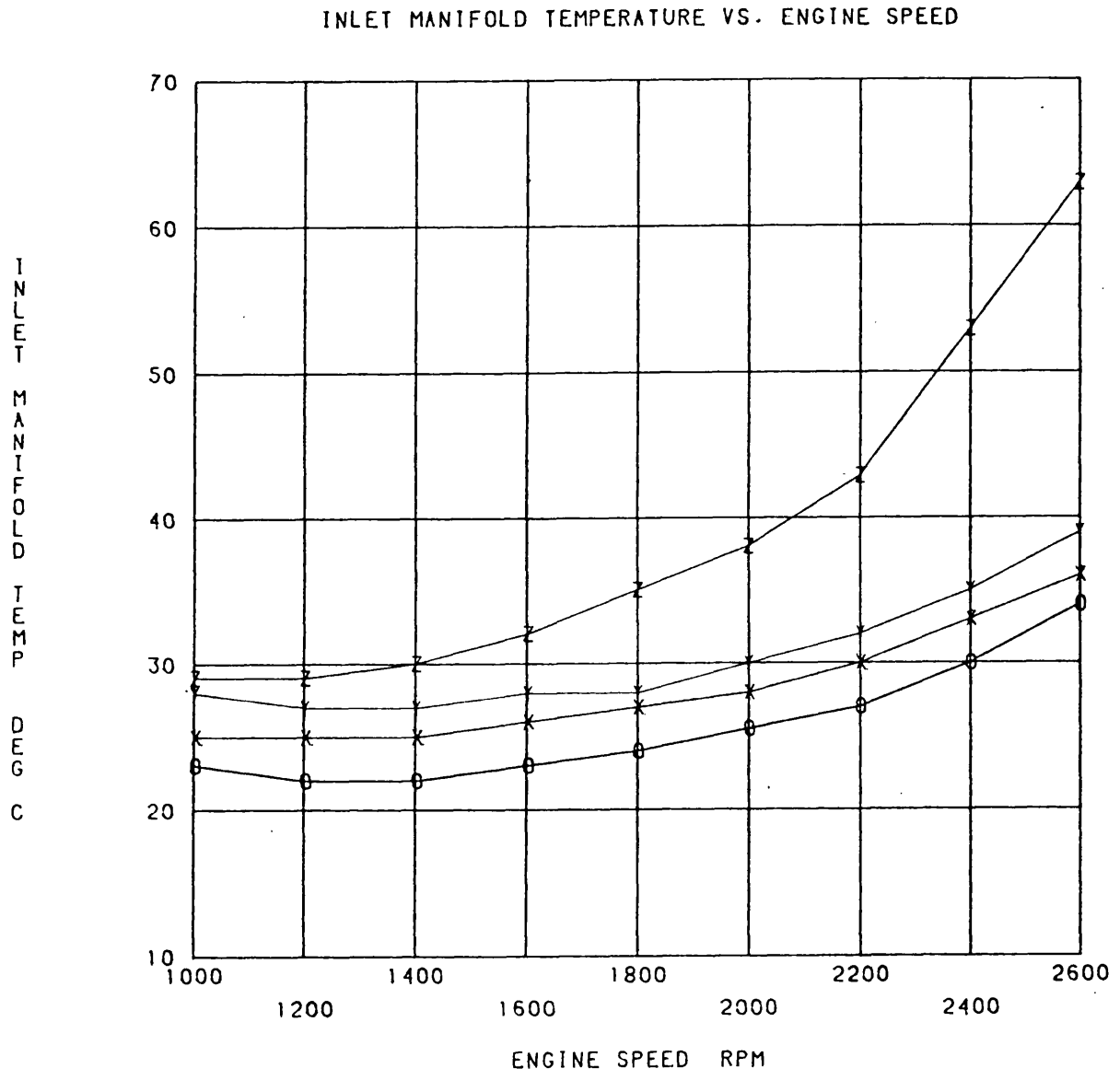

Fig. 3.13k 2 Bar BMEP Variable Geometry Engine Results,

O = 0%, X = 25%, Y = 40% and Z = 50% Restriction.

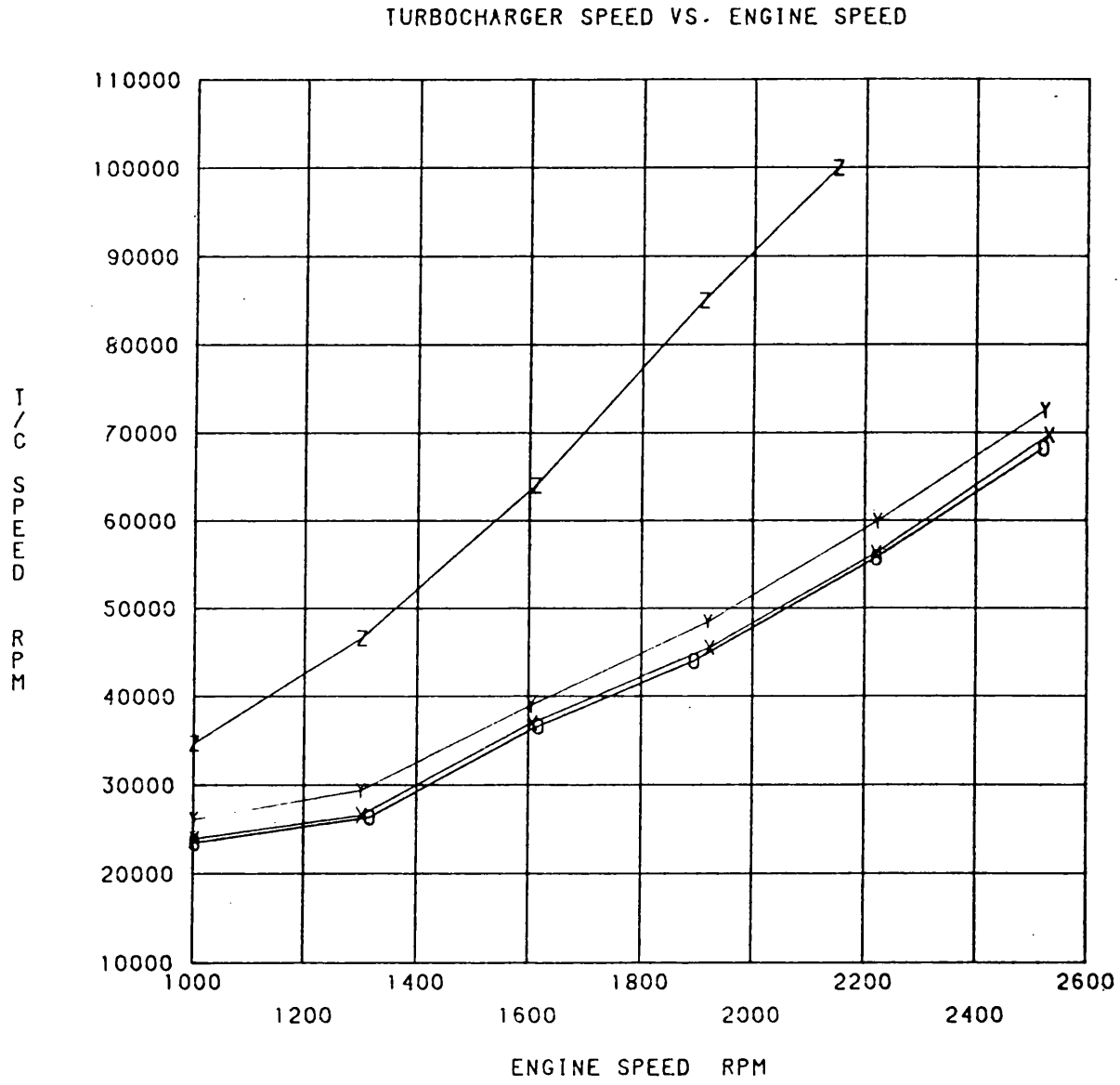

Fig. 3.14a 4 Bar BMEP Variable Geometry Engine Results,

O = 0%, X = 25%, Y = 40% and Z = 50% Restriction.

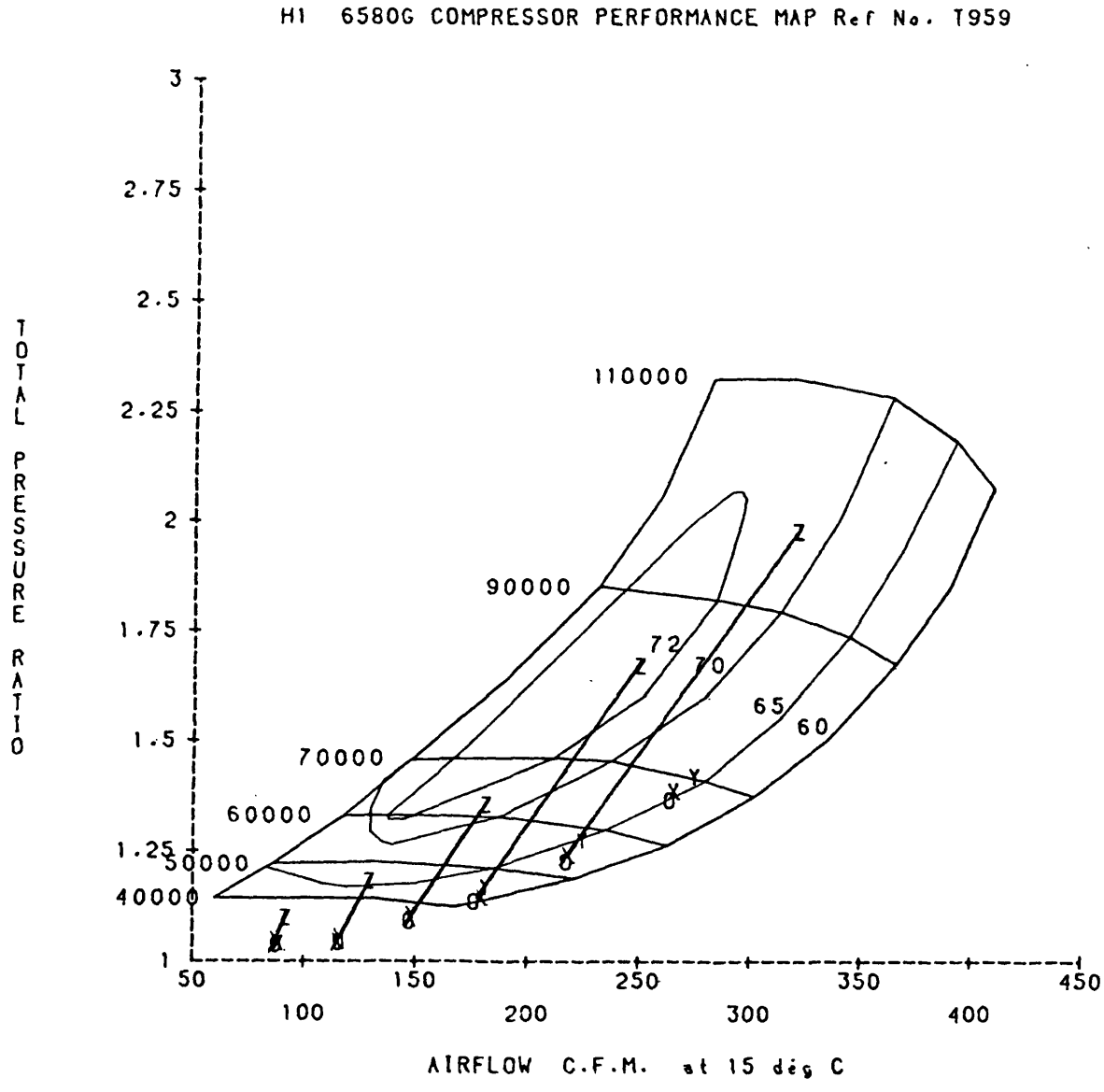

Fig. 3.14b 4 Bar BMEP Variable Geometry Engine Results,

O = 0%, X = 25%, Y = 40% and Z = 50% Restriction.

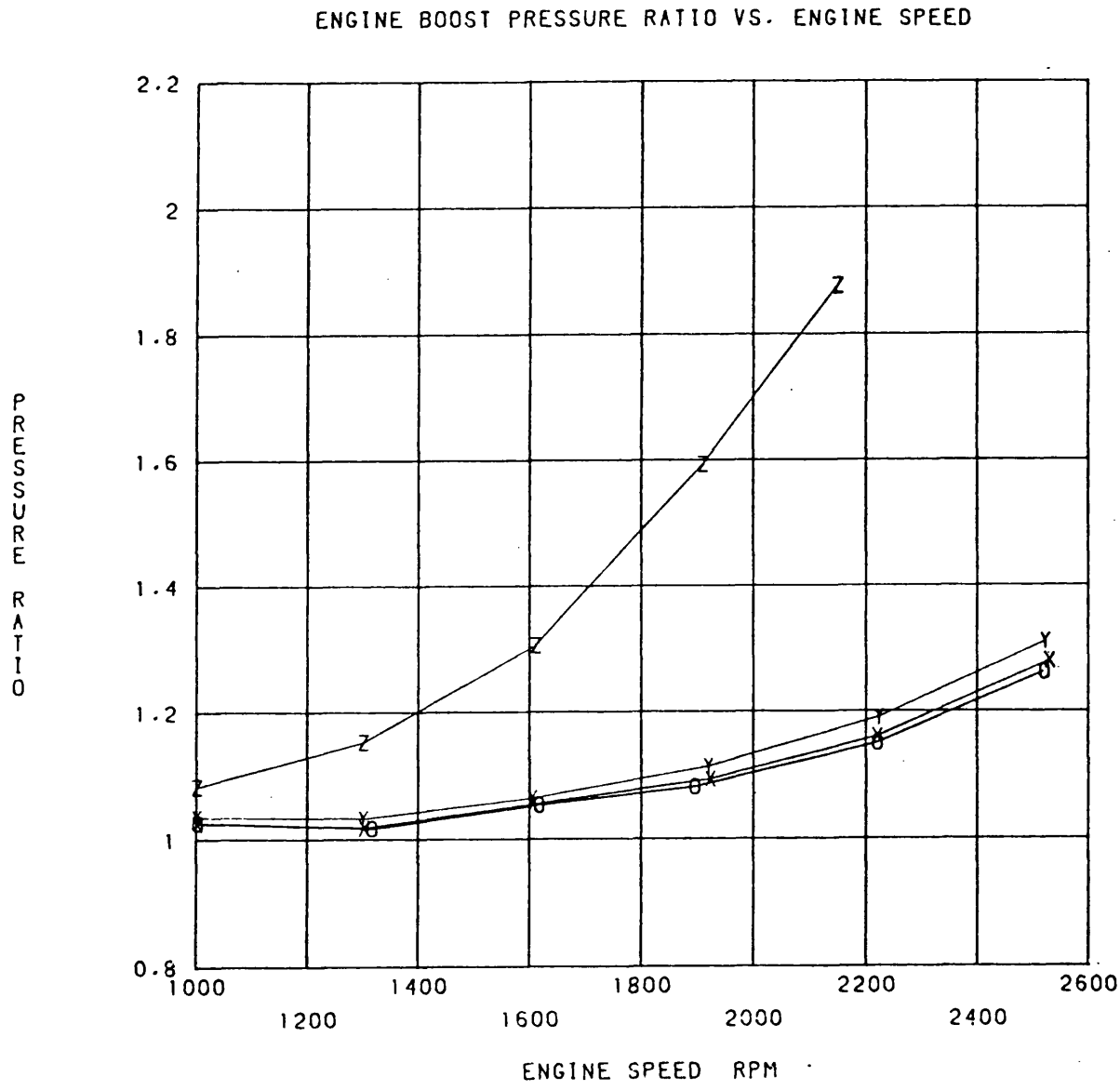

Fig. 3.14c 4 Bar BMEP Variable Geometry Engine Results,

O = 0%, X = 25%, Y = 40% and Z = 50% Restriction.

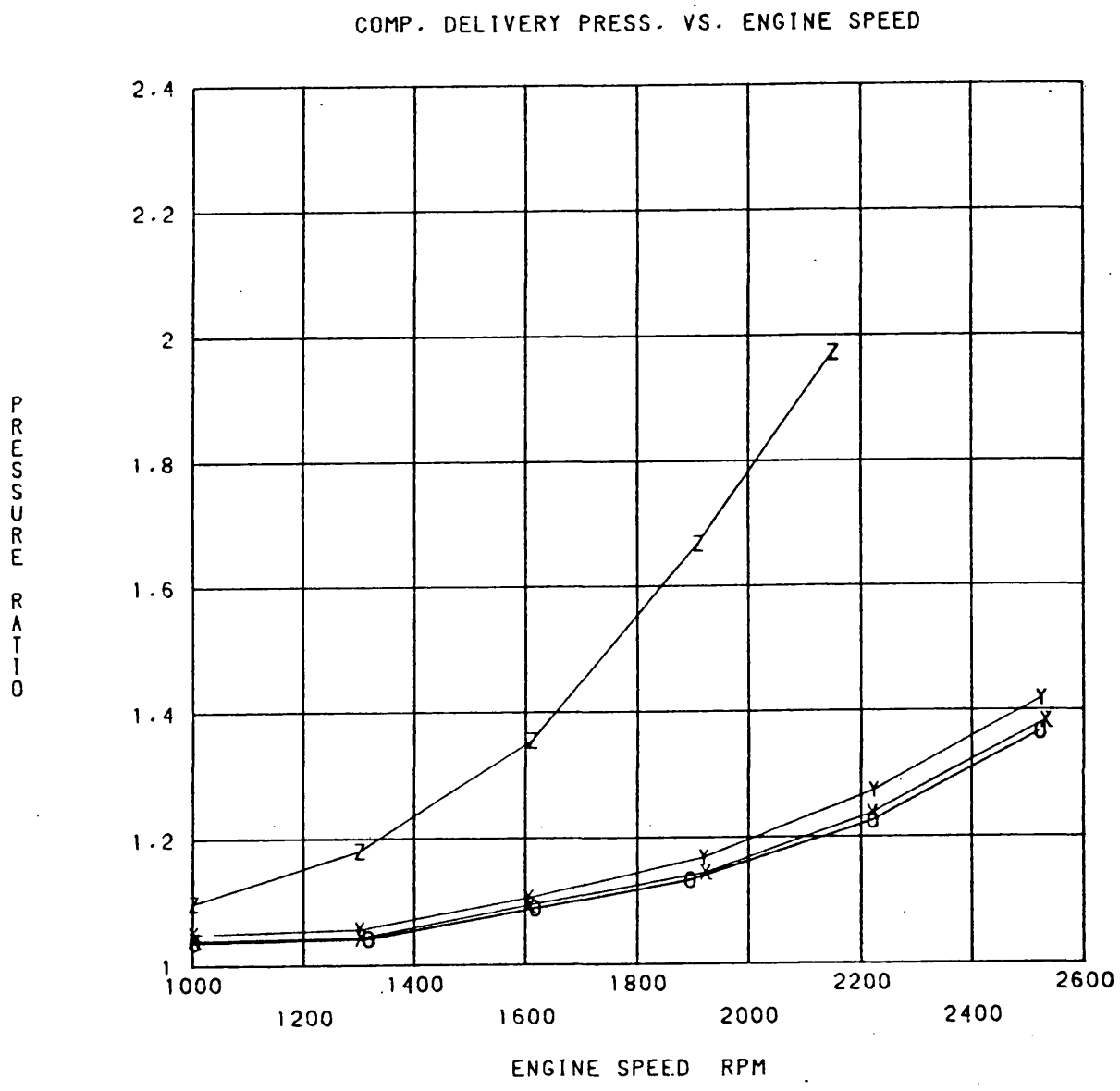

Fig. 3.14d 4 Bar BMEP Variable Geometry Engine Results,

O = 0%, X = 25%, Y = 40% and Z = 50% Restriction.

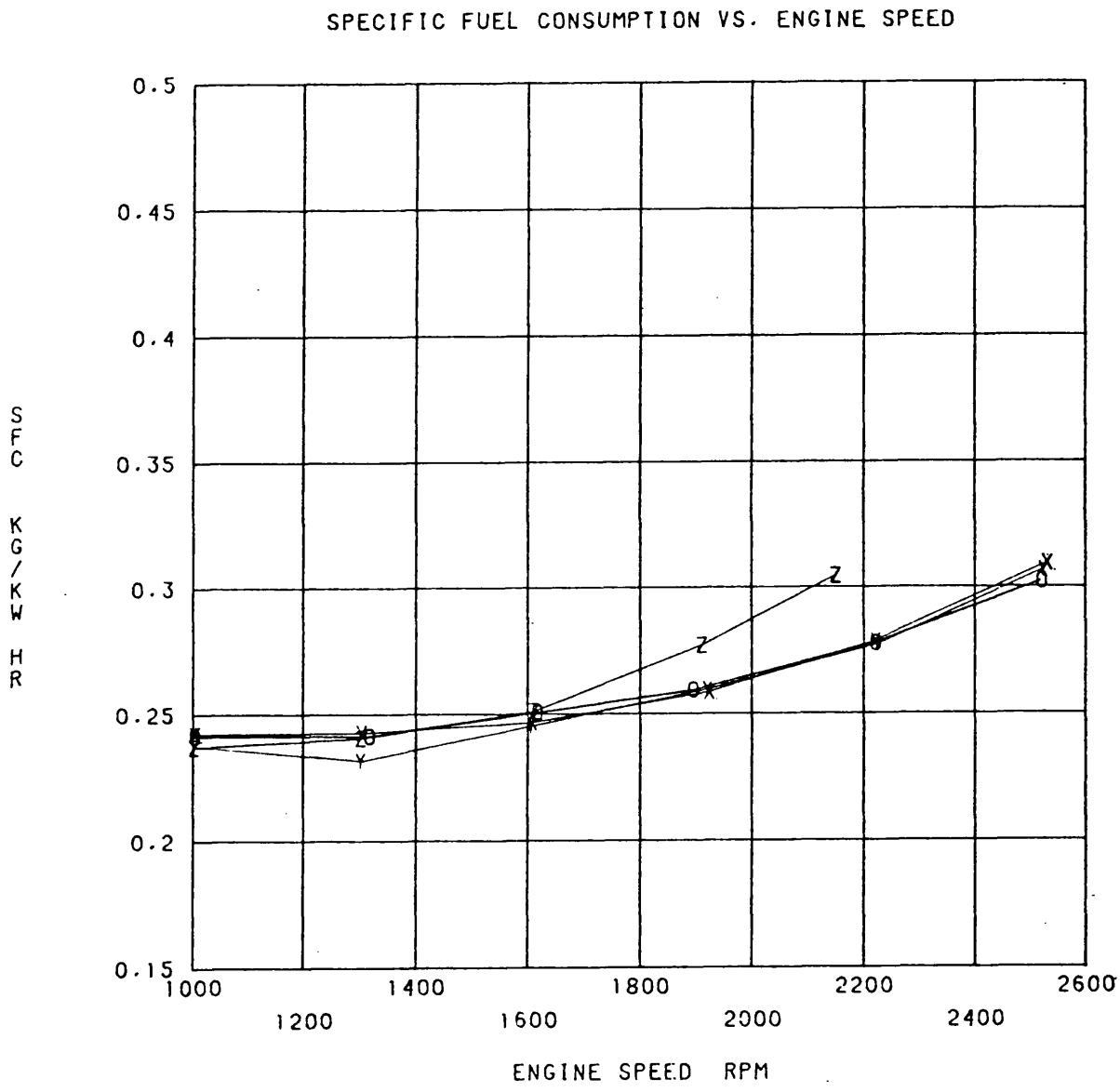

Fig. 3.14e 4 Bar BMEP Variable Geometry Engine Results,

O = 0%, X = 25%, Y = 40% and Z = 50% Restriction.

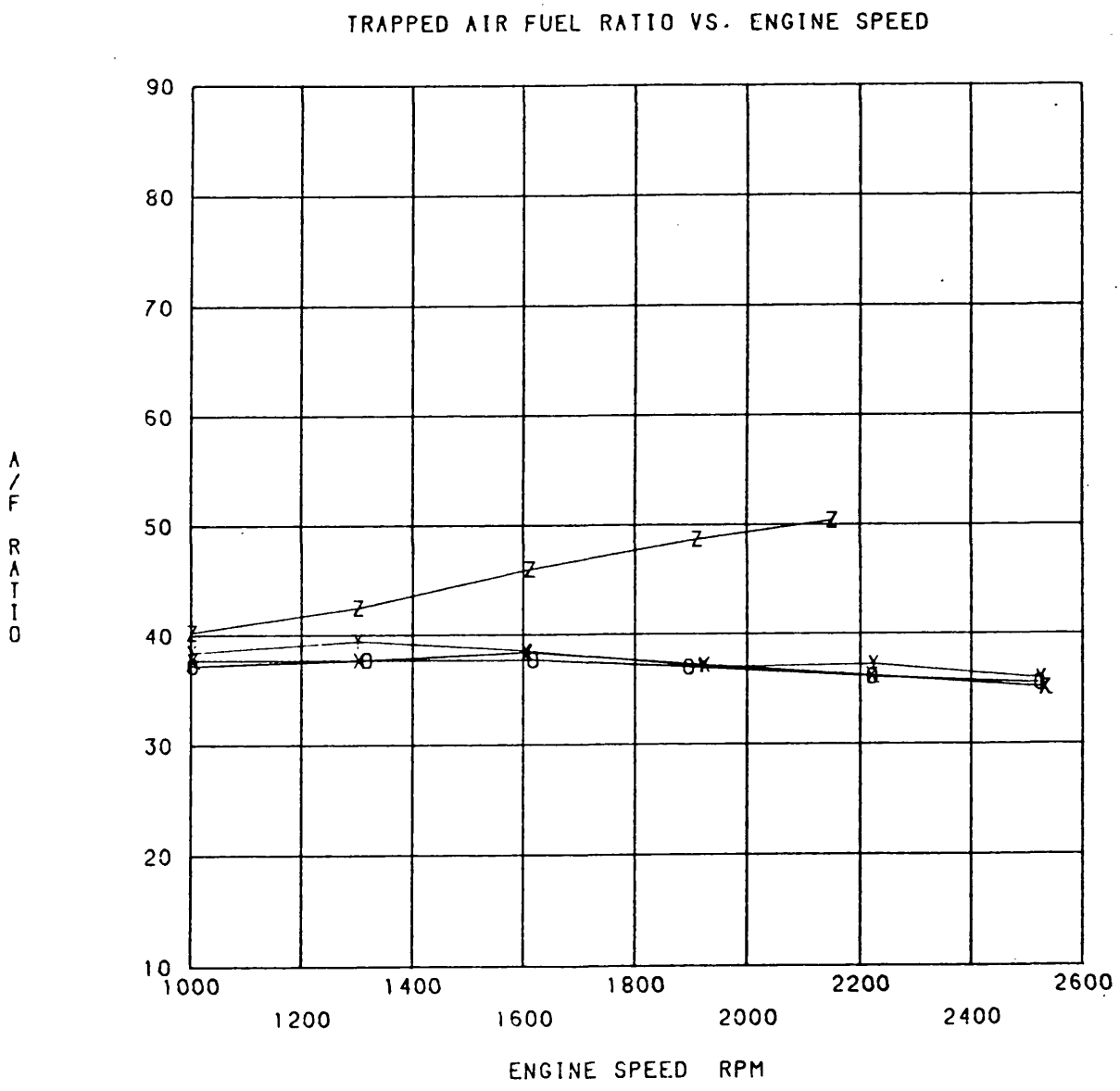

Fig. 3.14f 4 Bar BMEP Variable Geometry Engine Results,

O = 0%, X = 25%, Y = 40% and Z = 50% Restriction.

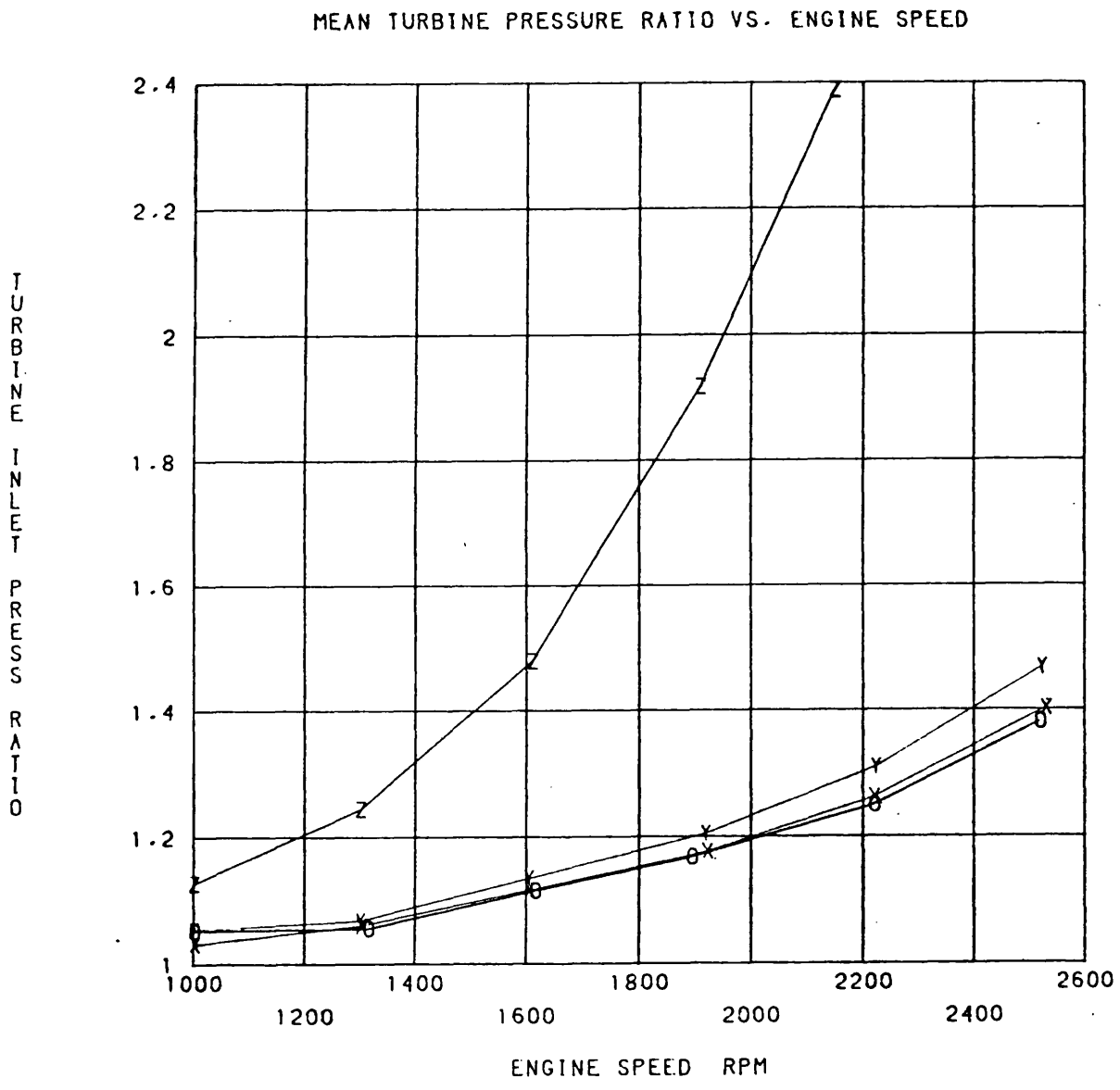

Fig. 3.14g 4 Bar BMEP Variable Geometry Engine Results,

O = 0%, X = 25%, Y = 40% and Z = 50% Restriction.

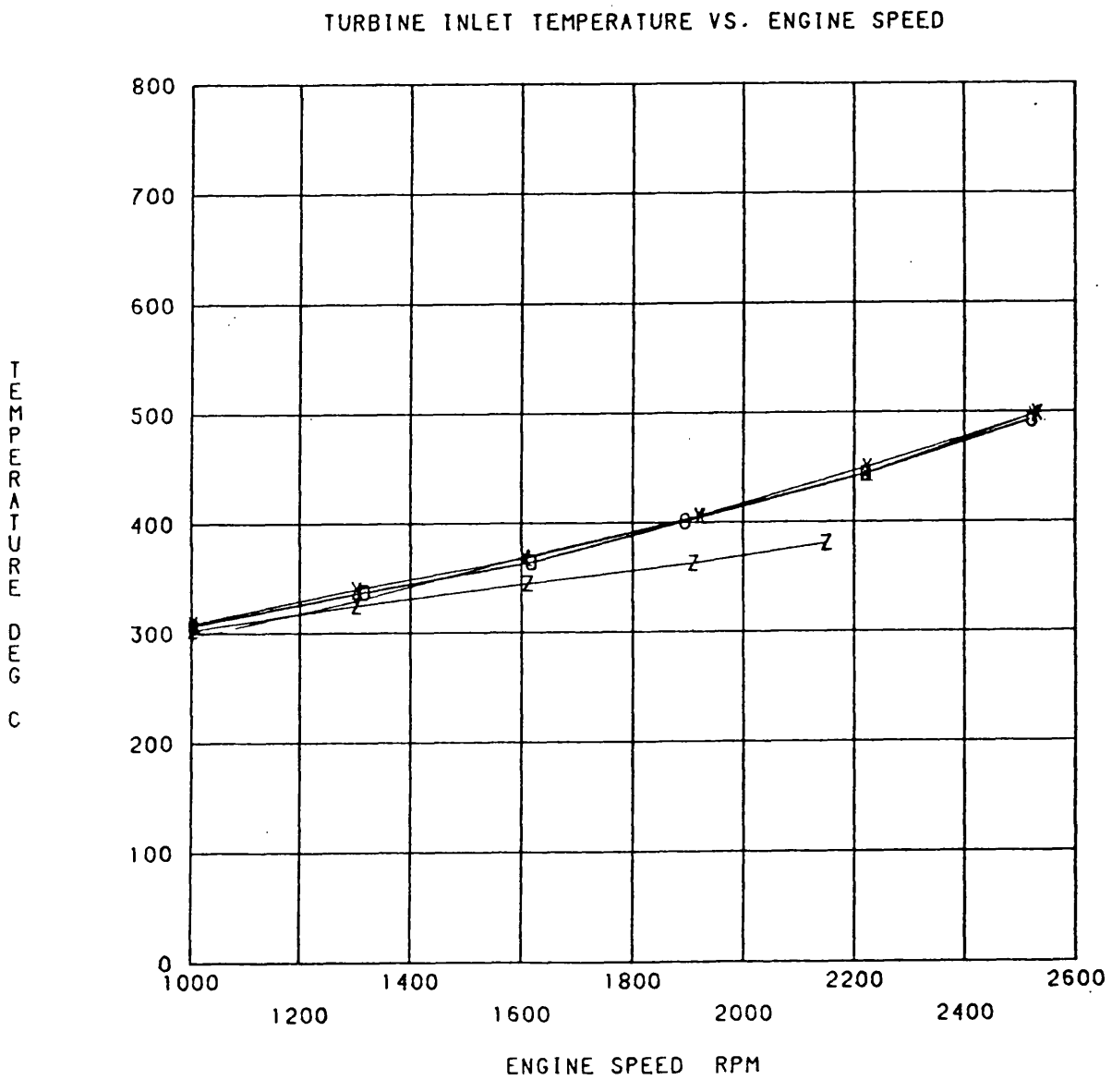

Fig. 3.14h 4 Bar BMEP Variable Geometry Engine Results,

O = 0%, X = 25%, Y = 40% and Z = 50% Restriction.

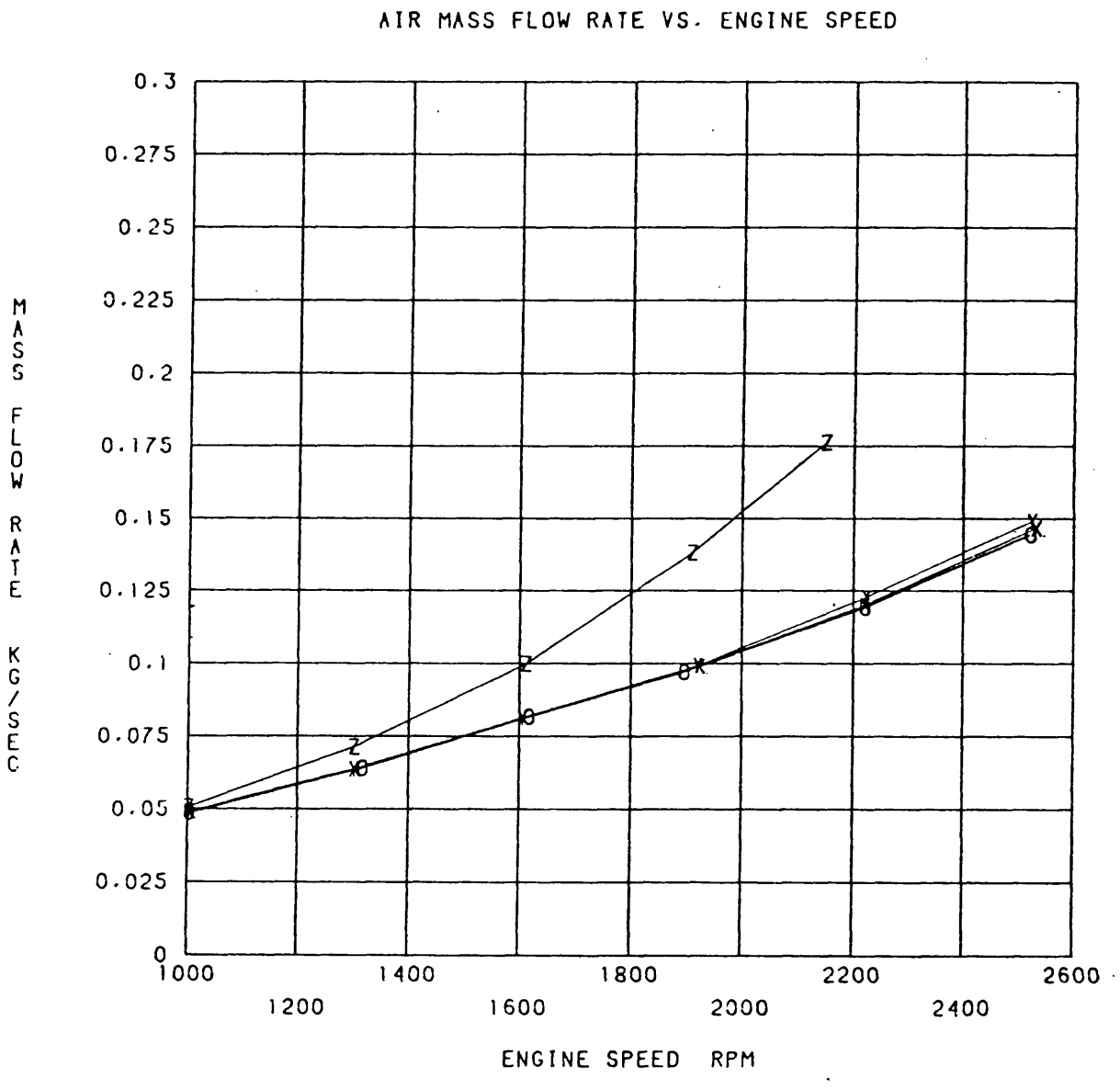

Fig. 3.14i 4 Bar BMEP Variable Geometry Engine Results,

O = 0%, X = 25%, Y = 40% and Z = 50% Restriction.

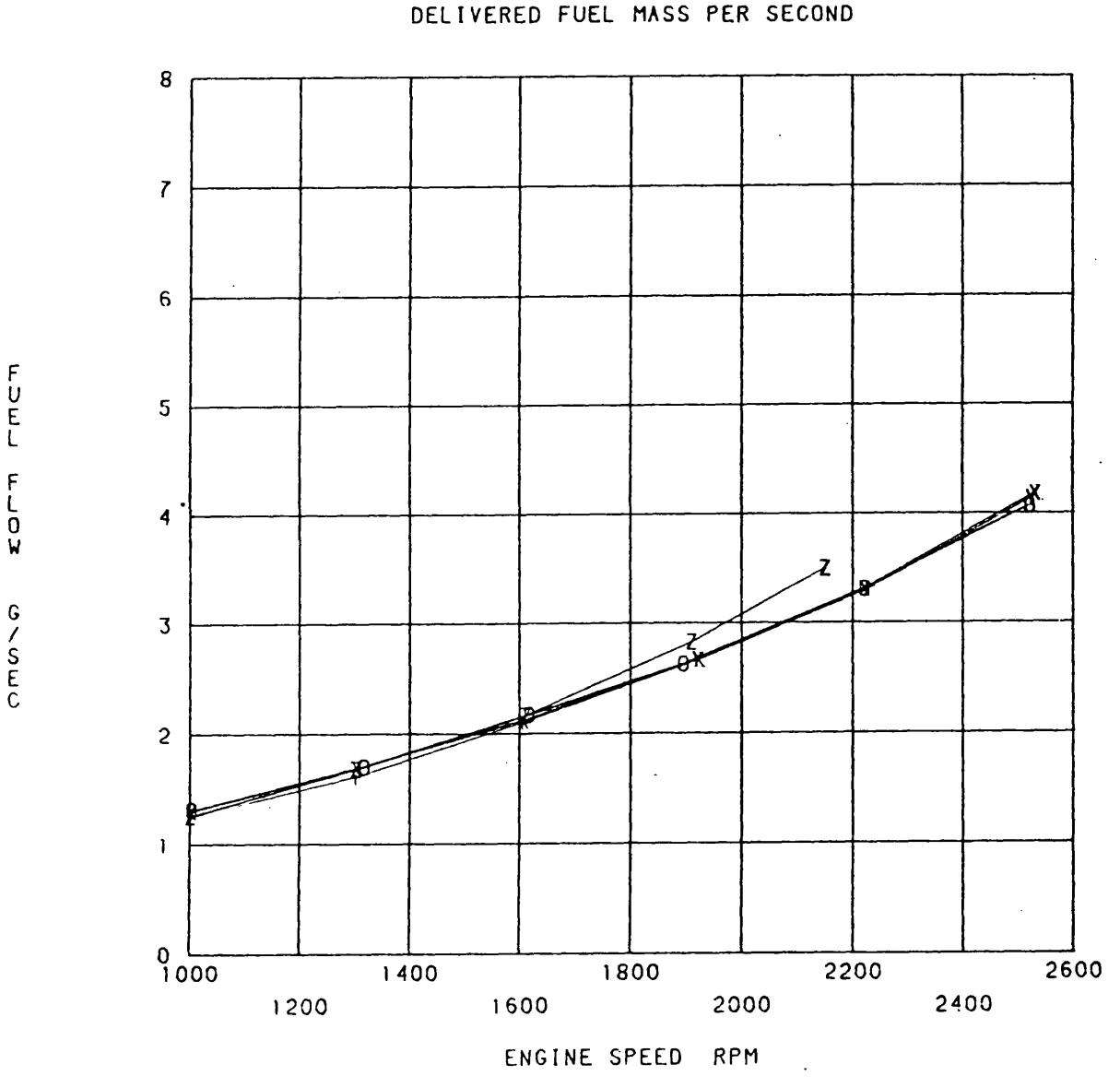

Fig. 3.14j 4 Bar BMEP Variable Geometry Engine Results,

O = 0%, X = 25%, Y = 40% and Z = 50% Restriction.

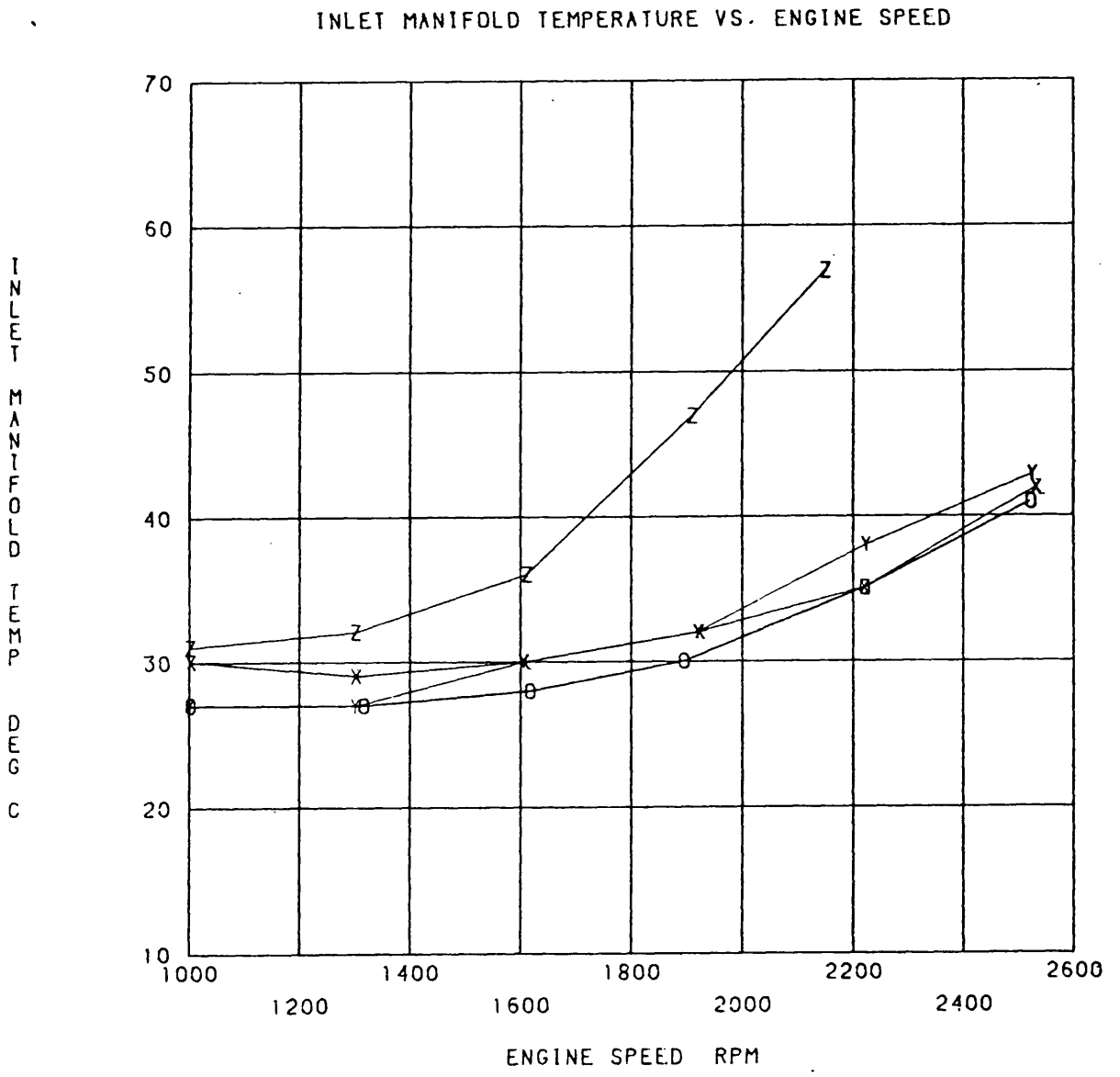

Fig. 3.14k 4 Bar BMEP Variable Geometry Engine Results,

O = 0%, X = 25%, Y = 40% and Z = 50% Restriction.

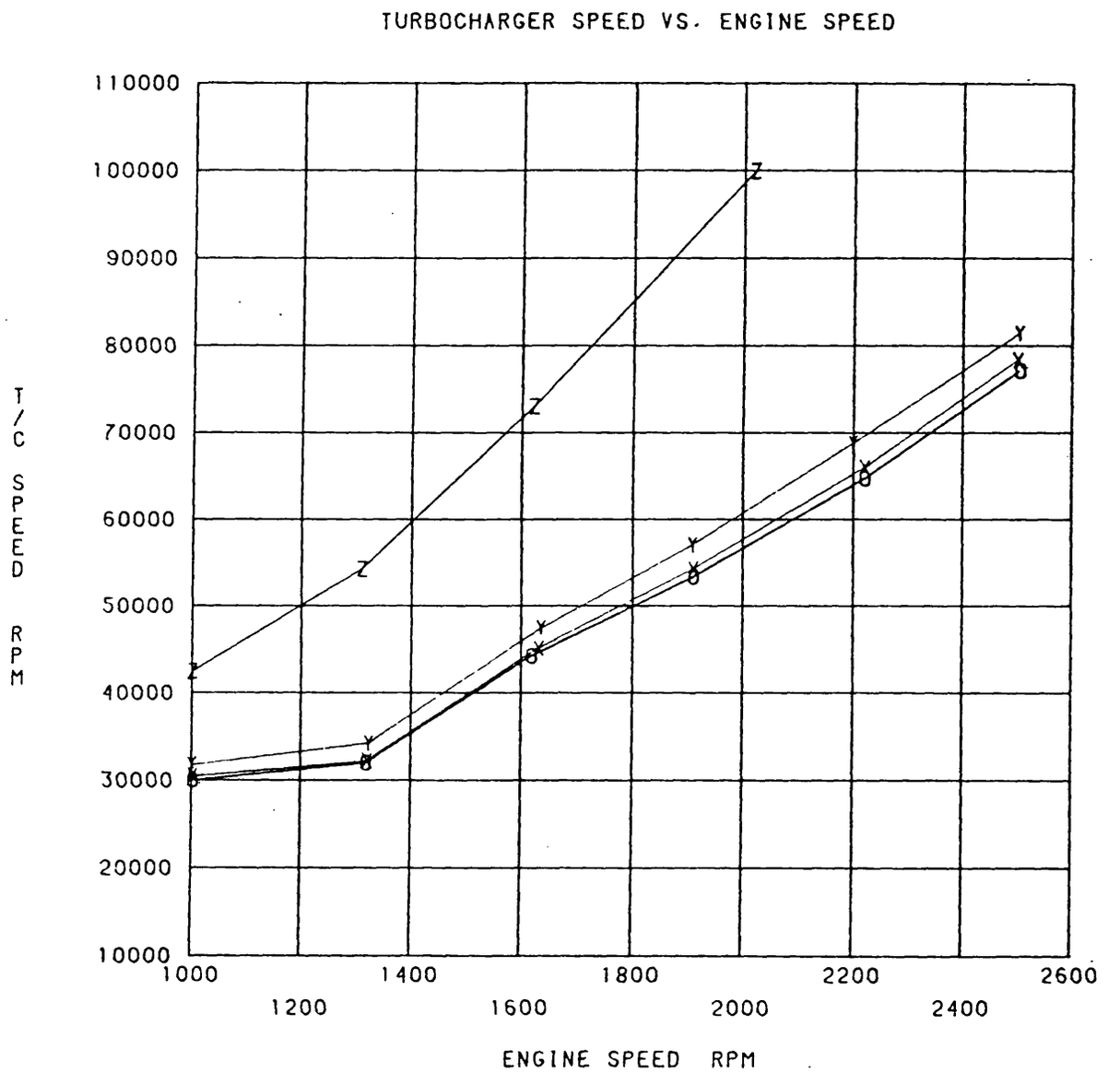

Fig. 3.15a 6 Bar BMEP Variable Geometry Engine Results,

O = 0%, X = 25%, Y = 40% and Z = 50% Restriction.

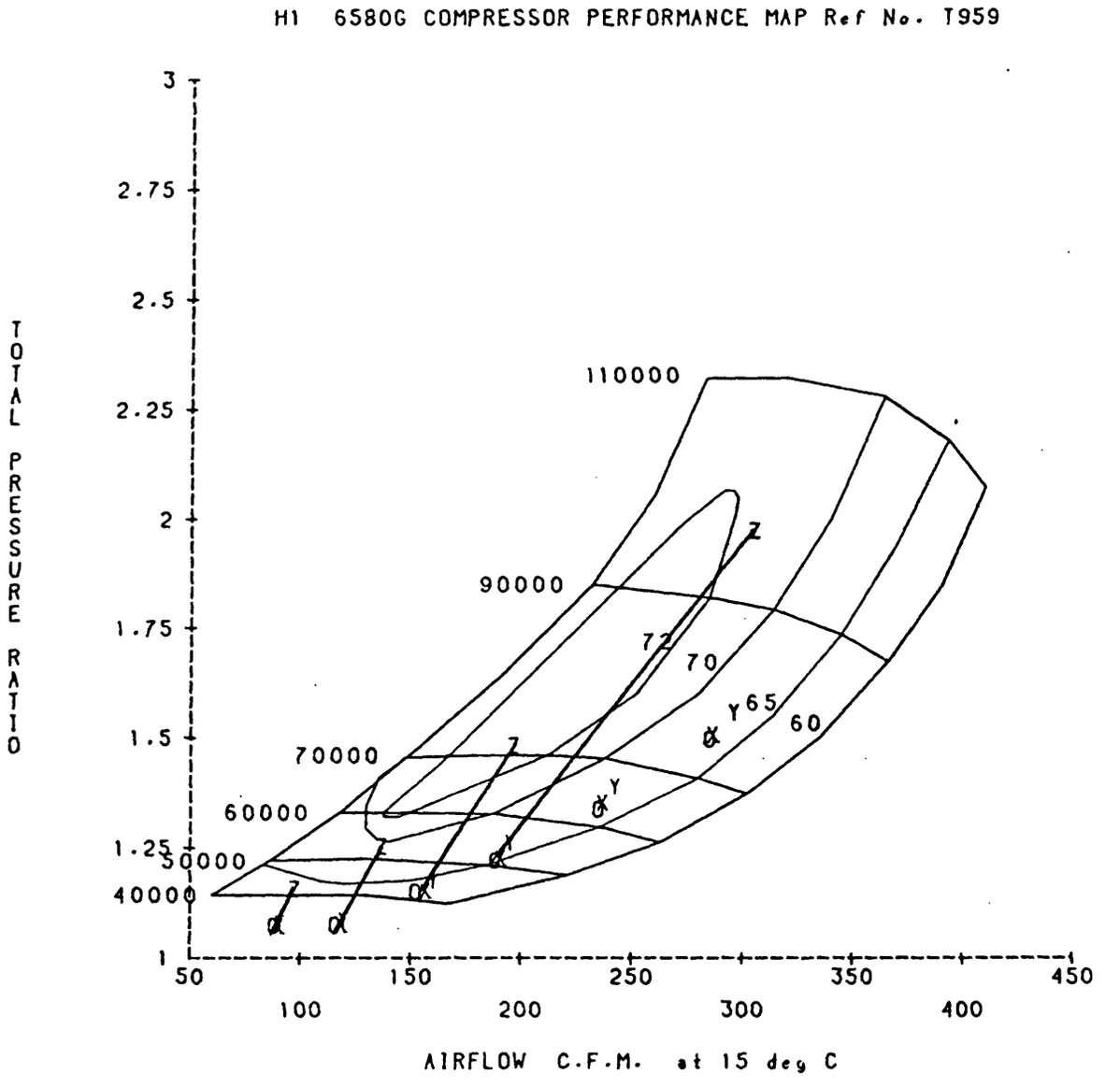

Fig. 3.15b 6 Bar BMEP Variable Geometry Engine Results,

O = 0%, X = 25%, Y = 40% and Z = 50% Restriction.

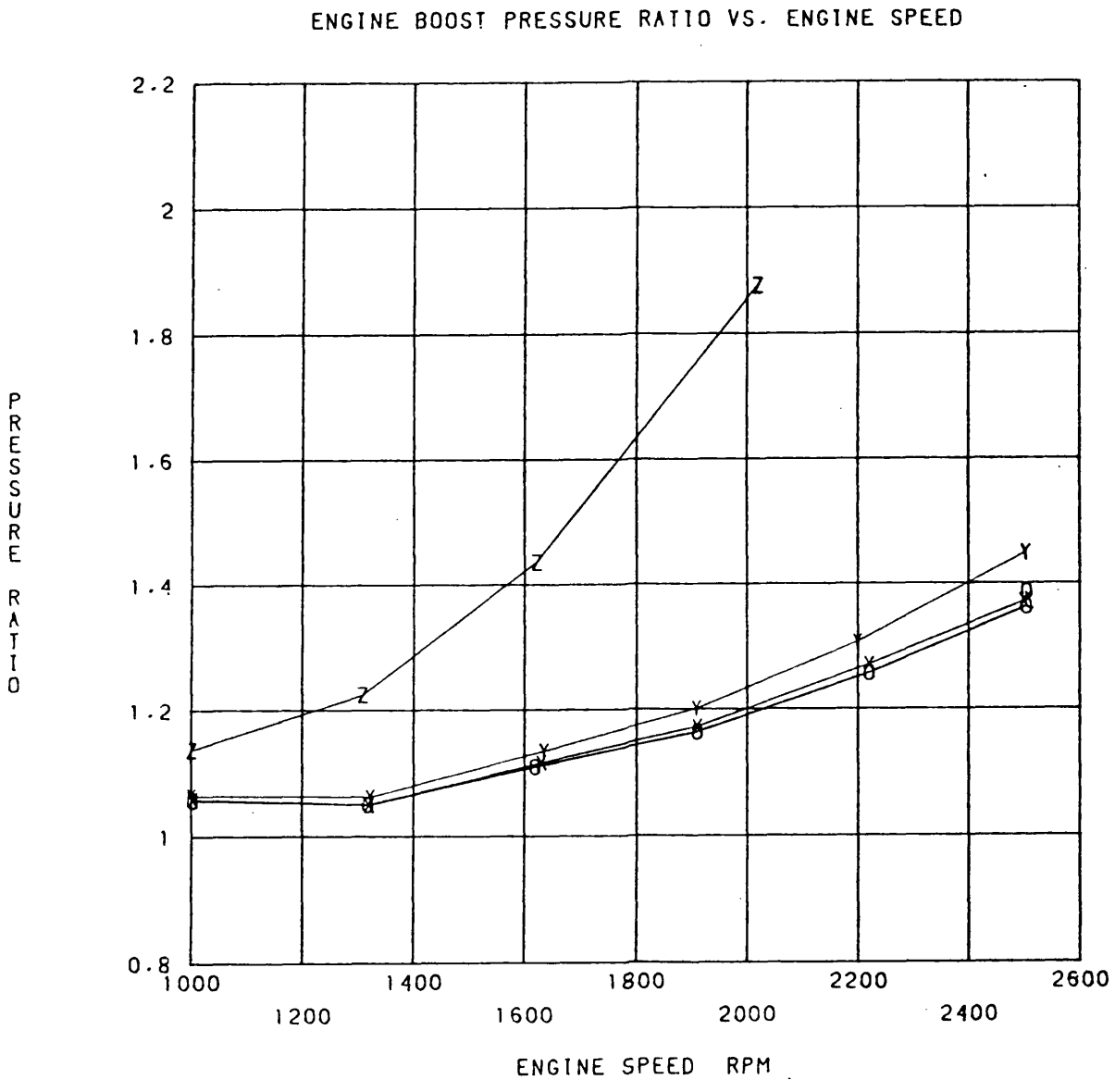

Fig. 3.15c 6 Bar BMEP Variable Geometry Engine Results,

O = 0%, X = 25%, Y = 40% and Z = 50% Restriction.

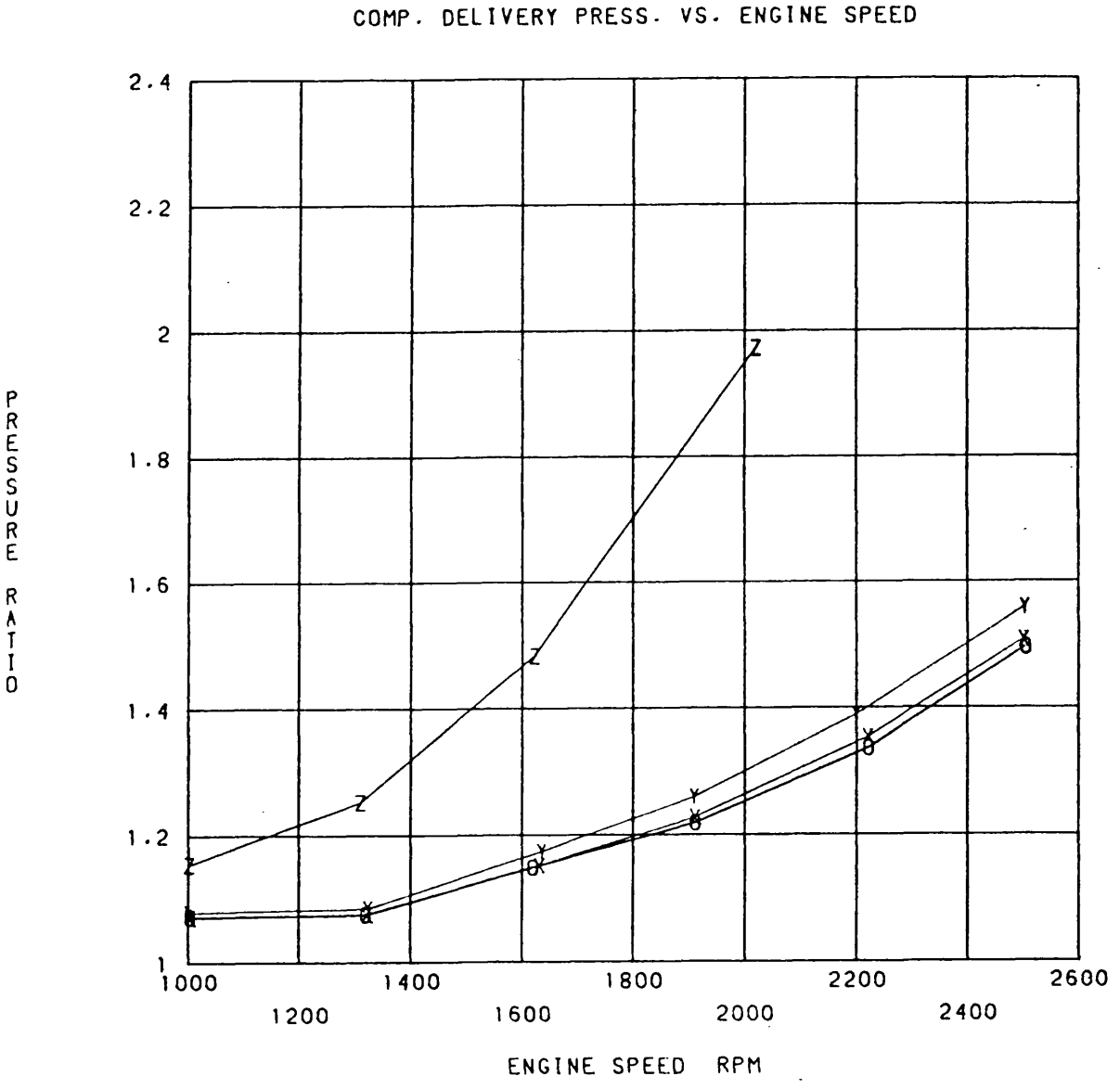

Fig. 3.15d 6 Bar BMEP Variable Geometry Engine Results,

O = 0%, X = 25%, Y = 40% and Z = 50% Restriction.

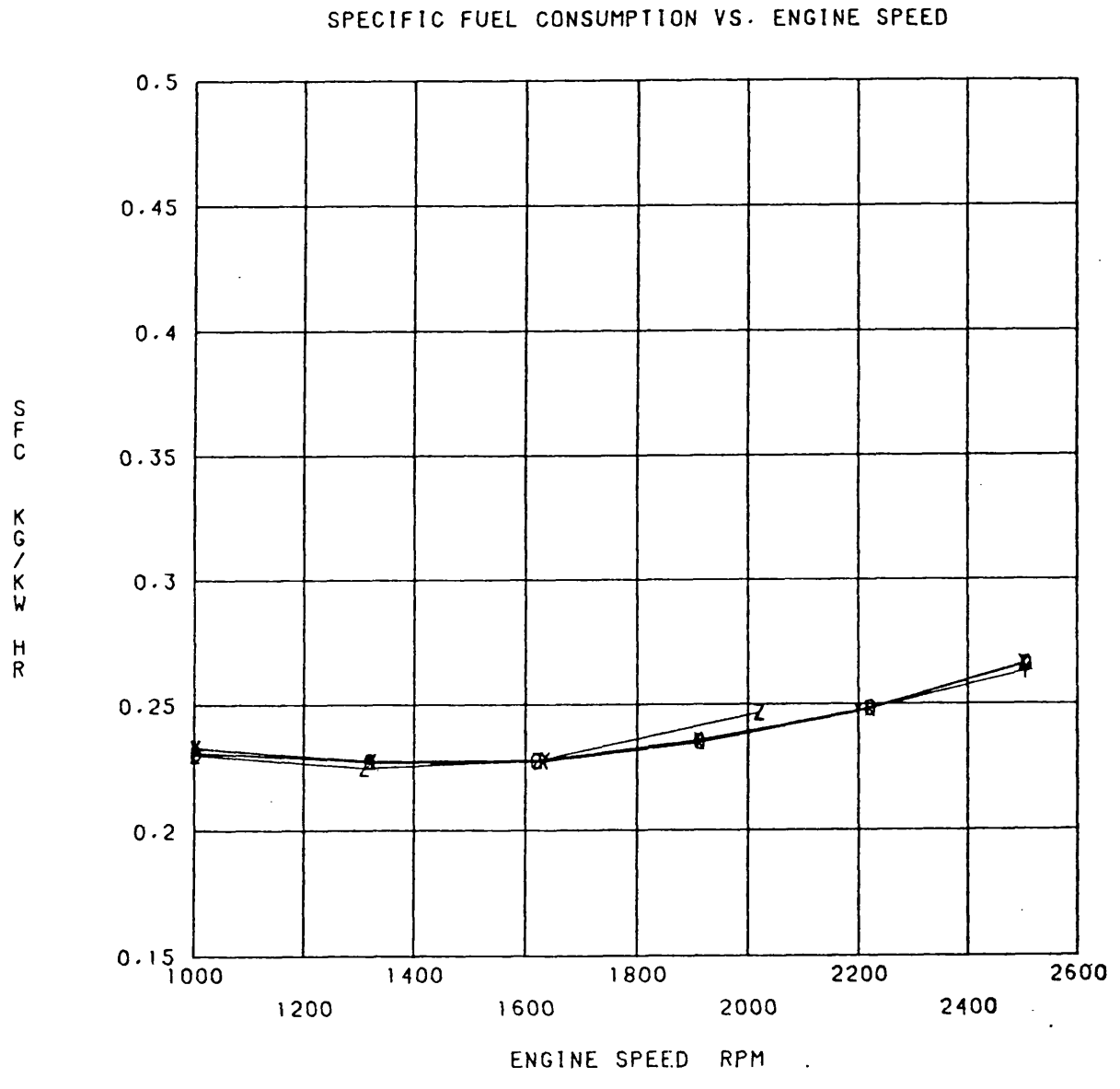

Fig. 3.15e 6 Bar BMEP Variable Geometry Engine Results,

O = 0%, X = 25%, Y = 40% and Z = 50% Restriction.

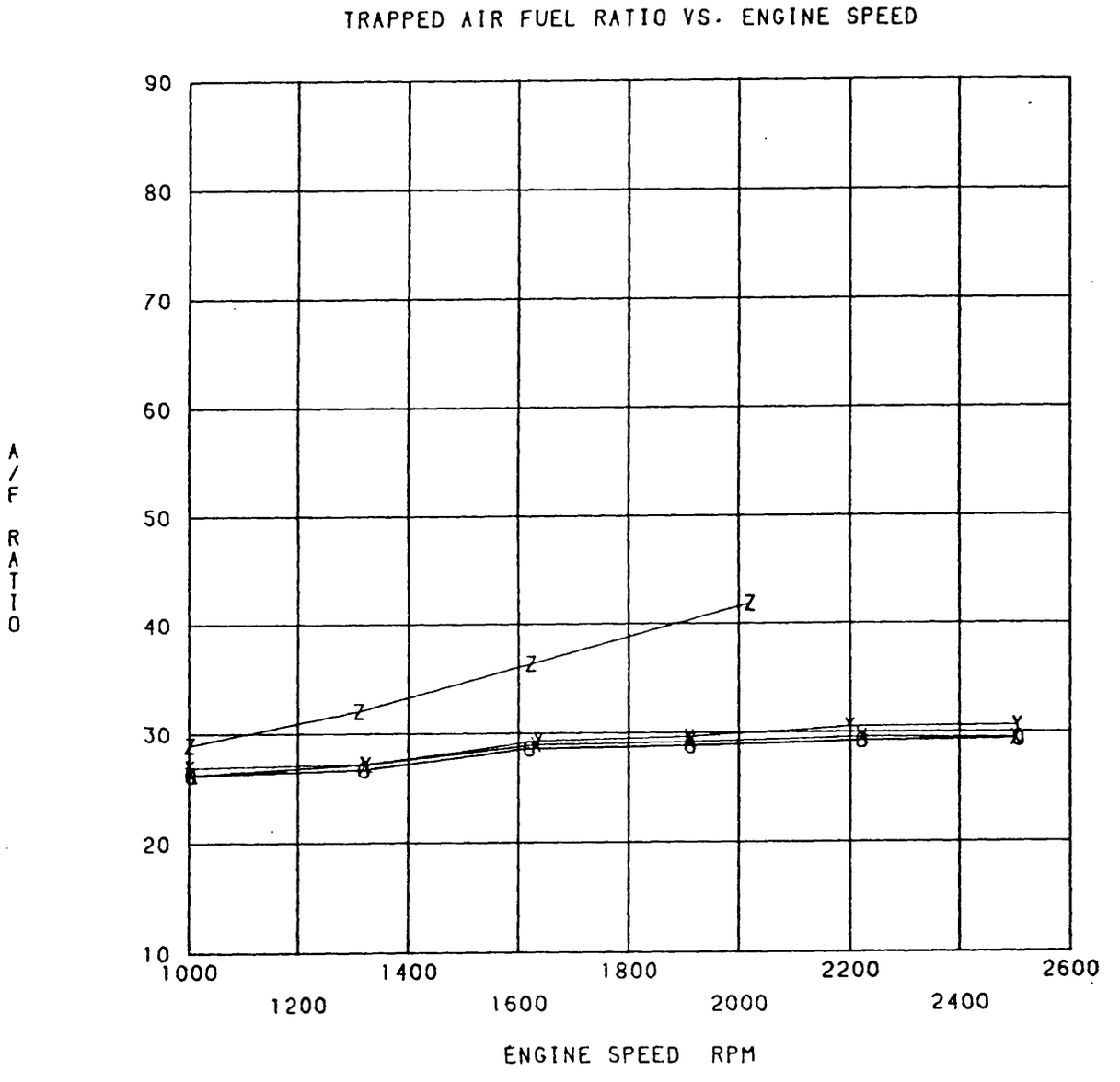

Fig. 3.15f 6 Bar BMEP Variable Geometry Engine Results,

O = 0%, X = 25%, Y = 40% and Z = 50% Restriction.

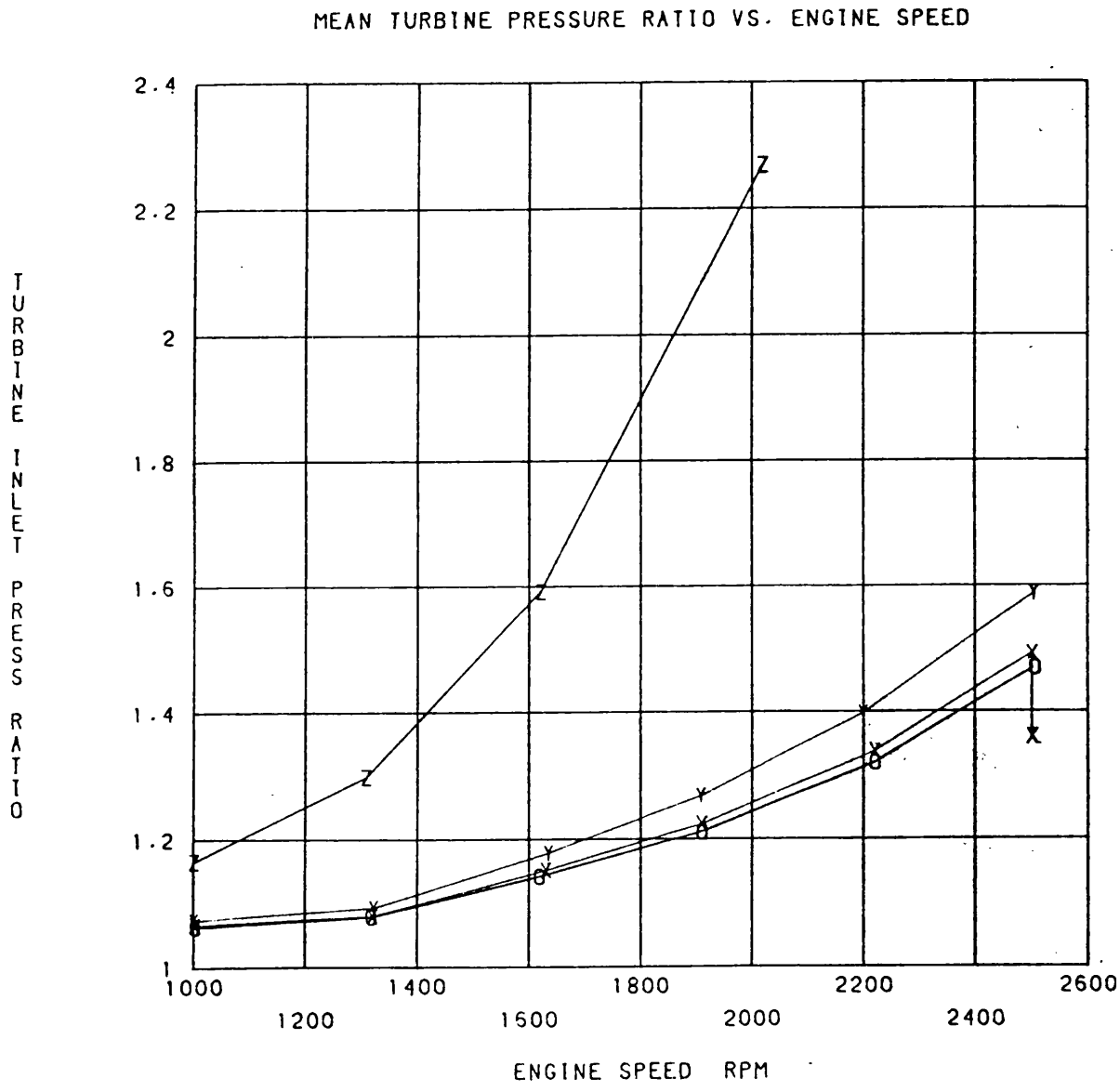

Fig. 3.15g 6 Bar BMEP Variable Geometry Engine Results,

O = 0%, X = 25%, Y = 40% and Z = 50% Restriction.

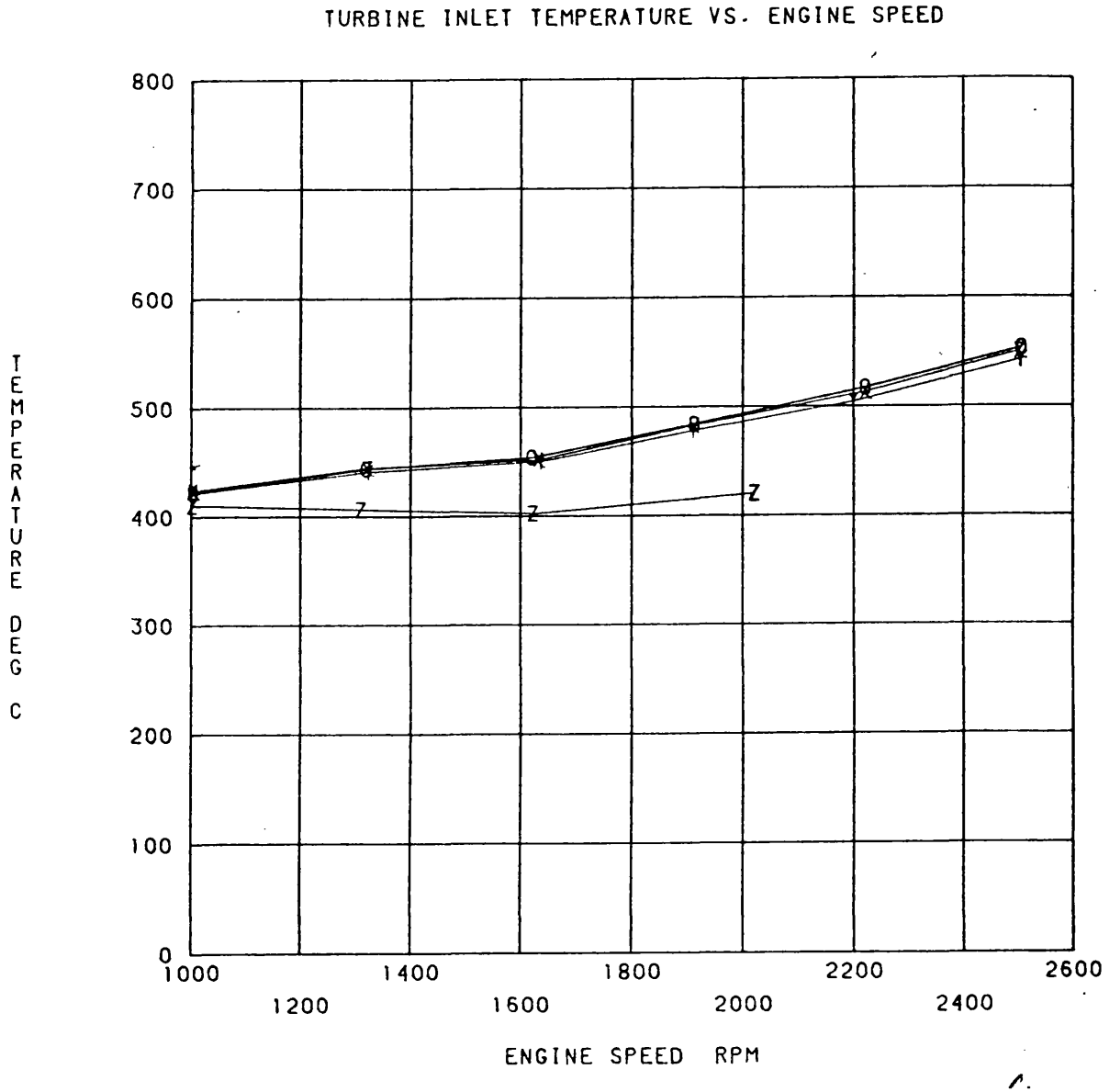

Fig. 3.15h 6 Bar BMEP Variable Geometry Engine Results,

O = 0%, X = 25%, Y = 40% and Z = 50% Restriction.

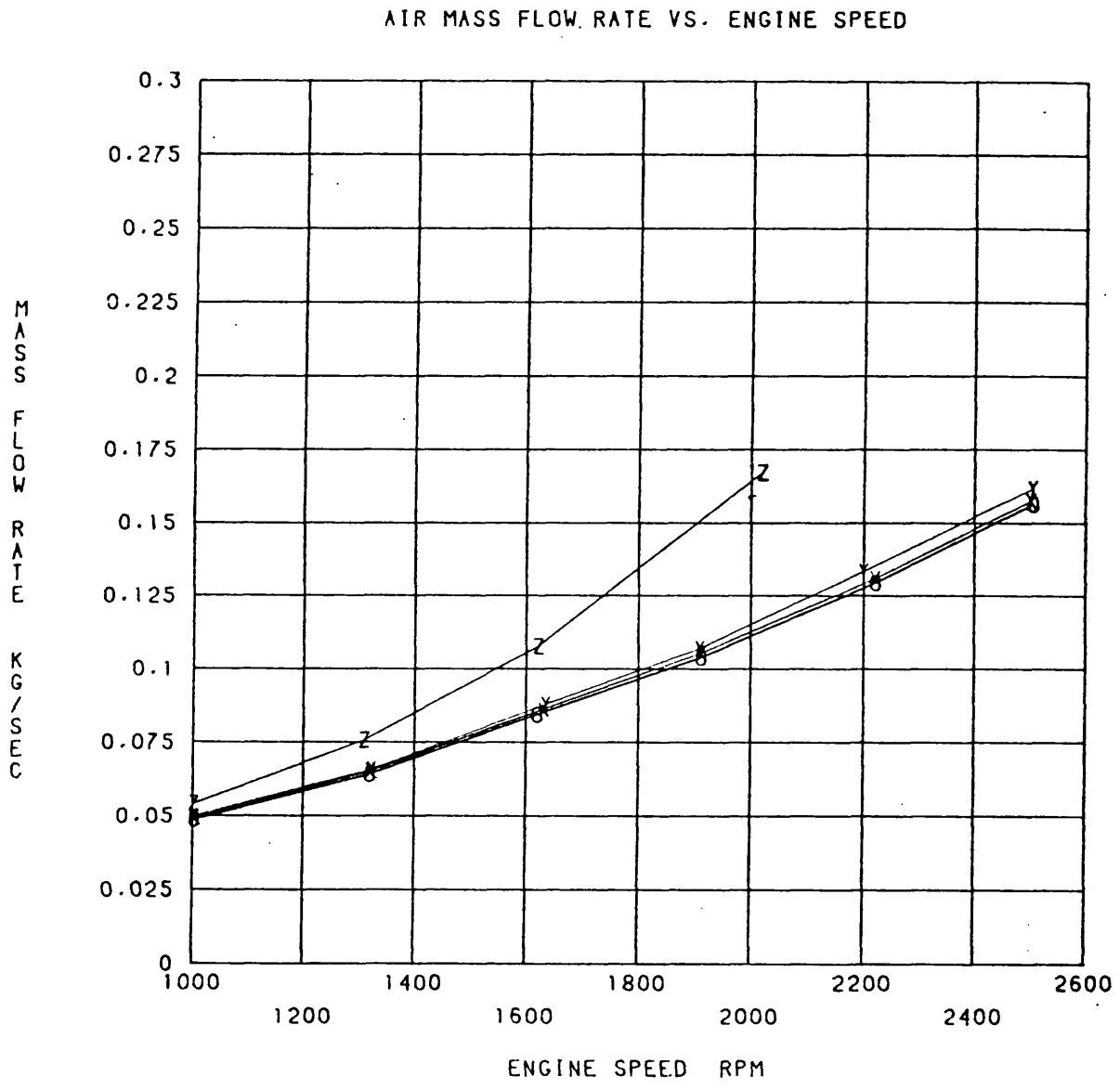

Fig. 3.15i 6 Bar BMEP Variable Geometry Engine Results,

O = 0%, X = 25%, Y = 40% and Z = 50% Restriction.

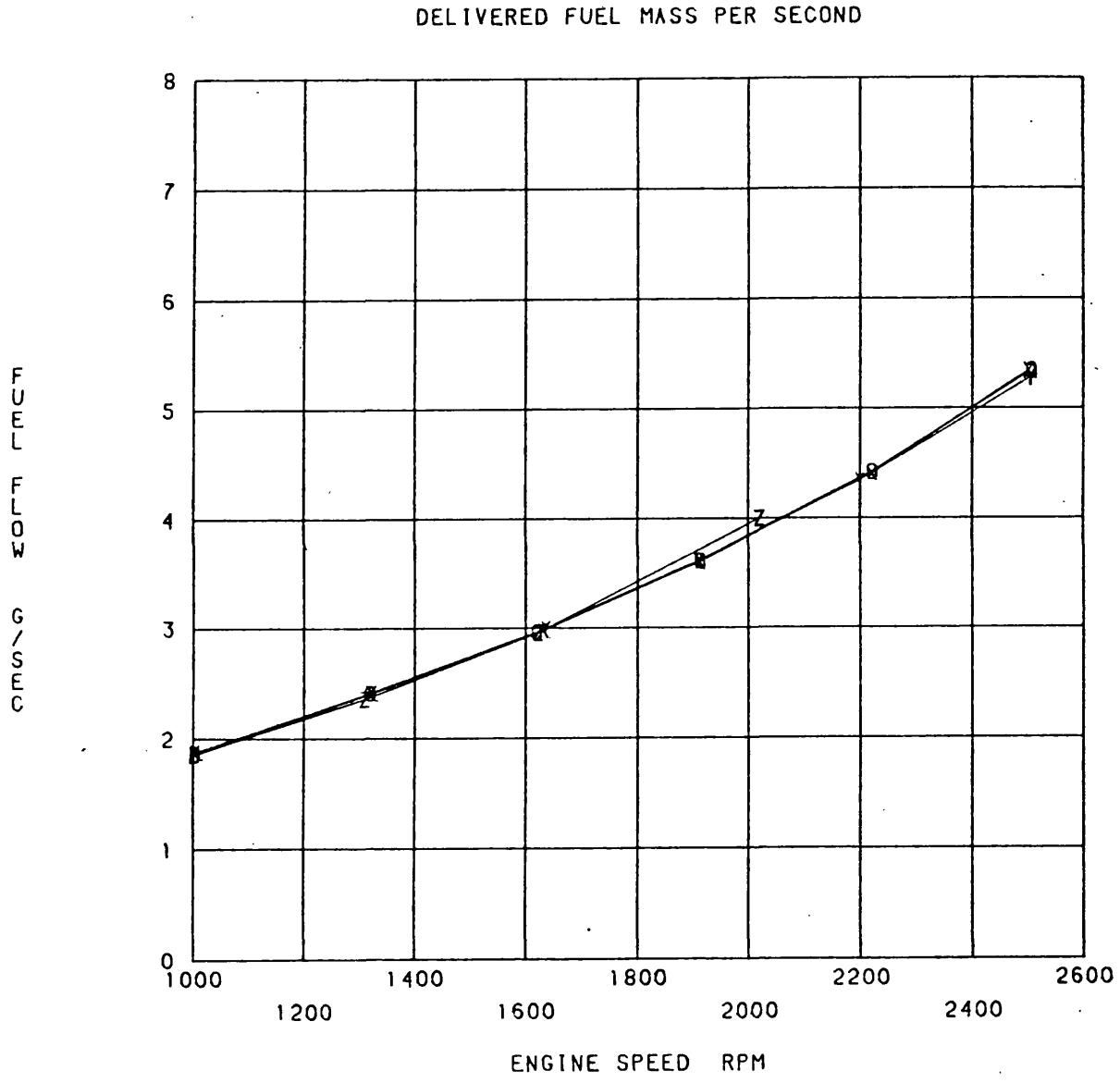

Fig. 3.15j 6 Bar BMEP Variable Geometry Engine Results,

O = 0%, X = 25%, Y = 40% and Z = 50% Restriction.

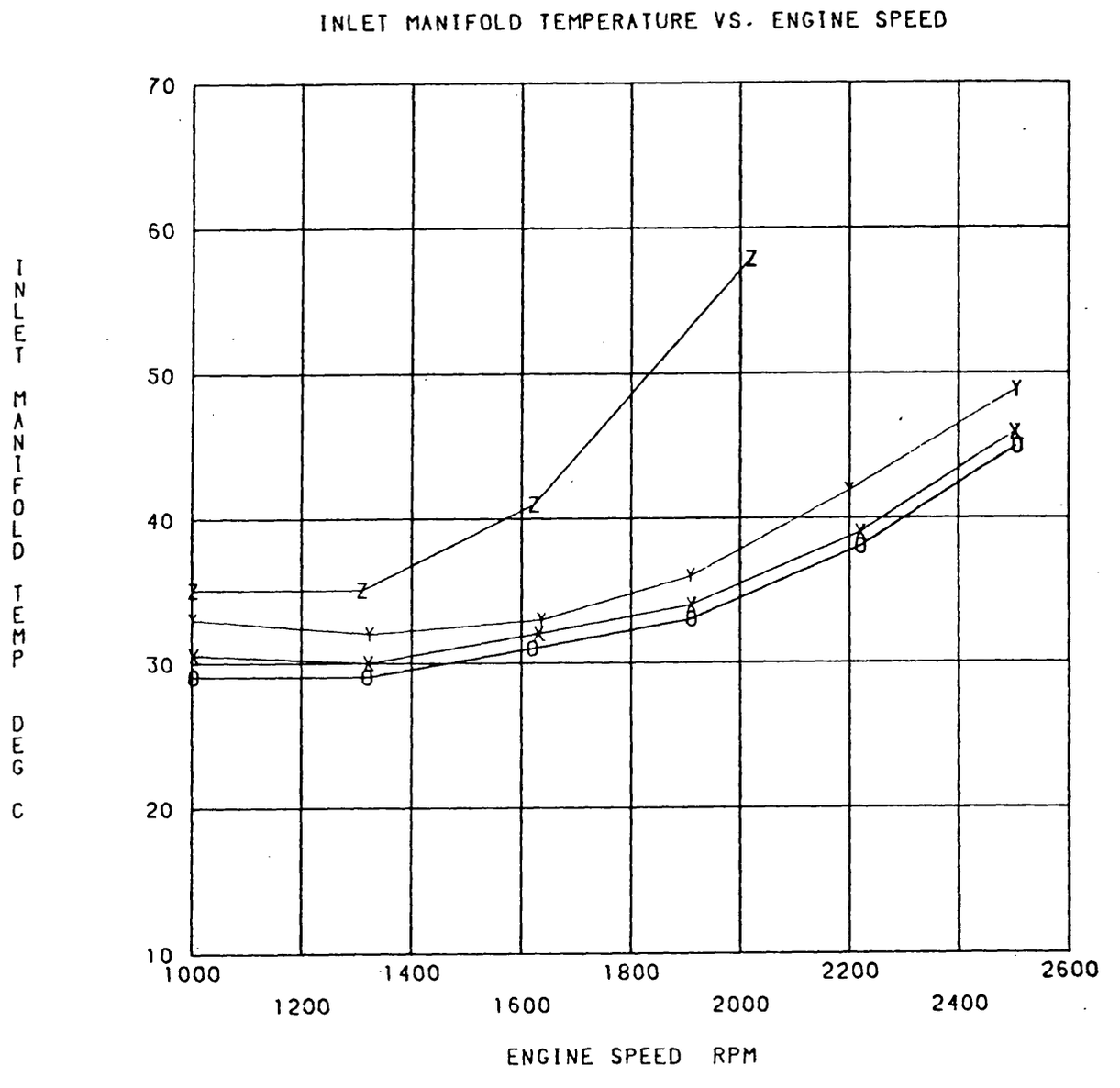

Fig. 3.15k 6 Bar BMEP Variable Geometry Engine Results,

O = 0%, X = 25%, Y = 40% and Z = 50% Restriction.

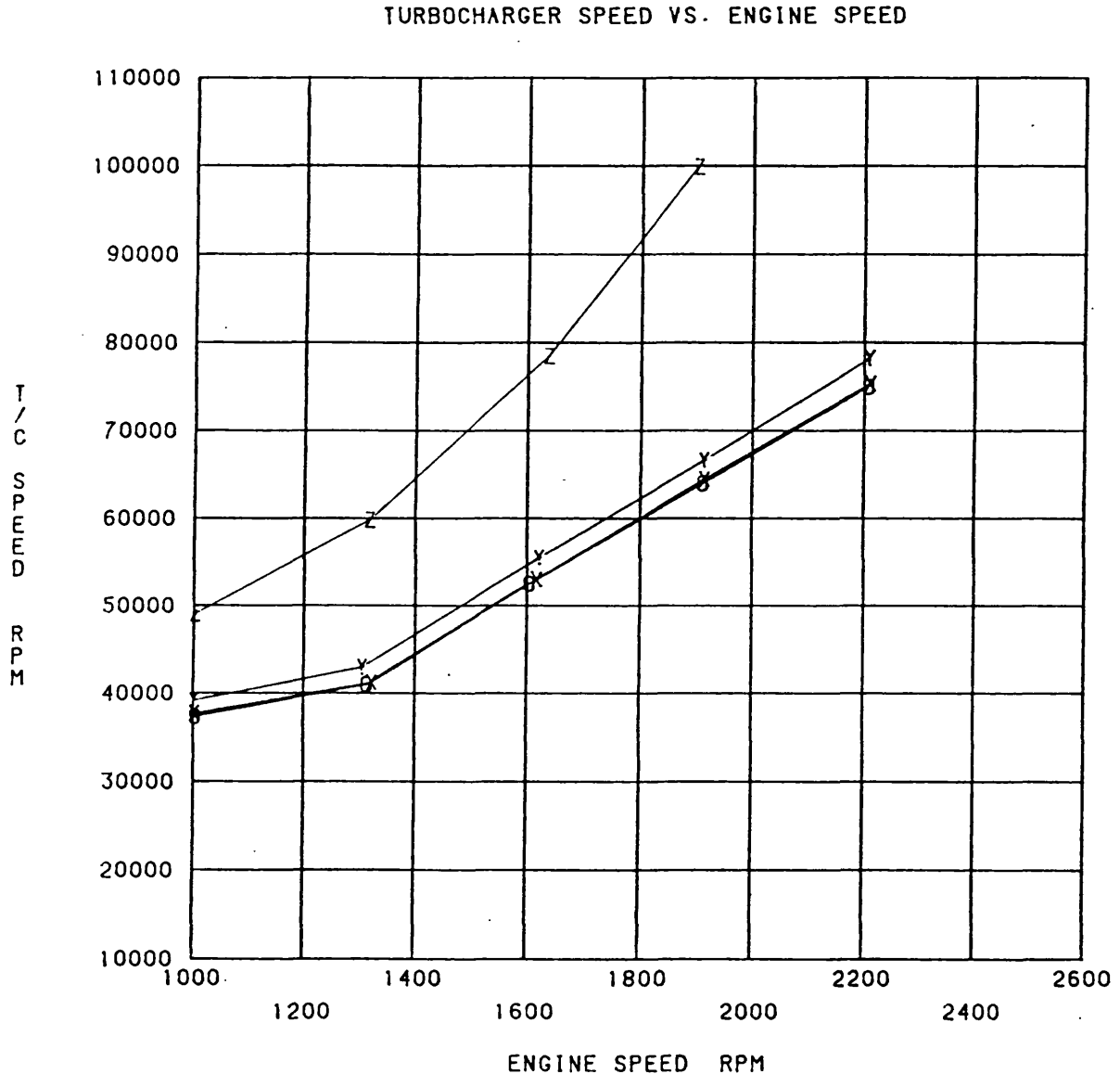

Fig. 3.16a 8 Bar BMEP Variable Geometry Engine Results,

O = 0%, X = 25%, Y = 40% and Z = 50% Restriction.

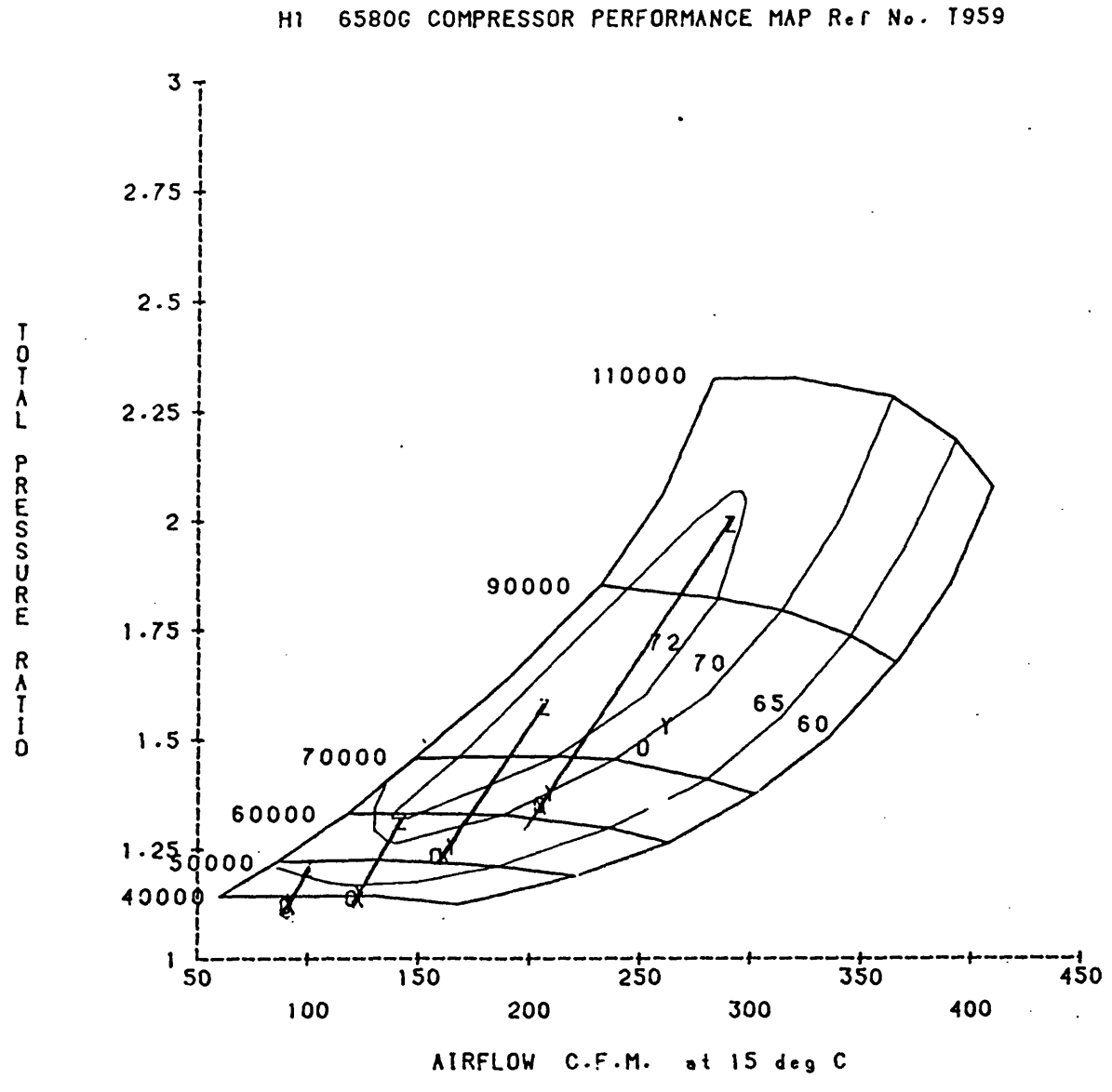

Fig. 3.16b 8 Bar BMEP Variable Geometry Engine Results,

O = 0%, X = 25%, Y = 40% and Z = 50% Restriction.

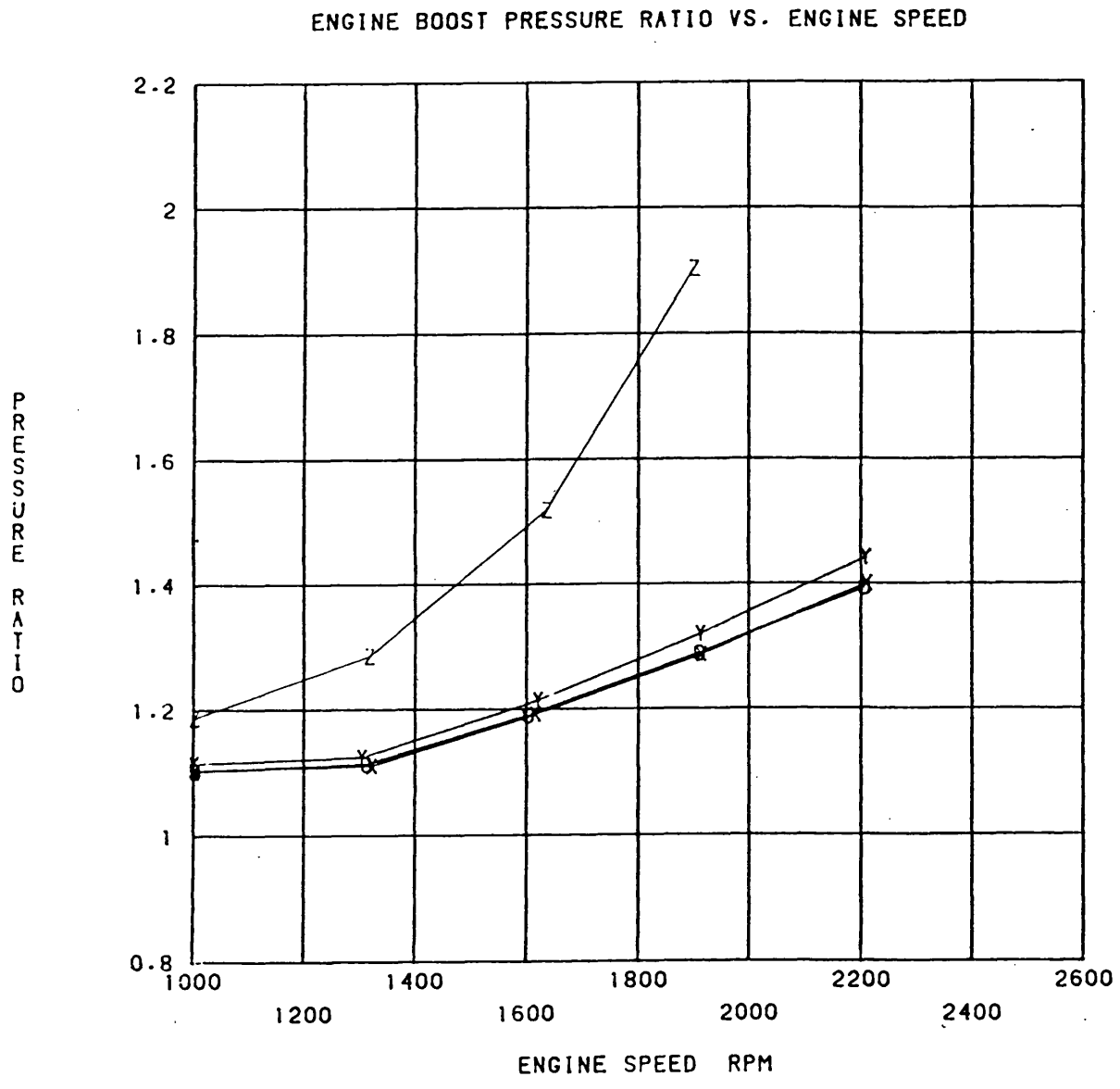

Fig. 3.16c 8 Bar BMEP Variable Geometry Engine Results,

O = 0%, X = 25%, Y = 40% and Z = 50% Restriction.

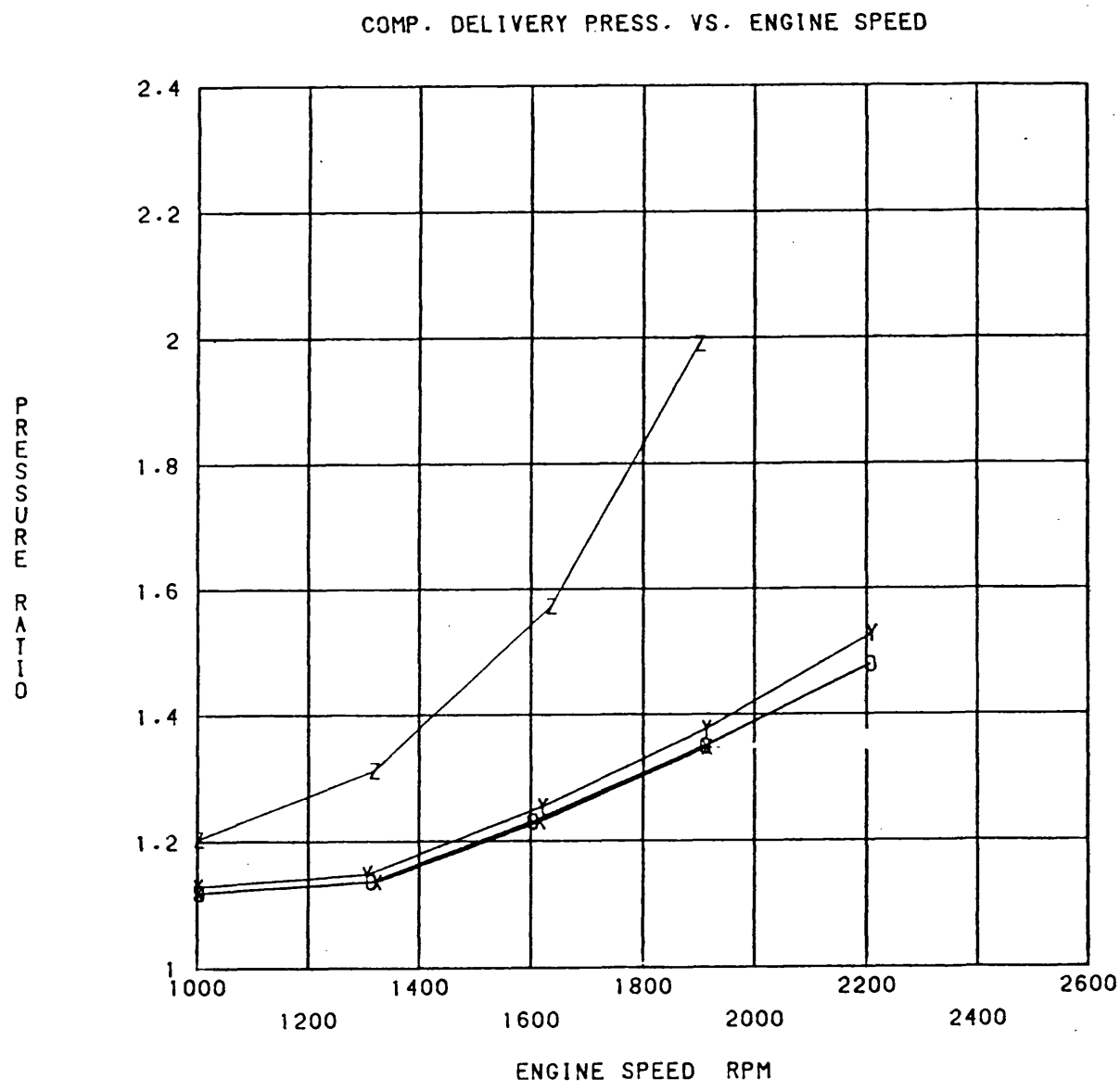

Fig. 3.16d 8 Bar BMEP Variable Geometry Engine Results,

O = 0%, X = 25%, Y = 40% and Z = 50% Restriction.

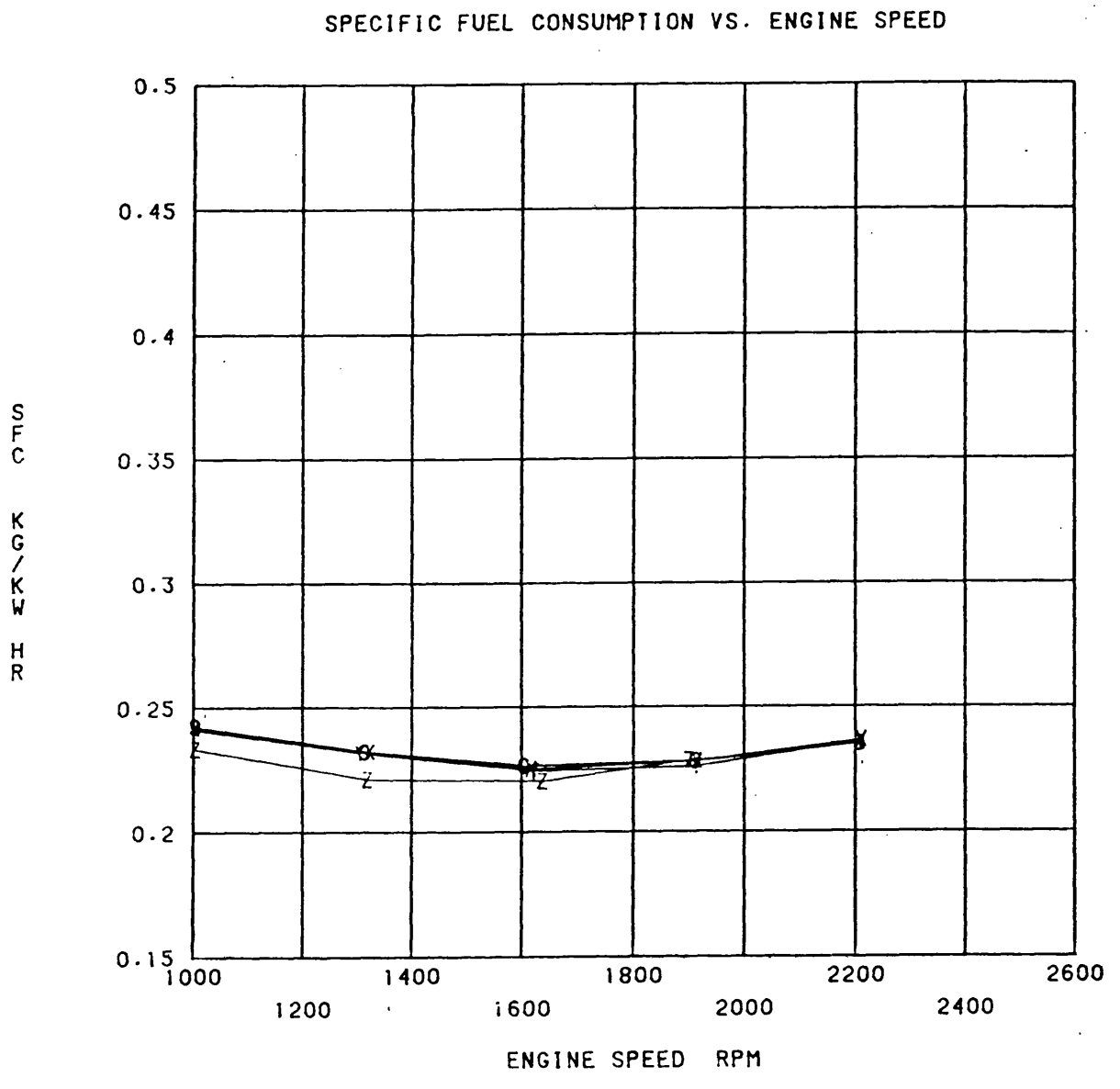

Fig. 3.16e 8 Bar BMEP Variable Geometry Engine Results,

O = 0%, X = 25%, Y = 40% and Z = 50% Restriction.

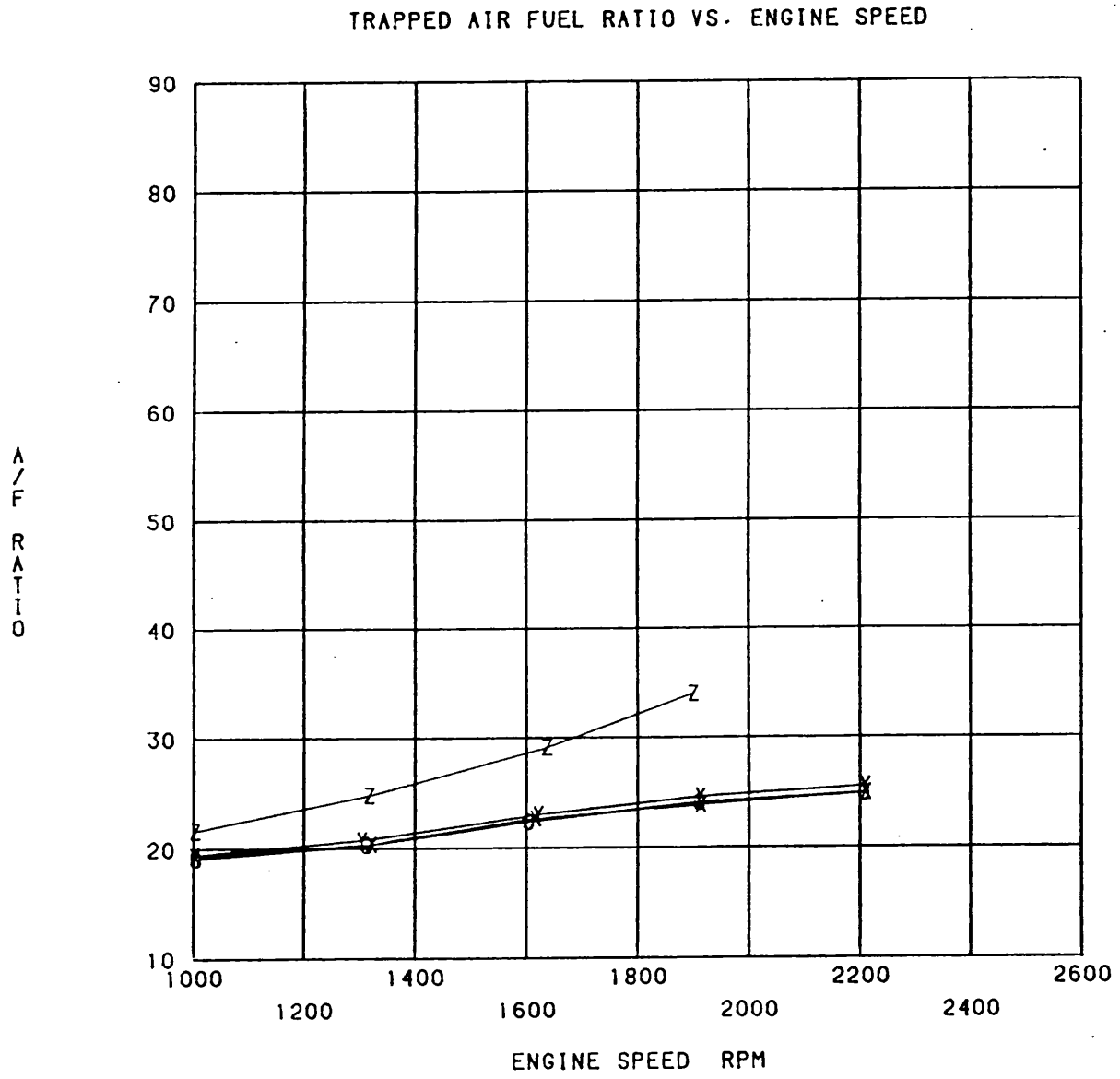

Fig. 3.16f 8 Bar BMEP Variable Geometry Engine Results,

O = 0%, X = 25%, Y = 40% and Z = 50% Restriction.

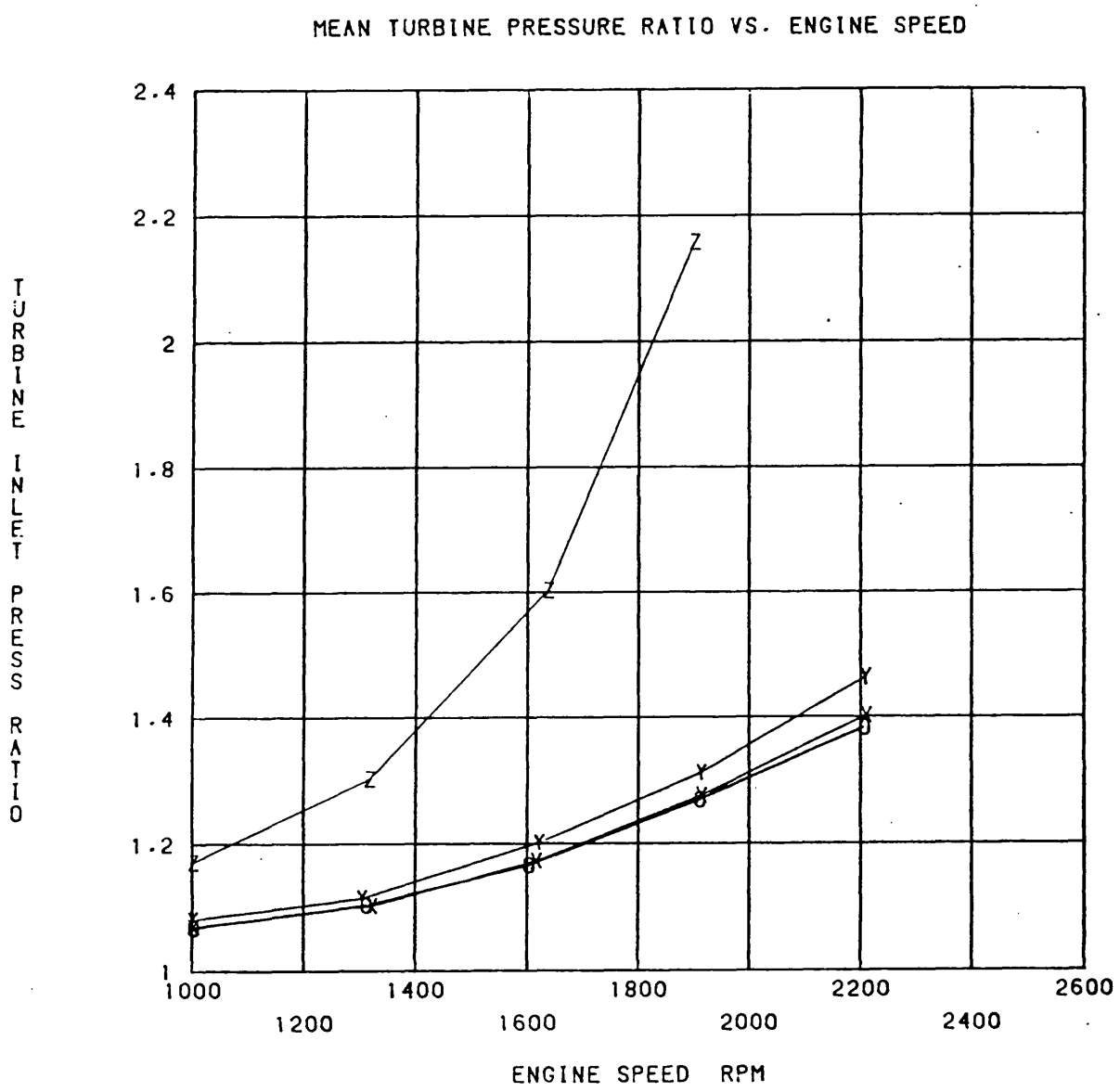

Fig. 3.16g 8 Bar BMEP Variable Geometry Engine Results,

O = 0%, X = 25%, Y = 40% and Z = 50% Restriction.

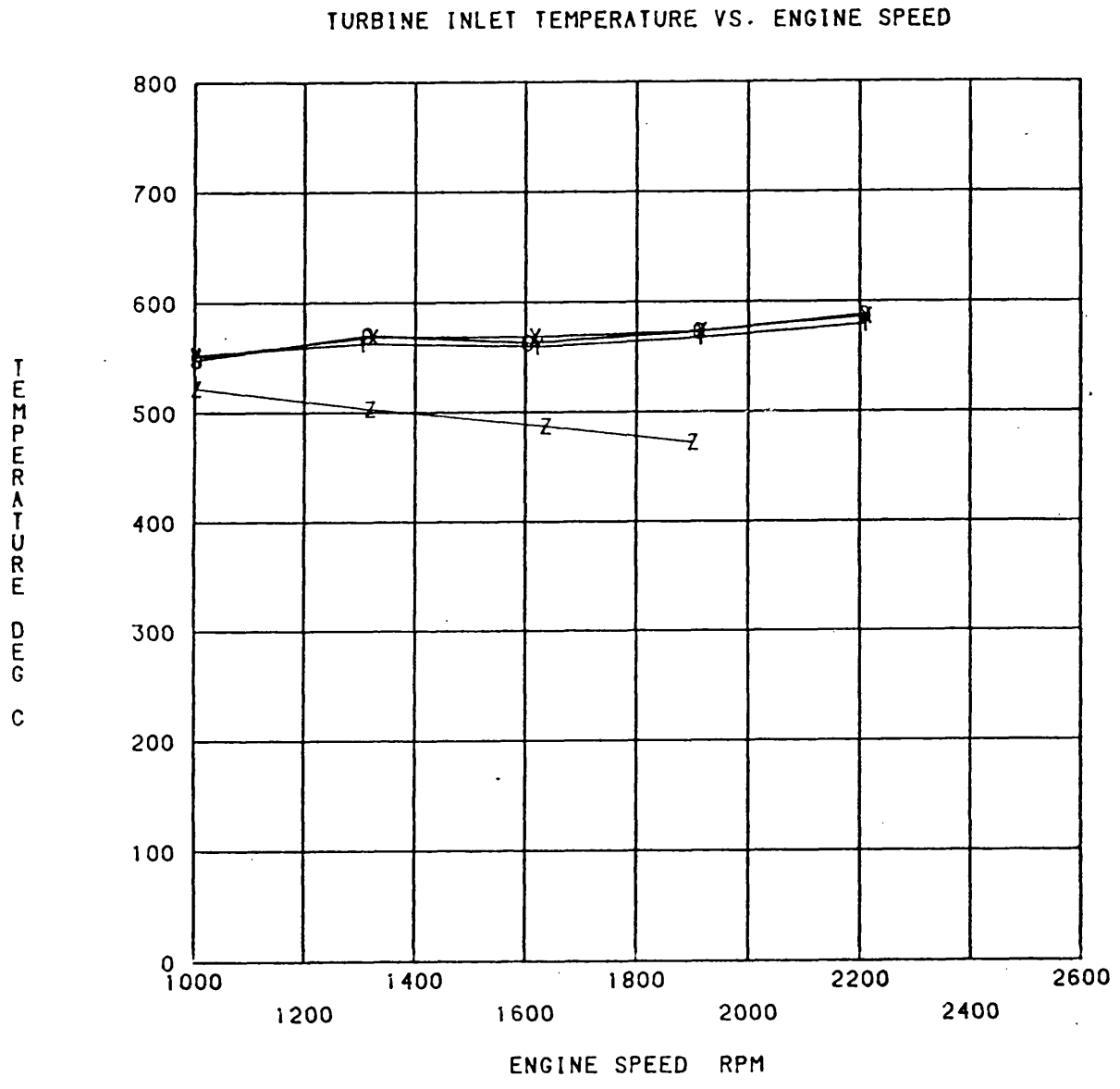

Fig. 3.16h 8 Bar BMEP Variable Geometry Engine Results,

O = 0%, X = 25%, Y = 40% and Z = 50% Restriction.

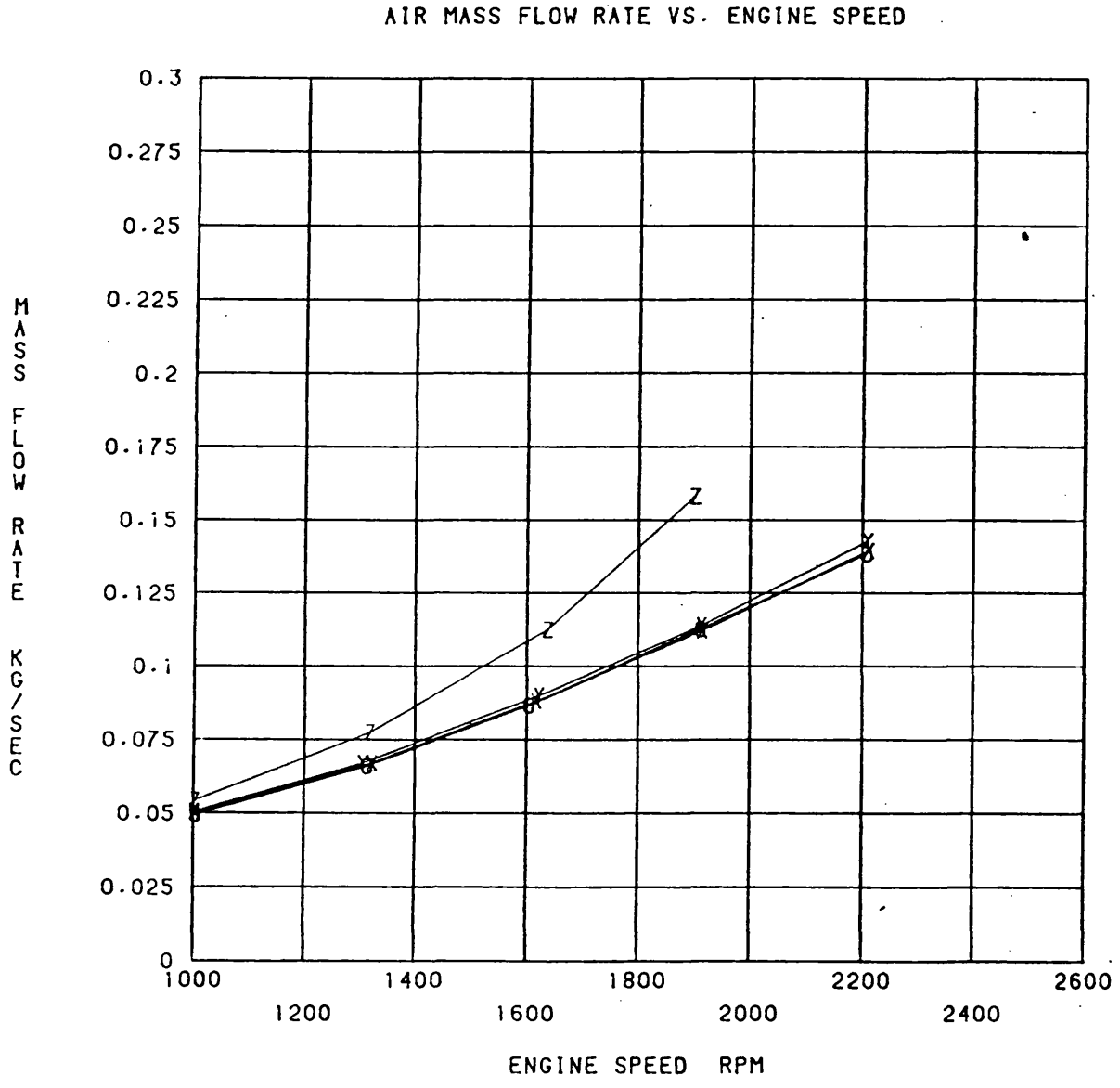

Fig. 3.16i 8 Bar BMEP Variable Geometry Engine Results,

O = 0%, X = 25%, Y = 40% and Z = 50% Restriction.

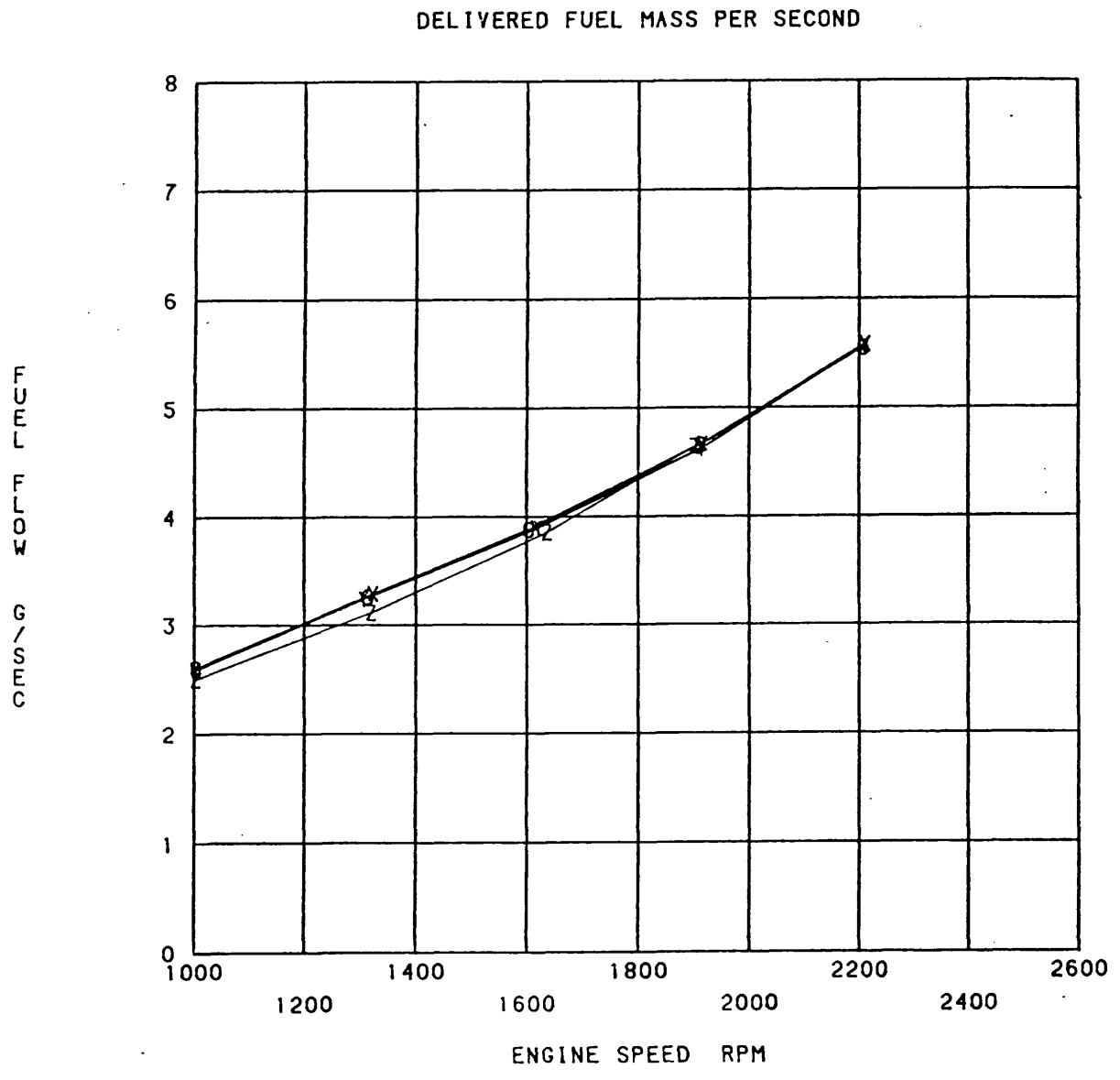

Fig. 3.16j 8 Bar BMEP Variable Geometry Engine Results,

O = 0%, X = 25%, Y = 40% and Z = 50% Restriction.

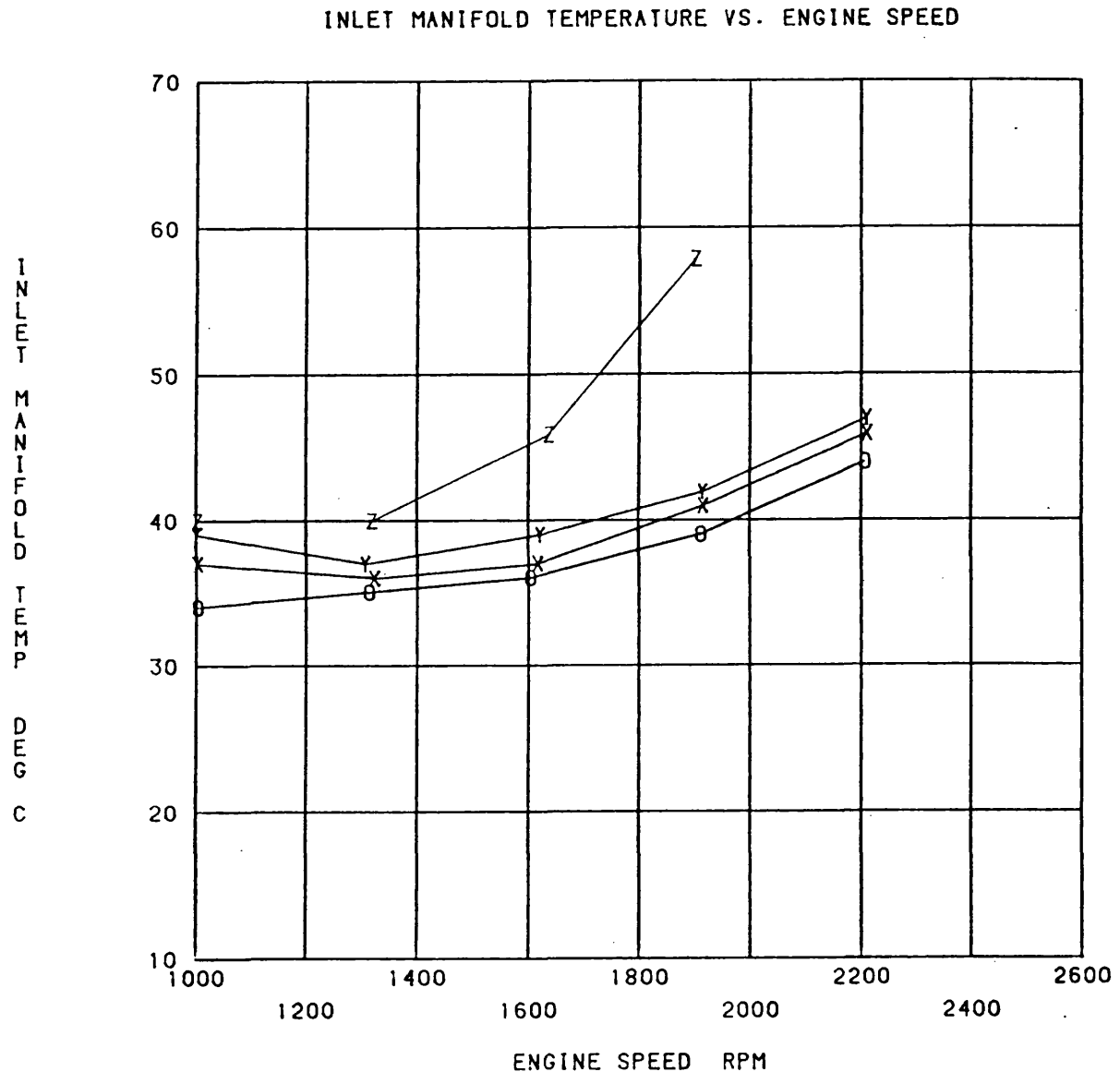

Fig. 3.16k 8 Bar BMEP Variable Geometry Engine Results,

O = 0%, X = 25%, Y = 40% and Z = 50% Restriction.

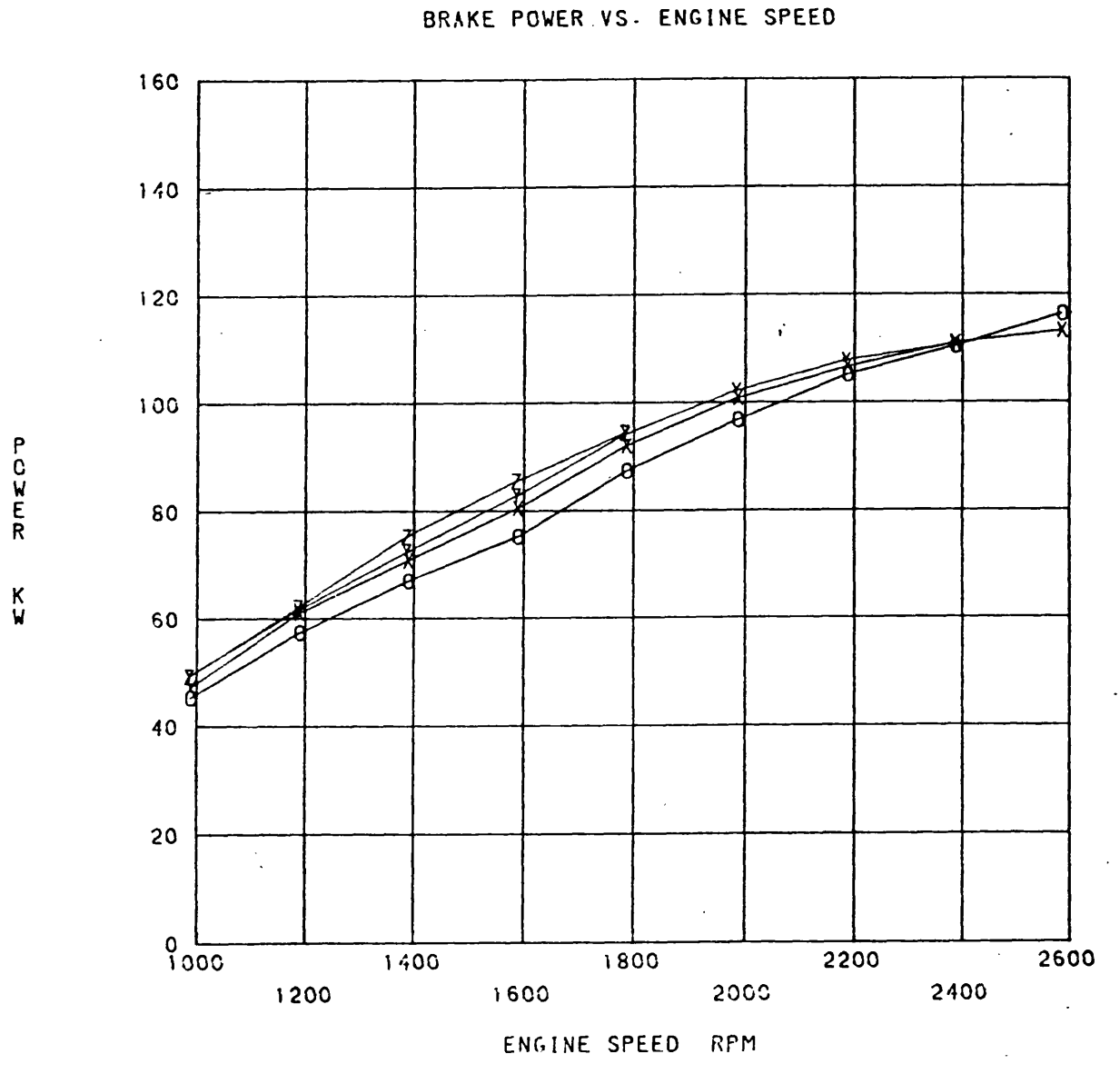

Fig. 3.17a Limiting Torque Variable Geometry Engine Results,

O = 0%, X = 25%, Y = 40% and Z = 50% Restriction.

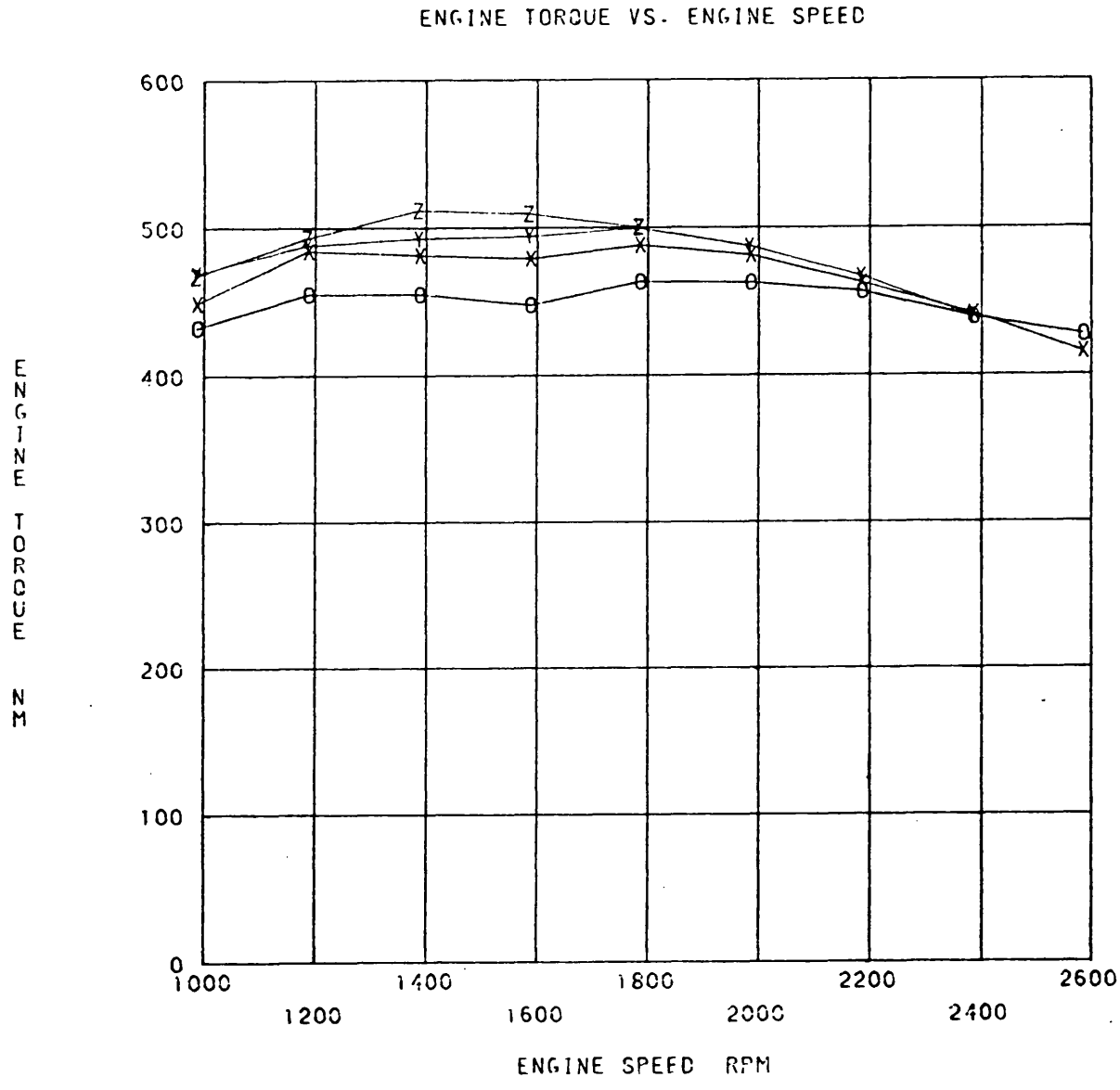

Fig. 3.17b Limiting Torque Variable Geometry Engine Results,

O = 0%, X = 25%, Y = 40% and Z = 50% Restriction.

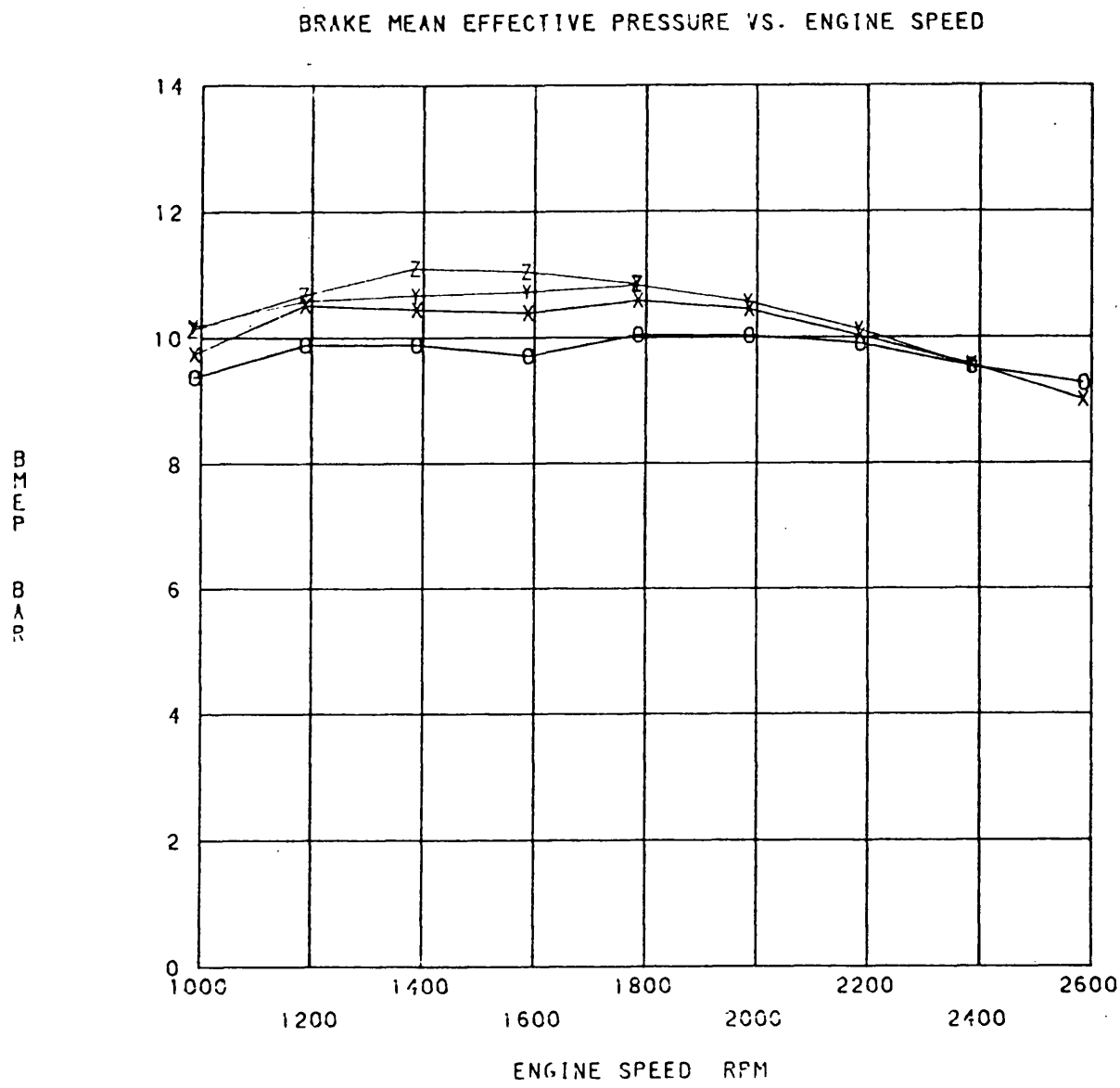

Fig. 3.17c Limiting Torque Variable Geometry Engine Results,

O = 0%, X = 25%, Y = 40% and Z = 50% Restriction.

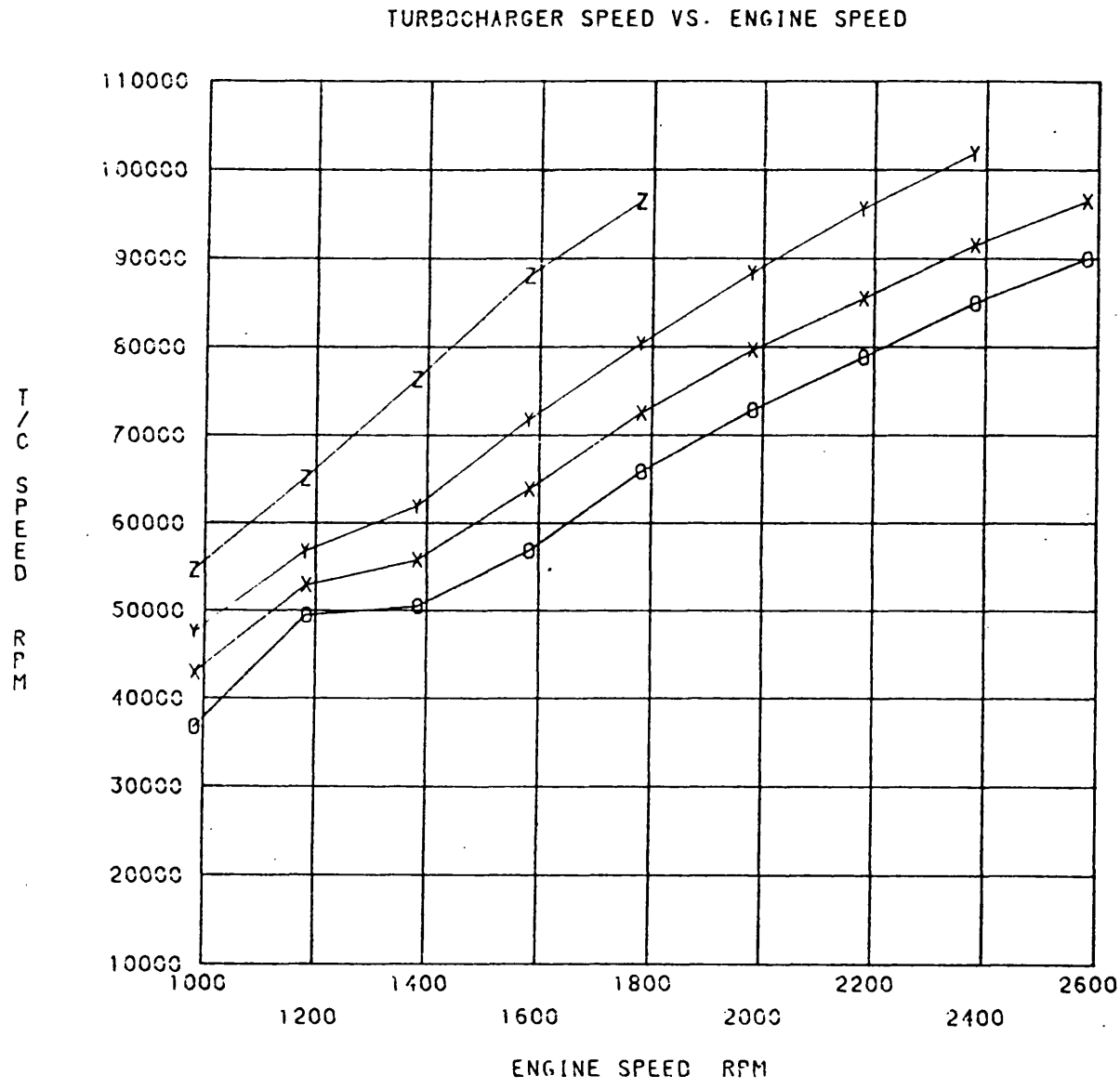

Fig. 3.17d Limiting Torque Variable Geometry Engine Results,

0 = 0%, X = 25%, Y = 40% and Z = 50% Restriction.

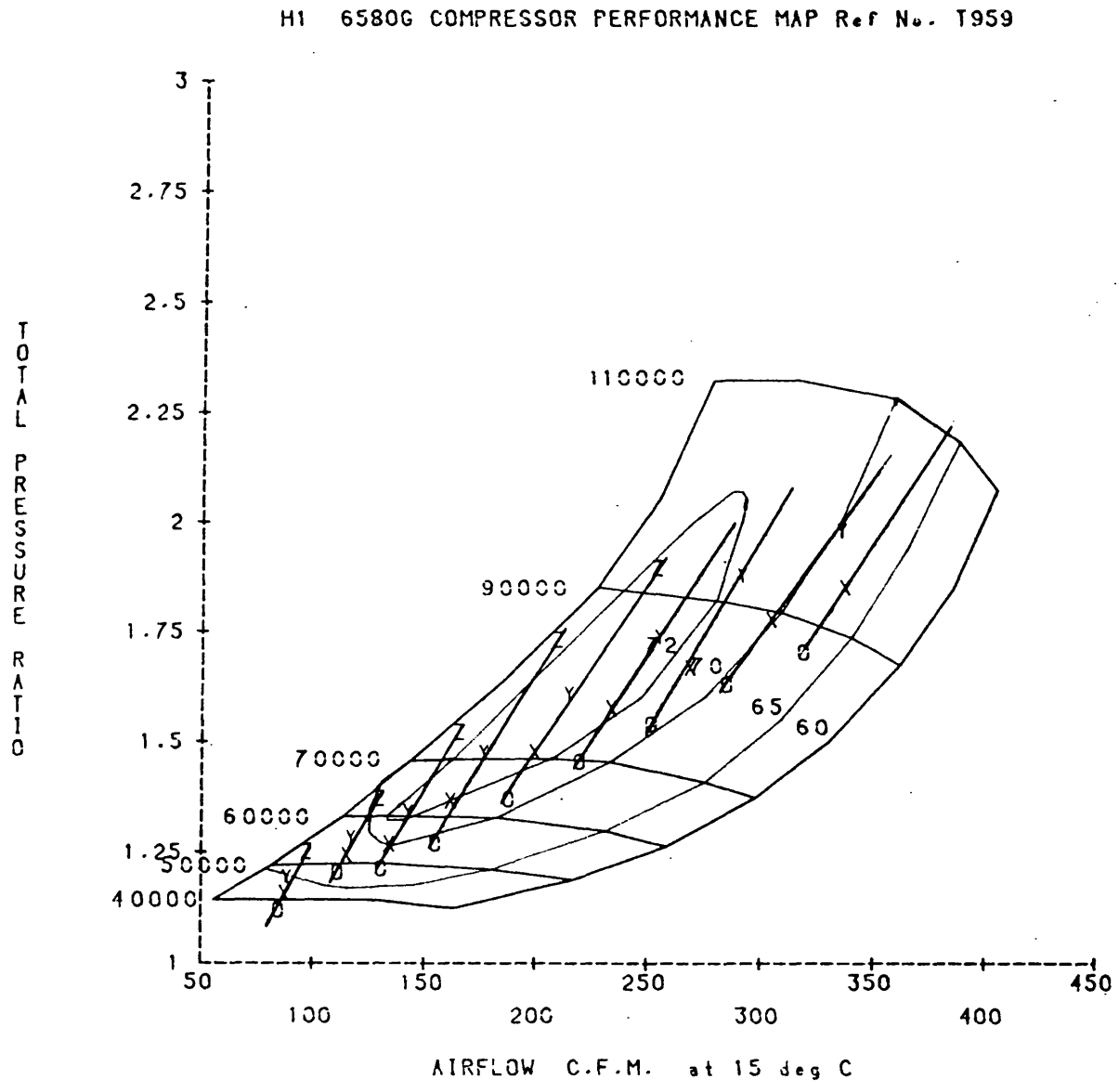

Fig. 3.17e Limiting Torque Variable Geometry Engine Results,

O = 0%, X = 25%, Y = 40% and Z = 50% Restriction.

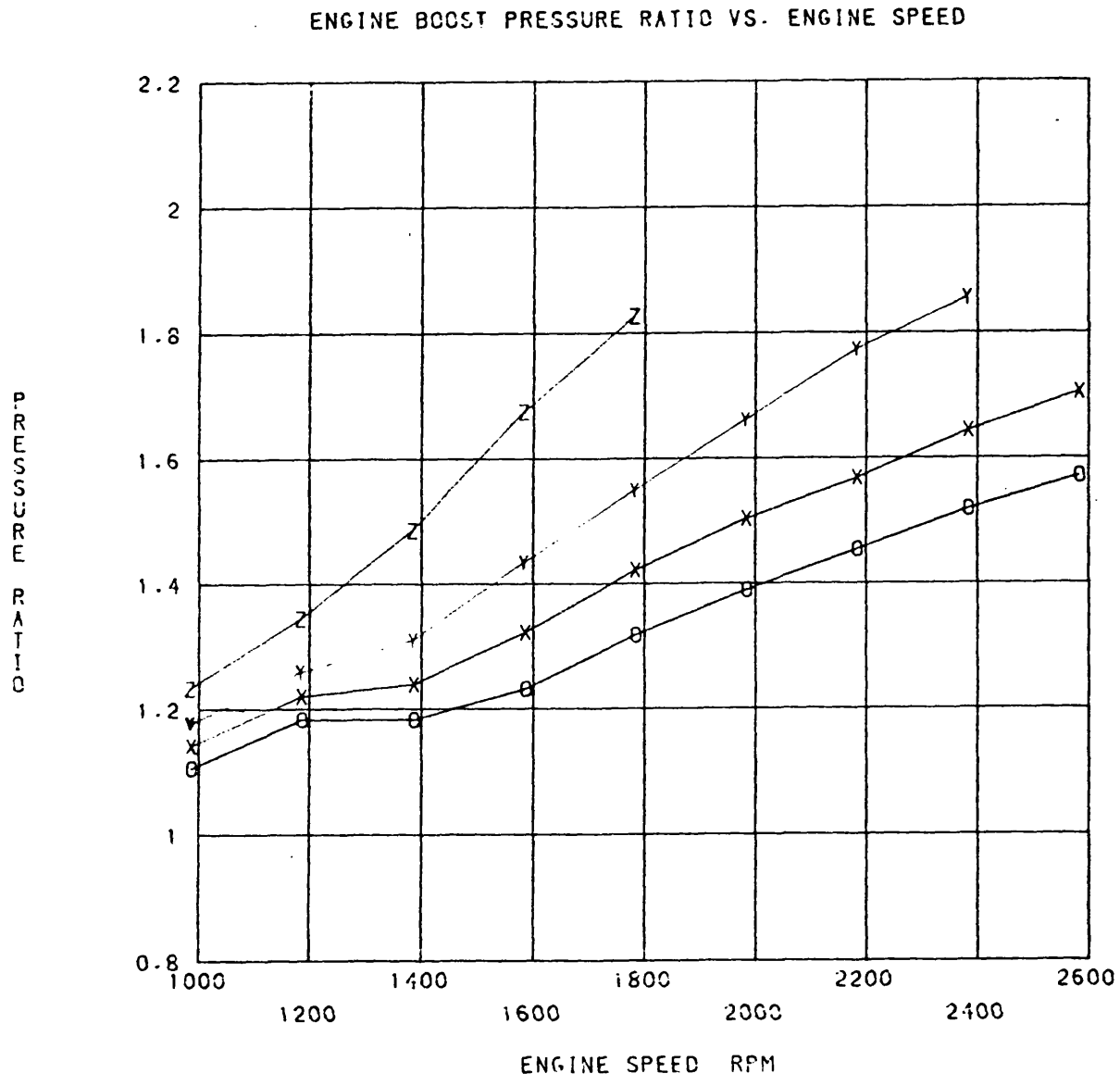

Fig. 3.17f Limiting Torque Variable Geometry Engine Results,

O = 0%, X = 25%, Y = 40% and Z = 50% Restriction.

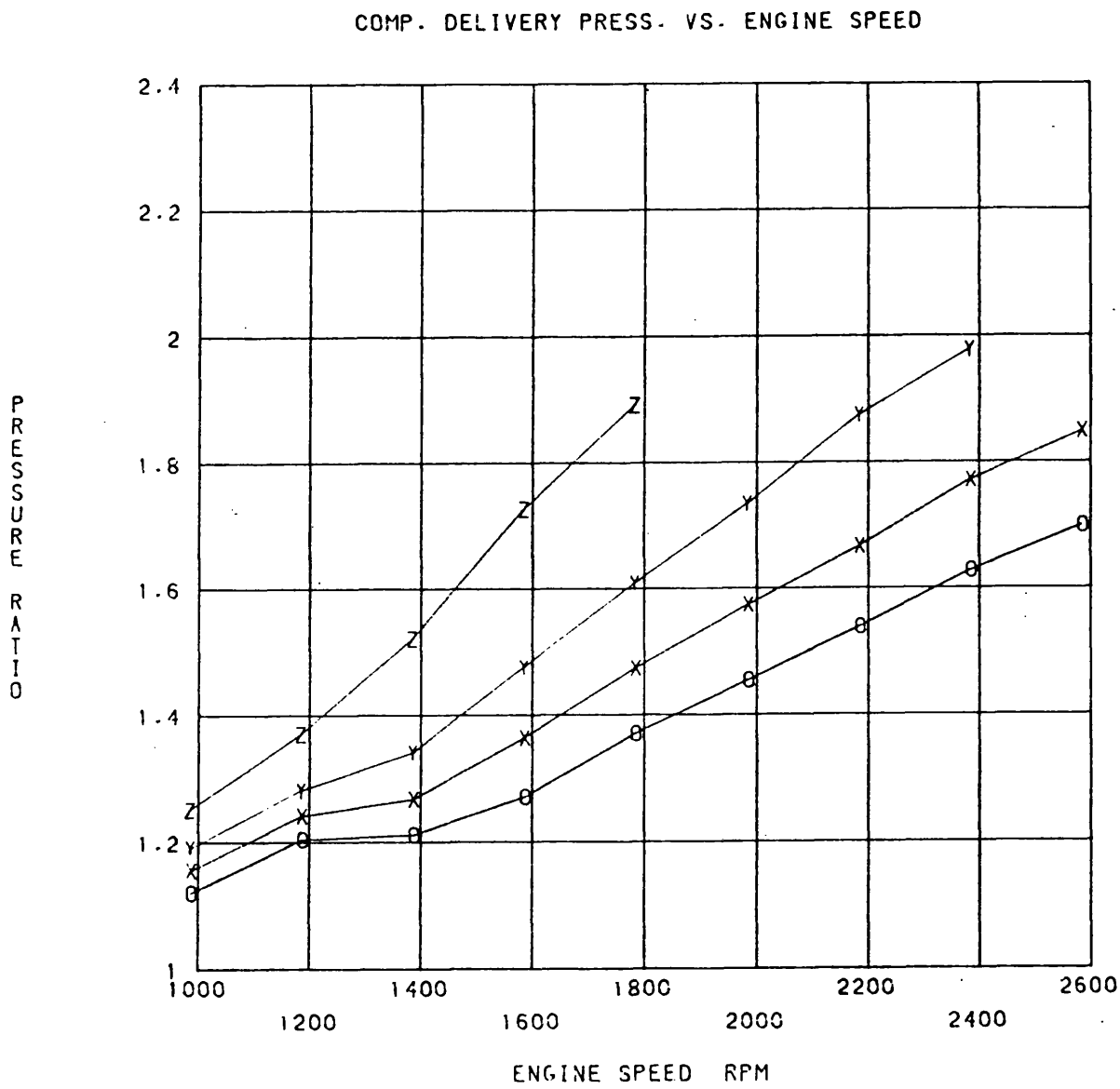

Fig. 3.17g Limiting Torque Variable Geometry Engine Results,

O = 0%, X = 25%, Y = 40% and Z = 50% Restriction.

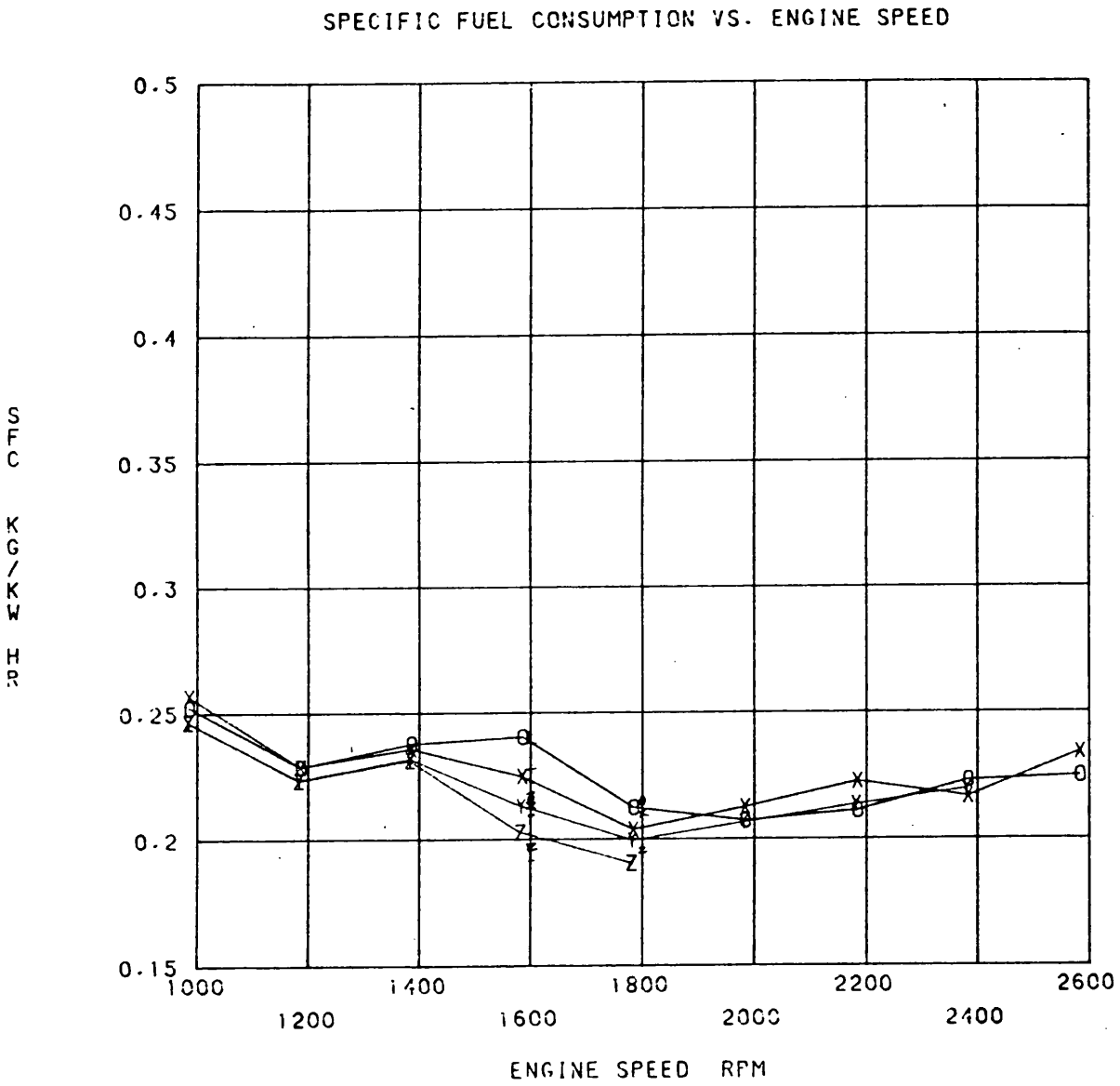

Fig. 3.17h Limiting Torque Variable Geometry Engine Results,

O = 0%, X = 25%, Y = 40% and Z = 50% Restriction.

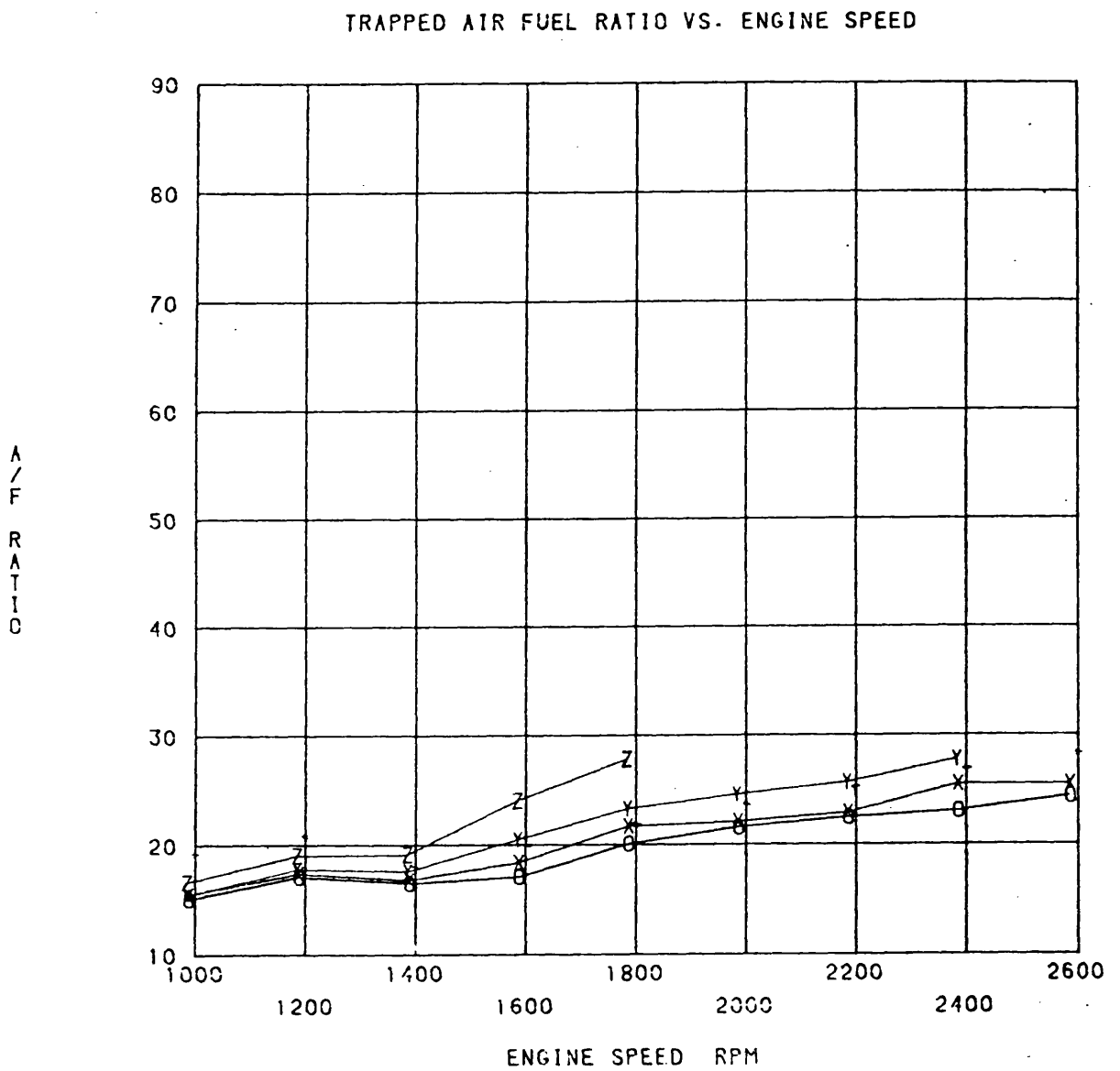

Fig. 3.17i Limiting Torque Variable Geometry Engine Results,

O = 0%, X = 25%, Y = 40% and Z = 50% Restriction.

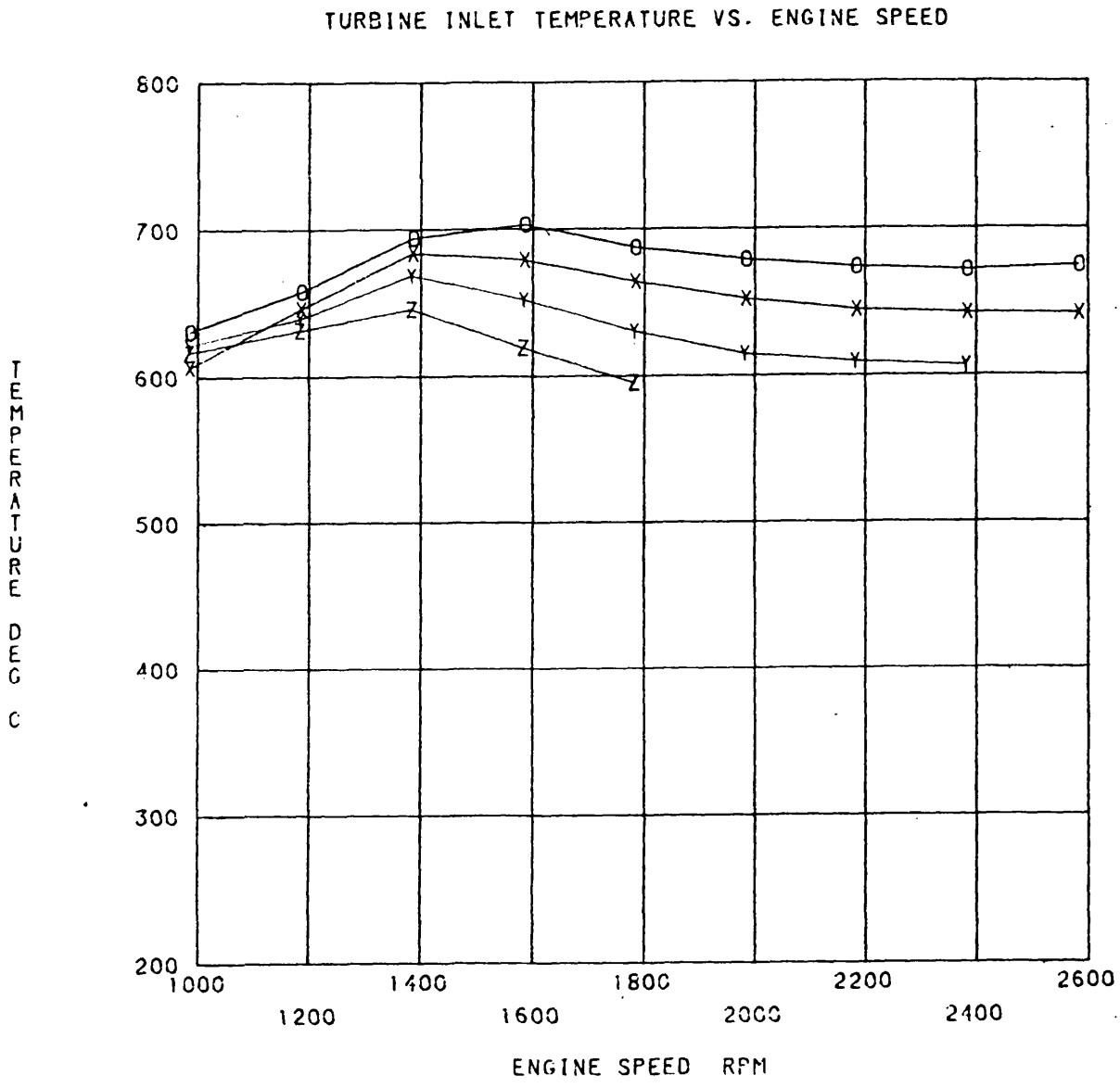

Fig. 3.17j Limiting Torque Variable Geometry Engine Results,

O = 0%, X = 25%, Y = 40% and Z = 50% Restriction.

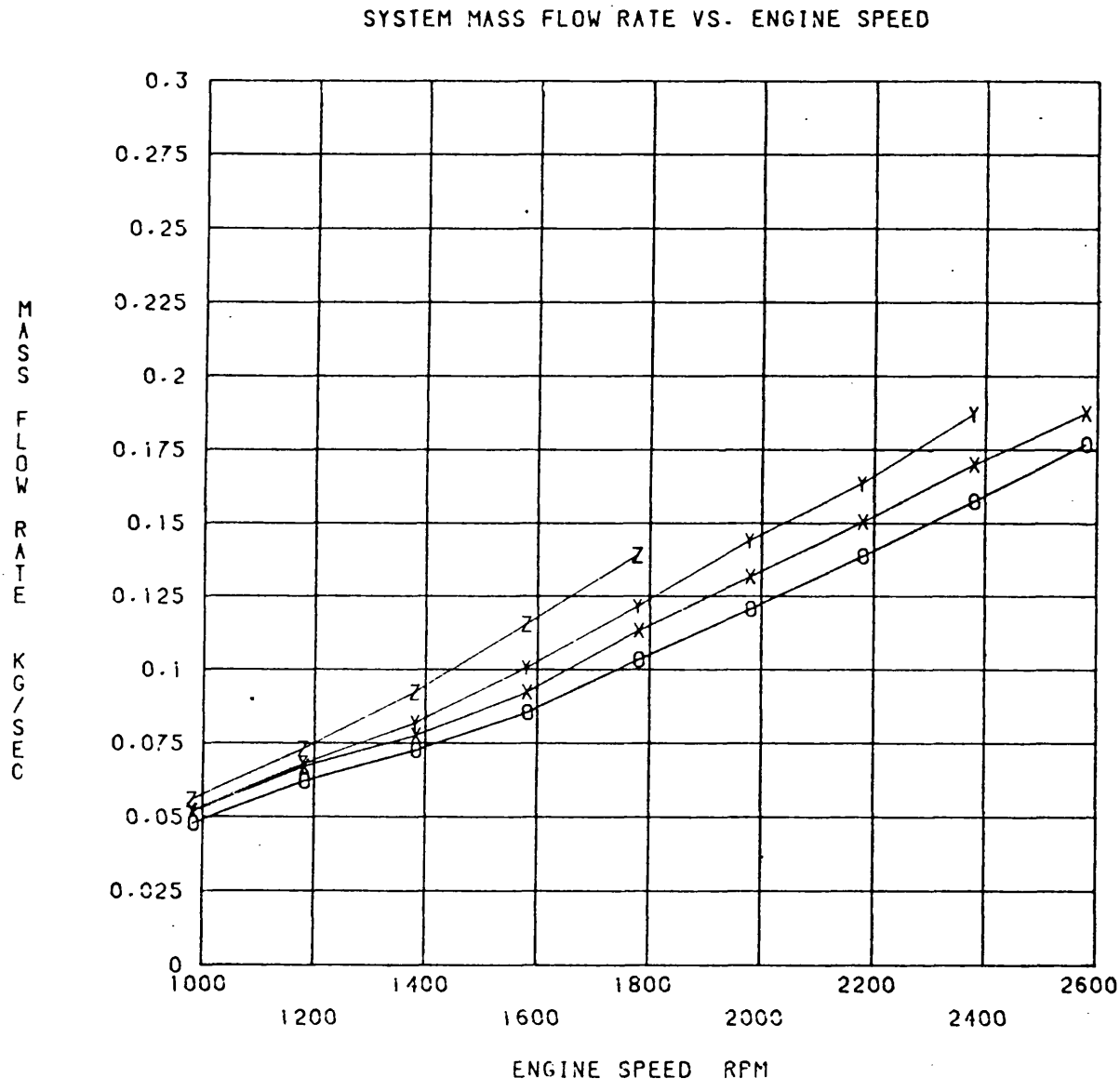

Fig. 3.17k Limiting Torque Variable Geometry Engine Results,

O = 0%, X = 25%, Y = 40% and Z = 50% Restriction.

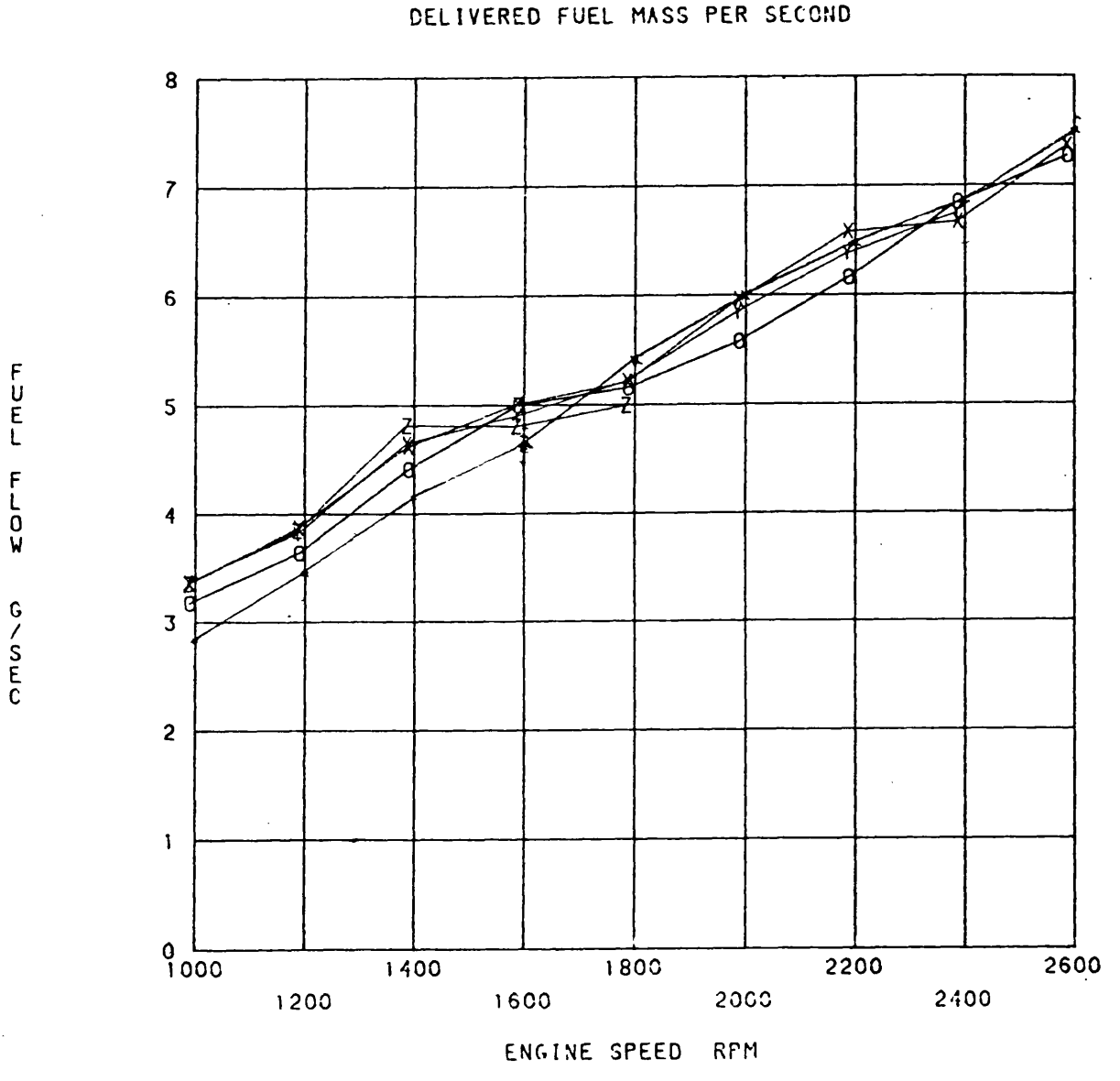

Fig. 3.171 Limiting Torque Variable Geometry Engine Results,

O = 0%, X = 25%, Y = 40% and Z = 50% Restriction.

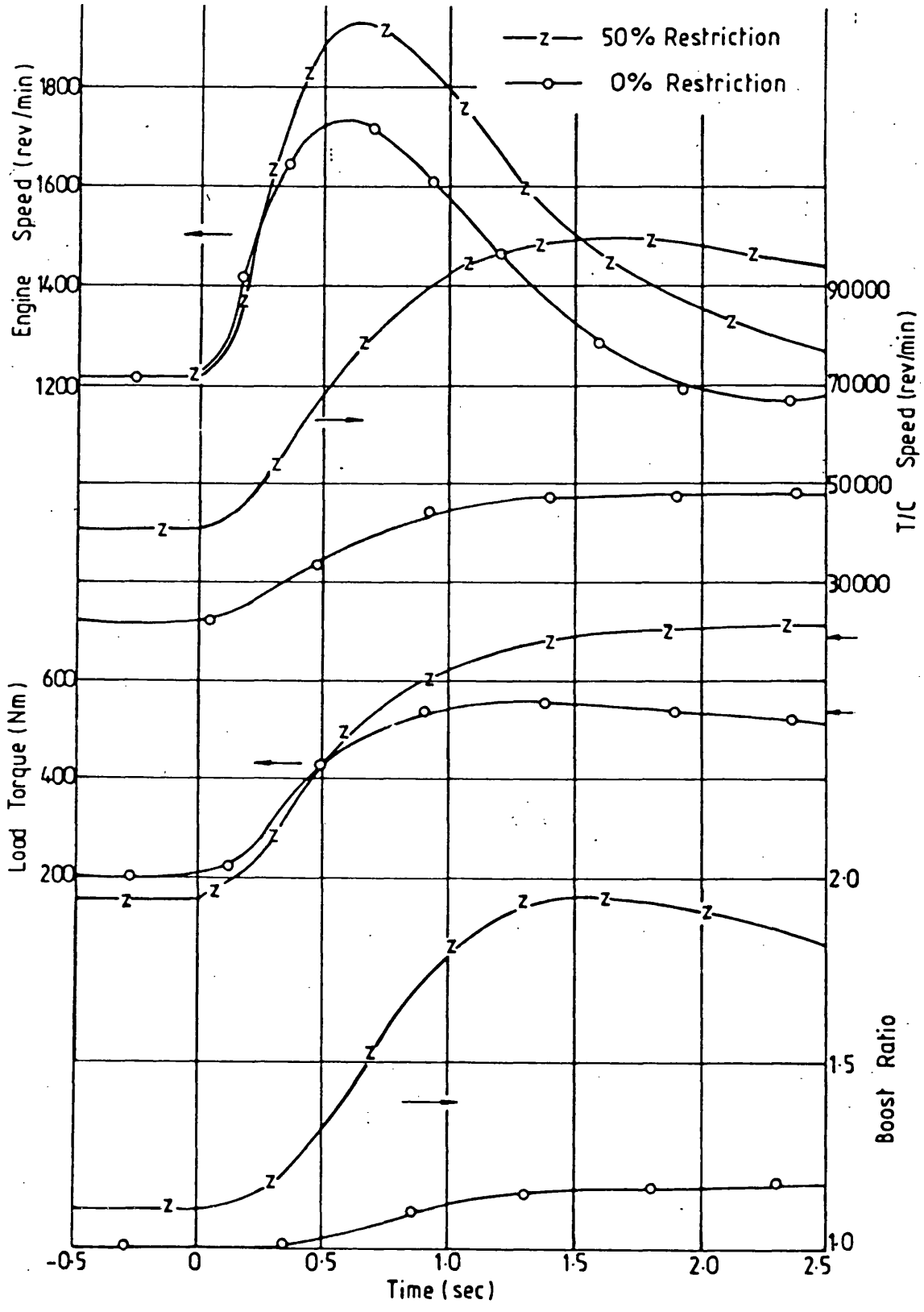

Fig. 3.18 Transient Engine-Turbocharger Response,

Nominal Engine Speed = 1200 rpm.

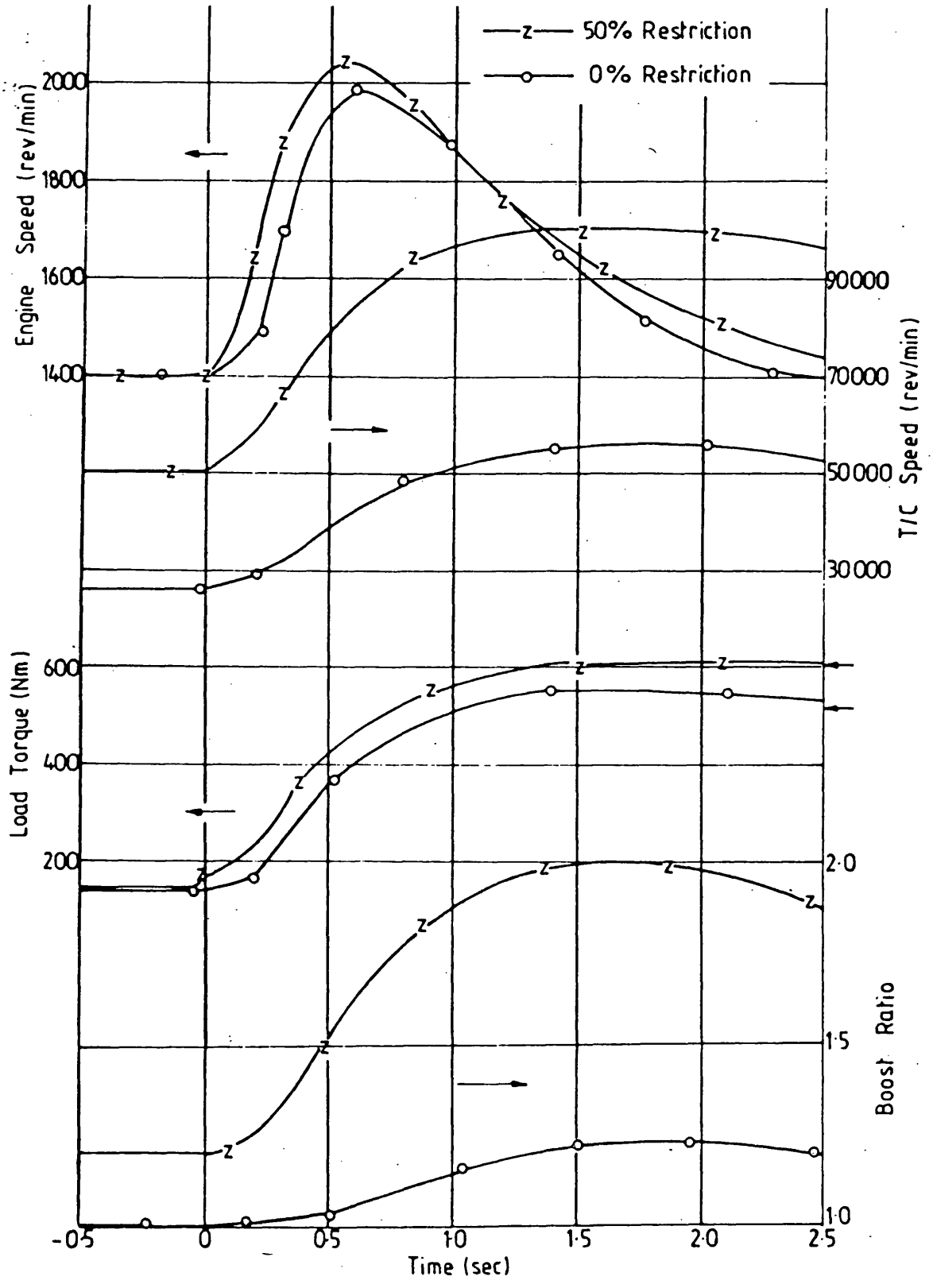

Fig. 3.19 Transient Engine-Turbocharger Response,

Nominal Engine Speed = 1400 rpm.

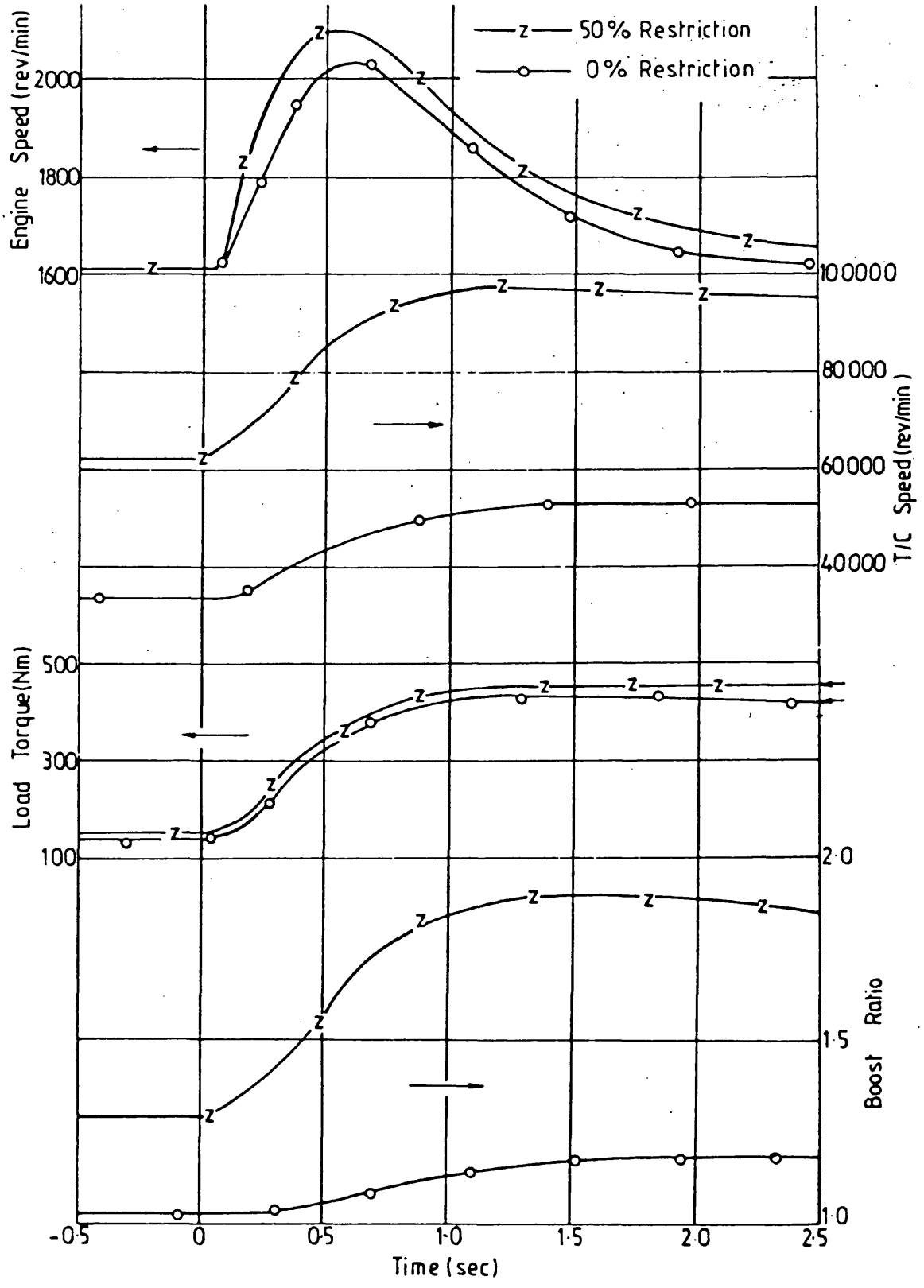

Fig. 3.20 Transient Engine-Turbocharger Response,

Nominal Engine Speed = 1600 rpm.

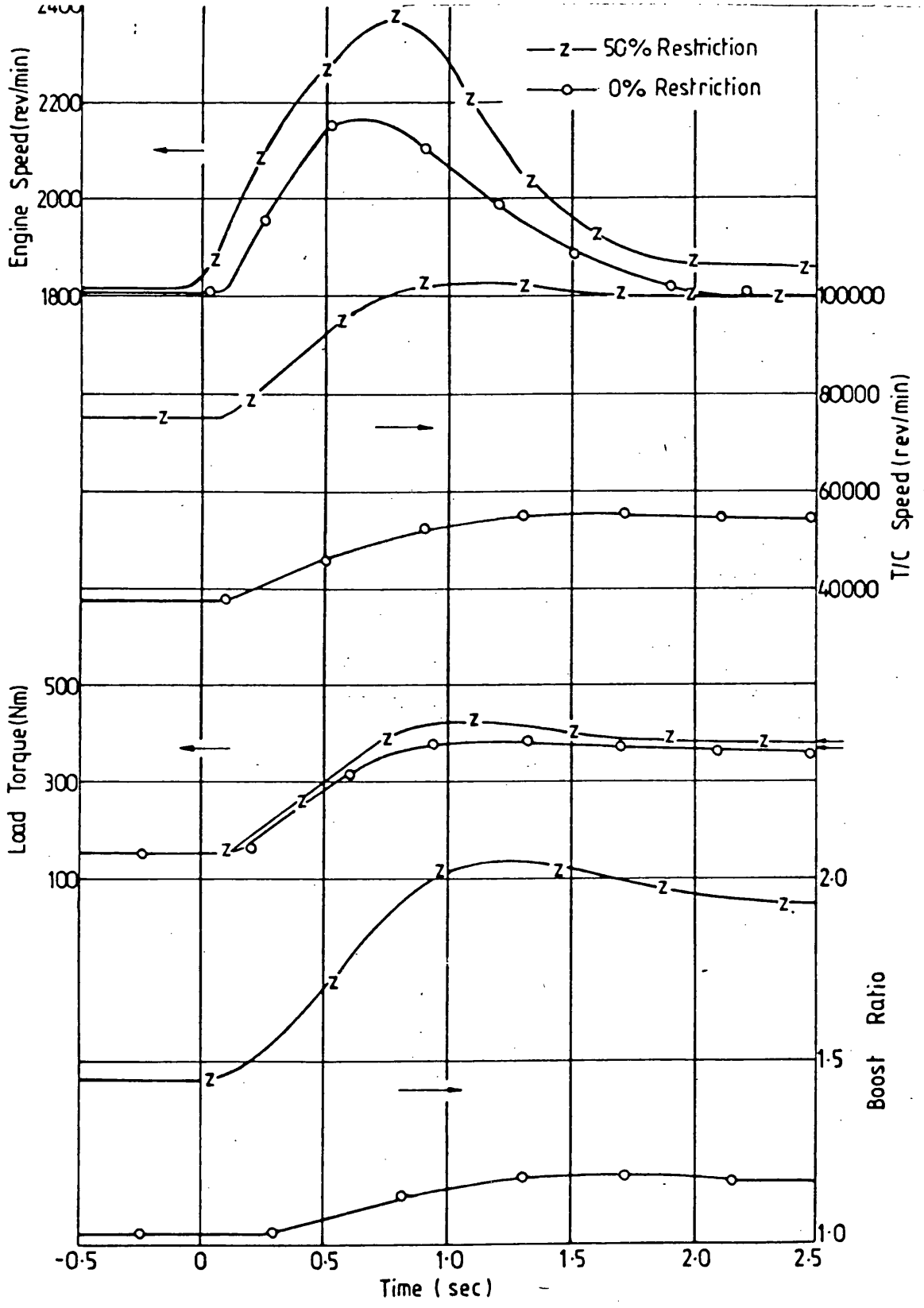

Fig. 3.21 Transient Engine–Turbocharger Response,

Nominal Engine Speed = 1800 rpm.

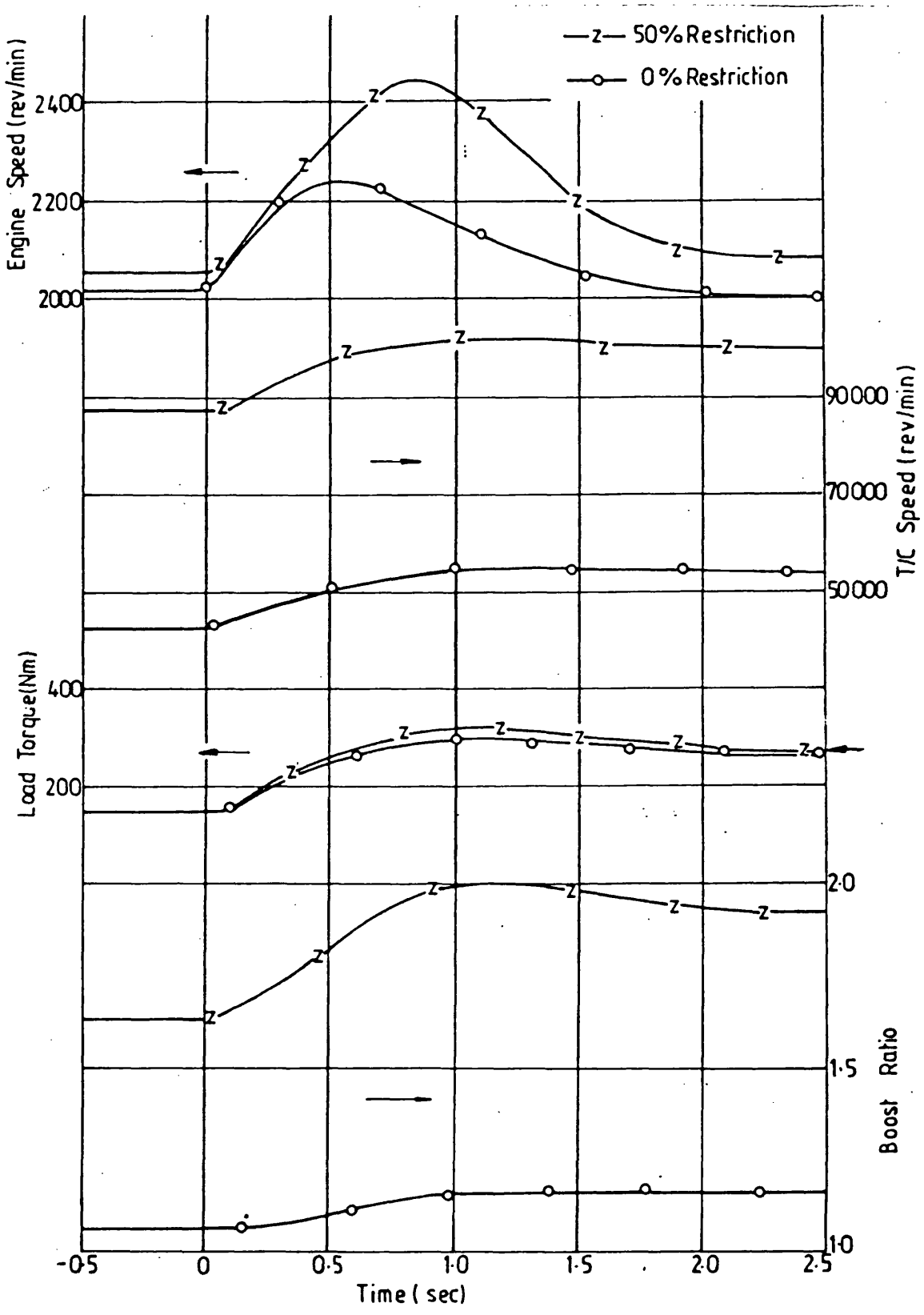

Fig. 3.22 Transient Engine-Turbocharger Response,

Nominal Engine Speed = 2000 rpm.

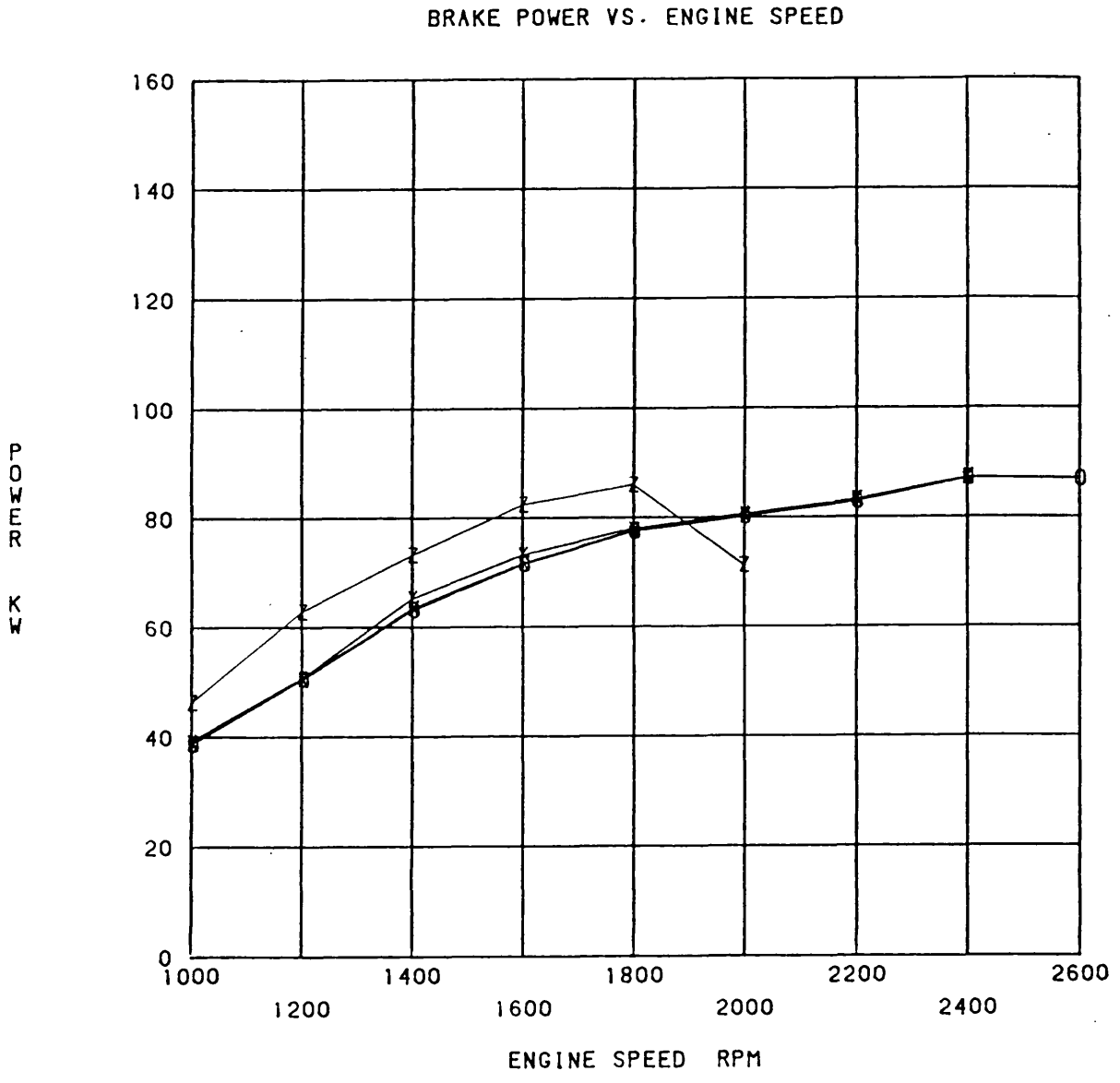

Fig. 3.23a Limiting Torque Variable Geometry Engine Results,

O = 0%, X = 25%, Y = 40% and Z = 50% Restriction.

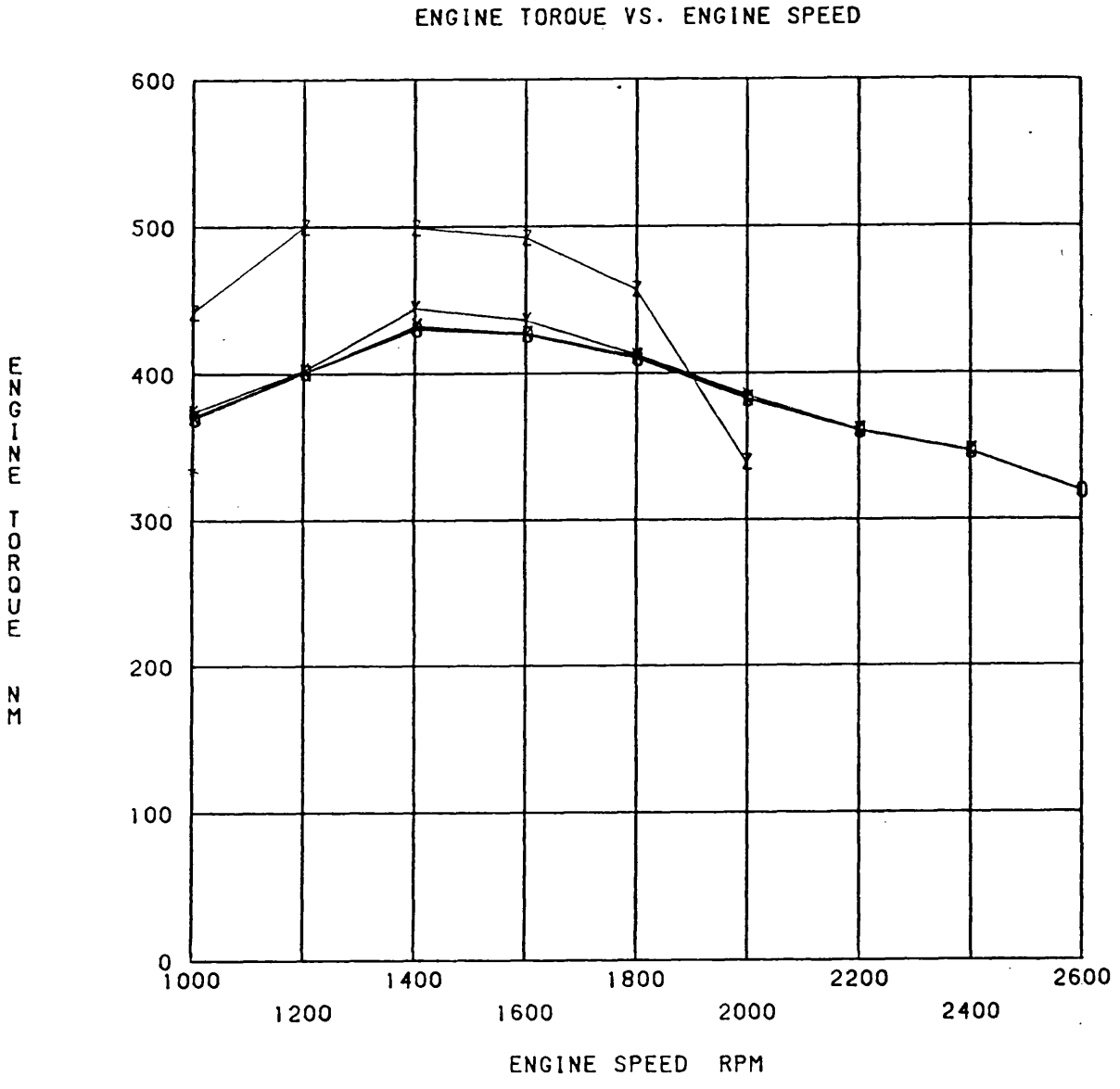

Fig. 3.23b Limiting Torque Variable Geometry Engine Results,

O = 0%, X = 25%, Y = 40% and Z = 50% Restriction.

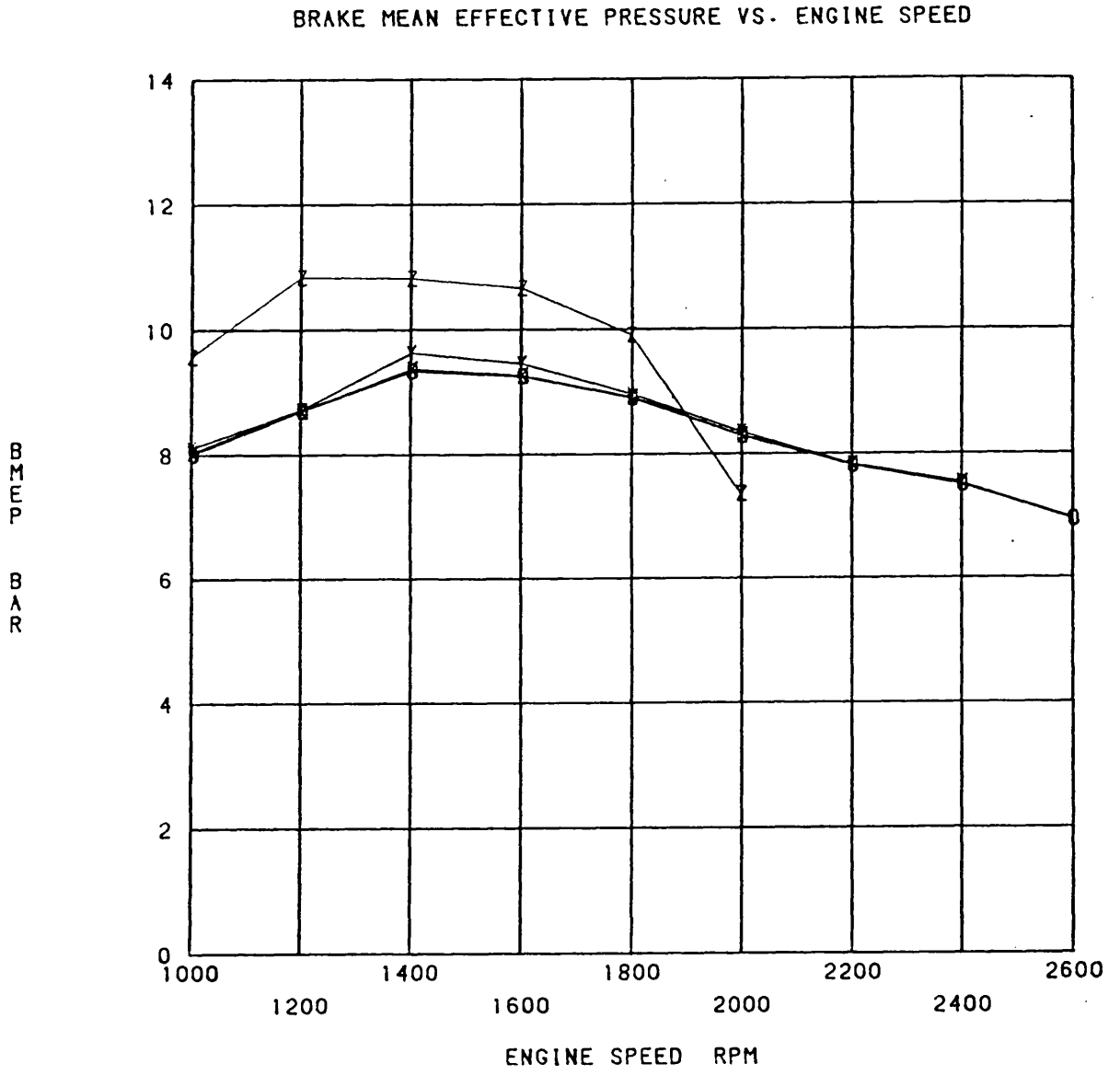

Fig. 3.23c Limiting Torque Variable Geometry Engine Results,

O = 0%, X = 25%, Y = 40% and Z = 50% Restriction.

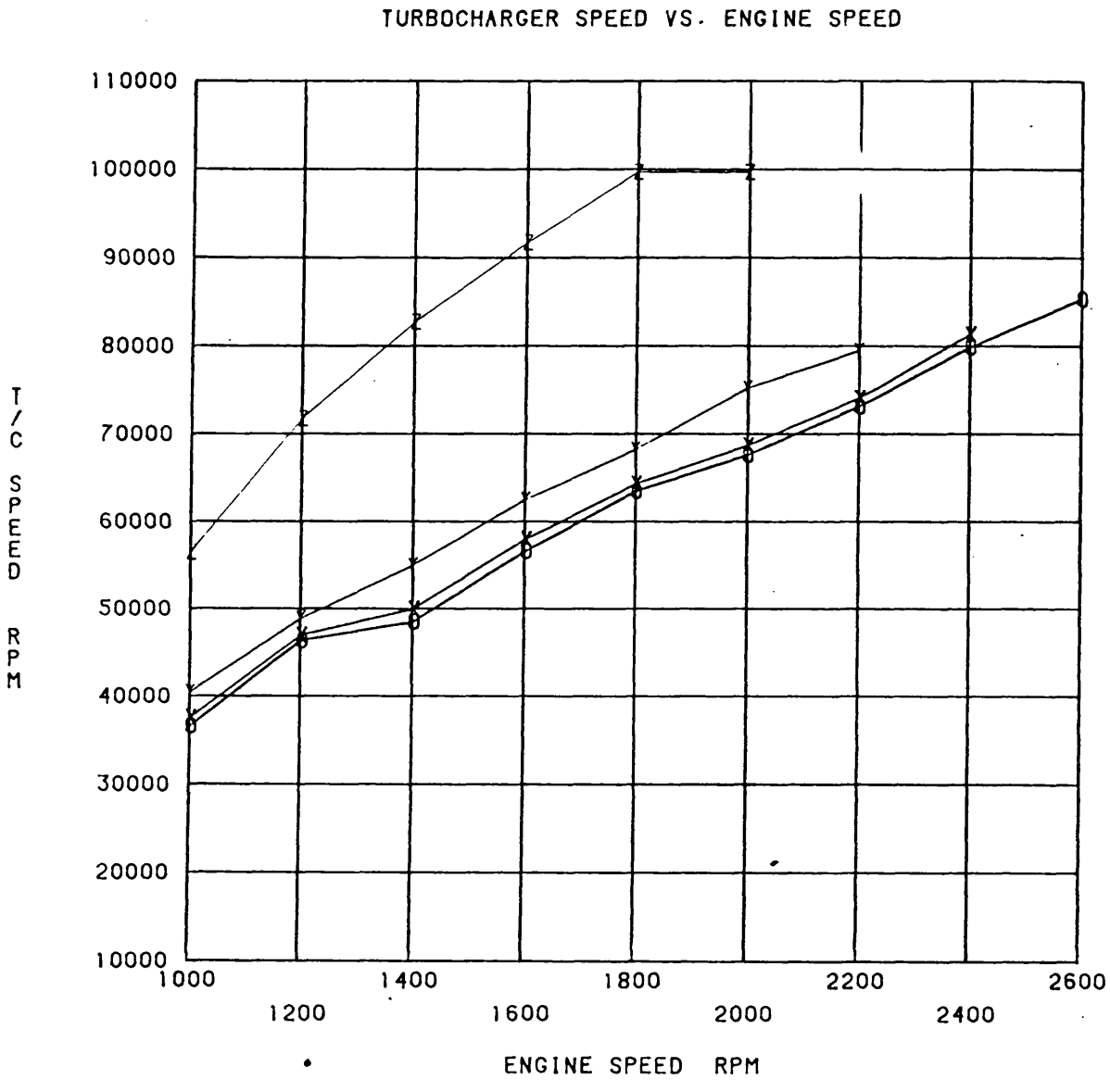

Fig. 3.23d Limiting Torque Variable Geometry Engine Results,

O = 0%, X = 25%, Y = 40% and Z = 50% Restriction.

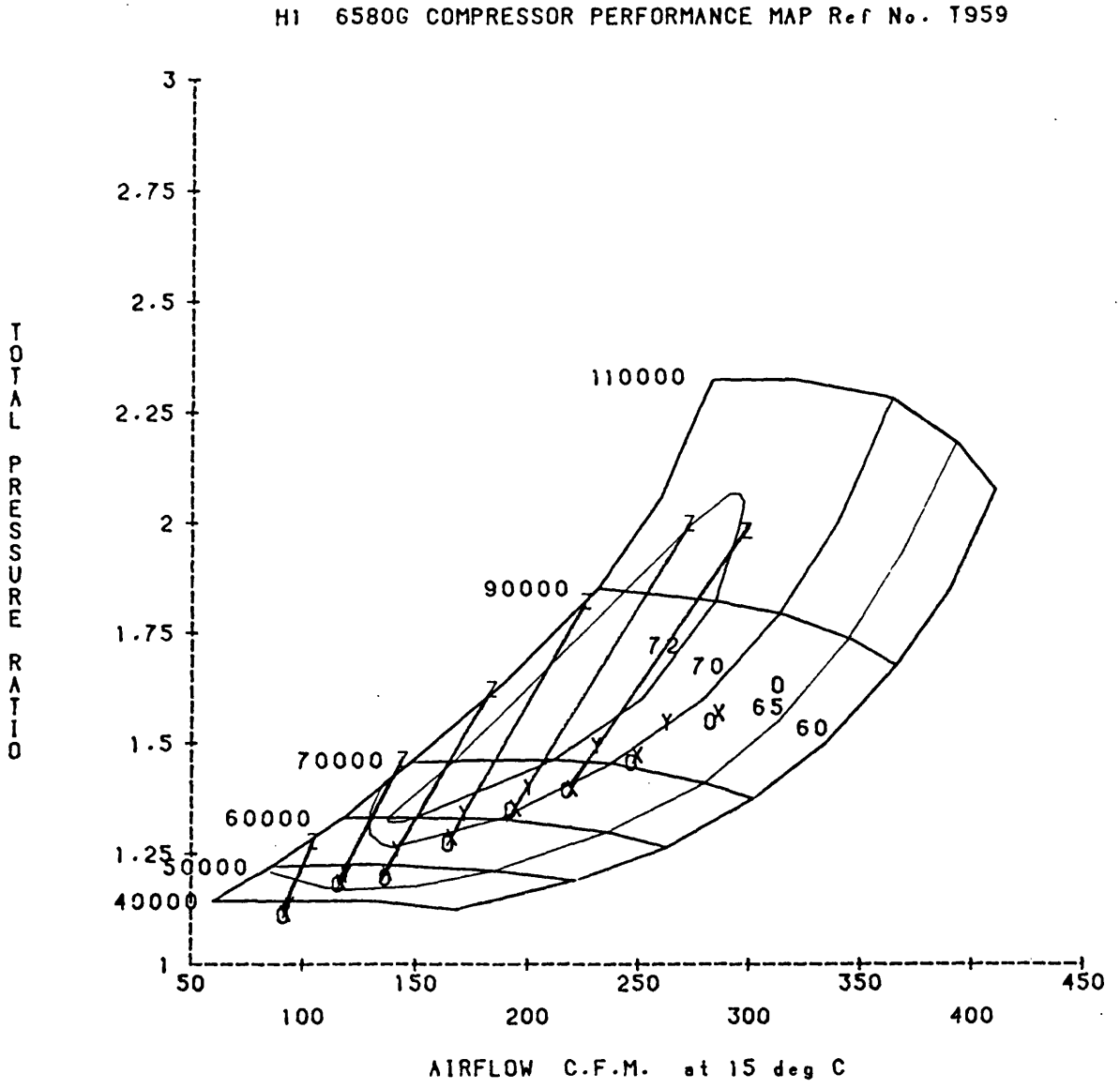

Fig. 3.23e Limiting Torque Variable Geometry Engine Results,

O = 0%, X = 25%, Y = 40% and Z = 50% Restriction.

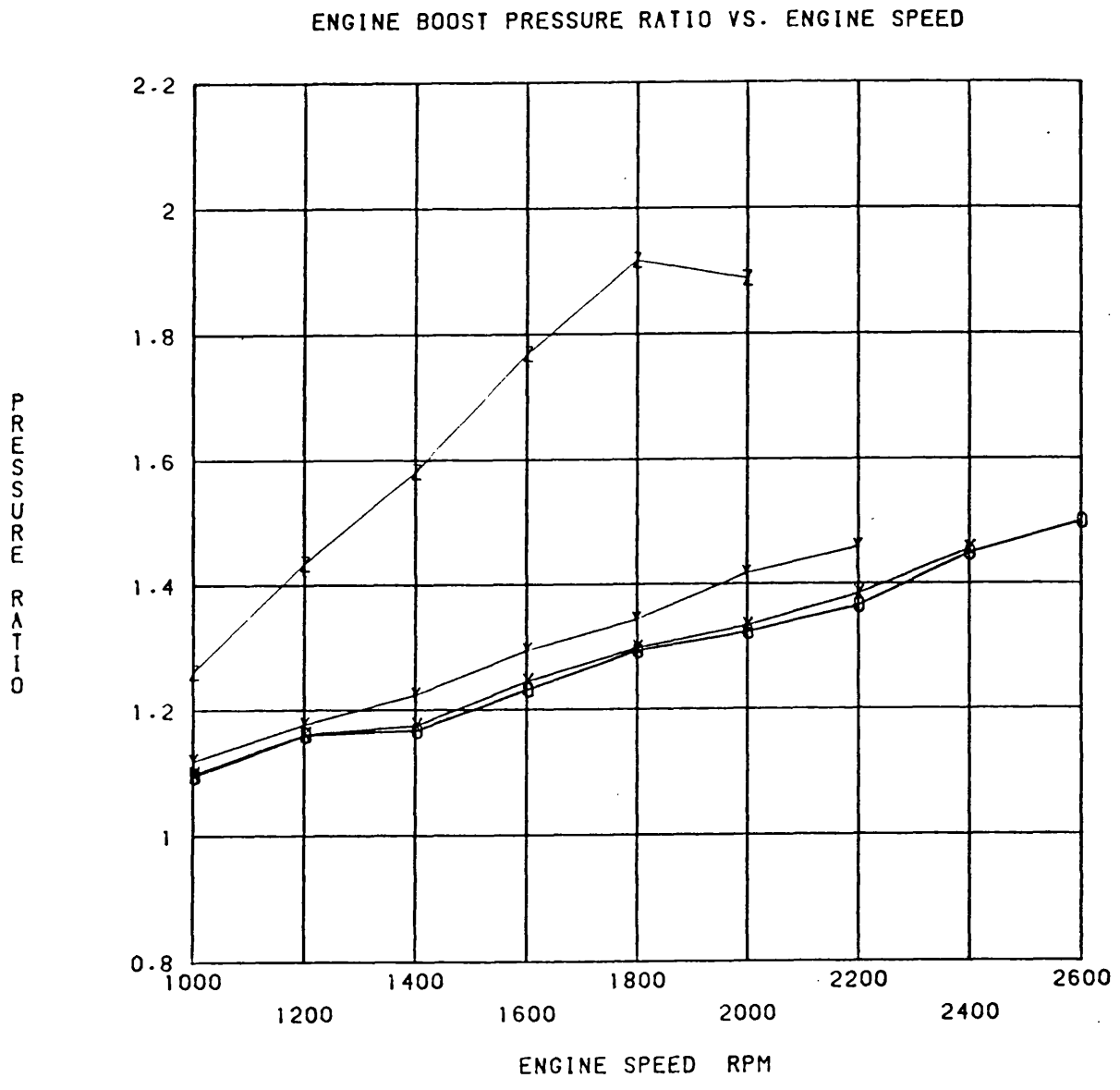

Fig. 3.23f Limiting Torque Variable Geometry Engine Results,

O = 0%, X = 25%, Y = 40% and Z = 50% Restriction.

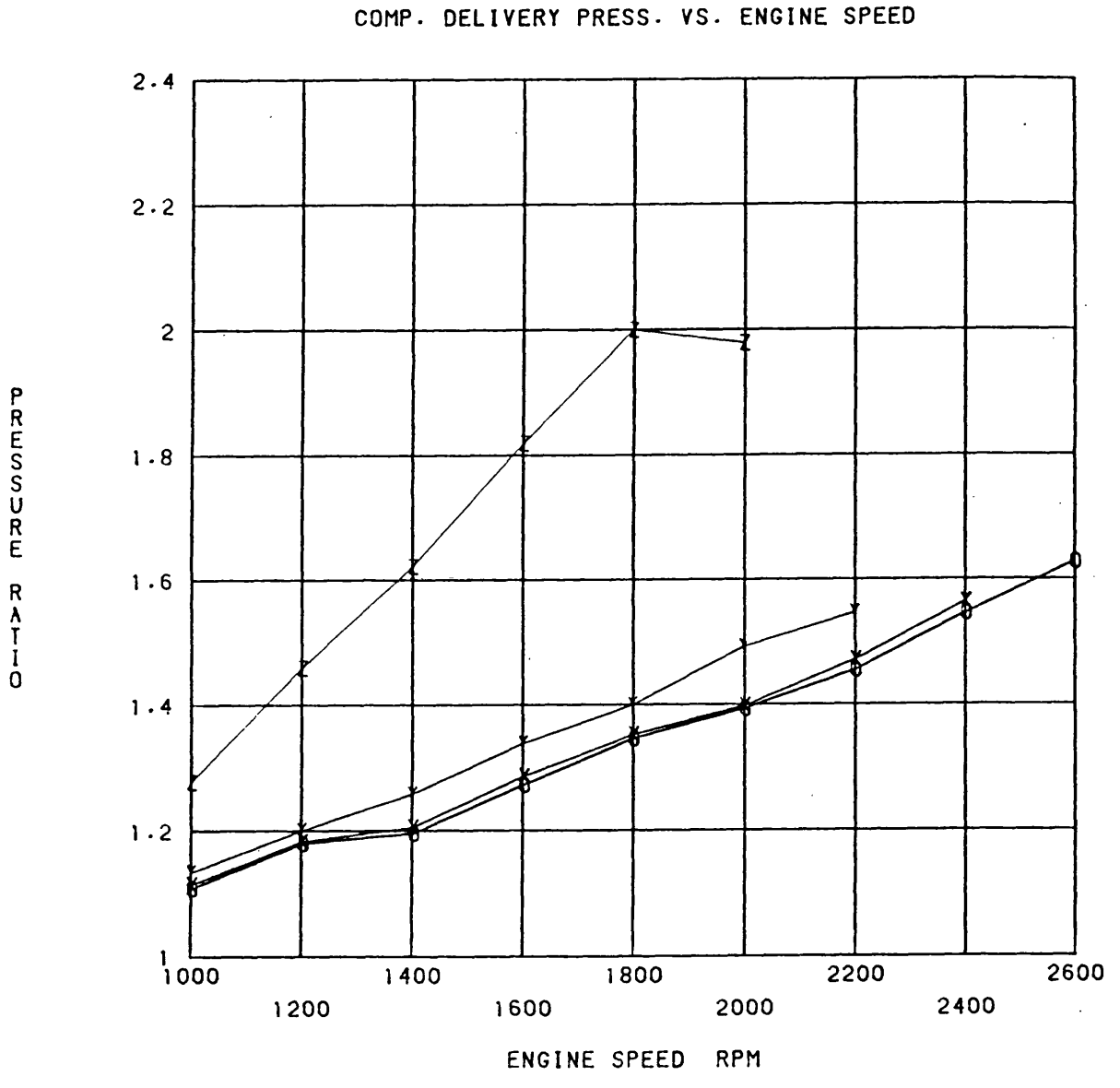

Fig. 3.23g Limiting Torque Variable Geometry Engine Results,

O = 0%, X = 25%, Y = 40% and Z = 50% Restriction.

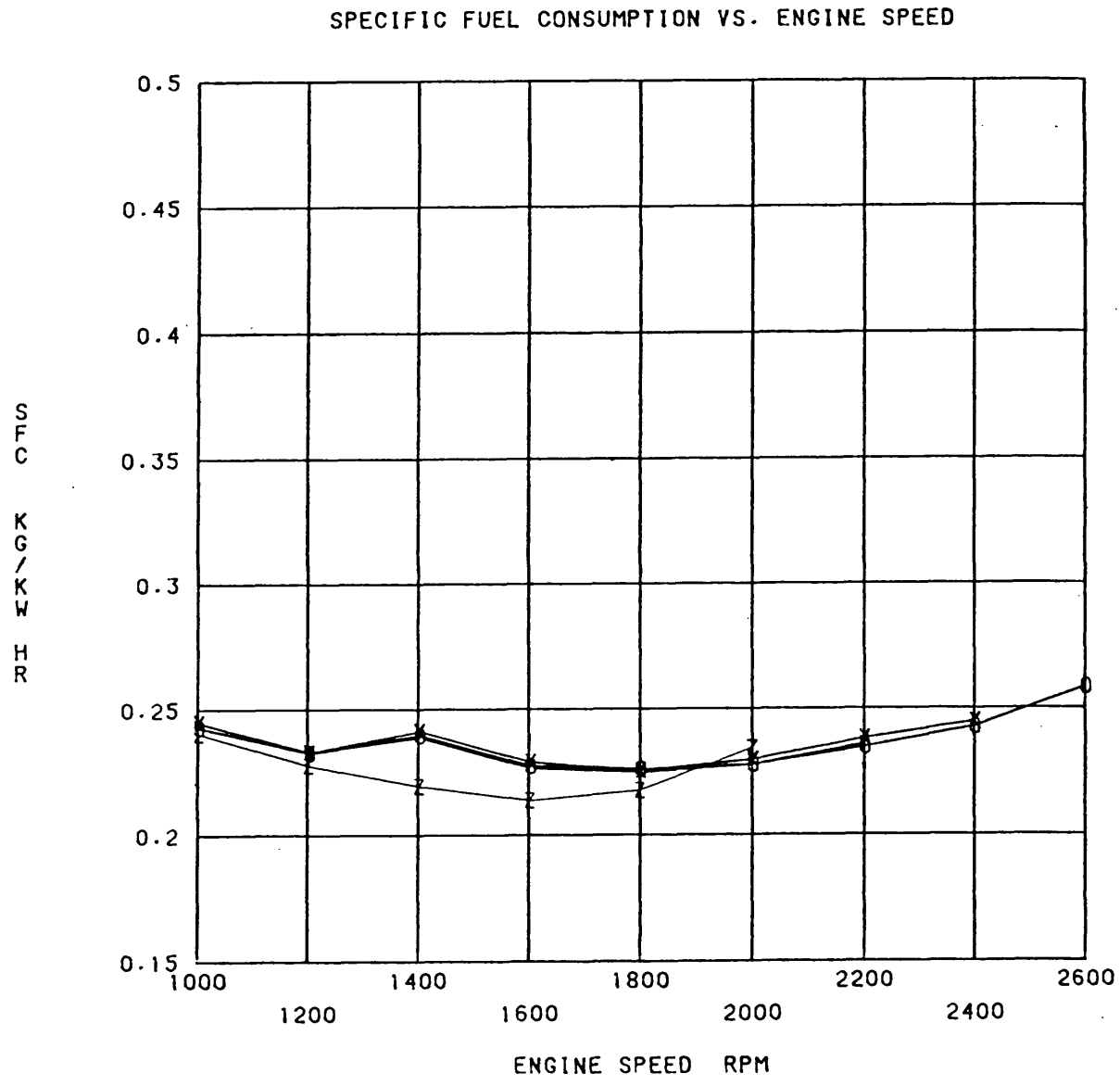

Fig. 3.23h Limiting Torque Variable Geometry Engine Results,

O = 0%, X = 25%, Y = 40% and Z = 50% Restriction.

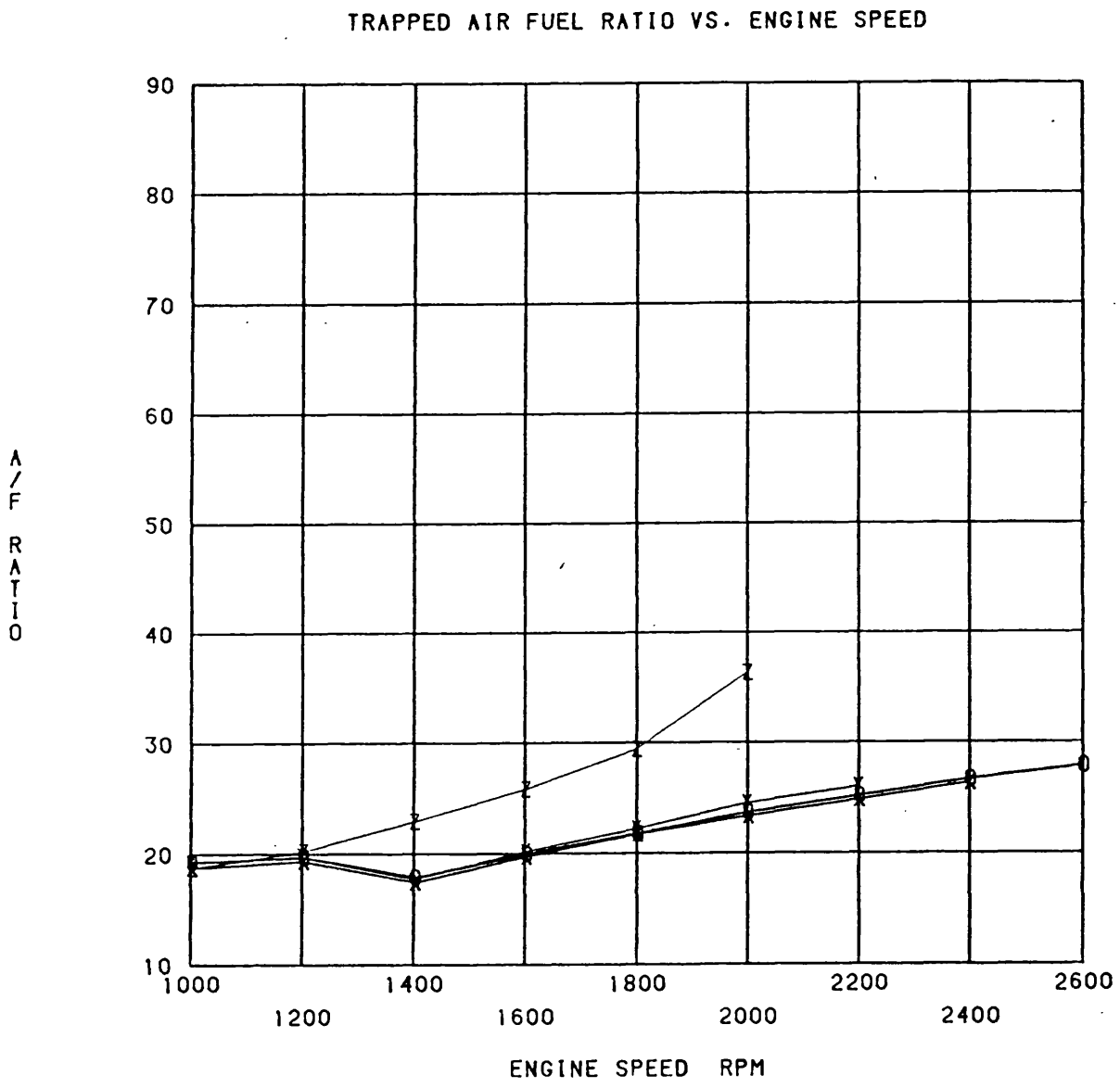

Fig. 3.23i Limiting Torque Variable Geometry Engine Results,

O = 0%, X = 25%, Y = 40% and Z = 50% Restriction.

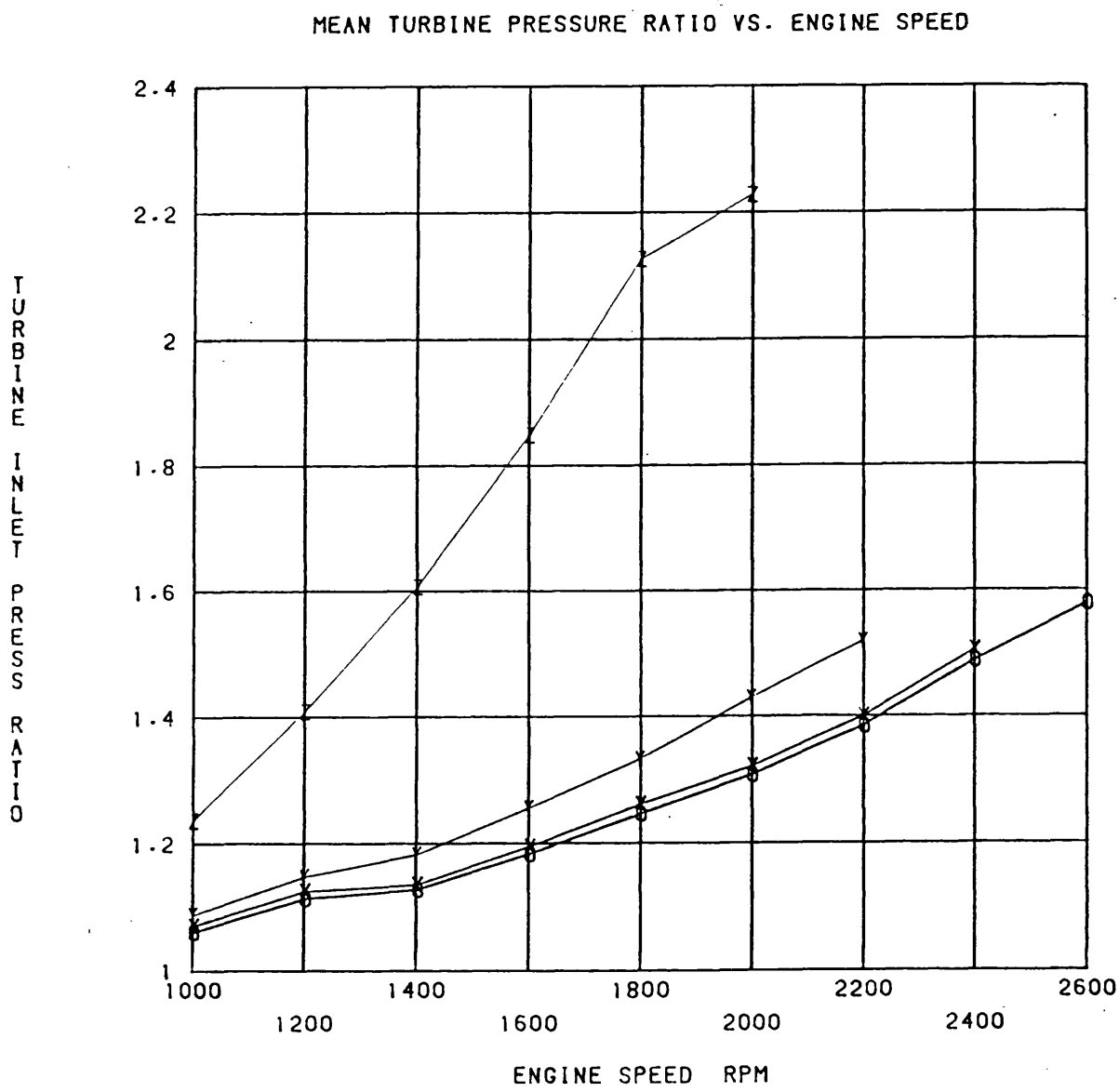

Fig. 3.23j Limiting Torque Variable Geometry Engine Results,

O = 0%, X = 25%, Y = 40% and Z = 50% Restriction.

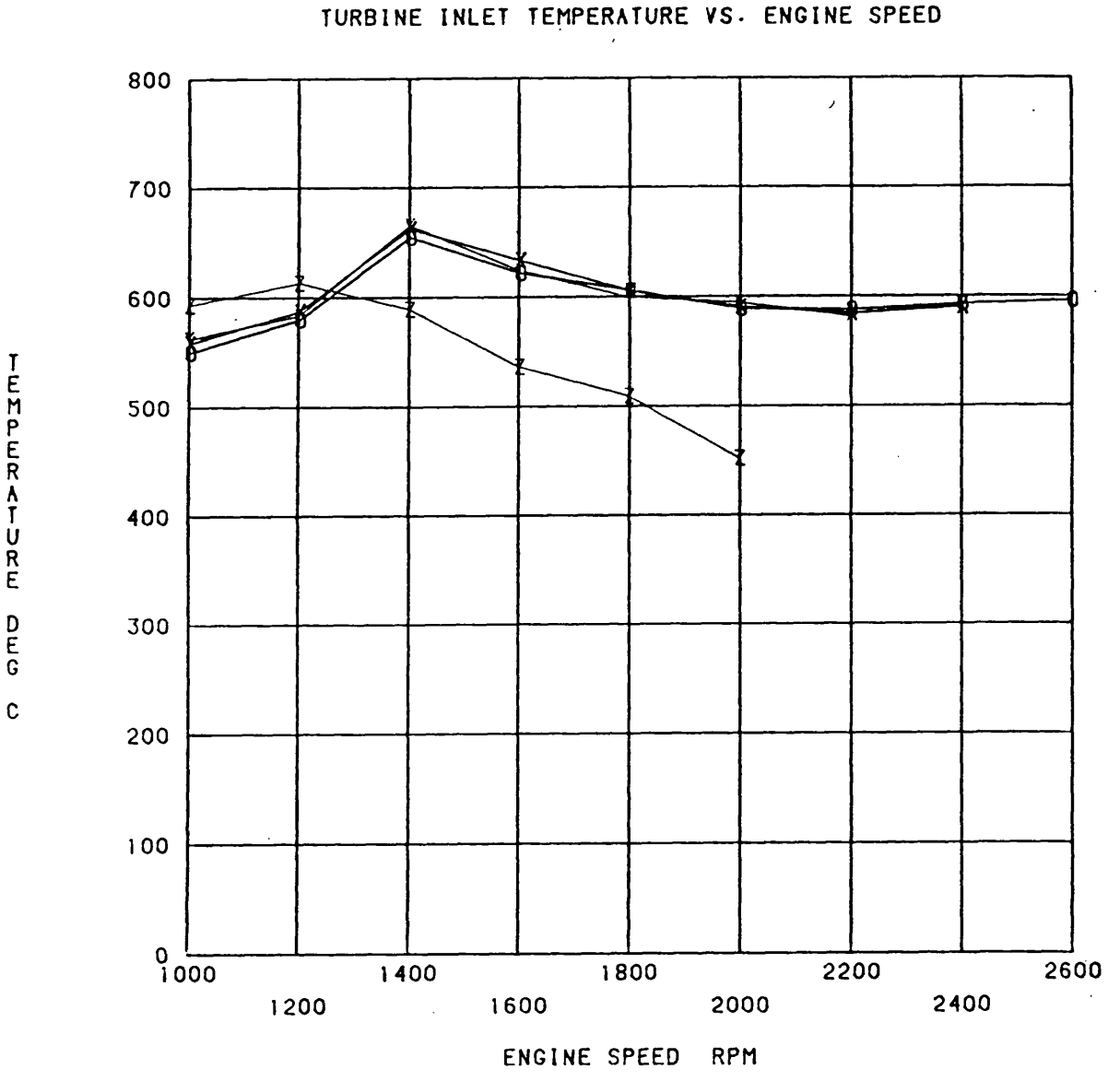

Fig. 3.23k Limiting Torque Variable Geometry Engine Results,

O = 0%, X = 25%, Y = 40% and Z = 50% Restriction.

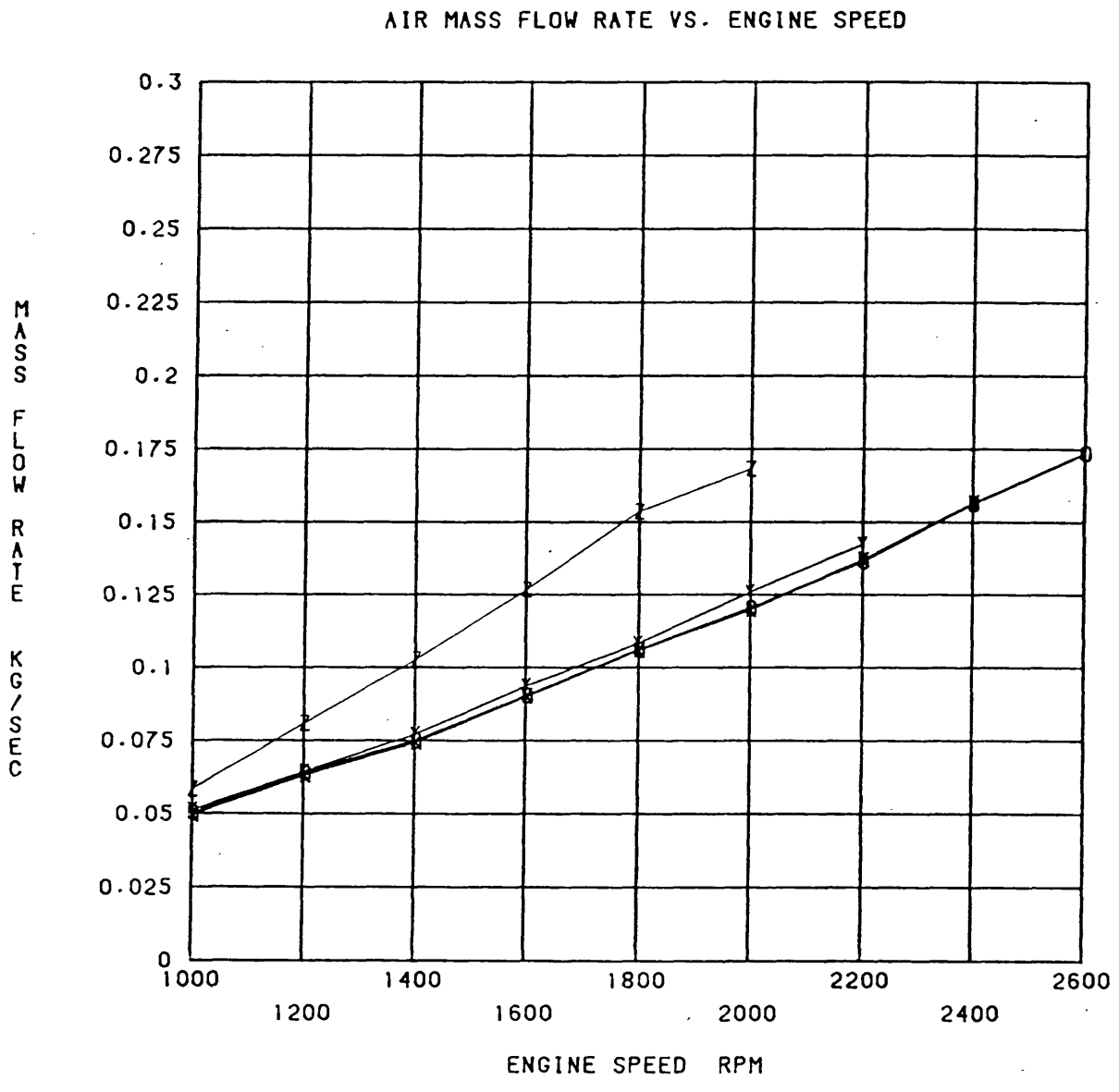

Fig. 3.231 Limiting Torque Variable Geometry Engine Results,

O = 0%, X = 25%, Y = 40% and Z = 50% Restriction.

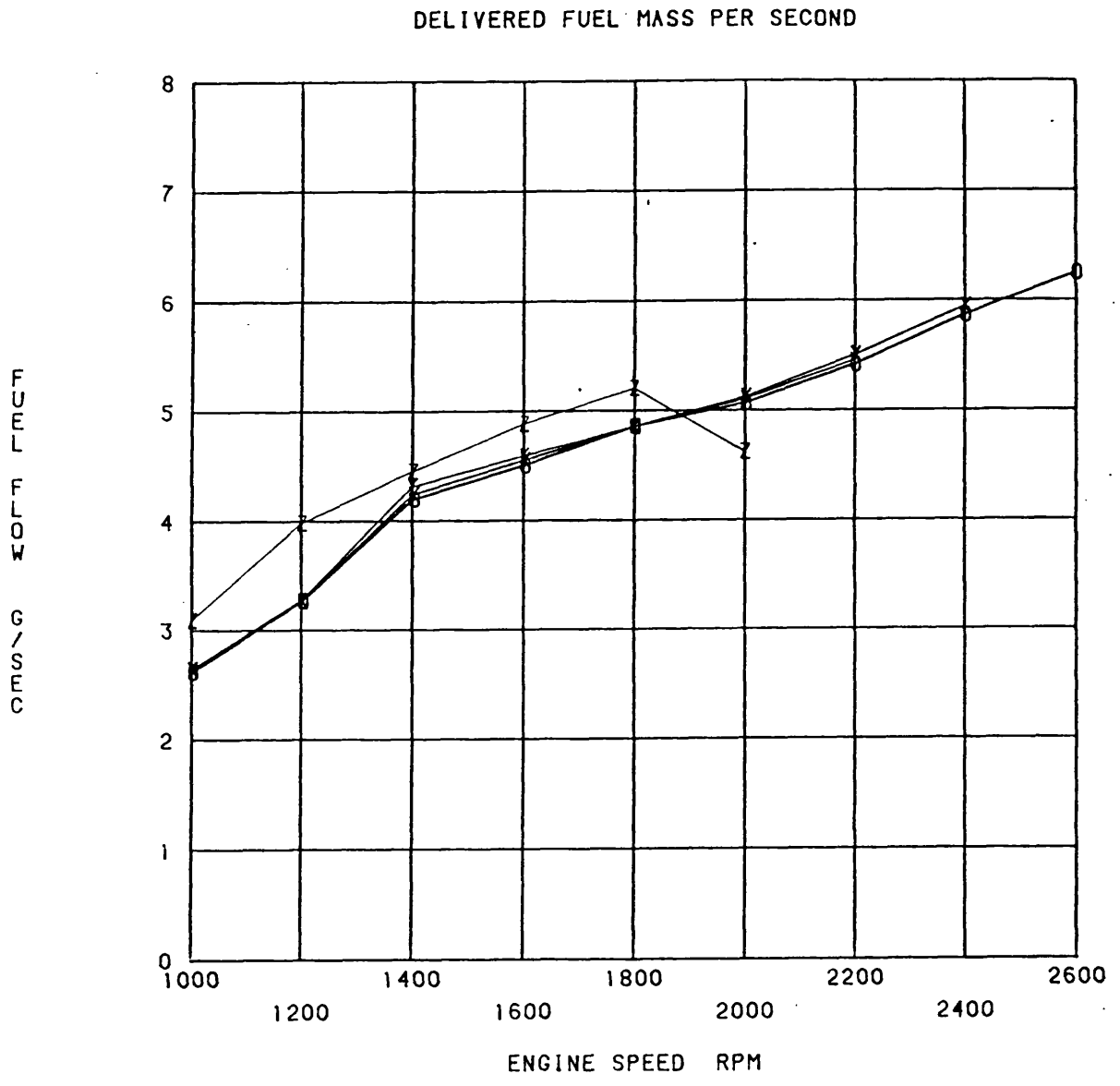

Fig. 3.23m Limiting Torque Variable Geometry Engine Results,

O = 0%, X = 25%, Y = 40% and Z = 50% Restriction.

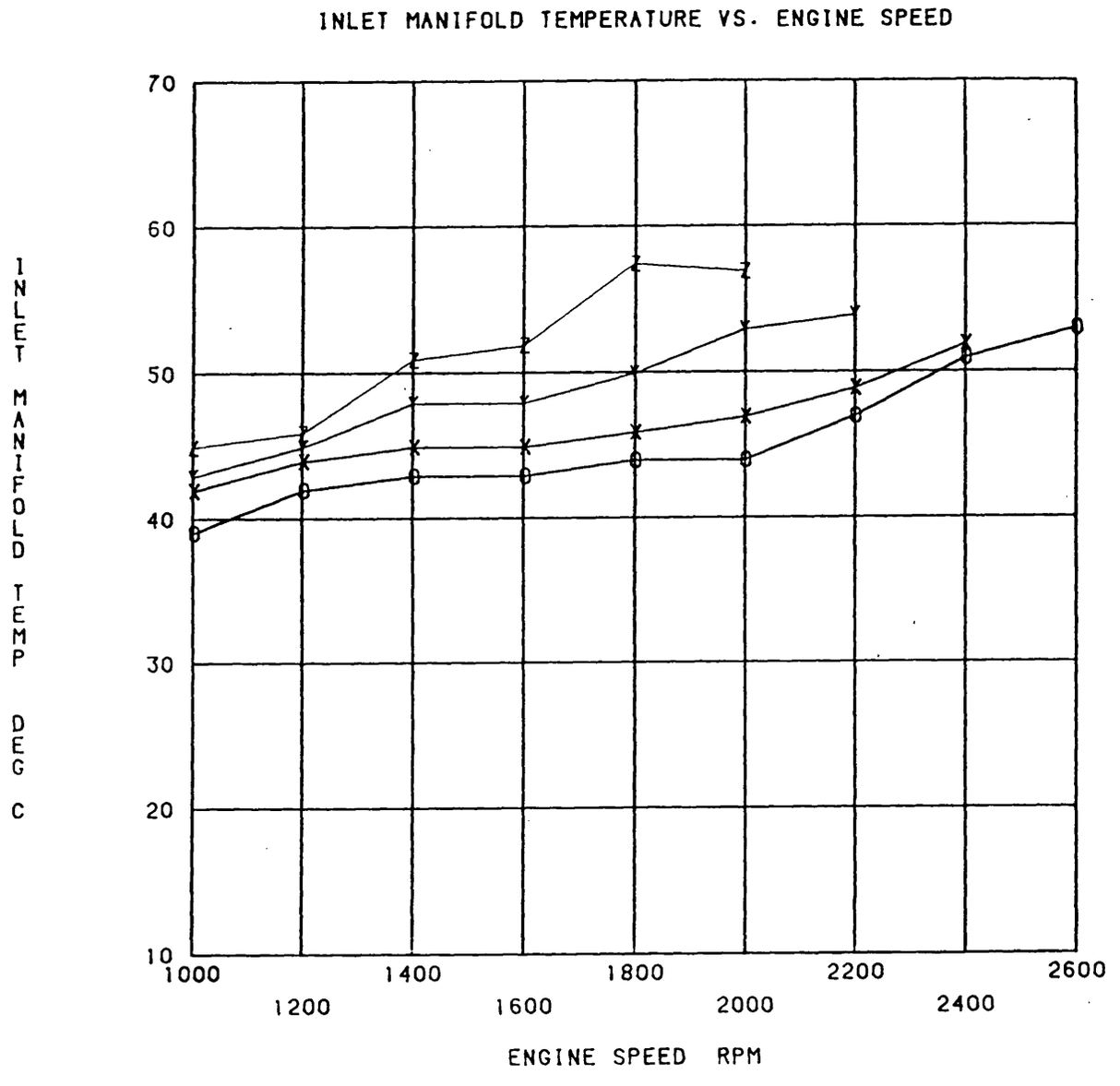

Fig. 3.23n Limiting Torque Variable Geometry Engine Results,

O = 0%, X = 25%, Y = 40% and Z = 50% Restriction.

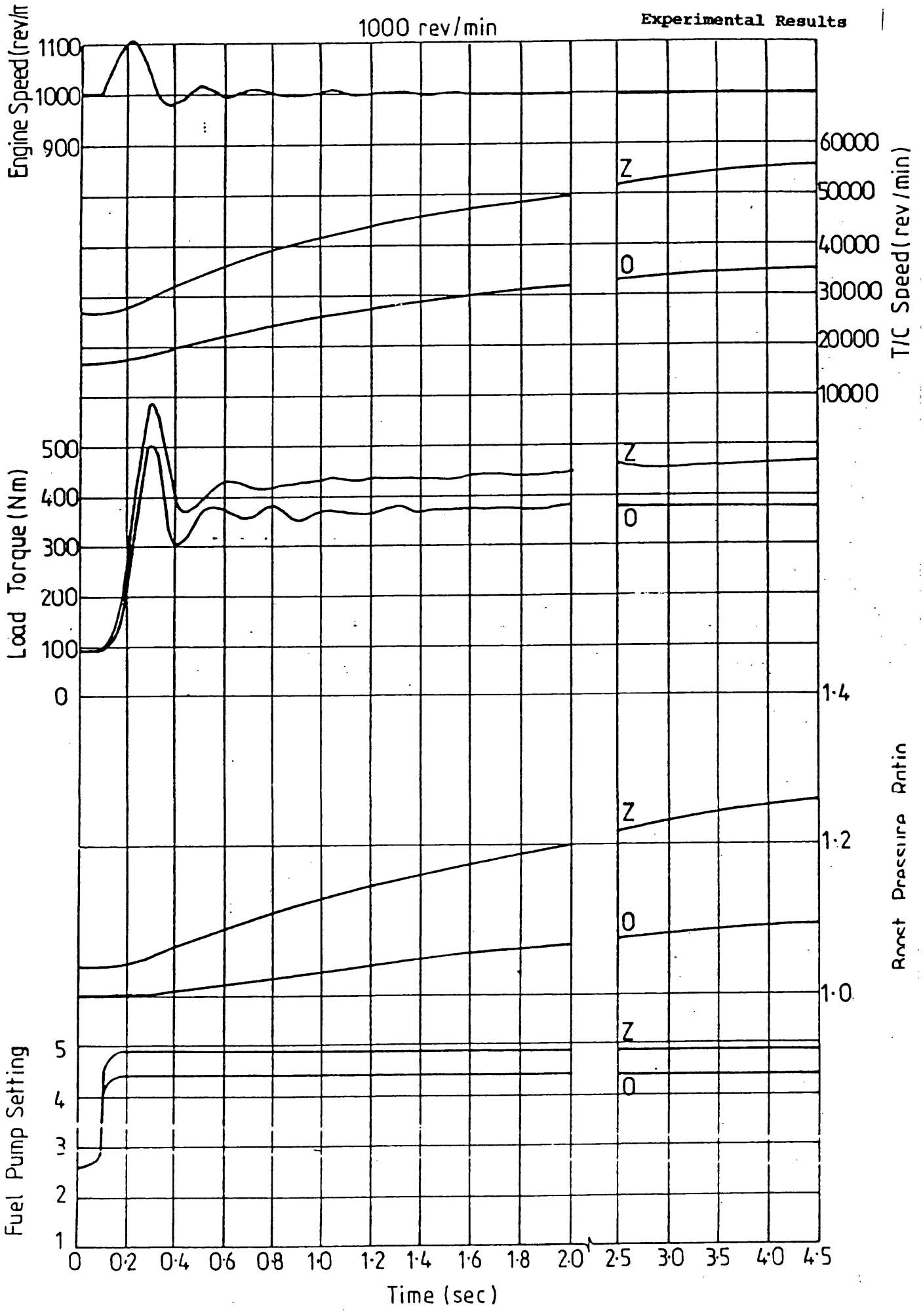

Fig. 3.24 Transient Engine Turbocharger Response With Improved Dynamometer Response,

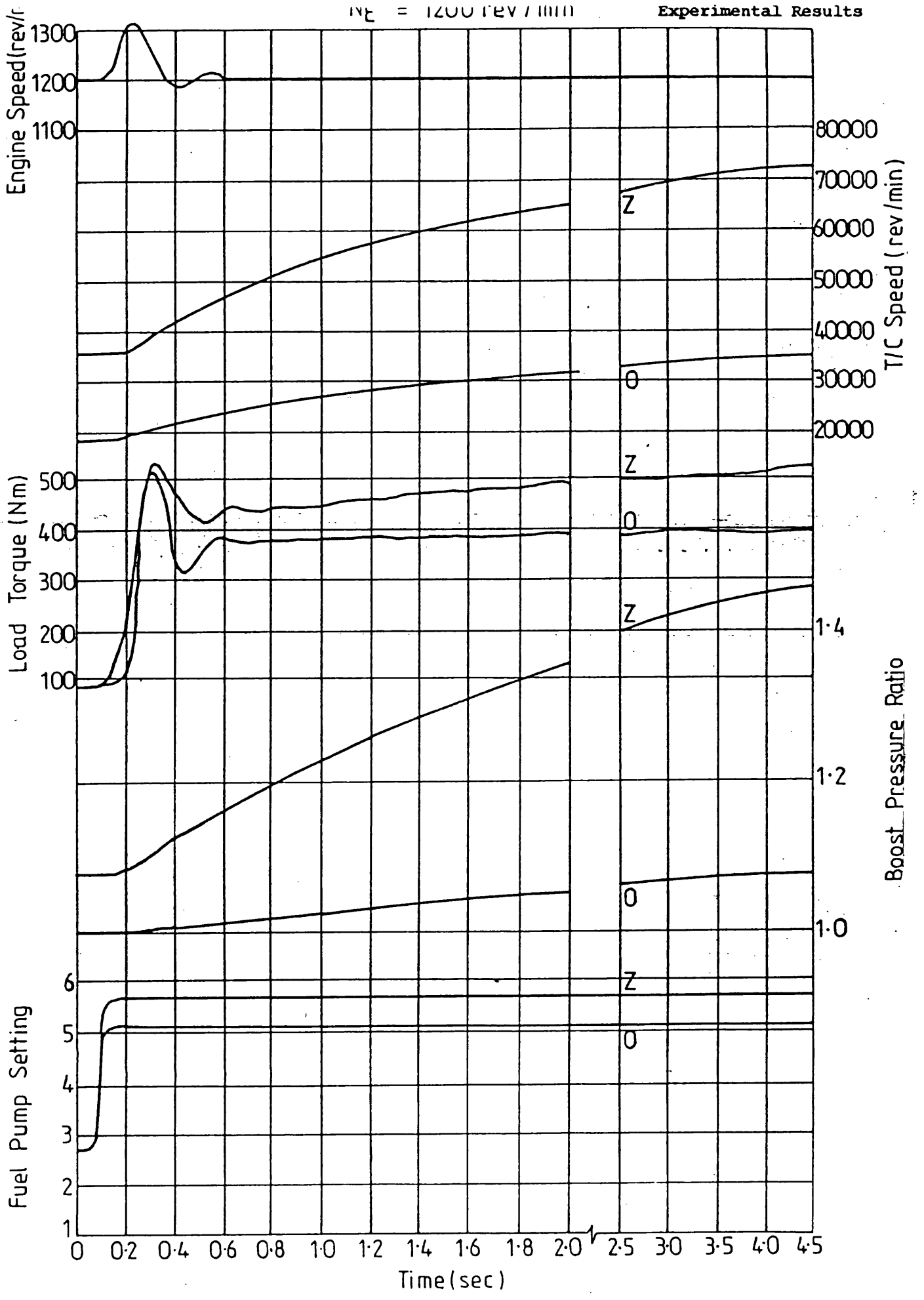

Fig. 3.25 Transient Engine Turbocharger Response With Improved Dynamometer Response, Nominal Engine Speed = 1200 rpm

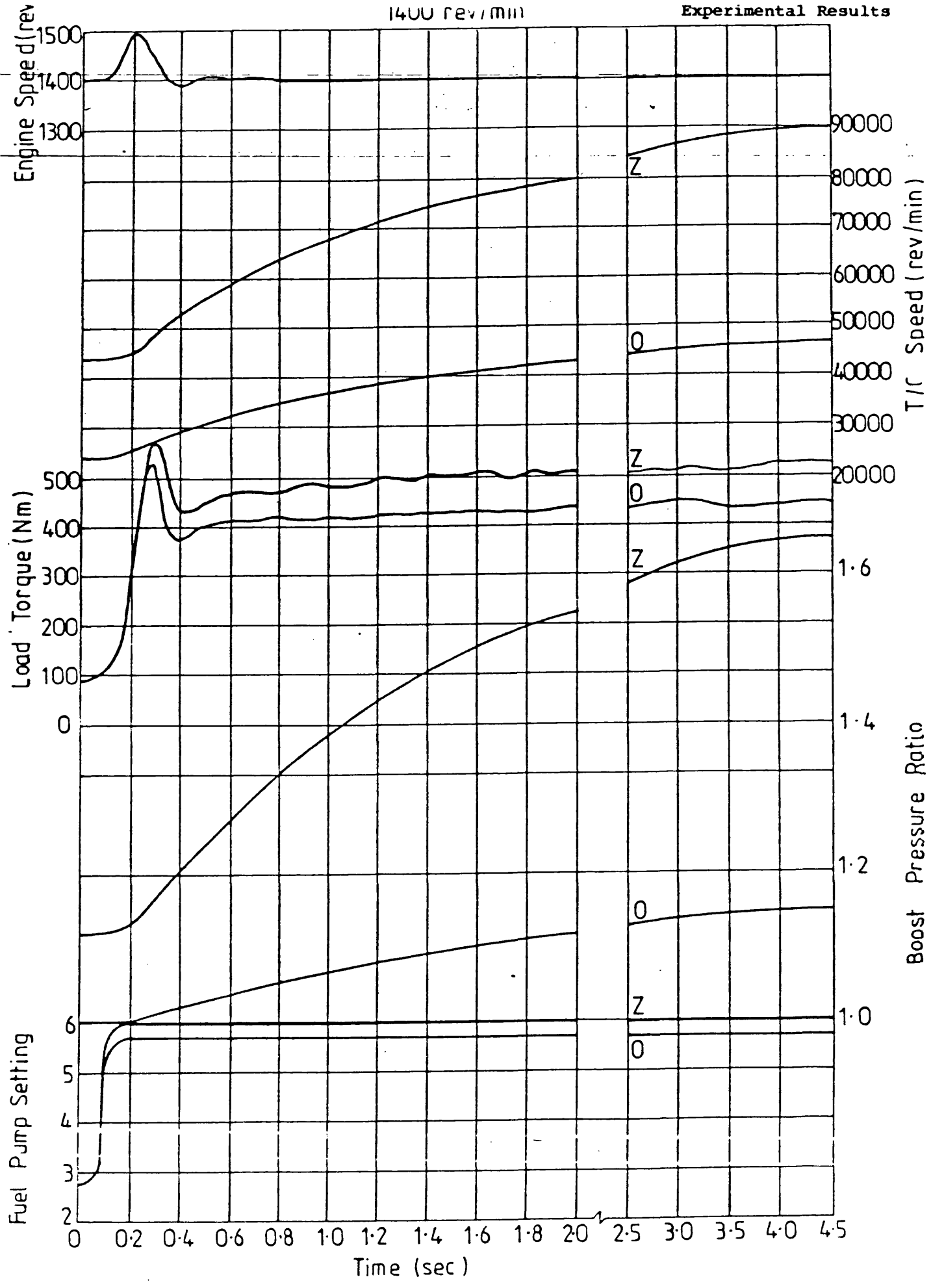

Fig. 3.26 Transient Engine Turbocharger Response With Improved Dynamometer Response,

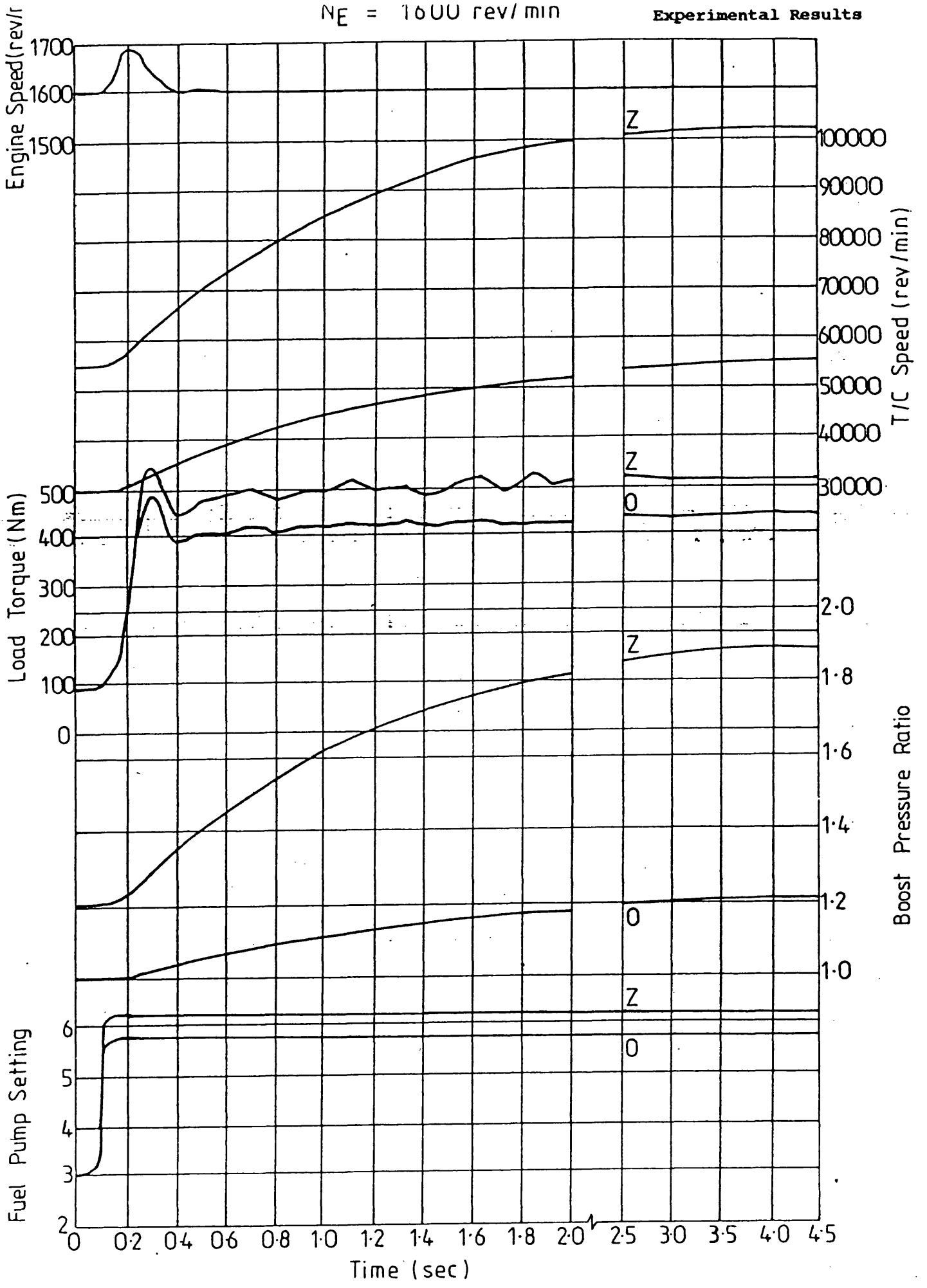

Fig. 3.27 Transient Engine Turbocharger Response With Improved Dynamometer Response,

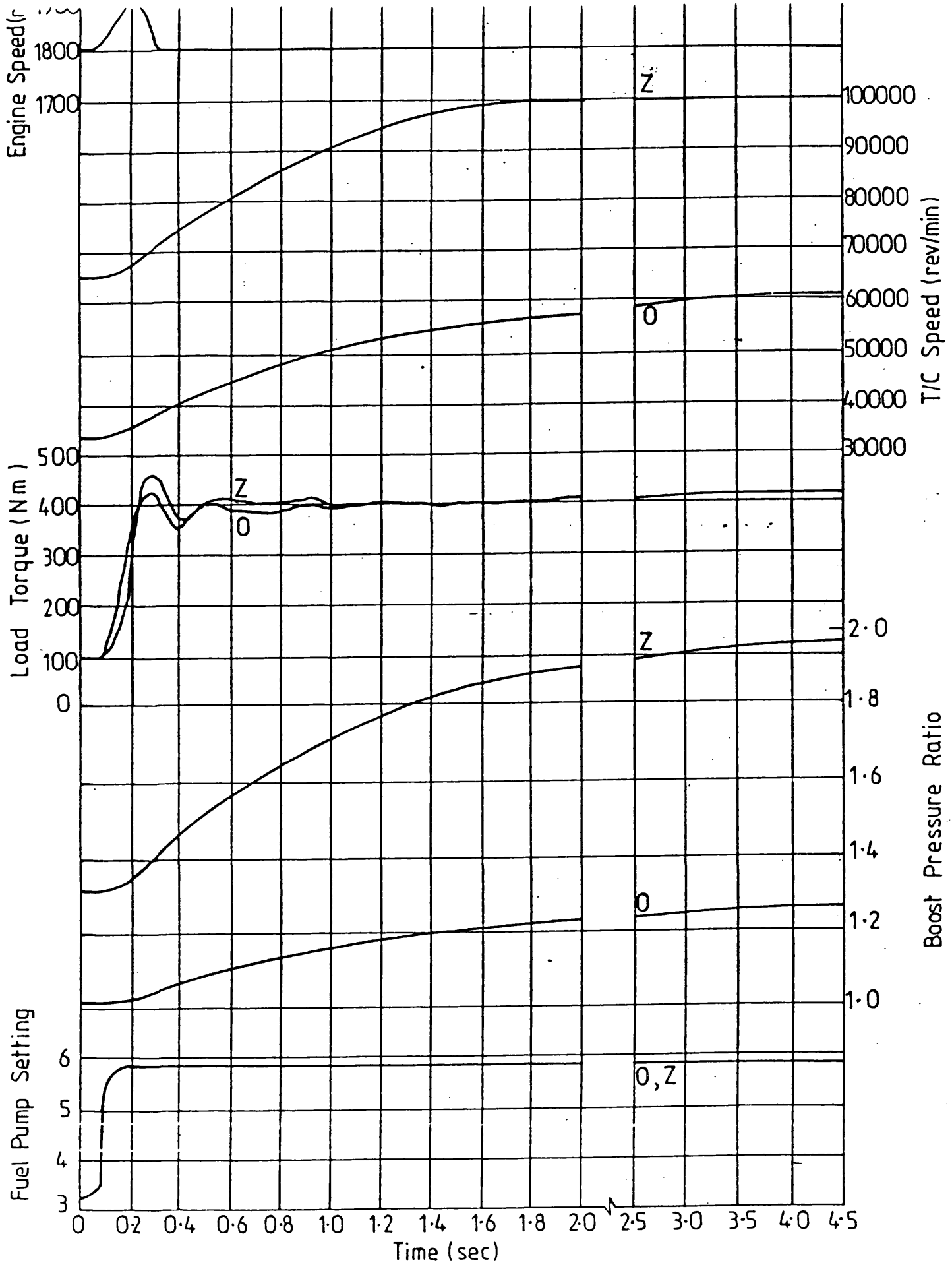

Fig. 3.28 Transient Engine Turbocharger Response With Improved Dynamometer Response, Nominal Engine Speed = 1800 rpm

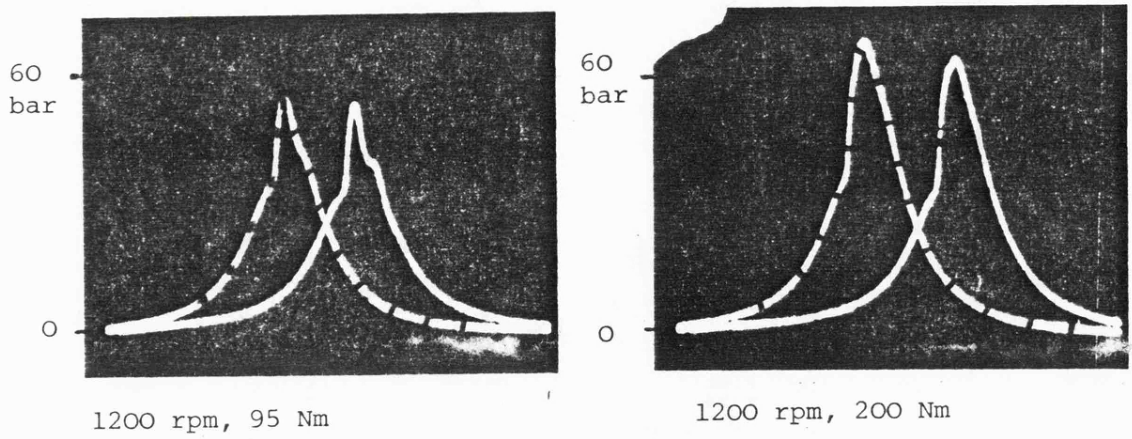

1200 rpm, 95 Nm

1200 rpm, 200 Nm

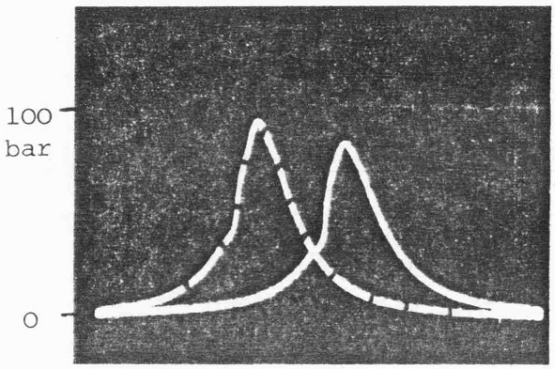

1200 rpm, 340 Nm

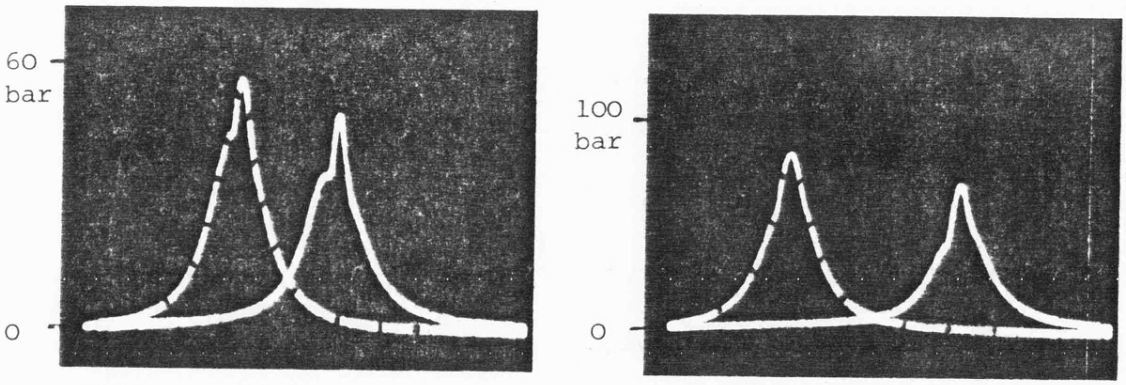

1800 rpm, 90 Nm

1800 rpm, 220 Nm

Solid lines : Fixed geometry

Broken lines: Variable geometry

Fig. 3.29 Effect of variable geometry on peak cylinder pressures for a few typical cases.

4. THEORETICAL INVESTIGATIONS

4.1 Survey of programming techniques and the existing programs

Mathematical modelling of complex physical systems comprising various components is accomplished in two steps. First, components are modelled individually hence creating a number of sub-models. Then, these sub-models are assembled and linked in such a way that for any given set of input data, an equilibrium solution - if physically possible - is found satisfying all the compatibility criteria.

In the turbocharged engine, the compatibility criteria are basically derived from mass flow continuity throughout the system and mechanical energy balance between appropriate components, e.g. the turbine and the compressor of the turbocharger. These, together with individual component sub-models, are incorporated in a main program to represent the whole system.

Two linking techniques are available for use in the main linking program:

1. A sequential iterative method, Fig 4.1

2. A parallel integrative method, Fig 4.2

Sequential iterative procedures involve combination of several 'nested loops' all of which have to be satisfied simultaneously to obtain equilibrium conditions. By contrast, in the second

technique, linking of different components of the system is done by using 'storage models' of either the mass or the energy type leading to a set of differential equations to be solved simultaneously.

4.2 The steady state iterative program, EMAT, Fig 4.3

4.2.1 General

In simulating the steady state operation of a single-stage turbocharged diesel engine iteratively, mass flow continuity throughout the system and power balance between the turbine and the compressor are essential. These will result in steady thermodynamic conditions such as temperature and pressure between every two adjacent components, and the whole system will then be operating in a steady state.

Since it would take prohibitive amounts of computing time to achieve absolute equalities, once the discrepancy is within a stipulated margin, E, steady state conditions are assumed.

This type of program does not necessarily have to employ a load absorption curve. The engine speed and fuel delivery are specified as data which produce a unique value of engine torque. This torque is assumed to be fully absorbed by the load.

In order to satisfy the equilibrium criteria, a compatible set of values of turbocharger speed, compressor mass flow and engine minimum exhaust pressure for a pulse turbocharged model must be achieved. To this end, initially guessed values are supplied as data to enable the program to enter the appropriate subroutines. Since the logical structure of the program is iterative, these three

variables are thus the iteration variables.

4.2.2 Structure of iterative linking technique

Due to the implicit nature of the unknown variables, it is not possible to obtain a matched set of results without iteration. Similarly, without initial guesses it is not possible to enter any of the subroutines representing the physical components. The iteration structure is determined by the requirements of the subroutines in terms of which variables are required as inputs and which as outputs. However, the iteration structure is not unique and other solutions are possible.

The values of the unknowns have to be found such that all the compatibility equations are satisfied. For instance, for a single-stage turbocharged engine, the turbocharger power balance criterion is:

$$E1 = TQt - TQc \qquad 4.1$$

and the mass flow continuity criterion is represented by:

$$E2 = \dot{M}t - (\dot{M}e + \dot{M}f) \qquad 4.2$$

A numerical iteration method is thus employed and for each compatibility criterion an iteration loop is set up which is not necessarily a physical loop but merely an algebraic loop that cannot be resolved explicitly.

In the simulation of the single-stage turbocharged engine turbocharger speed, Wt/c, and compressor mass flow rate, $\dot{M}c$, have been chosen as the two unknown variables in the two 'nested'

iteration loops. For a given simulation run the iterative method is started by making initial estimates for the unknowns and the program then proceeds to find the required equilibrium conditions.

Holding turbocharger speed, i.e. the outer loop variable, constant the inner loop unknown, i.e. compressor mass flow rate, is varied iteratively until the mass flow compatibility is established, (Fig. 4.1). Having satisfied the first compatibility equation, the mathematical procedure enters the outer loop to check the turbocharger torque balance compatibility; if the compressor torque and turbine torque are not balanced, the outer loop unknown i.e. $W_{t/c}$ is varied iteratively until a balanced condition is reached. However, since these loops are inter-related with each other, this disturbs the balance of the first loop; therefore once the outer loop has converged, the inner loop has to be re-entered to check the balance of the mass flow criterion. This process is continued repeatedly until a pair of values for $W_{t/c}$ and $\dot{M}_c$ are found which satisfy both the compatibility criteria. The accuracy of this method improves - if the iteration loops are stable - with each repetition of the operation. The solution is assumed to have been found when two successive approximations of the independent variables of each loop agree to within the allowable error whereby the iteration process is terminated.

As the complexity of the system and consequently the number of compatibility equations is increased, the iterative technique becomes less attractive to use. This is mainly because the number of successive calculations of the nested iteration loops and hence the computation time is increased exponentially with the number of

compatibility criteria.

The program structure is shown in more detail in Fig. 4.3. The use of the compressor subroutine (see section 4.2.3) demands knowledge of compressor speed and mass flow. In terms of these parameters the pressure ratio and efficiency are obtained directly from arrays while other parameters such as torque, power and outlet temperature are calculated from thermodynamic relations. If an after-cooler is used, the cooler subroutine calculates the outlet conditions in terms of the inlet conditions which are identical to the outlet conditions of the compressor if pipe losses are neglected. Therefore, in an iterative scheme the cooler subroutine can always follow the compressor subroutine directly with no need for any additional considerations.

The compressor flow is matched to the engine flow by means of the delivery ratio which is given as data as a function of engine speed and the ratio of mean exhaust pressure to inlet manifold pressure. The engine and compressor cannot be matched without a value for the mean exhaust pressure which can only be obtained by reference to the turbine flow characteristics. At this stage, however, the initial guess for mean exhaust pressure is used. As soon as the delivery ratio criterion is satisfied the engine subroutine can be entered. From the matching point of view the principal purpose of the engine subroutine is to provide the exhaust conditions. Other parameters such as power or fuel consumption are not involved in the matching of the components but are only required when the final solution is obtained.

The turbine subroutine requires as input, values of turbine speed, inlet pressure ratio and inlet temperature. From these and the turbine geometry the flow, efficiency and power are calculated. In this program the use of the turbine subroutine is complicated by the exhaust pulse model by which turbine inlet conditions are represented by five values of pressure ratio corresponding to different stages of the pulse. Thus the iterations are continued until turbine flow is equal to engine flow and the turbine power is equal to the compressor power.

4.2.3 Component models

The following sub-systems which are called in the main linking program, are represented by subroutines to describe the complete mathematical model of the turbocharged diesel engine.

1) the compressor

2) the charge cooler

3) the engine

4) the turbine.

In addition to these sub-models, there are other mathematical routines which represent various aspects of the system or processes associated with it. As these numerical and/or analytical routines are required many times in various parts of the simulation model, they are programmed as separate subroutines:

1) gas property calculations

2) numerical interpolation

3) numerical iteration

etc.

These subroutines have been in existence for a number of years and have not been modified in any significant way for the purpose of the present work.

4.2.3.1 Engine

In view of the prohibitive amounts of computing time associated with the step-by-step method of engine cycle analysis, especially in calculations of a repetitive nature, a cycle based on the modified form of the classical five-point P-V cycle has frequently been adopted, Fig. 4.4. Despite its oversimplifications, it has been commonly used for engine simulations and is normally modified by the inclusion of some empirical factor such as 'diagram efficiency' to produce acceptable results.

The present model, Fig. 4.4c, which includes provision for the most important features of the combustion process, gas property changes, heat transfer on simple aggregate basis, throttling losses through the valves etc. is thought to be a more representative model of the engine.

i) Closed period

The closed period is divided into the following distinct regions:

a) isentropic compression 1-2

b) constant volume combustion 2-3

c) constant pressure combustion 3-4

d) variable pressure combustion 4-5

e) isentropic expansion 5-6

Before the start of the cycle, the trapped conditions are estimated assuming that 39% of the energy released by the fuel during the 'previous' cycle is retained by the exhaust gases. This leads to an estimate for the exhaust temperature and density. Thus scavenge flow and scavenge efficiency is found using incompressible flow assumptions. Thus the amount of fresh air trapped in the cylinder at the beginning of the compression stroke is obtained. Compression and expansion strokes are assumed to take place isentropically.

The combustion process is greatly simplified by the assumption of the 'single - zone' model where the composition and state of the gases are assumed to be uniform throughout the cylinder. Instead of other more exact methods, the Whitehouse-Way formulation for combustion rate calculations, in which this rate depends upon the difference between the mass of fuel injected into the cylinder, and the mass prepared for burning, (42, 52), is adopted in the model as follows:

$$d(Mf)/d\theta = k.(Mfinj - Mf) \qquad 4.3$$

where Mf = mass of fuel prepared, i.e. ready for burning

Mfinj = mass of fuel injected

k = rate constant for fuel preparation

Combustion occurs at 'constant volume' (2-3 in Fig. 4.4c) which is assumed to occupy the period 5 deg. BTDC to 5 deg. ATDC, followed by a constant pressure phase 3-4 and finally a linear constant slope phase 4-5, such that the slope exactly matches the initial slope of the expansion curve 5-6.

The effective heat release is obtained by deducting the aggregate heat loss to coolant from the fuel heat release. The heat loss is obtained from empirical correlations appropriate to particular engines in order to avoid the need for time consuming step-by-step calculations (1, 18). An example of this is:

$$Hc = Kq.(Vs.Ncyl)^{0.6}.(\dot{M}e)^{0.4}.(1.13\dot{T}m - 21000/Rt - Tw) \qquad 4.4$$

This empirical equation assumes that the heat transfer coefficient is mainly a function of airflow and a mean temperature difference which is largely dependent on the air to fuel ratio but also affected by inlet manifold temperature and water temperature.

Equation 4.4 is not strictly dimensionless, so the constant kq will have a value dependent upon the units used and also to a small extent on the type of the engine.

Finally, calculation of the adiabatic expansion process 5-6 following completion of the combustion process 2-3-4-5 enables the release conditions p6, T6 to be determined.

ii) Open period

The mathematical representation of gas flow processes in the inlet and exhaust manifolds and through the associated valves presents

severe problems due to the unsteady nature of the flow and the complexity of wave action in the manifolds.

The flow through valves is widely treated on the basis of steady-state flow assumptions and the wave action is modelled by the use of numerical techniques. Generally, two methods are employed, viz.:

1) method of characteristics

2) 'filling and emptying' technique.

In the first method, the unsteady flow problem is solved by employing a numerical technique to analyse the 'wave characteristics diagram' which represents the superimposition of positive and negative waves in the exhaust manifold. In the second approach, the manifolds are treated as control volumes for each of which the energy and mass continuity equations are solved with varying gas conditions and simultaneous charging and discharging processes.

Since the method of characteristics requires detailed information of the engine cycle processes, and necessitates very large programs, for the purpose of the present investigations, a model based on the filling and emptying method is used to represent the flow processes in the exhaust and inlet manifolds.

The open period is divided into the following phases:

a) blowdown 6-7

b) exhaust 7-8

c) overlap 8-9

d) suction 9-10

e) 'supercharge' 10-1

The approximations involved in this treatment are the assumptions of constant mean valve areas and constant mean inlet and exhaust manifold pressures Pim and Pem. It is then possible to arrive at estimates of the cylinder pressure P7 = P8 during exhaust and P9 = P10 during suction, as well as of the scavenge air mass flow msc during the overlap period. The method gives consistent and reliable estimates of positive or negative loop work and of delivery ratio.

Completion of the open period calculations finally yields new values for the trapped conditions P1, T1 and a rapid overall iteration then enables the cycle condition to be fully established in terms of the estimated inlet manifold conditions Pim, Tim and the estimated mean exhaust pressure Pem.

4.2.3.2 Compressor

Although performance prediction programs for centrifugal or mixed flow type compressors are available (55), they are nevertheless too cumbersome for incorporation in matching programs. Instead multidimensional numerical arrays are used to represent given characteristics of the form of Fig. 4.5. Since any operating point on the map can be defined by the speed and mass flow values of that point, it is possible to find the corresponding values of efficiency and pressure ratio for any given values of speed and mass flow. Therefore, the mass flow axis is divided into a number of equally-spaced points for each of which the corresponding values of pressure ratio and efficiency at different speeds, are obtained from

the map. The use of a two-dimensional linear interpolation routine then enables the values of pressure ratio and efficiency to be determined for any operating point specified by its mass flow rate and speed.

The outlet temperature is then calculated from:

$$T2 = T1.[1 + (Rc^{\frac{\gamma-1}{\gamma}} - 1)/\eta c] \qquad 4.5$$

compressor power is given by:

$$CP = \dot{M}c.Cp.T1.[(Rc^{\frac{\gamma-1}{\gamma}} - 1)/\eta c] \qquad 4.6$$

and the compressor torque is calculated from:

$$Ct = CP/Cs \qquad 4.7$$

4.2.3.3 Turbine

Two alternative analytical turbine subroutines are available either of which can be used in the matching programs. The modelling has been approached by the application of the one-dimensional quasi-steady flow treatment in which the steady flow characteristics of the turbine are assumed to hold over suitably chosen small time intervals during the non-steady flow through the turbine. In effect, all performance parameters such as mass flow, power, efficiency etc. are calculated on the basis of the steady-state performance characteristics.

The first of these two models is based on the one-dimensional analysis for design and off-design performance of a radial turbine developed by Wallace (40, 41). Briefly, the theoretical assessment

of flow is based on non-isentropic expansions both in the nozzle and the rotor passages, while the power developed is derived from the momentum equation. To establish the magnitude and direction of the relative velocities in the stator-rotor interspace and rotor exit, an iteration routine is employed to find a compatible pressure distribution between stator and rotor.

The following losses are included in the model:

a) rotor exit loss

b) irreversibility loss designated by a polytropic loss factor

Finally to extend the analysis to the prediction of off-design conditions, the model also includes the incidence losses caused by the irreversible deflection of the gas at the rotor blade tips.

The second and more recent model is based on a unified approach where four expressions of continuity, energy, momentum and entropy are combined into a single equation of dimensionless groups of the form:

$$\dot{M}\sqrt{R.TOx}/Ay.POx\sqrt{\gamma} = f(My, \text{ state at } x, \text{ geometry}) \qquad 4.8$$

where x and y refer to inlet and exit conditions, respectively (39). The parameters in this expression are modified according to the nature of the component being modelled; namely rotating or stationary, and whether the flow is guided by vanes or blades or unguided.

This one-dimensional analysis includes a more sophisticated incidence model to account for flow deflection losses at the rotor

entry. All other known losses are accounted for by incorporation of semi-empirical expressions where analytical expressions are not available. Various loss factors are also available for final adjustments in order to match the routine to the particular build of turbine. Finally, these models are capable of simulating nozzled or nozzleless turbines with or without provisions for variable geometry.

4.2.3.4 Charge air cooler

The degree of cooling effect to which a heat exchanger can reduce the temperature is defined by its effectiveness incorporating a mean coolant temperature, Tcl:

$$e = (Tin - Tout)/(Tin - Tcl) \qquad 4.9$$

Therefore, for the air-to-water charge cooler used here, the charge cooler outlet temperature can be obtained from:

$$Tout = Tin - e.(Tin - Tcl) \qquad 4.10$$

The outlet pressure of the charge cooler is calculated from:

$$Pout = Pin - \Delta Pc \qquad 4.11$$

The values of cooler effectiveness and pressure drop are both functions of air mass flow. Hence, in the present charge air cooler model, the variation of cooler pressure drop and effectiveness based on experimental work carried out by previous workers have been used, Figs. 3.11 and 3.12.

4.2.3.5 Exhaust pulse model

Four distinct phases are normally associated with the discharge of cylinder contents into the exhaust manifold. At the moment of exhaust valve opening, the initial blowdown flow may become choked with sonic velocity at the minimum section. As the cylinder pressure falls, the blowdown flow becomes subsonic. Thirdly, after BDC the cylinder pressure gradually approaches exhaust manifold pressure. Finally, during the scavenging process, the cylinder pressure tends to rise to inlet manifold pressure.

In the present simulation studies, a simple version of the filling and emptying technique in conjunction with the modified 5-point engine cycle calculations is employed. The model treats the exhaust manifold as a single mass receiver of finite volume. In the case of a six cylinder engine, six pressure pulses, all of 120 deg. duration, are discharged from the cylinders into the exhaust manifold in every engine cycle, i.e. 720 deg. CA, Fig. 4.6. The model is based on neglecting divided manifolds and assuming that each cylinder discharges instantaneously into the exhaust manifold without allowance for interaction between pressure waves from other cylinders. On the other hand, volume changes in the cylinder connected to the manifold over any 120 deg. period are taken into account.

The state of the cylinder contents at release is known from engine cycle calculations (point 6 of the engine cycle). As the gas discharge process is instantaneous, the pressure, temperature and mass content of the exhaust manifold also increase instantaneously. To calculate the peak pressure, temperature and mass content of the exhaust manifold at the beginning of the pressure pulse, it is

assumed that the mixing process of the cylinder and the manifold gases can be treated as mixing of perfect gases under ideal adiabatic conditions. Considering the commencement of the pressure pulse from a cylinder (cylinder 1, Fig. 4.6), it is evident that there is another cylinder (cylinder 2) which has almost completed its pressure pulse discharge. It is assumed that the total mass content of the exhaust manifold is the sum of the mass content of cylinders 1 and 2, and the exhaust system viz:

$$M'ex = Mc1 + Mc2 + Mex \qquad 4.12$$

where

$$Mc1 = P6.V6/R.T6 \qquad 4.13$$

and the mass content of cylinder 2 is obtained at conditions related to the end of the exhaust release process of the engine cycle, therefore

$$Mc2 = Pex.Vc2/R.Tex \qquad 4.14$$

where Vc2 is the cylinder volume at EVO+120 deg. CA and Pex is the estimated value of exhaust minimum pressure used in the iteration process. Also

$$Mex = Pex.Vex/R.Tex \qquad 4.15$$

The exhaust peak temperature at the beginning of a pulse can be obtained by applying the energy equation for a closed system, viz:

$$T'ex = (Mc1.T6 + (Mc2 + Mex).Tex)/(Mc1 + Mc2 + Mex) \qquad 4.16$$

Perfect gas assumption leads to the peak pressure of the pulse given by:

$$P'ex = M'ex.R.T'ex/V'ex \qquad 4.17$$

where

$$V'ex = Vex + Vc2 + V6 \qquad 4.18$$

Following attainment of peak pressure and temperature (equations 4.16 and 4.17), the exhaust manifold is allowed to discharge into the turbine in a series of equally-spaced time steps. This process is accomplished within five steps for every 120 deg. CA and the length of each step is given by:

$$\Delta t = 20/5.es \qquad 4.19$$

At the end of first step, the exhaust manifold mass contents can be calculated (for the next step) as follows:

$$M''ex = M'ex - (\dot{M}t)step.\Delta t \qquad 4.20$$

The manifold pressure and temperature at the end of the step is obtained assuming isentropic processes:

$$P''ex = Pex^{1-\gamma}.((M'ex.R.Tex)/V'ex)^{\gamma} \qquad 4.21$$

$$T''ex = Tex.(P''ex/Pex)^{\frac{\gamma-1}{\gamma}} \qquad 4.22$$

where the instantaneous volume of the exhaust manifold is calculated from:

$$V''ex = V'ex - (V6-Vc)/5 \qquad 4.23$$

assuming that the total reduction of volume (i.e. V6-Vc) is linear over the whole interval.

This process is repeated over the 120 deg. CA interval, at the end of which the turbine performance parameters such as $\dot{M}t$ and TQt are taken as the sum and as the mean value over the complete interval.

4.3 The steady state and transient integrative program, TRANIC

4.3.1 General

In the integratively linked technique, the equilibrium conditions for each compatibility criterion is searched for by adjusting the unknown state variables through integration of a set of differential equations representing the system dynamics. The compatibility criteria are:

i) mass flow compatibility

ii) engine-load torque compatibility

iii) turbocharger torque compatibility

iv) pulse model compatibility

The important feature of this method is that it simulates the transient behaviour of the system; at the end of which steady state conditions are obtained. In the absence of equilibrium, all state variables are changed - proportionally to the imbalances in mass flow and torque - continuously and simultaneously. The steady-state mode can be regarded as a special case of the transient mode where the integration is continued until all compatibility criteria are satisfied. Furthermore, by supplying new information the

integration process can be re-started to find a new equilibrium condition.

This programming technique again relies on a series of mathematical models for performance prediction of individual components such as engine, compressor, turbine and air cooler that are linked to obtain the performance of the complete system. In a transient state the torque on either the turbocharger or engine - load shaft are not in balance. The additional nett torque causes an acceleration of the shaft so that the integration process predicts a change in shaft speed during the next time interval. Significant volumes are ascribed to the pipework between the cooler and engine and between the engine and turbine. Originally, a volume had been ascribed to the pipework between the compressor and the cooler. Experience has shown, however, that significant program stability improvements could be achieved by neglecting the latter volume without any significant effect on the performance prediction of the program. In a transient condition the compressor mass flow is not identical to that at engine inlet, and engine exhaust mass flow differs from that of the turbine. The difference results in a change of mass in the receiver volumes and hence to a change in pressure. Perfect mixing is assumed in the receivers so that the outlet temperature is assumed identical to the mean receiver temperature but not identical to the temperature at inlet. The receivers are assumed to be adiabatic so that temperature changes can be calculated using the energy equation.

4.3.2 Structure of integrative linking technique, Fig. 4.2

Each compatibility criterion is represented by a differential equation with 'time' as the independent variable. The mathematical procedure in this technique is such that it begins with arbitrary initial conditions for the 'storages'. The appropriate dynamic equations are then numerically integrated, the steady state compatibility criteria being checked at the end of each step. This process is continued, for as many steps as required, until all compatibility criteria are satisfied, i.e. all dynamic equations have settled down; the rate of change of all state variables being zero or to within a permissible tolerance. This, so called, quasi - steady state point provides the starting point for the 'true' transient which is then closely monitored if detailed transient response of the system is required for a particular fuel or load step application.

The receivers representing the pipework are of finite volume. A simplified representation of a receiver is shown in Fig. 4.7. At inlet, air enters at upstream conditions and at outlet, air is discharged to the downstream component.

The condition for mass flow continuity is:

$$\dot{M}r = \dot{M}in - \dot{M}out \qquad 4.24$$

Applying the first law of thermodynamics to the receiver yields:

$$\dot{Q} + \dot{W} + \dot{M}out.Hout - \dot{M}in.Hin + d(MU)r/dt = 0 \qquad 4.25$$

Assuming $\dot{W}=0$, $\dot{Q}=0$ and Tout=Tr the energy equation leads to:

$$A.\dot{T}r = B.Tr + C \qquad 4.26$$

where $A = Mr*Cv$

$B = -[\dot{M}out(Cp-Cv) + \dot{M}in*Cv]$

$C = \dot{M}in*Cp*Tin$

Under unsteady conditions, the temperature and pressure of the receiver change with time until equilibrium conditions are reached. Thus the differential equations 4.24 and 4.25 together with the perfect gas law Pv = mRT may be solved numerically for Tr and Pr.

Similarly for the engine load system, the dynamic equation for the behaviour of the shaft, (mechanical energy storage) is given by the conservation of momentum, Fig. 4.8.

$$TQe - TQl = I\dot{w} \qquad 4.27$$

This can be readily solved for the speed increment dw, provided a relationship between TQe, TQl and w is available. A crude approximation is to assume TQe to be constant and TQl to vary linearly with w, as in Fig. 4.8, such that:

$$TQl = TQe*(w/wf) \qquad 4.28$$

Therefore

$$\dot{w} + TQe/(wf.I).w - TQe/I = 0 \qquad 4.29$$

However, by specifying a load torque-speed schedule and using engine torque from the engine subroutine, equation 4.27 is solved numerically for $\dot{w}$. A full description of this program is found in ref. (34).

4.3.3 Component models

The program uses all of the components described earlier, including

the pulse model, in addition to a simple model of a governor. The formerly described subroutines are slightly modified for this program, in that the input-output information is slightly different and the appropriate alterations have been made before their incorporation into this program. The original structure of the program, however, has been altered during the past few years as follows.

4.3.4 Program improvements

A number of modifications have been made in the program to improve stability and run time. Only two significant component subroutines are retained, incorporating the rest into the main linking program. The calculations of the engine and turbine subroutines were sufficiently long to be kept as separate subroutines. In the case of the turbine calculations, both computation speed and program reliability were improved by using the turbine subroutine to generate two dimensional arrays for mass flow, torque and efficiency as functions of speed and pressure ratio. These arrays were then interpolated to get turbine performance during the transient calculations. The manufacturers' performance map was fed as data to provide numerical arrays for compressor pressure ratio and efficiency as functions of speed and mass flow (or volume flow). After-cooler performance was represented by two empirical relationships, one for pressure drop, the other for effectiveness, each of which includes an empirical coefficient that is supplied as input data. These values may be set to zero if no after-cooler is fitted.

The relations are:

$$P_{out} = P_{in} \cdot \left(1 - \frac{\frac{1}{2}(1 + Xloss).r.Xmf^2.T_{in}}{(6x10^6.P_{in}.P_a.\text{exit pipe area})^2}\right) \qquad 4.30$$

and

$$T_{out} = T_{in} - \frac{(T_{in} - T_a) \times 0.8^{(Xmf.\sqrt{T_{in}})}}{P_a \cdot P_{in} \cdot X_{eff}} \qquad 4.31$$

As stated earlier, the original program had an additional receiver between the compressor and the cooler. This method of calculation tended to be unstable as very small changes in receiver pressures caused relatively large fluctuations in flow. It was found more satisfactory to attach the cooler directly to the compressor and calculate the performance of the combined unit. This calculation is carried out at the start of the program; at each point in the compressor array the pressure and temperature from the after-cooler is calculated and stored in arrays for subsequent interpolation.

Instability was also encountered if the slope of the constant speed lines on the compressor map were not sufficiently negative. If the characteristic lines are horizontal - as may occur near the surge line - obtaining the flow into a receiver at a specified pressure is impossible as the flow is locally indeterminate. The addition of the cooler pressure drop made the slope of the characteristic lines more negative, so improving the stability. The stability was further improved by using the pipe diameter of the receiver to calculate the flow velocity and then to relate the stored mass to the static rather than the total pressure.

With guessed values for the conditions in the inlet and exhaust receivers and for turbocharger speed, a transient run can start from

this arbitrary condition and continue until equilibrium is approached. Some iterative modifications, however, were introduce into this procedure, partly to allow the steady state calculations to hold a specific engine speed and torque rather than accelerate to match engine to load torque, and partly to increase the rate of change of turbocharger speed which is otherwise unacceptably slow. At idling or very light load conditions it is impractical to obtain the steady state turbocharger speed by torque balance. Under these conditions the turbine and compressor torque are so low that the actual compressor speed depends crucially on details of the friction and the lower portion of the compressor map that are rarely known with sufficient accuracy, so it is necessary to hold constant the initial value of turbocharger speed that is either guessed or obtained by experiment.

The calculation procedure is restored to its purely integrative form for the 'true' transient simulation. As stated earlier, the usual procedure in running the program is to start by finding the steady state match at a specified speed and torque. The transient is then started by changing either the governor set point or the load-speed characteristics - or both together. A fixed time step is used throughout the calculations; this being chosen by experience to give a reasonable calculation time without program instability. A choice of integration methods is available ranging from first order (Euler) to fourth order (Runge - Kutta).

The physical components of the system are shown diagramatically in Fig. 4.9. For both turbocharger and engine - load, the inertia is represented by a flywheel concentrated at the centre of the shaft.

The volumes of the two manifold systems VOLce and VOLet are also shown as they play an important role in the transient analysis.

Fig. 4.10 - together with the notation given in table 4.1 - shows the flow of information between the different sections of calculation in the program. As an example, the engine subroutine requires as input the values of inlet mass flow ($\dot{M}i$), exhaust receiver pressure (Pt), inlet receiver pressure (Pim), inlet receiver temperature (Tim), engine speed (Ne) and fuel input ($\dot{M}f$). Values calculated within the subroutine are exhaust temperature (Te), torque (Te), exhaust mass flow ($\dot{M}ex$), cylinder contents temperature and pressure at release (Tr,Pr). Most constants and calculated values - such as horse power and efficiency - not required as input to the other sections are omitted from the diagram. Sections enclosed in rectangles are treated on a quasi steady basis using algebraic equations. Sections enclosed in boxes are dynamic and include differential equations with time as the independent variable. As an example, for each inertia the difference in torque gives a value of angular acceleration which must be integrated to obtain the shaft speed as output. In all, there are seven differential equations, two for each receiver (one for mass conservation, one for energy conservation), one for each inertia and one for the assumed first order differential equation to represent the response of the fuel rack to governor set point change.

4.3.5 Dynamic characteristics of pump-governor system

The mechanical governor is modelled simply by assuming that the rate

of change of rack movement is proportional to the imbalance between the instantaneous rack and the demanded rack i.e.

$$dr/dt = (rslope.(es - szero) - r)/T \qquad 4.32$$

where: rslope is the slope of the governor droop lines

es is the instantaneous engine speed

szero is the governor set point i.e. the demanded speed in rpm

r is the rack position (arbitrary scale)

T is the governor time constant

A simplified explanation of the above is as follows: Fig. 4.11 represents the assumed response of rack movement against time for a step increase in demand. Mathematically this behaviour is approximated by assuming that the rack will travel at a constant velocity equal to the initial slope of:

$$dr/dt = (rf - ri)/T \qquad 4.33$$

i.e. it travels to the final position from the initial position in T seconds.

If, however, the integration time interval, Δt, used in the program is less than T, then the new position of the rack after Δt sec. is found from:

$$r' = ri + ((rf - ri)/T).\Delta t \qquad 4.34$$

At the beginning of the next time interval it is again assumed that the rack will travel at a velocity equal to the new slope given by:

$$dr/dt = (rf - r')/T \qquad 4.35$$

and it will travel to the new position indicated by r'' after the next Δt sec. This process is repeated for every step and the final position is approached assymptotically. The shorter the integration interval, the more closely this response follows the original assumed response.

However, the rack response is also a function of engine speed and consequently the above treatment has to be modified to include this effect.

The steady state behaviour of rack against engine speed is shown in Fig. 4.12. The slope of each line is given by:

$$dr/dt = (rmax - rmin)/\Delta s = rslope \qquad 4.36$$

Therefore, for any given governor set point such as szero and engine speed, es, the rack position is found from:

$$R = rmin + rslpoe.(es - szero) \qquad 4.37$$

The overall rack movement for a new demanded governor set point is shown in Fig. 4.13. Had the rack response been instantaneous, such as when T is zero, the response would have followed the dotted line in Fig. 4.13. However, since a time constant has been assumed for the governor, the path is modified as follows: During the first integration step, the rack will move with a velocity given by equation 4.33. But rf can be substituted for from equation 4.37, i.e.:

$$rf = rmin + rslope.(es - szero2) \quad 4.38$$

Therefore

$$dr/dt = (rmin + rslope.(es - szero2) - ri)/T \quad 4.39$$

Assuming that the rack travel is from 0 to rmax

$$dr/dt = (rslope.(es - szero) - ri)/T \quad 4.40$$

Therefore rack position after Δt sec. is given by

$$r' = ri + ((rslope.(es - szero) - ri)/T).\Delta t \quad 4.41$$

But after Δt sec., es has been increased to es', thus the new rack position is at B in Fig. 4.13.

This process is repeated for every step with the modified expression, equation 4.40, which contains the instantaneous engine speed. Thus during the next step the rack will move with the new velocity (rf'-r')/T from r' towards rf' and not from r' to rf. Now

$$rf' = rslope.(es' - szero2) \quad 4.42$$

Therefore

$$dr/dt = (rslope.(es' - szero2) - r')/T \quad 4.43$$

This gives a new rack position after Δt as

$$r'' = r' + ((rslope.(es' - szero2) - r')/T).\Delta t \quad 4.44$$

which is represented by point C in Fig 4.13 which also shows that the engine speed has also increased to es''.

This procedure gives the general expression for rack velocity as

$$dr/dt = (rslope.(es - szero) - r)/T \qquad 4.45$$

and

$$r(new) = r(old) + ((rslope.(es - szero) - r(old))/T).\Delta t \qquad 4.46$$

where r and es are the instantaneous values of rack and engine speed respectively.

It was found that if this process is repeated enough times the rack will overshoot the demanded szero line and then spiral back towards the final steady state position. This effect is more pronounced as the size of the demanded governor set point increases. This is undesirable since engine speed fluctuates in phase with the spiral response leading to a sinosoidal transient response towards the end of the transient run, where this cross over occurs.

This was eliminated by assuming that when rack has reached its maximum value, it no longer is subject to the original step input and is totally speed dependent, i.e. more apt to be under a ramp input with assumed zero steady state lag rather than under a step input. Thus, when (dr/des)dynamic becomes zero, i.e. maximum rack has been reached, the following expression is used. ((dr/des)dynamic is the rate of change of rack with engine speed when there is engine acceleration.)

$$dr/dt = dr/d(es) \; . \; d(es)/dt \qquad 4.47$$

but

(dr/des)static = rslope 4.48

((dr/des)static is the slope of the governor droop lines, see Fig. 4.13)

Therefore dr/dt = slope*engine acceleration.

4.4 Program modifications for simulation of variable geometry turbocharging

4.4.1 General

Programs similar in structure to those described have been used extensively in a wide range of applications in simulating conventional and unconventional engine - turbocharger configurations such as single and two stage turbocharging and various compound schemes. It is also possible to use these programs, with some modifications, for such applications as variable geometry turbocharging. To this end, it is necessary to have a turbine subroutine capable of handling turbine throat area changes and a turbine throat area schedule according to which the nozzle ring position can be determined.

Both of the turbine subroutines available in these programs are capable of operating under restricted throat conditions. Attention has, thus, been paid to a controlling schedule and the mechanism by which it can determine the turbine nozzle ring setting. Since the most important factor in engine performance is the availability of air for the combustion of the fuel, a measure of air availability seemed the most obvious parameter to be chosen to control the turbine throat area. The mass of air trapped in the engine

cylinder is a direct function of the boost pressure ratio and the air temperature. In an after-cooled turbocharged engine, however, the overriding factor is the boost pressure level. For the current investigations, therefore, boost pressure ratio was chosen as the reference for nozzle control. For more practical schedules, it may be necessary to take account of the load by monitoring the fuel flow per revolution as delivered to the engine and the speed to optimize the nozzle ring setting so that the specific fuel consumption of the engine does not suffer at part load conditions when excessive boost is not required. These elaborate control schemes would necessitate transducers inputting into a central processing unit containing microprocessors etc. which can then set the nozzle ring using electro-hydraulic or pneumatic actuators.

However, it is desirable to maintain as high a level of boost in the midspeed range as is possible in order to obtain improved engine torque back-up without violating the engine physical limitations. For this purpose, a boost ratio of approximately 2 was thought to be sufficiently high in this engine since this pressure ratio coincides with the turbocharger speed limit of 100,000 rpm, while attempted higher levels would impose too large a back pressure on the engine due to higher turbine restrictions and the engine performance would suffer due to increased negative loop work. It is, therefore, desirable to reduce the swallowing capacity of the turbine for boost levels below two in some relation to boost deficiency. The value of 1.5 proved to be a compromise since higher values would have resulted in an almost abrupt change from fully restricted to fully open positions which could lead to nozzle ring instability, while on

the other hand, a lower value would not have offered the required effects by starting to open too early. The transition from fully restricted to fully open positions was given a smooth ramp as shown in Fig. 4.14. The above figures, however, were open to further refinement if this proved necessary. Previous experiments had shown that a restriction level greater than 50% is of no substantial benefit (57). Therefore, restrictions lower than this were not considered for the purpose of the computer simulations.

Finally, all the simulations were based on the Perkins T6.354 6-cylinder engine equipped with the Holset H1-6580 G/H 15A5 3" turbocharger unit, details of which were given in 3.1.3.

4.4.2 Steady state iterative program

Having decided on a boost controlled variable geometry scheme, the control schedule was then incorporated into the steady state matching program for simulation purposes. This was achieved by a series of 'if' statements to establish whether the boost level is below 1.5, above 2.0 or some value in between. The turbine throat width is set to its minimum position if boost is less than 1.5 and it is set to its maximum if boost is greater than 2.0. However, if the boost pressure ratio is in between these two values, the position of the turbine nozzle ring is determined from the equation representing the straight line connecting 1.5 and 2.0. This line is defined as follows for 1.5 < rm < 2.0 where rm is the boost pressure ratio:

```
hl = ((hlmax-hlmin).rm-hlmax.(rmjfr-rmjfo.(1-resmax)))          4.49
     /(rmjfo-rmjfr)
```

hlmax = Maximum turbine throat width

hlmin = Minimum turbine throat width

rmjfr = Boost at which turbine is just fully restricted

rmjfo = Boost at which turbine is just fully open

resmax = Maximum required restriction

and hl is the instantaneous value of turbine throat width determined by the instantaneous value of boost, rm.

Fig. 4.15 depicts the flow chart for the boost controlled variable geometry scheme.

The above three 'if' statements are placed just before the line where the main linking program calls either of the turbine subroutines. At this point, the value of boost is known. This is found from the compressor subroutine using the initial estimates of turbocharger speed and mass flow as supplied to the program. Knowing rm, a corresponding value of hl is chosen and the program continues as normal. The first value of compressor boost determined by using the initial guesses, is an underestimate and hence a tight turbine throat area is chosen. This will lead to an overestimate of the turbocharger speed which will cause an overestimate of boost when the program calls on the compressor subroutine next. This overestimate of boost will then cause the turbine to become less restricted than it would in the equilibrium position towards which the program will converge. It is obvious that this will lead to an underestimate of the next value of boost but normally greater than the initial value based on the supplied guesses for system mass flow rate and turbocharger speed. This is

essential if the solution is to converge towards the final equilibrium position.

This process is repeated as many times as necessary until all compatibility criteria are satisfied for any given fuelling and engine speed at which point the final position of the turbine nozzle ring has been found and the steady state operating results are printed. The process of converging towards the equilibrium position of the nozzle ring is speeded up by better estimates of the initially supplied values of turbocharger speed and system mass flow rate. No convergence problems, however, have been encountered in the course of running of this program. An alternative would have been to use the iteration subroutine as used to establish equilibrium values of the other iterating variables to achieve the nozzle ring position, but since the increase in run time was acceptable, the use of the iteration subroutine was avoided.

The performance of the turbocharged engine under different boost control schedules can be simulated by assigning any desired values to hlmax, resmax, rmjfr and rmjfo and running the program under these conditions.

4.4.3 Steady state and transient integrative program

The same variable geometry control schedule was incorporated in a similar position, i.e. before the turbine subroutine, in this program and the program could then run for transient simulation as required.

Having specified the initial conditions of the various receivers as

data, the program is able to determine the turbine throat area according to the inlet manifold receiver pressure and continue to do so after each time increment according to the new pressure. This is a much more gradual process than in the iterative program; since the turbine throat area is adjusted, as it would in practice, continuously with changing conditions until the quasi-steady state point is reached, after which the fuel step is applied and the nozzle ring is adjusted as before until the final steady state point is arrived at.

Since convergence presents greater problems in the integrative program , particularly as far as the quasi-steady state point is concerned, the initial guesses of the receiver conditions are critical in determining whether the program will converge. It was known that stipulating shorter time increments provided a means by which more stable operation of the program could be achieved; nevertheless, extremely accurate values of the initial conditions in the receivers are necessary to avoid instability in the program. This also has the effect of reducing the total run time, since less time is spent in arriving at the quasi-steady state point.

Table 4.1 Key to Symbols in Information Flow Chart

	Pressure	Temperature	Mass Flow	Torque	Speed
Atmosphere	Pa	Ta	-	-	-
Compressor Cooler	-	Ti	mi	Tc	Nt/c
Cooler-Eng Receiver	Pim	Tim	-	-	-
Engine Exh	Pex	Tex	mex	-	-
Eng-Turb Receiver	Pt	Tt	-	-	-
Turbine	Pt	Tt	mt	Tt	Nt/c
Engine	-	-	-	Te	Ne
Load	-	-	-	Tl	Ne

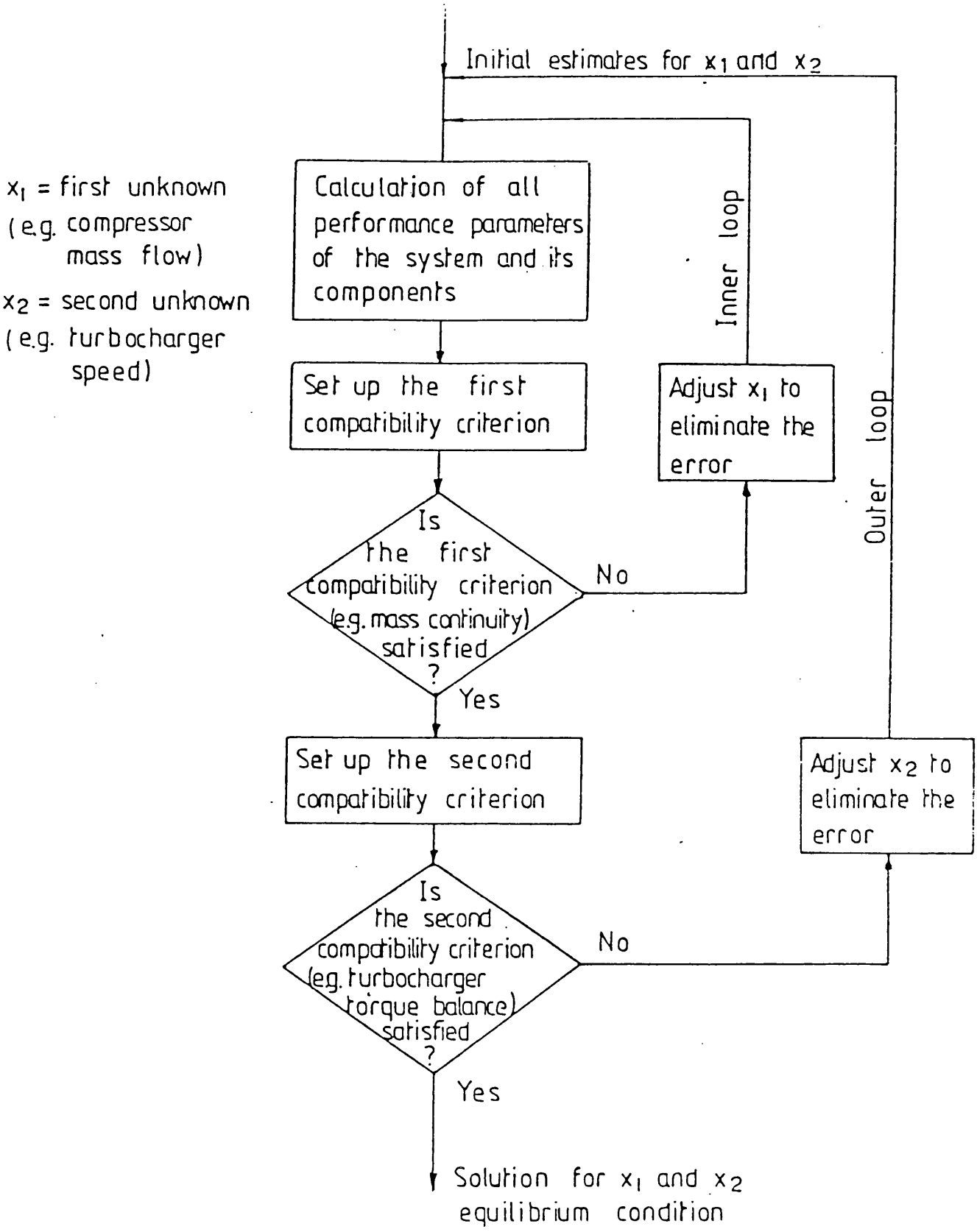

Fig. 4.1 General Iterative Linking Method With Nested Loops

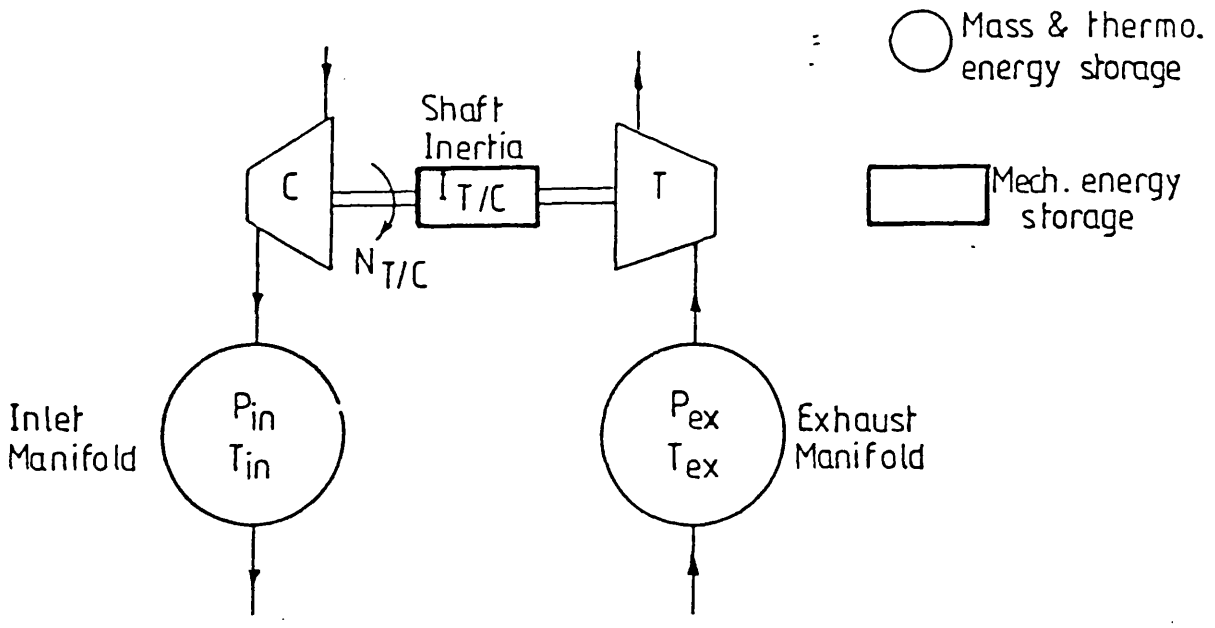

(a) Turbocharger and storage compliances

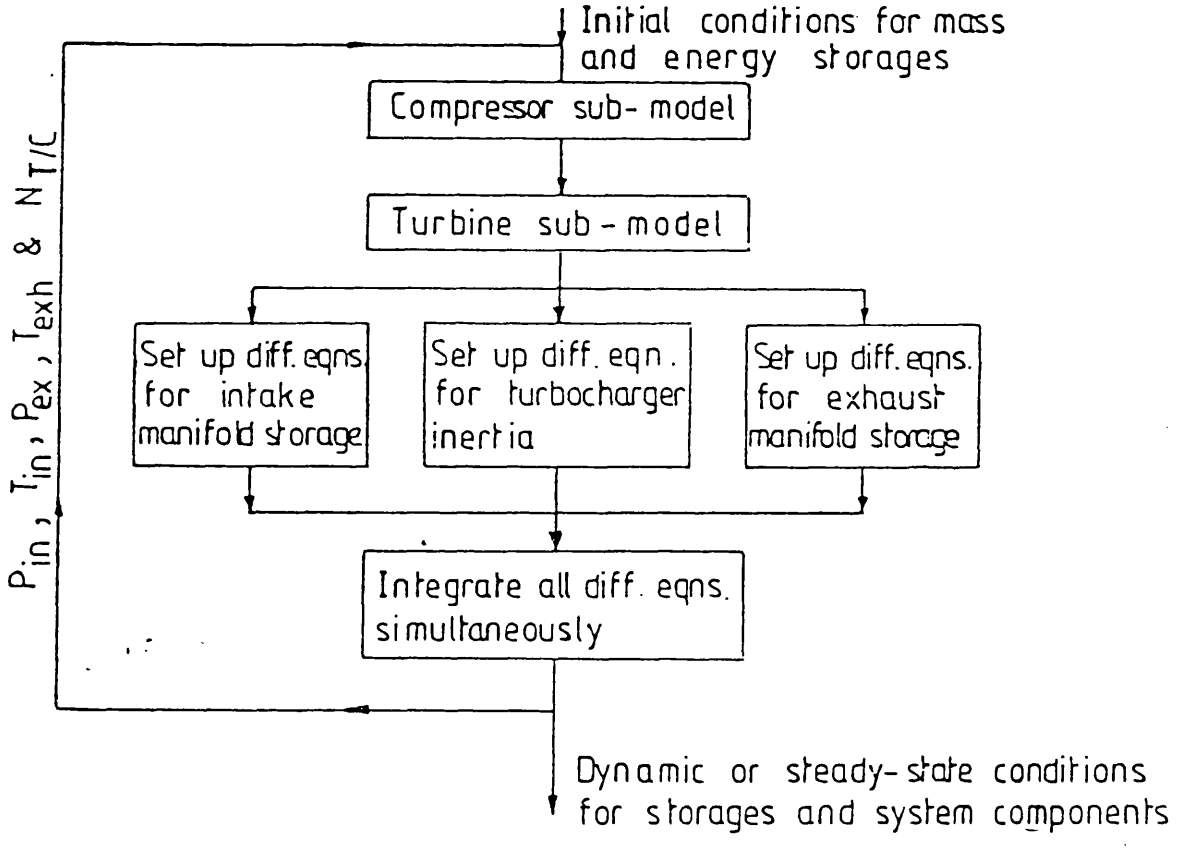

(b) Integratively linked model of turbocharger

Fig. 4.2 Illustration of the Integrative Technique.

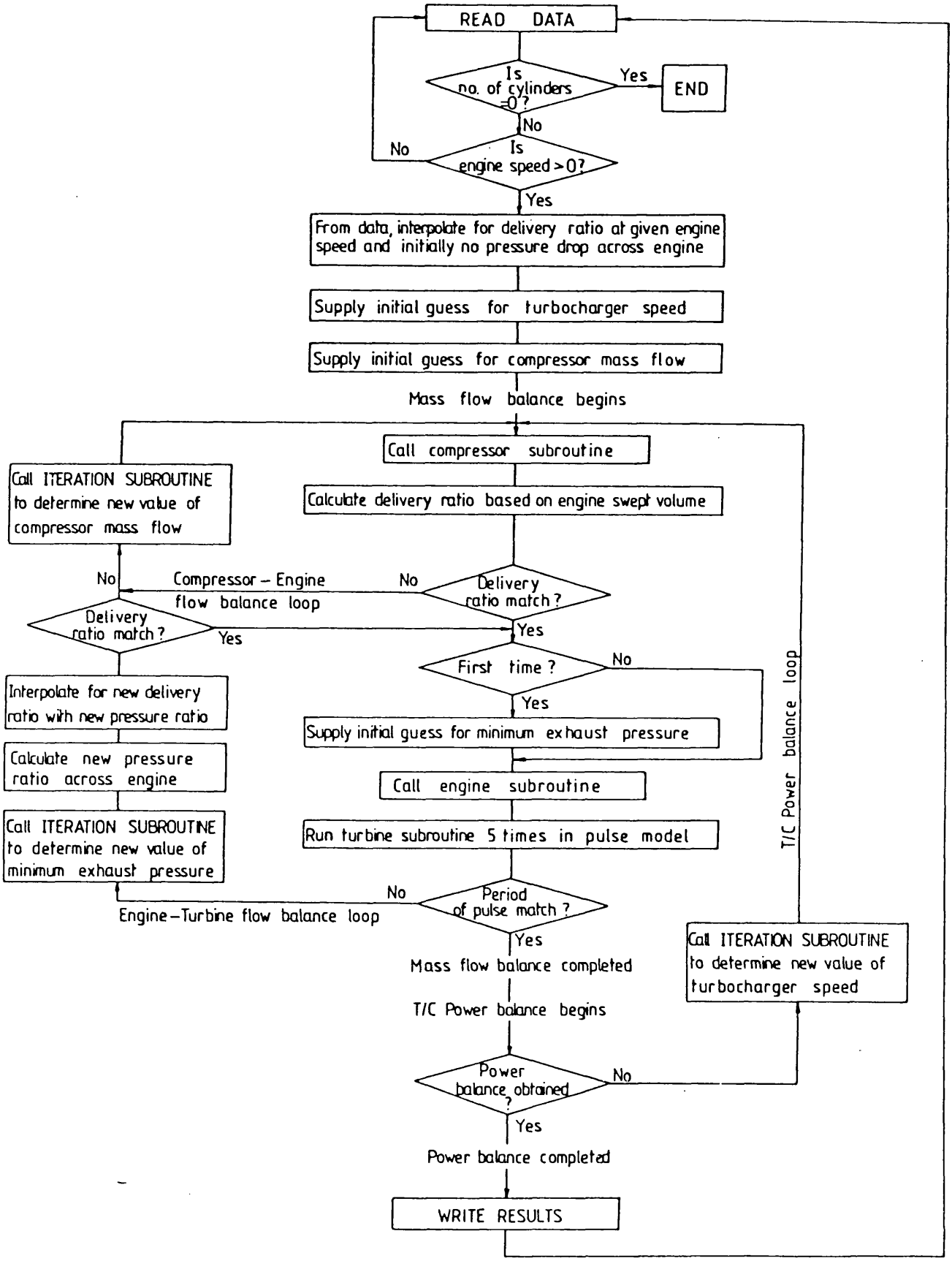

Fig. 4.3 Detailed Flow Diagram for Single Stage Turbocharged Diesel Engine Matching Program, EMAT.

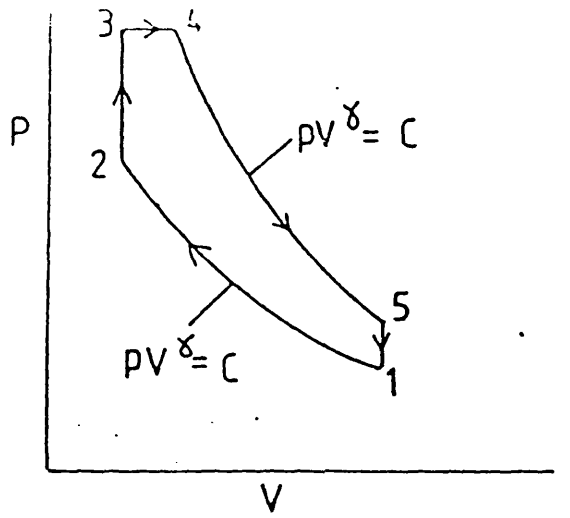

(a) AIR STANDARD CYCLE

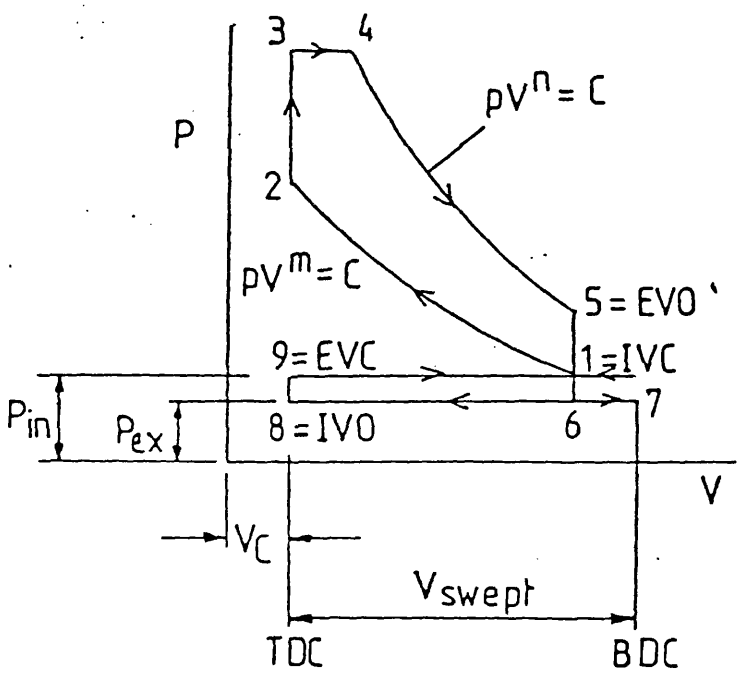

(b) MODIFIED AIR STANDARD CYCLE

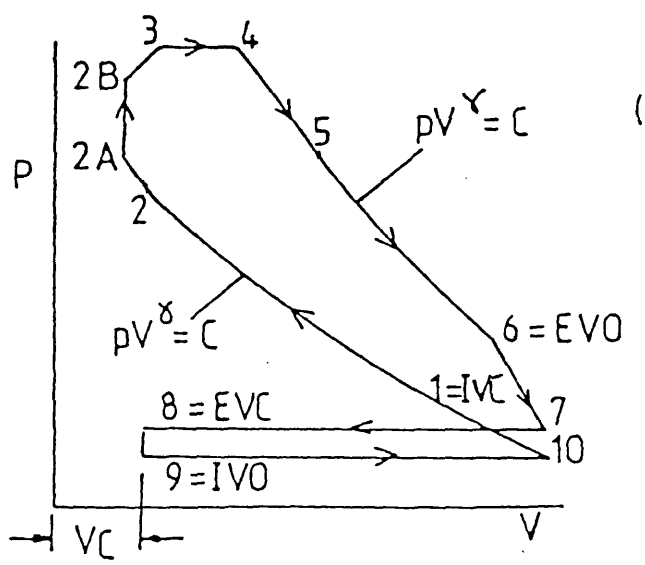

(c) FINAL FORM OF 'SIMPLE' CYCLE

Fig. 4.4 Variants of the Diesel Engine Cycle.

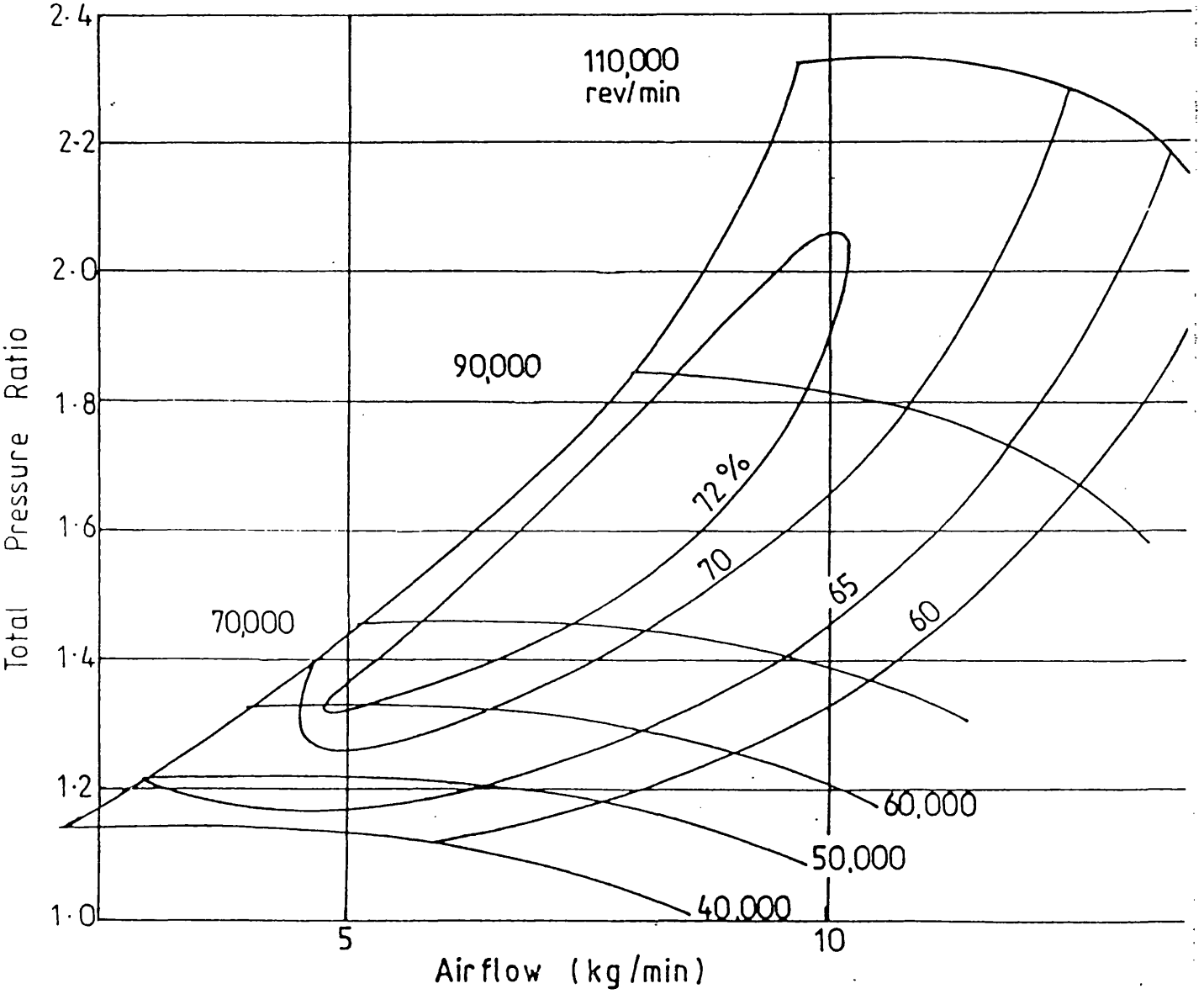

Fig. 4.5 H1/6580G Compressor Map.

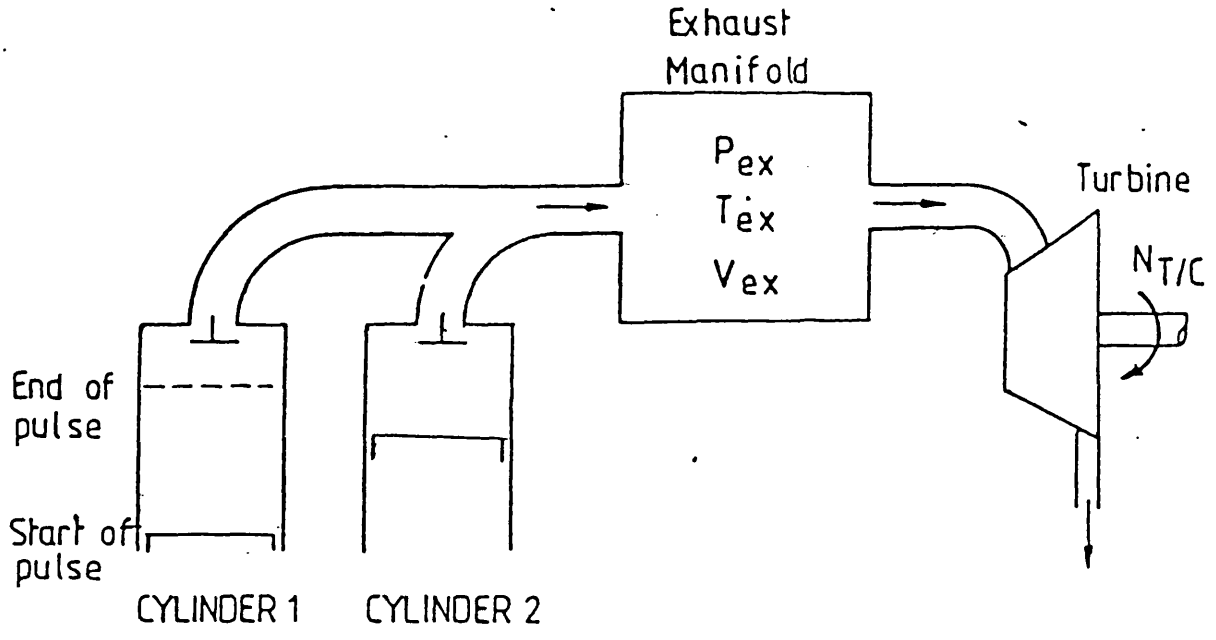

CYLINDER 1 ≡ about to discharge a pressure pulse to the manifold
CYLINDER 2 ≡ has almost completed its discharge to the manifold

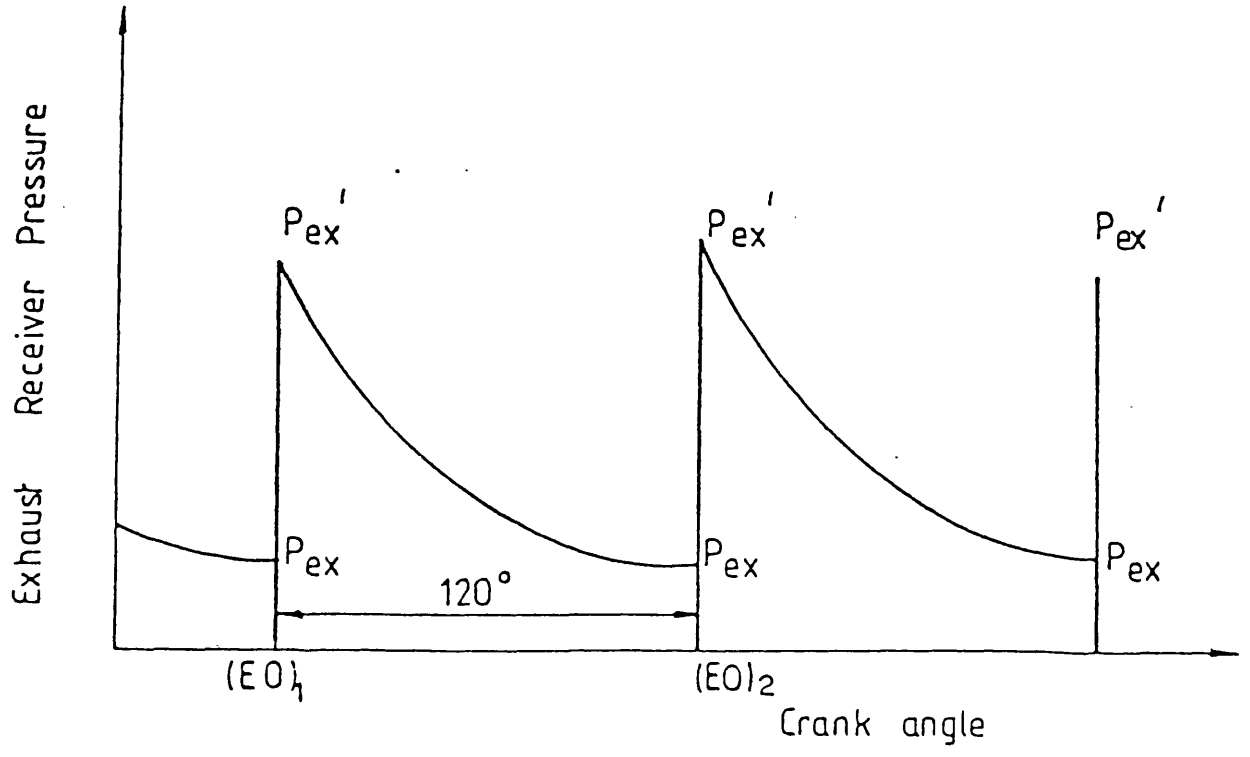

Fig. 4.6 simplified Exhaust Pulse Model.

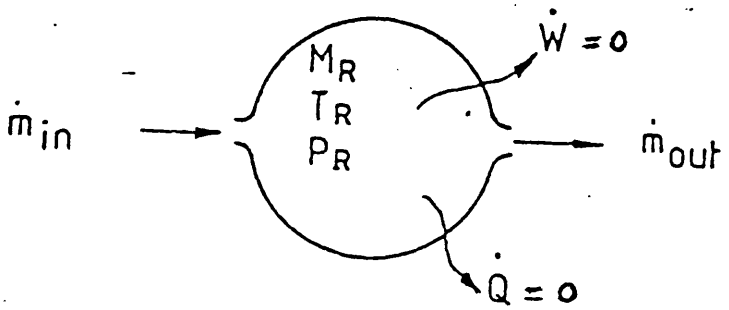

Receiver

Fig. 4.7 A Receiver Layout.

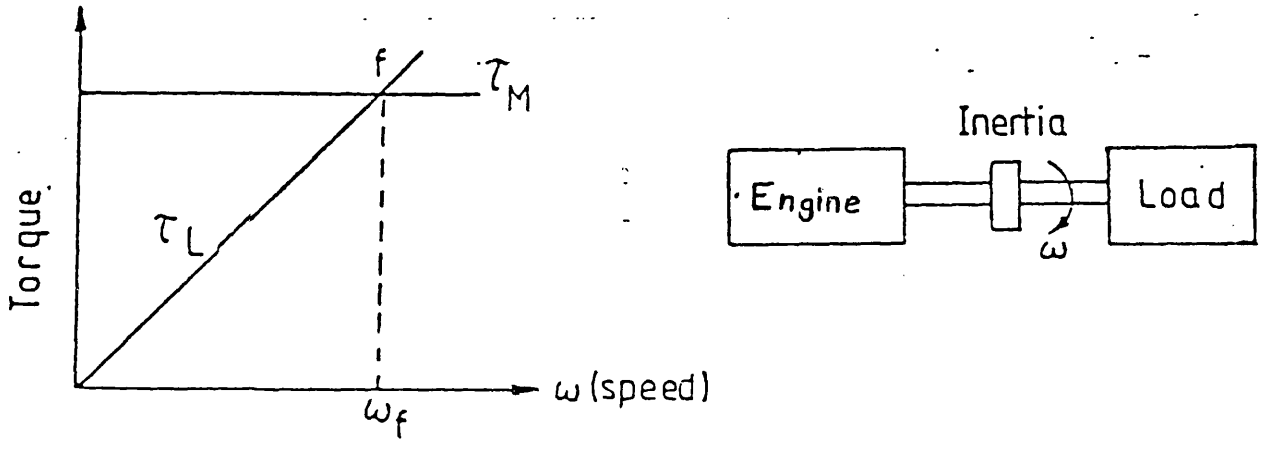

Fig. 4.8 A Simplified Engine-Load Dynamic System.

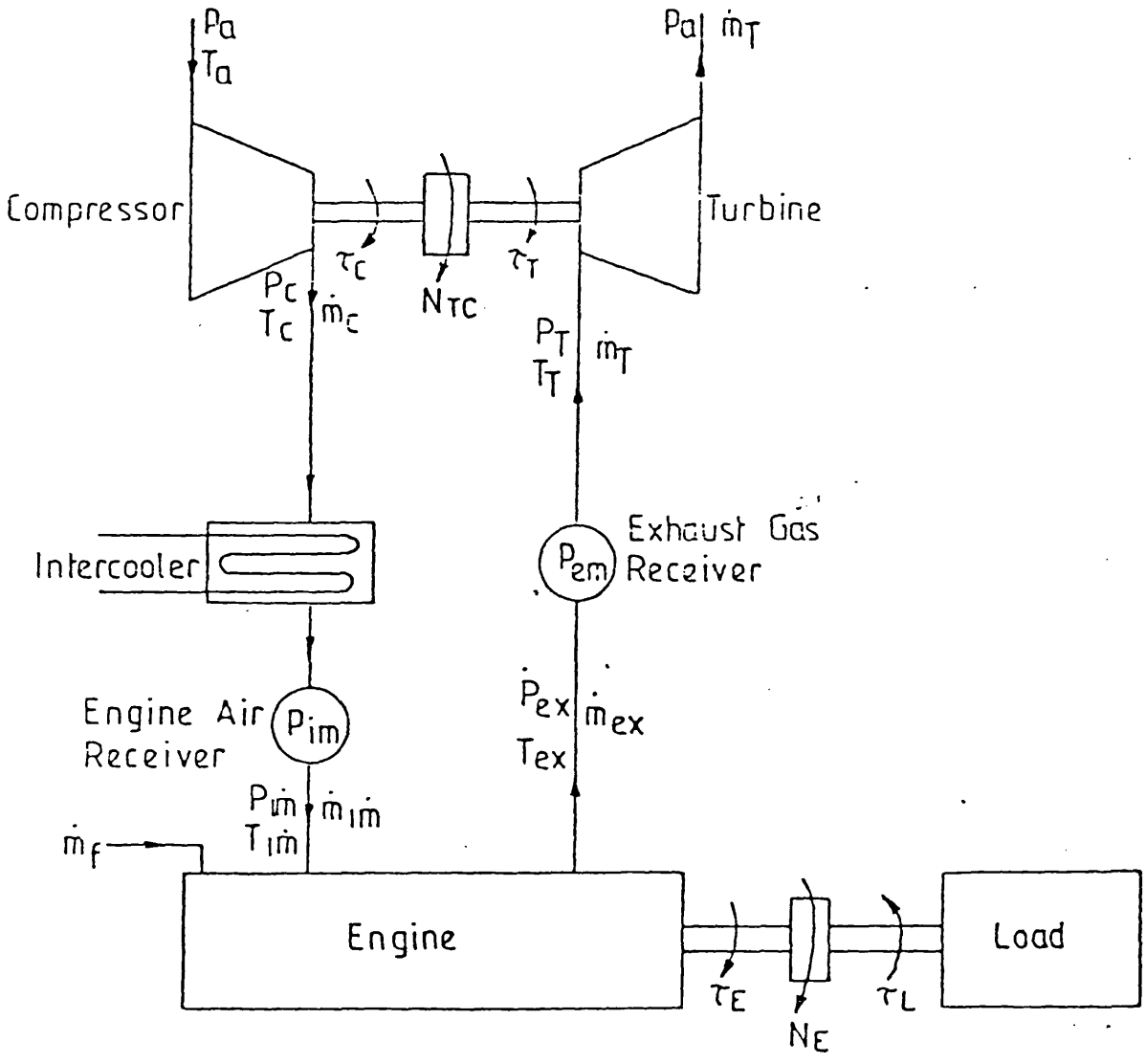

Fig. 4.9 Engine-Turbocharger Schematic Showing the Air Receivers, (Integrative Scheme).

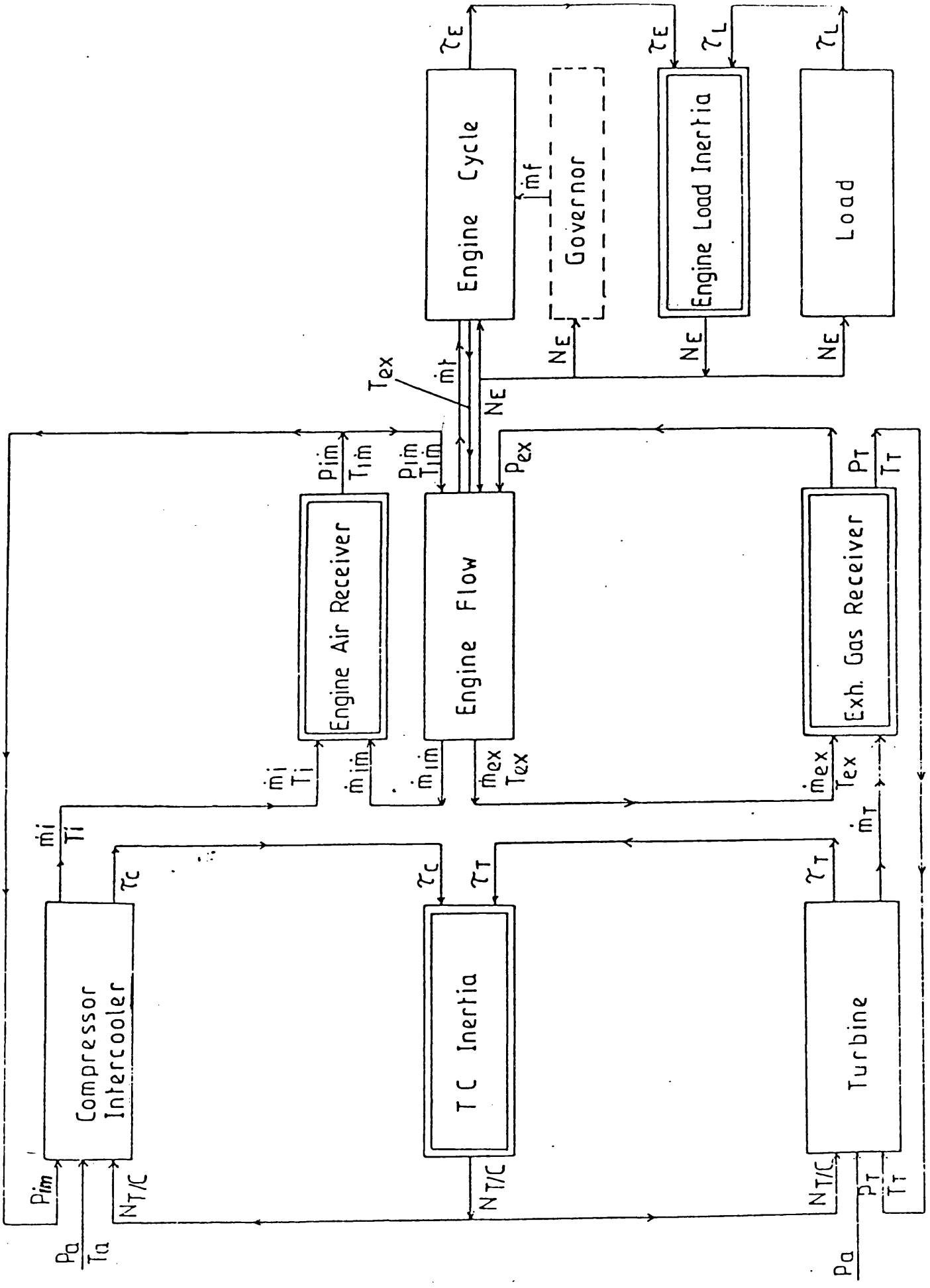

Fig. 4.10 Chart Showing the Flow of Information in the Integratively Linked Program.

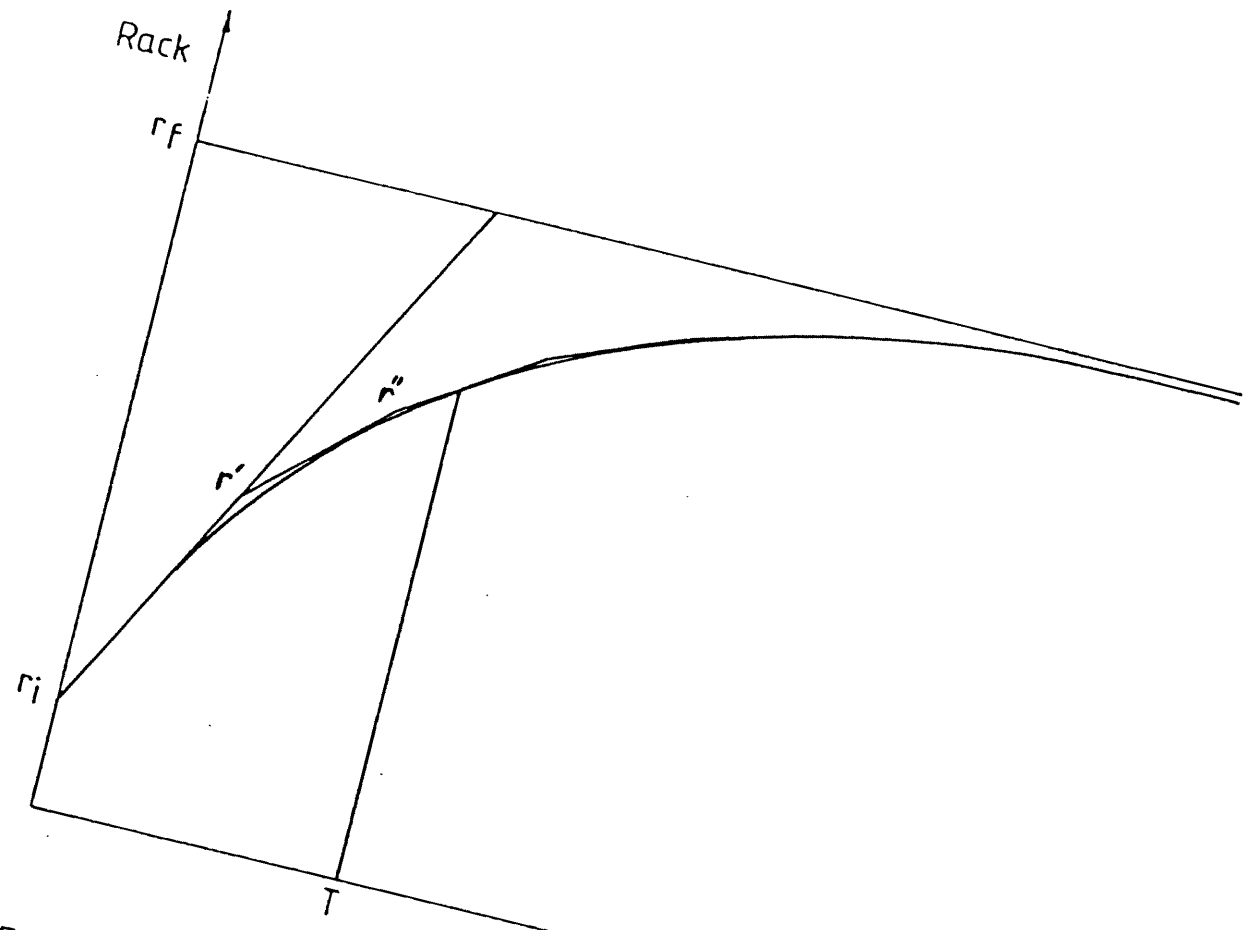

FIG. 4.11. ASSUMED GOVERNOR DYNAMIC RESPONSE

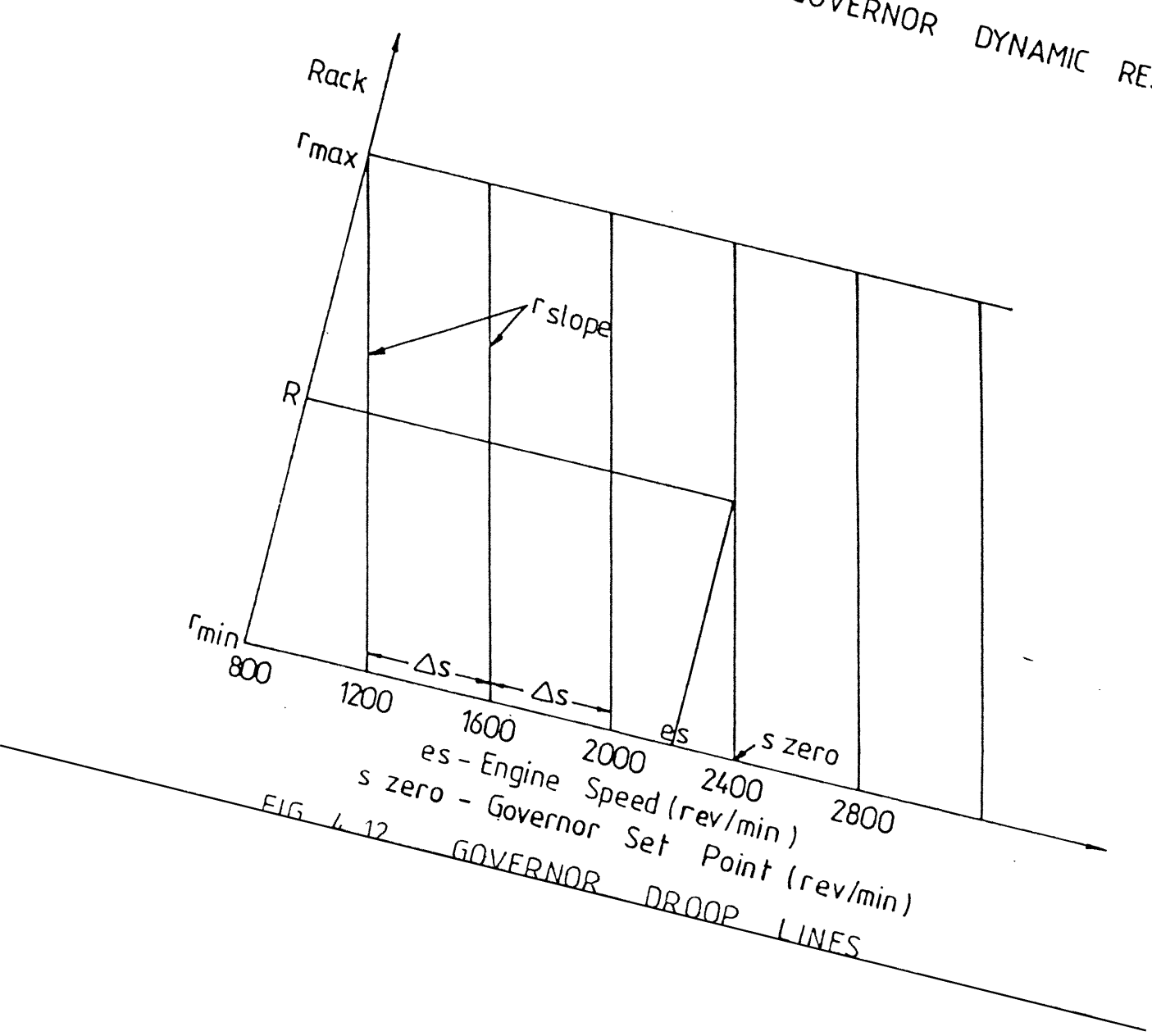

FIG 4.12 GOVERNOR DROOP LINES

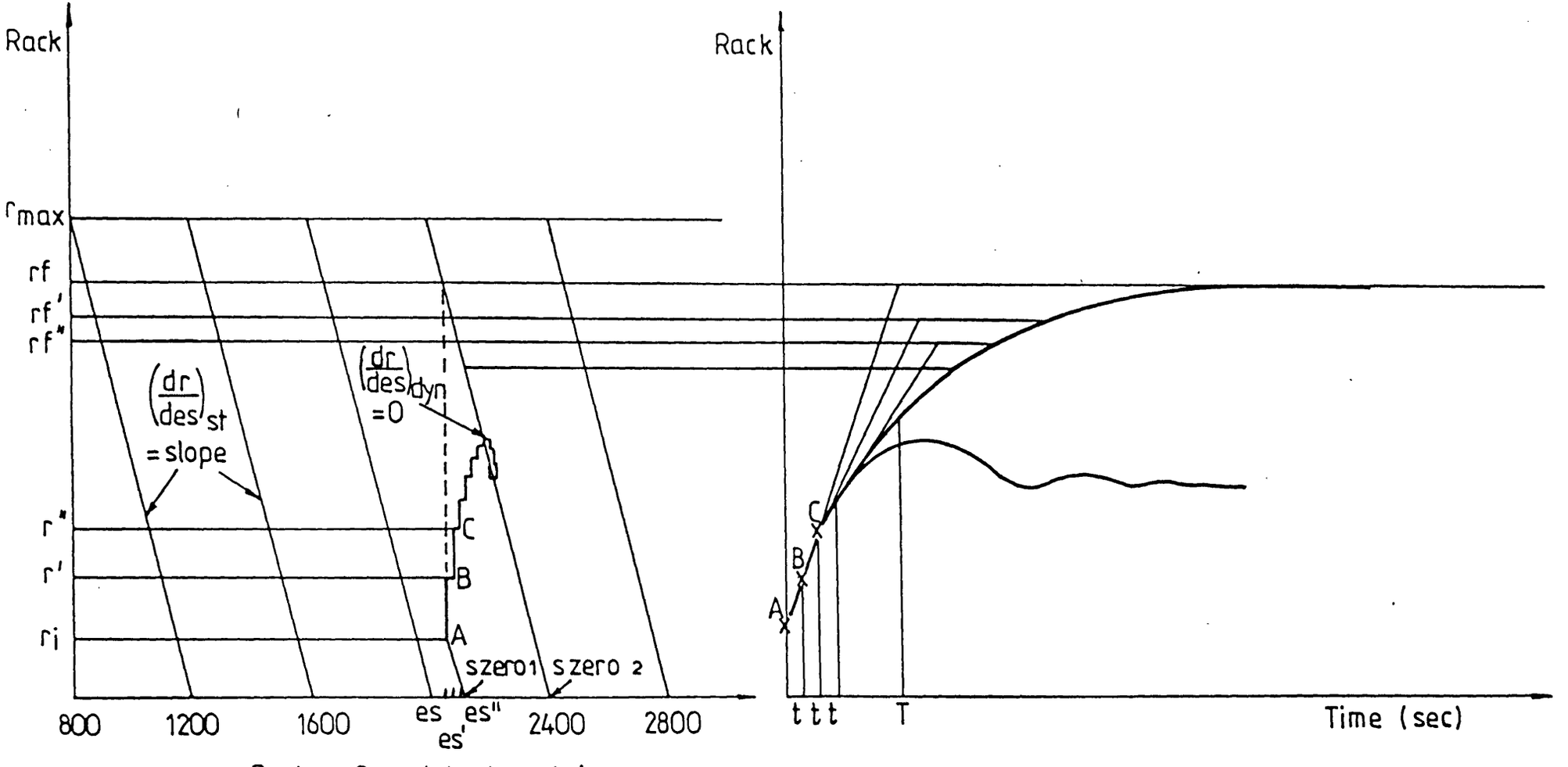

FIG. 4.13. GOVERNOR RESPONSE

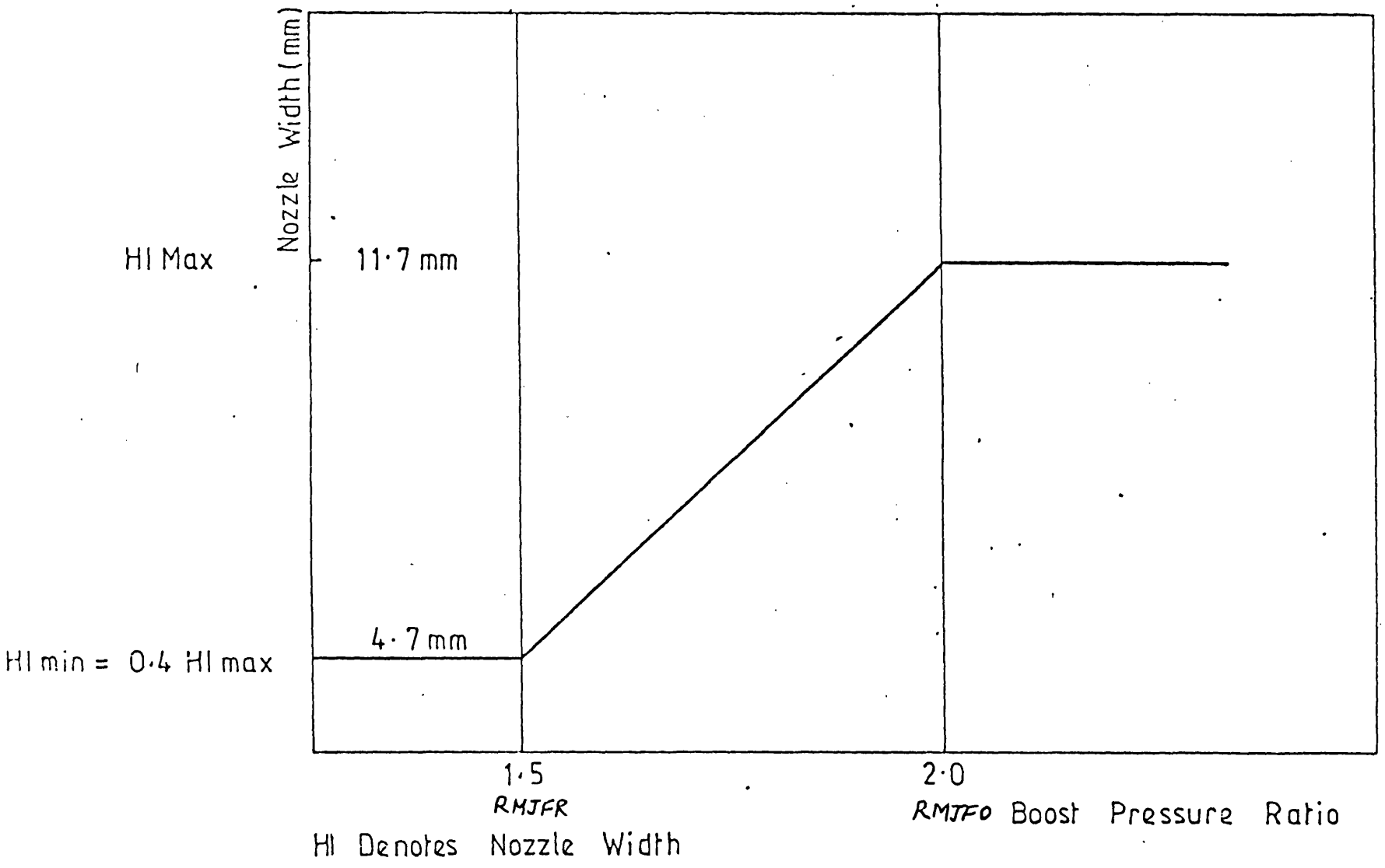

Fig. 4.14 Variable Geometry Boost-Restriction Schedule.

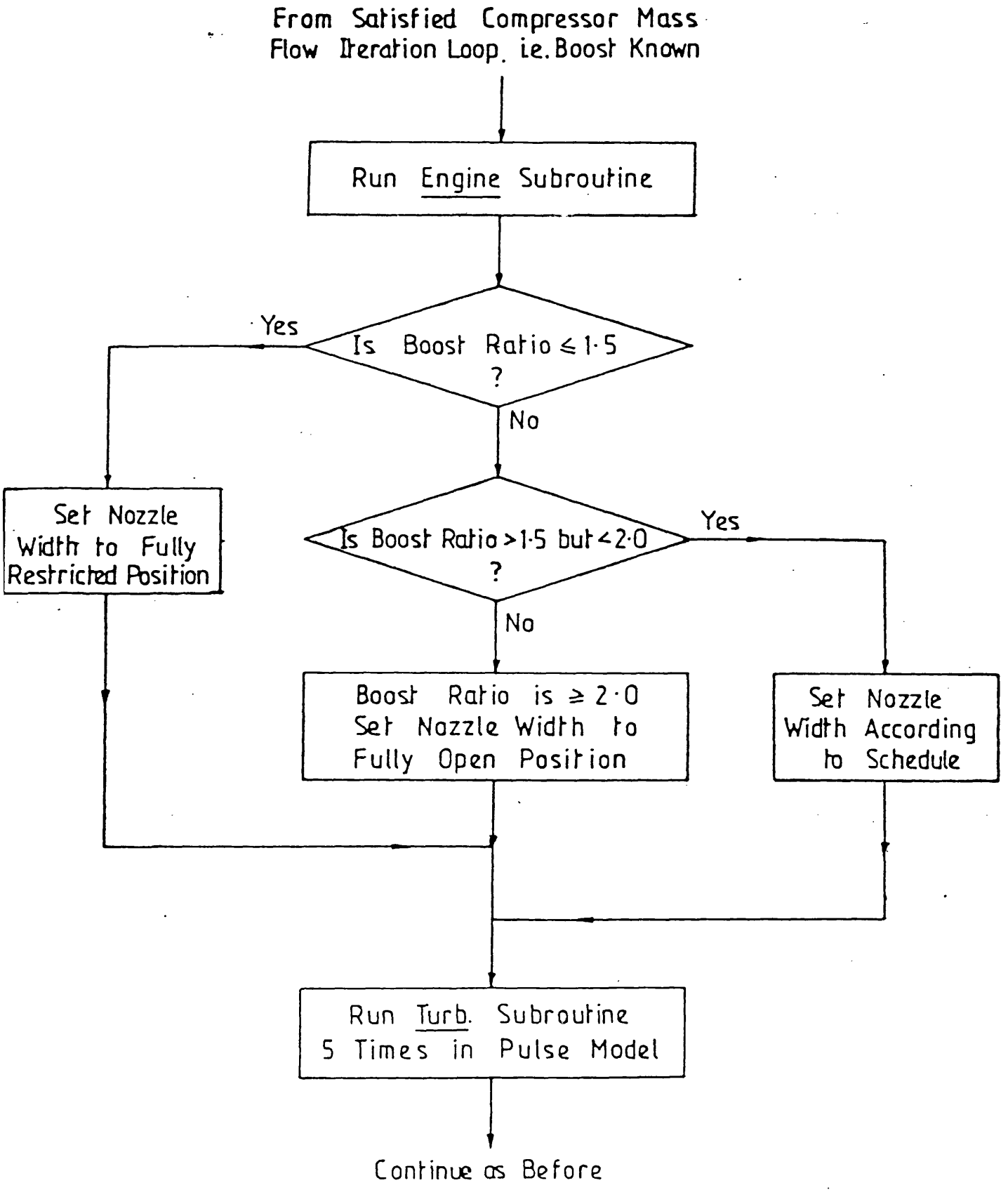

Fig. 4.15 Modified Section of the Steady State Matching Program to Accommodate Variable Geometry Turbine.

5. Computer program listings

5.1 Subroutines used in the iteratively linked program, EMAT

Most of the subroutines listed below have been in use for a number of years and are included for completeness. Most have been fully documented by other researchers and a comprehensive description of the subroutines used in this project can be found in ref. (34)

The subroutines are:

Component	Subroutine
compressor	clcoml
turbine	turbw
	turbz
engine	engine
cooler	cool
1-D interpolation	intxtl
2-D interpolation	intxt2
specific heat	cpg
specific heat ratio	g, ga
iteration	simpit

5.1.1 Compressor subroutine, clcoml

Centrifugal compressor model

Fortran X8 multics system

Program summary

The subroutine consists of a number of two dimensional arrays. This is a numerical representation of the compressor performance map supplied by the manufacturers, Fig. 4.5.

The linear interpolation routines are used to find pressure ratio and efficiency corresponding to specified values of compressor speed and mass flow. Compressor power, outlet temperature etc. are then computed from the standard thermodynamic relations given in subsection 4.2.3.2.

Associated subroutines: intxt1, intxt2, cpg, g and ga

Input variables		Units
cs	compressor speed	rpm
cmf	compressor mass flow	kg/min
msl	input marker (0 or 1)	
ta	ambient temperature	deg. k
pa	ambient pressure	bar

Output variables

rc	compressor pressure ratio	
tc	compressor outlet temp.	deg. k
cp	compressor power (absorbed)	kw
ce	compressor efficiency	
ct	compressor torque	nm

5.1.2 Engine subroutine, engine

diesel engine model

Fortran X8 multics system

Program summary

This is based on the modified 5-point diesel cycle calculation as described in ref. (34). Combustion occurs in three distinctive phases, namely a constant volume section followed by a constant

pressure section and finally the remainder of the fuel is assumed to burn on a constant slope line as shown in Fig 4.4c. Empirical factors such as diagram efficiency are employed to represent the deviation of the ideal cycle from the actual cycle performance. It accounts for negative loop work and the heat rejected to the coolant is obtained by using an empirically determined relationship.

Associated subroutines: cpg, h, g

Input variables		Units
es	engine speed	rpm
rc	boost pressure ratio	
tm	inlet air temperature	deg. k
pmaxl	max. press. limit	bar
cr	compression ratio	
rex	exhaust pressure ratio	
fprev	mass of fuel per revolution	kg/rev
amd	air mass flow delivered(input)	kg/min
fmep	friction mean effective pressure	bar

Output variables

rt	trapped air fuel ratio	
rd	delivered air fuel ratio	
amex	engine exh. mass flow rate	kg/min
tex	exhaust temperature	deg. k
bhp	engine power	kw
bte	brake thermal efficiency	

torque	engine torque	nm
pmax	maximum cylinder pressure	bar
bmep	brake mean effective press.	bar
sfc	specific fuel consumption	kg/kw-hr

5.1.3 Turbine subroutines, turbw and turbz

Radial inflow turbine models

Fortran X8 multics system

a) turbw

Program summary

This program is based on the one dimensional analysis for design and off-design performance prediction of radial flow turbines (40, 41). It can also handle variable geometry operation.

Associated subroutines: cpg, g, ga and h

Input variables		Units
s	turbine speed	rpm
pr	pressure ratio	
t0	inlet stagnation temp.	deg. k

and the geometric dimensions in meter.

Output variables

fl	mass flow	kg/min
tor	rotor torque	nm
hp	output power	kw
e	efficiency	
fm	corrected flow	$m\sqrt{t}/p$

fn	corrected speed	$n/\sqrt{t}$
fq	corrected torque	tq/p

b) turbz

Program summary

This subroutine is based on the unified one-dimensional analysis for design and off-design performance prediction of radial flow turbine, ref. (39). This subroutine can also simulate variable geometry operation. Associated subroutines: machn, volute, incid, rotor, itern, g, cpg, h

Input variables		Units
eni	rotor speed	rpm
ppi	pressure ratio	
t00	inlet stagnation temp.	deg. k

and the geometric dimensions in meter.

Output variables

fm	non-dimensional mass flow	
fq	non-dimensional torque	
fn	non-dimensional speed	
pwr	output power	kw
etats	total to static efficiency	
em	mass flow rate	kg/sec
q	torque	nm

5.1.4 Charge cooler subroutine, cool

Model of water-air charge cooler

Fortran X8 multics system

Program summary

This subroutine is based on employing the pressure drop - mass flow characteristics of a water to air charge air cooler, Figs. 3.11 and 3.12, to simulate its steady state behaviour. Empirical equations represent the variation of pressure drop and effectiveness against non-dimensional mass flow rate. Outlet temperature is then computed from the value of effectiveness at any mass flow condition.

Associated subroutines: none

Input variables		Units
enf	mass flow rate	kg/min
rc	inlet pressure ratio	
tc	inlet air temperature	deg. k

Output variables

tm	outlet air temperature	deg. k
rm	outlet pressure ratio	
e	cooler effectiveness	

5.2 Subroutines used in the integratively linked transient program, TRANIC

The components used in this program are:

Component	Subroutine name
compressor	(included in the main program)
turbine	turbw
engine	engint
cooler	(included in the main program)

5.2.1 Compressor

Since the compressor performance data is stored as arrays, this information is supplied as input data to allow easy replacement of the compressor by alternative builds, if necessary. It is essentially the same as that described in 5.1.1, but the calculations are carried out in the main program. The structural difference, however, is the input variables which are compressor speed and pressure ratio for this version as opposed to speed and mass flow rate for the earlier one. The mass flow rate and compressor efficiency are obtained through the use of the two-dimensional linear interpolation routine.

5.2.2 Engine subroutine, engint

The model is identical to that described in subsection 5.1.2.

5.2.3 Turbine subroutine, turbw

This program is also the same as that described in 5.1.3a.

5.2.4 Charge cooler

This is not a subroutine but is represented in the main program by two empirical relations representing pressure drop and temperature drop across the cooler. See section 4.3.4.

5.2.5. Differentiation, deriv

To set up a set of first-order differential equations

Program summary

In this subroutine the first derivatives of the dependent variables of the differential equations obtained in simulating the behaviour of the mass and energy storages, are calculated.

Associated subroutines: engine, turbw, intxt1, intxt2, g and h Input variables Units

tx independent variable (time) sec.

var array containing dependent variables of differential equations.

Output variables

Array containing first derivatives of dependent variables of differential equations.

5.3 Main iteratively linked program, EMAT (35)

This program simulates the steady state performance of a single-stage turbocharged diesel engine based on the iterative technique described in section 4.2.2. The two guessed iteration variables are turbocharger speed and compressor mass flow rate. These are iteratively altered until mass flow compatibility throughout the system and power balance between the compressor and turbine rotor is achieved.

Fortran X8 multics system

Associated subroutines: see section 5.1.

Input data Units

engine and turbine geometric dimensions in meter.

es	engine speed	rpm
fprev	fuel input per min.*10000/rev per min.	
injection timing and duration		deg. c.a.

Output information

bhp	engine power	kw
rm	boost	
rt	air fuel ratio	
torque	engine torque	nm
bmep	brake mean effective press.	bar
bte	brake thermal efficiency	
sfc	specific fuel consumption	kg/kw-hr
ts	turbocharger speed	rpm

5.4 Main integratively linked program, TRANIC (35)

This program is based on the integrative technique to solve the differential equations representing the dynamic behaviour of each mass and energy storage. These equations are solved by using one of the four numerical methods available. A first order , i.e. simple Euler, a second order, i.e. the improved Euler and the third or fourth order Runge - Kutta method of numerical integration can be used.

Fortran X8 multics system

Associated subroutines: see 5.2.

Input data	Units
receiver conditions	
engine speed	rpm

turbocharger speed	rpm
fuel flow rate	kg/rev
fuel or load step size	

Output information

Transient information such as engine acceleration, turbocharger acceleration, variation of the receiver conditions etc.

Finally, the auxiliary subroutines such as gas property subroutines, interpolation and iteration subroutines are fully described in ref. (34).

6. Theoretical predictions

6.1 General

Since programs similar to those described in chapters iv and v have been in use for some time and the basic programming philosophy is unchanged, it was decided not to include 'confirmation' runs which illustrate the prediction capability of the programs. Instead, it is proposed in this chapter to show the variable geometry projections beyond what has already been indicated by the experimental programme. To accomplish this objective, the program was 'calibrated' to reproduce approximately the limiting torque curve data given by the manufacturers. This was achieved by adjusting turbine nozzle angle to get the same air/fuel ratio and varying the fuelling to get the rated conditions. The values of fmep used were those deduced from the experimental results. Since the manufacturers' standard data could not be obtained for the H1 turbocharger series, comparisons have to be confined to a few parameters only. The data available was for the 3LD turbocharger series. Thus parameters such as turbocharger speed can not be compared. For this reason the standard data is not superimposed on Figs. 6.2a to 6.2h, with the exception of sfc. It is useful to note, however, that the bmep curves and the air/fuel ratio schedule in these figures are exact reproductions of the standard data.

Although maximum cylinder pressures were measured during the course of the experimental programme, this information was not sufficiently precise to be compared with the theoretical predictions accurately. However, the pressures predicted by the program were approximately

in agreement with the experimental observations. It was found from the theoretical predictions that cylinder peak pressures do not reach the limiting value of 138 bar under normal i.e. unrestricted conditions and thus enabled further fuelling under restricted conditions, provided compressor surge could be avoided. It was evident from the start that for a successful variable geometry scheme, a wide mass flow range compressor is essential. It was thus decided to increase the surge margin of the present compressor by 10% as shown in Fig. 6.7 to be able to take full advantage of the variable geometry scheme. A 10% improved surge margin is thought to be within the capability of the existing technology. Since peak torque under these conditions is limited by peak cylinder pressure only, provisions were made for lower compression ratio and retarded timing simulations to be performed to obtain maximum possible torque back up.

Since the programs use the analytical turbine subroutine, turbw, it was first necessary to establish whether the turbine performance under restricted conditions was predicted accurately enough. These results are discussed first.

6.2 Simulated turbine performance

Fig. 6.1 shows the variation of turbine efficiency with increasing pressure ratio at turbine speeds of 30000, 50000 and 70000 rpm for the 0% and 50% restriction cases. It is evident that there is close agreement between the experimental and the theoretically predicted results. The efficiencies for the 50% restricted case agree exceptionally well at every speed while the largest

discrepancy occurs in the unrestricted case at 50000 rpm at a pressure ratio of 1.5 to 1. It is thus seen that the use of the turbine subroutine in the program is justified to a large extent, especially since it saves storage of multi-dimensional arrays which would have to be employed if the experimental results were to be used. However, the agreement at the other restrictions was not as good. But as the investigations are mainly confined to the fully restricted and the fully open cases, these will not effect the results to be discussed here.

6.3 The engine calibration run

Figs. 6.2a to 6.2h show the results obtained after the data was adjusted to reproduce the manufacturers' standard curves. This was thought to be of practical value since the variable geometry experimental results showed that the engine had been derated. Thus to explore the full potential of the variable geometry system, the base curve was chosen to be the standard torque curve obtained by the manufacturers.

Fig. 6.2a shows engine power against engine speed. It is evident that the standard rating of 116 kw at 2600 rpm has been reached. Peak torque occurs at 1600 rpm engine speed corresponding to a 20.5% torque back up at 61.5% maximum engine speed. The corresponding torque values are shown in Table 6.1. The bmep curve is shown in Fig. 6.2b. Turbocharger speed and boost pressure ratio are shown in Figs. 6.2c and 6.2d. A maximum turbocharger speed of just over 100000 rpm is reached at 2600 rpm engine speed, while the corresponding compressor delivery and engine boost pressure ratios

are 1.92 and 1.82 respectively. Fig. 6.2e shows the engine operating points superimposed on the compressor performance map. It can be seen that this condition too is not an 'ideal' match. However, the large surge margin on the left of the operating points will be beneficial as far as the variable geometry operation is concerned. Specific fuel consumption variation is shown in Fig. 6.2f. A minimum of 0.216 kg/kw-hr occurs at an engine speed of 1800 rpm while this value is lower than the manufacturers' value by 0.015 kg/kw-hr. Since the trend of the sfc curves is in agreement with the manufacturers data the discrepancy may be due to auxiliary equipment on the manufacturers test engine. However, since the following comparisons are more qualitative than quantitative, this discrepancy will not be important.

Air/fuel ratio is shown in Fig. 6.2g. This is an exact reproduction of the standard data. Maximum exhaust temperature is about 650 deg. C which is shown together with other temperatures in Fig. 6.2h.

6.4 Fully restricted limiting torque projections

The results of this set of simulations are presented in Figs. 6.3a to 6.3h. From Fig. 6.3a it is evident that with the turbine fully restricted, there is a penalty on the maximum power produced by the engine. This is due to the negative loop work imposed on the engine by the tight turbine throat area. However, under continuously variable geometry scheme, the turbine throat area would be fully open at this engine speed leading to the attainment of the rated conditions. Under such conditions the engine will be

producing constant power down to a speed of approximately 1900 rpm.

Brake mean effective pressure is shown in Fig. 6.3b. The peak torque now occurs at 1400 rpm limited by the maximum cylinder pressure of 138 bar (Table 6.2). This corresponds to a torque back up of 50.2% at 54% maximum engine speed. This is a substantial increase over the unrestricted case described above. Table 6.2 shows that the air/fuel ratio at this speed is not the minimum permissible and thus, had the cylinder pressure not reached its limit, even a higher peak torque could have been achieved.

Fig. 6.3c shows the variation of turbocharger speed with engine speed. The maximum turbocharger speed is slightly over 110000 rpm and occurs at the maximum engine speed. However, this over-speeding will not occur when the continuously variable geometry scheme is employed. With the continuously variable geometry scheme it will be possible to maintain turbocharger speed around 100000 rpm under these conditions.

The corresponding compressor delivery pressure and engine inlet manifold pressures are shown in Fig. 6.3d. The maximum boost level of 2 is reached beyond speeds of 2150 rpm, indicating that a continuously variable geometry system would open to keep the boost and turbocharger speed down.

The limitations of the present compressor are clearly illustrated in Fig. 6.3e. Under fully restricted conditions, between engine speeds of 1200 and 1400 rpm inclusive, compressor surge is a problem that can be overcome by the use of wider mass flow range units or with compressor prewhirl. As it was mentioned earlier, a 10% increase

in the surge margin has been allowed to enable the program to run under the present conditions.

Specific fuel consumption, which is shown in Fig. 6.3f, has improved over the entire low and mid-speed range while in the higher speed range a considerable deterioration due to large negative pumping work has occurred (cf. Fig. 6.2f). This is mainly due to the increased power output while the fmep losses are the same as before. Air/fuel ratio is shown in Fig. 6.3g. It is evident that the very generous air/fuel ratio of 33 at 2600 rpm is unnecessary and occurs as a result of the excessive turbine restriction at this point. Had the turbine been unrestricted to keep the turbocharger speed down, the air/fuel ratio at this speed would still be sufficiently generous but not excessive. The air/fuel ratio at peak torque is still not the minimum permissible and has a value of 21. If peak cylinder pressures are kept down by lower compression ratio or retarded timing, higher peak torques can be reached.

The various temperatures are shown in Fig. 6.3h. Again the highest exhaust temperature occurs in the lowest air/fuel ratio region and is 630 deg. C at 1200 rpm engine speed.

6.5 Low compression ratio results

As it was indicated above, if a wide mass flow compressor is employed, the only constraint in peak torque will be the peak cylinder pressure limit. Air/fuel ratio is less of a problem if the minimum of 18 accepted by the manufacturers is also adopted here, (cf. Fig. 6.2g). Therefore, to overcome this limitation, two options were considered. Namely, the use of lower compression

ratio pistons or fuel injection retard. Both of these were investigated using the steady state program. Figs. 6.4a to 6.4h show the results for a compression ratio reduction from 16:1 to 14:1, maximum cylinder pressure occurring at 1400 rpm engine speed.

Fig. 6.4a shows the variation of engine power with engine speed. Peak power occurs at 1800 rpm, while there is a reduction of power at 2600 rpm due to excessive turbine restriction.

Brake mean effective pressure variation is shown in Fig. 6.4b. A maximum torque back up of 75.3% occurs at 1400 rpm, i.e. at 54% maximum engine speed. This is a substantial improvement over the standard compression ratio case.

The slight over-speeding of the turbocharger is shown in Fig. 6.4c. Again this can be avoided by the use of the continuously variable geometry scheme. The corresponding compressor delivery pressure ratio and inlet manifold pressure ratio is shown in Fig. 6.4d. The boost is well over 2:1 from an engine speed of 1600 rpm onwards, indicating the need for less turbine restriction in this region.

Fig. 6.4e shows the compressor performance map with superimposed engine operating lines. It can be seen that at an engine speed of 1200 rpm, the operating point is beginning to go beyond the extended surge region and thus represents the ultimate limit at this engine speed with this assumed compressor map. However, since 1200 rpm is below the peak torque speed of 1400 rpm, fuelling can be cut back at the expense of a sharp fall in engine torque below 1400 rpm.

Fig. 6.4f represents the sfc variation. There is a slight

deterioration in sfc at the lower and the higher speed range with no appreciable change in between these two extremes.

Air/fuel ratio and the various temperatures are shown in Figs. 6.4g and 6.4h. The air/fuel ratio at peak torque is still above the minimum of 18, while peak exhaust temperature is 660 deg. C and occurs at 1200 rpm.

6.6 Retarded timing results

Since a reduction in compression ratio will tend to lead to a reduction in the thermal efficiency of the engine as seen in Fig. 6.4f, particularly apparent in the lower and the higher speed range, together with the inevitable starting difficulties associated with low compression ratio, it may ultimately prove necessary to use a variable injection timing scheme to retard timing in the peak torque region to keep cylinder pressures below the specified limit of 138 bar. These results are obtained using the standard compression ratio of 16:1 while the injection timing is retarded by 3 degrees in the peak torque region. The same fuelling schedule as in the previous case has been used. These results are shown in Figs. 6.5a to 6.5h.

Similar performance to those obtained with the lower compression ratio are obtained, with a slight improvement in the power and the torque as a result of the better sfc values shown in Fig. 6.5f. Turbocharger speed and the engine operating points on the compressor map, Figs. 6.5c - 6.5e, are similar to the previous case and a maximum exhaust temperature of 650 deg. C occurs at 1200 rpm, Fig. 6.5h, where the air/fuel ratio is 18:1.

6.7 Continuously variable geometry simulations

After the fully restricted runs, it was necessary to investigate the behaviour of the variable geometry turbine under boost control. The same fuelling and injection timing as in the retarded timing runs were used, since this offered the best sfc. Runs using the original boost schedule, i.e. a transition from 1.5 to 2.0 bar boost pressure, proved to be unsatisfactory in this exceptionally high torque back up case as the turbine became unrestricted too early. Thus, it was found that to ensure sufficient boost in the mid-speed range, it was necessary to delay turbine nozzle opening. A schedule where the turbine is still fully restricted up to a boost ratio of 1.8 with the transition occurring between 1.8 and 2.0 was chosen to ensure sufficient boost in the mid-speed range. The results of this study are presented in Figs. 6.6i to 6.6j.

The boost schedule is shown in Fig. 6.6i and the nozzle width variation over the entire operating range is shown in Fig. 6.6j. The effect of this nozzle opening schedule on turbocharger speed and other parameters are now considered.

As the engine speed is reduced, a slight increase in power is observed down to 1600 rpm, beyond which point a sharp drop in power occurs. It is seen that the rated power at 2600 rpm is achieved, (Fig. 6.6a).

The brake mean effective pressure is depicted in Fig. 6.6b. The curve is very similar to the previous case, except in the high speed range where the drop in bmep due to negative loop work is eliminated.

Turbocharger speed is kept above the 90000 rpm line down to an engine speed of 1400 rpm, beyond which point the drop in speed is quite sharp, (Fig. 6.6c). The maximum turbocharger speed is slightly above 100000 rpm which is within the safe limit of operation of the turbocharger. The turbocharger is capable of rotating up to 125000 rpm but 100000 rpm was chosen to comply with manufacturers' recommendations.

The corresponding boost and compressor delivery pressure ratios are shown in Fig. 6.6d. In a pattern similar to the turbocharger speed, the boost is kept above 1.8:1 down to the same engine speed of 1400 rpm, with a sharp fall for lower engine speeds.

The position of the engine operating points on the compressor performance map is slightly improved, Fig. 6.6e. The 1200 and 1400 rpm points are now inside the extended surge margin. (see also Fig. 6.7).

Specific fuel consumption variation is shown in Fig. 6.6f. A minimum of 0.207 kg/kw-hr occurs at 1600 rpm, while a maximum of 0.241 occurs at 2600 rpm.

The air/fuel ratio at peak torque is near 19, Fig. 6.6g, and is closer to the limiting value of 18 than in the previous case. The maximum exhaust temperature is 670 deg. C and occurs at 1200 rpm.

6.8 Transient response simulations

The program TRANIC is capable of constant speed as well as variable speed fuel steps. The experimental programme was based on constant speed fuel steps. However, it became evident that these tests were

quite severe particularly as applied to truck engines. A certain amount of increase in speed can be expected in such applications and thus, it was decide to carry out the computer simulations, using some form of load-speed characteristic. It is quite reasonable to assume a propeller type load curve. The curve adopted is shown in Fig. 6.8. This figure together with the remaining figures show some of the important transient parameters. Tables 6.6 and 6.7 contain other variables not shown graphically.

The runs were carried out keeping everything identical in the two cases except for the turbine throat width. The same schedule as in Fig. 6.6i was used. The fuel pump characteristics were kept unaltered to illustrate the difference in transient response as a result of more air availability only. The compression ratio and injection timing are also identical to the standard values used in the steady state simulations.

The increase in engine torque due to variable geometry operation is clearly shown in Fig. 6.8. Although the nominal air/fuel ratio in both cases falls to 16 as seen in Fig. 6.9, the actual air/fuel ratio is different in the two cases as the fuel is injected into unequal amounts of air. The program takes a lower limit of 16, while the actual air/fuel ratio is lower than that indicated by the program but less acute in the variable geometry case. However, as it is seen from Fig. 6.9, the air/fuel ratio begins to rise much earlier in the case of the variable geometry turbocharger and reaches a value of 27 after 2.5 sec., while for the fixed geometry case, a much longer period of incomplete combustion is followed by only a rise to 20 after the same time. While black smoke is

expected in both cases under such large fuel steps, there is a clear improvement in the variable geometry case. As a result it is seen from Fig. 6.8 that the final equilibrium point is reached about half a second faster with the variable geometry case which represents approximately a 25% improvement.

Engine speed and turbocharger speed are shown in Figs. 6.10 and 6.11. Again the substantial improvement in both is clear, particularly so in the case of the turbocharger speed response. It is 10000rpm higher at the start of the transient period and reaches the limiting value of 100000rpm in less than 2 sec. while with the fixed geometry turbocharger, the speed is still rising and is just higher than 80000rpm.

These runs were an attempt to show the improvements possible without any modifications to the engine with the exception of the incorporation of the variable geometry turbocharger. However, if future experimental investigations confirm the need for revised timing and injection rates further theoretical work will have to be undertaken.

Note on theoretical predictions depicted in the following figures. The fuelling in each set has been adjusted as follows:

Fig. 6.2 series - Fuelling adjusted to reproduce manufacturers' data.

Fig. 6.3 series - Maximum fuelling limited by peak cylinder pressure at 1400 rpm engine speed.

Fig. 6.4 series - Maximum fuelling limited by peak cylinder pressure at 1400 rpm engine speed.

Fig. 6.5 series - Fuelling unchanged from 6.4 series.

Fig. 6.6 series - Fuelling unchanged from 6.4 series.

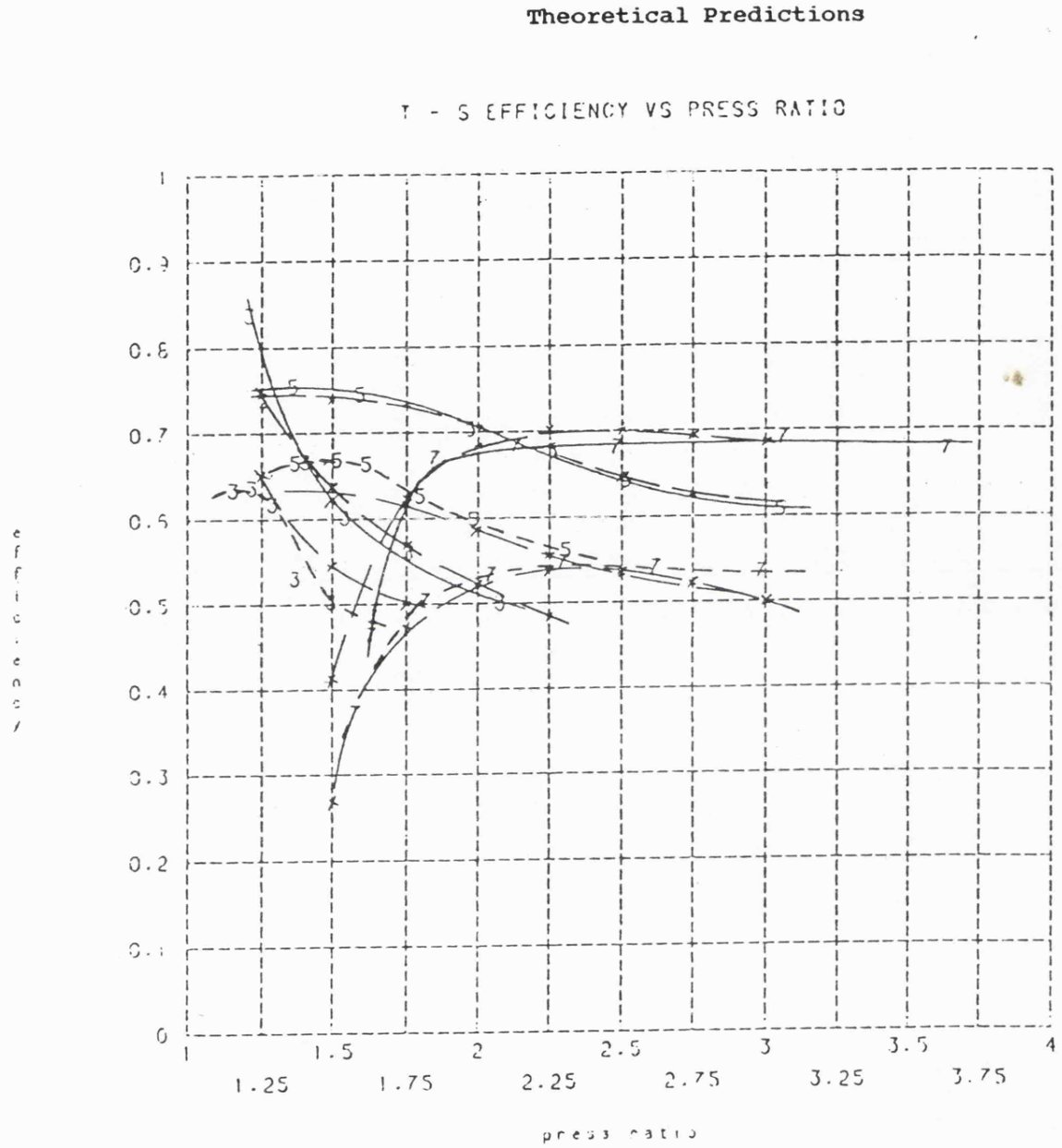

Fig. 6.1 Comparison of Experimental and Predicted Turbine Performance for 0 and 50% Restrictions.

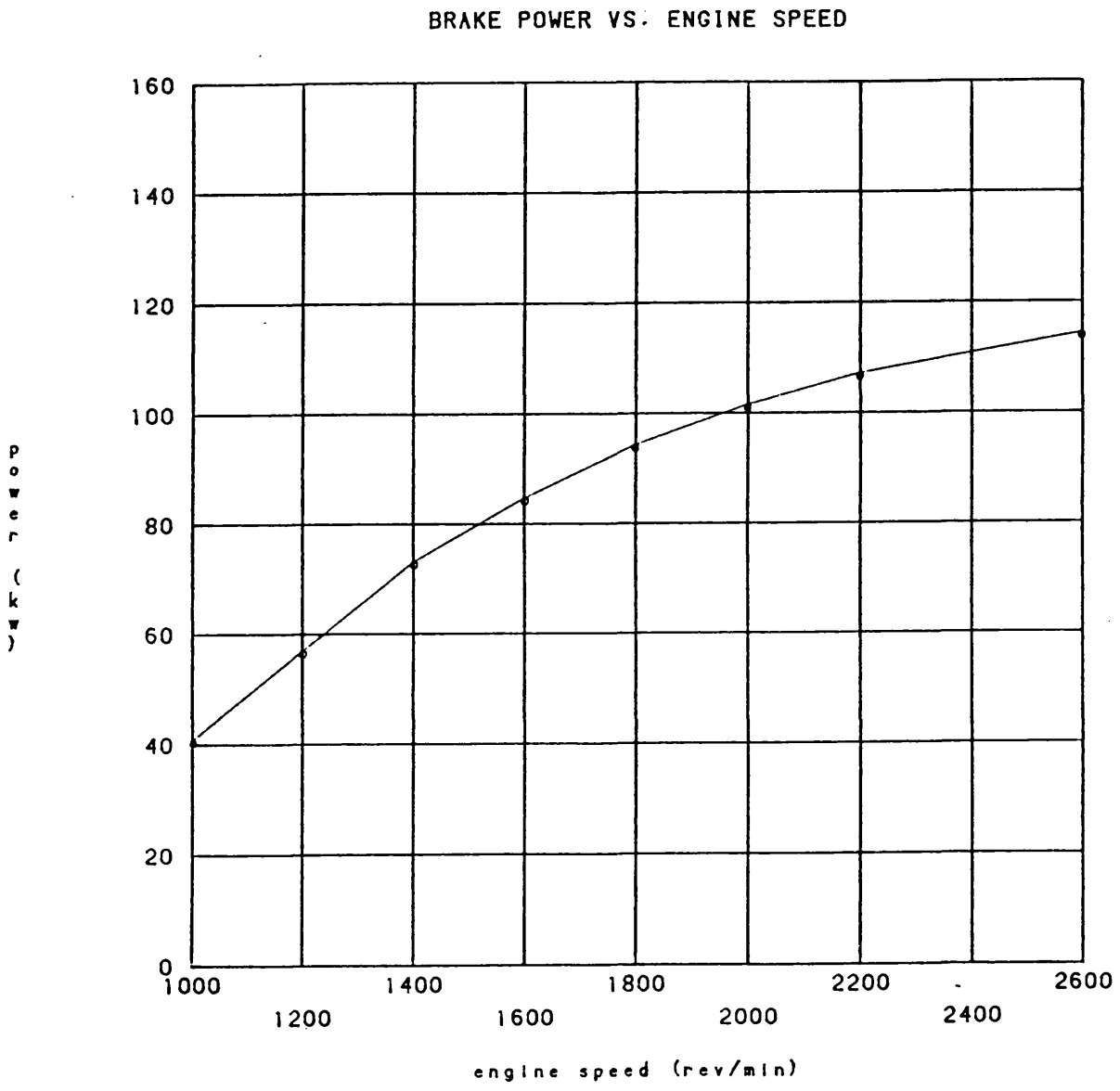

Fig. 6.2a Unrestricted Limiting Torque 'Calibration' Results, Standard Timing, Compression Ratio = 16:1.

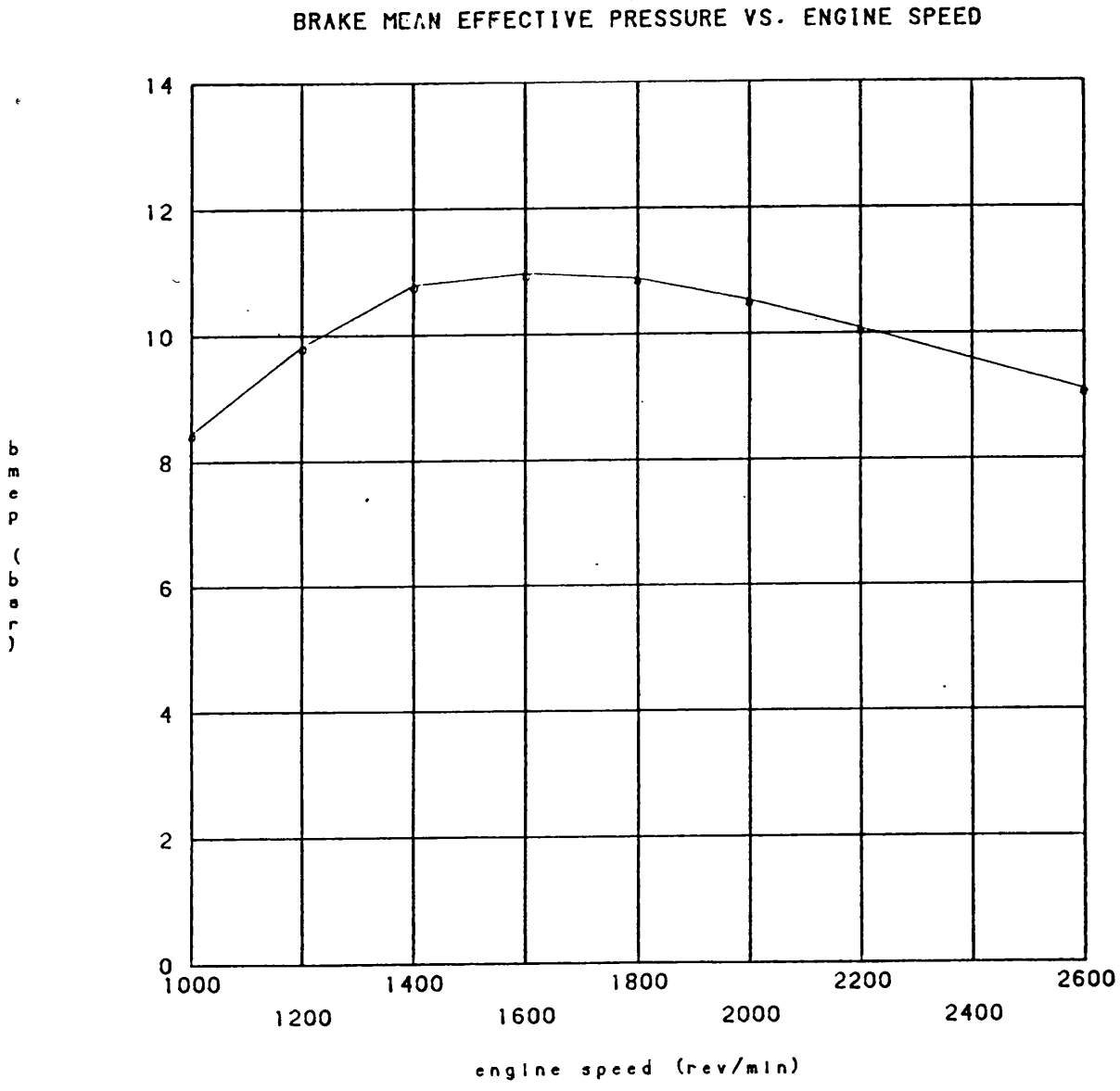

Fig. 6.2b Unrestricted Limiting Torque 'Calibration' Results,

Standard Timing, Compression Ratio = 16:1.

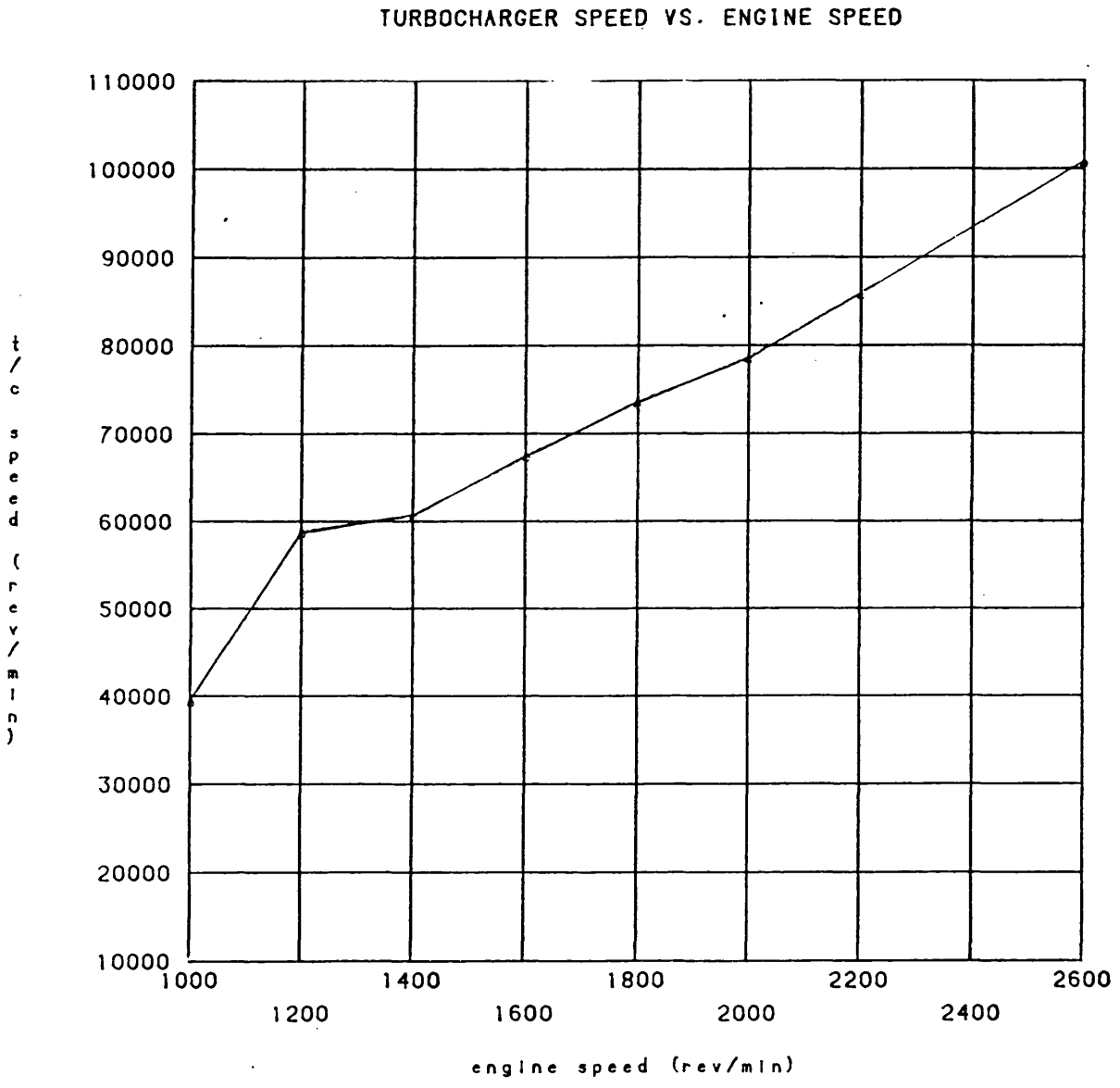

Fig. 6.2c Unrestricted Limiting Torque 'Calibration' Results,

Standard Timing, Compression Ratio = 16:1.

Theoretical Predictions

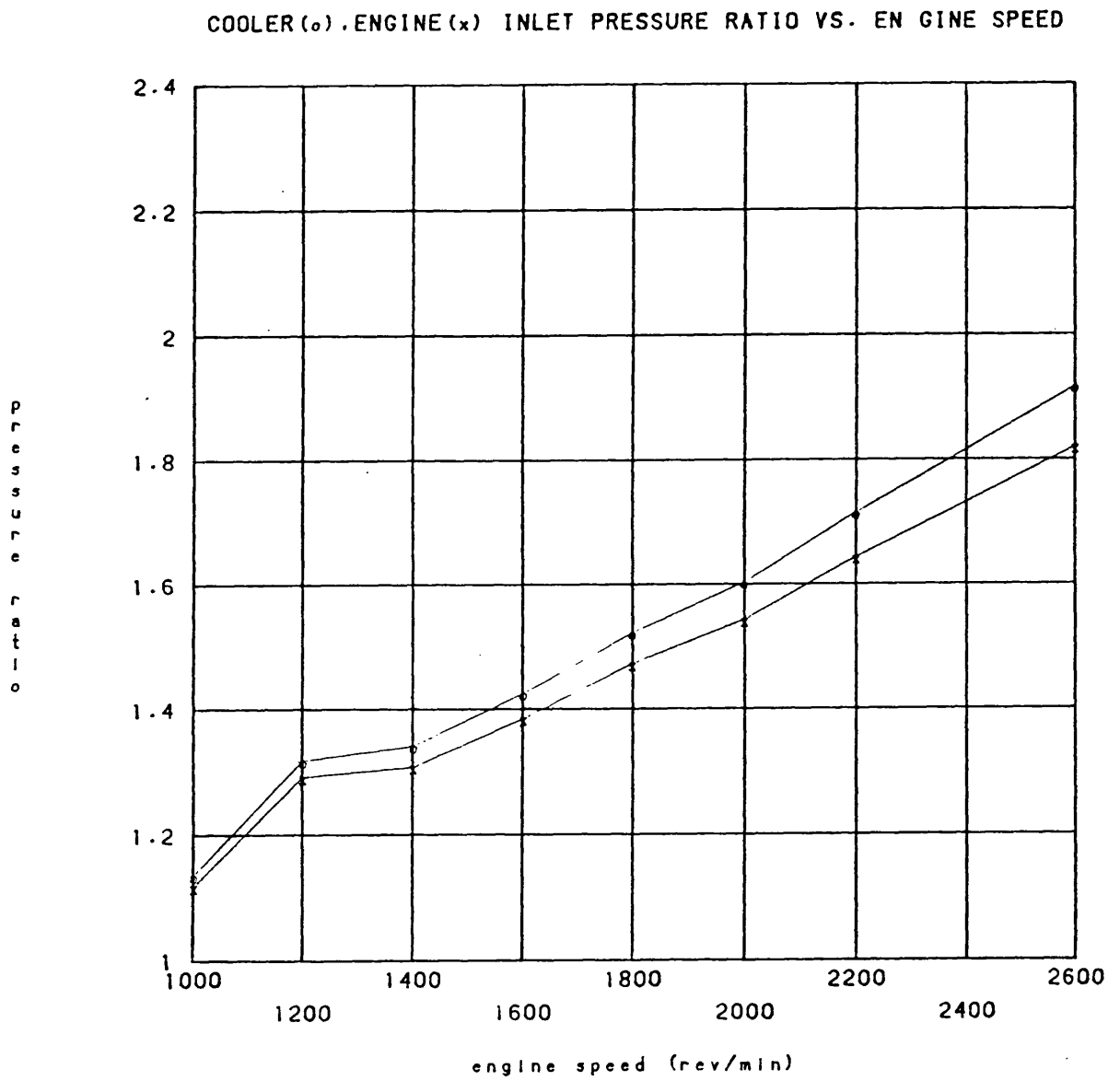

Fig. 6.2d Unrestricted Limiting Torque 'Calibration' Results,

Standard Timing, Compression Ratio = 16:1.

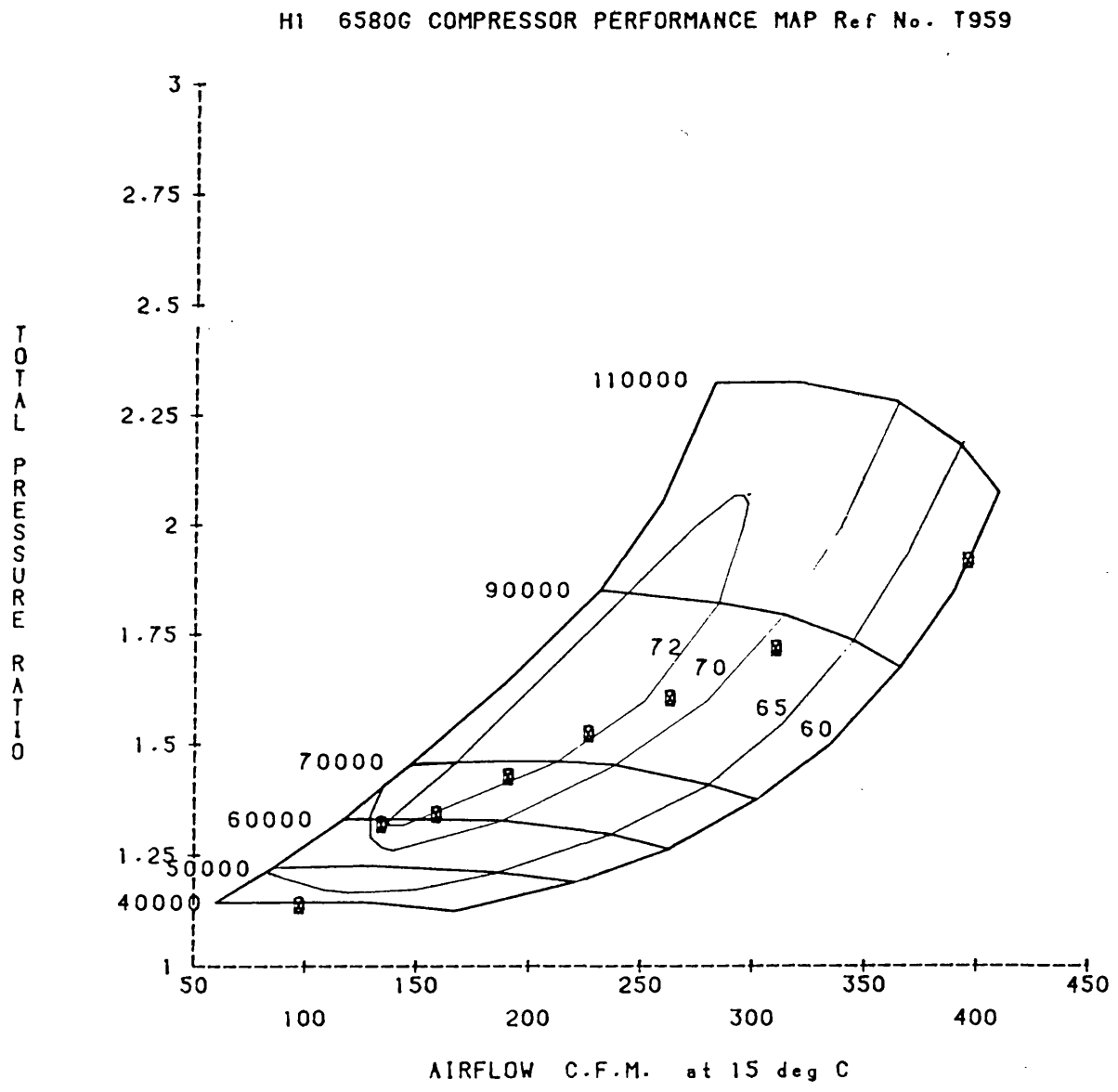

Fig. 6.2e Unrestricted Limiting Torque 'Calibration' Results,

Standard Timing, Compression Ratio = 16:1.

Theoretical Predictions

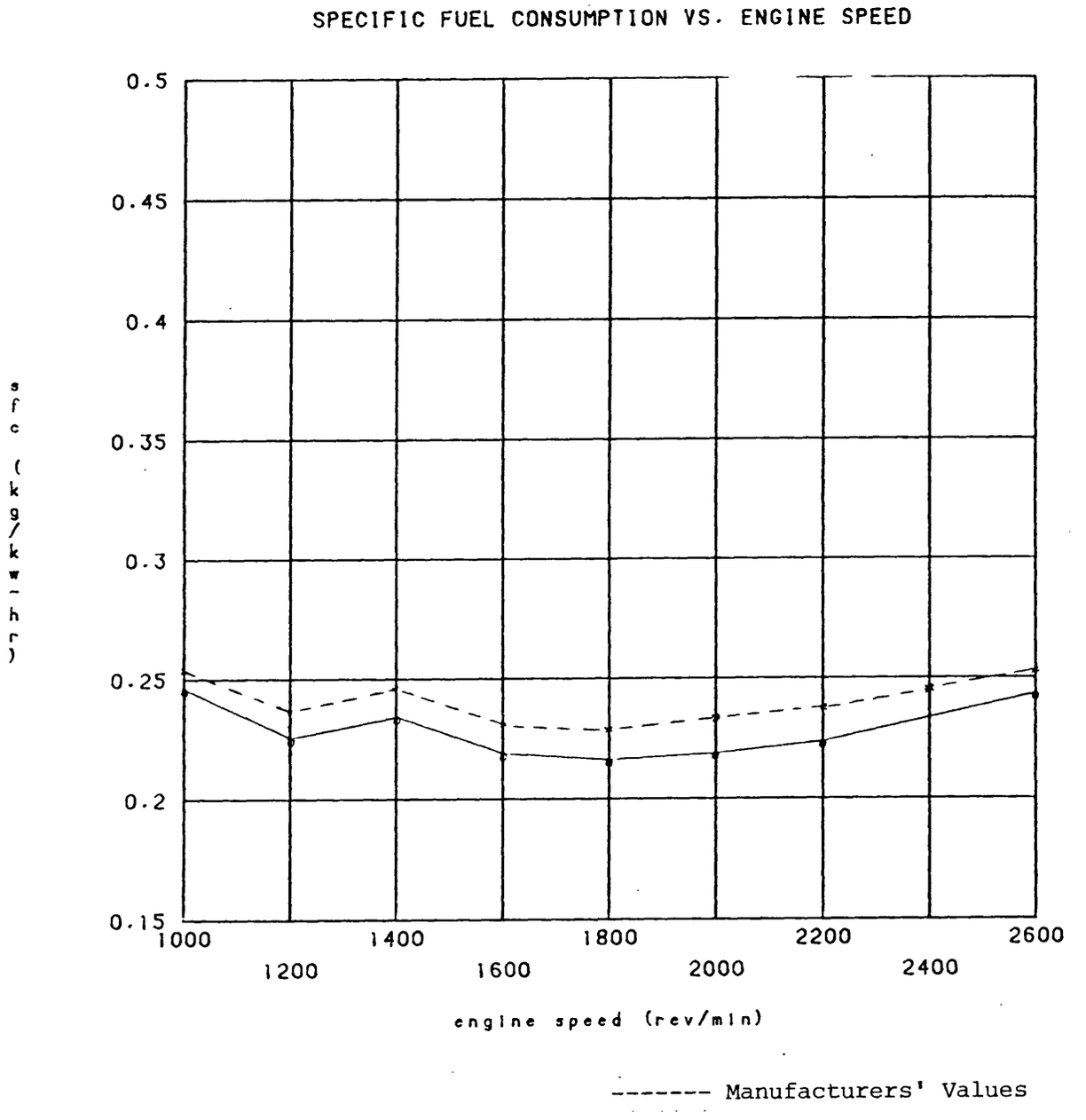

Fig. 6.2f Unrestricted Limiting Torque 'Calibration' Results,

Standard Timing, Compression Ratio = 16:1.

Theoretical Predictions

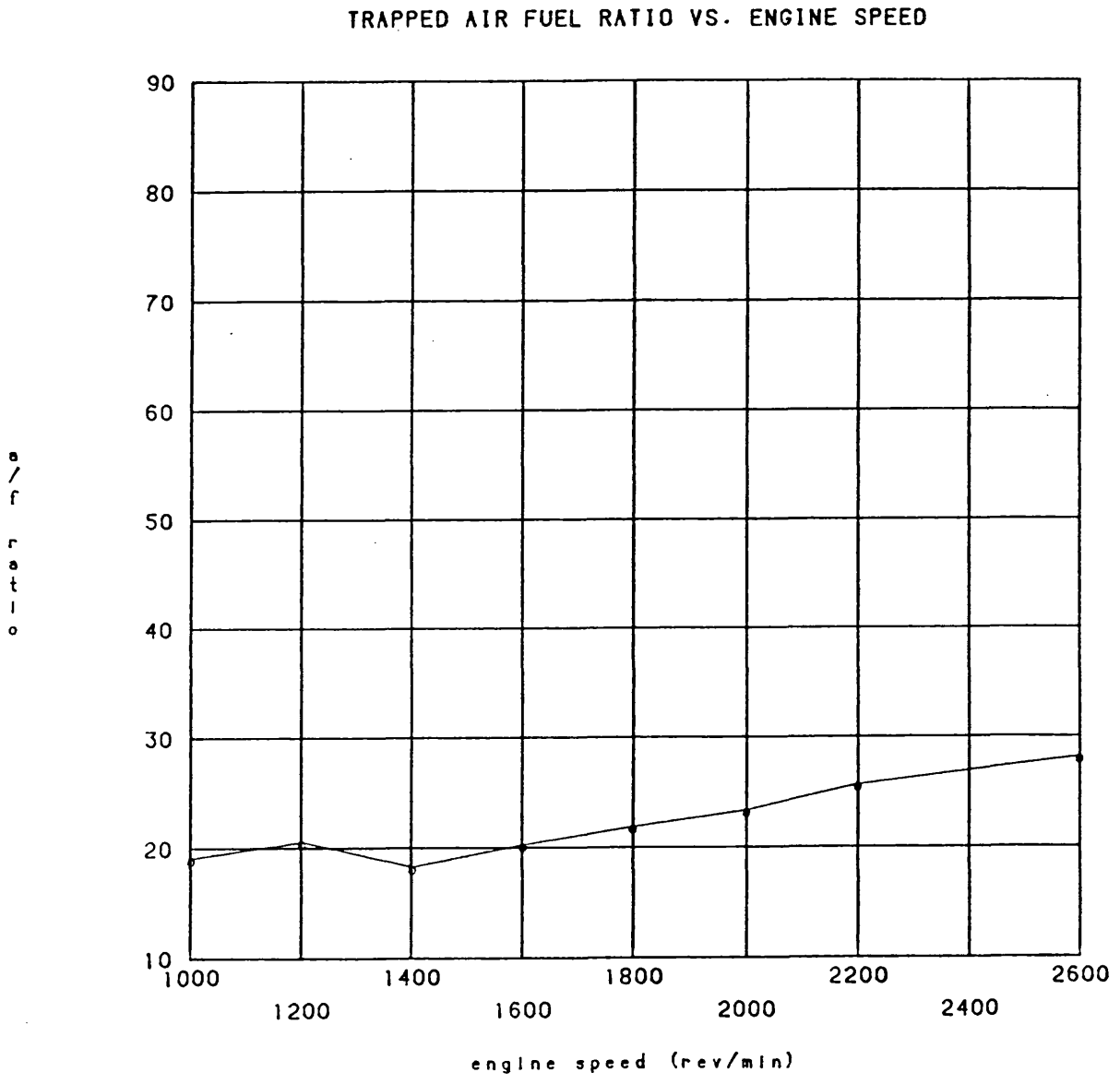

Fig. 6.2g Unrestricted Limiting Torque 'Calibration' Results,

Standard Timing, Compression Ratio = 16:1.

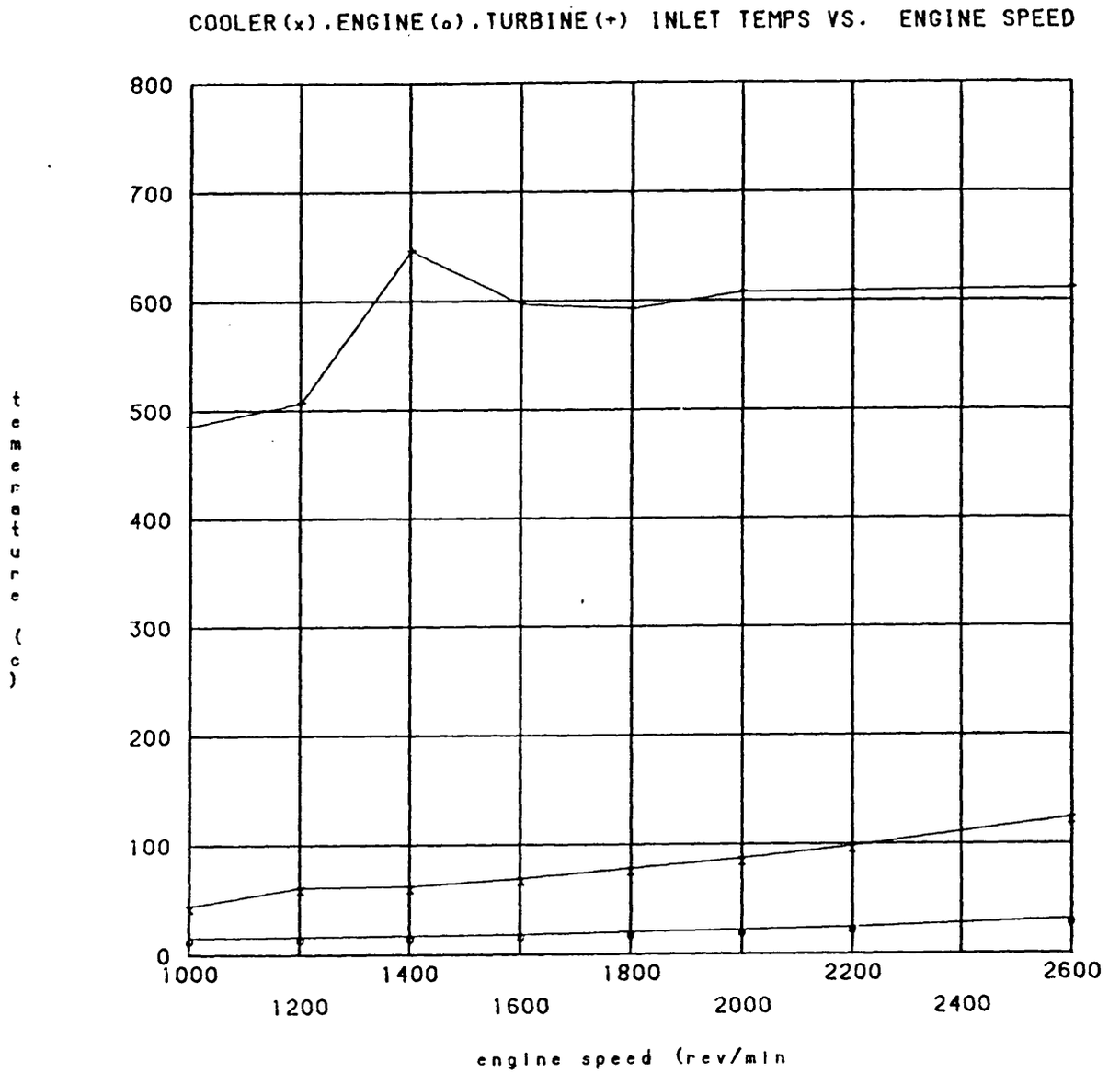

Fig. 6.2h Unrestricted Limiting Torque 'Calibration' Results,

Standard Timing, Compression Ratio = 16:1.

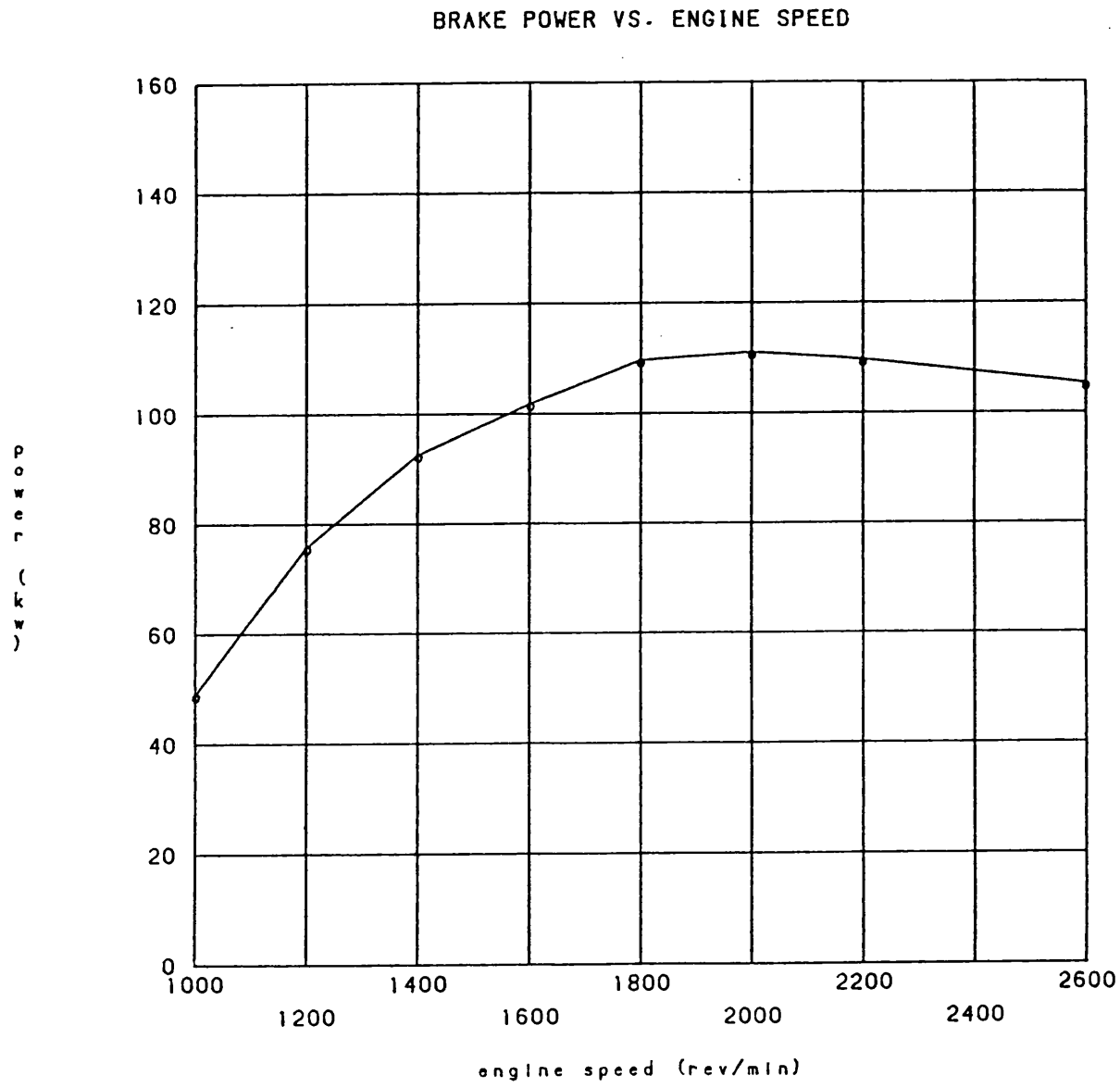

Fig. 6.3a Fully Restricted Limiting Torque Results, Pmax ≠ 138 bar, Standard Timing, Compression Ratio = 16:1.

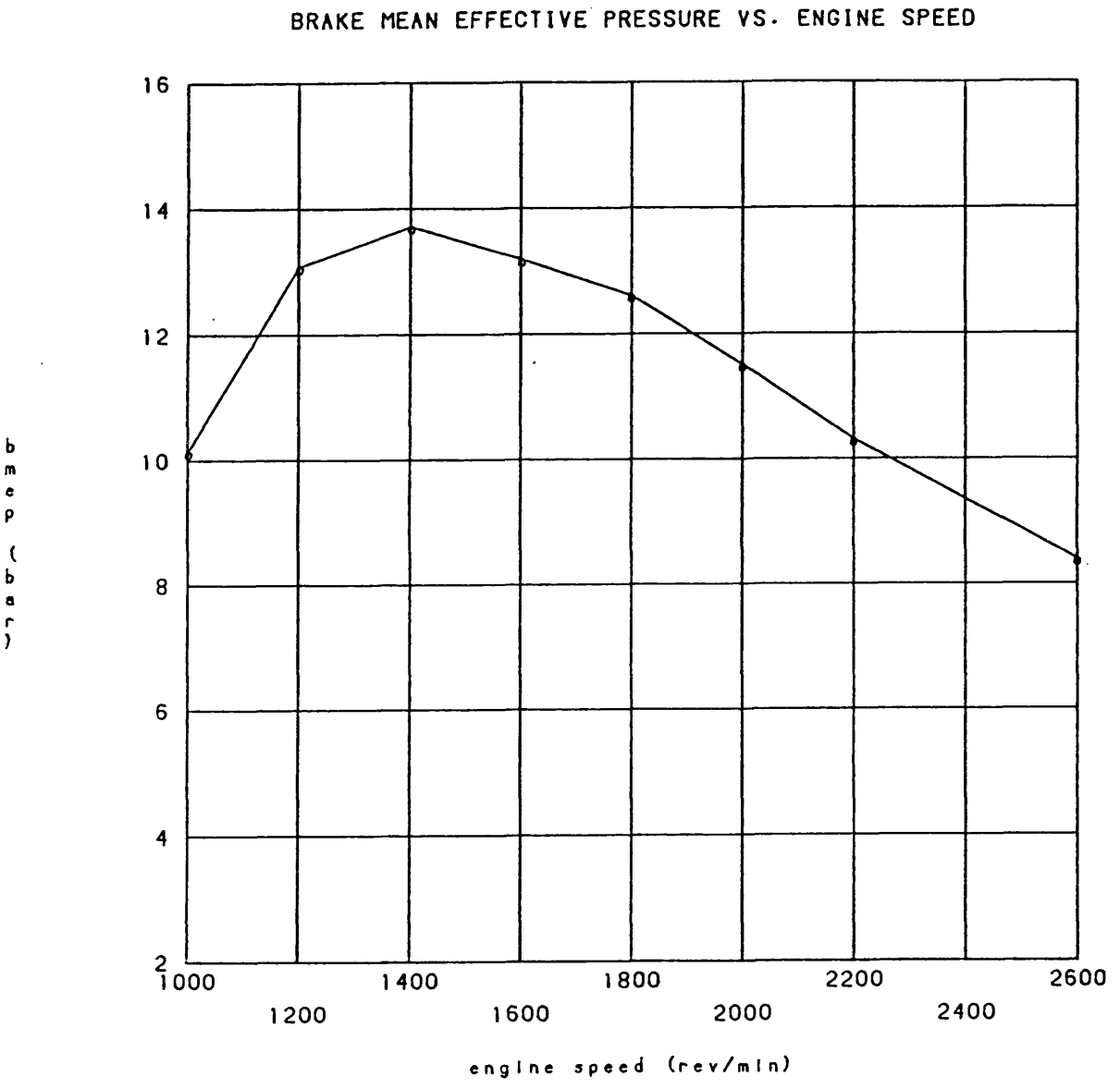

Fig. 6.3b Fully Restricted Limiting Torque Results, Pmax ≯ 138 bar, Standard Timing, Compression Ratio = 16:1.

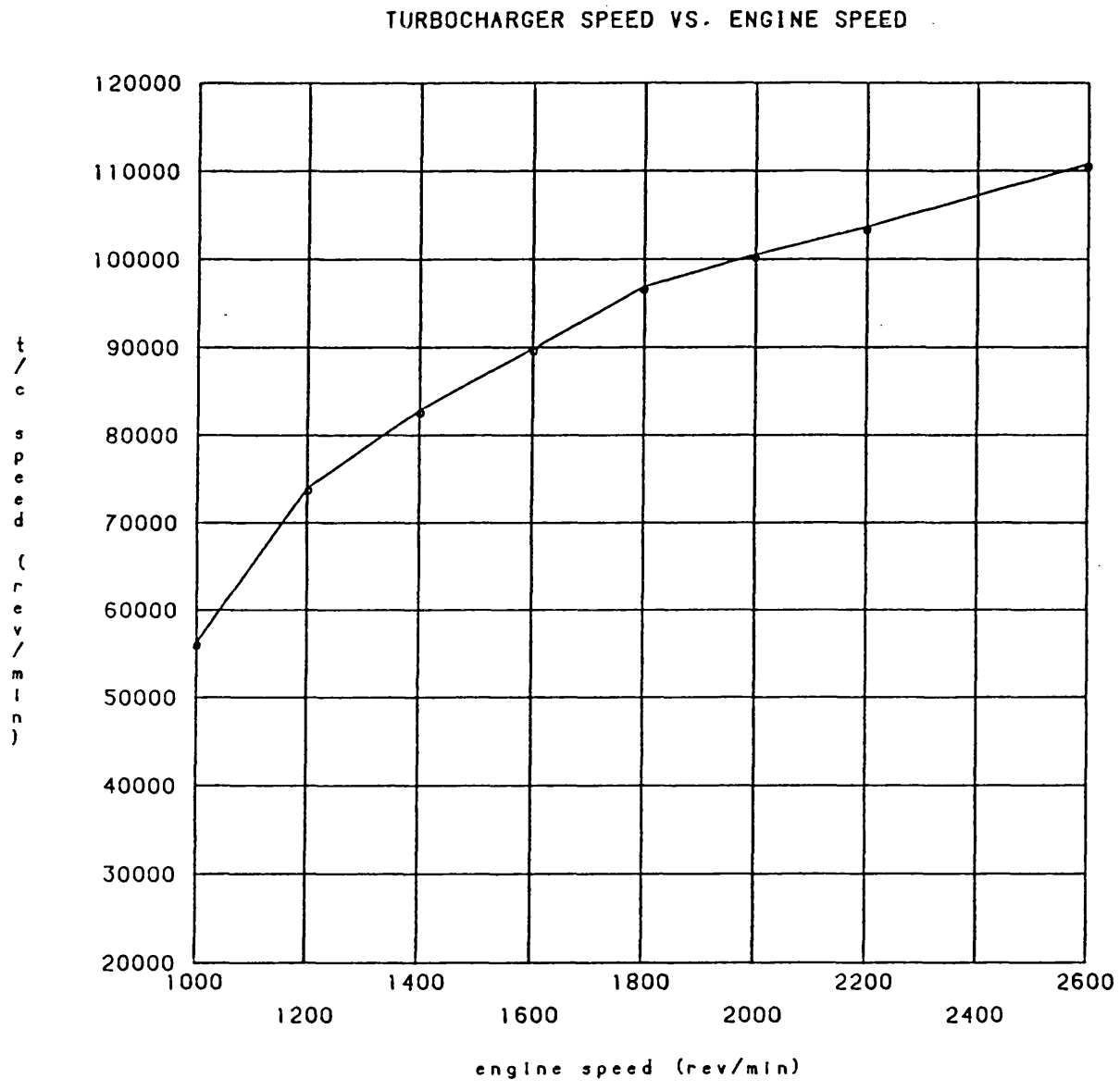

Fig. 6.3c Fully Restricted Limiting Torque Results, Pmax ≯ 138 bar, Standard Timing, Compression Ratio = 16:1.

Theoretical Predictions

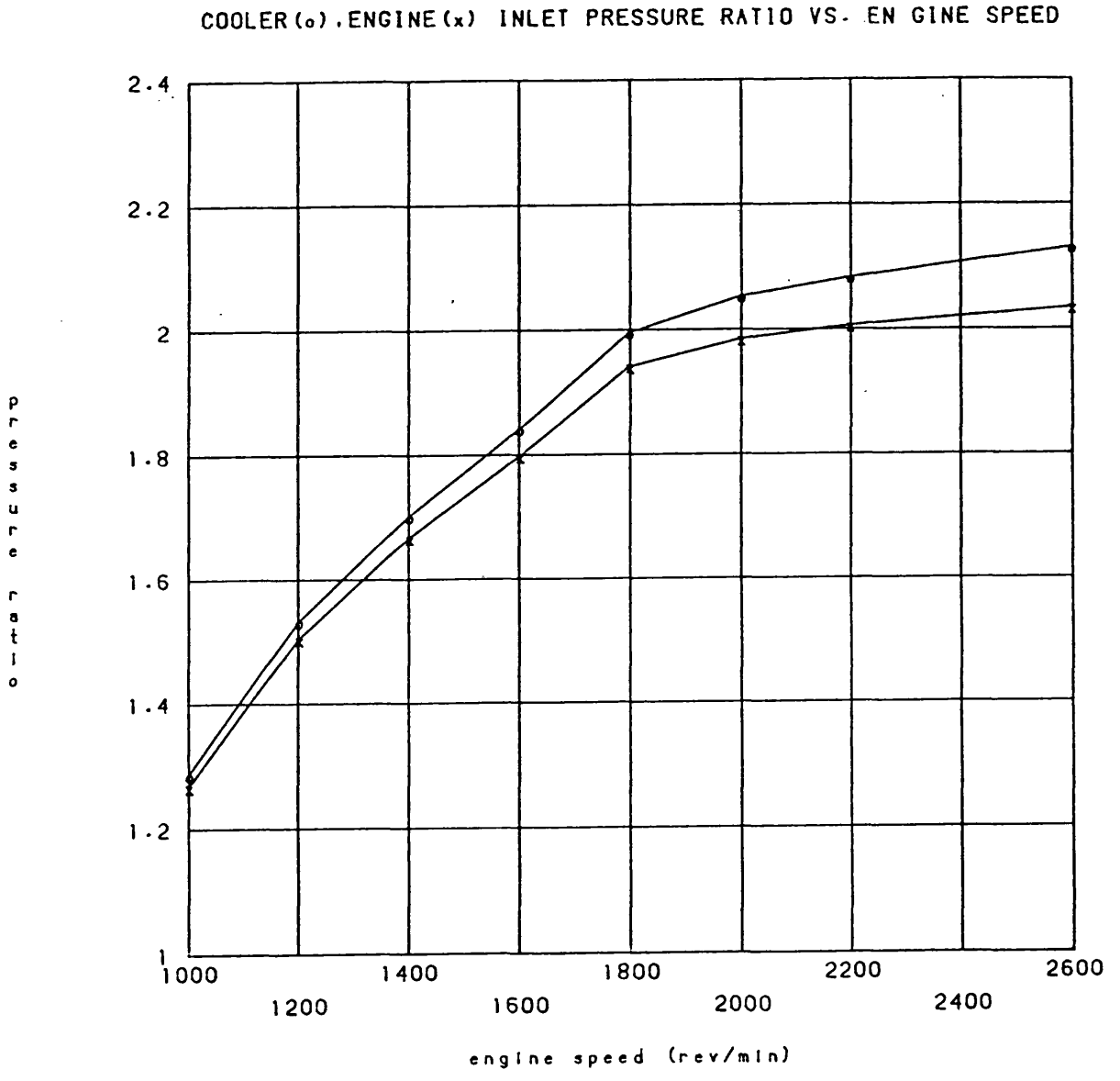

Fig. 6.3d Fully Restricted Limiting Torque Results, Pmax = 138 bar, Standard Timing, Compression Ratio = 16:1.

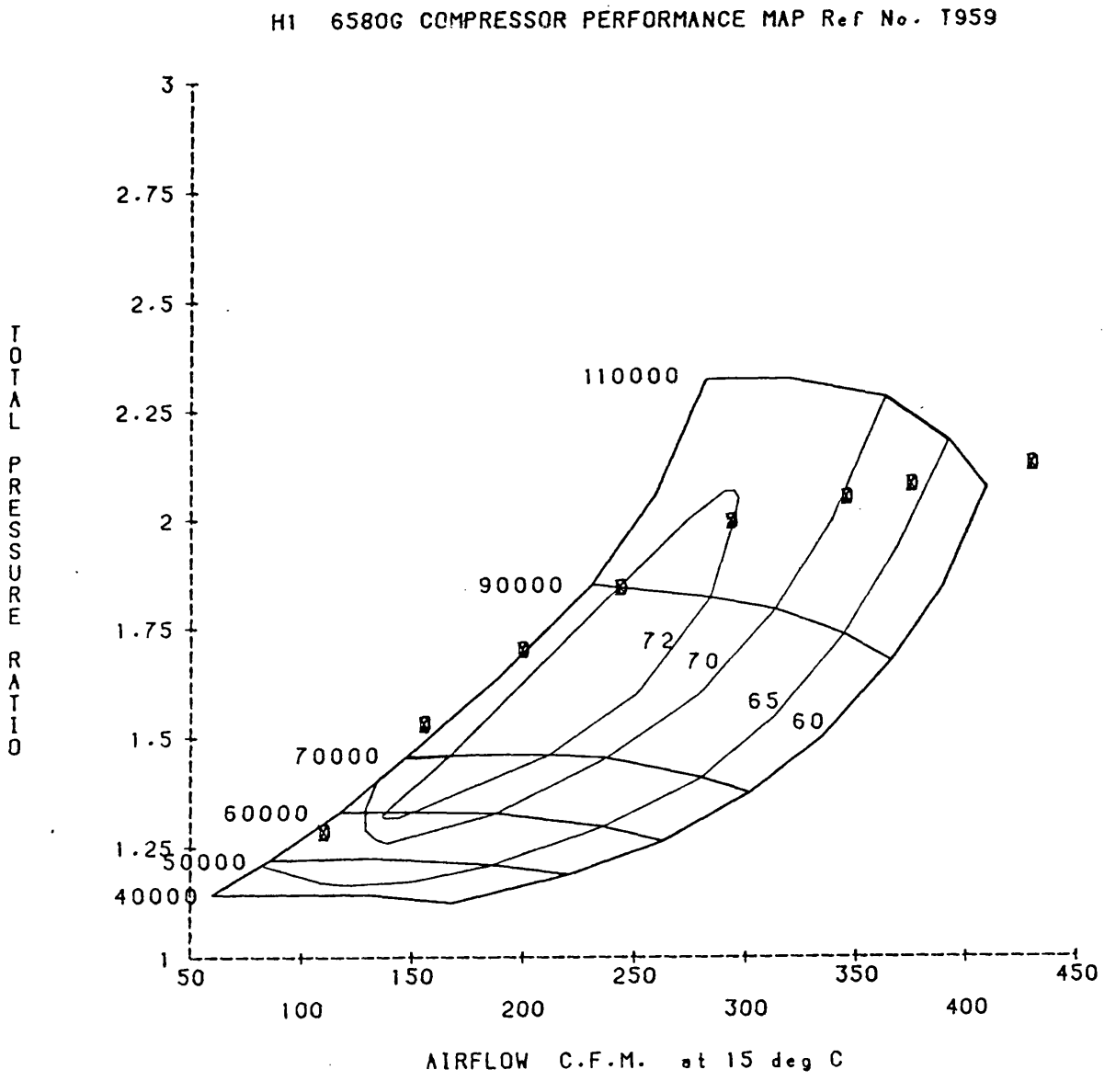

Fig. 6.3e Fully Restricted Limiting Torque Results, Pmax ≯ 138 bar, Standard Timing, Compression Ratio = 16:1.

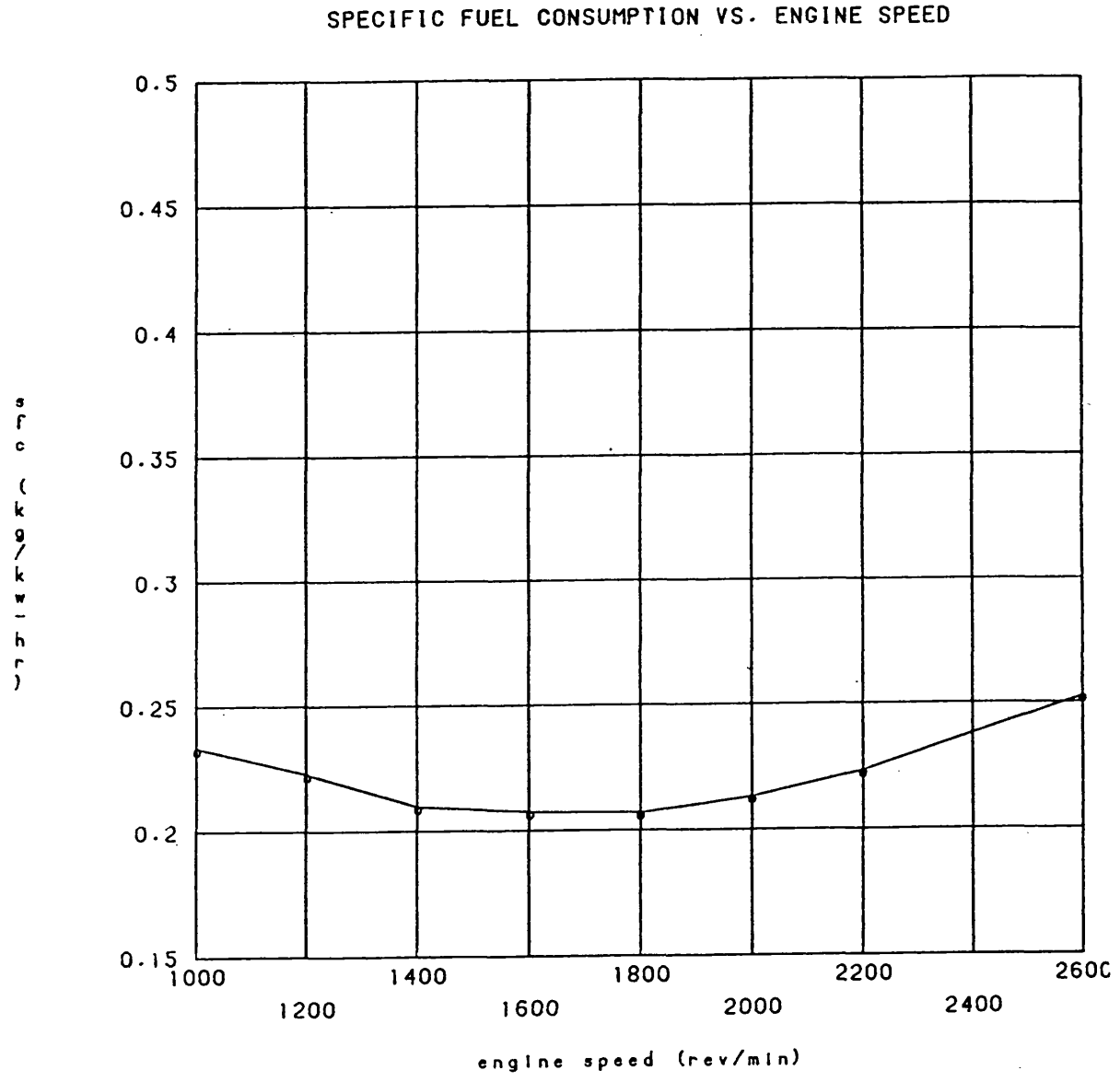

Fig. 6.3f Fully Restricted Limiting Torque Results, Pmax = 138 bar, Standard Timing, Compression Ratio = 16:1.

Theoretical Predictions

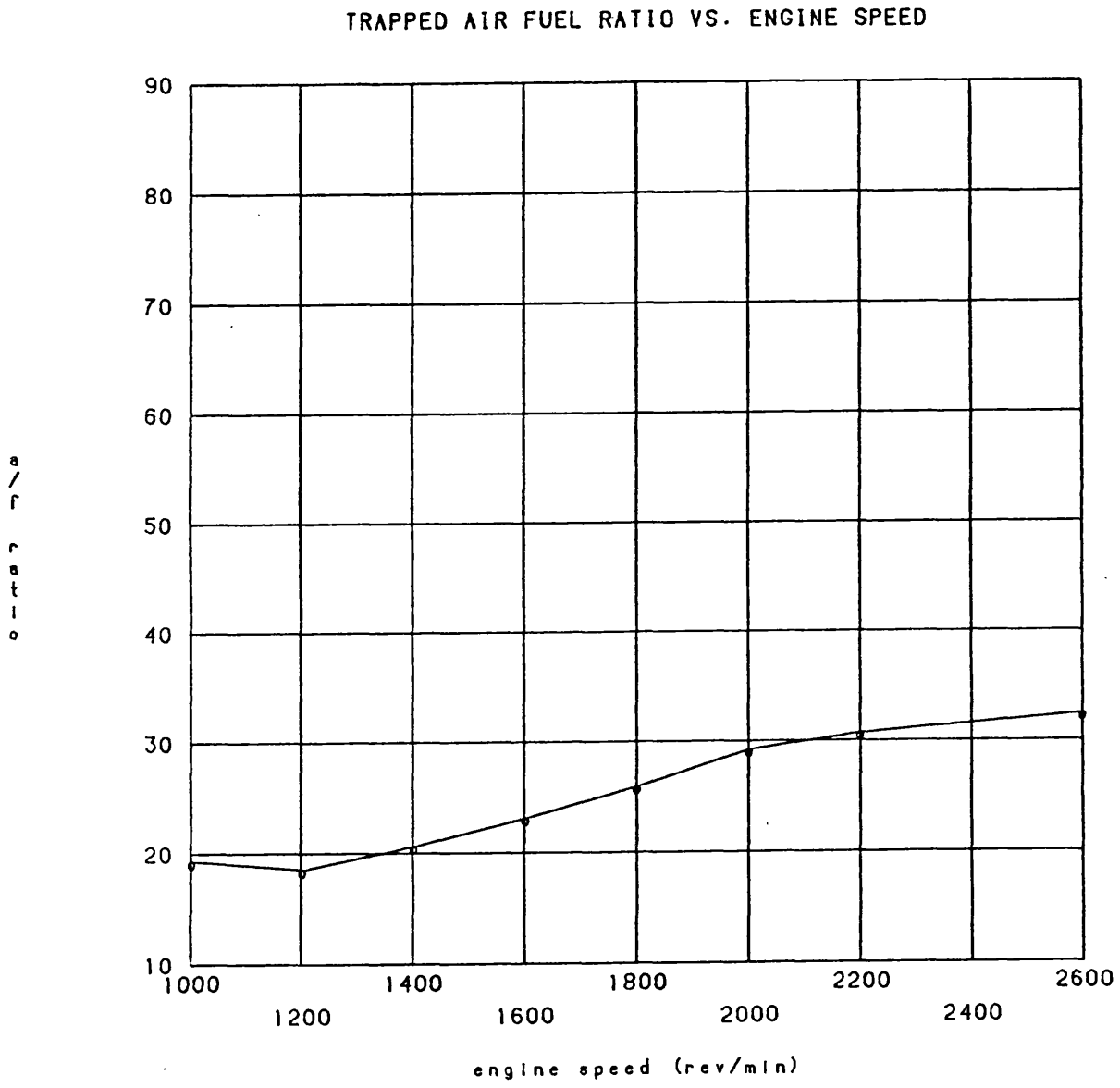

Fig. 6.3g Fully Restricted Limiting Torque Results, Pmax ≯ 138 bar, Standard Timing, Compression Ratio = 16:1.

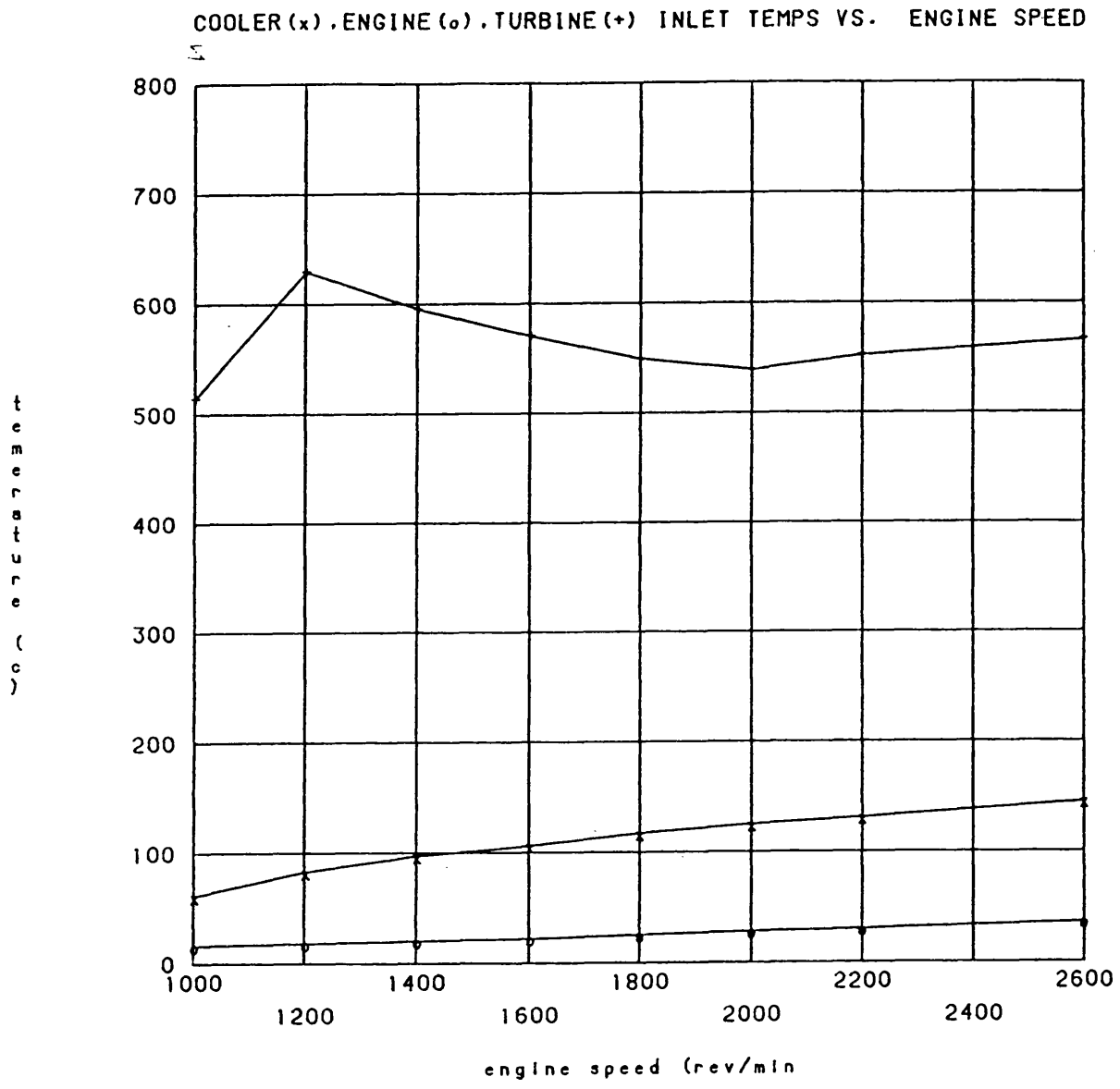

Fig. 6.3h Fully Restricted Limiting Torque Results, Pmax = 138 bar, Standard Timing, Compression Ratio = 16:1.

Theoretical Predictions

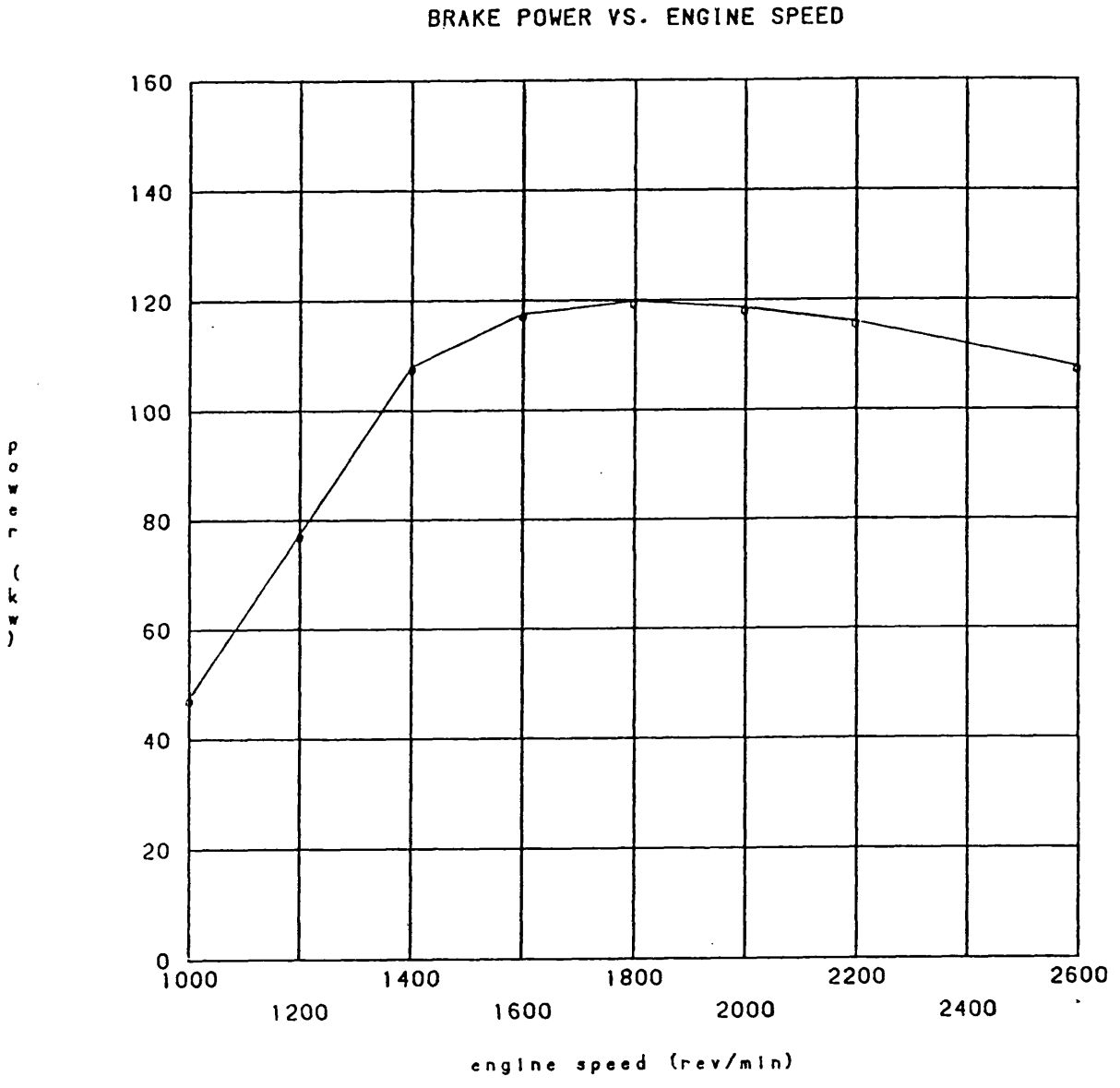

Fig. 6.4a Fully Restricted Limiting Torque Results, Pmax ≯ 138 bar, Standard Timing, Compression Ratio = 14:1.

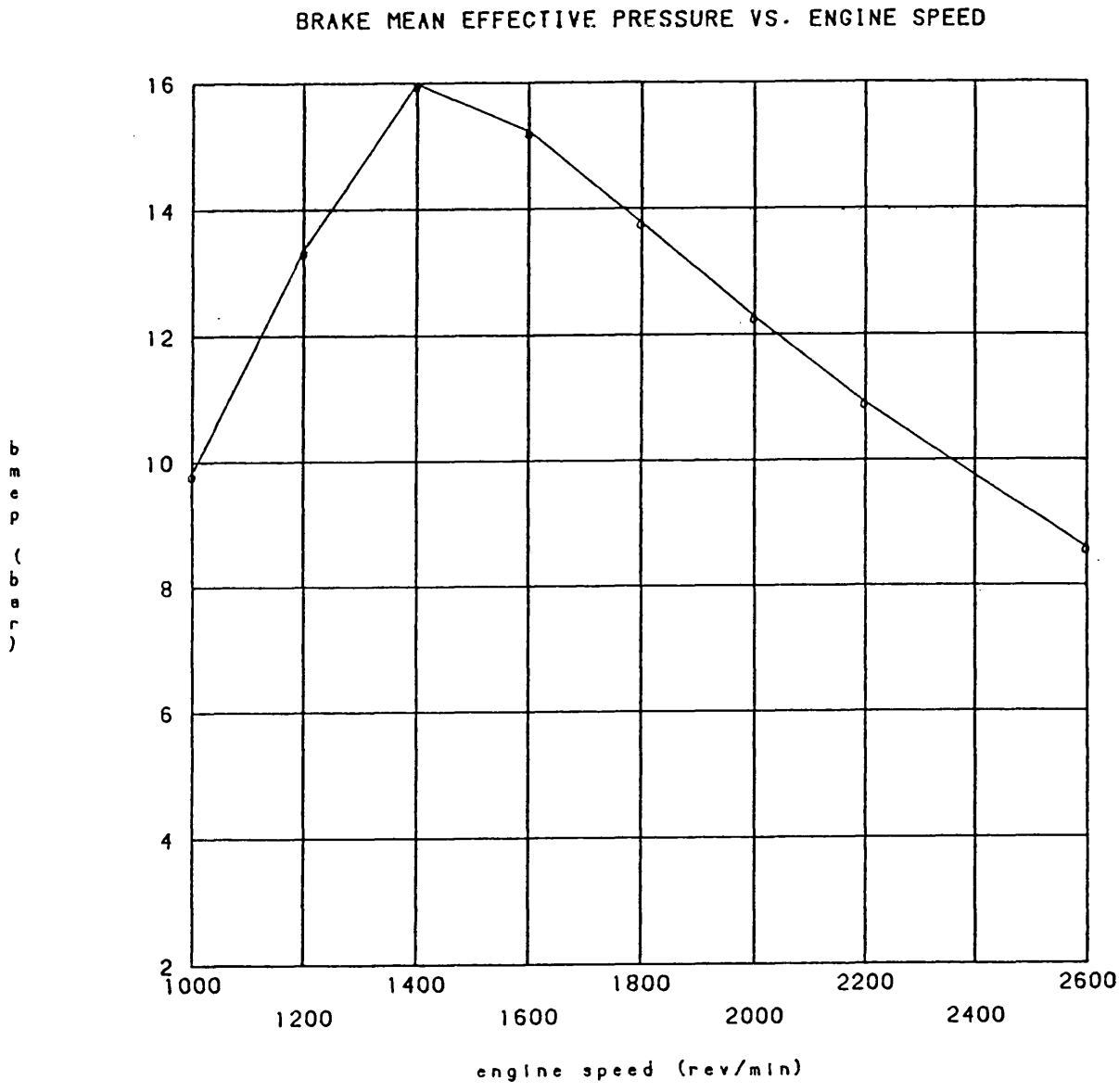

Fig. 6.4b Fully Restricted Limiting Torque Results, Pmax = 138 bar, Standard Timing, Compression Ratio = 14:1.

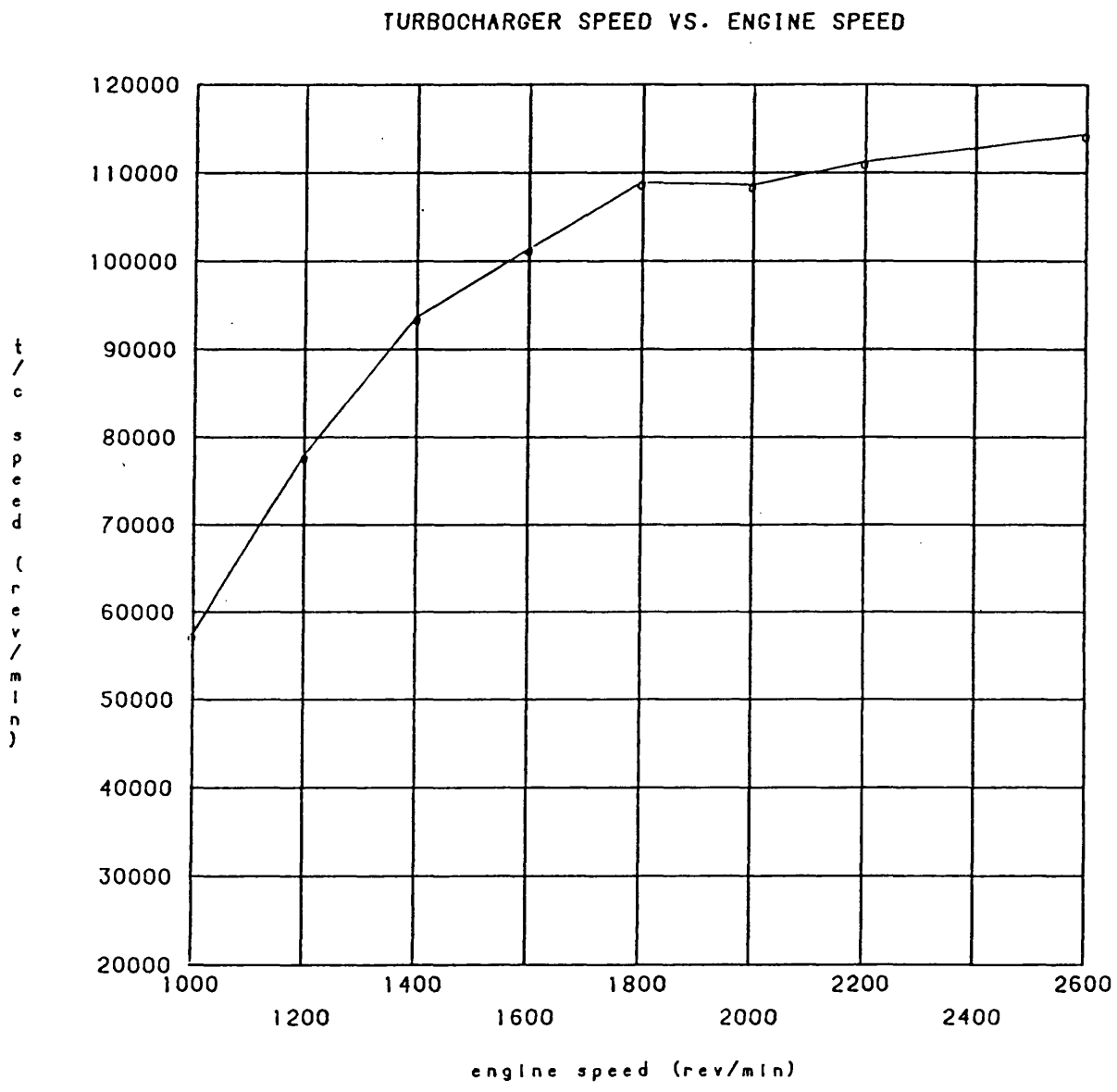

Fig. 6.4c Fully Restricted Limiting Torque Results, Pmax ≯ 138 bar, Standard Timing, Compression Ratio = 14:1.

Theoretical Predictions

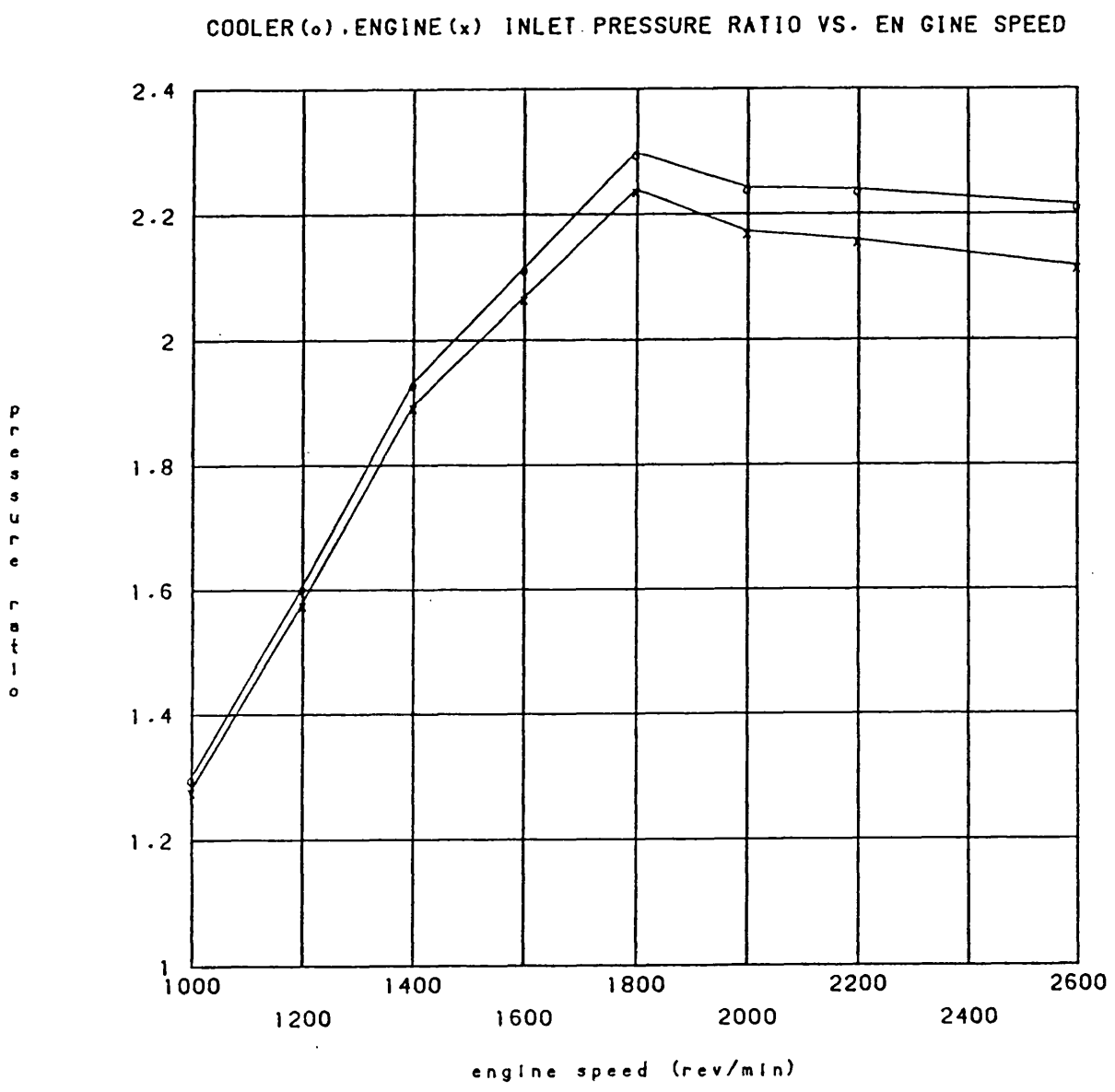

Fig. 6.4d Fully Restricted Limiting Torque Results, Pmax ≯ 138 bar, Standard Timing, Compression Ratio = 14:1.

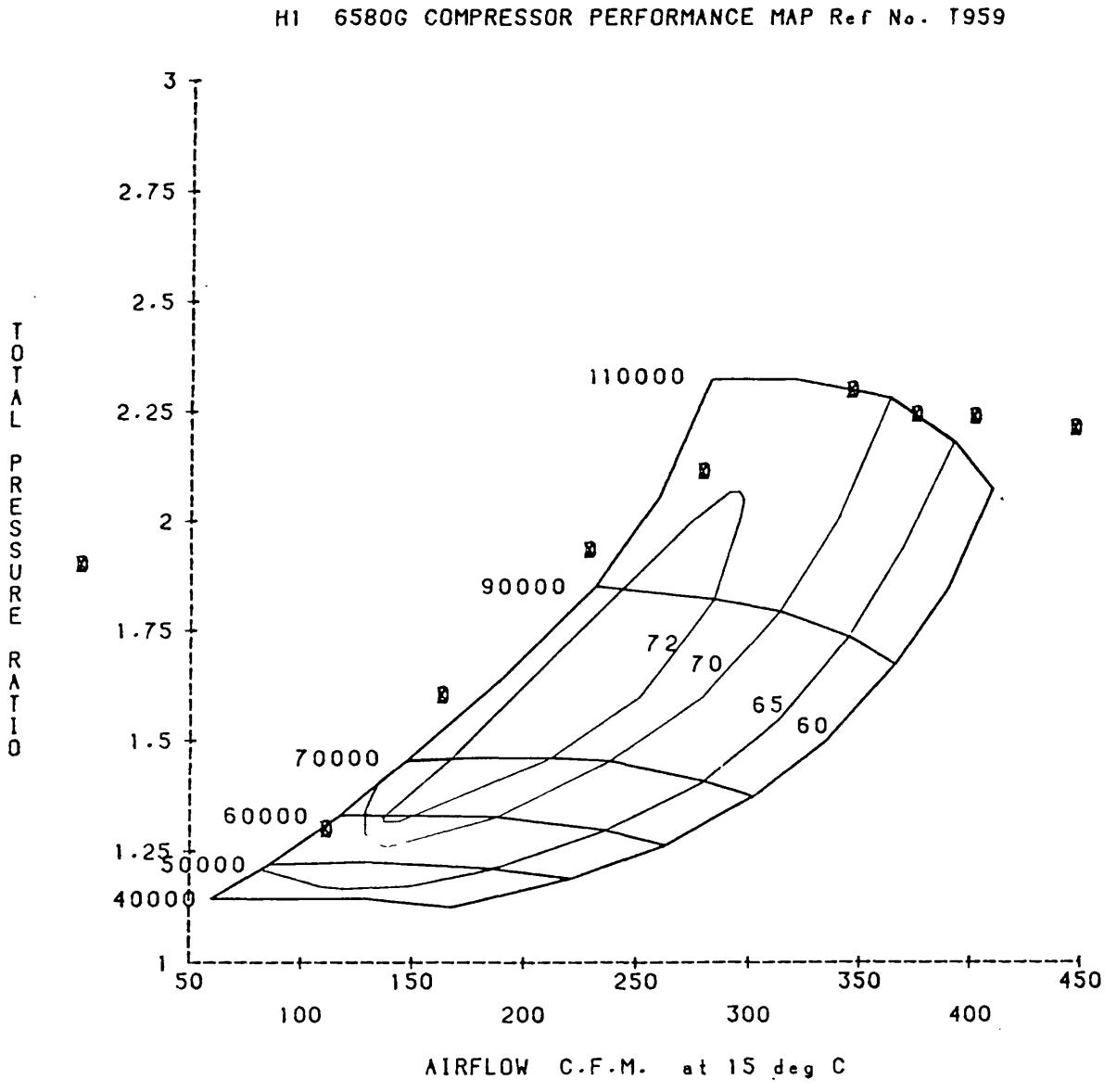

Fig. 6.4e Fully Restricted Limiting Torque Results, Pmax = 138 bar, Standard Timing, Compression Ratio = 14:1.

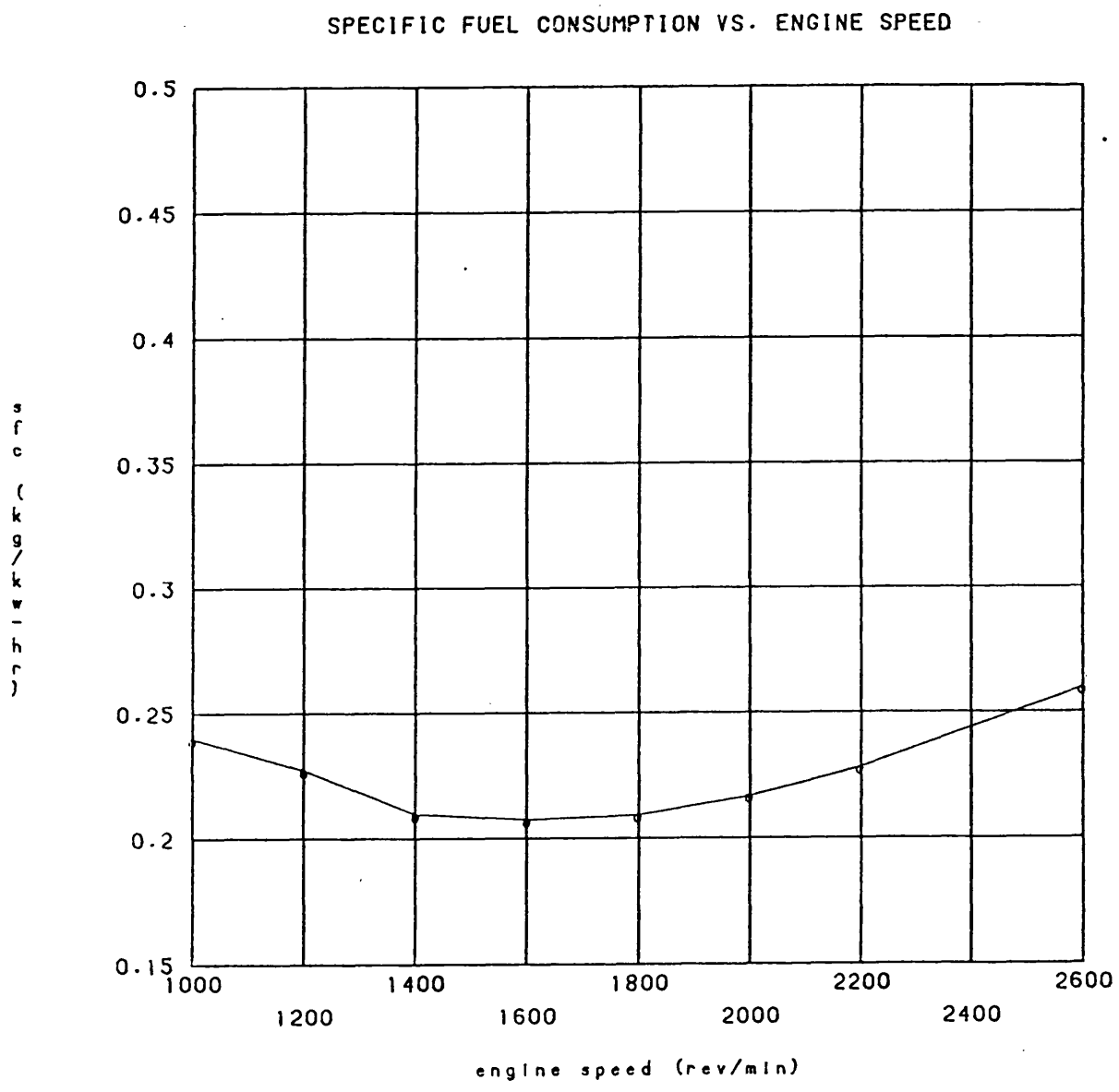

Fig. 6.4f Fully Restricted Limiting Torque Results, Pmax = 138 bar, Standard Timing, Compression Ratio = 14:1.

Theoretical Predictions

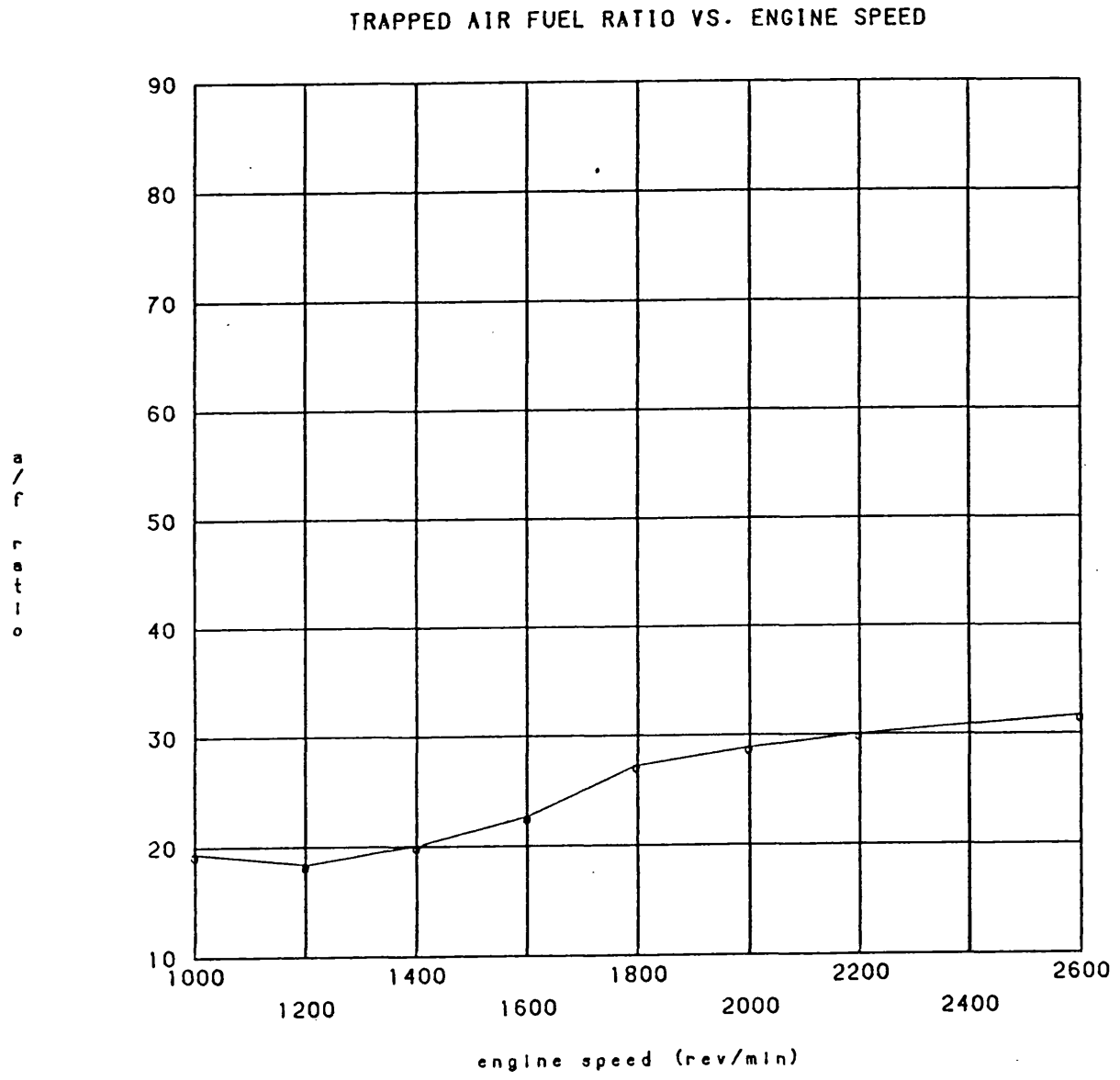

Fig. 6.4g Fully Restricted Limiting Torque Results, Pmax ≯ 138 bar, Standard Timing, Compression Ratio = 14:1.

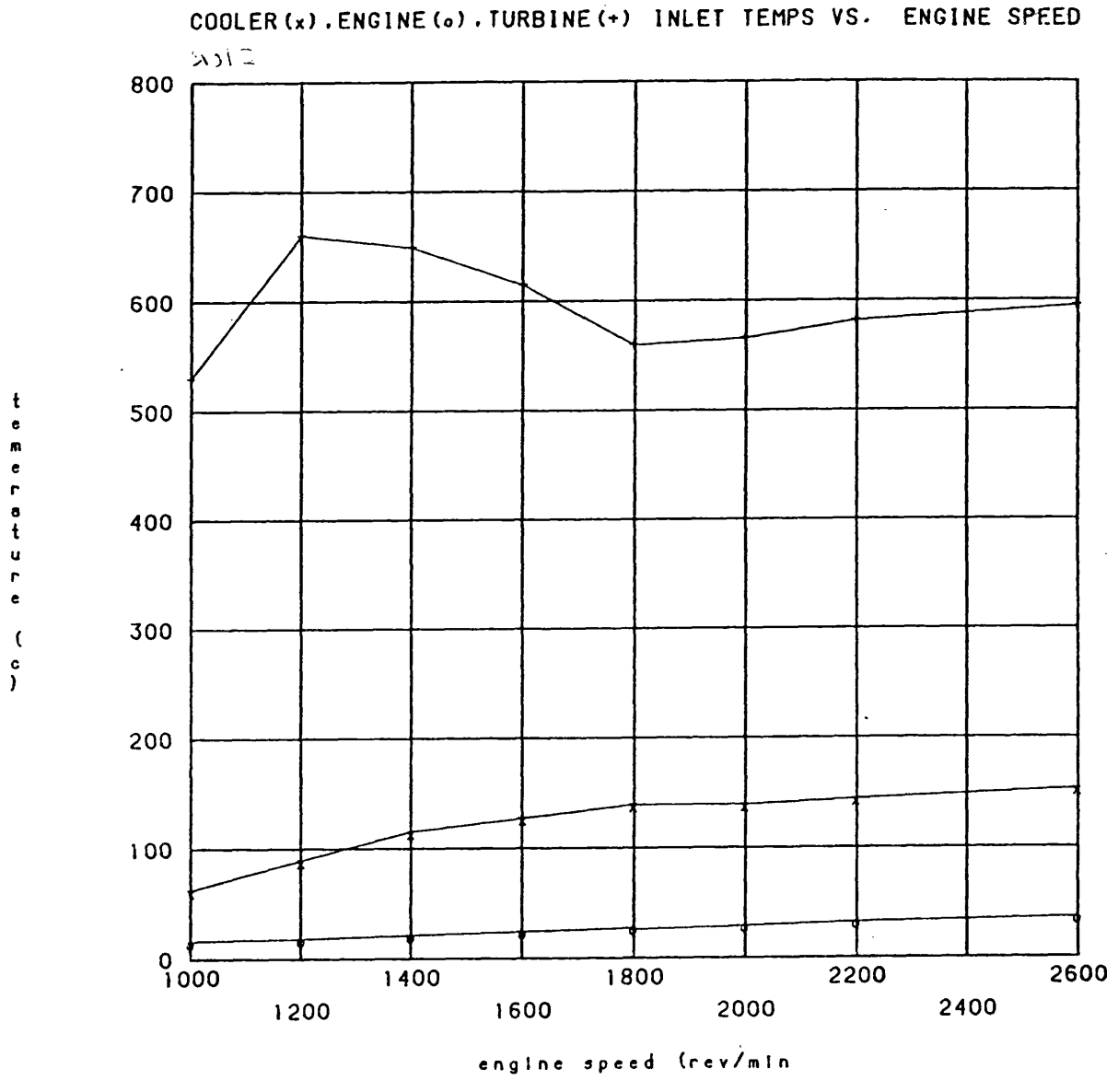

Fig. 6.4h Fully Restricted Limiting Torque Results, Pmax = 138 bar, Standard Timing, Compression Ratio = 14:1.

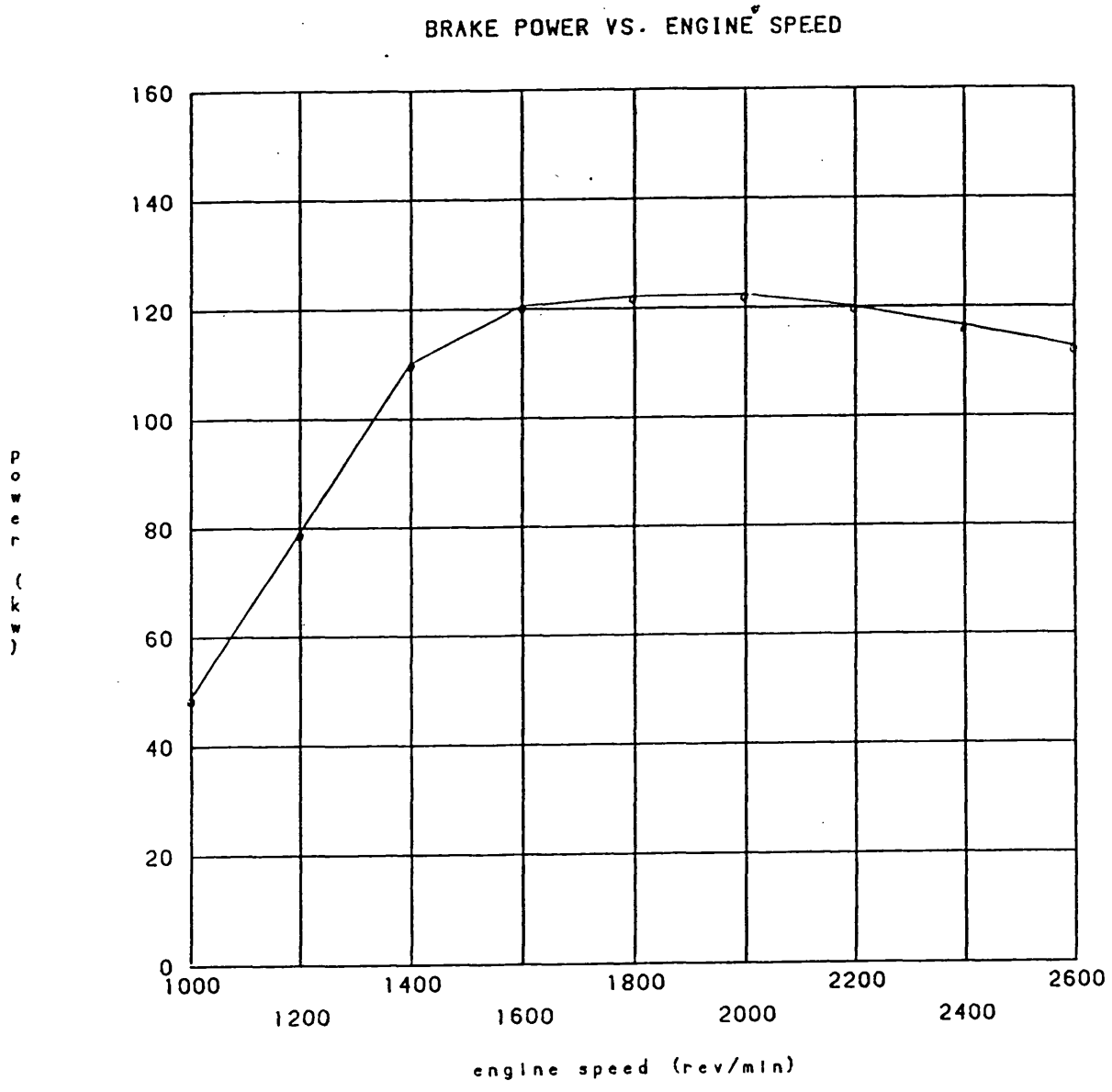

Fig. 6.5a Fully Restricted Limiting Torque Results, Pmax = 138 bar, Retarded Timing (3 deg.), Compression Ratio = 16:1.

Theoretical Predictions

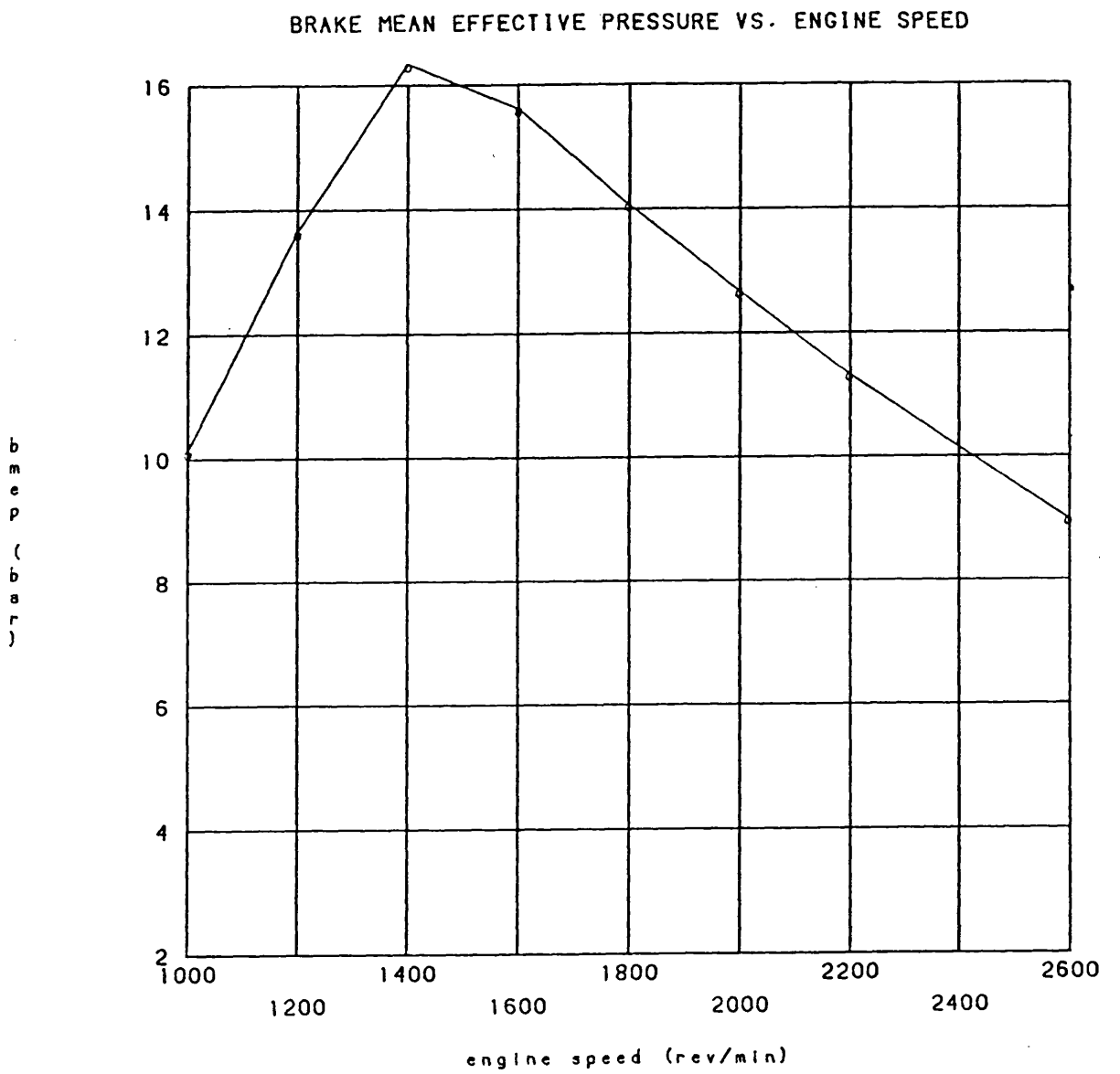

Fig. 6.5b Fully Restricted Limiting Torque Results, Pmax ≤ 138 bar, Retarded Timing (3 deg.), Compression Ratio = 16:1.

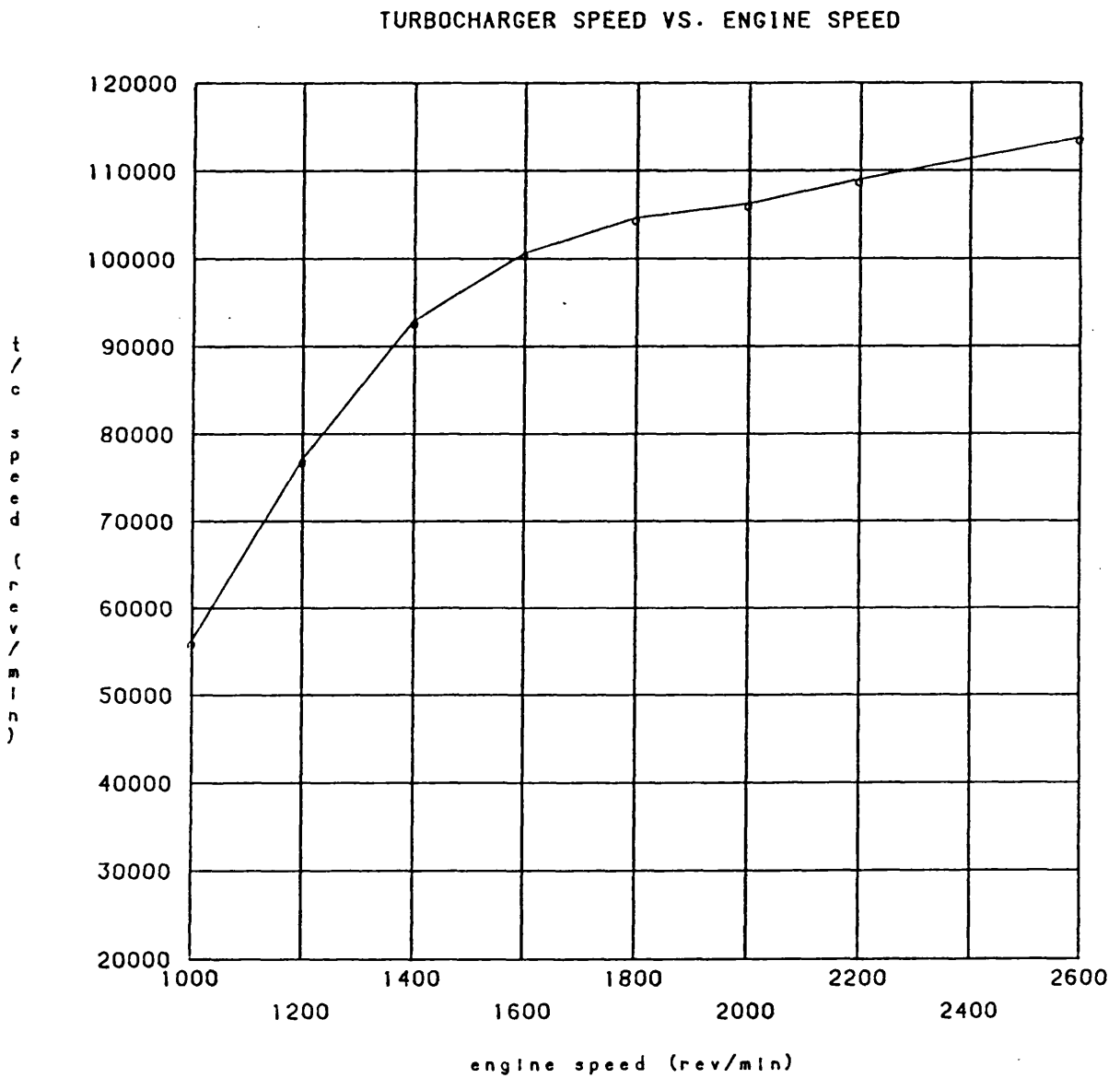

Fig. 6.5c Fully Restricted Limiting Torque Results, Pmax = 138 bar, Retarded Timing (3 deg.), Compression Ratio = 16:1.

Theoretical Predictions

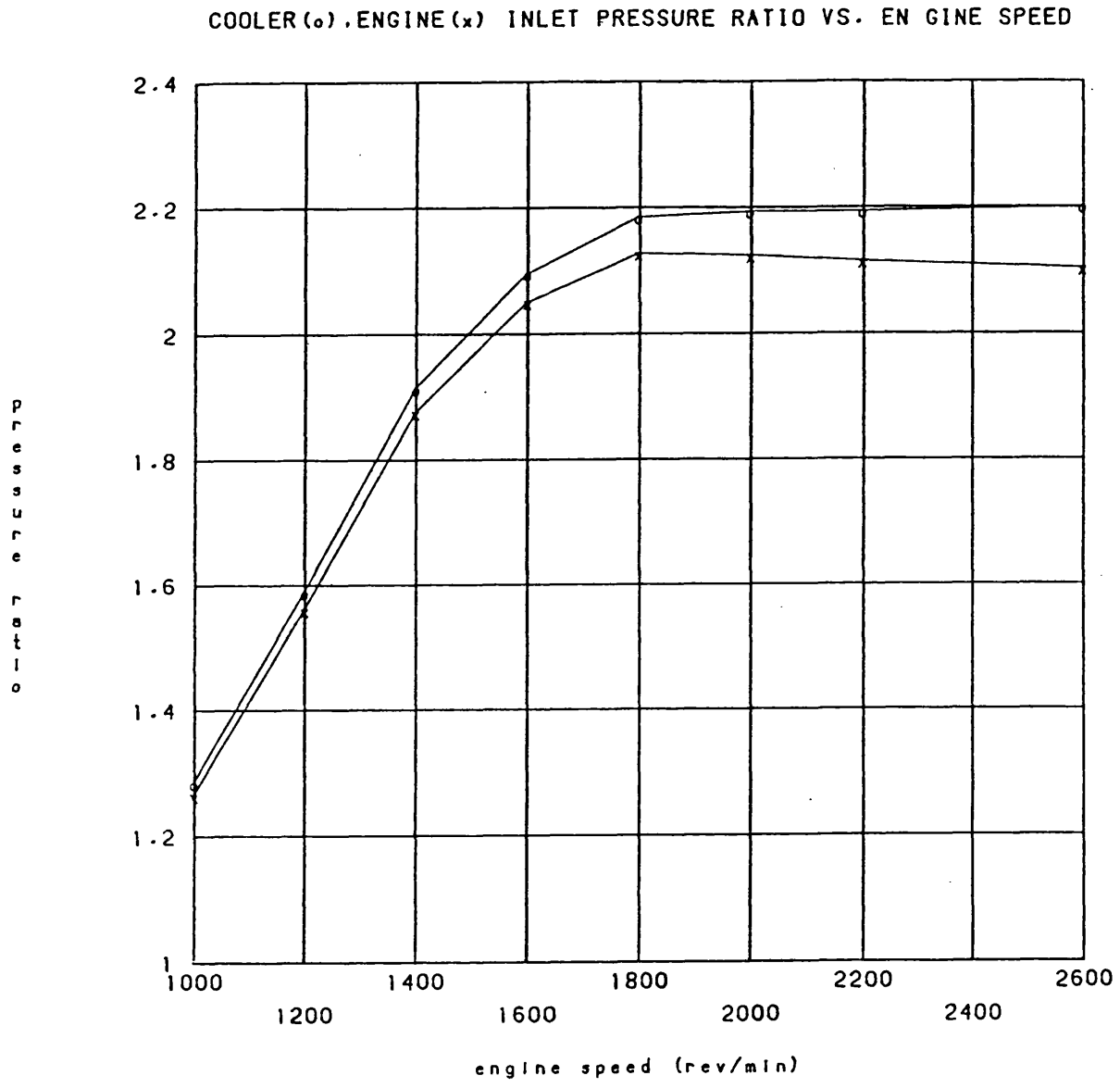

Fig. 6.5d Fully Restricted Limiting Torque Results, Pmax ≈ 138 bar, Retarded Timing (3 deg.), Compression Ratio = 16:1.

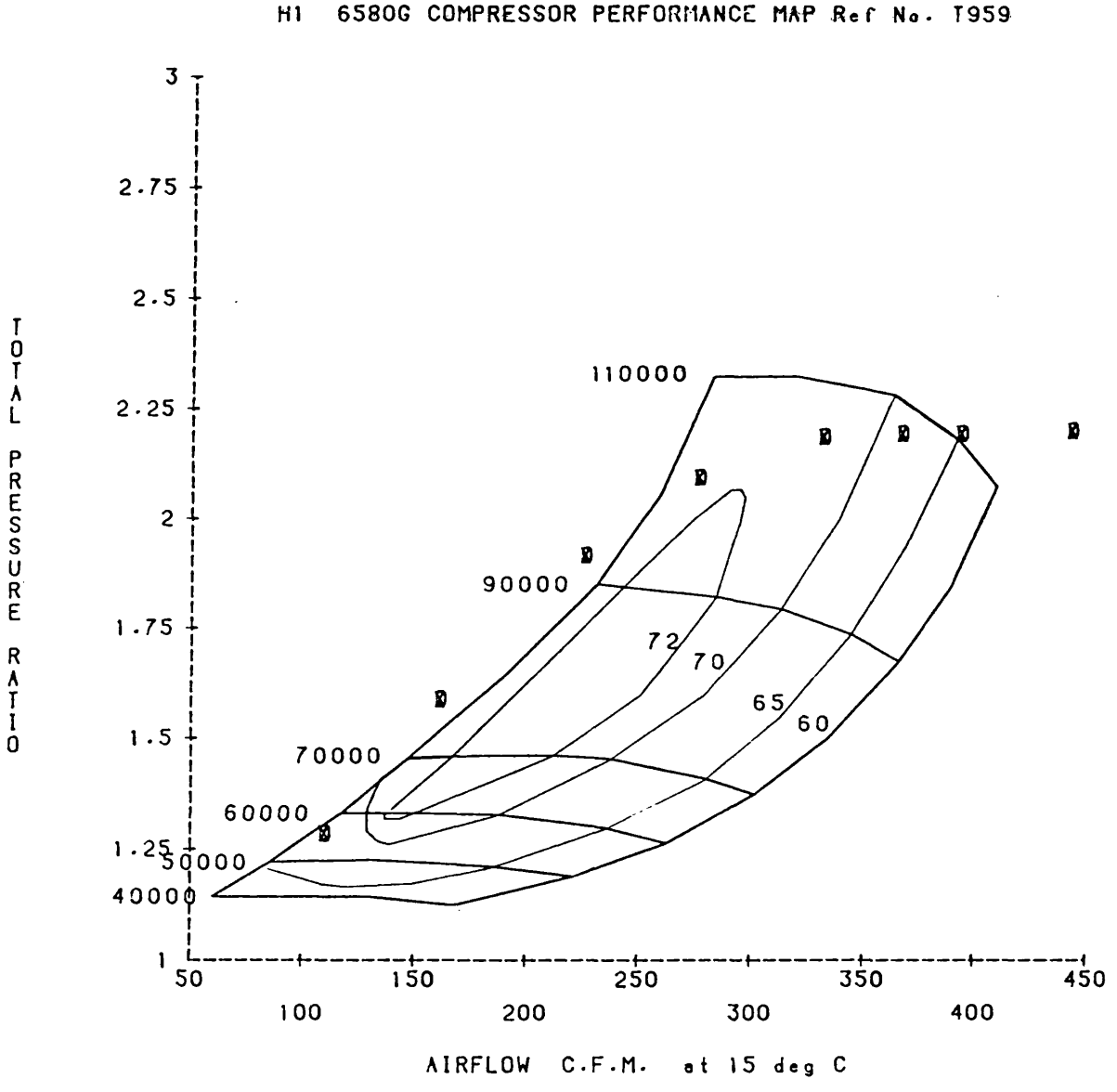

Fig. 6.5e Fully Restricted Limiting Torque Results, Pmax = 138 bar, Retarded Timing (3 deg.), Compression Ratio = 16:1.

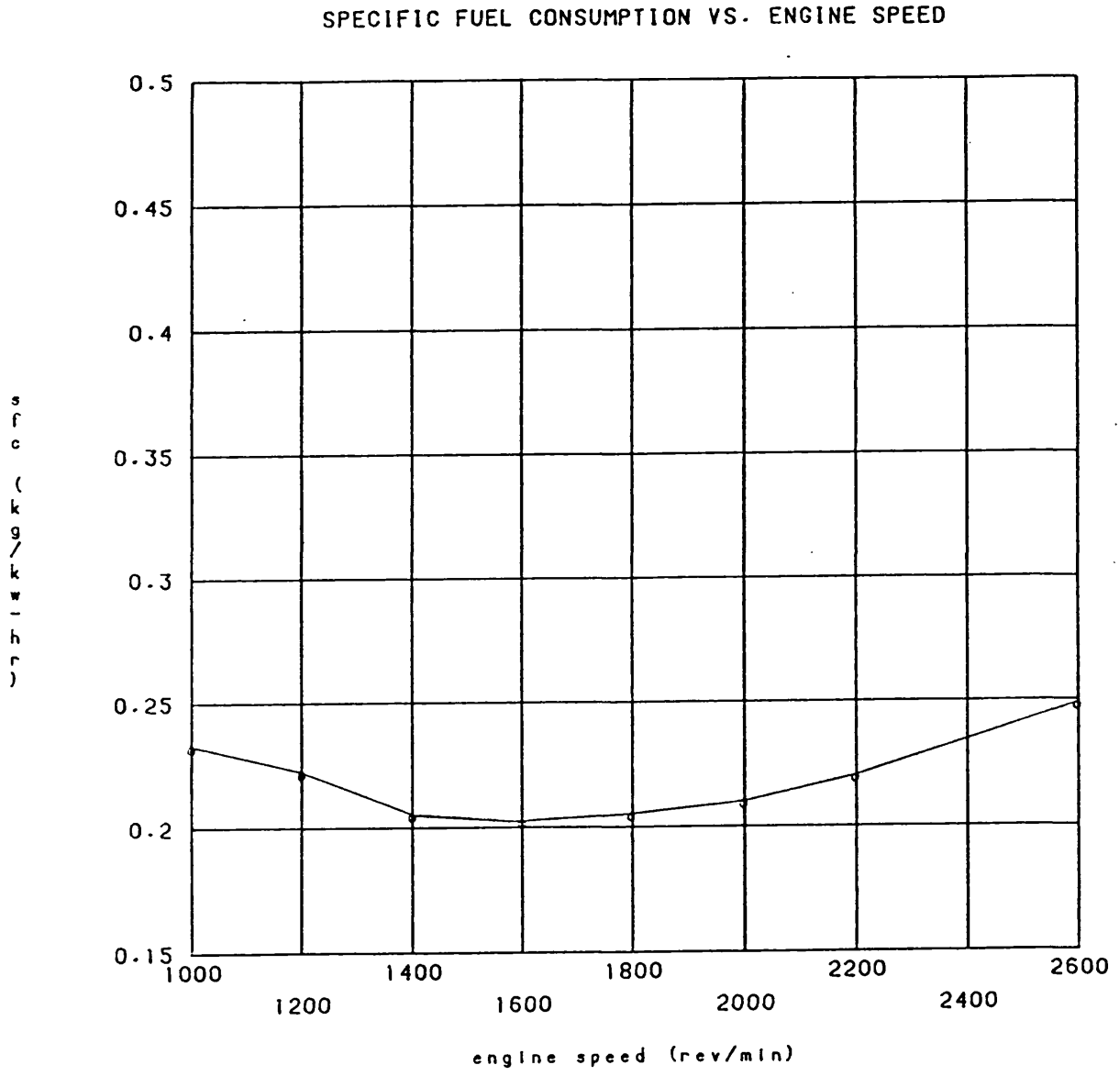

Fig. 6.5f Fully Restricted Limiting Torque Results, Pmax ≯ 138 bar, Retarded Timing (3 deg.), Compression Ratio = 16:1.

Theoretical Predictions

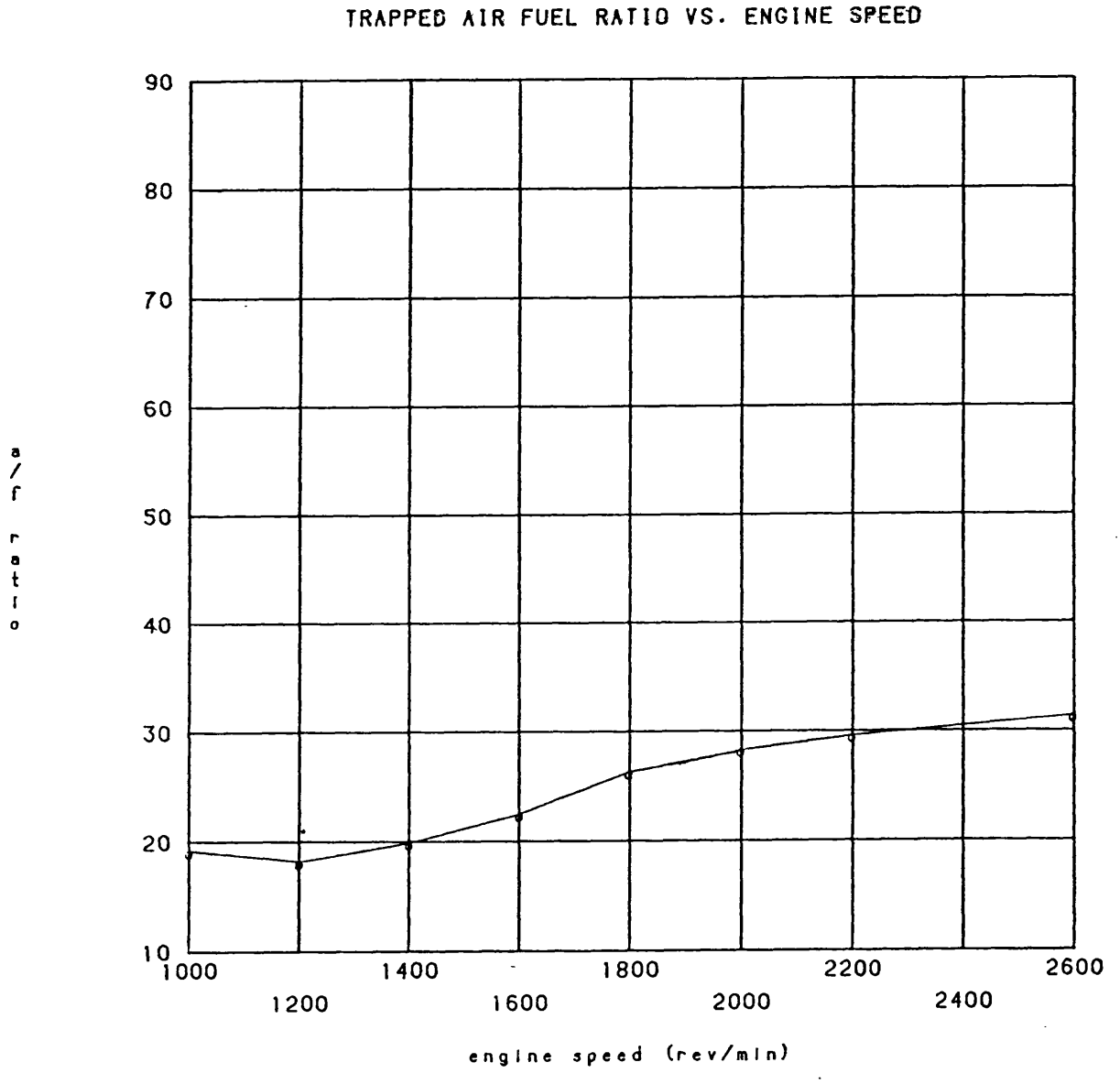

Fig. 6.5g Fully Restricted Limiting Torque Results, Pmax ≤ 138 bar, Retarded Timing (3 deg.), Compression Ratio = 16:1.

Theoretical Predictions

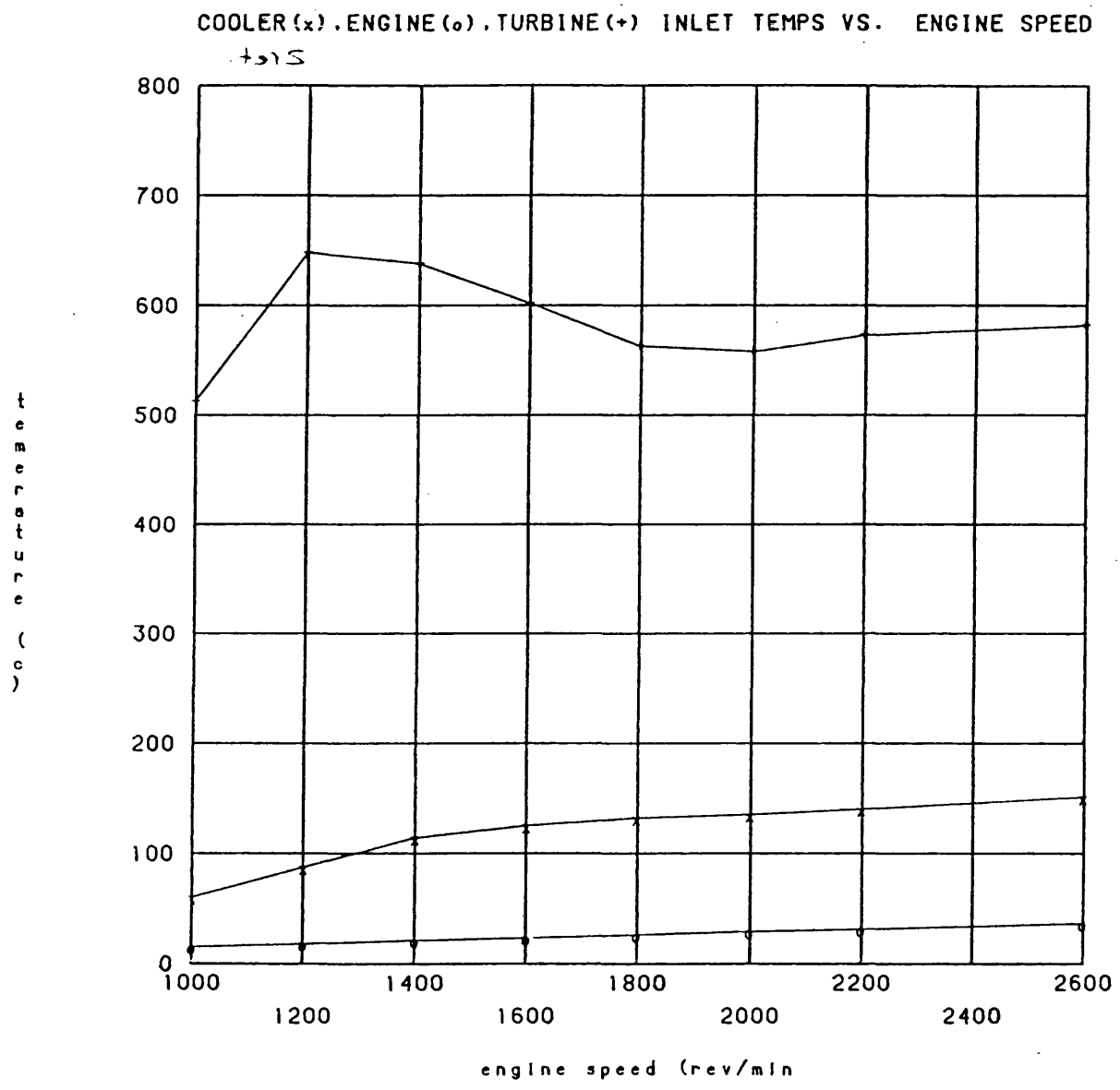

Fig. 6.5h Fully Restricted Limiting Torque Results, Pmax ≤ 138 bar, Retarded Timing (3 deg.), Compression Ratio = 16:1.

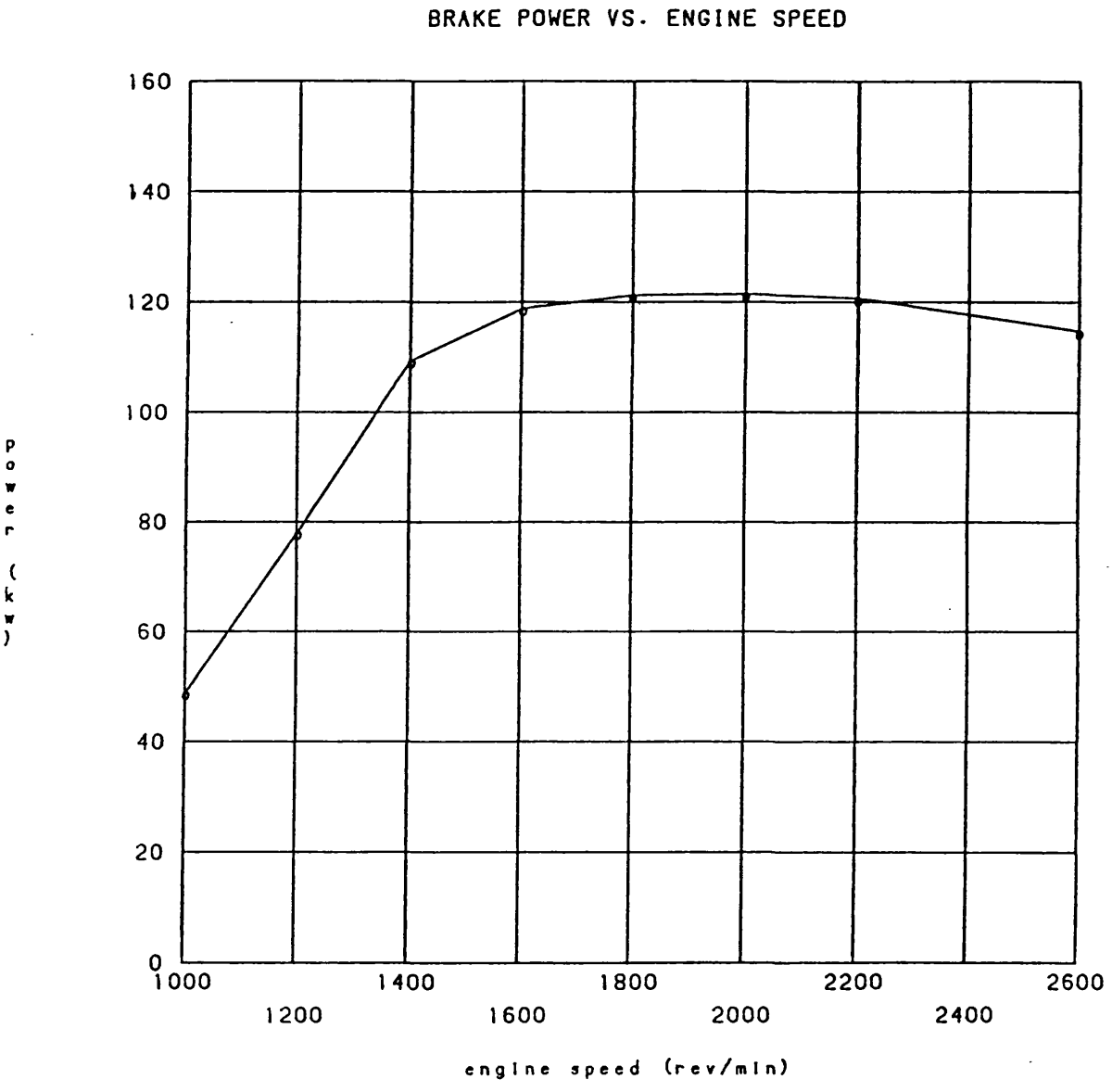

Fig. 6.6a Boost Controlled Variable Geometry Limiting Torque Results, Retarded Timing (3deg.), Comp. Ratio = 16:1.

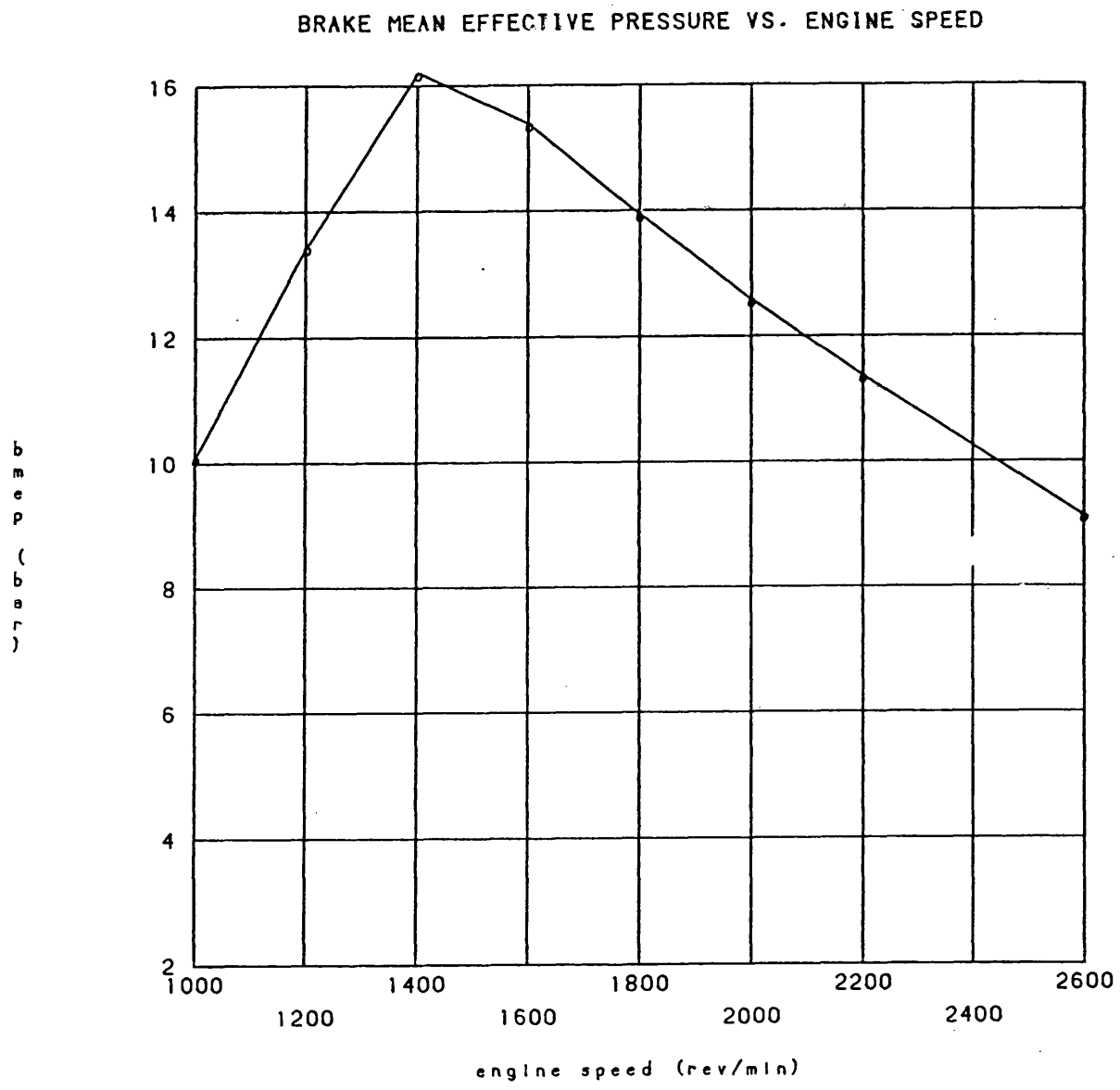

Fig. 6.6b Boost Controlled Variable Geometry Limiting Torque Results, Retarded Timing (3deg.), Comp. Ratio = 16:1.

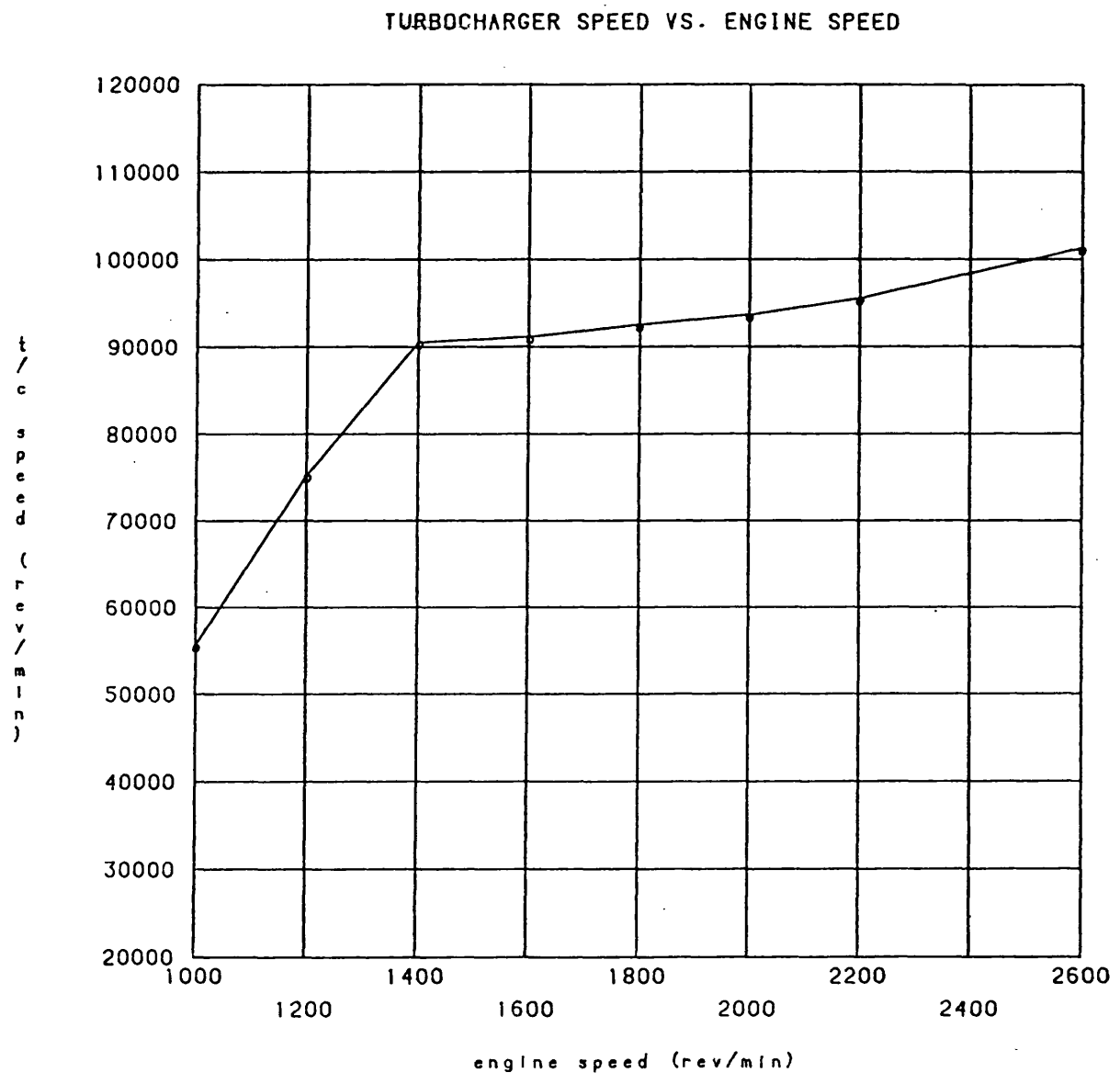

Fig. 6.6c Boost Controlled Variable Geometry Limiting Torque Results, Retarded Timing (3deg.), Comp. Ratio = 16:1.

Theoretical Predictions

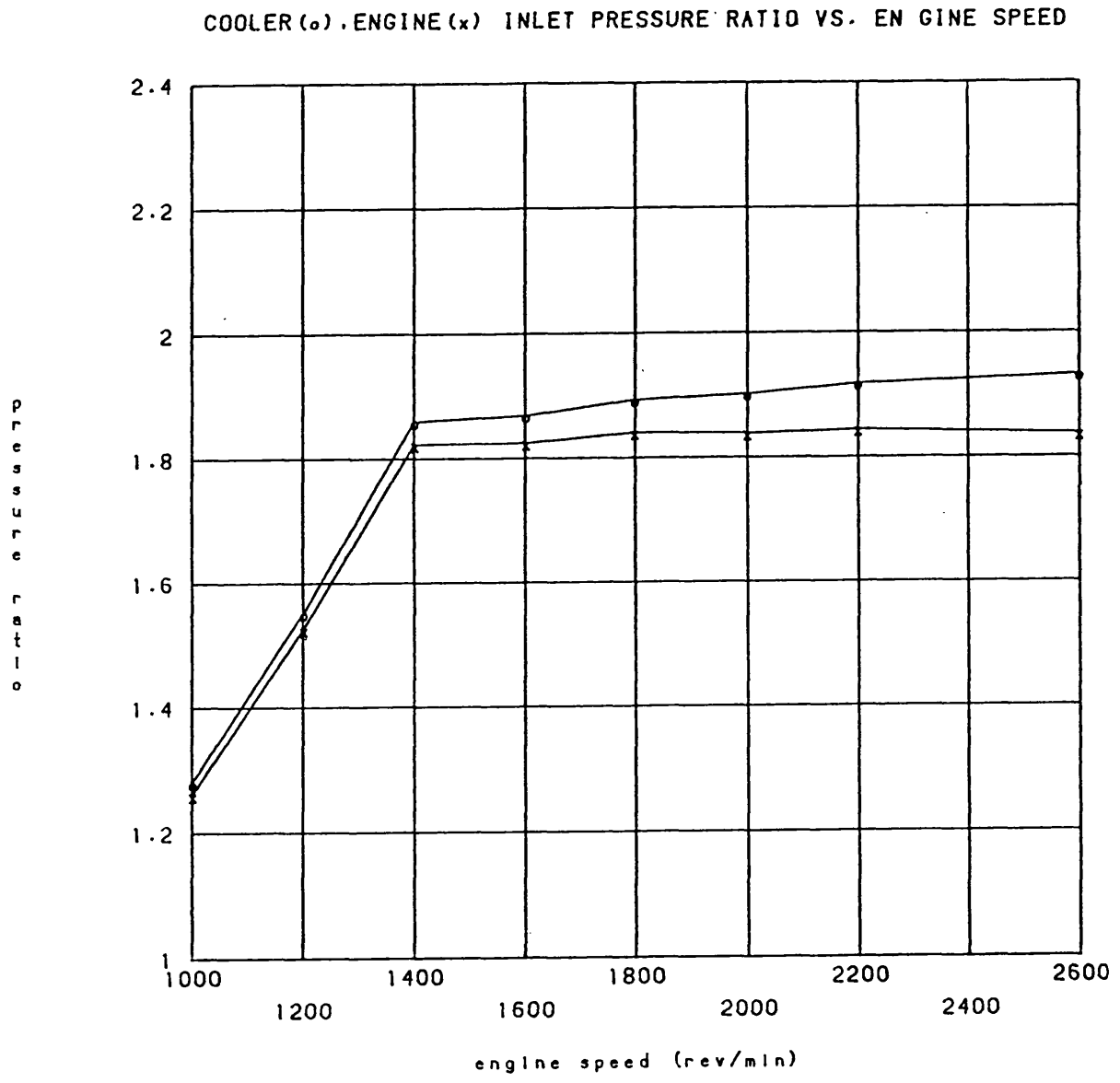

Fig. 6.6d Boost Controlled Variable Geometry Limiting Torque Results, Retarded Timing (3deg.), Comp. Ratio = 16:1.

Theoretical Predictions

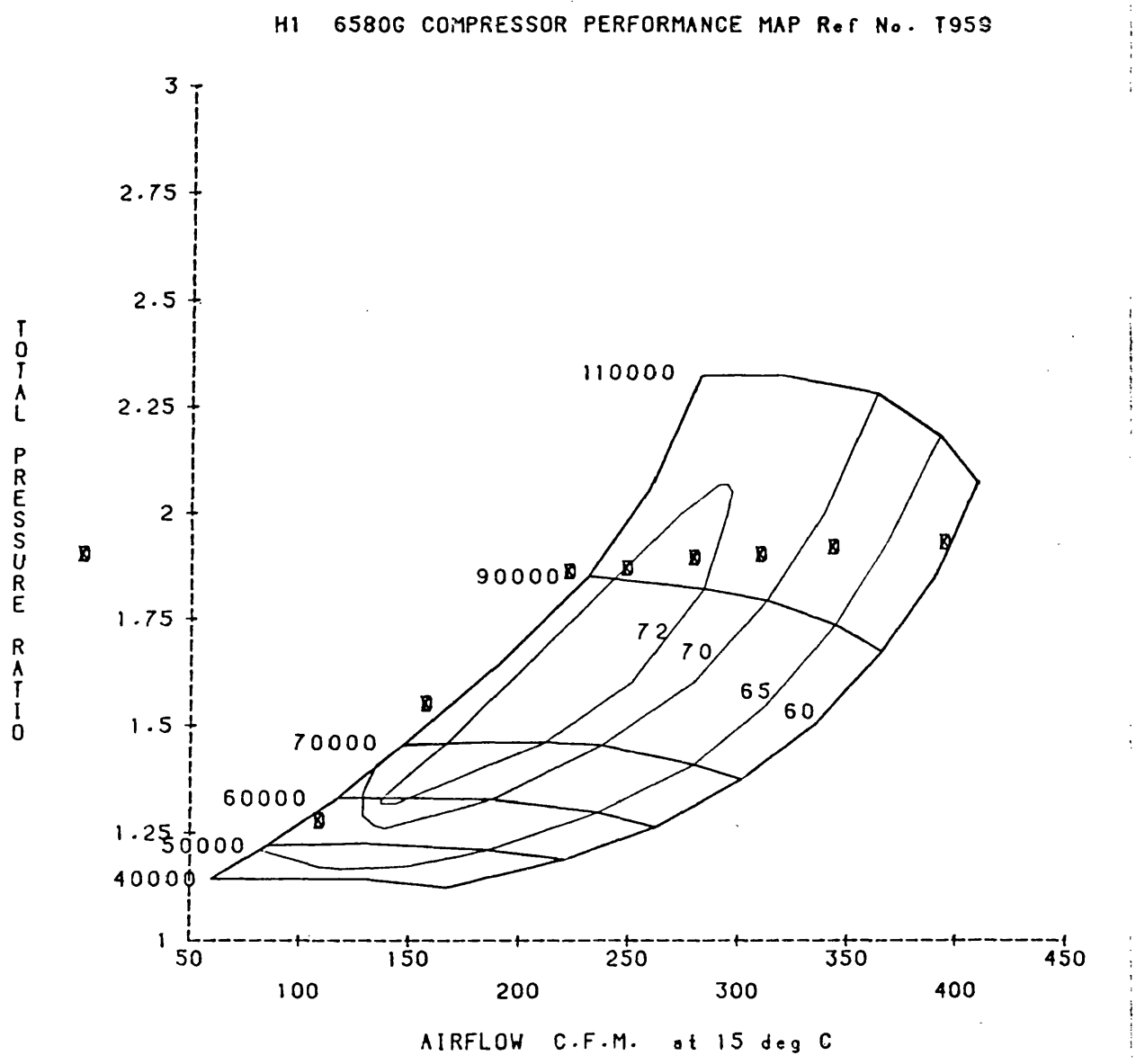

Fig. 6.6e Boost Controlled Variable Geometry Limiting Torque Results, Retarded Timing (3deg.), Comp. Ratio = 16:1.

Theoretical Predictions

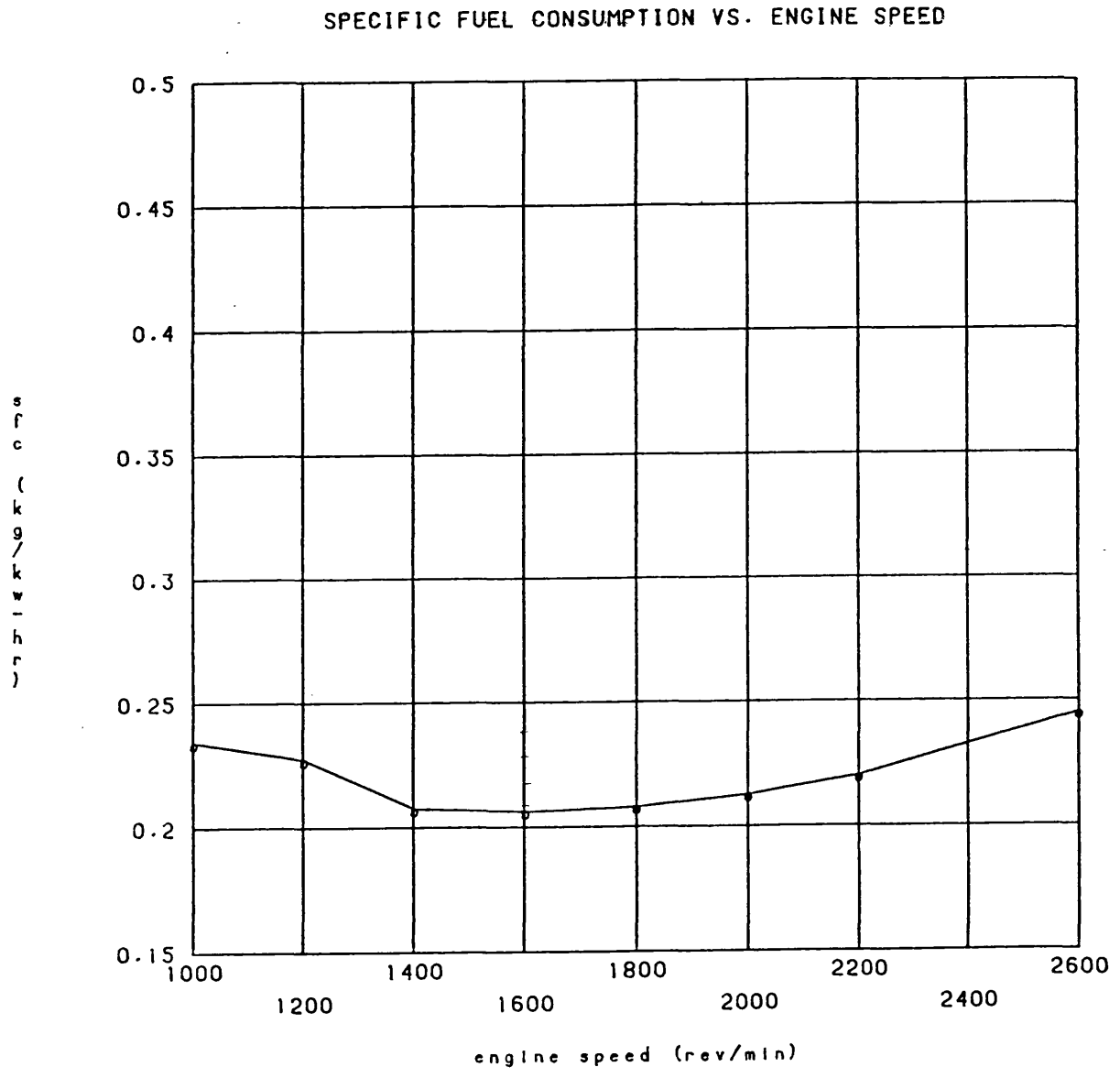

Fig. 6.6f Boost Controlled Variable Geometry Limiting Torque Results, Retarded Timing (3deg.), Comp. Ratio = 16:1.

Theoretical Predictions

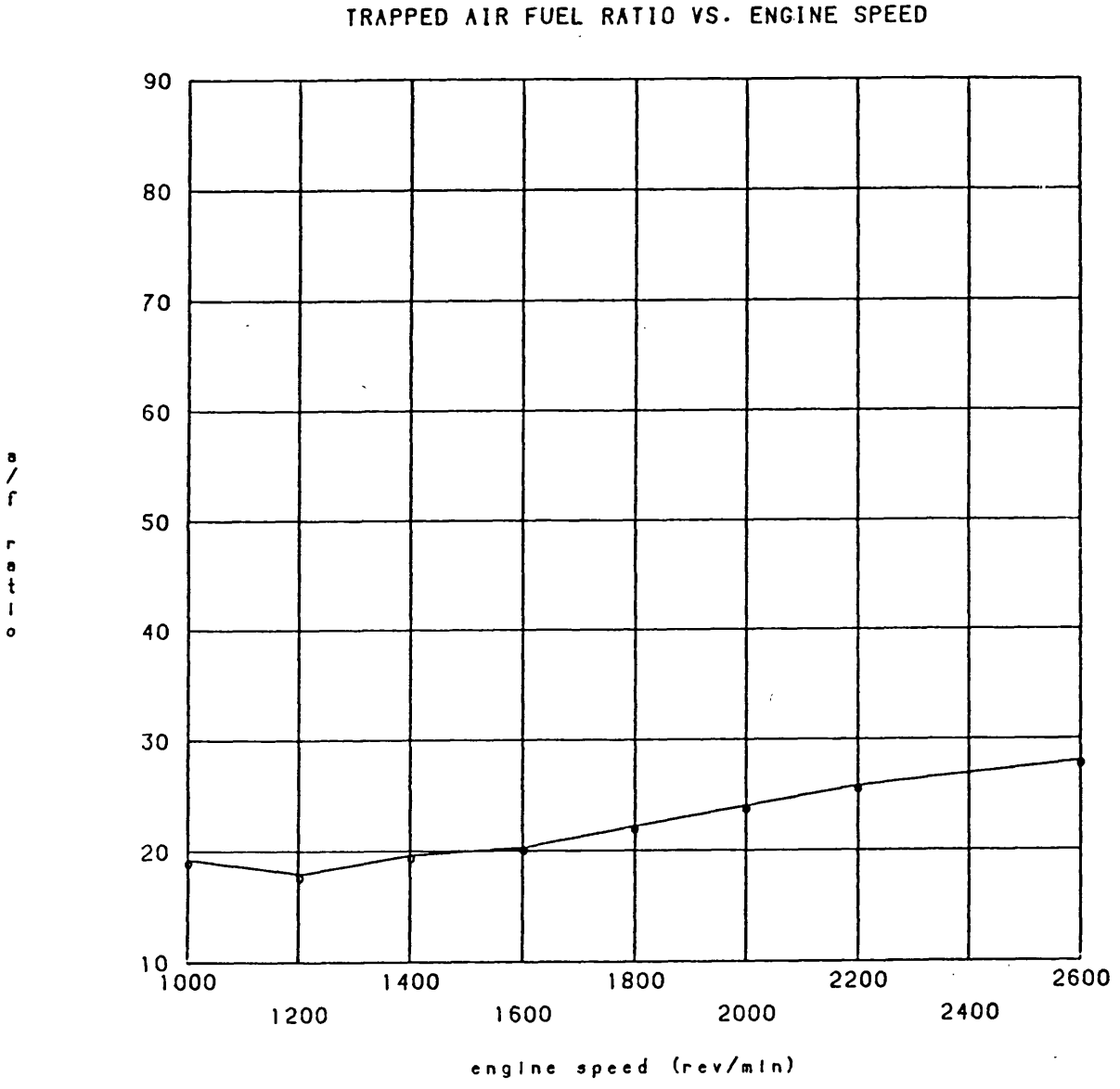

Fig. 6.6g Boost Controlled Variable Geometry Limiting Torque Results, Retarded Timing (3deg.), Comp. Ratio = 16:1.

Theoretical Predictions

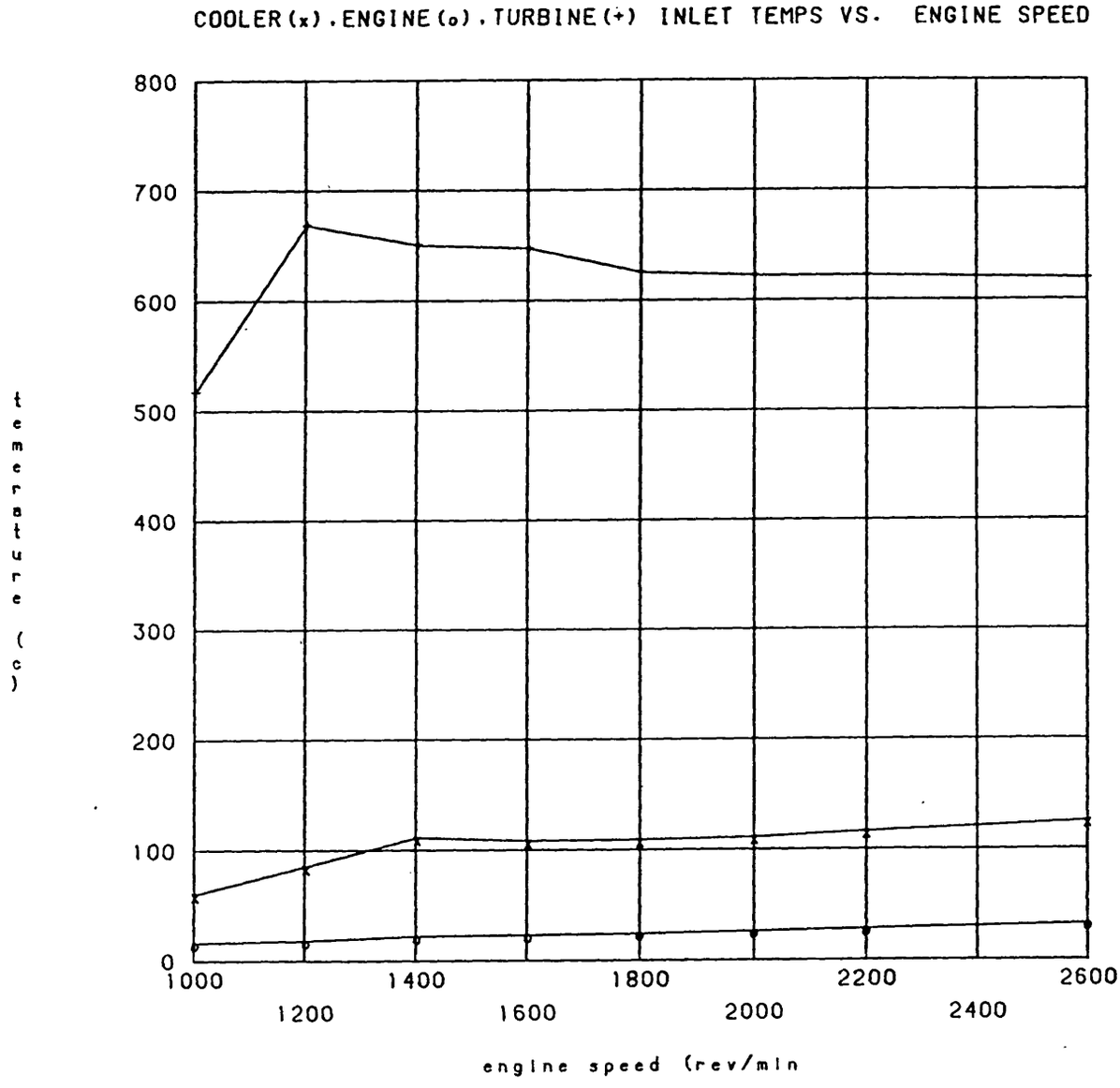

Fig. 6.6h Boost Controlled Variable Geometry Limiting Torque Results, Retarded Timing (3deg.), Comp. Ratio = 16:1.

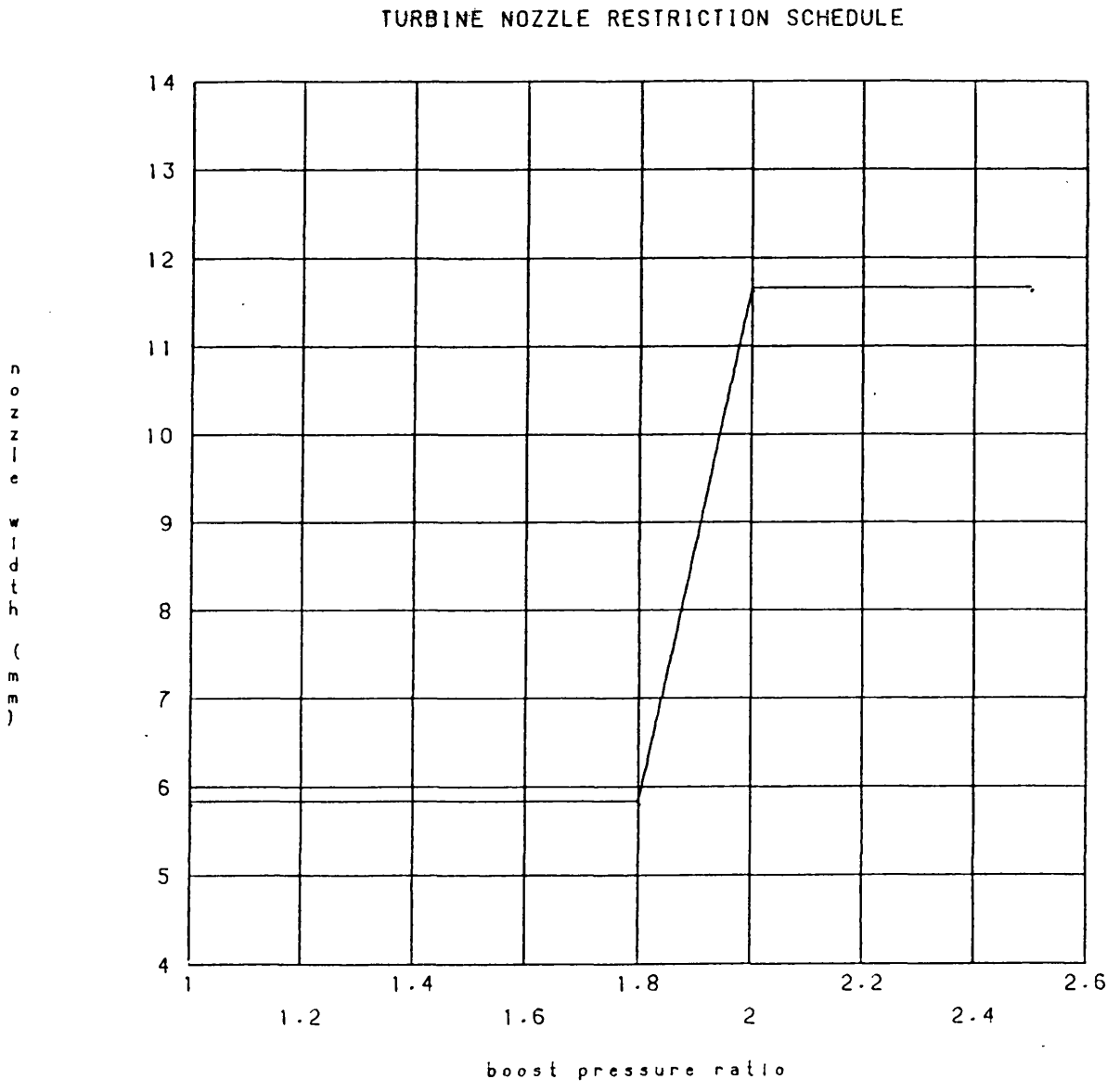

Fig. 6.6i Boost Controlled Variable Geometry Limiting Torque Results, Retarded Timing (3 deg.), Comp. Ratio = 16:1

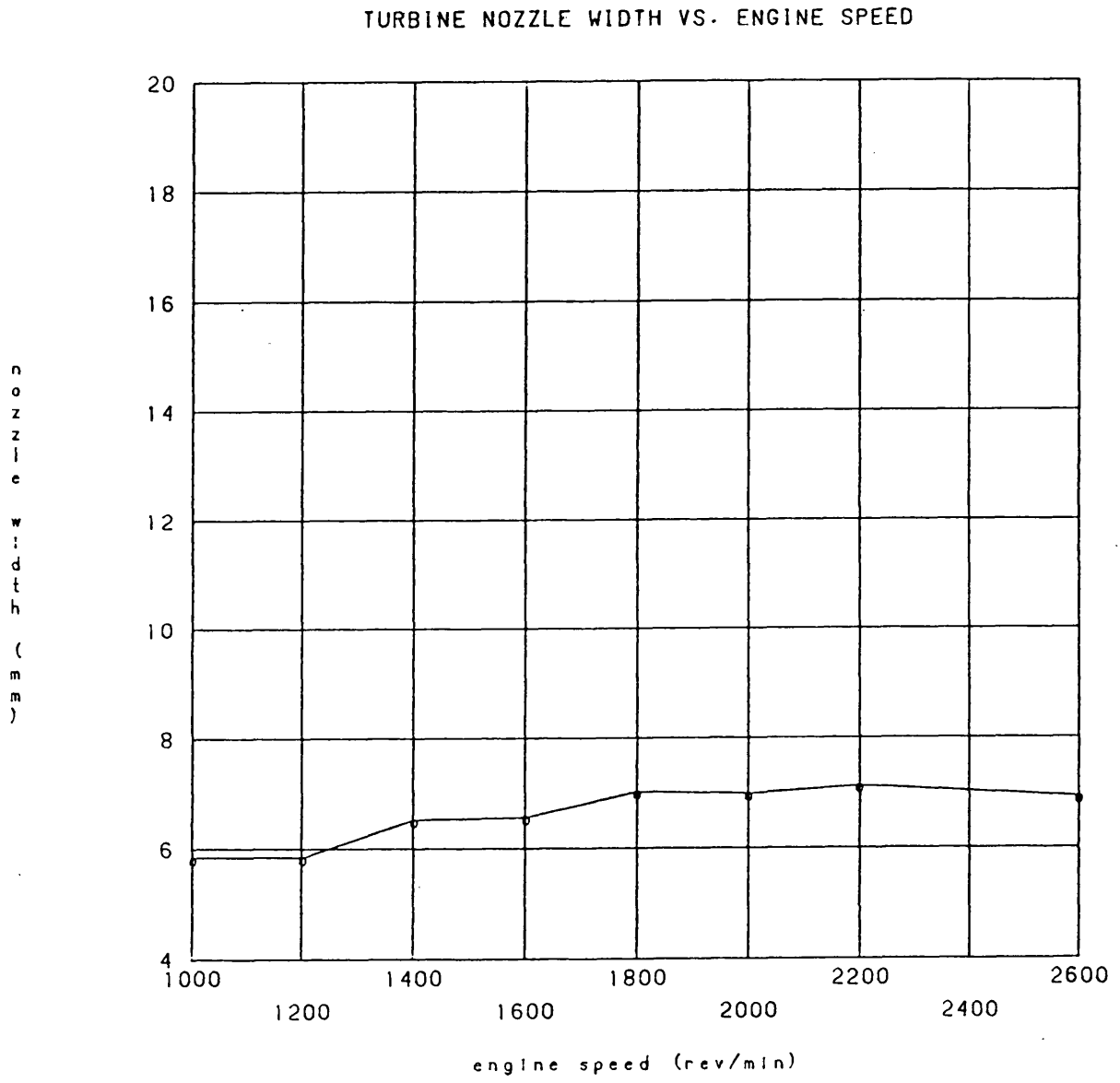

Fig. 6.6j Boost Controlled Variable geometry Limiting Torque Results, Retarded Timing (3 deg.), Comp. Ratio = 16:1

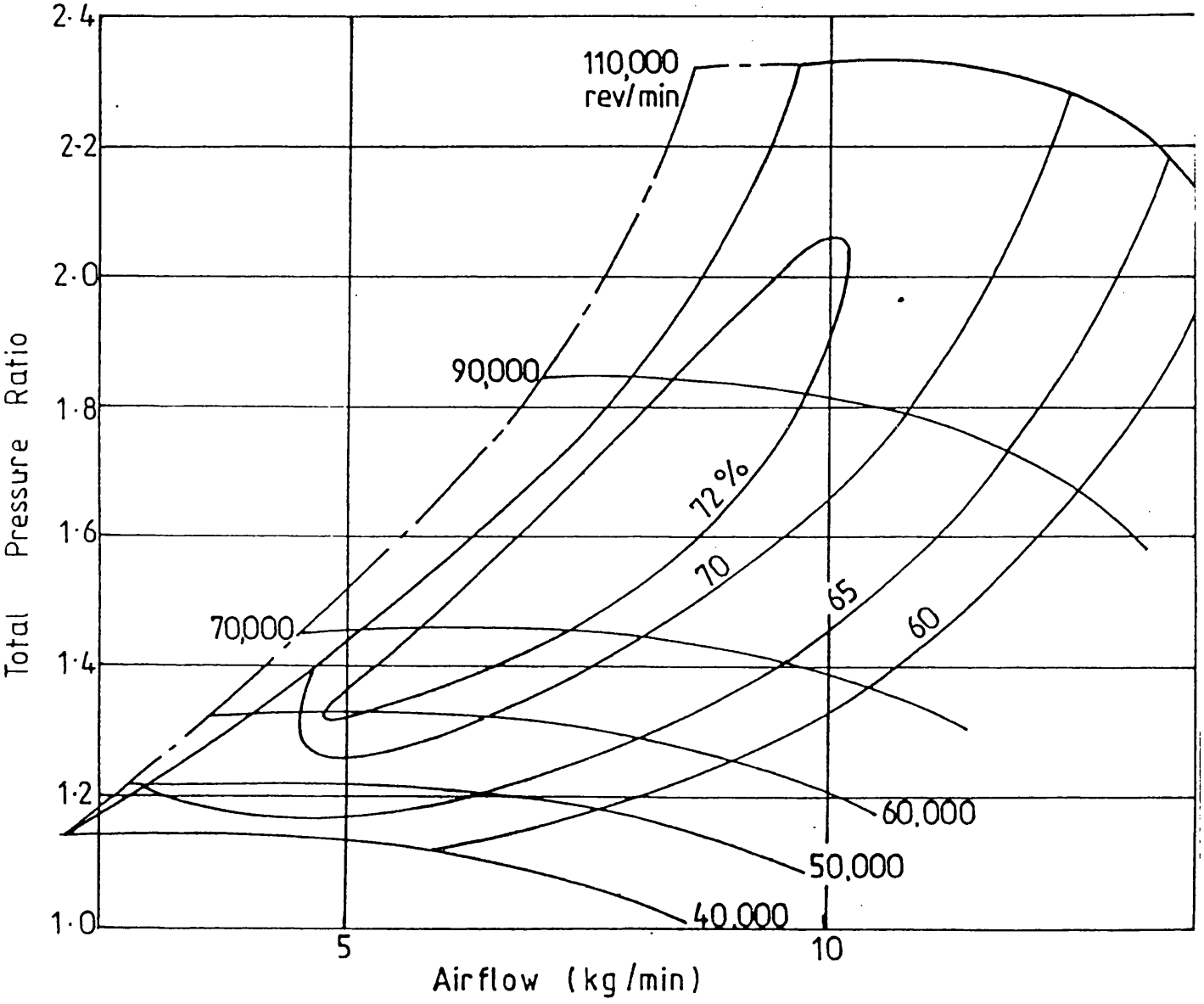

Fig. 6.7 Compressor Map Showing the Extended Surge Margin.

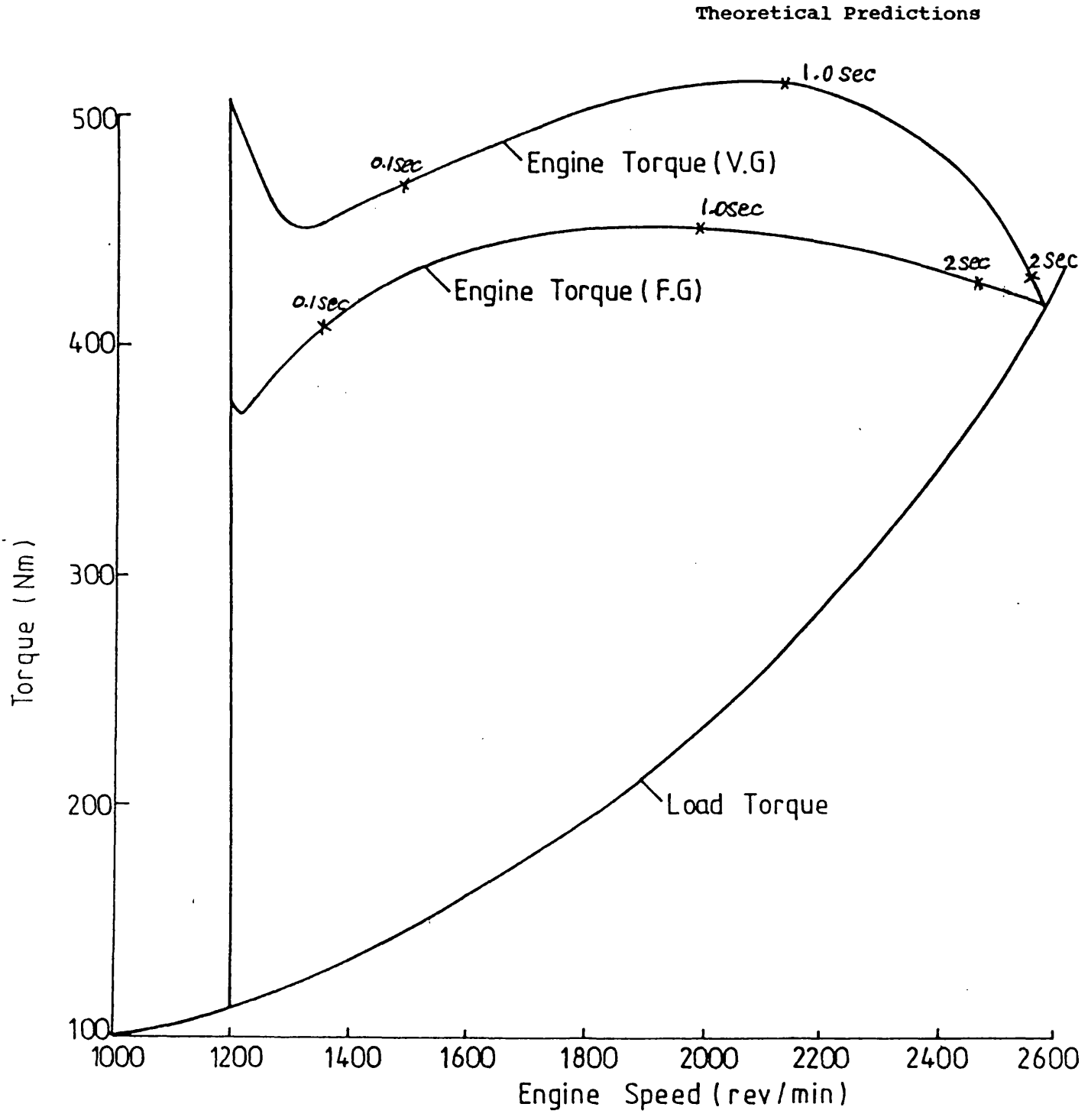

Fig. 6.8 Engine Acceleraion for a Fuel Step Operating on a Propeller Load absorption Curve.

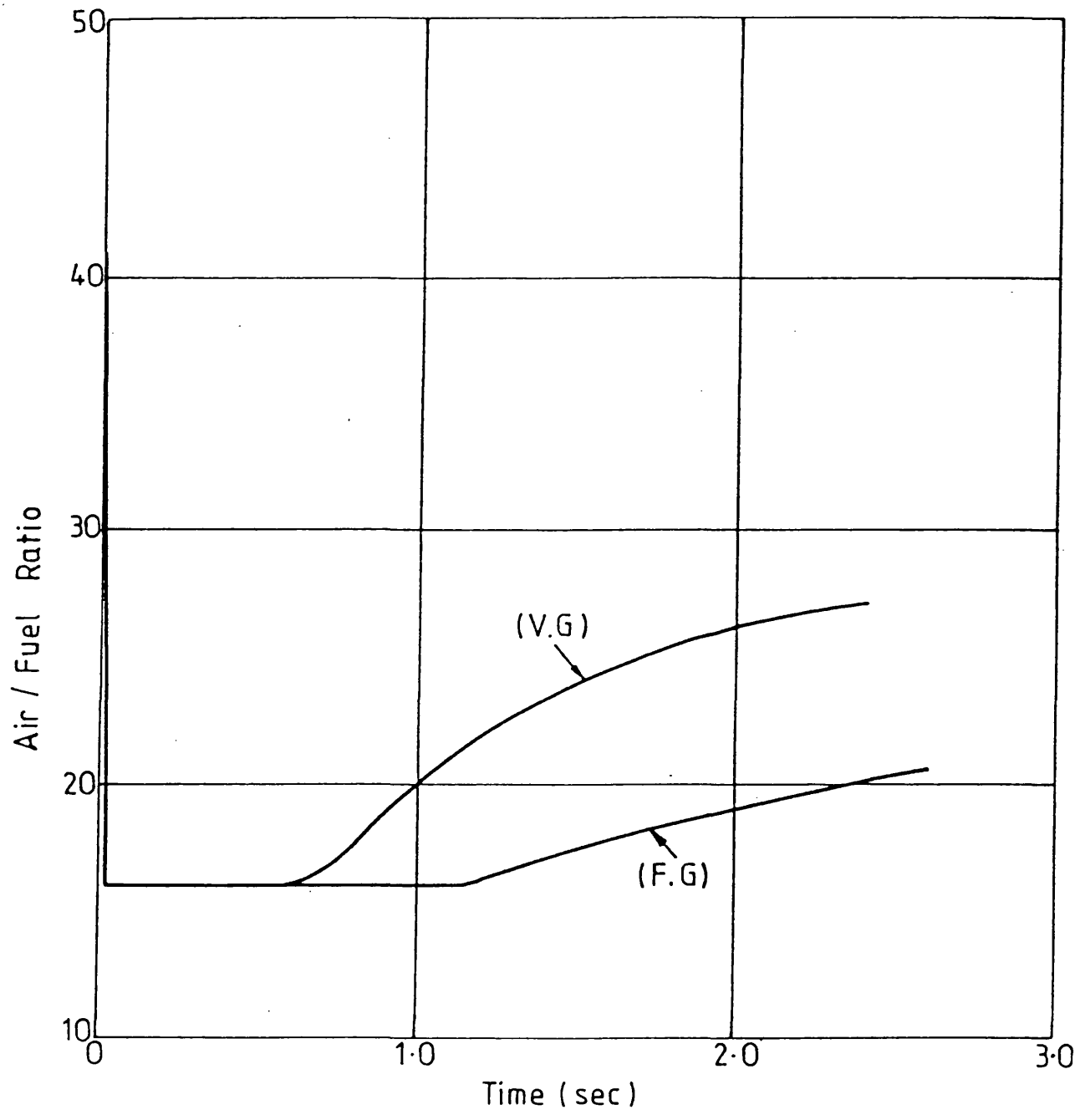

Fig. 6.9 The Transient Variation of Air/Fuel Ratio For a Fuel Step

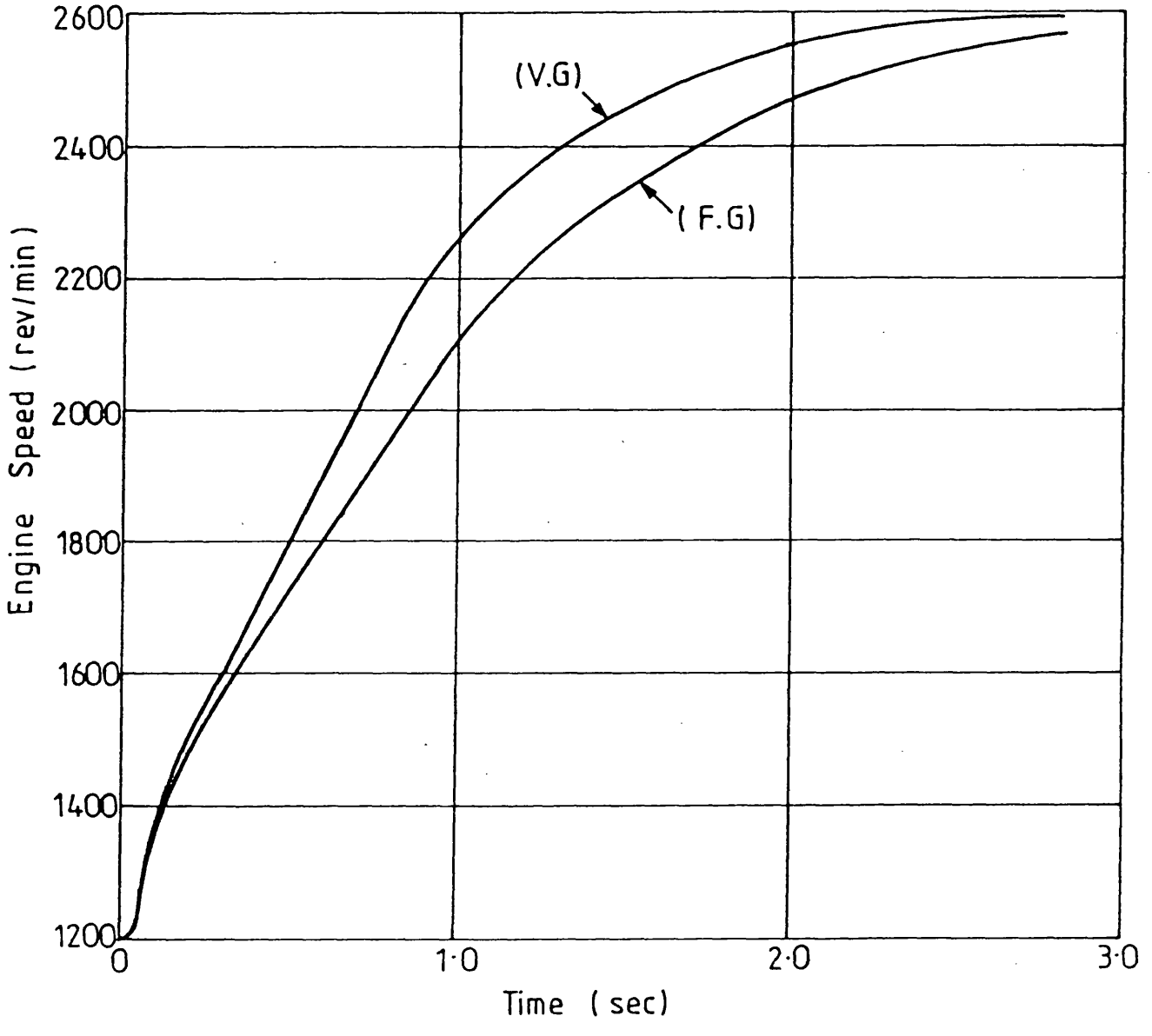

Fig. 6.10 Engine Speed Variation With Time for a Fuel Step.

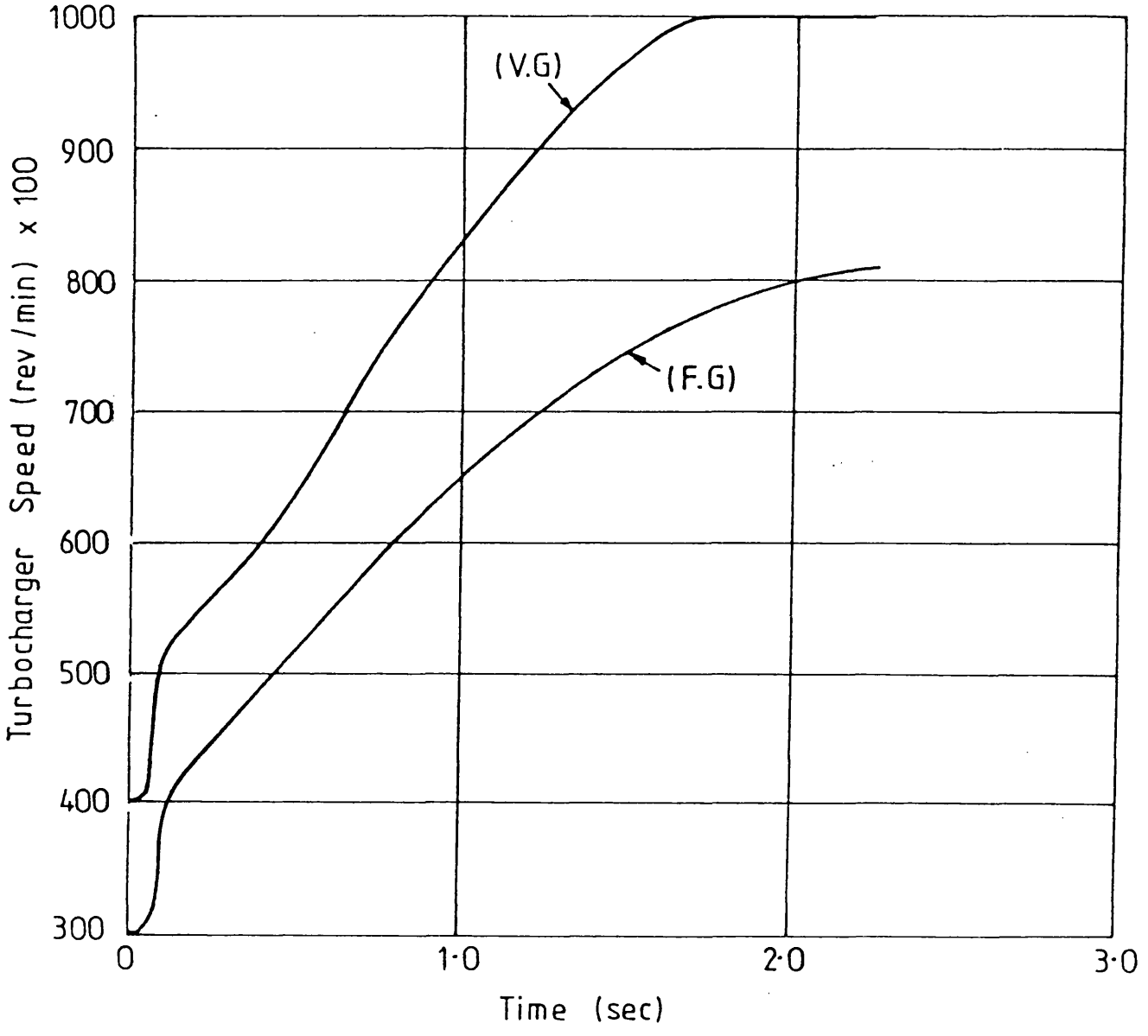

Fig. 6.11 Turbocharger Acceleration for a Fuel Step.

Perkins T6.354 Engine Data -- 0% Restriction 252 220 1100

number of cylinders	6.0	bore (m)	0.10	stroke (m)	0.12700			
con-rod length (m)	0.21908	inlet valve closing (degs)	229.0	number of turbochargers	1.0			
ambient temperature (deg k)	299.0	max. pressure limit (bar)	0.0000	ambient pressure (bar)	1.00530			
compression ratio	16.00	turbine nozzle angle (degs)	26.0000	turbine flow loss factor	0.8000			

engine speed(r.p.m)	1000.00	1200.00	1400.00	1600.00	1800.00	2000.00	2200.00	2600.00
boost pressure ratio	1.119	1.293	1.309	1.385	1.473	1.543	1.644	1.821
trapped a/f ratio	19.154	20.665	18.366	20.332	21.950	23.468	25.703	28.251
delivery ratio	0.820	0.820	0.822	0.820	0.819	0.823	0.836	0.834
manifold temp (deg k)	288.242	289.589	290.246	291.518	293.162	295.141	297.861	304.724
engine power (k w.)	40.95	57.14	73.21	85.01	94.79	101.92	107.46	114.66
engine torque (n.m.))	391.09	454.66	499.36	507.34	502.88	486.64	466.43	421.12
b.m.e.p (bar)	8.4811	9.8600	10.8291	11.0020	10.9053	10.5533	10.1149	9.1323
s.f.c. (kgs/kw hr)	0.246	0.226	0.234	0.219	0.216	0.219	0.224	0.244
b.thermal eff.	0.3390	0.3698	0.3564	0.3808	0.3854	0.3810	0.3732	0.3426
fuel / rev (kg.)	1.680	1.790	2.040	1.940	1.900	1.860	1.820	1.790
max cyl pressure (bar .)	80.81	109.32	114.32	112.24	110.06	106.26	104.35	105.36
max cyl temperature(deg k)	2108.10	2156.44	2294.14	2176.20	2082.50	1998.09	1896.65	1810.38
exhaust temperature(deg k)	760.39	781.68	920.38	871.26	867.98	882.75	883.35	885.28
percentage heat to coolant	32.97	27.17	24.68	22.04	19.85	18.13	16.44	14.30
compressor pressure ratio	1.1374	1.3189	1.3414	1.4264	1.5231	1.6037	1.7163	1.9173
delivery temperature(deg k)	317.43	334.78	335.46	342.91	351.52	360.18	371.05	397.36
delivery pressure (bar)	1.144	1.325	1.347	1.433	1.534	1.627	1.723	1.941
compressor speed (r.p.m.)	39600.0	58995.7	60979.7	67737.8	73766.9	78839.9	86039.0	101039.6
volume flow (cu m / min)	2.76	3.81	4.49	5.40	6.42	7.46	8.79	11.22
compressor power (kw.)	0.995	2.668	3.210	4.645	6.604	8.939	12.404	21.616
compressor efficiency	0.611	0.692	0.722	0.732	0.731	0.710	0.697	0.625
turbine speed (r.p.m)	39600.0	58995.7	60979.7	67737.8	73766.9	78839.9	86039.0	101039.6
turbine power (kw)	1.059	2.799	3.347	4.814	6.782	9.203	12.685	22.010
effective turbine efficiency.	0.478	0.662	0.565	0.613	0.625	0.632	0.636	0.642
fract of flow thro turbine.	0.000	0.000	0.000	0.000	0.000	0.000	0.000	0.000
first step. pressure ratio.	1.274	1.366	1.402	1.447	1.518	1.605	1.736	2.079
n.d. torque	0.9831	0.8786	1.0945	1.0508	1.0756	1.1323	1.1758	1.2420
n.d. mass flow.	251.0066	179.4994	237.1631	218.9408	216.8608	219.8333	219.9152	213.5270
n.d.speed	1245.2151	1899.3405	1868.1315	2134.2118	2366.5824	2564.9970	2860.0503	3414.3175
efficiency.	0.452	0.674	0.578	0.631	0.644	0.644	0.646	0.647
final step. pressure ratio.	1.021	1.087	1.078	1.131	1.201	1.289	1.421	1.777
n.d. torque	0.0000	0.0014	-0.0226	0.0534	0.1859	0.3575	0.5428	0.8609
n.d. mass flow.	0.0000	51.4983	48.8128	90.9206	124.3191	152.8778	174.4436	194.3359
n.d.speed	1279.3661	1953.1058	1926.7012	2198.1612	2434.3237	2633.6501	2930.1123	3480.2410
efficiency.	0.000	0.014	-0.261	0.232	0.443	0.546	0.590	0.628
compressor mass flow(kg/min).	3.23	4.46	5.26	6.33	7.52	8.74	10.30	13.15
delevered air to fuel ratio	19.22	20.76	18.43	20.39	21.99	23.49	25.72	28.25
v.g. nozzle width (m.m.)	11.6700	11.6700	11.6700	11.6700	11.6700	11.6700	11.6700	11.6700
cooler effectiveness	0.9592	0.9458	0.9330	0.9192	0.9045	0.8888	0.8708	0.8394
engine diagram factor	0.9800	0.9644	0.9500	0.9425	0.9300	0.8950	0.8600	0.8400

TABLE 6.1 UNRESTRICTED LIMITING TORQUE 'CALIBRATION' RESULTS

TABLE 6.2 FULLY RESTRICTED LIMITING TORQUE RESULTS

Perkins T6.354 Engine Data -- 50% Restriction 371 246 1230

number of cylinders	6.0	bore (m)	0.10	stroke (m)	0.12700			
con-rod length (m)	0.21908	inlet valve closing (degs)	229.0	number of turbochargers	1.0			
ambient temperature (deg k)	299.0	max. pressure limit (bar)	0.0000	ambient pressure (bar)	1.00530			
compression ratio	16.00	turbine nozzle angle (degs)	40.5000	turbine flow loss factor	0.8000			

engine speed(r.p.m)	1000.00	1200.00	1400.00	1600.00	1800.00	2000.00	2200.00	2600.00
boost pressure ratio	1.267	1.503	1.667	1.799	1.942	1.987	2.007	2.035
trapped a/f ratio	19.205	18.427	20.551	23.072	25.821	29.151	30.636	32.303
delivery ratio	0.820	0.822	0.822	0.820	0.818	0.856	0.843	0.819
manifold temp (deg k)	288.953	290.860	292.853	294.872	297.400	300.593	302.829	308.063
engine power (k w.)	48.97	75.79	92.72	101.98	109.69	111.11	109.65	105.24
engine torque (n.m.))	467.60	603.11	632.42	608.67	581.93	530.49	475.94	386.54
b.m.e.p (bar)	10.1403	13.0789	13.7145	13.1994	12.6197	11.5041	10.3210	8.3824
s.f.c. (kgs/kw hr)	0.233	0.222	0.209	0.207	0.207	0.213	0.223	0.252
b.thermal eff.	0.3583	0.3753	0.3986	0.4028	0.4035	0.3921	0.3746	0.3311
fuel / rev (kg.)	1.900	2.340	2.310	2.200	2.100	1.970	1.850	1.700
max cyl pressure (bar .)	92.39	136.36	138.12	137.35	134.71	129.83	120.55	111.21
max cyl temperature(deg k)	2121.20	2308.16	2179.73	2053.91	1931.20	1806.52	1750.75	1703.03
exhaust temperature(deg k)	787.72	902.62	868.00	843.70	822.39	812.35	825.50	839.78
percentage heat to coolant	30.55	24.86	21.37	18.93	16.95	15.39	14.69	13.65
compressor pressure ratio	1.2864	1.5303	1.7019	1.8427	1.9958	2.0549	2.0848	2.1312
delivery temperature(deg k)	333.29	355.32	369.26	378.70	389.76	397.46	403.40	417.86
delivery pressure (bar)	1.294	1.538	1.711	1.847	2.010	1.988	2.001	2.118
compressor speed (r.p.m.)	56223.3	74113.9	82944.0	89911.4	96948.4	100524.6	103680.0	110772.1
volume flow (cu m / min)	3.11	4.42	5.67	6.93	8.33	9.80	10.64	12.19
compressor power (kw.)	0.000	0.000	0.000	10.819	14.806	18.900	21.756	28.359
compressor efficiency	0.654	0.690	0.702	0.720	0.724	0.698	0.673	0.611
turbine speed (r.p.m)	56223.3	74113.9	82944.0	89911.4	96948.4	100524.6	103680.0	110772.1
turbine power (kw)	0.000	0.000	0.000	11.131	15.167	19.279	22.281	28.817
effective turbine efficiency.	0.595	0.604	0.613	0.617	0.618	0.620	0.620	0.617
fract of flow thro turbine.	0.000	0.000	0.000	0.000	0.000	0.000	0.000	0.000
first step. pressure ratio.	1.375	1.558	1.701	1.843	2.035	2.225	2.349	2.614
n.d. torque	0.7025	0.8216	0.8792	0.9136	0.9570	1.0043	1.0275	1.0635
n.d. mass flow.	146.9639	156.7934	161.0378	163.5999	165.9845	167.7561	168.4837	169.2967
n.d.speed	1761.2628	2280.2279	2622.8703	2933.3919	3254.2992	3476.2708	3610.2535	3863.5703
efficiency.	0.597	0.618	0.625	0.628	0.628	0.626	0.625	0.620
final step. pressure ratio.	1.077	1.180	1.317	1.472	1.679	1.892	2.045	2.358
n.d. torque	0.0056	0.1050	0.2800	0.4373	0.5962	0.7320	0.8106	0.9221
n.d. mass flow.	45.4930	85.6215	117.4819	136.4787	150.3769	158.7825	162.5245	166.5666
n.d.speed	1814.5223	2356.1194	2704.5328	3014.4967	3331.9266	3546.8390	3672.8145	3913.2867
efficiency.	0.067	0.387	0.527	0.570	0.592	0.605	0.610	0.613
compressor mass flow(kg/min).	3.65	5.17	6.65	8.12	9.76	11.49	12.47	14.28
delevered air to fuel ratio	19.21	18.43	20.55	23.07	25.82	29.15	30.64	32.30
v.g. nozzle width (m.m.)	5.5000	5.5000	5.5000	5.5000	5.5000	5.5000	5.5000	5.5000
cooler effectiveness	0.9578	0.9435	0.9288	0.9142	0.8988	0.8769	0.8640	0.8390
engine diagram factor	0.9800	0.9644	0.9500	0.9425	0.9300	0.8950	0.8600	0.8400

Perkins T6.354 Engine Data -- 50% Restriction 487 329 1645

number of cylinders	6.0	bore (m)	0.10	stroke (m)	0.12700			
con-rod length (m)	0.21908	inlet valve closing (degs)	229.0	number of turbochargers	1.0			
ambient temperature (deg k)	299.0	max. pressure limit (bar)	0.0000	ambient pressure (bar)	1.00530			
compression ratio	14.00	turbine nozzle angle (degs)	40.5000	turbine flow loss factor	0.8000			

engine speed(r.p.m)	1000.00	1200.00	1400.00	1600.00	1800.00	2000.00	2200.00	2600.00
boost pressure ratio	1.282	1.578	1.897	2.071	2.242	2.176	2.162	2.119
trapped a/f ratio	19.418	18.448	20.118	22.749	27.377	28.998	30.180	31.726
delivery ratio	0.820	0.822	0.831	0.820	0.842	0.855	0.843	0.822
manifold temp (deg k)	289.035	291.315	294.583	297.018	300.527	302.627	305.041	309.669
engine power (k w.)	47.50	77.57	108.25	117.87	120.17	118.98	116.32	108.10
engine torque (n.m.))	453.64	617.31	738.34	703.50	637.55	568.07	504.90	397.04
b.m.e.p (bar)	9.8375	13.3869	16.0114	15.2560	13.8257	12.3190	10.9491	8.6101
s.f.c. (kgs/kw hr)	0.240	0.227	0.210	0.208	0.209	0.217	0.228	0.260
b.thermal eff.	0.3476	0.3669	0.3982	0.4017	0.3984	0.3847	0.3657	0.3212
fuel / rev (kg.)	1.900	2.450	2.700	2.550	2.330	2.150	2.010	1.800
max cyl pressure (bar .)	79.90	123.23	137.70	136.22	133.28	121.47	111.54	99.92
max cyl temperature(deg k)	2086.37	2288.37	2192.39	2054.91	1859.13	1790.98	1742.62	1693.90
exhaust temperature(deg k)	804.79	934.50	923.33	889.24	834.31	840.68	856.92	869.50
percentage heat to coolant	30.34	24.18	19.76	17.53	15.42	14.70	14.16	13.37
compressor pressure ratio	1.3008	1.6049	1.9341	2.1165	2.3005	2.2452	2.2411	2.2171
delivery temperature(deg k)	335.07	362.37	388.79	400.09	412.08	412.03	417.46	426.18
delivery pressure (bar)	1.308	1.613	1.945	2.127	2.216	2.271	2.258	2.430
compressor speed (r.p.m.)	57486.5	78119.4	93821.6	101562.0	109034.4	108799.1	111437.5	114604.3
volume flow (cu m / min)	3.15	4.63	6.49	7.92	9.80	10.64	11.39	12.67
compressor power (kw.)	0.000	0.000	0.000	15.681	21.697	23.552	26.417	31.553
compressor efficiency	0.651	0.687	0.695	0.711	0.715	0.692	0.659	0.604
turbine speed (r.p.m)	57486.5	78119.4	93821.6	101562.0	109034.4	108799.1	111437.5	114604.3
turbine power (kw)	0.000	0.000	0.000	16.096	22.628	23.856	26.885	32.740
effective turbine efficiency.	0.595	0.606	0.615	0.617	0.618	0.617	0.616	0.617
fract of flow thro turbine.	0.000	0.000	0.000	0.000	0.000	0.000	0.000	0.000
first step. pressure ratio.	1.388	1.615	1.898	2.089	2.451	2.436	2.551	2.765
n.d. torque	0.7187	0.8646	0.9738	0.9983	1.0597	1.0393	1.0560	1.1013
n.d. mass flow.	148.1410	159.1629	165.1081	166.7517	168.8563	168.6482	169.0277	169.6845
n.d.speed	1783.6545	2369.3446	2895.8551	3244.2570	3665.2155	3702.4934	3808.0080	3923.9464
efficiency.	0.597	0.618	0.626	0.627	0.624	0.623	0.621	0.619
final step. pressure ratio.	1.079	1.203	1.425	1.638	2.043	2.057	2.208	2.482
n.d. torque	0.0055	0.1270	0.3684	0.5427	0.7808	0.7791	0.8471	0.9636
n.d. mass flow.	45.9223	91.3298	129.8626	146.7806	161.4446	161.5260	164.2281	167.5483
n.d.speed	1839.0655	2452.4237	2995.6183	3340.3855	3748.1776	3780.2119	3876.2766	3976.2479
efficiency.	0.064	0.410	0.545	0.579	0.604	0.602	0.607	0.614
compressor mass flow(kg/min).	3.69	5.42	7.60	9.28	11.48	12.47	13.35	14.85
delevered air to fuel ratio	19.42	18.45	20.12	22.75	27.38	29.00	30.18	31.73
v.g. nozzle width (m.m.)	5.5000	5.5000	5.5000	5.5000	5.5000	5.5000	5.5000	5.5000
cooler effectiveness	0.9577	0.9428	0.9255	0.9114	0.8919	0.8750	0.8617	0.8371
engine diagram factor	0.9800	0.9644	0.9500	0.9425	0.9300	0.8950	0.8600	0.8400

TABLE 6.3 FULLY RESTRICTED LIMITING TORQUE RESULTS, COMP. RATIO = 14

Perkins T6.354 Engine Data -- 50% Restriction 457 319 1595

number of cylinders	6.0	bore (m)	0.10	stroke (m)	0.12700		
con-rod length (m)	0.21908	inlet valve closing (degs)	229.0	number of turbochargers	1.0		
ambient temperature (deg k)	299.0	max. pressure limit (bar)	0.0000	ambient pressure (bar)	1.00530		
compression ratio	16.00	turbine nozzle angle (degs)	40.5000	turbine flow loss factor	0.8000		

engine speed(r.p.m)	1000.00	1200.00	1400.00	1600.00	1800.00	2000.00	2200.00	2600.00
boost pressure ratio	1.267	1.561	1.878	2.052	2.130	2.126	2.117	2.106
trapped a/f ratio	19.205	18.244	19.906	22.554	26.302	28.384	29.618	31.448
delivery ratio	0.820	0.822	0.830	0.820	0.850	0.854	0.843	0.819
manifold temp (deg k)	288.953	291.209	294.460	296.859	299.791	302.079	304.409	309.289
engine power (k w.)	48.97	79.29	110.55	120.83	122.50	122.67	120.53	112.89
engine torque (n.m.))	467.60	630.96	754.05	721.17	649.86	585.71	523.16	414.61
b.m.e.p (bar)	10.1403	13.6829	16.3522	15.6391	14.0928	12.7016	11.3452	8.9911
s.f.c. (kgs/kw hr)	0.233	0.222	0.205	0.203	0.205	0.210	0.220	0.249
b.thermal eff.	0.3583	0.3750	0.4066	0.4118	0.4061	0.3967	0.3790	0.3354
fuel / rev (kg.)	1.900	2.450	2.700	2.550	2.330	2.150	2.010	1.800
max cyl pressure (bar .)	92.39	126.43	137.13	137.39	133.91	134.44	128.51	115.89
max cyl temperature(deg k)	2121.20	2261.00	2157.88	2027.94	1872.27	1820.79	1784.64	1728.26
exhaust temperature(deg k)	787.72	922.99	912.58	876.85	837.17	832.96	847.58	856.36
percentage heat to coolant	30.55	24.34	19.89	17.62	15.80	14.89	14.31	13.44
compressor pressure ratio	1.2864	1.5880	1.9153	2.0974	2.1879	2.1955	2.1959	2.2030
delivery temperature(deg k)	333.29	360.80	387.49	398.53	405.04	408.24	413.43	424.59
delivery pressure (bar)	1.294	1.596	1.926	2.107	2.124	2.218	2.213	2.204
compressor speed (r.p.m.)	56223.3	77239.2	93000.2	100801.3	104849.5	106493.2	109224.0	113908.9
volume flow (cu m / min)	3.11	4.58	6.42	7.85	9.42	10.42	11.18	12.56
compressor power (kw.)	0.000	0.000	0.000	15.307	19.548	22.281	25.044	30.885
compressor efficiency	0.654	0.688	0.694	0.712	0.711	0.694	0.663	0.607
turbine speed (r.p.m)	56223.3	77239.2	93000.2	100801.3	104849.5	106493.2	109224.0	113908.9
turbine power (kw)	0.000	0.000	0.000	15.700	21.272	22.685	25.489	31.364
effective turbine efficiency.	0.595	0.605	0.615	0.617	0.622	0.618	0.617	0.616
fract of flow thro turbine.	0.000	0.000	0.000	0.000	0.000	0.000	0.000	0.000
first step. pressure ratio.	1.375	1.602	1.883	2.071	2.363	2.381	2.492	2.719
n.d. torque	0.7025	0.8548	0.9687	0.9922	1.0727	1.0350	1.0472	1.0802
n.d. mass flow.	146.9639	158.6443	164.9000	166.5764	168.8572	168.5180	168.8799	169.4814
n.d.speed	1761.2628	2350.2637	2874.2995	3227.3349	3499.8435	3636.5793	3756.4320	3935.6085
efficiency.	0.597	0.618	0.625	0.627	0.625	0.624	0.622	0.618
final step. pressure ratio.	1.077	1.198	1.416	1.626	1.962	2.014	2.161	2.447
n.d. torque	0.0056	0.1219	0.3623	0.5345	0.7801	0.7714	0.8363	0.9416
n.d. mass flow.	45.4930	90.0724	129.0536	146.1134	160.8655	161.0180	163.7697	167.0815
n.d.speed	1814.5223	2431.7144	2972.9174	3322.7643	3580.6682	3712.4322	3822.9807	3987.1272
efficiency.	0.067	0.405	0.544	0.578	0.610	0.604	0.608	0.612
compressor mass flow(kg/min).	3.65	5.36	7.52	9.20	11.03	12.20	13.10	14.72
delevered air to fuel ratio	19.21	18.24	19.91	22.55	26.30	28.38	29.62	31.45
v.g. nozzle width (m.m.)	5.5000	5.5000	5.5000	5.5000	5.5000	5.5000	5.5000	5.5000
cooler effectiveness	0.9578	0.9430	0.9258	0.9116	0.8916	0.8756	0.8623	0.8380
engine diagram factor	0.9800	0.9644	0.9500	0.9425	0.9300	0.8950	0.8600	0.8400

TABLE 6.4 FULLY RESTRICTED LIMITING TORQUE RESULTS, WITH RETARDED TIMING

Perkins T6.354 Engine Data

						404	300	1500
number of cylinders	6.0	bore (m)	0.10	stroke (m)	0.12700			
con-rod length (m)	0.21908	inlet valve closing (degs)	229.0	number of turbochargers	1.0			
ambient temperature (deg k)	299.0	max. pressure limit (bar)	0.0000	ambient pressure (bar)	1.00530			
compression ratio	16.00	turbine nozzle angle (degs)	40.5000	turbine flow loss factor	0.8000			

engine speed(r.p.m)	1000.00	1200.00	1400.00	1600.00	1800.00	2000.00	2200.00	2600.00
boost pressure ratio	1.260	1.524	1.823	1.825	1.841	1.839	1.844	1.837
trapped a/f ratio	19.104	17.827	19.569	20.293	22.157	23.958	25.787	27.993
delivery ratio	0.820	0.822	0.840	0.825	0.819	0.823	0.832	0.823
manifold temp (deg k)	288.912	290.985	294.198	295.100	296.465	298.115	300.311	304.595
engine power (k w.)	48.75	77.83	109.54	118.87	121.27	121.53	120.76	114.70
engine torque (n.m.))	465.50	619.31	747.14	709.46	643.35	580.26	524.17	421.28
b.m.e.p (bar)	10.0947	13.4303	16.2024	15.3851	13.9516	12.5835	11.3671	9.1357
s.f.c. (kgs/kw hr)	0.234	0.227	0.207	0.206	0.208	0.212	0.220	0.245
b.thermal eff.	0.3567	0.3681	0.4029	0.4051	0.4020	0.3930	0.3797	0.3408
fuel / rev (kg.)	1.900	2.450	2.700	2.550	2.330	2.150	2.010	1.800
max cyl pressure (bar .)	92.12	124.93	135.62	129.07	119.85	120.50	116.79	105.84
max cyl temperature(deg k)	2126.63	2287.32	2176.22	2136.62	2033.43	1972.75	1902.13	1818.58
exhaust temperature(deg k)	790.95	941.06	923.95	920.99	898.86	895.39	895.73	892.23
percentage heat to coolant	30.65	24.69	20.10	18.78	17.51	16.46	15.51	14.33
compressor pressure ratio	1.2795	1.5510	1.8602	1.8692	1.8936	1.9017	1.9179	1.9318
delivery temperature(deg k)	332.41	357.30	383.09	380.41	381.47	383.53	388.19	398.00
delivery pressure (bar)	1.287	1.559	1.870	1.879	1.903	1.910	1.870	1.932
compressor speed (r.p.m.)	55607.6	75256.0	90539.0	91158.7	92609.7	93647.0	95579.2	101284.7
volume flow (cu m / min)	3.10	4.47	6.31	7.07	7.93	8.79	9.73	11.18
compressor power (kw.)	2.027	0.000	0.000	11.266	12.809	14.555	16.999	21.676
compressor efficiency	0.657	0.689	0.694	0.723	0.730	0.717	0.690	0.629
turbine speed (r.p.m)	55607.6	75256.0	90539.0	91158.7	92609.7	93647.0	95579.2	101284.7
turbine power (kw)	2.141	0.000	0.000	11.813	12.918	14.973	17.161	22.032
effective turbine efficiency.	0.600	0.605	0.606	0.614	0.608	0.612	0.610	0.609
fract of flow thro turbine.	0.000	0.000	0.000	0.000	0.000	0.000	0.000	0.000
first step. pressure ratio.	1.368	1.568	1.772	1.823	1.838	1.904	1.978	2.148
n.d. torque	0.7364	0.8867	1.0415	1.0881	1.1056	1.1232	1.1525	1.1668
n.d. mass flow.	154.2641	166.0822	188.0662	191.1367	201.1161	201.3773	205.5793	203.1268
n.d.speed	1739.2214	2273.0926	2785.0396	2825.0900	2940.7196	3046.3883	3169.5748	3408.6028
efficiency.	0.599	0.619	0.627	0.626	0.622	0.621	0.616	0.613
final step. pressure ratio.	1.069	1.166	1.300	1.378	1.426	1.530	1.630	1.849
n.d. torque	-0.0038	0.0785	0.2116	0.3676	0.4339	0.5794	0.6940	0.8587
n.d. mass flow.	40.7325	82.4425	121.5652	142.7393	156.6106	170.2322	181.8329	190.3915
n.d.speed	1792.0648	2353.0634	2888.7639	2920.1296	3031.2396	3127.6879	3244.5230	3471.1824
efficiency.	-0.055	0.324	0.431	0.531	0.538	0.575	0.586	0.599
compressor mass flow(kg/min).	3.63	5.24	7.40	8.28	9.29	10.30	11.40	13.10
delevered air to fuel ratio	19.10	17.83	19.57	20.29	22.16	23.96	25.79	27.99
v.g. nozzle width (m.m.)	5.8350	5.8350	6.5015	6.5554	7.0177	6.9661	7.1052	6.9182
cooler effectiveness	0.9579	0.9433	0.9251	0.9133	0.8998	0.8848	0.8685	0.8415
engine diagram factor	0.9800	0.9644	0.9500	0.9425	0.9300	0.8950	0.8600	0.8400

TABLE 6.5 BOOST CONTROLLED VARIABLE GEOMETRY LIMITING TORQUE RESULTS WITH RETARDED TIMING

TABLE 6.6 UNRESTRICTED TRANSIENT RESULTS

time	0.000	0.010	0.020	0.030	0.040	0.050	0.060	0.070	0.080	0.090	sec
engine											
speed	1200.00	1200.00	1200.13	1208.44	1216.57	1224.64	1232.71	1240.85	1249.07	1343.50	rpm
load torq	120.00	115.93	115.94	116.63	117.32	118.02	118.72	119.44	120.17	129.41	n.m
eng torque	120.04	120.08	376.99	372.08	370.70	371.70	374.35	377.52	380.69	408.87	n.m
eng power	15.08	15.09	47.38	47.09	47.23	47.67	48.32	49.06	49.79	57.52	kw
b.m.e.p.	2.60	2.60	8.18	8.07	8.04	8.06	8.12	8.19	8.26	8.87	bar
s.f.c.	0.336	0.336	0.355	0.410	0.411	0.410	0.407	0.403	0.400	0.369	kg/kw.hr
th.effy	0.249	0.249	0.235	0.203	0.203	0.203	0.205	0.207	0.209	0.226	
boost rat	1.060	1.061	1.060	1.062	1.066	1.069	1.073	1.076	1.080	1.115	total
inlet temp	302.87	303.00	303.06	303.27	303.57	303.87	304.19	304.47	304.71	306.31	k
del rat	0.820	0.820	0.820	0.823	0.826	0.829	0.832	0.833	0.835	0.853	
tr af rat	41.40	41.40	16.00	16.00	16.00	16.00	16.00	16.00	16.00	16.00	
fuel/rev	70.31	70.33	233.74	266.28	266.13	265.98	265.83	265.67	265.52	263.28	kg*10e6
inl m.flow	3.49	3.49	3.49	3.54	3.58	3.63	3.67	3.71	3.75	4.23	kg/min
exh m.flow	3.58	3.58	3.77	3.86	3.90	3.95	4.00	4.04	4.08	4.59	kg/min
fuel flow	0.084	0.084	0.281	0.322	0.324	0.326	0.328	0.330	0.332	0.354	kg/min
max.press.	62.25	62.28	89.72	89.67	90.83	91.83	92.66	93.38	94.04	101.43	bar
max.temp.	1559.83	1559.96	2446.90	2448.93	2453.95	2457.88	2461.18	2464.03	2466.76	2493.18	k
exh.temp.	515.17	515.17	1100.96	1164.25	1170.19	1173.76	1175.46	1176.34	1176.99	1188.88	k
cool heat	30.97	30.97	31.83	31.60	31.37	31.14	30.92	30.72	30.52	28.41	%
fuel pump											
f.pump spd	600.00	600.00	600.07	604.22	608.29	612.32	616.36	620.43	624.53	671.75	rpm
gov set pt	1257.98	2800.00	2800.00	2800.00	2800.00	2800.00	2800.00	2800.00	2800.00	2800.00	engine rpm
rack posn	1.16	1.16	4.24	5.00	5.00	5.00	5.00	5.00	5.00	5.00	usually mm
fuel/strk	23.44	23.44	77.91	88.76	88.71	88.66	88.61	88.56	88.51	87.76	kg*10e6
inj start	355.35	355.35	350.54	349.37	349.16	348.96	348.76	348.56	348.36	346.34	deg atdco
duration	4.34	4.34	14.72	17.04	17.27	17.49	17.72	17.95	18.17	20.53	deg ca
compressor											
speed	30107.4	30190.5	30171.9	30461.4	30835.5	31266.8	31719.8	32164.9	32589.4	36738.7	rpm
press rat	1.085	1.086	1.086	1.086	1.087	1.089	1.091	1.092	1.094	1.113	total
out temp	310.47	310.53	310.58	310.54	310.73	310.89	311.14	311.37	311.61	314.04	k
mass flow	3.50	3.50	3.48	3.58	3.61	3.68	3.72	3.77	3.80	4.28	kg/min
torque	0.222	0.222	0.222	0.225	0.227	0.231	0.234	0.238	0.241	0.283	n.m
power	0.70	0.70	0.70	0.72	0.73	0.76	0.78	0.80	0.82	1.09	kw
effic	0.593	0.593	0.592	0.595	0.597	0.600	0.601	0.603	0.605	0.615	
cooler											
out p rat	1.016	1.017	1.018	1.017	1.019	1.021	1.024	1.026	1.029	1.052	static
out temp	299.88	299.88	299.88	299.90	299.92	299.95	299.98	300.01	300.03	300.36	k
effectvns	0.923	0.924	0.924	0.922	0.922	0.920	0.920	0.919	0.918	0.910	
turbine											
p rat max	1.326	1.326	1.671	1.805	1.902	1.948	1.952	1.937	1.917	1.933	total
p rat min	1.119	1.118	1.118	1.270	1.379	1.427	1.426	1.403	1.376	1.342	total
inl temp	501.23	503.85	505.98	648.53	786.41	896.79	980.16	1041.45	1085.70	1188.75	k
mass flow	3.68	3.66	5.89	5.57	5.27	5.09	4.90	4.71	4.56	4.55	kg/min
torque	0.23	0.23	0.67	0.80	0.89	0.92	0.91	0.89	0.86	0.89	n.m
power	0.71	0.71	2.13	2.55	2.86	3.02	3.04	2.99	2.94	3.44	kw
effic	0.525	0.525	0.391	0.346	0.318	0.306	0.302	0.303	0.305	0.322	

TABLE 6.6 Continued ...

time	0.190	0.290	0.390	0.490	0.590	0.690	0.790	0.890	0.990	1.090	sec
engine											
speed	1433.98	1525.14	1613.77	1698.44	1779.74	1858.76	1935.34	2007.63	2073.91	2134.16	rpm
load torq	139.12	149.98	161.96	174.39	187.45	201.74	217.56	234.23	250.79	266.74	n.m
eng torque	426.63	433.20	433.67	433.91	438.55	446.32	451.98	451.33	448.26	446.61	n.m
eng power	64.06	69.19	73.29	77.17	81.73	86.88	91.60	94.89	97.35	99.81	kw
b.m.e.p.	9.25	9.39	9.40	9.41	9.51	9.68	9.80	9.79	9.72	9.69	bar
s.f.c.	0.349	0.339	0.332	0.324	0.314	0.303	0.293	0.288	0.285	0.282	kg/kw.hr
th.effy	0.239	0.246	0.252	0.257	0.265	0.276	0.285	0.290	0.293	0.296	
boost rat	1.146	1.165	1.179	1.198	1.228	1.263	1.292	1.308	1.321	1.337	total
inlet temp	307.38	307.81	308.60	309.92	311.41	312.76	313.72	314.49	315.59	316.93	k
del rat	0.854	0.847	0.839	0.829	0.821	0.817	0.814	0.811	0.809	0.808	
tr af rat	16.00	16.00	16.00	16.00	16.00	16.00	16.00	16.00	16.00	16.00	
fuel/rev	260.21	256.17	251.04	245.61	240.61	235.84	231.24	226.95	223.06	219.55	kg*10e6
inl m.flow	4.63	4.96	5.25	5.53	5.85	6.22	6.58	6.87	7.13	7.38	kg/min
exh m.flow	5.01	5.35	5.65	5.94	6.28	6.66	7.03	7.33	7.59	7.85	kg/min
fuel flow	0.373	0.391	0.405	0.417	0.428	0.438	0.448	0.456	0.463	0.469	kg/min
max.press.	105.01	105.44	104.47	103.35	103.14	103.66	103.46	102.18	100.74	99.85	bar
max.temp.	2505.71	2509.08	2508.15	2505.49	2502.61	2499.27	2493.31	2485.99	2479.34	2474.09	k
exh.temp.	1196.76	1204.72	1212.28	1218.59	1223.19	1226.92	1232.33	1241.36	1250.86	1257.53	k
cool heat	26.91	25.82	24.98	24.23	23.43	22.58	21.84	21.28	20.84	20.41	%
fuel pump											
f.pump spd	716.99	762.57	806.88	849.22	889.87	929.38	967.67	1003.81	1036.96	1067.08	rpm
gov set pt	2800.00	2800.00	2800.00	2800.00	2800.00	2800.00	2800.00	2800.00	2800.00	2800.00	engine rpm
rack posn	5.00	5.00	5.00	5.00	5.00	5.00	5.00	5.00	5.00	5.00	usually mm
fuel/strk	86.74	85.39	83.68	81.87	80.20	78.61	77.08	75.65	74.35	73.18	kg*10e6
inj start	345.24	344.80	344.83	345.11	345.45	345.83	346.38	346.96	347.49	347.92	deg atdco
duration	21.97	22.81	23.19	23.29	23.33	23.29	23.12	22.92	22.76	22.67	deg ca
compressor											
speed	40631.2	44136.1	47441.6	50692.5	53977.6	57376.8	60685.6	63679.6	66330.5	68670.1	rpm
press rat	1.136	1.163	1.193	1.224	1.256	1.292	1.330	1.368	1.404	1.438	total
out temp	316.76	319.63	322.60	325.63	328.77	332.24	335.83	339.13	342.18	345.08	k
mass flow	4.68	4.98	5.26	5.56	5.90	6.28	6.61	6.88	7.13	7.39	kg/min
torque	0.327	0.371	0.418	0.467	0.520	0.581	0.641	0.693	0.741	0.793	n.m
power	1.39	1.72	2.08	2.48	2.94	3.49	4.08	4.62	5.15	5.70	kw
effic	0.625	0.639	0.655	0.667	0.677	0.683	0.690	0.699	0.706	0.710	
cooler											
out p rat	1.072	1.082	1.086	1.096	1.114	1.137	1.154	1.159	1.161	1.165	static
out temp	300.72	301.08	301.46	301.87	302.32	302.85	303.37	303.83	304.27	304.72	k
effectvns	0.903	0.899	0.896	0.892	0.888	0.884	0.881	0.880	0.878	0.876	
turbine											
p rat max	1.903	1.867	1.861	1.870	1.895	1.932	1.940	1.933	1.926	1.925	total
p rat min	1.275	1.220	1.208	1.214	1.227	1.246	1.233	1.212	1.195	1.181	total
inl temp	1192.22	1202.37	1211.11	1218.09	1223.14	1226.64	1230.95	1239.74	1249.55	1256.79	k
mass flow	5.07	5.38	5.66	5.94	6.27	6.66	7.05	7.35	7.60	7.86	kg/min
torque	0.90	0.90	0.94	0.99	1.06	1.14	1.16	1.16	1.17	1.18	n.m
power	3.84	4.18	4.67	5.26	5.99	6.83	7.37	7.77	8.11	8.49	kw
effic	0.351	0.378	0.398	0.413	0.425	0.435	0.446	0.456	0.465	0.470	

TABLE 6.6 Continued ...

time	1.190	1.290	1.390	1.490	1.590	1.690	1.790	1.890	1.990	2.090	sec
engine											
speed	2189.24	2239.03	2283.71	2323.63	2359.11	2390.55	2418.32	2442.81	2464.36	2483.30	rpm
load torq	281.96	296.37	310.05	322.71	334.21	344.49	353.59	361.59	368.59	374.68	n.m
eng torque	445.95	443.79	442.00	440.26	438.49	436.72	434.97	433.27	431.62	430.06	n.m
eng power	102.24	104.06	105.71	107.13	108.33	109.33	110.16	110.83	111.39	111.84	kw
b.m.e.p.	9.67	9.62	9.59	9.55	9.51	9.47	9.43	9.40	9.36	9.33	bar
s.f.c.	0.278	0.276	0.274	0.272	0.271	0.270	0.269	0.268	0.268	0.267	kg/kw.hr
th.effy	0.300	0.303	0.305	0.307	0.308	0.309	0.310	0.311	0.312	0.312	
boost rat	1.360	1.384	1.406	1.426	1.444	1.459	1.472	1.483	1.492	1.500	total
inlet temp	318.34	319.54	320.61	321.59	322.49	323.32	324.08	324.77	325.38	325.93	k
del rat	0.807	0.807	0.808	0.810	0.811	0.812	0.814	0.815	0.816	0.817	
tr af rat	16.16	16.61	17.04	17.43	17.79	18.10	18.38	18.62	18.84	19.02	
fuel/rev	216.39	213.60	211.16	209.03	207.16	205.52	204.08	202.82	201.71	200.73	kg*10e6
inl m.flow	7.66	7.94	8.22	8.47	8.69	8.89	9.07	9.23	9.36	9.48	kg/min
exh m.flow	8.13	8.42	8.70	8.95	9.18	9.39	9.57	9.72	9.86	9.98	kg/min
fuel flow	0.474	0.478	0.482	0.486	0.489	0.491	0.494	0.495	0.497	0.498	kg/min
max.press.	99.32	98.59	98.14	97.85	97.65	97.51	97.40	97.30	97.21	97.13	bar
max.temp.	2457.40	2420.59	2387.20	2358.02	2332.89	2311.36	2293.01	2277.39	2264.12	2252.82	k
exh.temp.	1253.66	1235.86	1217.84	1201.11	1186.12	1172.97	1161.59	1151.84	1143.54	1136.50	k
cool heat	19.97	19.54	19.15	18.81	18.51	18.26	18.05	17.87	17.71	17.58	%
fuel pump											
f.pump spd	1094.62	1119.51	1141.86	1161.81	1179.56	1195.28	1209.16	1221.41	1232.18	1241.65	rpm
gov set pt	2800.00	2800.00	2800.00	2800.00	2800.00	2800.00	2800.00	2800.00	2800.00	2800.00	engine rpm
rack posn	5.00	5.00	5.00	5.00	5.00	5.00	5.00	5.00	5.00	5.00	usually mm
fuel/strk	72.13	71.20	70.39	69.68	69.05	68.51	68.03	67.61	67.24	66.91	kg*10e6
inj start	348.24	348.45	348.60	348.71	348.79	348.85	348.90	348.94	348.98	349.01	deg atdco
duration	22.65	22.69	22.76	22.84	22.92	22.99	23.05	23.10	23.14	23.18	deg ca
compressor											
speed	70756.1	72520.8	73992.6	75226.8	76270.1	77157.3	77912.4	78555.1	79102.7	79570.0	rpm
press rat	1.469	1.496	1.518	1.537	1.552	1.565	1.575	1.584	1.592	1.598	total
out temp	347.88	350.37	352.49	354.29	355.81	357.10	358.20	359.12	359.90	360.56	k
mass flow	7.68	7.97	8.24	8.49	8.71	8.90	9.08	9.23	9.37	9.48	kg/min
torque	0.849	0.904	0.954	1.000	1.040	1.076	1.108	1.135	1.158	1.178	n.m
power	6.29	6.86	7.39	7.87	8.31	8.70	9.04	9.34	9.59	9.82	kw
effic	0.711	0.710	0.708	0.705	0.703	0.700	0.698	0.696	0.695	0.693	
cooler											
out p rat	1.175	1.187	1.197	1.206	1.213	1.219	1.223	1.226	1.228	1.229	static
out temp	305.19	305.64	306.06	306.43	306.77	307.06	307.32	307.54	307.74	307.91	k
effectvns	0.873	0.871	0.868	0.866	0.863	0.861	0.860	0.858	0.857	0.855	
turbine											
p rat max	1.926	1.922	1.920	1.920	1.922	1.924	1.926	1.928	1.930	1.931	total
p rat min	1.173	1.170	1.169	1.170	1.173	1.177	1.181	1.184	1.188	1.191	total
inl temp	1255.14	1237.54	1219.48	1202.62	1187.48	1174.15	1162.61	1152.71	1144.29	1137.14	k
mass flow	8.12	8.41	8.69	8.94	9.17	9.37	9.56	9.71	9.85	9.97	kg/min
torque	1.20	1.21	1.22	1.24	1.26	1.27	1.29	1.30	1.31	1.32	n.m
power	8.88	9.18	9.47	9.75	10.03	10.27	10.49	10.69	10.85	11.00	kw
effic	0.475	0.480	0.484	0.487	0.489	0.490	0.491	0.492	0.492	0.493	

TABLE 6.7 BOOST CONTROLLED VARIABLE GEOMETRY TRANSIENT RESULTS

time	0.000	0.010	0.020	0.030	0.040	0.050	0.060	0.070	0.080	0.090	sec
engine											
speed	1200.00	1200.00	1200.10	1212.55	1224.38	1236.06	1247.73	1259.41	1270.54	1383.93	rpm
load torq	120.00	115.93	115.94	116.98	117.99	119.01	120.05	121.11	122.15	133.64	n.m
eng torque	119.86	119.20	506.23	489.19	484.94	485.73	486.93	470.96	458.93	457.55	n.m
eng power	15.06	14.98	63.62	62.12	62.18	62.87	63.62	62.11	61.06	66.31	kw
b.m.e.p.	2.60	2.58	10.98	10.61	10.52	10.53	10.56	10.21	9.95	9.92	bar
s.f.c.	0.310	0.311	0.261	0.312	0.314	0.313	0.312	0.323	0.331	0.328	kg/kw.hr
th.effy	0.269	0.268	0.320	0.268	0.265	0.266	0.267	0.258	0.252	0.254	
boost rat	1.275	1.274	1.274	1.276	1.280	1.282	1.284	1.227	1.205	1.207	total
inlet temp	303.27	303.26	303.31	303.46	303.75	303.92	304.04	300.11	298.72	305.25	k
del rat	0.840	0.838	0.836	0.822	0.820	0.821	0.823	0.822	0.846	0.844	
tr af rat	55.26	55.12	16.00	16.00	16.00	16.00	16.00	16.00	16.00	16.00	
fuel/rev	64.82	64.78	230.42	266.21	265.98	265.76	265.54	265.32	265.09	262.02	kg*10e6
inl m.flow	4.30	4.29	4.28	4.26	4.29	4.34	4.40	4.30	4.39	4.69	kg/min
exh m.flow	4.38	4.37	4.55	4.58	4.62	4.67	4.73	4.63	4.73	5.05	kg/min
fuel flow	0.078	0.078	0.277	0.323	0.326	0.328	0.331	0.334	0.337	0.365	kg/min
max.press.	68.07	68.03	108.64	107.02	107.72	108.61	109.56	106.10	107.94	109.34	bar
max.temp.	1592.04	1595.56	2458.78	2459.74	2464.55	2468.63	2472.53	2472.81	2461.58	2500.53	k
exh.temp.	462.95	464.17	1022.28	1125.79	1132.27	1134.99	1137.53	1142.66	1157.89	1175.72	k
cool heat	26.98	27.02	28.21	28.28	28.14	27.94	27.73	28.13	27.40	26.69	%
fuel pump											
f.pump spd	600.00	600.00	600.05	606.26	612.19	618.05	623.86	629.70	635.27	691.96	rpm
gov set pt	1253.66	2800.00	2800.00	2800.00	2800.00	2800.00	2800.00	2800.00	2800.00	2800.00	engine rpm
rack posn	1.07	1.07	4.17	5.00	5.00	5.00	5.00	5.00	5.00	5.00	usually mm
fuel/strk	21.59	21.59	76.81	88.74	88.66	88.59	88.51	88.44	88.36	87.54	kg*10e6
inj start	355.52	355.52	350.64	349.26	348.97	348.68	348.39	348.11	347.85	345.72	deg atdco
duration	3.99	3.99	14.50	17.15	17.48	17.81	18.14	18.46	18.76	21.29	deg ca
compressor											
speed	39909.0	39848.9	39827.9	40513.9	40858.2	41427.0	41972.6	42515.4	43228.6	47953.6	rpm
press rat	1.135	1.134	1.134	1.137	1.141	1.145	1.149	1.227	1.115	1.205	total
out temp	316.54	316.48	316.47	316.81	317.26	317.72	318.15	354.93	316.09	323.55	k
mass flow	4.27	4.28	4.28	4.33	4.33	4.36	4.41	0.14	7.26	4.71	kg/min
torque	0.300	0.300	0.300	0.305	0.309	0.314	0.321	0.019	0.463	0.385	n.m
power	1.25	1.25	1.25	1.29	1.32	1.36	1.41	0.09	2.10	1.93	kw
effic	0.628	0.628	0.628	0.629	0.632	0.634	0.636	99999.000	99999.000	0.665	
cooler											
out p rat	1.221	1.220	1.220	1.220	1.224	1.226	1.227	1.227	1.026	1.156	static
out temp	299.90	299.90	299.90	299.93	299.94	299.97	300.00	299.03	300.97	300.25	k
effectvns	0.949	0.948	0.948	0.948	0.948	0.948	0.948	0.999	0.885	0.949	
turbine											
p rat max	1.329	1.338	1.844	1.955	1.996	2.000	2.011	1.978	1.972	1.957	total
p rat min	1.101	1.114	1.117	1.235	1.308	1.310	1.318	1.319	1.294	1.268	total
inl temp	439.72	445.89	450.11	593.64	747.79	872.99	973.63	1043.04	1082.48	1175.36	k
mass flow	4.44	4.49	7.93	7.37	6.71	5.91	5.48	5.21	5.12	5.29	kg/min
torque	0.50	0.51	1.05	1.14	1.18	1.15	1.15	1.10	1.09	1.08	n.m
power	1.24	1.29	4.37	4.80	5.04	4.99	5.07	4.90	4.93	5.41	kw
effic	0.596	0.596	0.482	0.447	0.420	0.410	0.404	0.407	0.409	0.433	

TABLE 6.7 Continued . . .

time	0.190	0.290	0.390	0.490	0.590	0.690	0.790	0.890	0.990	1.090	sec
engine											
speed	1486.97	1590.39	1693.68	1794.95	1891.48	1982.65	2068.03	2148.25	2223.48	2290.98	rpm
load torq	145.28	158.65	173.67	190.06	208.24	228.29	249.27	270.58	291.76	312.32	n.m
eng torque	469.55	483.92	496.16	501.02	501.82	504.56	508.29	514.07	519.05	505.78	n.m
eng power	73.12	80.59	88.00	94.18	99.40	104.76	110.08	115.65	120.86	121.34	kw
b.m.e.p.	10.18	10.49	10.76	10.86	10.88	10.94	11.02	11.15	11.26	10.97	bar
s.f.c.	0.515	0.299	0.284	0.274	0.267	0.259	0.252	0.244	0.237	0.239	kg/kw.hr
th.effy	0.265	0.279	0.294	0.304	0.312	0.322	0.331	0.342	0.352	0.349	
boost rat	1.239	1.280	1.320	1.348	1.374	1.426	1.499	1.579	1.654	1.715	total
inlet temp	307.20	308.70	309.74	310.28	311.43	313.60	315.52	316.95	318.06	319.00	k
del rat	0.840	0.834	0.826	0.820	0.816	0.813	0.811	0.811	0.811	0.815	
tr af rat	16.00	16.00	16.00	16.00	16.00	16.42	17.51	18.75	19.97	21.04	
fuel/rev	257.99	252.49	245.91	239.69	233.87	228.42	223.40	218.74	214.47	210.77	kg*10e6
inl m.flow	5.11	5.58	6.05	6.49	6.91	7.44	8.09	8.81	9.52	10.16	kg/min
max.press.	111.34	112.79	113.30	112.73	111.91	111.01	109.83	109.37	109.40	109.64	bar
max.temp.	2509.86	2511.67	2508.59	2503.13	2496.88	2456.37	2369.10	2281.76	2205.10	2144.44	k
exh.temp.	1183.73	1185.79	1184.43	1186.99	1194.53	1184.98	1147.31	1103.13	1059.58	1039.87	k
cool heat	25.37	24.08	22.95	21.99	21.17	20.28	19.27	18.30	17.45	16.77	%
fuel pump											
f.pump spd	743.49	795.20	846.84	897.48	945.74	991.32	1034.01	1074.12	1111.74	1145.49	rpm
gov set pt	2800.00	2800.00	2800.00	2800.00	2800.00	2800.00	2800.00	2800.00	2800.00	2800.00	engine rpm
rack posn	5.00	5.00	5.00	5.00	5.00	5.00	5.00	5.00	5.00	5.00	usually mm
fuel/strk	86.00	84.16	81.97	79.90	77.96	76.14	74.47	72.91	71.49	70.26	kg*10e6
inj start	344.92	344.79	345.09	345.51	346.05	346.76	347.45	348.01	348.39	348.62	deg atdco
duration	22.52	23.12	23.29	23.33	23.23	22.99	22.78	22.66	22.68	22.78	deg ca
compressor											
speed	51976.7	55776.6	59615.0	63570.8	67655.4	71822.5	75859.5	79751.9	83476.4	87055.1	rpm
press rat	1.241	1.278	1.321	1.370	1.426	1.490	1.553	1.615	1.675	1.735	total
out temp	326.98	330.46	334.49	338.93	343.76	349.28	355.02	360.73	366.21	371.65	k
mass flow	5.17	5.65	6.12	6.51	6.95	7.55	8.23	8.95	9.64	10.24	kg/min
torque	0.445	0.510	0.582	0.654	0.735	0.845	0.974	1.111	1.245	1.369	n.m
power	2.42	2.98	3.63	4.35	5.20	6.36	7.74	9.28	10.88	12.48	kw
effic	0.680	0.691	0.698	0.707	0.715	0.718	0.715	0.709	0.705	0.701	
cooler											
out p rat	1.155	1.181	1.208	1.222	1.231	1.261	1.310	1.365	1.413	1.450	static
out temp	300.50	300.77	301.06	301.30	301.55	301.87	302.25	302.65	303.02	303.34	k
effectvns	0.946	0.944	0.942	0.942	0.943	0.943	0.942	0.941	0.940	0.940	
turbine											
p rat max	1.885	1.890	1.909	1.935	1.969	2.009	2.052	2.103	2.156	2.216	total
p rat min	1.183	1.159	1.154	1.164	1.186	1.217	1.264	1.319	1.377	1.446	total
mass flow	5.52	5.99	6.47	6.91	7.34	7.84	8.48	9.19	9.91	10.57	kg/min
torque	1.05	1.12	1.21	1.30	1.41	1.51	1.63	1.74	1.86	1.97	n.m
power	5.73	6.54	7.55	8.68	9.96	11.39	12.92	14.57	16.22	17.94	kw
effic	0.458	0.477	0.494	0.508	0.520	0.531	0.543	0.553	0.560	0.564	

TABLE 6.7 Continued ...

time	1.190	1.290	1.390	1.490	1.590	1.690	1.790	1.890	1.990	2.090	sec
engine											
speed	2348.06	2395.95	2435.89	2469.52	2497.23	2520.47	2539.81	2555.34	2563.08	2566.27	rpm
load torq	330.61	346.26	359.34	370.19	379.12	386.48	392.61 447.4	397.53	399.97	400.99	n.m
eng power	121.32	121.01	120.67	120.30	119.85	119.41	119.00	115.71	111.25	109.35	kw
b.m.e.p.	10.70	10.46	10.26	10.09	9.94	9.81	9.70	9.38	8.99	8.82	bar
s.f.c.	0.241	0.244	0.246	0.248	0.250	0.252	0.253	0.255	0.257	0.257	kg/kw.hr
th.effy	0.346	0.342	0.339	0.336	0.334	0.331	0.329	0.327	0.325	0.324	
boost rat	1.758	1.785	1.803	1.813	1.819	1.822	1.824	1.825	1.823	1.821	total
inlet temp	319.71	320.58	321.06	321.64	322.22	322.75	323.22	323.60	323.88	324.05	k
del rat	0.814	0.816	0.818	0.820	0.821	0.822	0.823	0.824	0.825	0.825	
tr af rat	21.88	22.49	22.95	23.28	23.52	23.69	23.82	24.49	25.39	25.75	
fuel/rev	207.74	205.24	203.17	201.45	200.02	198.82	197.82	192.52	185.60	182.74	kg*10e6
inl m.flow	10.67	11.06	11.36	11.58	11.75	11.87	11.97	12.05	12.08	12.08	kg/min
exh m.flow	11.16	11.55	11.85	12.08	12.24	12.37	12.47	12.54	12.55	12.54	kg/min
fuel flow	0.488	0.492	0.495	0.497	0.499	0.501	0.502	0.492	0.476	0.469	kg/min
max.press.	109.77	109.67	109.49	109.18	108.82	108.47	108.16	107.06	105.64	105.00	bar
max.temp.	2100.27	2069.98	2047.85	2032.22	2021.38	2013.38	2007.25	1979.36	1944.46	1930.91	k
exh.temp.	1025.16	1015.34	1007.94	1002.90	999.95	998.10	996.88	981.26	959.87	951.56	k
cool heat	16.27	15.92	15.66	15.47	15.34	15.24	15.16	15.09	15.06	15.06	%
fuel pump											
f.pump spd	1174.03	1197.97	1217.94	1234.66	1248.61	1260.24	1269.91	1277.67	1281.54	1283.14	rpm
gov set pt	2800.00	2800.00	2800.00	2800.00	2800.00	2800.00	2800.00	2800.00	2800.00	2800.00	engine rpm
rack posn	5.00	5.00	5.00	5.00	5.00	5.00	5.00	4.89	4.74	4.67	usually mm
fuel/strk	69.25	68.41	67.72	67.15	66.67	66.27	65.94	64.17	61.87	60.91	kg*10e6
inj start	348.76	348.86	348.93	348.99	349.04	349.08	349.11	349.35	349.66	349.79	deg atdco
duration	22.89	23.00	23.09	23.15	23.21	23.25	23.27	22.74	21.94	21.60	deg ca
compressor											
speed	90479.1	93627.7	96415.9	98827.9	99814.2	100814.0	101558.1	102070.7	102043.0	101849.7	rpm
press rat	1.796	1.859	1.919	1.964	1.995	2.017	2.033	2.043	2.040	2.033	total
out temp	377.19	382.64	387.69	391.44	394.07	395.97	397.40	398.38	398.33	397.97	k
mass flow	10.71	11.07	11.36	11.57	11.73	11.86	11.96	12.03	12.06	12.07	kg/min
torque	1.480	1.578	1.666	1.733	1.783	1.820	1.849	1.871	1.875	1.872	n.m
power	14.02	15.47	16.82	17.87	18.63	19.22	19.67	19.99	20.03	19.97	kw
effic	0.698	0.695	0.693	0.690	0.688	0.686	0.684	0.683	0.682	0.681	
cooler											
out p rat	1.473	1.483	1.486	1.483	1.479	1.473	1.468	1.463	1.458	1.455	static
out temp	303.56	303.68	303.74	303.77	303.81	303.85	303.88	303.91	303.95	303.97	k
effectvns	0.942	0.944	0.947	0.948	0.949	0.950	0.950	0.951	0.950	0.950	
turbine											
p rat max	2.266	2.306	2.321	2.304	2.301	2.302	2.304	2.287	2.271	2.267	total
p rat min	1.506	1.556	1.576	1.559	1.559	1.563	1.569	1.570	1.580	1.588	total
inl temp	1027.49	1017.03	1006.71	1003.23	1000.24	998.35	997.08	985.01	961.52	952.24	k
mass flow	11.10	11.50	11.88	12.08	12.24	12.37	12.47	12.49	12.52	12.53	kg/min
torque	2.05	2.10	2.11	2.07	2.05	2.04	2.04	2.00	1.95	1.94	n.m
power	19.42	20.61	21.33	21.30	21.42	21.58	21.73	21.33	20.87	20.74	kw
effic	0.568	0.570	0.573	0.573	0.573	0.572	0.571	0.570	0.571	0.572	

7. Conclusions and suggestions for further work

7.1 Introduction

This project was concerned with the manufacture and development of a boost controlled, continuously variable geometry turbocharger prototype which was tested on the turbine dynamometer rig as well as by means of extensive engine-dynamometer experiments. These tests included steady state and transient tests. On the theoretical side, two programs were modified to provide the means of investigating theoretically, the areas of interest which the experimental programme did not include or which could not be covered by the present apparatus. The conclusions drawn from this work are divided into three subsections. The first deals with the experimental results. In the second, the theoretical predictions are considered and finally suggestions for further work are given.

7.2 Conclusions drawn from the experimental results

The benefits of variable geometry turbocharger application to a transport engine have been clearly demonstrated, in particular with regard to torque back up and reduced sfc on the limiting torque curve. With 50% restriction, 55.8% torque back up at an engine speed of 1200rpm corresponding to 46.1% maximum engine speed has been achieved which compares quite favourably with 34.3% torque back up at 53.8% maximum engine speed for the unrestricted case. There is a considerable improvement in sfc up to an engine speed of 1900rpm on the limiting torque curve beyond which point the sfc deteriorates due to the adverse pressure gradient across the engine. However, this can be avoided by the use of a boost-restriction

schedule to ensure less restriction in the high engine speed range. In the part load regime, the effect on sfc is negative which leads to an unacceptable drop in overall thermal efficiency. It is therefore, concluded that for best variable geometry utilization, a sfc optimization study will have to be undertaken to enable variable geometry setting for best sfc attainment. However, this will be in conflict with the transient response requirement of maximum air availability prior to a fuel step. This can also be allowed for in the control system where the turbine will be fully restricted under sudden metering valve increases. For such a system a simple boost controlled concept will be unacceptable and other parameters such as fuel flow rate and engine speed may have to be sensed and the variable geometry setting chosen according to a 'look up' table stored electronically. As it will be required to vary injection timing to keep maximum cylinder pressure within the safe limit, and as this has a primary effect on sfc and exhaust emissions, an additional dimension to the 'look up' table will have to be injection timing. Work concerning this parameter is under way at present by other researchers at Bath.

A manual override of the control system can provide the engine with an exhaust brake by restricting the turbine when required. The variable geometry device can also be used as a safety mechanism to control turbocharger speed in high altitude operations. This will require an initial throat area in excess of 100%. This can be allowed for in the design stage.

The effect on transient response has been less clearly shown due to the nature of the transient tests adopted. Nevertheless it is

evident that the engine response is substantially improved coupled with less smoke emission as a result of the extra air made available by the variable geometry turbocharger. However, as mentioned above, due to the fact that the part load sfc values have deteriorated due to variable geometry operation, the improvement in transient response has to be viewed in relation to the increased fuel consumption.

7.3 Conclusions drawn from the theoretical results

Since the engine turbocharger match was not completely satisfactory the experimental programme was not pursued as far as it was originally intended. Therefore, the computer programs have been used to indicate what can be expected with a well matched turbocharger and later with lower compression ratio and/or variable injection timing considerations. It is quite clear that a torque back up well in excess of 50% is possible when maximum cylinder pressures are contained using either of the above mentioned options. There is a small improvement in sfc in the low to mid-speed range while there is a sfc increase in the high speed region with a fully restricted turbine. Further, it has been shown that when a boost controlled restriction schedule is adopted the sfc penalties in this region will be avoided. In addition to wide mass flow range compressors, the need for variable injection timing has been clearly illustrated as reflected by the extra torque back up obtained by an injection retard of 3 degrees*. Although the peak cylinder pressures could not be measured accurately enough, the need for the control of this important parameter is clearly shown. It is also concluded that for a successful variable geometry scheme, it is of

* Fuelling increased to get maximum cylinder pressure at 1400 rpm

utmost importance to find compressors with as large a mass flow range as possible particularly if variable injection timing is envisaged. This requires the adoption of backward swept compressor blades or some type of compressor prewhirl device for schemes with exceptionally high torque back up requirements.

7.4 Suggestions for further work

The concept of variable geometry turbocharging has been confirmed using a technically and commercially viable design. However, the two areas where further work is necessary are:

i) Control aspects

This design was based on a boost controlled scheme. However, due to some difficulties encountered during this work, particularly with respect to sealing problems in the control cylinder, other mechanisms of control will have to be considered. A more suitable and more reliable choice may be the application of a solenoid actuated control system together with a suitable pressure transducer to indicate boost level or if more complex multi-variable control systems are envisaged, various transducers are necessary to indicate engine speed and fuel flow or load in addition to boost pressure. Alternatively, an electro-hydraulic system may be more appropriate. The same control variables can be used to achieve the required nozzle opening. Ultimately, it may prove necessary to adopt microprocessor control, particularly if a multi-variable scheme is chosen. Under these conditions it will be possible to optimize the nozzle opening schedule for best efficiency operation. The driver will demand either speed as is the case conventionally, or power,

and the optimized system will give optimum nozzle opening for the particular operating conditions.

ii) Engine considerations

To take full advantage of variable geometry turbocharging, it will be necessary to provide for variable fuel injection timing to avoid excessive pressures in the engine cylinders. This parameter too, can be controlled by the microprocessor for optimized running conditions.

It has also been clearly indicated that for a successful variable geometry scheme very wide mass flow range compressors are necessary. Endeavours in this area will be needed to ensure surge free compressor operation.

References

1. Annand, W.J.D.
"Heat transfer in the cylinders of reciprocating internal combustion engines"
Proc. I. Mech. E. Vol. 177, No. 36 1963 p973

2. Andre-Talamon, T.
"New aspects of turbocharger utilyzation with the hyperbar parallel supercharging"
I. Mech. E. C66/78 1978
Turbocharging and Turbochargers Conference.

3. Benson, R.S., Ledger, J.D., Whitehouse, N.D., and Walmsley, S.
"Comparison of experimental and simulated transient response of turbocharged diesel engines"
SAE 730666 1973

4. Berenyi, S.G., Raffa, C.J.
"Variable area turbocharger for high output diesel engines"
SAE 790064 SP-442, 1979

5. Brands., M.C.
"Helmholtz tuned induction system for turbocharged diesel engine"
SAE 790069 SP-442, 1979

6. Benson, R.S., Svetnicka, F.V.
"Two-stage turbocharging of diesel engines: A matching procedure and an experimental investigation"
SAE 740740, 1974

References

7. Bowns, D.E., Cave, P.R., Hargreaves, M.O.R., Wallace, F.J.
"Transient characteristics of turbocharged diesel engines"
Proc. I. Mech. E. 1973 p13

8. Bahmanpoor, D.
"Investigations on variable geometry nozzled radial inflow turbines"
M. Sc. Thesis, University of Bath, 1979

9. Chapple, P.M., Flynn, P.F., Mulloy, J.M.
"Aerodynamic design of fixed and variable geometry nozzleless turbine casings"
ASME Jl. of Engg. for power 1980 Vol 102 p141
79-GT-87

10. Curtil, R., Magnet, J.L.
"Exhaust pipes systems for high pressure charging"
I. Mech. E. C50/78 1978
Turbocharging and Turbochargers Conference.

11. Cser, G.
"Some results of combined charging applications"
I. Mech. E. C64/78 1978
Turbocharging and Turbochargers Conference.

12. Doerfler, P.K.
"Comprex supercharging of vehicle diesel engines"
SAE 750335 1975

References

13. Ghadiri-Zareh, M.S.
"Variable geometry single stage and two stage turbocharging of highly rated transport diesel engines"
Ph. D. Thesis, University of Bath, 1976

14. Ghadiri-Zareh, M.S., Wallace, F.J.
"Variable geometry vs two stage turbocharging of high output diesel engines"
Proc. I. Mech. E. 1978 C63/78 p119

15. Groenewold, G.M., Welliner, D.R., Kamo, R.
"Performance and sociability of Comprex supercharged diesel engine"
ASME 77-DGP-4 1977

16. Harp, J.L., Oatway, T.P.
"Centrifugal compressor development for a variable area turbocharger"
SAE 790066 SP-442 1979

17. Holler, H.G.
"The influence of induction and exhaust system design on power producing characteristics of diesel engines"
SAE 700535 1970

18. Holenberg, G.F.
"Advanced approaches for heat transfer calculations"
SAE 790825 SP/79-449

References

19. Janota, M.S., Watson, N.
"Pulse converters - A method of improving the performance of the turbocharged diesel engine"
Proc. I. Mech. E. 1973 Vol. 187 51/73

20. Kamo, R., Bryzik, W.
"Adiabatic turbocompound engine performance prediction"
SAE 780068 1978

21. Kyrtatos, N., watson, N.
"Application of aerodynamically induced prewhirl to a small turbocharger compressor"
Journal of Engg. for power 1980 Vol. 102 p943

22. Kyrtatos, N., Watson, N.
"An aerodynamic method for control and range improvement of rotary compressors"
ASME 80-GT-31 1980

23. Ledger, J.D., Benson, R.S., Farukawa, H.
"Improvement in transient performance of a turbocharged diesel engine by air injection into the compressor"
SAE 730665 1973

24. Monaghan, M.L.
"Boosting for a purpose"
I. Mech. E. C55/78 1978
Turbocharging and Turbochargers Conference.

References

25. Marzouk, M., Watson, N.
"Load acceptance of turbocharged diesel engines"
I. Mech. E. C54/78 1978
Turbocharging and Turbochargers Conference.

26. Rochford, K.G.
"Series turbocharging - A requirement for high specific output vehicular diesel engines"
SAE 790067 SP-442 1979

27. Robinson, R.R., Mitchell, J.E.
"Development of a 300 psi BMEP continuous duty diesel engine"
Proc. CIMAC 1965

28. Sanwalka, A.K.
"Investigation of alternative forms of variable geometry nozzleless turbine casings"
M.Sc. Thesis, University of Bath, 1976

29. Sivakumaran, K.
"Performance of diesel engines in association with variable geometry turbocharging"
Ph. D. Thesis, University of Bath, 1975

30. Schnurbein, Von., E.
"Constant-pressure turbocharging for medium-speed four-stroke engines"
I. Mech. E. C51/78 1978
Turbocharging and Turbochargers Conference.

References

31. Summerauer, I., Spinnler, F.S., Mayer, A., Hafner, A.
"A comparative study of the acceleration performance of a truck diesel engine with exhaust-gas turbocharger and with pressure-wave supercharger Comprex"
I. Mech. E. C70/78 1978
Turbcharging and Turbochargers Conference.

32. Smyth, R., Wallace, F.J.
"Comparative performance assessment by digital computers of various C.I. engine configurations in combination with compressors and turbines"
Proc. I. Mech. E. Vol. 181, Pt. 1, No. 12 p259 1966-67

33. Taylor, D.H.C., Whattam, M., Janota, M.S.
"Comparison of single and two stage turbocharging on a medium speed four-stroke diesel engine at high BMEP's"
CIMAC 1971 A-19

34. Veshagh, A.
"Steady state and dynamic simulation of single and two stage turbocharged diesel engines"
Ph. D. Thesis, University of Bath, 1979

35. Wallace, F.J., Way, R.J.B.
"A comprehensive suite of steady state and transient response engine-turbocharger performance prediction programs"
UNICEG/SRC conference, London, April 1980

References

36. Wallace, F.J., Hargreaves, M.R.O.
"The differential compound engine - Transient response of the dce compared with conventional t/cd engines"
SAE 1974 740722

37. Wallace, F.J., Whitfield, A., Atkey, R.C.
"Experimental and theoretical performance of a radial flow turbocharger compressor with inlet prewhirl"
Proc. I. Mech. E., 43/1975 Vol. 189 p177

38. Wallace, F.J.
"Matching of high output diesel engines with associated turbomachinary"
Proc. I. Mech. E. 48/1973 Vol. 187 p548
Two papers — Second paper:
"Differential compound engine"

39. Wallace, F.J., Baines, N.C., Whitfield, A.
"A unified approach to the one-dimensional analysis and design of radial and mixed flow turbines"
ASME March 1976 76-GT-100

40. Wallace, F.J.
"Theoretical assessment of the performance characteristics of inward flow turbines"
Proc. I. Mech. E. 1957 p931

41. Wallace, F.J., Cave, P.R., Miles, J.
"Performance of inward radial flow turbines under steady flow conditions with special reference to high pressure ratios and partial admission"

References

Proc. I. Mech. E. 1969

42. Whitehouse, N.D., Way, R.J.B.
"A simple method for heat release rates in diesel engines based on the fuel injection rate"
SAE Jan. 1971 710134

43. Whitfield, A., Patel, M.H., Wallace, F.J.
"Design and testing of two radial backward swept turbocharger compressors"
Proc. I. Mech. E. 1978

44. Whitfield, A., Wallace, F.J., Atkey, R.C.
"The effect of variable geometry on the operating range and surge margin of a centrifugal compressor"
ASME 76-GT-98 1976

45. Watson, N., Marzouk, M., Baazaari, Z.
"An evaluation of two stage turbocharging for efficient high output diesel engines"
ASME 78-DGP-2 1978

46. Winterbone, D.E., Benson, R.S., Closs, G.D., Mortimer, A.G.
"A comparison between experimental and analytical transient test results for a turbocharged diesel engine"
Proc. I. Mech. E. Vol. 190 22/76 p267

47. Watson, N., Holness, B.S.
"Engine and turbocharger interaction with multi-entry pulse converters"

References

I. Mech. E. C65/78 1978

Turbocharging and Turbochargers Conference.

48. Watson, N., Marzouk, M., Baazaari, Z.

"Turbocharger system options for vehicle engines"

I. Mech. E. C61/78 1978

Turbocharging and Turbochargers Conference.

49. Winterbone, D.E., Benson, R.S., Mortimer, A.G., Kenyon, P.

"Transient response of turbocharged diesel engines"

SAE 770122 1977

50. Wallace, F.J., Sivakumaran, K.

"Matching of high output turbocharged engines for maximum torque back up and emission reduction based on the use of variable geometry compressors and turbines"

SAE 740738 1974

51. Wallace, F.J., Sivakumaran, K.

"The differential compound engine - Part 1: Steady state and emission characteristics"

SAE 740721 1974

52. Whitehouse, N.D., Way, R.J.B.

"Rate of heat release in diesel engines and its correlation with fuel injection data"

Proc. I. Mech. E. 1969-70 Vol. 184 Pt. 3J

53. Wallace, F.J., Way, R.J.B., Baghery, A.

"Variable geometry turbocharging - The realistic way forward"

References

SAE 810336 Detroit Feb. 23-27 1981

54. Wallace, F.J.
"Performance of two-stroke compression ignition engines in combination with compressors and turbines"
Proc. I. Mech. E. 1963 177 p43-63

55. Whitfield, A., Wallace, F.J.
"Performance prediction for automotive turbocharger compressors"
Proc. I. Mech. E. 1975 Vol. 189 12/75

56. Wallace, F.J., Baghery, A., Ziarati, M.R.
"Variable geometry turbocharging for transport engines"
I. Mech. E. Conference on Turbocharging and Turbochargers
London, 1982.

57. Ziarati, M.R.
"Mathematical modelling and experimental testing of variable geometry inward radial flow turbines"
Ph. D. Thesis, University of Bath, 1979